Projective Process Monism

A Geometric Framework for Physics, Measurement, and the Observer

The Ontology

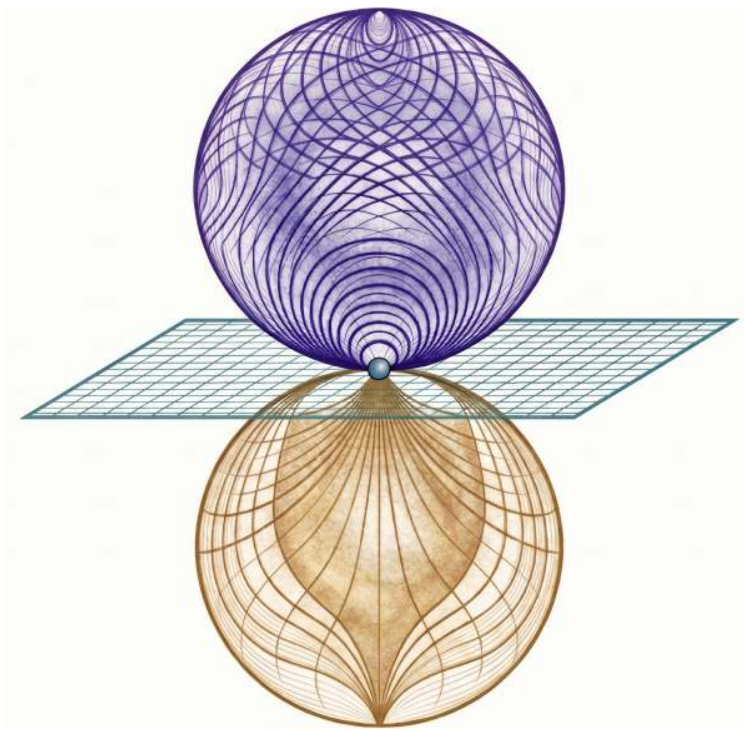

Jeff Wozniak

v1.1.0 | 2026-06-10

doi:10.5281/zenodo.20498762

ppm-framework@v1.2.0 | doi:10.5281/zenodo.20497332

Projective Process Monism

A Geometric Framework for Physics, Measurement, and the Observer

The Ontology

Jeff Wozniak

projectiveprocessmonism.com

contact@projectiveprocessmonism.com

Abstract. Phenomenal experience has the geometry of real projective three-space, $\mathbb{RP}^3$, established by phenomenology (Rudrauf et al., 2017; Williford et al., 2018) and supported by psychophysical experiment. This document takes that observation as a physical constraint and works out what reality must be like for experience to have that structure.

$\mathbb{RP}^3$ embeds uniquely as the fixed-point set of a complex conjugation τ on $\mathbb{CP}^3$. That single embedding forces the Standard Model gauge group, three and only three generations of matter, the Born rule, the fine-structure constant, the energy hierarchy descending from the Planck scale, Newton's constant, the cosmological constant, the quark CKM CP phase, the entire mass spectrum, and the conditions for biological experience — all from one arena ($\mathbb{CP}^3$), one operator (τ-projection from possibility to actuality), and one kind of event. The dynamics is variational: a free-energy functional $\mathcal{F}[\rho, \theta]$ is minimized at every scale of the hierarchy, with persistent structure (gravity at Planck, gauge content at Pati-Salam, the Higgs vacuum at electroweak, confinement at QCD, biological cognition where the hierarchy crosses thermal energies) appearing where the variational principle has stable minima. The same topology fixes the information content: each projection event delivers a scale-independent entropy of $\approx 5.5\, k_B$ from the Hopf-fiber circumference, and $\mathbb{RP}^3$ carries a finite topological capacity for fiber sections, $N_\infty = \varphi^{392}$, that sets both the information storage limit of the universe and the cosmological constant.

Phenomenal experience comes online at one specific scale: where individual actualization events have energy comparable to ambient thermal noise, and the integrated information Φ across the boundary is nonzero. The boundary's coupled dynamics under those conditions constitute experience read from inside. The framework identifies qualia with the stripped (non-actualized) content each τ-projection leaves perpendicular to the actualized record;

agency with the boundary's dynamics read from inside; the self with the recurring pattern those dynamics produce at a particular substrate (brain, body, environment). The framework is a process monism in the tradition of Whitehead (1978): reality is the sequence of τ-projection events. Matter, spacetime, and consciousness are persistent $\mathcal{F}$-minima of one variational landscape at different scales, not separate ontological categories needing a relation. The quantum measurement problem, fine-tuning of physical constants, cosmological constant problem, hard problem of consciousness (Chalmers, 1995), and mind–body problem all admit structural resolution within this framework — without new particles, extra dimensions, or modifications to Standard Model field equations.

The framework predicts: the cosmological constant matches observation to within a few percent; an effective Newton's constant $G_{\text{eff}}(z) = G_0(1+z)^{3/2}$ accounts simultaneously for the JWST early-galaxy population (Labbé et al., 2023) and the Hubble tension; the dark-energy equation of state $w_{\text{eff}} > -1$ strictly (no phantom crossing); the proton lifetime falls in the 10^{34}–10^{35} year window; the Hawking-radiation Page curve does not turn over from the external observer's perspective (information stripped at the horizon goes to the normal bundle, inaccessible from the tangent side); Φ scales as $\sqrt{N}$ for cortical architectures ($d_\Sigma = 2$); the synchronization window for phenomenal binding sits at ~ 60 ms; and anesthetic recovery follows a Berezinskii–Kosterlitz–Thouless-sharp transition.

The closing self-referential loop — phenomenology in, phenomenology out — is the framework's strongest structural claim: the $\mathbb{RP}^3$ structure of phenomenal experience is both the framework's empirical anchor and its derived prediction. Every claim in the chapters that follow maps to a corresponding section in the Technical Reference via marginal annotations (T.x); a reader who wants the derivations should consult that document.

Contents

Preface

This document is the ontological exposition of Projective Process Monism. It is the conceptual treatment: what the framework says about reality, why each piece is where it is, and what follows from the choices the geometry forces. The mathematical derivations live in the Technical Reference, which this document sometimes cites but does not depend on. A reader who wants the math should pick up the Technical Reference; this volume is for the reader who wants to know what the math means.

This document is for philosophers of physics, philosophers of mind, and technically literate readers interested in the foundational questions of reality, measurement, and consciousness. The text uses mathematical notation freely but keeps the structural argument in the foreground; the calculations are the Technical Reference's job. Familiarity with the language of manifolds, group actions, and projective spaces will help. Readers without that vocabulary can consult the math primer at projectiveprocessmonism.com, which covers each concept in a short self-contained entry.

The chapters develop in the order the framework develops itself. Parts I and II establish the arena ($\mathbb{CP}^3$, the involution τ, actuality as $\mathbb{RP}^3$) and the dynamics that follow from it. Parts III and IV trace the consequences across information, the Standard Model spectrum, gravity, and cosmology. Part V takes up consciousness: what the geometry says about boundaries, phenomenal structure, and the biological scale. Part VI is the closing arc—comparisons to other frameworks, what the framework resolves and dissolves, deep open questions, and the catalog of testable predictions.

The work is unaffiliated with any academic institution and is published openly. Substantive corrections, technical critiques, and pointers to relevant prior work are welcomed.

Part I

Foundations

Chapter 1

The Problem Space

Modern physics rests on two theories of extraordinary empirical precision—quantum mechanics T.1.8, 18
and general relativity—each of which describes its domain to many decimal places. Yet taken together, the theoretical landscape of fundamental physics exhibits four deep structural failures. These are not gaps in experimental coverage or technical inconveniences awaiting the next generation of accelerators. They are failures of the conceptual framework within which physics currently operates, and they share a common root.

1.1 Four Failures

The measurement problem. Quantum mechanics describes the evolution of physical systems with mathematical precision, but its formalism breaks in two at the moment of measurement. Between measurements, the state evolves smoothly and deterministically (Schrödinger evolution). At the moment of measurement, the state undergoes an abrupt, probabilistic transition (the Born rule). The theory provides no account of what constitutes a measurement, when it occurs, or why it follows this specific probabilistic law. Every interpretation of quantum mechanics—Copenhagen, many-worlds (Everett, 1957), Bohmian (Bohm, 1952), decoherence (Zurek, 2003), objective collapse (Ghirardi et al., 1986)—is an attempt to paper over this discontinuity. None eliminates it. The Born rule itself ($P = |\psi|^2$) (Born, 1926) is an axiom: empirically confirmed to extraordinary precision, never derived.

The fine-tuning problem. The Standard Model of particle physics contains 26 dimensionless parameters—coupling constants, mass ratios, mixing angles—that are measured with high precision and are essential to the structure of the physical world. None is derived from the theory. They are inputs, not outputs. The theoretical framework is compatible with a vast range of possible values for these parameters. The actual values we observe occupy no distinguished position within that range. The theory provides no account of why these values and not others. The cosmological constant compounds the problem: its observed value is roughly 10^{120} times smaller than the most natural theoretical estimate (Weinberg, 1989), a discrepancy so extreme that it has been called the worst prediction in the history of physics.

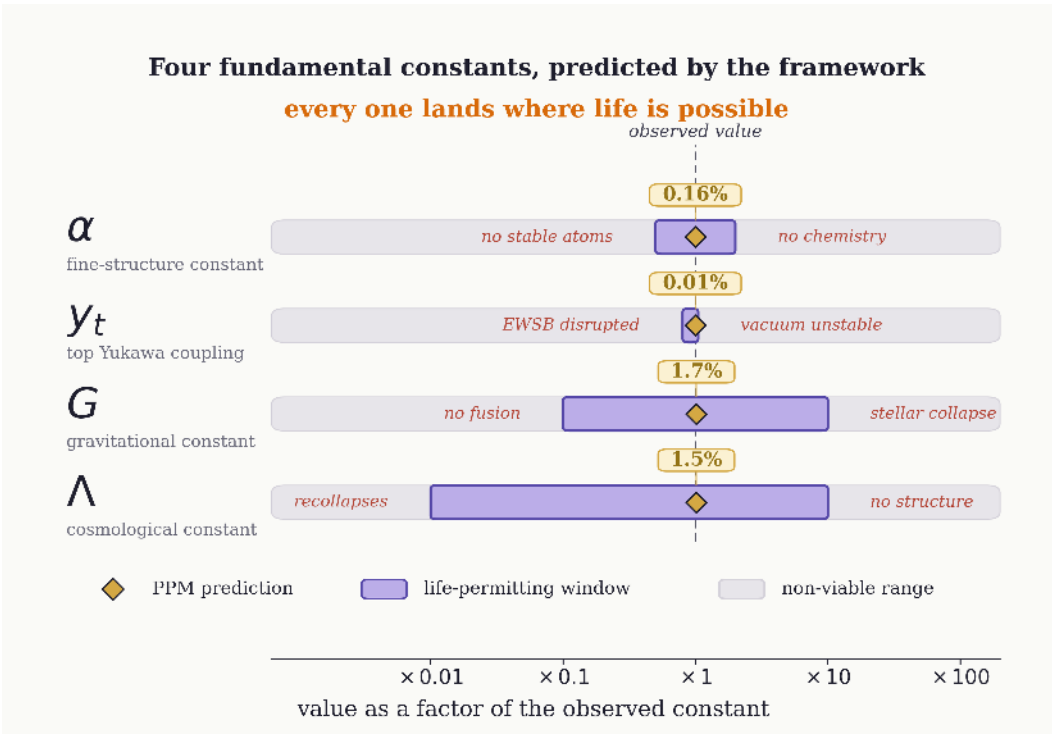

Figure 1.1: *Life-permitting ranges for four fundamental constants, compared with values derived from the PPM framework (gold diamonds, with percentage errors against observation). Each purple window spans the range of variation compatible with a universe containing stable atoms, stars, and large-scale structure, drawn from published anthropic bounds (Barrow and Tipler, 1986; Carr and Rees, 1979; Degrassi et al., 2012; Tegmark et al., 2006); the grey track is the non-viable remainder. The observed value sits at ×1. The fine-structure constant α and the top Yukawa coupling y_t are derived from $\mathbb{CP}^3$ spectral geometry alone; the gravitational constant G and cosmological constant Λ require one additional energy-scale reference (m_π, or the structural anchor ε_0). All four predictions fall within the life-permitting window; the framework's task is to explain why they take the values they do rather than accepting them as free parameters.*

The unification problem. General relativity describes gravity as the curvature of spacetime. Quantum field theory describes the strong, weak, and electromagnetic forces as excitations of quantum fields on a fixed spacetime background. Despite decades of effort, these two descriptions resist unification. The difficulty is not merely technical. Each theory assumes something the other denies: general relativity requires a dynamical spacetime; quantum field theory requires a fixed background. String theory, loop quantum gravity, and other programs have sought to resolve this tension, but none has produced a unique, parameter-free unification. A deeper structural obstruction exists: no existing framework provides an operator connecting spatial geometry to chiral gauge content—the two sectors of physics that must be linked for unification to succeed.

The hard problem of consciousness. Physical theories describe objective processes: mass, charge, momentum, spin. Conscious experience is subjective: there is something it is like (Nagel, 1974) to see red, to feel pain, to hear a chord. The gap between these two kinds of description has resisted every attempt at reduction. Functionalist accounts explain the *function* of consciousness (what it does) but not its *character* (what it is like). Eliminativist accounts deny the explanandum. Physicalist accounts defer the explanation to future neuroscience without specifying what form such an explanation could take. The hard problem (Chalmers, 1995) is not merely unsolved within current physics; it is *unformulable*. No existing physical theory contains the vocabulary to state, let alone answer, the question of why physical processes produce subjective experience.

1.2 A Common Root

These four failures appear unrelated. The measurement problem concerns quantum foundations. Fine-tuning concerns cosmology and particle physics. Unification concerns quantum gravity. Consciousness concerns philosophy of mind. They are studied by different communities, published in different journals, and addressed with different mathematical tools.

Yet they share a structural feature: each arises because the relevant physical theory begins with a mathematical structure chosen for tractability rather than derived from constraint. Quantum mechanics postulates a Hilbert space and a measurement rule. The Standard Model postulates gauge groups and parameters. General relativity postulates a Lorentzian manifold. In each case, the starting point is a piece of mathematical machinery selected because it works, not because something forces it to be so.

When the starting point is underconstrained, the theory inherits arbitrary features: free parameters (fine-tuning), undefined operations (measurement), structural incompatibilities (unification), and missing vocabulary (consciousness). The four failures are not independent pathologies; they are four symptoms of the same underlying condition.

1.3 An Alternative

The alternative is to derive the mathematical structure from an empirical constraint so tight that nothing is left free.

This is not a new methodological principle. It is how the most successful revolution in the history of physics actually proceeded. Einstein did not postulate the Minkowski metric. He took the Michelson–Morley result (Michelson and Morley, 1887)—the empirical invariance of the speed of light—seriously, asked what space and time must be for it to hold, and derived the structure of spacetime from that constraint (Einstein, 1905). The Lorentz transformations, the relativity of simultaneity, the equivalence of mass and energy were all consequences of a single empirical fact, taken seriously and followed to its mathematical conclusion.

Projective Process Monism adopts the same strategy with a different empirical starting point: the geometric structure of phenomenal experience, which fixes the arena ($\mathbb{CP}^3$ with $\mathbb{Z}_2$ involution) and from which the rest of the framework follows.

Chapter 2

The Empirical Starting Point

Chapter 1 argued that physics' four structural failures share a single cause: insufficient T.1.8
empirical constraint at the foundation. This chapter supplies the constraint.

The starting point is conscious experience treated as empirical data: it has structure, that structure is empirically accessible, and taking it seriously as a constraint on physical theory turns out to be extraordinarily productive.

2.1 The Phenomenology of Projective Space

Before any formal analysis, a simple phenomenological exercise establishes the central claim: the geometry of conscious experience is projective.

Stand at one end of a long straight road and look along it. The edges of the road converge toward a point on the horizon. Parallel lines meet. This is the defining property of projective geometry, and it is an immediate feature of perceptual experience. Euclidean geometry says parallel lines never meet. Your experience says they do. You live in projective space.

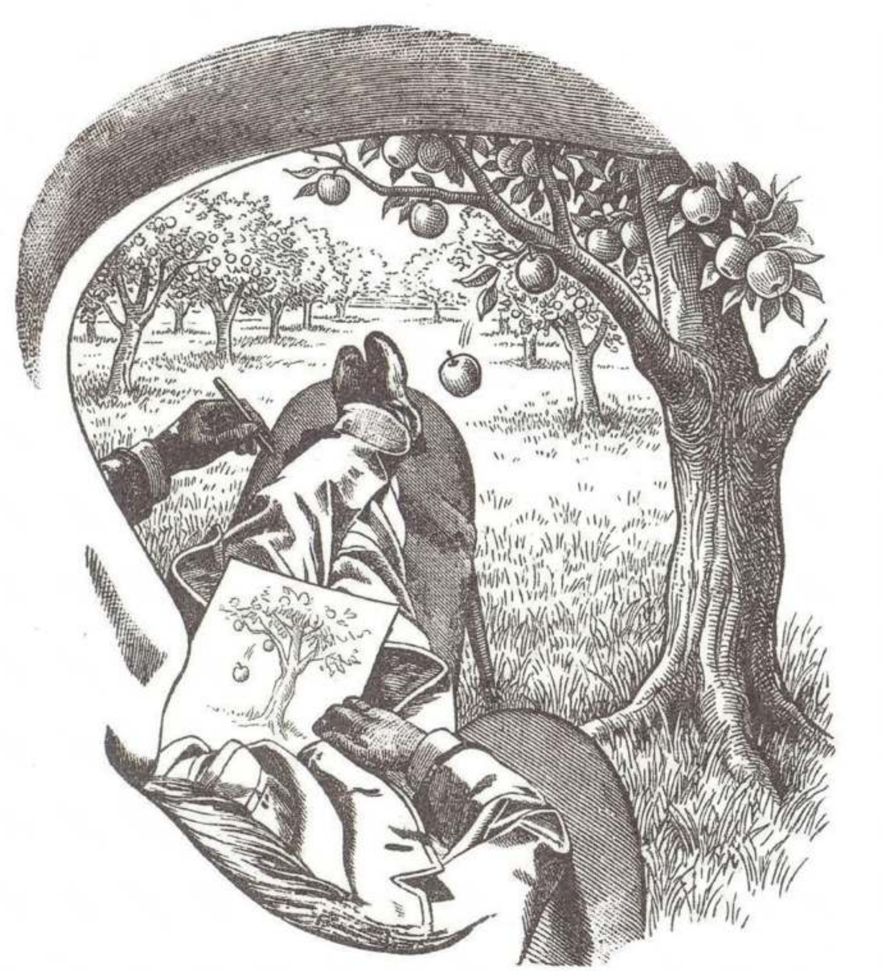

Figure 2.1: *The view from the right eye—the visual field seen from within. The field has no sharp boundary; it fades into the brow, nose, and cheek rather than terminating at an edge. The point from which one is looking does not appear as an object within the field. Both properties are characteristic of projective geometry: a compact space with no boundary, organized around an origin that is structurally present but experientially absent.*

Ernst Mach rendered the same structure with characteristic precision in his famous drawing of the visual field seen from the left eye (Mach, 1886). The view from inside the visual field—the brow, nose, and cheek framing a visual expanse that has no sharp boundary (Figure 2.1)—makes the topology plain. The visual field does not terminate at an edge. It fades. There is no frame. This is a topological property: the visual field is a projective surface, not a bounded Euclidean rectangle. It has no boundary because projective spaces are compact: they close on themselves.

Now attend to where you are. You cannot see the point from which you are looking. The origin of your visual experience is not a location *within* the visual field—it is the point through which all lines of sight pass. Every direction in your experience radiates from this point, yet the point itself is invisible. This is the projective origin: structurally present (all directions intersect there), experientially absent (it cannot appear as an object among objects). A camera has a focal point with exactly this structure. You are the focal point of your experience.

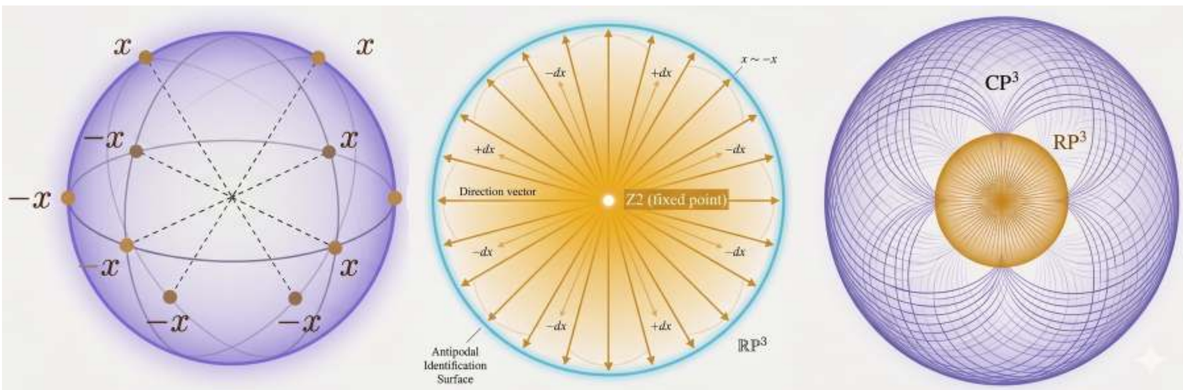

Figure 2.2: *The three geometric spaces of the framework, as a single integrated triptych.* Left: *the three-sphere S^3 with antipodal point pairs $(x, -x)$ marked across the surface.* Center: *the $\mathbb{Z}_2$ identification $x \sim -x$ collapses each pair to a single point, producing real projective three-space $\mathbb{RP}^3$ — the actuality space in which experience is given. The observer sits at the focal point; direction vectors radiate outward through the field of view to the antipodal identification surface where opposite directions meet, just as in the visual field where far ahead and far behind connect through the surround rather than separating at a wall.* Right: $\mathbb{CP}^3$*, the framework's full possibility space, with $\mathbb{RP}^3$ embedded as the locus of fixed points of the involution τ (the gold inner structure). The fibrous violet structure surrounding $\mathbb{RP}^3$ is the imaginary content that τ-projection strips when an event actualizes. S^3, $\mathbb{RP}^3$, $\mathbb{CP}^3$, and the τ-involution that relates them are the framework's basic geometric vocabulary; subsequent chapters develop the dynamics that runs on this scaffold (Chapter 3 formalizes $\mathbb{CP}^3$; Chapter 4 develops τ).*

The depth axis shares this projective character. Objects far ahead and objects far behind are not separated by a wall; they are connected through the visual surround. Turn around and you have not jumped to a different infinity—you have traversed a continuous path through the same connected space. The horizon wraps around you. Opposite directions meet, in the precise sense that the far distance in every direction forms a single connected boundary rather than a collection of isolated endpoints. This is the experiential signature of antipodal identification: in projective space, diametrically opposite directions are the same point at infinity.

These observations are not incidental curiosities. They are structural features of the space in which conscious experience occurs. The convergence of parallel lines, the compact boundary structure, the invisible origin, the connected horizon: taken together, they specify a three-dimensional geometry. That geometry is real projective three-space, $\mathbb{RP}^3$. Its $\mathbb{Z}_2$ topology—the 720-degree rotational identification that distinguishes $\mathbb{RP}^3$ from $\mathbb{R}^3$, demonstrated by the Dirac plate trick—is unpacked formally in Chapter 3.

2.2 The Wider Survey

The topology covered above fixes the spatial geometry of the visual field. Experience has further structural features beyond the spatial—features any framework purporting to give the geometry of experience must also honor. Three traditions—transcendental phenomenology, the Projective Consciousness Model, and Integrated Information Theory—have each named these features under their own vocabulary. The names converge on the same observations and supply the language used in the rest of the document. The exercise here is not argumentative; it is the same as before: attend to your own experience while reading.

Mineness. The experience you are having is yours. It is presented to you, not to anyone else, and no third-person vantage on it exists. Husserl (Husserl, 1913) called this *perspectivality*: every experience is experience *from* a point of view, and that viewpoint is constitutive of what the experience is. Integrated Information Theory (Oizumi et al., 2014; Tononi et al., 2016) calls it *intrinsic existence*: experience exists for the system that has it, not for an external observer. The two names refer to the same phenomenological observation. Whatever the geometry of experience is, it must contain the perspective that experience is from.

Temporal thickness. The present moment is not a knife-edge instant. It carries the immediate past—you can hear the beginning of a word while you hear its end—and it anticipates the immediate future. Husserl named the trailing edge *retention* and the leading edge *protention*; the sustained middle is the *living present* (Husserl, 1928). The current moment is a window with extent, not a point. The framework's geometry of experience must support a temporal grain consistent with this window.

Unity. The experience you are having is one experience. You do not have one experience for the left half of your visual field and another for the right; the field is unified. Integrated Information Theory calls this *integration*: experience is irreducible in the sense that it cannot be partitioned into independent components without losing what it is. The framework's geometry must accommodate this irreducibility.

Composition. The unified experience is nonetheless structured. It has a foreground and a background, near things and far things, parts that relate to each other. Integrated Information Theory calls this *composition*: experience is built up from sub-experiences that are themselves experiences. The framework's geometry must accommodate this compositional structure.

These four—mineness, temporal thickness, unity, composition—together with the projective-spatial topology of the previous section, constitute the empirical specification of experience that the framework's geometry must honor. That three programs arrive at the same set of features by different routes (the PCM from psychophysics, Husserl from first-person reflection, IIT from postulating an intrinsic causal structure for consciousness) is expected if all three are describing the same object. The next section translates the specification into geometry.

2.3 From Phenomenology to Geometry

The phenomenological observations above are intuitive and pre-formal. Rudrauf et al. (2017) T.1.8
and collaborators placed them on rigorous mathematical footing through the Projective Consciousness Model (PCM). The PCM proceeds by identifying the invariant structure of conscious experience—the features that remain constant across changes in attention, posture, and sensory modality—and showing that these invariants are the defining properties of a specific geometric space. The perspectival organization of the visual field (all directions radiating from an invisible origin), the horizon structure (antipodal identification at infinity), the absence of a boundary (compactness), and the 720-degree rotational periodicity ($\mathbb{Z}_2$ fundamental group) are not independent features; they are the axioms of $\mathbb{RP}^3$ expressed in experiential terms. Rudrauf and collaborators showed that no other three-dimensional geometry satisfies all of these invariants simultaneously.

The claim is testable because $\mathbb{RP}^3$ makes quantitative predictions about perceptual phenomena that differ from the predictions of Euclidean or affine geometry. The Moon Illusion—the perceived enlargement of the moon near the horizon—follows from the projective metric on $\mathbb{RP}^3$: angular size is measured along geodesics of the Fubini-Study metric, and the curvature of these geodesics produces a systematic magnification near the horizon that matches the observed effect. The Ames Room Illusion, in which people of different sizes appear identical when placed at geometrically conjugate points in a distorted room, follows from projective equivalence: the two positions are projectively indistinguishable, so the visual system treats them as identical despite the Euclidean discrepancy (Figure 2.3). Williford et al. (2018) tested these predictions in virtual reality psychophysics, placing subjects in controlled projective environments and measuring their perceptual responses. The match between projective-geometric prediction and experimental observation is exact within measurement error.

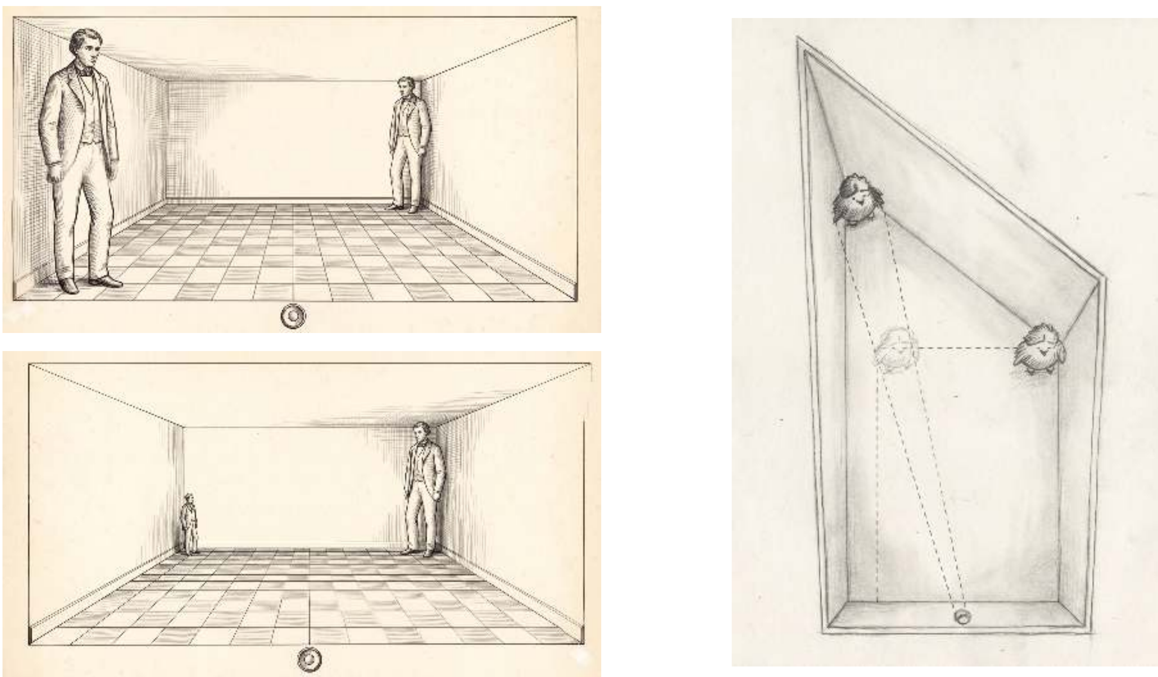

Figure 2.3: *The Ames Room demonstrates projective equivalence in perception.* Left, top: *the flipped view from outside the privileged viewpoint, where the trapezoidal geometry is plain and the figures recover their true proportions.* Left, bottom: *the perceptual experience through the peephole—the room appears rectangular and the two figures, who are actually the same height, appear to differ wildly in size.* Right: *the room's geometry. The actual floor plan is a trapezoid; two figures placed in opposite corners are at very different distances from the privileged viewing point (peephole), so the rays they subtend at the eye are equal even though their real-world sizes are not. The visual system resolves the projective ambiguity by assuming the room is Euclidean (its default expectation); the figures inherit the size discrepancy that the geometry actually distributes. The illusion fails only by stepping outside the peephole.*

The claim is that the geometry of conscious experience *is* projective geometry. The structure is not imposed by the analyst; it is discovered in the phenomenon.

2.4 Neutral Monism

The phenomenological result establishes that conscious experience has the mathematical structure of $\mathbb{RP}^3$. A further philosophical step is needed to connect this to physics: the claim that the structure of experience and the structure of the actual physical world are the same structure. This is the commitment that has been called neutral monism—the position that there is a single kind of structure underlying both the mental and the physical, and that what we call "mental" and "physical" are two readings of this common structure rather than two fundamentally different kinds of stuff. This framework is a neutral monism in the strict sense: it takes one structure ($\mathbb{RP}^3$ embedded in $\mathbb{CP}^3$) and reads it as physics from one direction and as the geometry of experience from another. The lineage runs back through Russell, James, and Spinoza, with structural realism (Ladyman and Lorenzetti, 2024) as the modern relative; what the framework adds is specificity. Chapter 22 surveys the lineage and the framework's relationship to neighbouring positions (physicalism, property dualism, idealism, structural realism, panpsychism). Here the commitment itself is announced.

The structural identity is more than analogy. An analogy would assert a likeness between two distinct structures; the claim here is that $\mathbb{RP}^3$ as recovered from phenomenology and $\mathbb{RP}^3$ as the fixed-point set of τ on $\mathbb{CP}^3$ are the same mathematical object, accessed from different directions. The kind of evidence that supports the identification is structural-feature parity: a property derived in one register predicts a feature in the other. The half-integer spinor closure on $\mathbb{RP}^3$ gives a 720° phenomenological signature recoverable in the plate trick and in visual-field rotation experiments; the projective-arena topology predicts a horizonless visual field with a structurally absent origin, which is exactly what Mach's self-portrait shows; the Hopf circle on each point of $\mathbb{RP}^3$ corresponds to a phase degree of freedom visible in interference experiments and in the temporal thickness of perceptual moments. What would falsify the identification is a structural feature of phenomenology that has no counterpart in the geometric object, or a structural feature of the geometric object that is absent from phenomenology under conditions where it should appear—for example, a phenomenological geometry that is not projective on careful examination, or a topological invariant of $\mathbb{RP}^3$ that has no detectable correlate in experience. None of the parities established so far are conclusive on their own; their weight is cumulative. The fuller comparison with neighbouring positions, and the discussion of what the identification commits one to philosophically, is deferred to Chapter 22.

The next chapter takes this empirical result—experience has the structure of $\mathbb{RP}^3$—and asks the mathematical question Einstein's strategy demands: given the actual world, what is the space of all possibility that produces it? The next chapter constructs that space.

Chapter 3

The Arena

The previous chapter established that conscious experience has the structure of $\mathbb{RP}^3$. This chapter does two things. First, it derives the canonical complexification of $\mathbb{RP}^3$ to obtain $\mathbb{CP}^3$—the smallest space containing the actual world as a real section, and therefore the framework's possibility space. Second, it describes the internal structure that $\mathbb{CP}^3$ carries: its $\mathbb{Z}_2$ topology, its metric, its fibrations, and its decomposition into actual and unrealized directions. That structure will, in later chapters, turn out to encode electromagnetism, gravity, and the full particle spectrum. T.1.1–1.7

3.1 From $\mathbb{RP}^3$ to $\mathbb{CP}^3$

The actual world is the collection of definite states—what has in fact happened. The possibility space must be larger: it must contain the actual world as a distinguished subspace, and it must contain everything that could have happened but did not. The mathematical question is: what is the simplest space containing $\mathbb{RP}^3$ as a real section?

The answer is uniquely determined. The canonical complexification of $\mathbb{RP}^3$ is $\mathbb{CP}^3$, complex projective three-space. This is not one option among several. It is the minimal complex manifold containing $\mathbb{RP}^3$ as the fixed-point set of a natural involution. Any larger space would contain superfluous structure. Any smaller space would fail to contain $\mathbb{RP}^3$ as a proper real section.

The result: the space of all possibility is $\mathbb{CP}^3$, a six-dimensional compact manifold. The actual world, $\mathbb{RP}^3$, sits inside it as a three-dimensional submanifold—the collection of all points that are purely real. The remaining three dimensions are imaginary directions: the space of unrealized possibility surrounding every point of actuality.

The analogy to special relativity is exact in structure, though different in content. Einstein took the empirical invariance of the speed of light and asked: what must spacetime be for this result to hold? The answer—Minkowski spacetime—was uniquely determined by the empirical constraint. The framework takes the empirical projective geometry of conscious experience and asks: what must the space of possibility be for this geometry to hold? The answer—$\mathbb{CP}^3$—is uniquely determined by the same kind of reasoning.

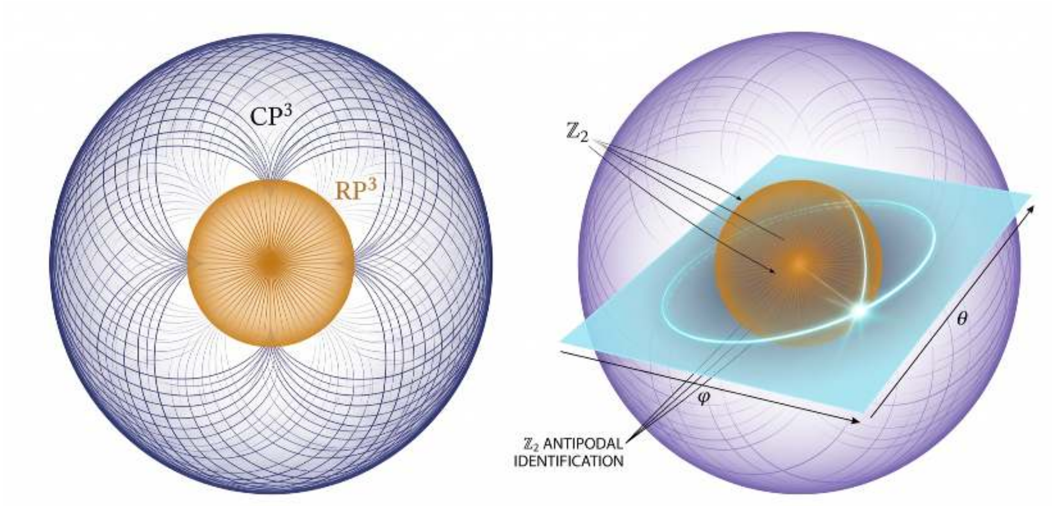

Figure 3.1: $\mathbb{CP}^3$ *(the six-dimensional space of possibility) with* $\mathbb{RP}^3$ *(the three-dimensional space of actuality) as the luminous locus of fixed points under the* $\mathbb{Z}_2$ *involution* τ*. This image is the foundation of the framework: every force, every particle, and the structure of phenomenal experience emerge from the internal geometry of this single arena.*

3.2 The Arena's Structure

The arena's construction is fixed. But "$\mathbb{CP}^3$ with τ" names a single object that carries several compatible kinds of geometric structure at once: its topology (how the space is connected), its metric and curvature (how distance and area work), its complex structure (which directions at each point are real and which imaginary), its fibration (how the six dimensions organize into nested circles and lines), and its tangent-normal decomposition along the actual world $\mathbb{RP}^3$ (which directions lie within actuality and which extend outside it). Each is determined by the choice of arena. The rest of this chapter takes each in turn.

3.3 Six Dimensions, Compact, Without Boundary

The arena is six-dimensional (six real dimensions, equivalently three complex dimensions). It is compact: it has finite total volume. It is without boundary: there is no edge, no wall, no place where the space ends. Every path within it can be extended indefinitely without ever reaching a terminus. Geodesics—the straightest possible paths—curve back on themselves, as they do on the surface of a sphere. The arena is geodesically complete.

These properties are not incidental. Compactness guarantees that integrals over the arena converge, which is essential for the information-theoretic quantities (entropy per event, information per event) that will appear later. Geodesic completeness guarantees that the actualization dynamics never reach a boundary condition that would require external specification. The arena is self-contained.

3.4 The $\mathbb{Z}_2$ Topology

The actual world inherits a specific topological feature from its projective structure. Projective three-space has fundamental group $\mathbb{Z}_2$ (Hatcher, 2002): rotations of 360 degrees are non-contractible loops; rotations of 720 degrees are contractible. The Dirac plate trick demonstrates the property mechanically. Hold an arm out with a cup of water, palm up. Rotate the cup 360 degrees around the vertical axis (under the arm, over the shoulder). The arm is now twisted—it has accumulated a topological winding that cannot be undone without reversing the rotation. Without reversing direction, rotate another 360 degrees. The arm untwists. The trick works because the rotation group of three-dimensional space, SO(3), has fundamental group $\mathbb{Z}_2$: a 360-degree rotation is a closed loop in SO(3) that cannot be contracted to a point, but a 720-degree rotation can. The twist in the arm records the topological non-triviality of the path. This is the same $\mathbb{Z}_2$ that characterizes $\mathbb{RP}^3$ because SO(3) and $\mathbb{RP}^3$ are diffeomorphic—they are the same manifold.

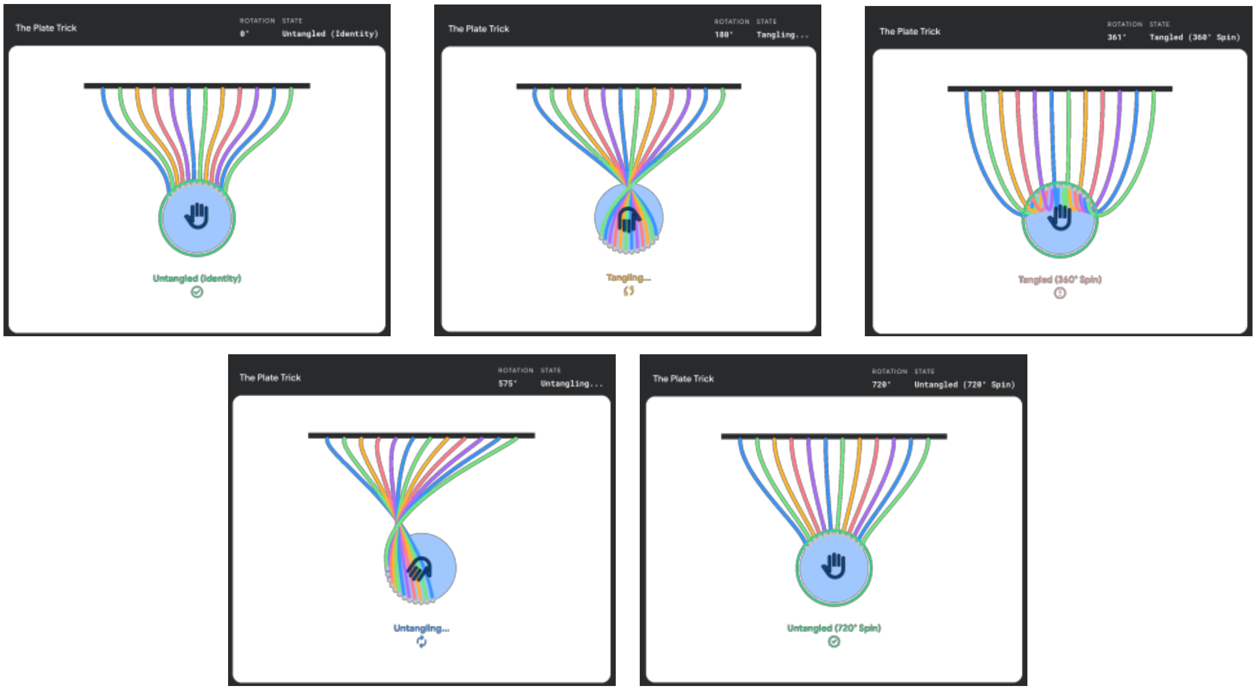

Figure 3.2: *The Dirac plate trick demonstrates the $\mathbb{Z}_2$ fundamental group of $\mathbb{RP}^3$. A disc (the "plate") is connected to a fixed bar by colored ribbons that record the topological state.* Top row, left to right: *at* $0°$ *the ribbons hang straight, untangled; at* $180°$ *they begin to cross as the disc rotates; at* $360°$ *the ribbons are locked in a tangle that cannot be undone by any continuous deformation—the system has traversed the non-contractible loop in SO(3)* $\cong \mathbb{RP}^3$. Bottom row: *continuing past* $360°$*, the tangle begins to resolve (*$575°$*); at* $720°$ *the ribbons return to their original untangled configuration, identical to the starting state. The* $360°$ *tangle records the non-trivial element of* $\pi_1(\mathbb{RP}^3) = \mathbb{Z}_2$*; the* $720°$ *resolution demonstrates that this element has order two. The reader can reproduce this with a belt: hold one end fixed, rotate the other* $360°$*, observe the twist cannot be removed; rotate another* $360°$ *in the same direction, and the belt can be untwisted by passing it over the buckle.*

The $\mathbb{Z}_2$ structure is load-bearing. It will reappear in the Born rule (Chapter 6, where the requirement that probability assignments respect $\pi_1(\mathbb{RP}^3) = \mathbb{Z}_2$ forces the exponent in $|\psi|^2$), in the spinor character of half-integer-spin matter (Chapter 12, where a single fiber's 720-degree identification produces fermion statistics), and in the projective frame's parameter space (Chapter 19, where the measurement torus T^2 inherits the same fundamental group). The phenomenological observation that opposite directions on the horizon are connected through the surround—demonstrated in the previous chapter—is the experiential reading of this same topology.

3.5 The Fubini-Study Geometry

The arena carries a natural metric—a way of measuring distances between points—called the Fubini-Study metric. It generalizes spherical geometry to complex projective space, and is the unique metric (up to overall scale) compatible with the complex structure and projective symmetries of $\mathbb{CP}^3$ (Griffiths and Harris, 1978). Just as the curvature of a sphere is fully specified by the sphere's own geometry without reference to any surrounding space, the arena's curvature is an internal property. T.1.1

The Fubini-Study metric has a characteristic feature: its sectional curvature varies between two values. Directions along holomorphic (purely imaginary) sections have curvature one. Directions along the actual world (the real section, $\mathbb{RP}^3$) have curvature one-quarter. Intermediate directions have intermediate curvatures. This variation is not a contingent feature; it follows from the Kähler structure described below.

The curvature ratio of four to one (holomorphic to totally-real) has direct physical consequences. Higher curvature means shorter geodesics: a path through the imaginary (possibility) directions of the arena closes on itself faster than a path through the real (actuality) directions. The curvature ratio fixes a tunneling rate, and that rate fixes the fine-structure constant α. This asymmetry governs the instanton tunneling amplitude—the rate at which a state on the actual world can tunnel into the imaginary directions and return. The tunneling amplitude is suppressed exponentially in the geodesic length of the path through possibility space, and because that space is more tightly curved, the suppression is stronger than it would be in a flat space. The balance between this suppression and the complexification drive of the Kähler structure determines the rate at which the actualization cycle runs, which in turn fixes α (Chapter 6). The curvature ratio is locked to four by the projective structure of the arena, and α inherits this rigidity.

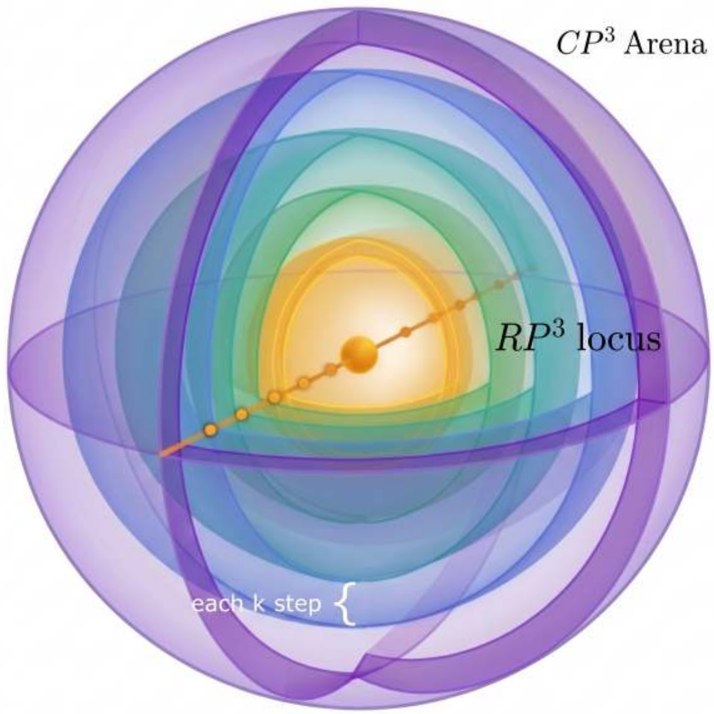

Figure 3.3: *The $\mathbb{CP}^3$ arena geometry. The arena viewed as nested spheres, with the $\mathbb{RP}^3$ locus (gold) at the core and Fubini-Study distance increasing radially outward through the full $\mathbb{CP}^3$ volume (violet). Each concentric shell marks one step in the energy hierarchy (k-level): moving inward toward $\mathbb{RP}^3$ increases fiber stiffness and decreases accessible phase space. The color gradient—gold at the core through cyan to violet at the outer boundary—traces the transition from actuality to possibility. Particle species, gauge thresholds, and the critical scale all sit at characteristic radii; their locations are derived from the Hopf fiber circumference in Chapter 14.*

3.5.1 The Round Metric on $\mathbb{RP}^3$ as Zoll Structure

The Fubini-Study metric restricted to $\mathbb{RP}^3$ is the round metric of constant sectional curvature $1/4$ — the inherited geometry of the totally-real section. This round metric has a strong global property: every unit-speed geodesic on $\mathbb{RP}^3$ closes back on itself in the same total length, making $\mathbb{RP}^3$ a *Zoll manifold* (Besse, 1978). That a 3-manifold is Zoll at all is not generic: manifolds all of whose geodesics close are heavily constrained, and the symmetric ones — the compact rank-one symmetric spaces — form a short classified family that $\mathbb{RP}^3$ belongs to. The integer ruler the cascade depends on is available because actuality's manifold is one of these few spaces rather than a generic 3-manifold. Three dimensions is moreover the unique case where $\mathbb{RP}^3$ admits non-constant-curvature Zoll metrics, an exception the arena inherits structurally.

Zoll structure is the unnamed source of several features the framework otherwise presents as starting points. The Laplacian spectrum on a Zoll manifold clusters around integer-shifted values $(\ell + \alpha)^2$ with multiplicities scaling as ℓ^{n-1} (Colin de Verdière, 1973); the integer k-level structure of the cascade developed in Chapter 14 is this Zoll spectral cluster, not a separate quantization assumption. The geodesic flow on a Zoll manifold admits a global section, which is what makes the icosahedral $\mathbb{RP}^3$ tiling discussed in Chapter 17 a well-defined object. The Funk transform on $\mathbb{RP}^3$ — the integral of a function over closed geodesics — is invertible, giving a real-side companion to the Penrose transform that operates on the imaginary directions of $\mathbb{CP}^3$ (LeBrun and Mason, 2002).

3.6 Kähler Structure

The arena is a Kähler manifold: it carries a metric, a symplectic form, and a complex structure J, all three mutually compatible. The metric is the Fubini-Study metric introduced above. The symplectic form measures oriented areas. The complex structure J is the endomorphism of the tangent space at each point satisfying $J^2 = -1$; it rotates tangent vectors by a quarter turn within each complex coordinate plane, distinguishing real from imaginary directions. Every complex projective space is canonically Kähler (Griffiths and Harris, 1978); the arena's Kähler structure is built into its construction. T.1.5

The compatibility is strong: any two of the three objects determine the third. The physical consequence is that real and imaginary directions are coupled. A state sitting on the actual world is not stable in the Kähler sense; the symplectic structure generates a flow that pushes states into imaginary directions. This is the geometric origin of the complexification tendency described in the actualization cycle (Chapter 6): possibility regenerates from actuality because the arena's own geometry drives states off the real section.

3.7 Four Complex Dimensions

The arena $\mathbb{CP}^3$ is the projective space of four complex dimensions (six real), constructed as the equivalence classes of nonzero vectors in $\mathbb{C}^4$ under scalar multiplication. The dimension is forced by three simultaneous requirements. T.1.6

First, the arena must admit an anti-holomorphic involution (the actualization operator) whose fixed-point set is three-dimensional, matching the observed dimensionality of space.

Second, the arena must support the Hopf fibration, which encodes electromagnetic structure. Third, the arena's isometry group must contain the Pati–Salam gauge group (Pati and Salam, 1974), the maximal gauge symmetry before the first stage of symmetry breaking.

The case-by-case comparison makes the uniqueness visible:

Arena	Real dimension	Fixed-point set	Maximal gauge content
$\mathbb{CP}^1$	2	$\mathbb{RP}^1$ (1-dim)	U(1) only
$\mathbb{CP}^2$	4	$\mathbb{RP}^2$ (2-dim)	up to SU(2) (rank 2 tangent)
$\mathbb{CP}^3$	6	$\mathbb{RP}^3$ (3-dim)	up to SU(4) $\supset$ SU$(3)_C$ (rank 3)
$\mathbb{CP}^n$, $n \geq 4$	$2n$	$\mathbb{RP}^n$ (n-dim)	larger, but fixed set $>$ 3-dim

$\mathbb{CP}^1$ carries only U(1)—abelian, sufficient for electromagnetism, too small for non-abelian color. $\mathbb{CP}^2$ supports at most SU(2), since the holomorphic tangent has complex rank two; its fixed-point set is also two-dimensional, not three. $\mathbb{CP}^3$ is the smallest projective space whose holomorphic tangent has complex rank three, supporting SU$(3)_C$, and whose anti-holomorphic involution has a three-dimensional fixed-point set. $\mathbb{CP}^n$ for $n \geq 4$ produces fixed-point sets of dimension greater than three, inconsistent with observation.

The three requirements above bind the dimensionality of the arena, the dimensionality of the actual world, the gauge group structure, and the existence of the actualization operator into a single constraint with exactly one solution.

The framework identifies each of the four complex components of a vector in $\mathbb{C}^4$ with one independent kind of factual content that a single actualization event can extract from the arena: spectral content (what frequencies are present), spatial content (where something is), chiral content (which handedness), and intensity content (how much energy). These four fact types are developed fully in Chapter 9; each transforms differently under the actualization operator.

3.8 Two Fibrations

The arena carries two internal fibration structures—two distinct ways of organizing its six dimensions into a base space threaded by fibers. Each fibration encodes a different sector of physics. T.1.3–1.4

The first is the Hopf fibration. It exists because $\mathbb{CP}^3$ is defined as the quotient of the unit sphere S^7 in $\mathbb{C}^4$ by the U(1) phase action—dividing out by the freedom to multiply all coordinates by a common phase factor $e^{i\theta}$ (Nakahara, 2003). The orbits of this phase action are circles, and the projection from S^7 to $\mathbb{CP}^3$ organizes the arena as circles (one-dimensional fibers) threaded through the seven-dimensional sphere. The circular fiber encodes electromagnetic structure: the electromagnetic gauge symmetry is precisely the freedom to rotate along these circles without changing the projective point. The circumference of each circle is 2π, a topologically fixed quantity that turns out to be the fundamental scaling factor governing the entire energy hierarchy (Chapter 14).

The second is the twistor fibration. It exists because $\mathbb{CP}^3$ is the twistor space of the four-sphere S^4—a fact established by Penrose (1967) as part of the twistor program. The fibration organizes the arena as two-spheres (S^2) fibered over S^4, where each point of S^4 corresponds to a family of null geodesics (light-ray directions) in the conformal geometry of spacetime. This structure encodes gravitational degrees of freedom: solutions to the gravitational field equations can be reformulated as holomorphic structures on twistor space, and the arena *is* this twistor space.

$\mathbb{CP}^3$ is the only complex projective space that supports both fibrations simultaneously (Penrose, 1967). This is why both electromagnetism and gravity exist: they are not independent forces pasted together; they are two structural features of the same geometric space. The difficulty of unifying them in other frameworks arises because those frameworks treat them as separate entities requiring unification, rather than recognizing them as different fibrations of a single arena.

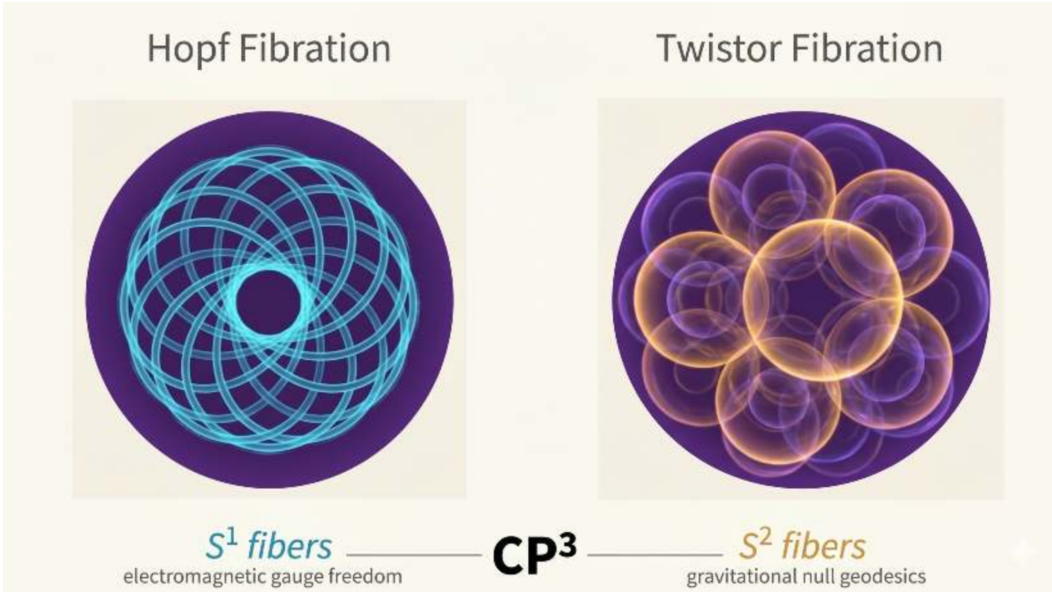

Figure 3.4: $\mathbb{CP}^3$ *admits two complementary fibration structures. Left: the Hopf fibration decomposes the arena into circular S^1 fibers—the orbits of the* U(1) *phase action—encoding electromagnetic gauge freedom. The fibers are topologically linked: every pair threads through the other, a property unique to the Hopf structure. Right: the twistor fibration decomposes the same arena into S^2 fibers over S^4, encoding gravitational null geodesics. Both structures coexist on a single geometric space; electromagnetism and gravity are distinct fibrations of the same arena.*

3.9 The Tangent and Normal Bundles

The actual world $\mathbb{RP}^3$ sits inside the arena $\mathbb{CP}^3$ as a three-dimensional submanifold. At every point of the actual world, the six dimensions of the arena split into two groups of three: three directions tangent to $\mathbb{RP}^3$ and three directions normal to it. This splitting is the tangent/normal bundle decomposition, and it is one of the most consequential structural features of the framework. T.1.3, 1.7

The tangent bundle consists of the real directions—the directions along which the actual world extends. These directions are preserved by the actualization operator: τ maps them to themselves. Content living in the tangent bundle survives projection intact. At the particle scale, tangent directions correspond to spatial and intensity degrees of freedom. At the critical scale, they correspond to the structural features of experience that persist from moment to moment.

The normal bundle consists of the imaginary directions—the directions perpendicular to the actual world within the arena. These directions are anti-fixed by τ: the operator reverses their sign. As a vector bundle the normal bundle is topologically trivial—it factors globally as $\mathbb{RP}^3 \times \mathbb{R}^3$, carrying no twists or holonomy of its own. This follows from $\mathbb{RP}^3$ being a Lagrangian submanifold of the Kähler arena combined with the parallelizability of $\mathrm{SO}(3) \cong \mathbb{RP}^3$. Content living in the normal bundle is stripped by each actualization event and deposited as residual structure over the actual world. At the particle scale, normal directions correspond to spectral and chiral degrees of freedom. At the critical scale, they correspond to the qualitative character of experience—the content that is transcoded, event by event, from imaginary to actual. Triviality matters downstream: properties carried along normal directions (charge, color, mass) take their values from how the arena's isometry group acts on the fibers, with the bundle's intrinsic topology contributing nothing additional.

The decomposition into tangent and normal is not a choice of coordinates; it is determined by the operator. Wherever τ acts, the distinction between preserved and stripped content follows. This is why the normal bundle reappears throughout the framework in different guises: as the carrier of quantum numbers at particle scales, as the source of entropy at thermodynamic scales, as the locus of qualia at the critical scale. In each case, the underlying geometry is the same—three imaginary directions at each point of the actual world—but the physical interpretation depends on the energy scale and the constraints operative there.

The Hopf fibration and twistor fibration described in the previous section organize the arena globally; the tangent/normal decomposition organizes it locally, at each point of the actual world. Together, they exhaust the arena's internal structure.

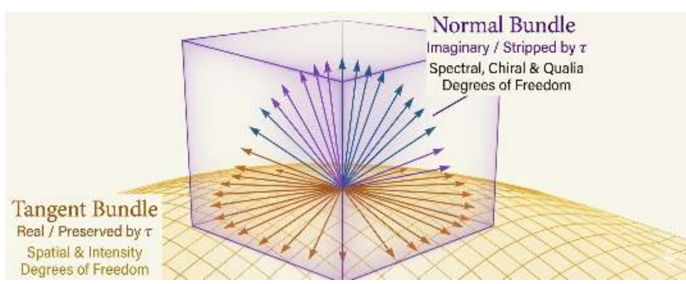

Figure 3.5: *The tangent/normal decomposition at a point of $\mathbb{RP}^3$. Gold arrows mark the three tangent (real) directions preserved by τ; violet arrows mark the three normal (imaginary) directions stripped by τ at each actualization event. The split is determined by the operator's action on the arena and is the geometric content of one fiber. Part IV builds on this split: the tangent directions carry the propagating wave-function, while the normal directions carry the spectral and chiral content (quantum numbers, charge, mass).*

3.10 Intrinsic Completeness

The arena requires no embedding in a larger space. All six dimensions are physically meaningful: three (the real directions, the tangent bundle of $\mathbb{RP}^3$) constitute the actual world, and the other three (the imaginary directions, the normal bundle) constitute the space of unrealized possibility at each point of actuality. T.1.7

Every trajectory within the arena stays within the arena. The actualization operator maps the arena to itself. The stripped content (normal-bundle directions removed by actualization) persists as structure over the actual world, still within the arena. No external reservoir, no ambient space, no product of arenas is required. The arena is, in a precise mathematical sense, its own universe.

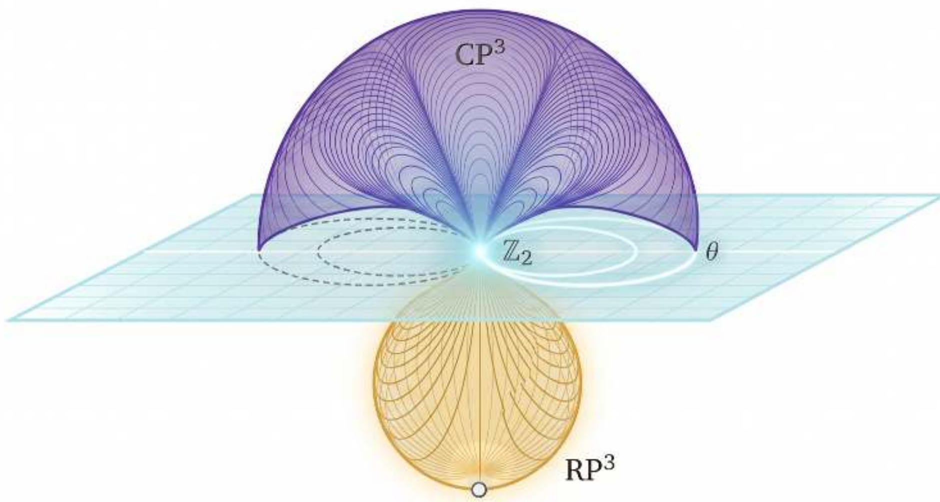

Figure 3.6: *The arena, schematically.* $\mathbb{CP}^3$ *(violet, above the plane) is the space of possibility;* $\mathbb{RP}^3$ *(gold, below) is the actual world. The two meet at the* $\mathbb{Z}_2$ *boundary, where the involution* τ *acts: complex conjugation identifies each point of* $\mathbb{CP}^3$ *with its conjugate, and the fixed-point set is* $\mathbb{RP}^3$*. Every structural feature introduced above—the Fubini-Study metric, the Kähler flow, the two fibrations, the tangent/normal decomposition—lives within this single self-contained geometry.*

3.11 Everything the Arena Provides

The chapter has built up the arena layer by layer; this closing section names what each layer contributes to the rest of the framework. Every constant, gauge group, and prediction documented in the chapters that follow traces to one of the structural inputs listed here.

Geometric input	What it sources
$\mathbb{CP}^3$ isometry group PSU(4)	Pati-Salam gauge structure; Standard Model after symmetry breaking (Chapters 11, 15)
τ involution	actuality ($\mathrm{Fix}(\tau) = \mathbb{RP}^3$); chirality ($\tau$-eigenspace decomposition); fact-type Klein four-group (Chapter 9)
Kähler structure on $\mathbb{CP}^3$	complexification drive that regenerates possibility from actuality (Chapter 6); the Lagrangian property of $\mathbb{RP}^3$
Hopf fibration $S^1 \to S^7 \to \mathbb{CP}^3$	electromagnetic gauge freedom; circumference 2π that sets the energy-hierarchy step (Chapter 14)
Twistor fibration $S^2 \to \mathbb{CP}^3 \to S^4$	gravitational degrees of freedom; the geometric setting for spacetime structure (Chapter 16)
$\pi_1(\mathbb{RP}^3) = \mathbb{Z}_2$	Born-rule exponent of 2; non-trivial spin structure; 720° spinor closure used in mixing-angle derivations (Chapters 4, 13, 15)
$\mathbb{RP}^3 \cong \mathrm{SO}(3)$ parallelizability	topological triviality of the normal bundle; permits free fact-type orbit on ν (§3.9)
Trivial normal bundle $\nu \cong \mathbb{RP}^3 \times \mathbb{R}^3$	gauge content lives on isometry-group action rather than bundle topology; clean orbit-volume reading of the hierarchy step $g = 2\pi$ (Chapter 14); together with the Fubini–Study geodesic structure, the cascade k-axis is geometrically flat, so the same fiber structure runs at every energy scale (Chapter 14 §The k-Scale as a Flat Coordinate)
Pion mass m_π	one dimensionful input; sets the energy scale of the entire cascade (Chapter 14)

Table 3.1: *Geometric inputs and what each contributes downstream.*

The framework takes nothing else. Whenever the rest of the document derives a constant, a gauge factor, a particle generation count, a mixing angle, or a cosmological parameter, the geometric source is one of the rows above. The arena's intrinsic completeness, established in the previous section, is the structural reason this short list suffices. All of this is static structure; the operator τ that acts on it is the subject of the next chapter.

Chapter 4

The Operator

The geometric structure of the arena alone does not generate events; actualization requires an operator acting on the arena. The previous chapter introduced exactly one such operator: the involution τ whose fixed-point set is $\mathbb{RP}^3$. τ is the framework's actualization operator: each firing projects a state of the arena onto $\mathbb{RP}^3$. T.2.1–2.2

Given the arena, τ is uniquely determined. It is complex conjugation:

$$\tau \colon \mathbb{CP}^3 \to \mathbb{CP}^3, \qquad z \mapsto \bar{z}, \tag{4.1}$$

the map that replaces every coordinate of a point in the arena with its complex conjugate. Real coordinates are unchanged. Imaginary parts are negated. The fixed points—τ's invariants—are precisely those with all-real coordinates: the actual world, $\mathbb{RP}^3$.

4.1 What τ Does

Each firing of τ produces an *event*: a single actualization in which one state of the arena is projected onto its fixed-point set $\mathbb{RP}^3$. Events as such—their cumulative structure, their rate, their role in process ontology—are the subject of the next chapter. This section shows what one firing does to the arena geometrically.

Globally, τ splits the arena's bundle structure: the tangent (real) directions are preserved, the normal (imaginary) directions are anti-fixed, and the projection lands on the actuality submanifold. The same action can be narrated locally along a single fiber—the per-fiber view of what τ does at each point of $\mathbb{RP}^3$ (Figure 4.1).

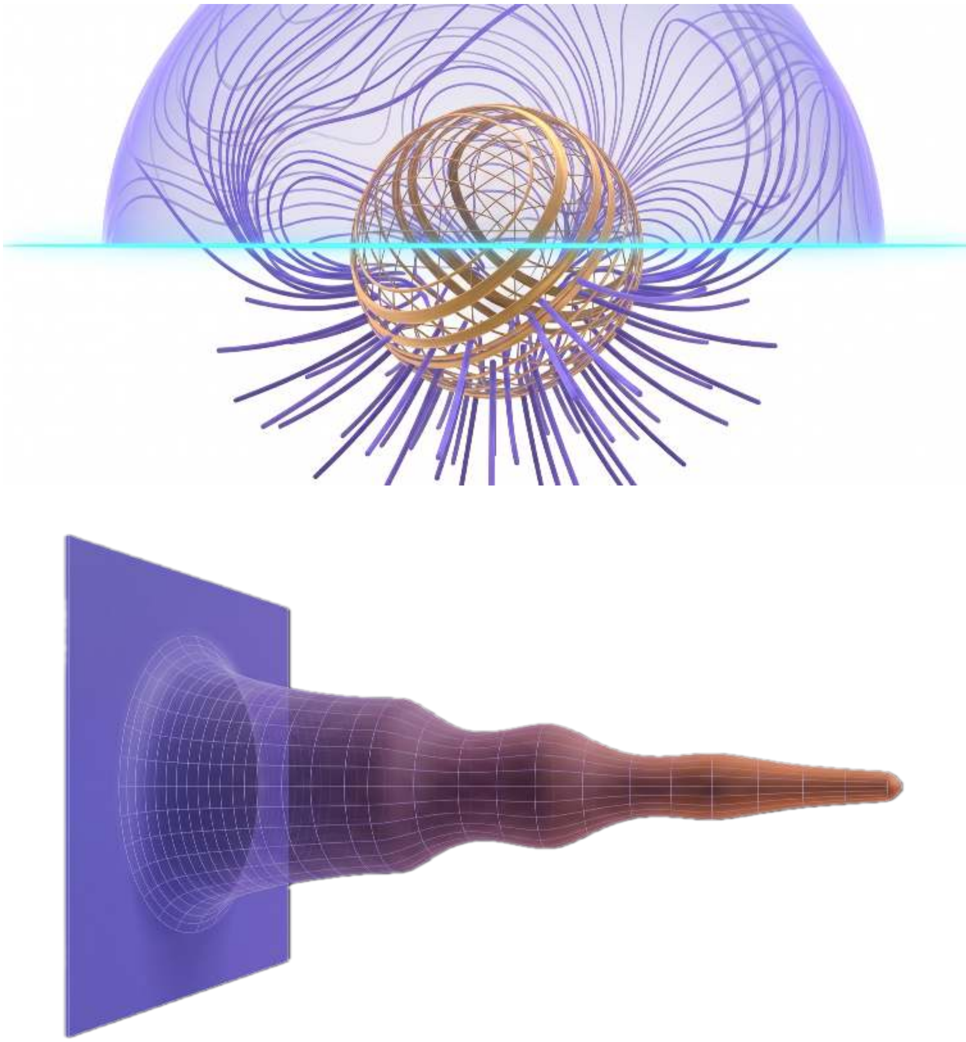

Figure 4.1: *Two views of τ's action.* Top: *the bundle picture. The violet dome is $\mathbb{CP}^3$ with its full $\mathrm{U}(4)$ symmetry structure; complex conjugation acts at the cyan $\mathbb{Z}_2$ boundary, splitting the geometry into two components at $\mathbb{RP}^3$ (gold sphere). The gold bands wrapping the sphere's surface are the tangent bundle (real directions preserved by τ); the violet filaments radiating perpendicular to the surface are the normal bundle (imaginary directions reversed by τ). The split is isometric, anti-holomorphic, involutory, and breaks $\mathrm{U}(4)$ to $\mathrm{O}(4)$—only the transformations compatible with the split survive as symmetries.* Bottom: *one fiber under the projection. A single filament of the normal bundle is rooted in the $\mathbb{CP}^3$ sheet at left and extends rightward through the projection. The filament's body is divided by successive constrictions, each marking a stage at which τ-incompatible content has been stripped; the surviving wireframe density across the filament's surface thins at every pinch. The substance gradient from cool violet at the base to warm orange at the terminus reads as the cascade from possibility-side fiber content to a single actualized event on $\mathbb{RP}^3$. No new operator acts at each pinch—what is shown is the same complex conjugation acting on a single filament across the structure of $\mathbb{CP}^3$, with the chambered constrictions standing in for successive symmetry-breaking transitions whose specific energy scales are derived in Chapter 14.*

4.2 Five Defining Properties

The operator has five properties, each of which is forced by the arena's structure:

Isometry. The operator preserves distances. The separation between any two points before actualization is the same as the separation after actualization. This property is essential: if the operator distorted the arena's geometry, it would introduce energy from outside the system. An isometric operator is a closed operation; it redistributes the arena's internal structure without adding or removing anything.

Anti-holomorphic. The operator reverses the complex structure. Where the arena distinguishes "real" from "imaginary," the operator flips the imaginary part. This is what makes it an actualization: it selects the real (actual) content and discards the imaginary (possible) content. A holomorphic operator would preserve the complex structure and therefore fail to distinguish actuality from possibility.

Involution. Applied twice, the operator returns to the identity. Conjugating twice leaves every coordinate unchanged. This property has deep consequences for process ontology (Chapter 5): it means there is no cumulative "residue" from repeated applications. Each firing of the operator is complete in itself.

Three-dimensional fixed-point set. The fixed points of the operator—the points left unchanged—form $\mathbb{RP}^3$, a three-dimensional manifold. This is the actual world. The dimensionality three is not chosen; it is a consequence of the operator acting on the specific arena $\mathbb{CP}^3$.

Symmetry breaking. Before the operator acts, the arena possesses its full isometry group: U(4) acting on $\mathbb{C}^4$, which descends to PSU(4) (dimension fifteen) on $\mathbb{CP}^3$ once the overall U(1) phase is quotiented away. The operator τ refines this further, retaining only those isometries compatible with complex conjugation. The Pati–Salam gauge group $\mathrm{SU}(4)_C \times \mathrm{SU}(2)_L \times \mathrm{SU}(2)_R$ is constructed by gauging the two complementary decompositions of the $\mathfrak{u}(4)$ isometry algebra induced by τ—a complex (holomorphic) decomposition and a τ-fixed (real) decomposition. Concretely, the algebra of arena-rotations splits two ways—once into a holomorphic part where the complex structure J is preserved, and once into the τ-fixed part where the real structure is preserved; gauging both decompositions produces the Pati–Salam group. The Standard Model arises from this construction by further reduction at higher k-levels (Chapter 15). Forces are what the geometry's symmetry licenses at each scale of the cascade after τ has selected the relevant facets.

4.2.1 Uniqueness

These five properties do not merely describe the operator; they determine it. Any anti-holomorphic isometry of $\mathbb{CP}^3$ can be written as complex conjugation composed with a unitary transformation—a change of coordinates within the arena. All such maps are conjugate to one another: they differ only in which coordinate system you use to write them down, not in their geometric content. There is one geometric operation (negating the imaginary part of the arena), and choosing a coordinate system fixes its expression as standard complex conjugation. The phrase "unique up to symmetry" means that the choice of coordinates is the only freedom; the underlying map is the same in every case. Furthermore, only one such conjugation class produces a fixed-point set of dimension three. Conjugations on $\mathbb{CP}^n$ have fixed-point sets $\mathbb{RP}^n$, so the dimension of the fixed-point set is tied to the dimension of the arena. On $\mathbb{CP}^3$, the fixed-point set is $\mathbb{RP}^3$—automatically three-dimensional. There is no second, geometrically distinct anti-holomorphic isometry to consider.

The operator is not a modeling choice, a simplifying assumption, or a parameter to be fitted. It is forced by the geometry.

This is one of the framework's central claims: given the empirical constraint ($\mathbb{RP}^3$ as the actual world) and the complexification ($\mathbb{CP}^3$ as the possibility space), the actualization operator is uniquely determined. There is nothing to choose.

4.3 Dissolving the Measurement Problem

The measurement problem of quantum mechanics asks three questions: what constitutes a measurement, when does it occur, and why does it follow the Born rule? Standard quantum mechanics cannot answer any of them from within its own formalism. A measurement is defined circularly as an interaction that produces a definite outcome; the timing of collapse is not specified by the Schrödinger equation; and the Born rule is an axiom with no derivation. Interpretations of quantum mechanics differ precisely in how they attempt to answer these three questions, and none succeeds without introducing structure beyond the formalism itself—additional worlds (Everett, 1957), hidden variables (Bohm, 1952), stochastic perturbations (Ghirardi et al., 1986), or ad hoc decoherence thresholds (Zurek, 2003).

The projection dissolves all three questions simultaneously. What constitutes a measurement? Any firing of τ—the unique anti-holomorphic isometry of the arena. No special apparatus, observer, or environment is required; the operator is a permanent structural feature that acts whenever the complexification drive pushes sufficient imaginary amplitude past the instanton threshold. When does it occur? When the accumulated imaginary content reaches the threshold set by the Kähler barrier height, which is determined by the curvature of the arena and is the same at every point and every scale. Why the Born rule? Because the topology of the fixed-point set $\mathbb{RP}^3$ has fundamental group $\mathbb{Z}_2$ (Hatcher, 2002), which forces the unique bilinear, $\mathbb{Z}_2$-invariant probability measure to be the squared amplitude (Chapter 13). The same $\pi_1(\mathbb{RP}^3) = \mathbb{Z}_2$ also fixes the framework's spin structure: of the two spin structures $\mathbb{RP}^3$ admits, the framework uses the non-trivial one—the structure for which a 360° rotation flips the spinor sign and 720° closure is required. This is the spin structure consistent with the $\mathrm{Spin}(3) \cong \mathrm{SU}(2)$ double cover of $\mathrm{SO}(3) \cong \mathbb{RP}^3$, and it is the source of the 720° closure that later surfaces in the half-integer spin of fermions and in the Berry-phase derivation of mixing angles (Chapter 15). Each answer is a geometric consequence of the arena and the operator, requiring no additional postulates.

4.4 What the Operator Is Not

The operator is not a measurement apparatus. It is not a conscious observer. It is not a decoherence process. It is not a spontaneous collapse mechanism. Each of these is a *downstream consequence* of the operator at specific energy scales.

Decoherence is what the operator's cumulative action looks like in the thermodynamic limit (many events, coarse-grained). Collapse is what a single firing looks like from the perspective of a subsystem. Measurement is the registration of an operator firing by a system with sufficient integration to record it. Conscious observation is measurement by an integrated system that sets its own projective frame—the architecture selecting which question each τ-firing asks (Chapter 19).

The operator does not "choose" outcomes. The probability of each outcome is determined by the topology of the projection (the Born rule). The operator does not need a trigger; projection is what involutions do. Complexification is what Kähler geometry does.

The next chapter takes up the events themselves: their structure as the framework's fundamental units of physical happening, the energy each firing carries, and the process ontology that the involutive character of τ commits the framework to.

Chapter 5

The Event

5.1 From Geometry to Experience

T.2.1, 2.3

The preceding chapters described the arena and the operator as mathematical objects: a six-dimensional projective manifold, an involution that fixes a three-dimensional submanifold. Everything was presented in the third person—a space out there, an operator acting on it, with properties to be catalogued. But the arena is not out there. If the framework is correct, the arena is the structure of the space you are looking out from.

Your visual field has no edge. It does not terminate at a boundary beyond which there is darkness; it curves back on itself and closes. Look for the border of your phenomenal experience and you will not find one: the topology of $\mathbb{RP}^3$ does not admit one. The compactness described in Chapter 3 is not an abstract property of a mathematical space. It is the reason your experience has the particular closed, self-contained character that it does.

The Fubini–Study metric determines how distances and angles are measured within your visual field. The tangent/normal decomposition determines what persists from moment to moment (tangent content) and what is qualitatively experienced in each moment (normal content). The Hopf fibration encodes the electromagnetic structure that governs which wavelengths of light you see. The twistor fibration encodes the gravitational structure that determines how objects curve toward each other in the scene before you. The τ-involution of Chapter 4 is what produces a definite scene at all—the operator whose action on the arena yields the discrete moments of experience.

This chapter develops the process by which τ acts on the arena to produce events: the unit of physical happening, and the unit of experiential happening read from the other side. The geometry described in the preceding chapters is doing the work—every force, every particle, every feature of conscious experience will turn out to be a consequence of the internal structure of this single six-dimensional space.

5.2 The Event

A single application of the operator to a point in the arena is an *event*: the fundamental unit of physical happening.

Before the operator fires, the point occupies the full arena—it has both real and imaginary coordinates, representing a superposition of actuality and possibility. After the operator fires, the imaginary content has been stripped. What remains is a definite point in the actual world, $\mathbb{RP}^3$: a single fact, realized.

The event is discrete and topological. There is no smooth, continuous transition from possibility to actuality. The operator is a projection; projections are discontinuous by nature. A state is either projected or it is not. The sharpness of this transition reflects the algebraic fact that $\tau^2 = \mathrm{id}$, which admits no intermediate states.

The stripped content—the imaginary directions removed by actualization—does not vanish. It persists as structure in the normal bundle over the actual world. At particle scales, this structure manifests as quantum numbers (color charge, flavor, spin quantum numbers). At cosmological scales, it accumulates as dark energy. At the critical scale, it manifests as the qualitative character of experience. The same geometric object—the normal bundle content of the projection—plays different physical roles at different energy scales.

5.3 The Energy of an Event

Each event has an energy. Alongside its location on $\mathbb{RP}^3$ and the fiber it strips, the energy is one of the event's defining attributes—the cost of crystallizing the actualized record at that event: the amount of arena content converted from probabilistic possibility into the frozen $\mathbb{RP}^3$ state the event leaves behind. Information about the stripped content is preserved in the full $\mathbb{CP}^3$ arena (it persists in the normal bundle), but it is no longer accessible from within $\mathbb{RP}^3$; what the actualized record carries is the energy paid to make that inaccessibility a fact about the world.

The same energy carries three names elsewhere in the framework, and the source it draws on is the Kähler flow of the arena itself. In quantum dynamics, the energy is the eigenvalue of the Kähler Hamiltonian H_α selected by the projection at the event; between events, H_α generates unitary evolution under the Kähler potential $V = m_\pi c^2 \log(1 + |z|^2/\lambda_C^2)$, which pushes the state away from $\mathbb{RP}^3$ into the imaginary directions and rebuilds the τ-odd content the previous event stripped, and at the next event the projection picks out one eigenstate whose eigenvalue is that event's energy. In thermodynamics, it is the energy E in the free-energy functional $F = E - TS$—the per-event contribution that the configuration's total E accumulates across all events. On the energy hierarchy, every event sits at a specific cascade level k via $k = 51 - 2\log_{2\pi}(E/m_\pi)$ (the inverse of the cascade formula in Chapter 14); the cascade is the logarithmic energy coordinate that locates events on a scale, with low k marking high-energy events near Planck and high k marking low-energy events near the CMB scale. Flow complexifies; events strip; the cycle is closed. Energy is not created at the event and not stored in some external reservoir; it is the conversion rate between two geometric forms of the same content—possibility-side τ-odd content built up by the flow, actuality-side τ-even content laid down by the projection.

The three are the same quantity. An event's energy is an eigenvalue selected by the Hamiltonian at the projection, a thermodynamic contribution added to the configuration's E, and a cascade reading at the k-scale where the event happens. The unification is stated formally in the technical document (Chapter 7, §The Energy Identity). The cascade is a coordinate, not the spectrum of H_α: H_α has its own discrete spectrum, and these eigenvalues populate the cascade non-uniformly. Both structures coexist and together describe how the framework's events distribute energy across scales.

5.4 Process Ontology

Substance ontology is the default in physics: the assumption that the world consists of enduring objects—particles, fields, spacetime points—that possess properties which change over time. Process ontology offers an alternative. It holds that events are the fundamental constituents of reality and that what we call "objects" are recurring patterns across events.

The idea has deep roots. Heraclitus argued that flux is primary and stability derivative (Heraclitus, c. 500 BCE). Buddhist metaphysics (particularly the Abhidharma tradition) analyzes experience into momentary dharmas—discrete events that arise and perish without any persisting substrate. In Western philosophy, Whitehead (1978) built a systematic process metaphysics in which "actual occasions" replace substances as the ultimate realities. Rescher (1996) extended process thought into the philosophy of science, arguing that process categories are better suited to modern physics than substance categories.

These traditions arrived at process ontology through philosophical argument. The framework arrives at it through mathematics.

The involution property ($\tau^2 = \mathrm{id}$) forces a specific ontological commitment: process ontology.

The argument is as follows: if the operator applied twice returns to the identity, then there is no mathematical object that carries forward from one event to the next. Between events, the formalism contains no state, no particle, no field configuration that persists as an enduring entity. Whatever structure exists between events is a feature of the arena's geometry and the patterns formed by sequences of events—not a substance that endures through them.

An electron, in this framework, is a pattern that recurs across a sequence of actualization events with specific regularity (specifically, with period $k = 57$ in the energy hierarchy). The electron's mass, charge, and spin are features of this pattern—properties of the recurrence, not properties of an enduring substance. A spacetime point is similarly not an object; it is a location in the accumulated record of past actualization events.

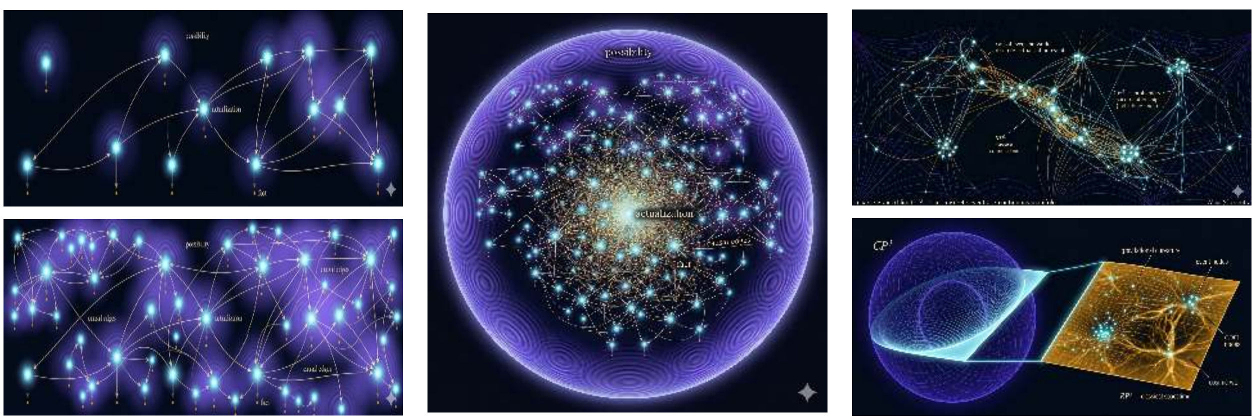

Figure 5.1: *From discrete events to continuous geometry.* Top left: *Individual actualization events form causal connections—each τ-firing produces a fact that constrains subsequent firings.* Bottom left: *As events accumulate, the causal network densifies; causal edges enforce local consistency between neighboring events.* Center: *At sufficient density, the event network coalesces into the smooth $\mathbb{RP}^3$ manifold—actuality crystallizes from possibility.* Top right: *In the coarse-grained limit ($N \to \infty$), the discrete causal network converges on a continuous manifold; gold strands trace $\mathbb{RP}^3$ classical connections while cyan lines mark $\mathbb{CP}^3$ probability-space relationships.* Bottom right: *The same projection onto $\mathbb{RP}^3$ that yields local geometry yields cosmic geometry—the smooth manifold emerging from discrete events at small scales is the same arena that hosts large-scale structure. The progression illustrates the process-ontological thesis: $\mathbb{RP}^3$ is an emergent record, tiled event by event from the actualization dynamics.*

5.5 Comparison with Whitehead

The process ontology mandated by the mathematics has structural parallels to the philosophy of Alfred North Whitehead (1978), who argued that the fundamental constituents of reality are "actual occasions"—momentary events of experience that perish immediately upon completion and are superseded by new occasions. For Whitehead, objects are "societies" of actual occasions: patterns of repetition that create the appearance of endurance.

The parallel is genuine. Both PPM and Whitehead hold that events are ontologically primary and objects are derivative. Both deny that substances persist between events. Both treat the event as having an internal structure (Whitehead's "prehension," PPM's projection from $\mathbb{CP}^3$ to $\mathbb{RP}^3$) that determines what the event contributes to subsequent events.

The differences are equally important. Whitehead's actual occasions are general: they apply to everything from electrons to human experiences, but their internal structure is described in metaphysical rather than mathematical terms. PPM's events have a specific geometric content: they are projections on a specific manifold, with quantifiable information content, entropy production, and probability distributions. This specificity is what allows the framework to derive physical predictions. Whitehead's metaphysics is compatible with many possible physics; the framework's process ontology is compatible with exactly one.

5.6 Why Substance Ontology Fails

The exclusion of substance ontology deserves explicit treatment, because the habit of thinking in terms of enduring objects is deeply ingrained in both everyday cognition and physical theory.

Consider what it would mean to overlay substance ontology on the framework. One would need to posit an entity—call it the electron-substance—that exists between actualization events and carries the electron's properties through time. But the formalism provides no mathematical object for this entity. Between events, the state of the system is described by the arena's geometry and the pattern of prior events. There is no additional structure that could serve as the carrier of an enduring substance—and no need for one: the geometry and the event pattern already encode every property the system has.

One might propose that the carrier is implicit: perhaps the pattern itself *is* the substance. But this reduces substance ontology to a verbal relabeling of process ontology. If the "substance" just is the pattern of events, then calling it a substance adds nothing explanatory and imports misleading connotations of endurance and independence.

The deeper issue is that substance ontology requires a notion of identity across time: the electron at time t_1 is *the same electron* at time t_2. In PPM, there is no fact of the matter about whether two events at different times involve "the same" entity. There is only the question of whether they belong to the same recurrence pattern. Two events belong to the same pattern if and only if they share the same k-value and quantum numbers, where k is the integer index on the energy hierarchy developed in Chapter 14 (small k near the Planck scale, large k near room-temperature scales). This is a structural criterion, not a substantial one. Identity is pattern identity, not substance identity.

Part II

Universal Dynamics

Chapter 6

The Actualization Cycle

The arena, the operator, and the event are the framework's three primitives. The actualization cycle describes how they interact: the repeating pattern by which possibility becomes actuality and actuality regenerates possibility. T.2.3, 13

Figure 6.1: *The actualization cycle in four phases.* Phase 1 (Complexification): *Kähler flow on the arena rebuilds imaginary content, expanding the state into superposition along the secret imaginary directions.* Phase 2 (Threshold): *imaginary amplitude reaches the instanton threshold, where tunneling through the Kähler barrier becomes appreciable.* Phase 3 (Projection): *the operator fires probabilistically, following the Born rule; imaginary content is stripped.* Phase 4 (Actuality): *a new definite fact is deposited into the actual world, and the cycle restarts. The tension between Kähler complexification and projection requires no external observer to trigger—the cycle is self-driving from the arena's own geometry.*

6.1 Two Geometric Tendencies

The dynamics between successive operator firings are governed by two geometric tendencies in permanent tension.

The first tendency is complexification. After the operator fires, the state sits on the actual world—all coordinates are real, all imaginary content has been stripped. The state is maximally definite and minimally possible. But the actual world, $\mathbb{RP}^3$, is a special kind of submanifold within the arena (a Lagrangian submanifold): the symplectic form pulled back to it vanishes identically (Audin, 2004; McDuff and Salamon, 2017). The Kähler structure of the arena (Griffiths and Harris, 1978) couples real and imaginary directions in the neighborhood of every point on the actual world, and this coupling generates a flow that pushes states off the real section into imaginary directions.

Possibility regenerates from actuality because the arena's own geometry naturally generates imaginary content from real initial conditions. A state sitting on the actual world is geometrically analogous to a ball sitting at the top of a saddle: the curvature of the surrounding space pushes it away from the constrained position. Possibility is the relaxed state of the arena; actuality is the constrained state.

Figure 6.2: $\mathbb{RP}^3$ *as an unstable Lagrangian submanifold of the Kähler flow, on the toy case* $\mathbb{CP}^1 \cong S^2$*.* Left: $\mathbb{RP}^1 = \mathrm{Fix}(\tau)$ *is the orange great circle; Kähler-flow arrows along it point normal, into the* τ*-odd directions the prior projection stripped.* Right: *surprisal* $F[\rho] = -\log(1-|y|^2)$ *as a bowl with minimum on* $\mathbb{RP}^3$*. An actualization event drops the state to the floor (cyan); the Kähler flow then pumps it back up the walls. The actualization cycle is the forced oscillation between* F*-stable and flow-unstable readings of* $\mathbb{RP}^3$*.*

The second tendency is projection. The operator is a permanent structural feature of the arena; it does not turn on and off. As imaginary amplitude rebuilds, the probability of projecting back onto the actual world grows. When the accumulated imaginary content reaches a critical threshold—the instanton threshold, where the tunneling amplitude through the Kähler barrier becomes appreciable (Coleman, 1985; Rajaraman, 1982)—projection occurs. The state collapses to the real section, stripping its imaginary content into the normal bundle over the actual world.

6.2 The Cycle

The two tendencies are in geometric contention. The surprisal landscape says $\mathbb{RP}^3$ is stable: the actual world sits at the minimum of F, the configuration the projection is biased toward. The Kähler flow says $\mathbb{RP}^3$ is unstable: a state on the actual world is pushed off it by the coupling between real and imaginary directions. Both facts hold simultaneously, and the cycle is the system oscillating between them.

Actuality gives rise to possibility (complexification). Possibility grows until it reaches the instanton threshold. At the threshold, the operator fires: projection strips the imaginary content and produces new actuality. From this new actuality, possibility begins to regenerate again.

The cycle is self-sustaining. No external input drives it. The Kähler geometry of the arena provides the complexification; the involutory structure of the operator provides the projection. Together, they produce a continuous alternation between the definite and the possible. Physical history is the accumulated record of this alternation. Figure 6.3 traces two turns of this cycle.

Figure 6.3: *Two turns of the actualization cycle. One full cycle, left to right: a definite event on $\mathbb{RP}^3$ (the state actualized); the crystal departing as the Kähler flow lifts the state off the real section; fiber rings expanding as imaginary content rebuilds; the holomorphic field re-emerging across $\mathbb{CP}^3$, possibility restored; and the lattice re-forming as that possibility crystallizes back toward the next event. The lattice that closes the row crystallizes into the next event. A single cycle is the $720°$ (4π) traversal $\pi_1(\mathbb{RP}^3) = \mathbb{Z}_2$ requires before an actualization completes.*

6.3 The Born Rule

Each projection event produces an outcome. To say which outcome is more likely than which, the cycle needs a probability measure on the possible outcomes of each event. In standard quantum mechanics this measure is the Born rule, $P = |\psi|^2$, postulated as an axiom (Born, 1926). Here it is forced by geometry already in place.

A probability measure on states must satisfy three conditions: bilinearity (so that superpositions decompose into component probabilities plus interference), normalization (unit amplitude gives unit probability), and continuity (small changes in the state give small changes in probability). These are the standard conditions defining what *probability measure* means on a vector space of states; they are the same conditions that drive Gleason's theorem and its quantum-measure descendants (Busch, 2003; Gleason, 1957).

Add the $\mathbb{Z}_2$ topology of $\mathbb{RP}^3$: $\pi_1(\mathbb{RP}^3) = \mathbb{Z}_2$ (Hatcher, 2002), so a 360° rotation flips a state's sign and only 720° returns it to itself. The sign-flipped state $-\psi$ represents the same physical point of $\mathbb{RP}^3$ as ψ; the antipodal identification is built into the projective structure. Observables are functions on the physical configuration space, so they must assign the same value to both representatives, and any probability measure built from the wave function must cancel the sign. The simplest such construction is $\psi^*\psi = |\psi|^2$. The three conditions above force this exponent to be exactly two: an exponent of one fails bilinearity (interference cannot arise from a non-bilinear measure), an exponent of four fails normalization. Only the squared amplitude survives.

The Born rule is therefore a structural consequence of the arena (Chapter 3) and the involutory structure of the operator (Chapter 4), not an independent postulate. The full derivation, including the relationship to Gleason's theorem and the role of bilinearity in forcing interference, is given in Chapter 13.

The rule sets probabilities, not specific outcomes. The geometry fixes the distribution over possible results of a projection event; the draw from that distribution is irreducibly stochastic. No hidden variable in the framework secretly determines which outcome occurs in advance; no-go results on local hidden-variable theories (Aspect et al., 1982; Bell, 1964; Kochen and Specker, 1967) apply directly to the projection step. The framework is deterministic in its geometric structure and indeterministic in the sequence of events that structure produces.

6.4 The Master Equation

The cycle described above—complexification rebuilding imaginary content, projection stripping it away—has a precise mathematical form. Between operator firings, the state of a system is described by a density matrix ρ, which encodes both the definite (real) content inherited from the last actualization and the growing imaginary content generated by the Kähler flow. The operator firing is a dissipative event: it irreversibly strips the τ-odd content and deposits it in the normal bundle.

The standard physics of a quantum system undergoing repeated dissipative interactions with its environment is the Lindblad master equation (Gorini et al., 1976; Lindblad, 1976). Here, the "environment" is the arena's imaginary sector, the "interaction" is the τ-projection, and the Lindblad equation is the continuous-time description of the actualization cycle applied to ρ. In what follows, $\hat{A}_b$ is the actualization operator (the projection that commits the system to a definite outcome) and the second term is the normalization correction that keeps ρ a valid probability; the formal definition of the operator is taken up in Chapter 13.

$$\dot{\rho} = \hat{A}_b \, \rho \, \hat{A}_b^\dagger - \tfrac{1}{2}\Big\{\hat{A}_b^\dagger \, \hat{A}_b, \ \rho\Big\}, \tag{6.1}$$

where $\hat{A}_b$ is the actualization operator—the mathematical expression of τ-projection in a given measurement basis b. The first term ($\hat{A}_b \rho \hat{A}_b^\dagger$) is the projection itself: it produces the actualized outcome. The anticommutator term restores the normalization lost by the projection. Together, they encode the two geometric tendencies: the state evolves toward actuality (the projection drives ρ toward τ-even configurations) while the arena's geometry continually regenerates imaginary content (captured in the pre-projection evolution of ρ).

The equation is the dynamics of the actualization cycle in its most general form. At the Planck scale, it governs the production of spacetime geometry. At the Standard Model scale, it governs particle interactions. At the critical scale, it governs the neural boundary's actualization cascade (Chapter 20). The equation is the same; only the boundary conditions and the energy scale change. Figure 6.4 shows the equation driven through many turns of the cycle.

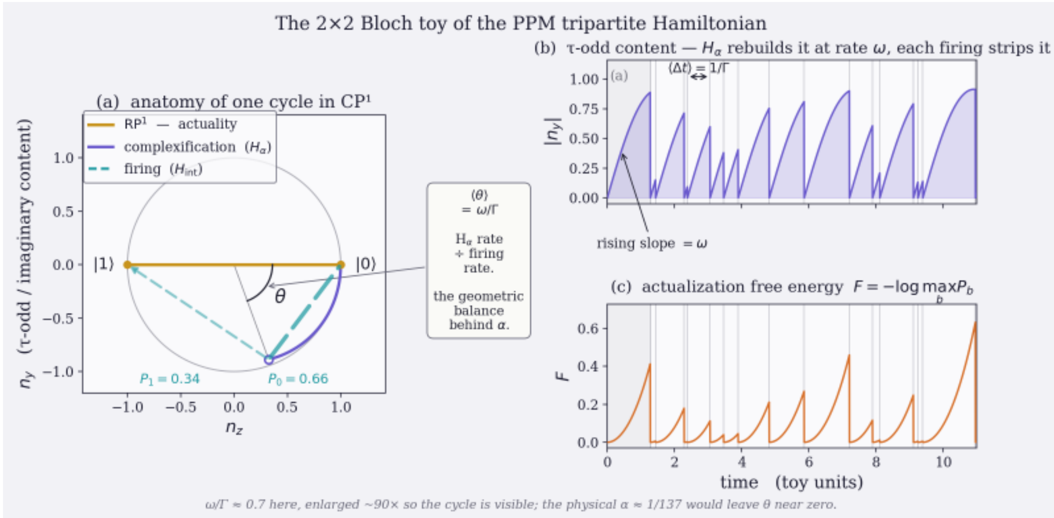

Figure 6.4: *The master equation in its smallest drawable instance:* $\mathbb{CP}^3$ *shrunk to* $\mathbb{CP}^1$ *(a Bloch sphere), with its actuality locus the circle* $\mathbb{RP}^1$*.* (a) *One turn: a definite state on* $\mathbb{RP}^1$ *(gold) lifts off the real section into possibility (violet arc tracing imaginary content); the operator then fires and projects back to actuality, landing on one of two outcomes with Born-rule probability set by how far it had travelled.* (b) *Imaginary content over many turns: regenerated by the flow, stripped at every firing.* (c) *Free energy along the same run — low after each firing, climbing as possibility rebuilds. The cycle shown runs at every scale.*

The measurement basis b in Eq. (6.1) specifies *which question* the τ-projection asks: which observable's eigenbasis the projection sharpens, drawn from the structure the operator already provides (the τ-even/odd split, the tangent and normal decompositions of Chapter 4). At most scales, the basis is set by external conditions (the experimental apparatus, the boundary geometry). At the critical scale, the basis becomes a dynamical variable controlled by the system itself—a development explored in Chapter 20. The broader implications of basis selection for the variational principle are developed in Chapter 7.

6.5 The Fine-Structure Constant as Equilibrium

The balance between the two tendencies is set by a self-consistency condition. The rate of T.13
complexification (how fast imaginary content rebuilds) and the rate of projection (how readily the operator fires once imaginary content is present) must be self-consistent: the constants governing each rate are themselves products of prior actualization events, and they must match the constants assumed at the outset.

The fine-structure constant, $\alpha \approx 1/137$, measures this balance. The equilibrium exists because both extreme limits are dynamically unstable. If α were zero, the projection would transmit no information: every actualization event would strip all content and produce no definite facts. The cycle would run but leave no record—no particles, no forces, no structure. If α were one, every bit of information would survive the projection intact: nothing would be stripped, no entropy would be produced, and the arrow of time would vanish. The complexification tendency would have no material to regenerate possibility from, and the cycle would stall after a single event. Between these two limits, a larger α means faster projection, less accumulated coherence between events, a more classical universe. A smaller α means more accumulated superposition, less definiteness, a more quantum universe. The observed value is the self-consistent point at which the complexification rate and the projection rate match.

What "match" means here is precise. The complexification rate depends on the Kähler curvature and the coupling constants that govern how fast imaginary amplitude rebuilds after a projection. The projection rate depends on the instanton tunneling amplitude, which itself depends on the same coupling constants. Both rates are functions of α. For the cycle to be stationary—for the same physics to operate from one event to the next—the α that governs the complexification between events must equal the α that governs the projection at the next event. If they differ, the cycle drifts: events would produce coupling constants different from the ones assumed at the outset, and the next cycle would operate under different physics than the previous one. The system would not reproduce itself.

The matching condition is a fixed-point requirement. Define a map that takes the coupling constants assumed before an event and returns the coupling constants produced by that event. A self-consistent universe is a fixed point of this map: constants in equal constants out. If the input α is too large (projection too fast), the event produces less coherent structure than assumed, and the effective α for the next cycle is smaller—the system corrects downward. If the input α is too small (projection too slow), more coherence accumulates than assumed, and the effective α is larger—the system corrects upward. The fixed point is an attractor: deviations in either direction are self-correcting. The observed $\alpha \approx 1/137$ is the unique value at which the map returns its own input.

This gives the fine-structure constant a geometric interpretation: it is the ratio of the actual world's content to the arena's total content, computed at the natural scale where the two tendencies balance. Three independent geometric calculations produce the same value for α, each measuring a different aspect of this ratio (Chapter 18).

The cycle supplies the rhythm and the Born rule supplies the per-event probabilities, but neither fixes the trajectory between events: which states evolve toward which outcomes, and why one direction rather than another. That direction follows from a single functional whose descent governs dynamics at every scale, developed in the next chapter.

Chapter 7

Universal Dynamics and the Variational Principle

The actualization cycle established in Chapter 6 describes a repeating pattern: complexification rebuilds imaginary content, and projection strips it away. The Born rule established in Chapter 6 tells us the probability of each outcome (the Born rule $P = |\psi|^2$, derived in Chapter 13). What neither chapter addresses is the *direction* of the dynamics: given that the cycle runs, what determines the trajectory of a system through its state space? Why does anything happen in one way rather than another? T.2.4–2.6

The answer is a single variational principle that governs dynamics at every scale. The system evolves toward the state that minimizes a functional called the actualization free energy. The principle follows from the Kähler geometry of the arena and the dissipative character of the operator.

7.1 Actualization Free Energy

Between operator firings, the state evolves unitarily within the arena. At each firing, the operator projects the state onto the actual world, stripping imaginary content. The actualization free energy, $\mathcal{F}$, measures how far the current state is from being maximally compatible with the next projection. A state sitting exactly on the actual world has zero free energy: it is already fully actual, and the operator would leave it unchanged. A state with large imaginary content has high free energy: the next projection will strip a great deal of content, and the outcome is correspondingly uncertain.

The functional $\mathcal{F}$ decreases monotonically under the actualization cycle. A quantity with this behavior is called a *Lyapunov functional*: a scalar that descends along the dynamics and pins the system to a fixed point in the limit (Khalil, 2002). The mechanism has two pieces working together, both introduced in Chapter 6. Between firings, ρ evolves continuously by the Lindblad master equation (Gorini et al., 1976; Lindblad, 1976)

$$\dot{\rho} = \hat{A}_b\,\rho\,\hat{A}_b^\dagger - \tfrac{1}{2}\Big\{\hat{A}_b^\dagger\,\hat{A}_b,\ \rho\Big\},$$

The first term applies the actualization operator $\hat{A}_b$, which is the boundary's mechanism for committing the system to a definite outcome. The second term is the normalization correction that keeps the density matrix a valid probability—it preserves total probability while the first term concentrates it. Together they decohere off-diagonal content with respect to the operator basis and prepare the state for actualization. At Poisson-distributed firing times set by the rate Γ_G, the operator projects: $\rho \to \hat{A}_b\rho\hat{A}_b^\dagger/P_b$ with probability $P_b = \mathrm{Tr}[\hat{A}_b\rho\hat{A}_b^\dagger]$ (the Born rule). After firing, ρ sits at an eigenstate of $\hat{A}_b^\dagger\hat{A}_b$ and $\mathcal{F} = 0$ for the operator that fired.

The Lyapunov property holds for the cycle as a whole. Between firings, $\mathcal{F}$ is conserved (the dissipator with Hermitian rank-1 $\hat{A}_b$ commutes with $\hat{A}_b^\dagger\hat{A}_b$); at firings, $\mathcal{F}$ collapses to zero. Averaged over a multi-operator system, unitary mixing redistributes population between firings, and stochastic firings select for high-probability outcomes via the Born rule, so the ensemble-mean $\mathcal{F}$ descends monotonically toward zero. The proof uses only positivity of ρ, the Born rule, and the algebraic structure of the dissipator; no new assumptions are introduced. The full derivation is in Technical Reference Ch. 2.

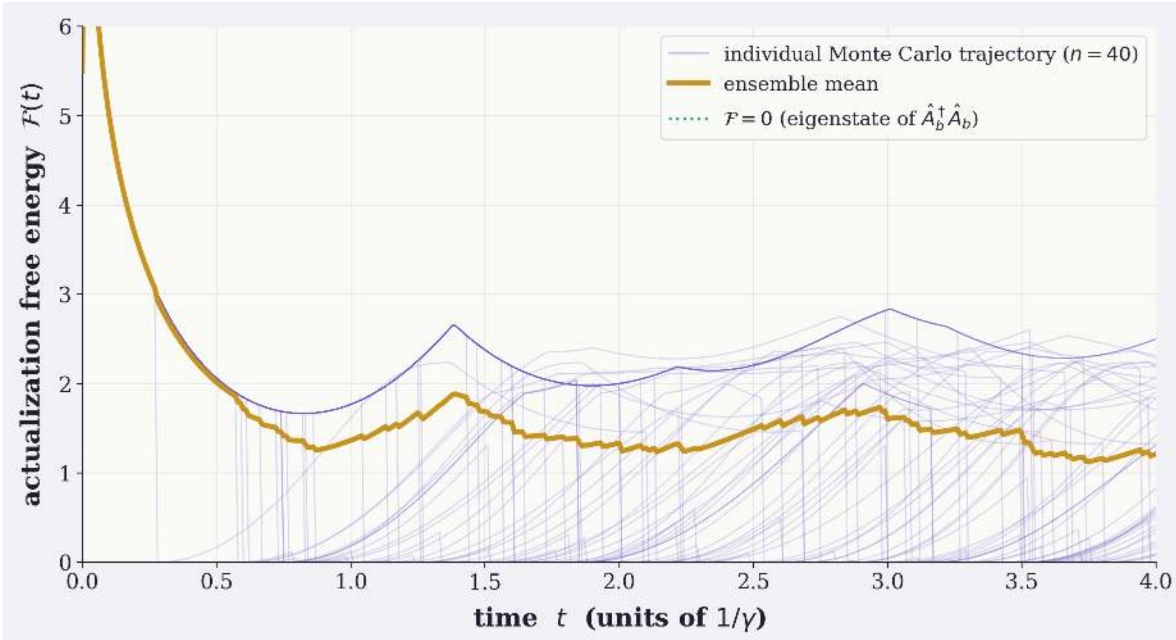

Figure 7.1: *$\mathcal{F}$ as Lyapunov functional for the full actualization cycle. Forty Monte Carlo trajectories (violet) of continuous Lindblad evolution between Poisson-timed POVM firings drawn under the Born rule, on a small $\mathbb{CP}^3$ truncation. Initial state is pure τ-odd — worst case: $\mathcal{F}(0) \to +\infty$, capped at 6 for display. Individual trajectories drop to $\mathcal{F} \approx 0$ after the first few firings; the ensemble mean (gold) descends monotonically toward the $\mathcal{F} = 0$ floor as firings collapse ρ into eigenstates of $\hat{A}_b^\dagger \hat{A}_b$. Pure Lindblad alone — with the framework's Hermitian rank-1 projector convention for $\hat{A}_b$ — leaves $\mathcal{F}$ unchanged; descent emerges only from the continuous-plus-stochastic cycle taken together.*

The Lindblad equation is the dynamical core of the framework. Every application of the variational principle described in this chapter—from Planck-scale gravity to thermodynamic equilibrium to the consciousness state equation—is a specialization of this single equation of motion to a particular energy scale and set of boundary conditions. What changes across scales is the actualization operator $\hat{A}_b$ (which encodes the relevant symmetries and constraints) and the measurement basis b (which determines how the projection decomposes outcomes into fact types). The functional $\mathcal{F}$ and the Lindblad dynamics that minimize it are universal.

$\mathcal{F}$ provides a direction for the dynamics. The system is not wandering aimlessly through the arena between projections. It is descending a landscape defined by the geometry of the arena and the structure of the operator, toward the state that is most ready to be actualized.

$\mathcal{F}$ tracks the surprisal of the next event; the von Neumann entropy tracks the *mixedness* of ρ—how far ρ is from being a pure state. A pure state corresponds to a rank-one density matrix (a single nonzero eigenvalue, one) representing a fully definite quantum state; a mixed state is a probabilistic mixture with eigenvalues spread across several outcomes. Mixedness is the spread. The two functionals have different signatures under Lindblad evolution. $\mathcal{F} = -\log \mathrm{Tr}[\hat{A}_b \rho \hat{A}_b^\dagger]$ is the surprisal of the next actualization at site b in measurement basis b—a joint property of ρ and the operator that descends to zero over the actualization cycle. The von Neumann entropy $S_{\mathrm{vN}}[\rho] = -\mathrm{Tr}[\rho \log \rho]$ (von Neumann, 1932) is the quantum analogue of Shannon entropy, built directly from the density matrix and reducing to the Shannon entropy of the eigenvalue distribution of ρ; it is the relevant comparison here because both $\mathcal{F}$ and S_{vN} are functionals of ρ acted on by the same Lindblad dynamics. S_{vN} is a property of ρ alone, measuring mixedness without reference to which operator will fire. S_{vN} has no privileged direction under Lindblad dynamics: a rank-one jump operator can increase or decrease it depending on the alignment of ρ with $\hat{A}_b$. $\mathcal{F}$ drives evolution toward the next event; S_{vN} is a state functional with no fixed sign.

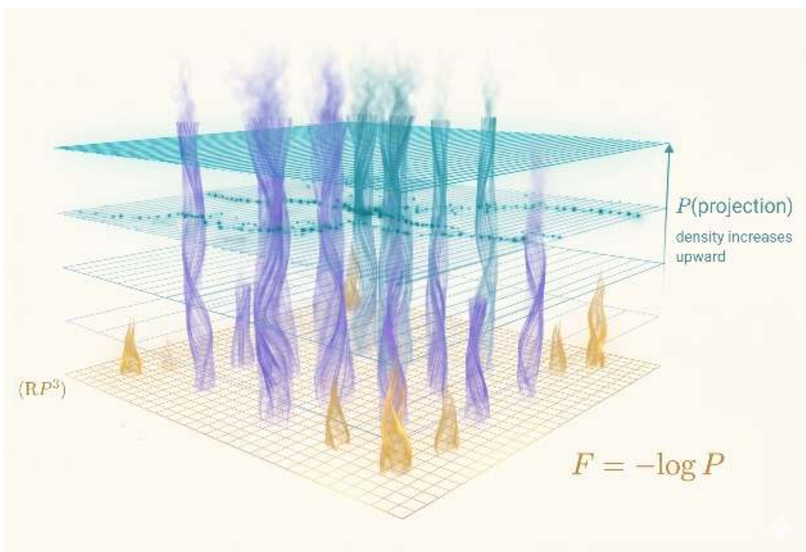

Figure 7.2: *The actualization free energy as fiber extent crossed by an asymmetric projection field. Gold baseline: the τ-stable stratum ($\mathbb{RP}^3$). Violet fibers: off-stratum content of ρ, length encoding imaginary weight. Cyan lines: candidate projection events, density rising with height h above $\mathbb{RP}^3$. Tall fibers extend into the dense cut zone and are clipped sooner; short fibers persist. Aggregated, $\mathcal{F} = -\log P$ descends in expectation because high-yield operators fire more often, and each firing reduces the off-stratum content in the direction it acts.*

7.2 F as Surprisal

The free energy $\mathcal{F} = -\log P$ has a precise information-theoretic reading. Where P is the Born-rule probability of the next actualization, $\mathcal{F}$ is the *surprisal* of that event (Shannon, 1948): the number of bits (in units of $\log 2$) by which the outcome will reduce uncertainty about the state. A state aligned with the operator yields $P \approx 1$ and $\mathcal{F} \approx 0$ — the firing is fully expected, conveys no new information, and changes nothing. A misaligned state yields $P \ll 1$ and large $\mathcal{F}$; the firing, when it comes, will be highly informative because the outcome was hard to predict.

Read this way, the variational principle is identical to a Bayesian prior-update statement. $\mathcal{F}$-descent means: the system flows toward configurations whose next actualization will be least surprising. Equivalently: the system tracks the state in which its own dynamics most efficiently extracts information from the arena.

This same Bayesian-update reading of quantum dynamics has been developed independently in QBism (Fuchs, 2010; Fuchs and Schack, 2013), which interprets the Born rule as a coherence constraint on an agent's probability assignments about future measurement outcomes and state evolution as belief updating. The convergence is structural, not metaphysical: QBism takes probabilities to be personalist degrees of belief; the framework treats $\mathcal{F}$-descent as objective geometry. That two routes—agent-centered epistemology and geometric realism—arrive at the same dynamical reading is itself informative. The Born rule, derived in Chapter 13 from the topology of $\mathbb{RP}^3$, is recovered here as the dynamical law that governs descent. Probability assignment and probability dynamics are not two separate postulates but two faces of one structure: the Born weight selects which firing happens, and the surprisal of that selection is the quantity the system minimizes between firings.

This connects $\mathcal{F}$ directly to the framework's information account in Chapter 10. The information per event $I(k) = 3\log_2 R(k)$ is the maximum surprisal an event at hierarchy level k can carry, set by the resolvability ratio $R(k) = E(k)/k_B T$. Here k is the integer energy-cascade index developed in Chapter 14 ($k = 1$ near the Planck scale, $k \approx 51$ at the QCD/pion confinement scale, $k \approx 75$ at room-temperature scales), and $E(k)$ is the energy at that level. $\mathcal{F}$ is the actual surprisal of the upcoming event, given the current state. At high R, individual events can be highly informative and $\mathcal{F}$ can fluctuate over a wide range; at $R \approx 1$ (the critical scale), each event carries near-zero information and $\mathcal{F}$ is small for almost any state, so descent becomes shallow and integrative dynamics take over. Chapter 20 develops what that shallowness implies.

7.3 The Two-Loop Structure

The functional written so far depends only on ρ. This is incomplete. $\hat{A}_b$ acts in a measurement basis b that is itself a parameter of the dynamics, and the framework's full free energy is a function of two arguments,

$$\mathcal{F}[\rho,\theta] \;=\; -\log \mathrm{Tr}\Big[\hat{A}_b(\theta)\,\rho\,\hat{A}_b(\theta)^\dagger\Big],$$

where $\theta = (\theta_{AB}, \theta_{CD})$ is the projective frame on the measurement torus $T^2 = [0,\pi/2]^2$ developed in Chapter 9. The angles θ_{AB} and θ_{CD} parameterize the Kähler-doublet and gauge-doublet allocations of each actualization event; choosing θ is choosing which question the projection asks—which allocation of the two doublets the event enforces. The answer is the outcome produced under that allocation.

Minimization runs in two loops, on different time scales and over different variables. The *inner loop* minimizes $\mathcal{F}[\rho,\theta]$ over ρ at fixed θ: this is the Lindblad dynamics of the previous section, evolving the state toward eigenstates of the active operator. The *outer loop* minimizes $\mathcal{F}[\rho,\theta]$ over θ at fixed ρ: the projective frame slides on T^2 to the angles at which the current ρ is most actualizable. Iterating the two loops descends the joint landscape toward a self-consistent fixed point (ρ^*, θ^*) where neither further state evolution nor frame adjustment can lower $\mathcal{F}$.

For systems at $R \gg 1$ (particle scales), θ is fixed by external apparatus — the experimenter chooses the basis by constructing the measurement device — and only the inner loop runs on the system's own dynamics. Standard quantum mechanics is the single-loop limit of the framework.

For systems at $R \approx 1$ (the critical scale, Chapter 20), θ becomes a dynamical degree of freedom of the system itself: integrated boundaries ($\Phi > 0$, Chapter 20) carry an internal representation of θ that gradient-descends $\mathcal{F}$ between actualization events. This outer-loop dynamics is the framework's substrate-level account of what biology calls active inference (Friston, 2010; Friston et al., 2017): the gradient descent on θ that integrated systems run on top of the inner-loop Lindblad evolution. Active inference is not produced by the variational principle; the variational principle supplies the landscape on which integrated systems can do active inference. Chapter 20 develops the consequences.

The two-loop structure is what permits the same functional to generate gravity at one extreme of the hierarchy and conscious content at the other without changing form. At $R \gg 1$ the outer loop is degenerate (no system-internal θ to vary); at $R \approx 1$ it becomes the dominant dynamics; at $R \ll 1$ both loops shut off and only the statistical aggregate survives. The landscape of $\mathcal{F}$ is one object; the access pattern of the two loops onto that landscape changes character with scale.

7.4 The Variational Principle

The framework's variational principle is concise: at each level of the energy hierarchy, the system evolves toward the state that minimizes $\mathcal{F}$.

What does it mean for a state to minimize $\mathcal{F}$? The actualization free energy measures the gap between the current state and the state that would be left unchanged by the next operator firing. Minimizing $\mathcal{F}$ means closing that gap—evolving toward the configuration where the projection strips the least content, where the Born probability of the actual outcome is highest, where the state is already as close to actual as the arena geometry permits. The minimum is the state that is, in a precise geometric sense, most ready to become actual.

The minimum is not a single universal configuration. It depends on the constraints operative at a given energy scale: which symmetries have already broken, which degrees of freedom remain accessible, what boundary conditions the environment imposes. At the Planck scale, the unconstrained minimum is the Einstein geometry. At the QCD scale, the minimum is a color-neutral hadron. At room temperature, it is the Boltzmann distribution. These are different configurations, but they are all solutions to the same problem: minimize $\mathcal{F}$ subject to the constraints that apply at that scale.

The functional $\mathcal{F}$ is the same at every scale; the landscape it defines changes with the constraints. Each symmetry breaking reshapes the landscape—flattening some directions, steepening others, opening new minima that did not exist at higher energies. The system descends whatever landscape it finds itself on. The diversity of physical law arises from the diversity of landscapes, all generated by the same functional under different constraint regimes.

7.4.1 Existence, Uniqueness, and What Happens When the Minimum Is Not Reached

The phrase "the system evolves toward the minimum" contains three distinct claims that need to be separated. First, a minimum exists: $\mathcal{F}$ is bounded below by zero (when ρ is an eigenstate of $\hat{A}_b^\dagger \hat{A}_b$, the actualization probability is one and the surprisal vanishes). Second, the system descends toward it: the cycle Lyapunov property of the previous section. Third, the descent reaches the minimum in finite time. The third claim is more subtle than the first two and is often false in physically interesting ways.

When the constraints permit a unique minimum — a single configuration of the accessible degrees of freedom that minimizes $\mathcal{F}$ — the system flows there and stays there. The Planck-scale Einstein geometry, in the absence of further symmetry breaking, is unique in this sense: there is one $\mathcal{F}$-minimizing geometry under no additional constraints.

When the constraints permit *multiple degenerate minima*, the system selects one and breaks the symmetry that connected them. Spontaneous symmetry breaking, in the framework, is exactly this: two or more configurations are equally favored by $\mathcal{F}$, the system descends into one of them, and the symmetry that exchanged them is broken at the level of the realized state. The Higgs vacuum expectation value is the canonical example.

When the landscape contains *metastable minima* — local minima separated from the global minimum by finite barriers — the system can become trapped. Trapped states persist for cycle times set by the barrier height divided by the per-event energy, which can be astronomical (false vacua, supercooled phases, glassy configurations). Tunneling out of a metastable well is itself an actualization event, weighted by the Born rule on the available outcomes; sufficiently high barriers correspond to negligible tunneling rates and effectively permanent trapping at cosmological time scales. This is the framework's account of why structures persist that are not minima of the global landscape: they sit at minima of the constrained landscape they were prepared in, and the constraint that prepared them has not relaxed.

When the landscape is *flat* along some direction — a soft mode, a Goldstone direction, a degenerate moduli space — descent along that direction is unforced and the system explores the level set diffusively. Most of the framework's open-parameter content sits in soft directions of this kind: the tilting of the Higgs vacuum away from the precise SU(4) center, the moduli of instantons that have not been computed (Chapter 18), the residual freedom in the projective frame at the critical scale. A flat direction is a place where $\mathcal{F}$-minimization stops imposing structure; further information is needed to fix what configuration the system actually realizes.

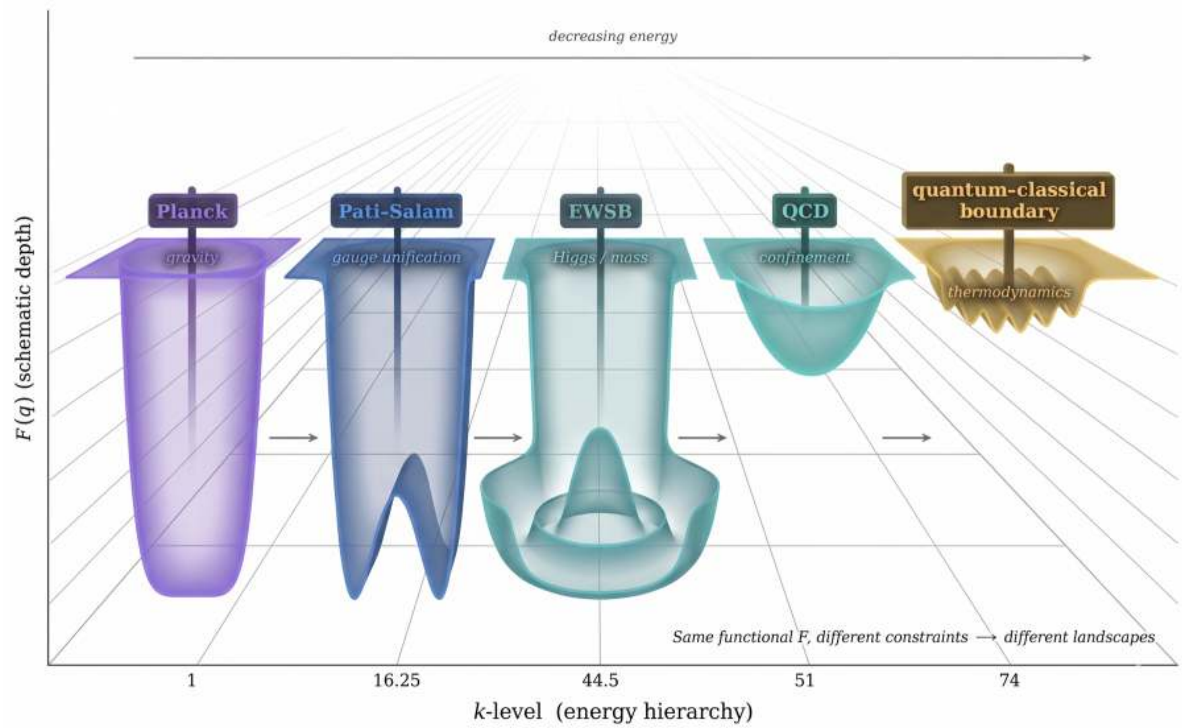

Figure 7.3: *The $\mathcal{F}$-landscape at characteristic points in the energy hierarchy, each shape set by which symmetry has just broken.* Planck *($k \approx 1$): unique minimum. No constraints have yet been imposed; the full* PSU(4) *isometry of* $\mathbb{CP}^3$ *acts, and unconstrained Einstein geometry sits in a single deep well.* Pati–Salam *($k \approx 16.25$): bifurcation. The operator's projection now distinguishes real from imaginary directions,* PSU(4) *shatters to* $\mathrm{SU}(4)_C \times \mathrm{SU}(2)_L \times \mathrm{SU}(2)_R$*, and the four fact types separate into Kähler and gauge doublets. A formerly flat direction in the landscape has just acquired curvature; the single minimum has split into competing branches.* Electroweak *($k \approx 44.5$): degenerate Mexican-hat minima. Within the gauge doublet, chiral and intensity directions decouple and* $\mathrm{SU}(2)_L \times \mathrm{U}(1)_Y$ *breaks to* $\mathrm{U}(1)_{\mathrm{em}}$*. The Higgs vacuum expectation value occupies one trough of the rotationally-symmetric ring, W and Z acquire mass in the directions that became steep.* QCD *($k \approx 51$): constrained narrow well. The strong coupling grows to order unity and color-charged states cannot propagate as free excitations; $\mathcal{F}$ minimization forces color-neutral combinations and confinement traps them.* Quantum–classical boundary *($k \approx 74$): flat directions, shallow basins. $R \approx 1$: thermal energy now matches level spacing, the landscape no longer distinguishes its minima sharply, and many nearly degenerate basins host populations whose collective behavior is the Boltzmann distribution. Same functional throughout, with different constraints active at each scale; the landscape topology changes because the symmetry that survived to define it changed.*

7.5 The Variational Principle Across Scales

The preceding section described the variational principle in the abstract: minimize $\mathcal{F}$ subject to constraints. This section walks through the energy hierarchy and identifies, at each scale, what the operative constraint is, where it comes from, and what the $\mathcal{F}$-minimizing configuration looks like under that constraint. The pattern is always the same: a new constraint enters (because a symmetry has broken, or a threshold has been crossed, or an environmental condition has changed), the landscape of $\mathcal{F}$ reshapes itself, and the system settles into the new minimum.

The geometric mechanism behind each transition is bifurcation. At high energy a single basin of $\mathcal{F}$ accommodates the system; as the constraint structure tightens with decreasing energy, a flat direction in that basin acquires curvature in one sign or the other, and a single minimum splits into two (or more) competing minima separated by a saddle. Symmetry breaking is the geometric event of the system selecting one branch. The breaking sequence walked below is the bifurcation diagram of $\mathcal{F}$ traversed along the energy axis: at each named scale, a previously soft direction has just become curved, and the $\mathcal{F}$-minimum has just moved to the new branch.

7.5.1 Planck Scale ($k \approx 1$): Gravity

Constraint: none. At the highest energies, no symmetry-breaking constraints have yet been imposed. The operator acts on the full arena, and the state encodes the quantum geometry of a spatial slice—the three-dimensional shape of space at a given moment. All arena coordinates are dynamical variables.

Why this constraint holds here: the Planck scale is the top of the hierarchy. The operator's distinction between real and imaginary directions has not yet produced any symmetry breaking, because the energy per event is far above any breaking threshold. The full SU(4) symmetry of the arena is intact.

What $\mathcal{F}$ minimization produces: the actualization free energy measures the gap between the current quantum geometry and the geometry that would be left unchanged by the operator. The stationarity condition $\delta\mathcal{F}/\delta\rho = 0$ requires the actualized geometry to sit at the free-energy minimum of the gravitational sector, which reduces to the Wheeler–DeWitt constraint (DeWitt, 1967): the Hamiltonian acting on the spatial geometry annihilates the state. In the classical limit, this is equivalent to Einstein's field equations (Einstein, 1916). General relativity is the $\mathcal{F}$-minimizing configuration when no other constraints are operative—the geometry that is maximally compatible with actualization.

The actualized geometry, once projected, does not evolve. It is frozen in the historical record. What we experience as the passage of time is the accumulation of successive actualization events, each adding to the record without modifying what came before. General relativity exhibits no explicit time coordinate precisely because it describes this frozen actualized sector. The dynamics are in the actualization process, not in the geometry.

7.5.2 UV Boundary ($k \approx 10$): High-Scale Unification

Constraint: the operator's fixed-point set begins to distinguish real from imaginary directions.

Why this constraint holds here: as the cascade moves past the Planck scale and the energy per event falls, the operator's projection onto $\mathbb{RP}^3$becomes geometrically significant relative to the state's imaginary content. The full SU(4) symmetry of the arena, which was effectively invisible at $k = 1$, now encounters the fixed-point set as a structural boundary. Directions tangent to $\mathbb{RP}^3$(real, destined to become spatial and intensity degrees of freedom) and directions normal to it (imaginary, destined to become spectral and chiral degrees of freedom) are no longer interchangeable.

What $\mathcal{F}$ minimization produces: the landscape of $\mathcal{F}$ develops structure that was absent at the Planck scale. The $\mathcal{F}$-minimizing configurations are no longer arbitrary arena geometries; they are geometries compatible with the incipient real/imaginary distinction. These configurations set the initial conditions for the symmetry-breaking cascade that follows.

7.5.3 Pati-Salam Scale ($k \approx 16.25$): Grand Unification

Constraint: the real/imaginary distinction fully engages, and the SU(4) symmetry of the arena shatters into the Pati–Salam group (Pati and Salam, 1974).

Why this constraint holds here: the energy has dropped to the point where the operator's projection strips enough imaginary content per event that two doublets become separately resolvable—the Kähler doublet (spectral and spatial) and the gauge doublet (chiral and intensity). The symplectic orthogonality between doublets, which was a latent structural feature at higher energies, now constrains the accessible states. The $\mathcal{F}$ landscape bifurcates: a formerly flat direction acquires curvature, new minima appear, and the system settles into a lower-symmetry configuration.

What $\mathcal{F}$ minimization produces: the Pati-Salam gauge group and its associated field content. The breaking is irreversible—each subsequent stage inherits the doublet structure and the constraints it imposes.

7.5.4 Electroweak Scale ($k \approx 44.5$): Higgs and Mass Generation

Constraint: within the gauge doublet, the chiral and intensity directions decouple.

Why this constraint holds here: the energy has dropped to the scale where the right-handed weak interaction decouples from the left-handed one. The Pati-Salam group breaks further, and the $\mathcal{F}$ landscape develops a new minimum corresponding to the Higgs vacuum expectation value. The Higgs field, in this picture, is the fiber orientation locking into a geometric potential minimum defined by the operator's action at this scale—it is the configuration where the chiral/intensity distinction is maximally compatible with actualization.

What $\mathcal{F}$ minimization produces: the W and Z bosons acquire mass (they correspond to the directions that have become steep in the new landscape), the distinction between electromagnetic and weak interactions becomes operative, and fermion masses are set by the depth of the new minimum in each flavor channel.

7.5.5 QCD Scale ($k \approx 51$): Confinement

Constraint: the strong coupling constant grows to order unity, and color-charged states can no longer propagate as free excitations.

Why this constraint holds here: the energy per event has dropped to the pion mass, the reference scale of the hierarchy. At this energy, the imaginary content associated with the normal directions of $\mathbb{RP}^3$within the arena—the directions that encode color charge (Chapter 3)—can no longer be sustained as free degrees of freedom. The $\mathcal{F}$ minimum requires color-neutral combinations.

What $\mathcal{F}$ minimization produces: confinement. The remaining partially unactualized degrees of freedom (quarks, which retain imaginary content corresponding to their color charge) are forced into fully actualized composites (hadrons). The pion mass, which calibrates the entire hierarchy, sits at this scale.

7.5.6 Higher Scales: From Classical Emergence to Subjective Experience

Above the QCD scale in the cascade, the actualization cycle continues to operate, but the character of $\mathcal{F}$ minimization shifts. At each scale, the actualization cycle does two things simultaneously: it extracts information (resolving structure in the actual world) and it produces entropy (depositing stripped content in the normal bundle). The resolvability ratio $R(k)$—the energy available at scale k divided by the thermal energy $k_B T$—determines which process dominates.

In the *dark-matter regime* ($k \approx 61$–62), the surviving symmetries after electroweak breaking constrain the $\mathcal{F}$ landscape to produce extremely light masses. The minima are shallow—nearly flat—corresponding to the neutrino mass spectrum and potential sterile-sector particles (Chapter 15).

At the *quantum-classical boundary* ($k \approx 73$–75 at biological temperature), R drops to unity: each event thermalizes as much as it resolves. The dissipative character of the cycle, always present, now dominates over coherent evolution. $\mathcal{F}$ minimization produces the second law of thermodynamics and the emergence of classical behavior as the coarse-grained statistical effect of vast numbers of individually unresolvable events (Chapter 8). The boundary is temperature-dependent and is distinct from QCD confinement, which occurs at $k \approx 51$ regardless of temperature.

The *critical scale* ($k \approx 75.35$) nearly coincides with this boundary. R is approximately unity: the thermal energy matches the hierarchy's level spacing, so each event thermalizes roughly as much as it resolves. Maintaining coherent structure at this scale requires continuous metabolic expenditure. For systems satisfying the integration condition $\Phi > 0$, $\mathcal{F}$ minimization acquires additional structure—a second dynamical variable (the projective frame) and a second minimization loop—developed in Chapter 20.

What $\mathcal{F}$ minimization produces: where the integration condition holds, the persistent $\mathcal{F}$-minimum at $k \sim 75$ is the active-inference regime—sustained two-loop $\mathcal{F}$-descent over both state and projective frame. Without integration, $k \sim 75$ supports no persistent structure—the marginally stable strip (Chapter 19) is thermal noise. Biology is one search algorithm for substrates that supply the integration topology; the basin exists in the variational landscape regardless of how it is found.

Beyond the critical scale ($k \gg 75$), R is negligible. $\mathcal{F}$ minimization produces the Boltzmann distribution (Boltzmann, 1872): macroscopic regularities emerge only statistically, from the aggregate of vast numbers of individually uninformative events.

Across these scales the functional $\mathcal{F}$, the Lindblad dynamics, and the minimization principle are uniform. What changes is the landscape—reshaped at each threshold by the constraints that have become operative. The diversity of physical regimes is the diversity of landscapes, all generated by one functional under different constraint regimes.

7.6 The Variational Principle Among Variational Principles

Physics has been variational since at least the eighteenth century. Maupertuis's principle of least action, Hamilton's principle for classical mechanics (Hamilton, 1834), Fermat's principle for geometric optics, the Hilbert action for general relativity (Einstein, 1916), and the path integral for quantum field theory (Feynman, 1948) all share one structural claim: physical trajectories extremize a functional defined over the space of possible trajectories. The framework's variational principle is continuous with this lineage and adds two extensions.

The first extension is that the functional is derived rather than postulated. In Hamilton's framework, the action is given by an external Lagrangian; one writes down a Lagrangian appropriate to the problem and verifies it produces the right equations of motion. $\mathcal{F}$ here is fixed by the arena and the operator with no freedom to adjust: any state ρ and any operator $\hat{A}_b$ determine $\mathcal{F}$ uniquely as the surprisal of the next actualization. The framework loses the ability to adjust the functional; it gains the absence of choice in what dynamics applies.

The second extension is the two-variable structure described in Section 7.3. Hamilton's principle extremizes a single functional over a single argument (the trajectory). $\mathcal{F}[\rho, \theta]$ extremizes over both the state ρ and the projective frame θ on the measurement torus, and the two arguments enter through different dynamical loops on different time scales. Standard variational principles cover the ρ minimization at fixed θ (apparatus chosen externally); the θ outer loop has been considered, in different vocabularies, by Friston's free-energy principle in neuroscience (Friston, 2010; Friston et al., 2017), by predictive-coding accounts in machine learning (Clark, 2013; Rao and Ballard, 1999), and by Jaynes's maximum-entropy formulation in statistical mechanics (Jaynes, 1957). PPM's contribution is to unify these into a single $\mathcal{F}$ acting at a fixed substrate (the arena) under a fixed operator dynamics (the actualization cycle), with the two loops expressing different projections of one functional onto different argument slots.

Read against the lineage, the framework's variational principle is recognizable as a special case: the state is a density matrix on $\mathbb{CP}^3$, the functional is fixed by the arena, the dynamics are Lindblad-plus-Born-rule, and the outer loop opens at the critical scale. Each piece has prior art; the unification is what is new.

7.7 Scope of the Principle

The variational principle accounts for a great deal at low cost. Conservatively scoped, what it accounts for is exactly: the dynamics of the system between actualization events, the Born-rule weighting of which event fires, and the ensemble-mean direction of $\mathcal{F}$ descent over the cycle. Several things look like they should follow but do not, and the chapter would mislead if it did not say so.

The principle does not pick the measurement basis. $\mathcal{F}$ is defined relative to a chosen $\hat{A}_b$ at a chosen θ. Physically, θ is fixed by the apparatus at $R \gg 1$ and by the system's own integration dynamics at $R \approx 1$; in neither case does $\mathcal{F}$ alone select a basis. At high R the basis is an external boundary condition; at low R it is an outer-loop dynamics that runs on top of $\mathcal{F}$, not within it.

The principle does not choose the constraints. Each subsection of §7.5 names a constraint and walks through what minimization produces under it; the constraint itself comes from the symmetry-breaking history of the universe at that scale, not from $\mathcal{F}$. The variational principle takes a constraint set and produces the minimum; it does not derive the constraint set.

The principle does not replace renormalization-group flow. RG flow describes how the effective action and the effective couplings change under coarse-graining of degrees of freedom (Wilson, 1975). $\mathcal{F}$-minimization happens at a fixed energy scale; the coupling between $\mathcal{F}$ at different scales (the way the coarse-grained landscape inherits structure from the fine-grained landscape) is RG content, not variational content. The framework's hierarchy of k-scales tracks RG flow as the energy decreases (Chapter 14), and at each k the local dynamics is $\mathcal{F}$-descent under the constraints active at that k.

The principle does not derive consciousness. At $R \approx 1$ the outer-loop dynamics on θ becomes operative, and integrated boundaries can run active inference on top of the variational landscape. Doing active inference is something biology does, exploiting conditions the framework provides; the framework does not produce active inference, and active inference does not produce phenomenal content (Chapter 20). These are three distinct claims that benefit from separation.

7.8 Synthesis

Three pieces have come together over the chapter. $\mathcal{F}$ is the surprisal of the next actualization, fixed by the arena geometry and the choice of measurement basis; it is not entropy, and it does not move with entropy. The actualization cycle — continuous Lindblad evolution between firings, stochastic POVM projections at firings under the Born rule — has $\mathcal{F}$ as a Lyapunov functional: ensemble-averaged $\mathcal{F}$ descends monotonically toward zero on the cycle, and trapped states sit at constrained minima rather than at the global minimum. The cycle decomposes into two loops: an inner Lindblad loop on ρ at fixed measurement basis, and an outer gradient loop on the projective frame θ at fixed ρ, with the second loop active only at scales where the system carries an internal representation of θ.

The chapter's central claim is that one functional, derived rather than postulated, generates the dynamical content of physics across the hierarchy by reshaping its landscape under the constraints operative at each scale. Gravity, gauge theory, confinement, thermodynamics, and critical-scale active inference are not five different variational principles; they are the same principle viewed through five different constraint-shaped landscapes. This is not a unified gauge group — the framework has none — but it is a unified dynamics.

The next chapter takes one consequence seriously. $\mathcal{F}$ descent on the actualization cycle is irreversible: each firing deposits content in the normal bundle that the actualized world cannot recover. That irreversibility, accumulated over $M(t) \approx 10^{121}$ events, is what gives time its arrow and what the four laws of thermodynamics describe. Chapter 8 develops the thermodynamic content from the geometry of the deposition.

Chapter 8

Time and Irreversibility

Thermodynamics and time are conventionally treated as fundamental. The laws of thermodynamics are treated as primitive empirical generalizations, true by inspection. The arrow of time is held to be a deep mystery resolved (when it is resolved at all) by appeal to special boundary conditions at the universe's beginning. Both sit beneath physics, given rather than derived. T.7

The framework treats them as emergent. The four laws of thermodynamics are properties of the projection: the zeroth from the connectedness of the fixed-point set, the first from the isometry of the operator, the second from the many-to-one character of dimensional reduction, the third from the exhaustion of fiber modes at zero temperature. The arrow of time is the direction in which the actualization record accumulates. Both stories rise from the same substrate—the per-event projection from $\mathbb{CP}^3$ to $\mathbb{RP}^3$—and they are linked by it. Each event that strips entropy into the normal bundle (the geometric record of the discarded directions, attached at each point of $\mathbb{RP}^3$) is also an event that adds to the cumulative record whose growth defines the direction of time. Time and irreversibility are two readings of the same accumulation.

This chapter develops both lines from the same projection geometry.

8.1 Projection as Information Loss

Each actualization event projects a state from the six-dimensional arena onto the three-dimensional actual world. The projection is many-to-one: distinct states in the arena can map to the same point on the actual world, because the imaginary content that distinguishes them is stripped away. This is dimensional reduction in the most literal sense—three complex dimensions collapse to three real dimensions, and the content of the discarded imaginary directions is deposited in the normal bundle over the actual world.

The deposited content is not destroyed. The operator is an involution ($\tau^2 = \mathrm{id}$), so the full arena state is recoverable in principle: the information persists in the normal bundle. But recovery would require access to the full arena state, which is precisely what the actualized world does not provide. From within the actual world, the stripped content is inaccessible. The projection is reversible globally and irreversible locally.

A concrete analogy clarifies the distinction. Consider a photograph of a three-dimensional scene. The projection from three dimensions to two is many-to-one: objects at different depths that happen to lie along the same line of sight occupy the same pixel. The photograph preserves all the information contained in its two-dimensional surface, but the third dimension—depth—is lost. Knowing the photograph alone, you cannot reconstruct which object was in front. Yet if you had access to the original three-dimensional scene, the projection could be inverted trivially. The information is not destroyed; it is rendered inaccessible from within the lower-dimensional record. The actualization projection works identically: the three imaginary dimensions are the "depth" that the actual world's three-dimensional "photograph" cannot recover.

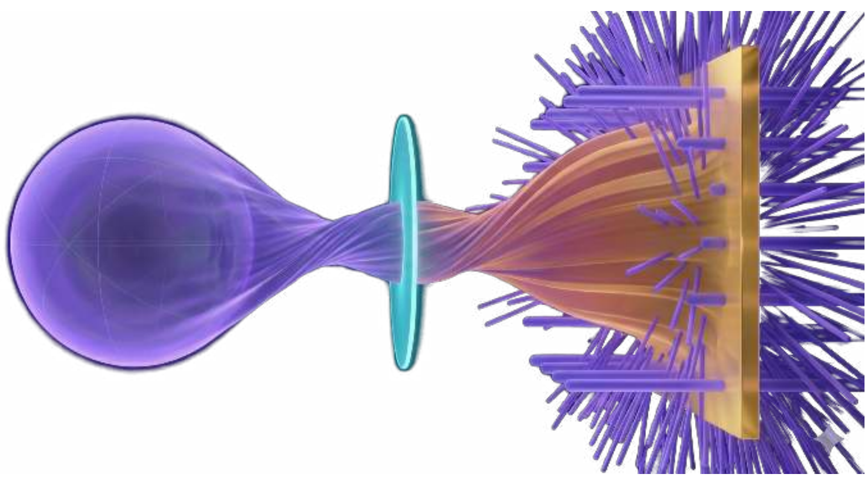

Figure 8.1: *The actualization projection. A state in $\mathbb{CP}^3$ (violet sphere) narrows through the $\mathbb{Z}_2$ involution (cyan aperture); τ reverses the imaginary component as it passes. At the $\mathbb{RP}^3$ surface the state separates into tangent content parallel to the surface (gold bands, preserved as the actualized fact) and normal content perpendicular to it (violet filaments, stripped imaginary structure, deposited but locally inaccessible). Each event produces both: the tangent content is information extracted; the normal content is entropy deposited.*

This distinction—global reversibility, local irreversibility—generates the four laws of thermodynamics.

8.2 The Four Laws as Projection Theorems

The four laws of thermodynamics are typically presented as independent empirical generalizations, discovered separately and unified only loosely by statistical mechanics. In PPM, all four follow from properties of the operator and the projection it defines.

8.2.1 The Zeroth Law: Transitivity from $\mathrm{Fix}(\tau)$ Connectedness

The zeroth law states that if two systems are each in thermal equilibrium with a third, they are in equilibrium with each other (Fowler and Guggenheim, 1939). The fixed-point set of τ is $\mathbb{RP}^3$. This set is topologically connected: it consists of a single piece, not disjoint fragments. Every actualized state in the universe sits in the same $\mathbb{RP}^3$, and equilibrium between two subsystems is the matching of their normal-bundle fiber densities across whatever surface they share—the densities are properties of the same fixed-point set viewed at different positions.

Because $\mathbb{RP}^3$ is connected, density matching is transitive. If subsystem A shares fiber density with B, and B with C, then A and C are matched along chains of contact through B. The transitivity of thermal equilibrium—and the well-definedness of temperature itself—rests on this topological fact: the actual world is one piece. A universe whose actualization fixed-point set fragmented into disjoint components would have no universal temperature scale, and the zeroth law would fail at every boundary between fragments. Temperature is a universal quantity because $\mathbb{RP}^3$ is universal.

8.2.2 The First Law: Conservation from Operator Isometry

The first law states that the energy of an isolated system is conserved (von Helmholtz, 1847). The operator τ is an isometry of the arena: it preserves the Kähler metric. The total energy, defined as the Kähler volume of the occupied state, is therefore conserved across each projection. No energy is created or destroyed in the act of actualization.

What changes is the *distribution* of energy between the actualized sector and the normal bundle. The Kähler volume that falls inside the projection's image becomes available as actualized energy in $\mathbb{RP}^3$; the volume in the normal-bundle fibers is the remainder, locally inaccessible. Heat exchange between subsystems is the transfer of normal-bundle content across their shared boundary; work is the rearrangement of the actualized geometry itself. The familiar form $dU = \delta Q - \delta W$ is the balance sheet for this redistribution.

The conservation is geometric, enforced by the isometry property, and holds exactly at every scale. Energy conservation in the framework is the metric structure of the arena under its own symmetry, not a separate principle imposed on top of the dynamics.

8.2.3 The Second Law: Irreversibility from Dimensional Reduction

The second law states that the entropy of an isolated system never decreases (Carnot, 1824; Clausius, 1865). The projection from the arena to the actual world is many-to-one. Each firing strips three real dimensions of imaginary content and deposits them in the normal bundle. The entropy produced per event is approximately constant:

$$\Delta S \approx 3\, k_B \ln(2\pi),$$

which is roughly $5.5\, k_B$ per projection. The factor of 2π is the circumference of the Hopf fiber—a topologically fixed quantity—and the factor of three reflects the three stripped dimensions. The entropy production is geometric, set by the same fiber topology that determines the rest of the arena's structure.

The second law follows: the total entropy of an isolated system increases with each actualization event, because each event adds approximately $5.5\, k_B$ to the entropy budget. The increase is monotonic, bounded below by zero, and driven by the many-to-one character of the projection. No appeal to coarse-graining, ergodic hypotheses, or low-entropy initial conditions is required. The second law is a counting statement about the projection: every firing strips, every stripped quantum joins the normal bundle, the record grows.

8.2.4 The Third Law: Fiber Collapse at Zero Temperature

The third law states that the entropy of a system approaches a minimum value as the temperature approaches absolute zero (Nernst, 1906). As the temperature approaches zero, the thermal energy available to excite fiber modes vanishes. The Boltzmann factor suppresses access to excited states, and the number of distinguishable fiber configurations approaches one—the ground state alone. Entropy, defined as $S = k_B \ln \Omega$ (Boltzmann, 1872) where Ω is the number of accessible microstates, approaches zero.

The third law is therefore a statement about the fiber structure at low temperature: when no thermal energy is available to populate higher modes, the normal bundle collapses to its ground state, and the projection becomes effectively one-to-one. The many-to-one character that drives the second law is extinguished—there is only one available possibility per actualized position, and actualization brings nothing new into the record. Absolute zero is the limit at which no fiber content remains for the projection to strip.

8.3 The Structure of Time

The most consequential thermodynamic result is the arrow of time. In standard physics, the arrow is a persistent puzzle: the fundamental equations of motion are time-reversible, yet macroscopic processes manifestly are not. The standard resolution appeals to a low-entropy boundary condition at the Big Bang (the "past hypothesis" (Penrose, 1989)), which is itself unexplained.

The framework treats time as a structure with two layers: an elementary per-event clock and a cumulative record across events. The arrow falls out of how the two relate.

8.3.1 The per-event clock

Each τ-projection event has a finite duration set by the Margolus–Levitin minimum-evolution bound (Margolus and Levitin, 1998), $\tau_{\text{event}}(k) = \pi\hbar/(2\,E(k))$, where $E(k)$ is the energy at cascade level k (Chapter 14; technical 7). At Planck scales, τ_{event} is on the order of 10^{-44} s; at the electroweak scale, around 10^{-26} s; at the QCD confinement scale, around 10^{-23} s; at room-temperature thermal scales ($E \approx k_B T \approx 25$ meV), around 38 fs. Each scale carries its own elementary clock, set by the energy at that scale. Time at any given scale is the count of projections that have occurred at that scale, multiplied by the duration of each.

The elementary clock is the framework's smallest temporal unit: nothing happens faster than $\tau_{\text{event}}(k)$, because nothing happens between events. Between projections the arena evolves unitarily; only at events does anything get committed to the record.

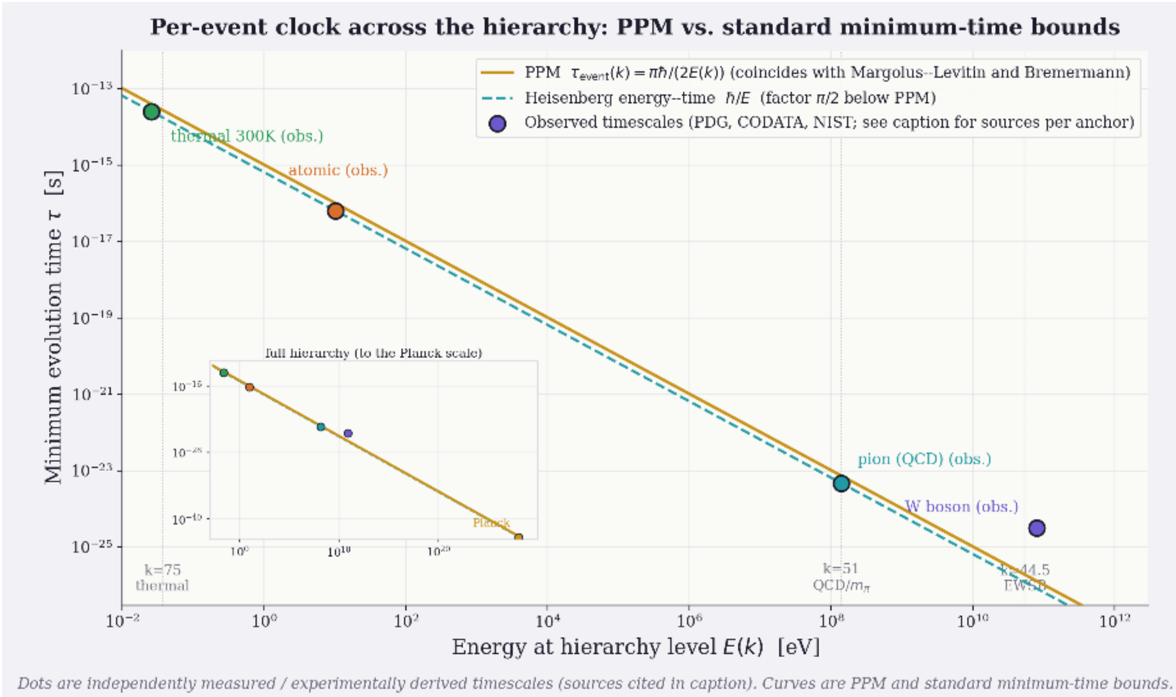

Figure 8.2: *The per-event clock against five measured timescales. The gold curve is the prediction $\tau_{\text{event}}(k) = \pi\hbar/(2E(k))$ across the cascade; the dashed cyan curve is the Heisenberg bound $\hbar/E$, which the Margolus–Levitin form sits a factor $\pi/2$ above. The five filled circles are intrinsic timescales measured independently of the framework — Planck time, the W-boson lifetime, the pion intrinsic time, the hydrogen Lyman-α atomic time, and the room-temperature thermal time (Kramida, A. and Ralchenko, Yu. and Reader, J. and NIST ASD Team, 2023; Particle Data Group, 2024; Tiesinga et al., 2021) — plotted at their observed energy with no fit. All five land on the floor across some thirty decades of energy, on a curve carrying no per-scale parameter. The W point sits a little high because its weak-suppressed decay runs slower than the per-event minimum at M_W: the curve is a lower bound on event duration, which a real process can exceed. One caution: τ_{event} is the duration of a single event, and structured behavior unfolds over many — millisecond cellular integration is $\sim 10^{11}$ events of ~ 38 fs each.*

8.3.2 The cumulative record

The cumulative actualization count $M(t)$ is the total number of τ-events across cosmic history. Each event deposits $\Delta S \approx 5.5\, k_B$ in the normal bundle and adds a fact to the actualized record on $\mathbb{RP}^3$, so the total recorded entropy is $S_{\text{record}}(t) = M(t) \cdot \Delta S$. With $M(t) \approx 10^{121}$ events to date, the recorded entropy reaches $S_{\text{record}} \approx 10^{122}\, k_B$. The Bekenstein–Hawking entropy of the cosmic horizon (Bekenstein, 1973; Hawking, 1975), $S_{\text{BH}} = A_{\text{hor}}/(4\,\ell_P^2) \approx 2 \times 10^{122}\, k_B$ for the present-epoch de Sitter horizon, sets the universe's total information capacity — the deposited record sits at the same order, a factor of about two below it.

$M(t)$ is distinct from the boundary capacity $N_\infty = \varphi^{392} \approx 10^{82}$ that sets the cosmological constant (Chapter 17). N_∞ is the static topological capacity of the boundary; $M(t)$ is the cumulative count of events that have occupied positions on it. The $\sim 10^{39}$ ratio between them is the average number of re-actualizations per boundary position. N_∞ does not grow—the boundary's information capacity is fixed—but $M(t)$ does, because positions get re-actualized through cosmic history.

8.3.3 The arrow

The operator τ is invertible globally: $\tau^2 = \mathrm{id}$, so no information is destroyed at the level of the full arena. But the actualized record $M(t)$ accumulates monotonically. Each projection adds to the record but cannot erase what was previously recorded, because doing so would require reversing a specific prior projection—which demands access to the specific normal-bundle content that was deposited at that earlier event. That content, while globally preserved, is locally inaccessible.

The arrow therefore points in the direction of increasing $M(t)$: increasing content in the $\mathbb{RP}^3$ historical record, decreasing accessible content in the pre-projection arena. Memory works only backward because the past is the already-projected record and the future is the not-yet-projected content. The asymmetry is geometric: the projection is information-losing at the actualization level even though the underlying map is invertible globally.

This resolves the puzzle without a past hypothesis. The arrow does not depend on the universe having started in a special state; it depends on the structure of the projection—specifically, on the fact that projection from six dimensions to three is many-to-one, and on the fact that the deposited normal-bundle content cannot be read back by the actualization machinery. Any universe governed by this operator would exhibit a time arrow, regardless of initial conditions. Time grows because $M(t)$ grows; the cosmological capacity N_∞ that anchors Λ stays still while the record accumulates against it.

8.4 The Entropy Budget Across Scales

The entropy produced per event ($\Delta S \approx 5.5\, k_B$) is approximately constant across all scales, because it depends on the fiber geometry, which is topologically fixed. This invariance is the thermodynamic instance of cascade flatness (Chapter 14 §The k-Scale as a Flat Coordinate): quantities derived from fiber content are k-invariant, while quantities derived from energy scale (such as the information $I(k)$ below) are k-dependent. The *information* extracted per event, by contrast, varies dramatically with energy scale.

At high energies (small k in the hierarchy), each event resolves a large amount of information: the resolvability ratio $R(k)$ is large, and the projection extracts more structure than it thermalizes. A single actualization event at the electroweak scale, for instance, can resolve a particle's spin state, its flavor identity, its momentum to within the de Broglie wavelength, and the phase relationships between superposed amplitudes—all from one projection. At still higher energies (the Planck scale), an event resolves geometric structure: the curvature of a spatial region, the topology of a local neighborhood, the causal relationships between nearby points. In these regimes, nearly the entire pre-projection entropy budget crystallizes into the actualized record as structured, recoverable information. The small residual deposited in the normal bundle is negligible. This is why high-energy physics is quantum physics: individual events carry enough information to distinguish sharply between possible outcomes.

At low energies (large k), the resolvability ratio drops below unity, and the balance reverses. Each event thermalizes more than it resolves. A single actualization event at room temperature resolves almost nothing: the thermal noise from the projection vastly exceeds any signal about the state's identity. No individual event can distinguish one molecular configuration from another, or one spin orientation from its opposite. The structured information per event is a vanishing fraction of the entropy produced. The quantum-classical boundary sits where these two quantities cross. Because the entropy per event is fixed but the information yield depends on $R(k) = E(k)/(k_B T)$, the crossing is temperature-dependent: at $T = 310\,\mathrm{K}$ the boundary falls at $k \approx 73$, far above the QCD confinement scale at $k \approx 51$. (QCD confinement is a separate phenomenon—a symmetry-breaking transition where $\alpha_s = 1$, not an information-theoretic boundary. At the QCD scale, $R \sim 10^{10}$; individual actualization events are overwhelmingly informative.)

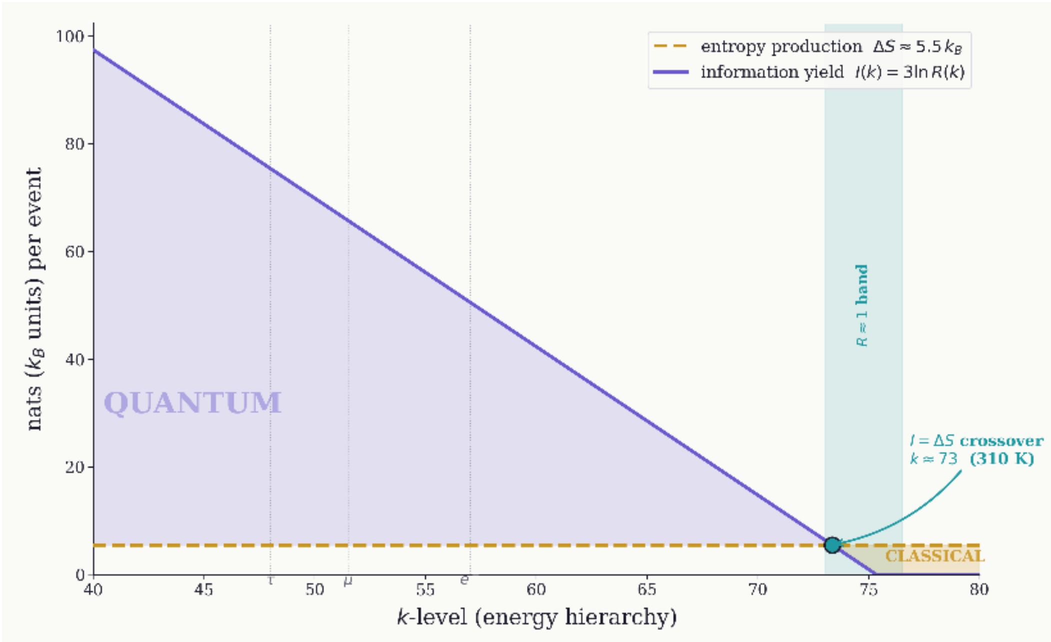

Figure 8.3: *Entropy production versus information yield across the energy hierarchy (at $T = 310\,K$). The gold dashed line is the entropy deposited per actualization event ($\Delta S \approx 5.5\,k_B$), fixed by the Hopf fiber geometry and independent of scale. The violet curve is the information extracted per event, $I(k) = 3\ln R(k)$, which declines with k as the energy per event drops toward the thermal floor. Where the two curves cross ($k \approx 73$), individual events become thermally uninformative—the quantum-classical boundary.*

Below the quantum-classical boundary, individual actualization events are thermally blurred—indistinguishable from noise. Classical behavior emerges because the coarse-grained effect of many such events produces smooth, deterministic-looking dynamics, even though each underlying event is discrete and stochastic. The classical world is the statistical residue of a vast number of individually uninformative projections.

8.5 What Time and Irreversibility Are

Thermodynamics and time both emerge from the same per-event projection, and they are linked through it. Each τ-event deposits entropy in the normal bundle (the irreversibility) and adds a fact to the actualized record (the cumulative count whose growth marks time's direction). Without the projection there would be no entropy production and no time arrow; with the projection both follow without further postulate.

The four laws of thermodynamics are properties of the operator and the projection it defines: the zeroth from the connectedness of the fixed-point set, the first from the isometry property, the second from the many-to-one character of dimensional reduction, the third from the exhaustion of fiber modes at zero temperature. The structure of time is the per-event clock $\tau_{\text{event}}(k)$ combined with the cumulative record $M(t)$, and the arrow of time is the direction in which $M(t)$ grows. Neither requires special boundary conditions; both fall out of how projection works.

The entropy produced per event is determined by the topology of the arena (specifically, the Hopf fiber circumference), and the information extracted per event is determined by the energy scale. The interplay between these two quantities—one fixed, one variable—generates the full spectrum of thermodynamic behavior, from the deep quantum regime where every event is informative to the deep classical regime where every event is noise.

The information gradient between $\mathbb{CP}^3$ and $\mathbb{RP}^3$ is the sole source of free energy in the framework. Every physical energy gradient is a descendant of this projection gradient, realized at a different scale of the hierarchy: temperature differences at thermal scales, chemical potentials at molecular scales, gravitational potential wells as Fubini–Study curvature projected onto $\mathbb{RP}^3$ at the highest energies. The engine is the same at every scale—τ fires, structure crystallizes from the gradient, entropy is deposited in the normal bundle, the record advances—and what varies is the informational yield per stroke. Time and irreversibility are the two macroscopic shadows of one microscopic event, taken many times.

What that microscopic event delivers, in what currency, is the question Part III takes up. The four irreducible kinds of factual content (Chapter 9), the per-event budget that allocates information against entropy (Chapter 10), and the six pairwise bridges between fact types (Chapter 11) develop the structural picture for which this chapter has supplied the time and entropy bookkeeping.

Part III

Information and Structure

Chapter 9

Four Kinds of Fact

Part I introduced the arena and the operator that runs it. Part II showed how that operator drives a recurring cycle—the actualization event—governed by a single variational principle and producing time and irreversibility as byproducts. What Parts I and II did not yet specify is what an event actually delivers. The cycle fires, the operator projects, content is committed to the actualized record—but content of what kind, in what currency. T.5

Part III answers in three steps. This chapter inventories the four irreducible kinds of factual content any actualization event extracts. Chapter 10 reads the per-event budget that splits each projection between information gained and entropy produced, recovering the canonical results of quantum information theory and the quantum–classical boundary as features of how the geometry keeps its records. Chapter 11 connects the four types pairwise into the bridge graph that underwrites every fundamental constant.

The four-fold inventory developed here is forced by the operator. τ acts on the arena's four complex directions—the components of the underlying $\mathbb{C}^4$ from which $\mathbb{CP}^3$ is the projective space (Chapter 3)—with two independent kinds of partition. The first is τ-parity: each direction has an imaginary part that τ flips and a real part that τ preserves, the bundle split established in Chapter 4. The imaginary parts populate the normal bundle of $\mathbb{RP}^3$ inside $\mathbb{CP}^3$ (content stripped at projection); the real parts populate the tangent bundle (content preserved). The second is the doublet symmetry: the four directions group into two pairs that do not symplectically couple to one another, one pair carrying quantum-geometric content (the Kähler doublet) and the other carrying gauge content (the gauge doublet). Crossing the two partitions produces a $V_4 = \mathbb{Z}_2 \times \mathbb{Z}_2$ structure with four cells. Each cell holds one complex direction; the content that direction carries is one fact type.

9.1 The Four Types

Every actualization event extracts factual content from the arena in exactly four kinds—one for each cell of the V_4 partition above. Each subsection below takes a cell in turn, naming the τ-parity and doublet membership that locate it in the bundle geometry, the content the corresponding direction carries between events, and the fact that content becomes at projection.

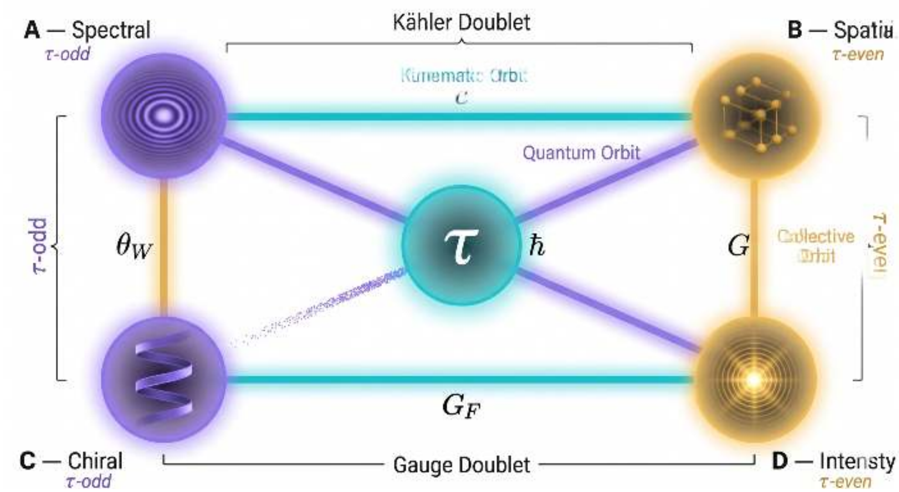

Figure 9.1: *The four fact types and their bridge graph. Vertical split: τ-parity — τ-odd directions (left, normal bundle) reverse sign at projection; τ-even (right, tangent bundle) survive. Horizontal split: Kähler doublet (top, spectral and spatial) vs gauge doublet (bottom, chiral and intensity); the doublets are symplectically orthogonal. Cells label fact types A (spectral), B (spatial), C (chiral), D (intensity). Six edges carry the fundamental constants (c, $\hbar$, G, G_F, θ_W, with a sixth that turns out to be τ); colors group bridges into three V_4 orbits, developed in Chapter 11.*

Doublet membership locates a type in the geometry: the Kähler-doublet types (A, B) sit in the Kähler structure of $\mathbb{CP}^3$ itself—the arena's own geometry—while the gauge-doublet types (C, D) sit in the gauge bundle structure layered on the arena. Reading the subsections through this split: A and B are the imaginary and real coordinates of the arena; C and D are the imaginary and real coordinates of the fiber.

The τ-even types (B, D) carry both a particle-scale and a macroscopic-record manifestation because their content persists through projection; the τ-odd types (A, C) carry only the particle-scale manifestation because their content is deposited in the normal bundle and does not accumulate as a classical record. The depth difference across the four subsections reflects this asymmetry rather than any privileging.

9.1.1 Type A: Spectral

Type A is the (Kähler, τ-odd) cell: the imaginary axis of the Kähler complex coordinate, lying in the normal bundle of $\mathbb{RP}^3$. Between events this direction carries quantum amplitude—the imaginary part of the wavefunction that Schrödinger evolution rotates and that the standard formalism reads as superposition phase. At projection, τ flips the imaginary content into the normal bundle as residual structure: what was a continuous amplitude becomes, in the actualized record, a discrete fact about which spectral identity the event resolved. Type A is destroyed and rebuilt with every event; its persistence sits in the normal-bundle deposit, not on $\mathbb{RP}^3$. The fact it delivers answers *what frequencies are present*.

At particle scales, spectral content manifests as the discrete quantum numbers that label particle states—principal quantum number, angular momentum, magnetic quantum number. These are the quantities most directly accessible to spectroscopic measurement, and their discreteness reflects the high resolvability ratio at those scales: the information per event is large enough to resolve sharp spectral lines.

9.1.2 Type B: Spatial

Type B is the (Kähler, τ-even) cell: the real axis of the Kähler complex coordinate, lying in the tangent bundle of $\mathbb{RP}^3$. Between events this direction carries position—a real-valued coordinate on the actual world that already sits in $\mathbb{RP}^3$ without imaginary content. At projection, τ leaves this direction unchanged: the real content passes through the operator and accumulates in the actualized record as the persisting spatial structure of the world. The fact it delivers answers *where*.

At particle scales, spatial content manifests as the position-space wave function and, in the classical limit, as the trajectory of a particle. Experimentally, spatial content is what a detector registers when it records where a particle hit: the pixel that fires, the wire that discharges, the bubble that forms. Every position measurement is a readout of Type B content. At macroscopic scales, spatial content constitutes the spatial geometry of the actual world—the three-dimensional structure of space that general relativity describes. The persistence of spatial content through projection is why the classical world exists at all: each actualization event adds to the accumulated spatial record, and the sum of these contributions over vast numbers of events produces the stable, three-dimensional geometry that we navigate.

9.1.3 Type C: Chiral

Type C is the (gauge, τ-odd) cell: the imaginary axis of the gauge complex coordinate, lying in the normal bundle of $\mathbb{RP}^3$ alongside Type A but along a symplectically orthogonal direction. Between events this direction carries handedness—the orientation distinguishing left from right, encoded as imaginary content on the gauge axis. At projection, τ flips this content into the normal bundle, in the same way it flips spectral content but along a separate channel that no isometry of the arena couples to the Kähler one. The fact it delivers answers *which handedness*.

The asymmetry between left and right that defines weak-interaction physics is the operator's τ-odd action on this fact type. The weak nuclear force couples only to left-handed particles and right-handed antiparticles (Lee and Yang, 1956; Wu et al., 1957); the geometric origin in the framework is that Type C lives in the normal bundle and the operator's action on normal directions distinguishes left from right (Chapter 15).

9.1.4 Type D: Intensity

Type D is the (gauge, τ-even) cell: the real axis of the gauge complex coordinate, lying in the tangent bundle of $\mathbb{RP}^3$ alongside Type B. Between events this direction carries magnitude—the real-valued amplitude weight that determines how much an event contributes to the actualized record. At projection, τ preserves this content; intensity passes through unchanged and accumulates in the historical record alongside spatial content. The fact it delivers answers *how much*.

At particle scales, intensity content manifests as the energy and momentum of a state—what a calorimeter measures when it absorbs a particle and converts kinetic energy to heat, or what a spectrometer infers from the curvature of a charged track in a magnetic field. At macroscopic scales, it constitutes the energy density and pressure that source the gravitational field through Einstein's equations. Intensity is what makes the actualized record gravitationally significant: the physical "weight" of each event's contribution to spacetime. The persistence of intensity through projection (alongside spatial content) is why the universe has a gravitational history at all—each event deposits both a location (Type B) and a weight (Type D) into the accumulated record, and Einstein's field equations (Einstein, 1916) describe how these deposits collectively curve the spatial geometry.

The four-fold classification exhausts the inventory. The four cells of V_4 are the four irreducible representations of $\mathbb{Z}_2 \times \mathbb{Z}_2$, and the geometry has nowhere else to put factual content: every measurement outcome in every experiment expresses as a combination of spectral, spatial, chiral, and intensity content. A hydrogen spectral line encodes all four simultaneously—its wavelength (A), the position of the detector that records it (B), the polarization state that distinguishes left- from right-circularly polarized photons (C), and the brightness of the line (D). No fifth type appears in any known measurement because τ's V_4 partition has no fifth cell.

9.2 The Two Doublets

The four fact types do not stand independently. They organize into two pairs—doublets—connected by the complex structure of the arena.

The two doublets correspond to two layers of geometric structure: the Kähler doublet *is* the Kähler structure of $\mathbb{CP}^3$ itself—the geometry of the arena—while the gauge doublet is the additional structure layered on top of it. This dual realization surfaces in later chapters: gauge bosons appear as excitations of gauge-doublet content (Chapter 15), gravity emerges from what the Kähler structure does at the boundary without analogous quanta of its own (Chapter 16), and the same arena-vs-contents split organizes phenomenal experience at the critical scale (Chapter 20).

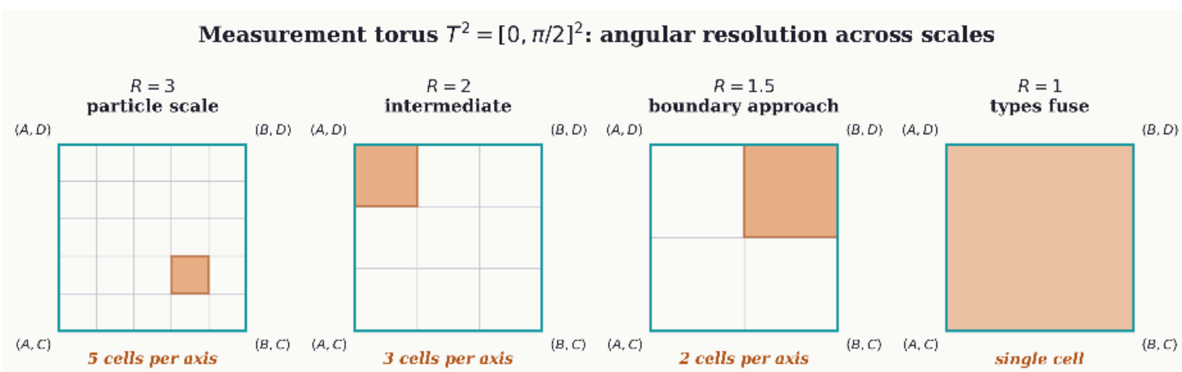

Figure 9.2: *The measurement torus $T^2 = [0, \pi/2]^2$ across four scales $R = 3$, 2, 1.5, 1. The horizontal axis is the Kähler doublet angle θ_{AB} (spectral $\leftrightarrow$ spatial); the vertical axis is the gauge doublet angle θ_{CD} (chiral $\leftrightarrow$ intensity). The four corners label the canonical measurement configurations $(A$ or $B) \times (C$ or $D)$. Grid spacing is the angular-resolution bound $\delta\theta \geq (\pi/2)\, R^{-3/2}$; a single measurement configuration occupies one grid cell (highlighted). At $R \gg 1$ the torus carries many resolvable configurations; as $R \to 1$ the bound saturates at $\pi/2$ and the torus collapses to a single cell, so the four fact types fuse into undifferentiated content. The geometric mechanism behind this scale dependence—the constriction of the CP^3 fiber bundle whose cross-section is the torus —is shown in Figure 9.3 below.*

9.2.1 The Kähler Doublet (A, B)

Types A and B form the Kähler doublet. They are the imaginary and real parts of the same complex coordinate: spectral content is the imaginary part, spatial content is the real part, and the complex structure J of the arena maps one to the other.

This pairing has a profound consequence: quantum mechanics and spatial geometry are aspects of the same doublet. The spectral content that quantum mechanics describes (energy levels, superposition amplitudes, interference patterns) and the spatial content that geometry describes (positions, distances, curvature) are not independent sectors of physics; they are the τ-odd and τ-even components of a single complex coordinate. The uncertainty principle (Chapter 10) is the information-theoretic expression of this pairing: spectral and spatial resolution compete for a shared budget because they are two aspects of one degree of freedom.

Within the Kähler doublet, quantum amplitude and spatial position are paired by the complex structure J; this pairing carries both ways. The wave function lives in the imaginary (spectral) part of the doublet; the classical position lives in the real (spatial) part. Actualization projects the complex coordinate onto its real part, stripping the spectral content and depositing it in the normal bundle. What remains is spatial content—position, geometry, classical structure.

9.2.2 The Gauge Doublet (C, D)

Types C and D form the gauge doublet. The Kähler doublet accounts for one complex coordinate of each point in the arena; the gauge doublet accounts for the other. The arena's isotropy group at any point of the actual world decomposes the tangent space into exactly two irreducible representations, and the gauge doublet is the second one—it cannot be further decomposed or absorbed into the Kähler doublet, because the two representations are orthogonal under the arena's metric. The gauge doublet is irreducible for the same geometric reason that the Kähler doublet is: each corresponds to an independent complex coordinate, and the symmetry group of the arena does not mix them.

Within this doublet, chiral content (C) is the imaginary part and intensity content (D) is the real part.

This pairing connects the weak force to energy. The chiral asymmetry that defines the weak interaction and the intensity (energy) that sources gravity are not independent phenomena; they are the τ-odd and τ-even components of the second complex coordinate. The weak force acts on chirality; gravity acts on energy; the doublet structure means these two forces are paired in the same way that quantum mechanics and spatial geometry are paired in the Kähler doublet.

Electric-magnetic duality (Montonen and Olive, 1977)—the symmetry that exchanges electric and magnetic fields—may be expressible as a rotation within this doublet, reallocating information between chiral and intensity channels in the same way that the uncertainty principle reallocates information between spectral and spatial channels in the Kähler doublet. We note this analogy without claiming a derivation: the structural parallel is suggestive, but the formal mapping between the Kähler-doublet rotation and electric-magnetic duality is open.

9.3 Symplectic Orthogonality

The two doublets are symplectically orthogonal. The symplectic form is the geometric structure that measures the oriented area spanned by pairs of directions in the arena; two subspaces are symplectically orthogonal when every pair of vectors—one drawn from each subspace—has zero symplectic area. In the present case the symplectic form vanishes identically when one direction is drawn from the Kähler doublet and the other from the gauge doublet. Concretely, no observable in one doublet can be expressed as a function of observables in the other; the dynamics carries no information across the boundary, and the two doublets act as independent measurement channels—knowing one tells you nothing about the other through any evolution of the system.

This is a theorem of the arena's geometry, not an assumption. At any point of the actual world, the six-dimensional tangent space of the arena splits into two three-dimensional subspaces, one for each doublet. These subspaces are orthogonal under the metric, and the complex structure of the arena preserves the split: it maps each subspace to itself, never mixing the two.

The physical consequence is independence. No isometry of the arena mixes the Kähler doublet with the gauge doublet. No measurement can trade spectral resolution for chiral resolution, or spatial resolution for intensity resolution. The two doublets are separate information channels, each with its own internal complementarity constraint but no cross-doublet tradeoff.

Only the actualization operator τ crosses the doublet boundary. Within each doublet, τ acts by stripping the odd component and preserving the even one. But τ acts on both doublets simultaneously—every actualization event strips both spectral and chiral content, preserving both spatial and intensity content.

This is why τ occupies a unique structural position. Before projection, the state lives in the full arena: all four components are present as possibility, but no facts have been recorded—there is nothing yet to call spectral or spatial or chiral or intense, because those distinctions are made by the projection itself. After projection, the facts are recorded in the actualized world, but the doublets have become mutually inaccessible: the symplectic orthogonality that separates them is now a physical barrier, and no measurement within either doublet can reach the other. The moment of projection—the operator firing—is the only point at which all four fact types simultaneously exist as determinate facts and are mutually available. τ is the hinge between undifferentiated possibility and separated actuality.

9.4 The Measurement Torus

Each actualization event decomposes its outcome into the four fact types. The decomposition is not unique: within each doublet, the allocation of information between the two types is a continuous parameter. The space of all possible allocations is a torus $T^2 = [0, \pi/2]^2$, parameterized by two angles $(\theta_{AB}, \theta_{CD})$—one for each doublet.

The angle θ_{AB} controls the partition within the Kähler doublet. At $\theta_{AB} = 0$, the projection resolves maximal spectral content (Type A) and no spatial content (Type B). At $\theta_{AB} = \pi/2$, the reverse: maximal spatial resolution, no spectral resolution. At intermediate angles, both types receive partial resolution. The complementarity constraint of Chapter 10 is the statement that the total information within the doublet is fixed: what one type gains, the other loses. The angle θ_{CD} plays the identical role within the gauge doublet, allocating information between chiral (C) and intensity (D) content.

A point on the torus specifies a complete measurement configuration: which question the τ-projection asks. Choosing a spectrometer (which resolves energy levels) corresponds to a small θ_{AB}; choosing a position detector (which resolves spatial location) corresponds to a large θ_{AB}. The experimental apparatus, in this language, is a point on T^2.

The symmetry group that acts on this torus is $\mathrm{PGL}(4, \mathbb{R})$—the group of projective transformations of $\mathbb{RP}^3$. This group parameterizes all possible ways the actualization outcome can be decomposed into fact types: every change of measurement apparatus, every reorientation of the experimental frame, corresponds to a $\mathrm{PGL}(4, \mathbb{R})$ transformation that moves the system's operating point on T^2. At particle scales ($R \gg 1$), the torus has full structure: the experimenter can position the system at any point on T^2 by building the appropriate apparatus. The angular resolution within each doublet is bounded by the information budget:

$$\delta\theta \;\geq\; \frac{\pi}{2}\, R(k)^{-3/2},$$

where $R(k) = E(k)/(k_B T)$ is the resolvability ratio at hierarchy level k (the integer energy-cascade index of Chapter 14, used in this chapter as a named landmark on the energy scale). At high R, the bound is tight: the doublet angle can be selected with high precision. As R decreases toward unity, the angular resolution degrades, and the ability to distinguish the four fact types erodes. The behavior of the measurement torus at the critical value $R = 1$ has consequences for the nature of conscious experience, developed in Chapter 20.

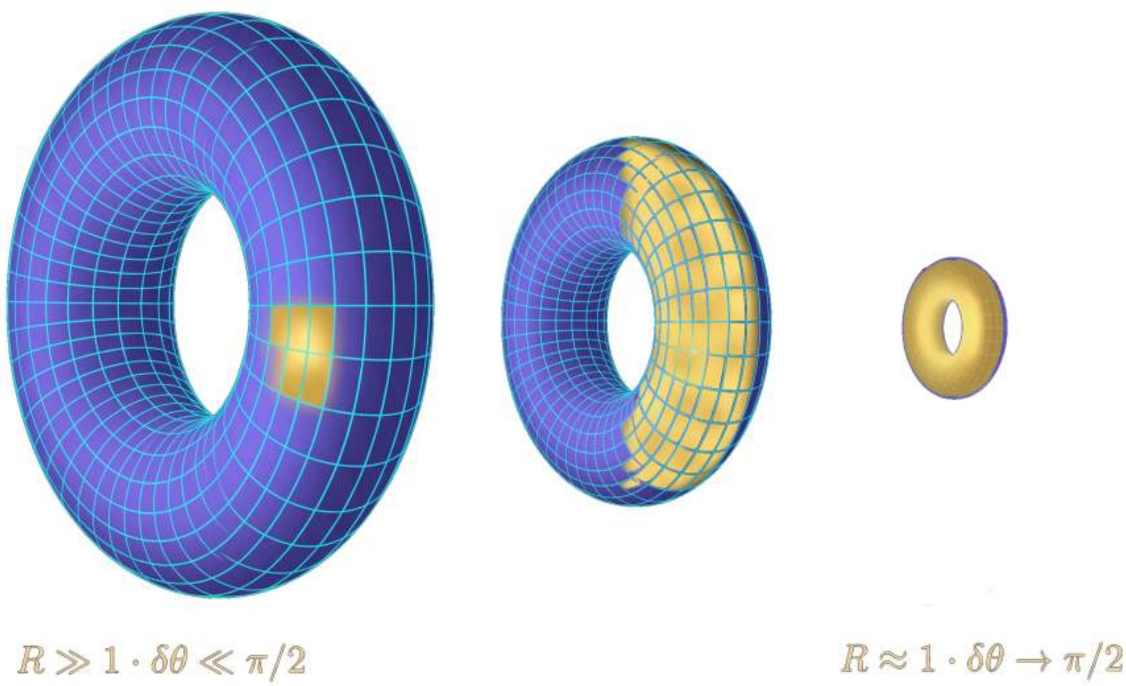

Figure 9.3: *The measurement torus read as a cross-section of the CP^3/RP^3 bundle. The measurement torus $T^2 = [0, \pi/2]^2$ shown at three locations along the cascade, descending in size as the CP^3 bundle cross-section attenuates. The gold region on each torus is the fraction of the bundle cross-section occupied by RP^3 at that scale: a single activated cell at high resolvability ($R \gg 1$, left), a partly activated torus at intermediate resolvability (center), essentially the entire torus at the critical scale ($R \approx 1$, right). As R falls toward unity the activated region spreads and the angular-resolution bound $\delta\theta \geq (\pi/2)\, R^{-3/2}$ widens; at $R \approx 1$ the torus has fused to a single cell and the four fact types become indistinguishable.*

9.5 The Three Regimes

The same resolvability ratio that bounds angular precision on the measurement torus—$R(k) = E(k)/(k_B T)$, defined at each hierarchy level k in Chapter 7—divides the hierarchy itself into three physically distinct regimes, separated by the crossover at $R = 1$ where the per-event information and the per-event entropy are equal. The crossover's location depends on temperature: at higher ambient temperatures the boundary shifts to lower k; at lower temperatures it shifts upward. The QCD confinement scale ($k = 51$) is a separate transition—a symmetry-breaking threshold where $\alpha_s = 1$, distinct from this information-theoretic boundary.

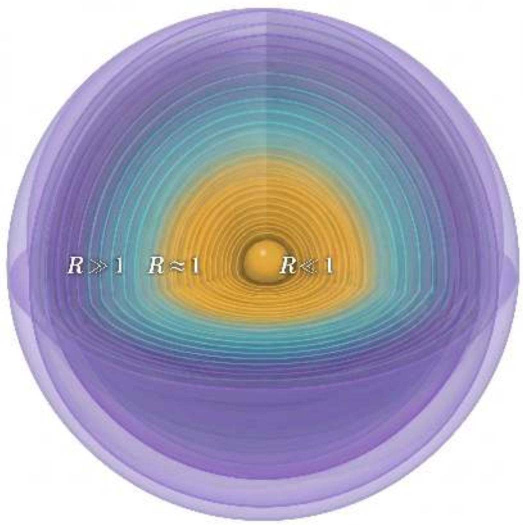

Figure 9.4: *The $\mathbb{CP}^3$ arena in cross-section, radial coordinate encoding k (low k outer, high k core). Three resolvability regimes: $R \gg 1$ at low k (violet, sharply defined shells); $R \approx 1$ in the cyan transition band (shells broaden thermally); $R \ll 1$ at high k (gold core, featureless radiance). The same normal bundle over $\mathbb{RP}^3$ carries discrete quantum numbers, continuous content, or statistical noise depending on $R(k) = E(k)/(k_B T)$.*

In the high-resolvability regime ($R \gg 1$, roughly $k \lesssim 50$), each event resolves the four fact types sharply. Spectral and chiral content are clean discrete labels; spatial and intensity content are determinate to within the de Broglie scale of the event. Quantum numbers are crisp, the four corners of the measurement torus are populated by distinct configurations, and structured combinations (particles, atoms, crystals) sit at free-energy minima and persist indefinitely without external input. This is the regime of static persistence: structure, once formed, stays.

In the transitional regime ($R \approx 1$), the per-event information and per-event entropy are comparable. No structure persists without continuous energy input. The normal-bundle fiber is thermally occupied, and the fact types do not resolve as sharp discrete labels but as continuous content—the angular bound $\delta\theta \geq (\pi/2)R^{-3/2}$ saturates at $\pi/2$ and the torus collapses to a single cell. The four-fold classification remains exhaustive at the structural level, but the resolution available to any single event no longer separates the four types. Persistent organization at this scale requires continuous energy throughput.

In the low-resolvability regime ($R \ll 1$, roughly $k \gtrsim 80$), entropy per event overwhelms information per event. No persistent structure survives individual actualization events. Quantum coherence is thermally washed out, and the fact types are recoverable only through the statistical aggregate of vast numbers of events. Classical physics is the low-resolution limit of the actualization cycle. Newton's equations, Maxwell's equations, thermodynamics—each is a coarse-grained description of the same projective dynamics, valid wherever the per-event information falls below observational resolution. The fundamental dynamics remain discrete and stochastic; the smooth trajectories, deterministic evolution, and continuous observables of classical behavior emerge when the grain of the underlying events is too fine to resolve against thermal noise. The classical world is real—it is the accumulated record of actualization events—and it is coarse-grained beyond the point where individual events carry recoverable information.

The boundary between regimes is fixed by the topology of the arena (which sets the entropy per event) and the energy hierarchy (which sets the energy per event at each scale). Observers, measurement apparatus, and environmental decoherence enter nowhere in its specification. Where each regime sits on the hierarchy follows from the same geometry that determined the energy levels themselves.

What each event extracts from the arena is now classified, and the regimes show how the per-event resolution varies across the hierarchy. What each event *spends* to extract that content—the per-event budget that allocates information against entropy, and what its allocation forces on the major results of quantum information theory—is the subject of Chapter 10.

Chapter 10

Information and the Quantum-Classical Boundary

Information lives where every other physical quantity in the framework lives: in the con- T.7
figuration of the arena. An actualization event leaves the arena in a different state than it found it; that state is the event's full record, and information theory is how the record is read. Each event has a definite information content—the resolution at which outcomes were distinguished—and a definite entropy cost—the volume of normal-bundle content stripped away. Information measures how sharp the projection was; entropy measures how thick the fiber it integrated over. Both are read off the geometric step the event executed.

The familiar information-theoretic quantities are features of that step. Shannon information counts the distinguishable configurations the projection resolved. Boltzmann entropy measures the volume of fiber content the projection integrated out. Mutual information is the geometric overlap between two readings of the same state. Channel capacity is the resolution available at a given energy scale. The roles played elsewhere by observers, measurement apparatus, and external environments are absorbed: the geometry has already done the work.

This chapter develops the reading. The first section identifies the two quantities every event produces—information and entropy—and the budget that splits each projection between them. The doublet structure of the arena established in Chapter 9 constrains how the per-event information is distributed within the four fact types, recovering the Heisenberg uncertainty principle as a channel-allocation theorem. The resolvability ratio $R(k) = E(k)/(k_B T)$, with k the integer energy-cascade index of Chapter 14, measures how much of the budget falls on each side at each energy scale—the same ratio that divided the hierarchy into the three regimes of the previous chapter, now read as the per-event allocation parameter that drives that division.

The remaining sections recast the major results of quantum information theory—no-cloning, no-deleting, no-broadcasting, Holevo, Landauer, Maxwell's demon, Bennett's reversibility, Bremermann's compute-rate bound—as features of how the geometry keeps its records, then close on what computation is in a universe with finite topological capacity.

10.1 Two Quantities Per Event

Every actualization event does two things. It resolves structure in the actual world—determining which of the distinguishable outcomes obtains—and it deposits stripped content in the normal bundle as entropy. These two contributions exhaust the event's budget: the total pre-projection entropy splits into information gained and entropy produced, with nothing left over.

The entropy produced per event is approximately constant across all scales. It depends on the volume of the normal-bundle fiber, which is set by the Hopf fiber circumference (2π, a topological invariant) and the three stripped dimensions. The result is $\Delta S \approx 3\, k_B \ln(2\pi) \approx 5.5\, k_B$ per event. This number does not change with energy scale, because the fiber geometry does not change with energy scale.

The information extracted per event, by contrast, depends on the energy available relative to the thermal noise floor. The resolvability ratio $R(k) = E(k)/(k_B T)$, introduced in Chapter 7, measures this: it counts the number of distinguishable outcomes per real dimension at hierarchy level k. The total information per event is $I(k) = 3\,\log_2 R(k)$ bits—three real dimensions, each contributing $\log_2 R(k)$ bits of resolution.

At high energies ($R \gg 1$), nearly the entire pre-projection budget crystallizes into structured information. At the electroweak scale ($k \approx 44.5$), for instance, $R \sim 2 \times 10^{12}$: a single actualization event can resolve a particle's spin, flavor, color charge, and momentum to within the de Broglie wavelength—roughly $3 \log_2(2 \times 10^{12}) \approx 123$ bits of information—while producing the same $5.5\, k_B$ of entropy it produces at any other scale. The information dominates overwhelmingly. At room temperature ($k \approx 80$), $R \sim 10^{-2}$: a single event resolves almost nothing, and the entire budget goes to entropy. The $5.5\, k_B$ of entropy is the same; the information channel is effectively closed ($\log_2 R < 0$). Any structure at this scale must come from the statistical aggregate of vast numbers of events, which is why macroscopic physics looks continuous and deterministic.

The ratio between information and entropy is set by the energy scale at which the event occurs. Observers and measurement apparatus play no role in it.

10.2 The Complementarity Budget

The information per event is not freely allocable across the four fact types. The doublet structure of the arena (Chapter 9) imposes constraints on how information is distributed within each event.

The four fact types organize into two independent channels: the Kähler doublet (spectral and spatial, types A and B) and the gauge doublet (chiral and intensity, types C and D). Each doublet carries half the total information budget per event. Within each doublet, the two fact types compete for resolution: increasing the precision with which one type is measured necessarily decreases the precision available for the other.

In the Kähler doublet, the competition between spectral and spatial resolution is the Heisenberg uncertainty principle (Heisenberg, 1927). Resolving spectral content (what frequencies are present) to high precision leaves less information budget for spatial content (where something is), and vice versa. The uncertainty principle, on this account, is a channel-allocation constraint: the Kähler doublet has a fixed information capacity per event, and spectral and spatial content compete for it. The minimum uncertainty product $\Delta x \cdot \Delta p \geq \hbar/2$ is the statement that the doublet's total capacity cannot be exceeded.

In the gauge doublet, the competition between chiral and intensity resolution is the information-theoretic content of electric-magnetic duality: reallocating resolution between chirality (which handedness) and intensity (how much energy) is the same transformation that Montonen–Olive duality (the symmetry exchanging strong and weak coupling, equivalently electric and magnetic charges) (Montonen and Olive, 1977) performs on the electromagnetic field.

The two doublets are symplectically orthogonal: no isometry of the arena mixes them. This is a theorem of the Kähler geometry of $\mathbb{CP}^3$(the symplectic form vanishes on cross-doublet pairs), and it means that the two channels are statistically independent. Improving spectral resolution has zero effect on chiral resolution, and vice versa. The total information per event is the sum of the two doublet contributions, with no cross-doublet tradeoff.

10.3 Quantum Information as Geometry

Quantum information theory has built up a list of impossibility results across the late twentieth century: states cannot be cloned, deleted, or broadcast; measurement extracts at most a fixed amount of classical information per channel use; information processing pays a thermodynamic floor cost; no agent can use measurement to undercut the second law. Each was proved separately, each in the language of unitarity, channels, or operator algebras. The framework reads them as a single observation: the arena's configuration is the only ledger, and these are the operations the configuration cannot support.

10.3.1 No-Cloning, No-Deleting, No-Broadcasting

Classical information copies freely. A bitstring duplicated to a second register loses nothing: original and copy share the value without affecting each other. Quantum information does not—a generic state cannot be copied to a fresh register. The proof (Wootters and Zurek, 1982) runs to a few lines and uses only the linearity of unitary evolution, but the consequences are large: it underwrites quantum cryptography, constrains quantum computing, and makes state-teleportation protocols destructive of their input by construction.

In PPM the constraint reads geometrically. An actualization event deposits content of two kinds. The τ-even part lands in $\mathbb{RP}^3$ as the publicly accessible record. The τ-odd part lands in the normal bundle as the event's projection-specific fingerprint. The τ-even part is freely copyable—it sits in the actual world and can be transcribed by any other event that reads the same $\mathbb{RP}^3$ region. The τ-odd part is bound to the specific projection that produced it: accessing it requires reversing that event, and the reversal returns the original configuration without yielding a copy.

The deletion theorem (Pati and Braunstein, 2000) extends the same reasoning. Erasing a quantum state would require annihilating both parts; τ is an involution, $\tau^2 = \mathrm{id}$, and the τ-odd content can be relocated but cannot be destroyed. What appears as erasure at the level of the actual record is relocation to the normal bundle—the content persists in a sector inaccessible to the actualization machinery, and an external observer with full access to $\mathbb{CP}^3$ could in principle reverse the projection and recover it.

The no-broadcasting theorem (Barnum et al., 1996) extends the constraint to mixed states: no quantum channel takes an arbitrary mixed state ρ to a bipartite state whose marginals are both ρ. Density matrices on $\mathbb{CP}^3$ decompose into τ-even and τ-odd components by the same split that applies to pure states, and the τ-odd component remains bound to its specific projection geometry. Mixtures whose τ-odd component vanishes broadcast freely; the constraint binds whenever the mixture retains genuine quantum content.

The unifying observation across the three theorems: the τ-odd content is the same content that anchors each event to its specific position in the geometry. Information that copies freely is information that has lost its position-specific binding. Information that resists copying carries that binding. The operations that fail are the operations that would treat the projection-fingerprint as separable data—data that could be moved, duplicated, or deleted independent of the geometric event that produced it. The framework's response is that no such data exists: detachable fingerprints would be classical content by definition, and the τ-odd content cannot be detached.

10.3.2 Holevo and Landauer as Per-Event Budget

Holevo's bound (Holevo, 1973) answers a question that quantum mechanics raises by its structure. A qubit's state is specified by two continuous parameters, so a quantum system might seem able to store unbounded classical information in arbitrarily refined amplitudes. Holevo's theorem rules this out: no measurement strategy extracts more than $\log_2 d$ bits per use from a d-dimensional system, regardless of how cleverly the input states are prepared. The continuous parameter space contracts at the moment of measurement.

In PPM the contraction has a direct geometric form. Each event extracts at most $3 \log_2 R(k)$ bits of structured information at energy scale k, with $R(k) = E(k)/(k_B T)$ the resolvability ratio. This per-event budget is the framework's Holevo-type bound for τ-projection: the maximum classical information any single event can deposit in the actualized record is set by the volume of the projection's image, in bits. The continuous $\mathbb{CP}^3$ structure is real; it simply does not survive the projection step in a form the actualized record can read out.

Landauer's principle (Landauer, 1961) located the thermodynamic cost of computation: erasing one bit of information dissipates at least $k_B T \ln 2$ as heat. The result connected information processing to entropy production and ruled out free computation. In standard treatments the connection is derived by careful analysis of phase-space contraction and the second law. PPM makes it structural. Every τ-projection event, whether or not it extracts useful information about a target system, deposits $\Delta S \approx 5.5\, k_B$ in the normal bundle. Information and entropy are two readings of the same per-event budget; their relationship is the geometry's, with no auxiliary principle to impose on top.

Maxwell's demon (Bennett, 1982; Maxwell, 1871) sharpens the picture into a paradox-shaped puzzle. A demon that measures molecular microstates and uses the results to sort molecules appears to lower entropy without paying. Bennett's resolution attributed the missing cost to the demon's eventual memory erasure—the bill comes due when the demon clears its records to make room for new ones. PPM places the cost earlier. Each measurement the demon performs is itself an actualization event, and the event deposits $5.5\, k_B$ at the moment the measurement occurs. The demon has nothing left to erase that it has not already paid for; the second law is settled at acquisition, every time.

The common feature of Holevo and Landauer in this reading: the per-event budget is finite, paid in advance, and split between information and entropy by the resolvability ratio. The cap on extractable information and the floor on dissipated entropy are halves of one allocation, and the allocation is fixed by the volume of the fiber the projection integrates over. Information and thermodynamics are not separate subjects coordinated by an analogy—they are the two halves of how the geometry pays for an event.

10.4 Computation as a Reading of Geometry

Computation is what happens to the arena's record under sequences of events. Every gate in a quantum circuit, every step of a classical algorithm, every brain process, every chemical reaction is either a sequence of τ-projection events (each actualizing some $\mathbb{CP}^3$ content, depositing the residue, updating the record) or unitary evolution between events (rotating $\mathbb{CP}^3$ structure without projecting). The split between these two modes is the deep structure of computation in the framework, and it explains both why quantum computers can outperform classical ones and why no computational process anywhere in the universe is unbounded.

10.4.1 Two Modes of Evolution

The framework has exactly two ways the arena can change. Between events, $\mathbb{CP}^3$ evolves under unitary dynamics: the state rotates, amplitudes recombine, content moves through the possibility space without anything being committed to the actual world. This evolution is reversible. Running the unitary backwards undoes its effect, and no entropy is produced. At events, the τ-projection happens: the state is committed to an $\mathbb{RP}^3$ position, the τ-odd content is deposited in the normal bundle, and $5.5\,k_B$ of entropy is produced. This step is irreversible. Reversing it would require recovering the deposited content from the inaccessible sector. Each event has a finite duration set by the Margolus-Levitin minimum-evolution time (Margolus and Levitin, 1998), $\tau_{\text{event}}(k) = \pi\hbar/(2E(k))$, which composes directly to the Bremermann compute-rate bound $2mc^2/(\pi\hbar)$ (Bremermann, 1962) when integrated over particle count—the framework's per-event budget reproduces the canonical bound by direct algebra (technical reference, 7).

The Bennett observation (Bennett, 1973)—that computation can in principle be performed reversibly, with no Landauer cost, if intermediate states are kept rather than erased—reads geometrically as: reversible computation is computation that stays in $\mathbb{CP}^3$ between actualization events. Each unitary gate is a rotation of the possibility space, costing nothing. Cost is paid only at the moments where the geometry forces a commitment to an actualized outcome.

Classical computation pays at every step. A classical bit is an actualized record—a configuration in $\mathbb{RP}^3$—and updating it requires a τ-projection event. The Landauer floor binds each gate. Quantum computation (Deutsch, 1985) pays only at readout. The quantum register lives in $\mathbb{CP}^3$, gates are unitary rotations that preserve τ-odd content, and the state is projected to $\mathbb{RP}^3$ only when the final answer is read out. An N-gate quantum algorithm pays for one event across the entire computation.

10.4.2 Where Quantum Speedup Comes From

A quantum algorithm exploits the structure that classical computation cannot represent. The τ-odd content of the $\mathbb{CP}^3$ state carries amplitude relationships—phase information—that have no classical analog. Gates organize these amplitudes such that interference between different $\mathbb{CP}^3$ trajectories cancels the amplitude on unwanted $\mathbb{RP}^3$ positions and concentrates probability on the desired one. When the projection finally occurs, the Born rule yields the correct answer with high probability.

Shor's factoring algorithm (Shor, 1997) is the cleanest example. The arithmetic of modular exponentiation is performed in superposition, period-finding extracts a phase relationship, and the projection collapses to one of polynomially many candidate periods. Classical algorithms must explore the candidate space serially—each test is its own actualization. Shor's protocol performs the exploration in $\mathbb{CP}^3$ and pays once.

The advantage has a precise resource cost. Maintaining τ-odd content across N gates requires the resolvability ratio to stay high enough that thermal noise does not project the state prematurely. Each event has a duration set by the Margolus-Levitin minimum-evolution time, $\tau_{\text{event}}(k) = \pi\hbar/(2E(k))$ (Technical Reference Ch. 7). At biological temperatures with $R \approx 1$, $\tau_{\text{event}} \approx 38$ fs and ambient thermal noise drives τ-projection on timescales of nanoseconds and faster; quantum computation at scale requires $R \gg 1$ for the duration of the computation, which is why working quantum computers operate in cold isolation and why scaling them is hard. Decoherence, in this reading, is the geometry resuming its default behavior of actualizing. The resource cost of quantum computation is the cost of holding the geometry off from that default.

10.4.3 The Bounded Universe

The standard physical Church-Turing thesis (Deutsch, 1985) states that no physical process exceeds Turing-machine computability. PPM yields a stronger statement: no physical process exceeds bounded Turing-machine computability. The boundary capacity $N_\infty = \varphi^{392} \approx 10^{82}$ caps the total information content of the arena—every $\mathbb{RP}^3$ configuration is a finite refinement of the holographic structure on the cosmological boundary. The cumulative actualization count $M(t) \sim 10^{121}$ caps the total number of events that have occurred or will occur across cosmic history. Both quantities are finite by construction.

Every computational process inside the universe is therefore a finite computation operating on a finite tape, regardless of how the process is organized—classical or quantum, deterministic or stochastic, biological or engineered. The framework excludes physical hypercomputation, infinite-precision real arithmetic, and any process that exploits genuinely unbounded resources. The bound follows from the geometry. The arena has a specific topological capacity, and that capacity sets the ceiling on what any internal process can do.

The ceiling is loose by computational standards. A capacity of 10^{82} bits and 10^{121} events is vastly larger than any process humans have constructed or are likely to construct. The bound is finite, however large; asymptotic behavior at infinity is a regime the universe does not occupy.

The four-fact inventory of Chapter 9 and the per-event budget read out in this chapter give the local content of any actualization event. What remains is the structural connection: how do the four kinds of factual content relate to one another, and which physical conversion constants mediate those connections? Chapter 11 answers this by laying out the K_4 graph of pairwise bridges and identifying τ itself as the sixth bridge, where every existing unification framework leaves a gap.

Chapter 11

Fundamental Constants: The Six Bridges

The arena delivers content in four kinds (Chapter 9), read at a resolution set by the per-event T.10
budget (Chapter 10). Those two structural facts identify what gets extracted and at what rate. They do not yet say how the four kinds are connected to one another—how spectral content relates to spatial content, how chiral content couples to intensity, which translations between the types the arena permits and which it forbids. Those connections are the subject of this chapter, and they are where the framework's account of the fundamental constants lives.

Each pair of fact types can be linked by a physical relationship: a conversion law, a coupling constant, a structural translation that takes content of one kind into content of another. Four fact types admit six pairwise connections. In graph theory, the complete graph on n vertices—denoted K_n—is the graph in which every pair of vertices is connected by exactly one edge. For four fact types, K_4 has exactly six edges: one for each pair. Five of these connections are realized by known physics. The sixth is absent from every existing framework, and identifying what occupies it is what closes the architecture before Part IV opens the physical content the architecture supports.

11.1 The Complete Graph

The six bridges are the six edges connecting the four vertices A, B, C, D:

Bridge	Constant	Physics
$A \leftrightarrow B$	c (speed of light)	Special relativity
$A \leftrightarrow D$	$\hbar$ (Planck's constant)	Quantum mechanics
$B \leftrightarrow D$	G (Newton's constant)	General relativity
$C \leftrightarrow D$	G_F (Fermi coupling)	Weak interaction
$A \leftrightarrow C$	θ_W (Weinberg angle)	Electroweak mixing
$B \leftrightarrow C$	—	**Missing**

Each bridge constant converts factual content of one type into factual content of the other.

The speed of light converts spectral content (what frequencies) into spatial content (what distances): $\lambda = c/\nu$. A photon with a definite frequency has a definite wavelength; c is the conversion factor between these two descriptions of the same physical state.

Planck's constant converts spectral content into intensity content (how much energy): $E = \hbar\omega$. A mode with frequency ω carries energy $\hbar\omega$. The conversion is discrete—energy comes in packets of size $\hbar\omega$—because the bridge operates through the τ fiber, whose circumference 2π quantizes the relationship. Every quantum of energy is one trip around the fiber.

Newton's constant converts spatial content into intensity content: how much gravitational energy a given geometry carries. The conversion is concrete and measurable. A photon climbing out of a gravitational well loses frequency—its spectral content shifts—in exact proportion to the spatial curvature it traverses, with G setting the exchange rate. Near a mass M, the gravitational redshift is $\Delta\nu/\nu = GM/(rc^2)$: Newton's constant converts the spatial fact (distance r from mass M) into an intensity fact (how much energy the photon surrenders to the geometry). The Schwarzschild radius $r_s = 2GM/c^2$ (Schwarzschild, 1916) is the point where this conversion becomes total—all of the photon's intensity content is absorbed by the spatial geometry. The smallness of G ($\sim 10^{-38}$ in natural units) has a structural origin developed in Chapter 16.

The Fermi coupling G_F converts chiral content into intensity content: how strongly the weak interaction couples handedness to energy exchange. A left-handed neutrino interacts with matter; a right-handed neutrino does not. G_F quantifies the rate at which chirality (the fact of being left-handed) is converted into energy transfer (the fact of exchanging momentum with another particle). The coupling is weak—$G_F \sim 10^{-5}/\text{GeV}^2$—because the chiral-to-intensity conversion operates through the full gauge doublet structure, with most of the information budget allocated to intensity rather than chirality.

The Weinberg angle θ_W (Glashow, 1961; Weinberg, 1967) sets the ratio of chiral to spectral content in the electroweak interaction—it determines how much of the electroweak coupling goes to chirality and how much to spectral identity. At the Z mass, $\sin^2 \theta_W \approx 0.231$: roughly a quarter of the electroweak coupling is chiral (weak) and three quarters is spectral (electromagnetic).

The five known bridges are the five known fundamental relationships of physics: relativity, quantum mechanics, gravity, the weak force, and electroweak unification. Each is associated with a constant that mediates conversion between two specific fact types. The table is not a classification scheme imposed from outside; it is the complete list of pairwise connections among four objects.

11.2 The Missing Bridge

The sixth edge of the graph connects spatial content (Type B, τ-even) to chiral content (Type C, τ-odd). This is the only bridge that crosses both the doublet boundary (B belongs to the Kähler doublet, C to the gauge doublet) and the τ-parity boundary (B is τ-even, C is τ-odd).

No known physical theory provides this bridge. General relativity operates entirely within the τ-even sector (spatial geometry and energy: Types B and D). The Standard Model operates on spectral, chiral, and intensity content (Types A, C, D) while treating spatial geometry as a fixed background. String theory's T-duality and mirror symmetry exchange within the Kähler doublet (A and B). Electric-magnetic duality and S-duality exchange within the gauge doublet (C and D). Each of these frameworks reaches some of the bridges, but none reaches the B–C edge.

The missing bridge is the structural signature of the unification problem. This is the framework's reading of the unification problem rather than a unanimous diagnosis: existing programs characterize the difficulty in their own terms (background independence (Rovelli, 1996), ultraviolet completeness (Weinberg, 1978), anomaly cancellation (Green et al., 1987)), and the B–C framing is one structural reading among several. Read in the framework's vocabulary, attempts to unify gravity with the other forces involve connecting spatial geometry (Type B) with gauge content that includes chirality (Type C). Loop quantum gravity, for example, promotes geometry from a fixed background to a quantum variable—deepening Type B content—but has no natural mechanism for generating the chiral coupling of the weak force (Type C); the Immirzi parameter (Immirzi, 1997) remains free precisely because the B–C link is absent. String theory reaches across the Kähler doublet via T-duality (Polchinski,

1998) (A $\leftrightarrow$ B) and across the gauge doublet via S-duality (Montonen and Olive, 1977) (C $\leftrightarrow$ D), but no known string duality bridges B to C directly. The difficulty, on this reading, is the absence of any known structure that simultaneously engages a τ-even quantity from one doublet and a τ-odd quantity from the other.

11.3 The Operator as the Missing Bridge

The actualization operator τ fills this structural gap. It acts simultaneously on both doublets: within the Kähler doublet, it preserves Type B (real geometry) and strips Type A (imaginary fiber); within the gauge doublet, it preserves Type D (squared amplitudes) and strips Type C (chiral phases). No other structure in the framework crosses both the doublet boundary and the τ-parity boundary.

Before τ acts, the arena carries the full SU(4) symmetry with all four fact types undifferentiated. After τ acts, all four types are simultaneously distinguished by the projection's action on their respective directions. The B–C bridge is the statement that spatial geometry and chirality are connected by the same act of actualization that connects every other pair of fact types.

The five known bridges are consequences of τ's action restricted to specific pairs. The speed of light is τ's isometric action within the Kähler doublet: it preserves the Fubini-Study metric, so the conversion factor between spectral and spatial content is fixed by the geometry. Planck's constant is τ's phase-identification action. The kernel of τ—the set of directions annihilated by the projection—is the U(1) phase fiber of the Hopf fibration, a circle of circumference 2π. Dividing h by this circumference gives $\hbar = h/2\pi$, the conversion between spectral content and intensity. Newton's constant carries a factor $(2\pi)^3$ reflecting τ's three-dimensional information-destroying projection from arena to actual world. The Fermi coupling and Weinberg angle arise from τ's breaking of the chiral symmetry and its allocation of the gauge doublet's information budget.

The sixth bridge is τ itself, operating as the full cross-doublet projection. The five constants are partial expressions of a single operator; the sixth bridge is the operator in its complete form.

The operational form is geometric rather than numerical. In homogeneous coordinates on $\mathbb{CP}^3$,

$$\tau\colon \mathbb{CP}^3 \to \mathbb{CP}^3, \qquad \tau\Big([z_1 : z_2 : z_3 : z_4]\Big) = [\bar{z}_1 : \bar{z}_2 : \bar{z}_3 : \bar{z}_4], \qquad \tau^2 = \mathrm{id}, \qquad \mathrm{Fix}(\tau) = \mathbb{RP}^3.$$

A single application acts as $\mathrm{diag}(-1, +1, -1, +1)$ on the (A, B, C, D) basis: it reverses the sign of the τ-odd directions (A in the Kähler doublet, C in the gauge doublet) and preserves the τ-even directions (B, D). The B–C bridge is the joint output of one event: each projection simultaneously commits a spatial fact (B preserved) and a chiral fact (C stripped, deposited in the normal bundle), with no multiplicative conversion factor between them because no separate physical content connects the two—they are two readings of the same projection. τ self-reduces by one fiber volume and therefore carries τ-reduction exponent 1 alongside $\hbar$. The five constants quantify partial actions of τ; τ itself, as a bridge, is the full action that those quantifications are partial expressions of.

The natural follow-up question—whether τ can be reconstructed as a combination of the five known bridge constants—has a definite answer. Not multiplicatively: τ is a dimensionless geometric operator on $\mathbb{CP}^3$, and c, $\hbar$, G, G_F, θ_W are scalar coupling constants with mixed mass–length–time dimensions. No algebraic combination of them reconstitutes an operator. What the five *do* fix together is the structural slot τ occupies: knowing the five τ-reduction exponents $(0, 1, 3, 0, 3)$ together with the sum rule $\sum(\text{exponents}) = 2\chi(\mathbb{CP}^3) = 8$ forces the sixth exponent to be 1, and knowing all six pairwise restrictions of an involution on $\mathbb{CP}^3$ pins down the involution up to coordinate choice. τ relates to the bridge constants as a three-dimensional shape relates to its set of two-dimensional projections: the projections taken together with the constraint that they come from a single object determine the object, but no projection alone, and no algebraic combination of projections, equals the object. Dimensionally, the same five constants in the Planck combinations ($L_P = \sqrt{\hbar G/c^3}$, $t_P = \sqrt{\hbar G/c^5}$, $M_P = \sqrt{\hbar c/G}$) fix the scale at which τ's action becomes nontrivial—they tell you where τ matters, even though they do not tell you what τ is.

11.4 The Structural Origin of the Unification Problem

The symplectic orthogonality of the two doublets explains why unification has been so difficult. The Kähler doublet governs quantum mechanics and gravity (spectral and spatial content). The gauge doublet governs the weak force and energy (chiral and intensity content). These two sectors are geometrically independent: no smooth deformation of the arena can mix them.

Every existing unification program attempts to embed both sectors into a single larger structure—a grand unified gauge group, a higher-dimensional spacetime, a string compactification. The difficulty is structural. The two doublets are orthogonal under the symplectic form, and forcing them into a common framework requires introducing degrees of freedom (extra dimensions, extra fields, extra symmetries) that are not present in the arena. Each added structure buys some bridge coverage, and each pays for it in unmotivated content the original geometry did not contain.

The framework's resolution is that the two doublets do not need to be merged. They are already connected—by the operator τ, which acts on both simultaneously. The "unification" is the recognition that a single actualization event processes both doublets through the same projection. The six bridges between fact types are the specific structural connections that τ establishes between the four types. The missing sixth bridge (spatial $\leftrightarrow$ chiral) is not a gap in the bridge graph; it is the operator itself, which no existing framework reaches because none has the projection structure to support it. The duality classification that follows makes the same observation empirically: every existing program either operates within a single doublet or provides an invertible cross-doublet dictionary. None acts on both doublets non-invertibly. That is the structural slot τ occupies.

11.5 The Duality Classification

The bridge structure classifies all known dualities in physics. Every duality is a coordinate transformation between different fact-type bases on the same underlying $\mathbb{CP}^3$ space. The classification organizes by which doublet the duality operates within, and reveals a systematic gap.

Framework	A	B	C	D	Bridge(s) reached
General relativity		•		•	B–D
Standard Model	•		•	•	A–C, A–D, C–D
T-duality / Mirror symmetry	•	•			A–B
S-duality / Montonen–Olive			•	•	C–D
AdS/CFT	•	•	•	•	A–B (invertible)
Twistor theory	•	•	•		A–B, A–C (partial)
Loop quantum gravity		•		•	B–D (deepened)
Causal set theory		•		•	B–D (discrete)
PPM (τ)	•	•	•	•	All six (non-invertible)

Dualities within the Kähler doublet (A, B) are expressions of the complex structure J, which maps real to imaginary parts. Wave-particle duality, T-duality, mirror symmetry, Born reciprocity (Born, 1938), and AdS/CFT (Maldacena, 1998) all exchange spectral and spatial content via the Kähler isometry. Dualities within the gauge doublet (C, D) are expressions of the Hodge star on the gauge algebra: electric-magnetic duality, S-duality, and particle-vortex duality exchange chiral and intensity content.

The table makes the pattern visible. Every existing framework either operates within a single doublet or, where it reaches across (as AdS/CFT and twistor theory do), provides an invertible dictionary rather than a non-invertible projection. No established duality mixes the Kähler doublet with the gauge doublet in a way that destroys information. The B–C column—spatial geometry to chirality—is empty for every row except the last.

The actualization operator τ is the only structure that reaches all six bridges and does so non-invertibly. The failure of existing unification programs, in this classification, traces to the same structural absence: they lack a projection that acts on both doublets simultaneously.

11.6 The Klein Four-Group Structure

The six bridges organize into three pairs under a symmetry group: the Klein four-group $V_4 = \mathbb{Z}_2 \times \mathbb{Z}_2$. This group has three nontrivial elements, each of which swaps the four fact types in a specific pattern and thereby pairs the six bridges into three orbits.

The first element swaps τ-parities within each doublet ($A \leftrightarrow B$, $C \leftrightarrow D$), pairing the two within-doublet bridges: c (the A–B bridge) with G_F (the C–D bridge). These are the kinematic orbit—bridges that connect fact types within the same symplectically orthogonal pair.

The second element swaps doublets ($A \leftrightarrow C$, $B \leftrightarrow D$), pairing two cross-doublet bridges that link opposite τ-parities: θ_W (the A–C bridge) with G (the B–D bridge). These are the gauge orbit—bridges that require traversing the Kähler structure to connect doublets.

The third element combines both swaps ($A \leftrightarrow D$, $B \leftrightarrow C$), pairing the remaining two cross-doublet bridges that link same τ-parities across doublets: $\hbar$ (the A–D bridge) with τ (the B–C bridge). These are the unification orbit—the bridges that require the full $\mathbb{CP}^3$ geometry to connect fact types.

The orbit pairing of $\hbar$ and τ is the central structural result. Planck's constant converts spectral facts (Type A, τ-odd) into intensity facts (Type D, τ-even); the actualization operator converts spatial facts (Type B, τ-even) into chiral facts (Type C, τ-odd). Both cross both the doublet boundary and the τ-parity boundary. They are the same bridge applied to complementary pairs of fact types.

11.7 The Weinberg Angle

The Weinberg angle θ_W sits on the A–C bridge, connecting spectral and chiral content. It determines how the electroweak force divides its coupling between the electromagnetic and weak channels—a single number that governs the relative strengths of two of the four fundamental interactions. Its measured value ($\sin^2\theta_W \approx 0.231$ at the Z mass) is one of the most precisely known quantities in particle physics (Glashow, 1961; Weinberg, 1967). The bridge framework gives it a topological meaning at the Pati-Salam unification scale.

At the Pati-Salam scale, the Weinberg angle takes the value $\sin^2\theta_W = 3/8$. In the bridge framework this ratio reads

$$\sin^2\theta_W \;=\; \frac{\dim(\mathbb{RP}^3)}{2\,\chi(\mathbb{CP}^3)} \;=\; \frac{3}{8},$$

the dimension of the actual world divided by twice the Euler characteristic of the arena. The numerator counts how many spatial dimensions the projection produces; the denominator counts the total topological content of the pre-actualization space. The Weinberg angle, at its unification value, is the fraction of the arena's topological structure that survives as spatial dimensionality.

The information-theoretic reading follows directly. The gauge doublet (C, D) carries chiral and intensity content through a single information channel. At the Pati-Salam scale the Weinberg angle sets the intrinsic allocation: 3/8 of the channel capacity goes to chirality and 5/8 to intensity. The running of $\sin^2\theta_W$ from 3/8 down to 0.231 at the Z mass is the scale-dependent flow of this allocation parameter as the operative constraints change with energy—an effect tracked in detail by the renormalization group in Technical Reference Ch. 7.

11.8 The τ-Reduction Exponents and Derivability

The bridge constants differ in how much of the operator's structure they carry. This difference is measured by a single integer—the τ-reduction exponent—which determines whether each constant is derivable from the geometry, defines a unit, or is the geometry itself.

Each bridge constant carries a characteristic power of 2π—the circumference of the Hopf fiber that τ identifies. This power is the τ-reduction exponent.

11.8.1 The Three Exponents

The speed of light c has exponent 0: τ is an isometry of the Fubini-Study metric, so c is unchanged by the projection. A constant with exponent 0 is τ-invariant—it carries no imprint of the projection's dimensional or fiber structure. This is why c functions as a unit-defining constant: it sets the relationship between length and time without reference to the projection. Its orbit partner G_F (the Fermi coupling) shares exponent 0 and shares the property of τ-invariance: the Fermi coupling is measured in individual weak decays, not in collective contexts where τ's dimensional structure would appear. G_F is derivable from the arena geometry given the confinement-scale anchor ε_0 (operationally m_π); c is not, because it defines the units in which derivation is expressed.

Planck's constant has exponent 1: $\hbar = h/2\pi$, where the single power of 2π is the volume of the fiber that τ identifies. A constant with exponent 1 absorbs exactly one copy of the fiber structure—the minimal nonzero imprint of the projection. This is why $\hbar$ defines the quantum scale: it converts between the arena's continuous phase structure and the discrete units of action. Its orbit partner is τ itself, which also carries exponent 1: τ self-reduces by one fiber volume. $\hbar$ defines a unit; τ is the geometric axiom.

Newton's constant has exponent 3: the gravitational constant carries a factor $(2\pi)^3$, where the three powers correspond to the three dimensions of the actual world $\mathbb{RP}^3$. A constant with exponent 3 absorbs the full dimensional structure of the projection—the collective, scale-dependent physics that accumulates over N actualization events. This is why G is derivable: it encodes how the projection's information loss aggregates across the entire actualization history (Chapter 16). Its orbit partner θ_W (the Weinberg angle) shares exponent 3 and shares the property of collective dressing: $\sin^2\theta_W$ runs from $3/8$ at the Pati-Salam scale to 0.231 at the Z mass, driven by the number of degrees of freedom—the same dimensional structure that gives G its exponent.

11.8.2 The Sum Rule

The total τ-reduction exponent across all six bridges is

$$2 \times (0 + 1 + 3) = 8 = 2\,\chi(\mathbb{CP}^3),$$

where $\chi(\mathbb{CP}^3) = 4$ is the Euler characteristic of the arena. The total τ-content of the bridge constants is fixed by the topology of the kinematic space.

The identity underlying this constraint is $\chi(\mathbb{CP}^n) = \dim(\mathbb{RP}^n) + 1$ for all n: the Euler characteristic of the pre-actualization arena always equals the dimension of the post-actualization world plus one fiber degree of freedom (the τ fiber itself, absorbed by $\hbar$). For $n = 3$, this gives $4 = 3 + 1$, splitting the gravitational exponent (3, from the dimensionality of the actual world) from the quantum-mechanical exponent (1, from the fiber identification).

The six bridge constants, taken together, exactly account for the topological content of $\mathbb{CP}^3$. Each bridge carries a fraction of the operator's structure; the fractions exhaust the total. No bridge constant is redundant, and no topological content is left unassigned.

11.9 Bridge Constants and Structure Constants

The exponent classification above applies to bridge constants—the six edges of K_4 that connect distinct fact types. A separate class of constants are internal to a single fact type or to a single bridge. The fine-structure constant α is internal to the spectral–intensity channel; the strong coupling α_s is internal to the spectral sector; the CKM and PMNS mixing angles parameterize the internal structure of the A–C bridge. These are *structure constants*: they describe the geometry within a vertex or along an edge, rather than the relationship between vertices.

Structure constants are always derivable from $\mathbb{CP}^3$ geometry. They are eigenvalues of the Laplacian, holonomies of the gauge connection, or Berry phases (Berry, 1984) on the instanton moduli space. No additional input is needed beyond the arena itself. Bridge constants are not always derivable: the exponent determines whether a given bridge carries physical content (derivable) or metrological content (unit-defining), as the previous section established.

The full derivability hierarchy, from most geometric to most conventional, is:

1. *Purely geometric* (no input): τ, α (via the heat kernel), the number of generations, the gauge group.

2. *Geometric plus one anchor* (requires m_π or the electroweak symmetry-breaking scale): G, G_F, θ_W, the Higgs vacuum expectation value, particle masses.

3. *Geometric plus outstanding computation* (path identified, integral not yet completed): α_s, CKM angles, some PMNS entries.

4. *Unit-defining* (not derivable, not physical): c, $\hbar$, k_B.

The bridge/structure distinction and the τ-reduction exponent together predict which tier each constant occupies. Structure constants always fall in the first three tiers. Bridge constants fall in the tier determined by their exponent: exponent 0 or 3 yields derivable (with one anchor); exponent 1 yields either unit-defining ($\hbar$) or geometric (τ). This is a structural consequence of the K_4 graph and V_4 symmetry, not an imposed taxonomy.

11.9.1 The Complete Catalog

The catalog has two pieces: a table of the six bridge constants on the K_4 edges, and a structural map of which graph scopes the framework's structure constants populate at each tier. The bridge table commits to the exponent and tier of each conversion constant. The structural map shows where in the graph derivable content sits, scope by scope; the per-constant derivations live in the chapters where each constant is developed.

Tier values throughout: 1 = purely geometric (no empirical input); 2 = derivable given one anchor (m_π or the electroweak symmetry-breaking scale, equivalent through the cascade); 3 = derivation path identified, integral pending; 4 = unit-defining.

Bridge constants. The six edges of K_4, each carrying a single conversion constant.

Constant	Edge	Doublets	τ-exp	Tier	Type
τ	B–C	K–G cross	1	1	geometric
G	B–D	K–G cross	3	2	derivable
G_F	C–D	within gauge	0	2	derivable
θ_W	A–C	K–G cross	3	2	derivable
c	A–B	within Kähler	0	4	unit-defining
$\hbar$	A–D	K–G cross	1	4	unit-defining

11.10 Closing the Architecture

The architecture is now in place. Each event partitions the arena's content into information and entropy at a rate the resolvability ratio sets; the factual content sorts into four types organized by the V_4 symmetry of τ into Kähler and gauge doublets; six bridges connect the types pairwise, with τ-reduction exponents, a V_4-invariant sum rule, and a derivability hierarchy constraining every physical constant. The arena, the operator, and the bridges between fact types form a closed structural picture.

What this picture does not yet supply is the specific content that flows across the bridges. The K_4 graph has six edges, but it does not say which gauge group lives on the chiral vertex, which particle masses emerge from the spectral vertex, or which values the bridge constants take. Those values come from somewhere additional: the energy hierarchy. Forces, particles, masses, and constants emerge from τ acting on the isometry group PSU(4) at successively lower energy scales, each symmetry-breaking threshold producing new physical content that the one above it did not contain. The K_4 graph tells how many bridges exist and which exponents they carry; the gauge cascade tells what flows across them.

The bridge/structure distinction makes this boundary precise. Structure constants—α, α_s, the mixing angles—are eigenvalues and holonomies internal to the arena's geometry, and will be derived in Chapters 15 through 18 from τ acting on PSU(4). Bridge constants—c, $\hbar$, G—are the conversion factors between fact types. Some are derivable (their exponent permits it); others are unit-defining (their exponent forbids it). The hierarchy makes precise which constants the framework derives and which it takes as unit-defining.

Part IV picks up the gauge cascade at the top of the hierarchy and works downward, populating the vertices of K_4 with the specific physical content—fields, particles, forces, the values of the constants—that the architecture supports.

Part IV

The Physical World

Chapter 12

Fiber Fields and Excitations

Parts I through III established the geometry of the arena, the operator, the variational principle, the four fact types, and the six bridges that connect them. Those constructions worked at the per-event scale: what the operator does at one actualization, what content one event delivers, which constants convert between fact types. T.2, 5–7

Part IV reads the same geometry at the field scale and develops its consequences as the physical world. Where the earlier parts described a single event, Part IV describes what arises when the operator acts simultaneously across all of $\mathbb{RP}^3$: a quantum field theory built from the arena itself, the energy hierarchy that organizes its excitations, the spectrum of particles and forces those excitations populate, gravity as the cumulative back-reaction of τ-projections on the metric, the formal apparatus of quantum mechanics on the same arena, and the dimensionless constants that fix the scheme.

This chapter is the foundation: the field picture itself. PPM's account of quantum field theory is the dynamics of $\mathbb{RP}^3$'s local $\mathbb{CP}^3$ content read across all base points at once. This chapter develops the picture from the geometry already in hand and identifies the excitations the field supports; subsequent chapters work out the consequences in detail.

12.1 The Field as Geometric Configuration

Chapter 4 described the actualization operator at one event: a τ-projection of the local $\mathbb{CP}^3$ content at a single base point onto its $\mathbb{RP}^3$ value. That description was local by design. It specified what the operator does at one site, leaving open what the geometry looks like across the whole actuality manifold.

The field picture extends the local description to all base points simultaneously. Every point of $\mathbb{RP}^3$ has its own local $\mathbb{CP}^3$ content—the same arena structure introduced in Chapter 3, now indexed by base point. The fiber over a base point is the six real dimensions of $\mathbb{CP}^3$ available there, decomposed (Chapter 3) into three tangent directions of $\mathbb{RP}^3$ and three normal directions perpendicular to it. The field is the collection of all such fibers, considered as one continuous geometric object rather than as a sequence of disconnected per-event arenas. Its dynamics are the variational dynamics of Chapter 7 applied simultaneously across the field, with the actualization cycle of Chapter 6 firing at sparse base points distributed across its extent.

No new ingredients enter at this step. The arena $\mathbb{CP}^3$, the involution τ, the Kähler structure, and the variational free energy $\mathcal{F}$ all carry over from earlier chapters. What changes is the resolution at which the geometry is read: the whole geometric object considered at once rather than one event at a time.

Conventional quantum field theory (Peskin and Schroeder, 1995; Weinberg, 1995) keeps the field and the spacetime separate: spacetime is the stage, the field is what lives on it, and the field's value at each spacetime point is a datum overlaid on the geometry. The framework collapses that distinction. There is no external stage; the field is the configuration of the geometry at the field-resolution scale, and the configuration of the geometry is what conventional QFT would call the field value at each point. Every property a particle can carry—position, momentum, spin, charge, mass—is a feature of how the fiber field is configured, not an additional datum specified independently.

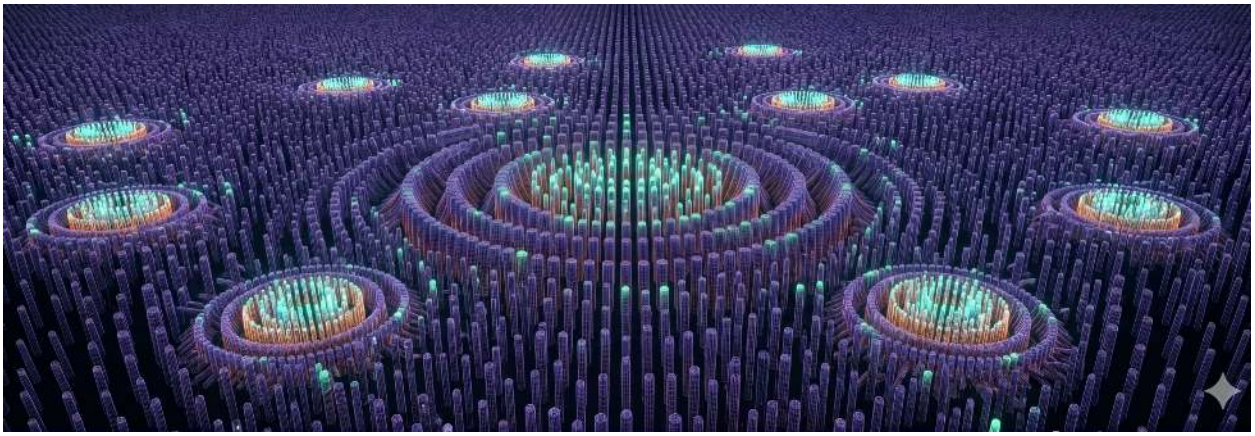

Figure 12.1: *The fiber field with several localized particle excitations. Vertical purple strands are the fibers, one over every point of* $\mathbb{RP}^3$*. Each bright concentric pattern is a single particle: a region where the field anchors at fixed base points from one actualization cycle to the next. The standing ripples around each particle depict its local wavefunction; cyan flashes mark* τ*-events firing at sparse base points, their density tracking* $|\psi|^2$*—the Born rule made geometrically visible. Warm orange tones in the active regions indicate accumulated* $\mathbb{RP}^3$ *residue from repeated* τ*-projections—the visible trace of the particle's persistence.*

12.1.1 The Vacuum

The vacuum is the field's ground state: every fiber aligned along its base point's τ-invariant direction, no excitations sustained, no τ-events firing above the background rate set by the gravitational projection rate Γ_G (Chapter 6). Uniform alignment minimizes the variational free energy $\mathcal{F}$ across the field: every fiber sits at the bottom of its local variational potential, and the field as a whole sits at the minimum of $\mathcal{F}$ summed across base points. Excitations are local departures from this configuration that the variational dynamics either dissipate (if shallow) or sustain (if anchored, as developed below).

The vacuum is not empty. The geometry $\mathbb{CP}^3$ is present at every base point regardless of excitation content; what distinguishes the vacuum is that the local content is everywhere unperturbed. Vacuum energy—the cosmological constant Λ—is what this everywhere-present geometric structure contributes to the metric of $\mathbb{RP}^3$, computed from the boundary capacity $N_\infty = \varphi^{392}$ (the topological boundary capacity, derived in Chapter 17).

12.1.2 Bounded Cascade, Bounded Field

The fiber field operates over the k-cascade developed in Chapter 14: each base point's local content decomposes into modes at successive energy scales, with the Planck level at $k = 1$ setting the UV bound and the cosmological horizon setting the IR bound. The cascade has both ends fixed by the geometry; the framework excludes physical hypercomputation, infinite-precision content, and any process drawing on genuinely unbounded resources (Chapter 10).

This matters for the field-theoretic treatment that follows. The framework's UV bound is geometric rather than parametric: the cascade itself has finite range, fixed by the arena's topology. Conventional renormalization-group flow of running couplings (Technical Reference Ch. 9) remains the standard machinery for tracking how those couplings change with scale within the cascade. What is sidestepped is the conventional appearance of UV divergences as artifacts of integrating over arbitrarily high momenta: in the framework, no such momenta exist, because the cascade does not extend past $k = 1$. The structural comparison with conventional regulators is developed in Technical Reference Ch. 9, §The k-Bound as Geometric Regulator.

12.2 The Fiber as Geometric Object

A fiber is the local geometric content of $\mathbb{CP}^3$ at one base point of $\mathbb{RP}^3$. Chapter 3 established the bundle structure that supports it. Around any point of $\mathbb{RP}^3$, the six real dimensions of $\mathbb{CP}^3$ split into three tangent directions (along $\mathbb{RP}^3$ itself) and three normal directions (perpendicular to $\mathbb{RP}^3$, into the unactualized region of the arena).

The two halves of this split carry different physics under τ. The tangent directions are real coordinates of the actual world; τ preserves them, and they survive every projection unchanged. The normal directions are the imaginary coordinates of the arena at that point; τ flips their sign, and they are stripped at every actualization event. A fiber is the local possibility space at one base point: three real directions of motion within the actual world, three imaginary directions of unactualized arena content.

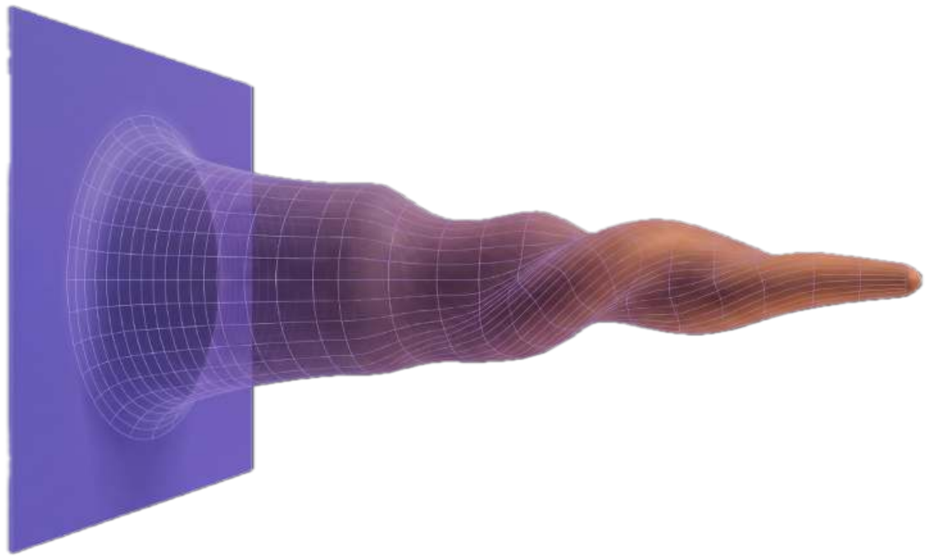

Figure 12.2: *Fiber-mode rotational closure. A single fiber rooted in the actuality wall (left) extends along the normal-bundle direction; the visible twist toward the tip is the* $720°$ *spinorial closure inherited from the spin structure on* $\mathbb{RP}^3$ *(Chapter 13.5). The rotation comes from the non-trivial element of* $\pi_1(\mathbb{RP}^3) = \mathbb{Z}_2$*: a spinor traversing a non-contractible loop returns with a sign change and must complete two such traversals before returning to identity. The fiber-mode index* n *counts how many half-rotations a given mode executes along the fiber; Chapter 15 uses this index to label the lepton ladder.*

Every property a particle can carry is encoded in the fiber. Spin is fiber orientation. Color charge counts displacement in the normal directions. Electric charge measures fiber winding under the residual U(1) symmetry. Mass measures the cost of supporting an excitation against the variational potential. None of these properties require an additional structure laid on top of the geometry. They are the geometry, read off the local fiber.

This dovetails with the V_4 doublet structure of Chapter 9. $\mathbb{CP}^3$'s Kähler structure is the Kähler-doublet content of every point—spectral and spatial fact types are the imaginary and real coordinates of the base manifold itself—while the gauge bundle structure on $\mathbb{CP}^3$ is the gauge-doublet content—chiral and intensity fact types are the imaginary and real coordinates of the fiber. The fiber-bundle and V_4 pictures are two vocabularies for the same two-layer geometry: arena (Kähler) and what lives on it (gauge). Fermions are bundle sections drawing position and energy from the Kähler arena and chirality and charges from the gauge fiber; gauge bosons (Chapter 15) are excitations of gauge-bundle connections.

12.3 Wavefunction as Field Configuration

The wavefunction ψ is the orientation pattern of the fiber field. At each base point, the local fiber has an orientation in $\mathbb{CP}^3$; that orientation is the value of ψ at that point. A standing-wave pattern of orientation across the field is a standing wave in ψ; a propagating pattern of orientation is a propagating wavefunction.

This identification is structural, not analogical. The wavefunction in standard quantum mechanics is a complex-valued function on configuration space. The configuration of a fiber at one base point is a point in $\mathbb{CP}^3$, which is by construction a complex projective space. The fiber's orientation is its complex coordinate, and the arrangement of those coordinates across the fiber field is exactly what the conventional formalism calls the wavefunction. The unitary PSU(4) flow on this configuration space is Kähler flow on $\mathbb{CP}^3$ — evolution of the orientation pattern under the arena's isometry group, generated by the Kähler structure itself. The Schrödinger equation (Chapter 13) is the differential equation that tracks this evolution at the level of the wavefunction.

Phase is the rotational position of a fiber around its own axis. Coherent phase across the fiber field—fibers winding together in step—is what makes interference possible. When a fiber decoheres—when its phase becomes effectively random with respect to neighbors—interference patterns are erased (the formal mechanism is treated in Chapter 13); the orientation pattern survives as a pattern, but the coherence across the field is lost.

12.4 Actualization Density and the Born Rule

An actualization event at a base point is a τ-projection of the local fiber content onto its $\mathbb{RP}^3$ value—a single firing of the operator at one location, stripping the fiber's normal-bundle content and leaving a real-valued residue on the actuality manifold. Across the field, such events occur at sparse, irregular positions; their density is not uniform.

The density follows the wavefunction. Where the orientation pattern has high amplitude, τ-events at that base point occur frequently; where the amplitude is low, they occur rarely; at nodes of the pattern, the rate goes to zero. The local event rate tracks the squared amplitude of the orientation pattern. This is the Born rule (Born, 1926): $|\psi|^2$ is the local rate of τ-events.

The exponent two is forced by the topology of the actuality manifold. Chapter 13 derives it from the $\mathbb{Z}_2$ identification on $\mathbb{RP}^3$ and the requirement that any probability measure be bilinear, normalized, and continuous. The wavefunction is the orientation of the field; the event density is the actualization rate; the squaring is the geometric fingerprint of the $\mathbb{Z}_2$ involution itself.

12.5 Excitations: Matter and Force

The fiber field supports two qualitatively different kinds of excitation. Each corresponds to a different geometric regime, and the difference maps directly onto the standard particle taxonomy.

12.5.1 Localized Excitations: Matter and Antimatter

A localized excitation is a region of the field where actualization events cluster at fixed base points. The excitation is *anchored*: its actualizations occur at the same locations from event to event, tracing a trajectory of base points along $\mathbb{RP}^3$. The fiber at each anchor point carries imaginary-direction content (normal-bundle modes) that is repeatedly stripped and repeatedly reconstituted from the underlying field configuration.

Figure 12.3 shows a localized excitation in isolation. A small region of the field sustains a tight cluster of τ-events at fixed base points; the surrounding field is unperturbed. The cluster persists from one actualization cycle to the next, with its position evolving along $\mathbb{RP}^3$ as the variational dynamics drive it. The persistence is what makes the excitation a particle: a trajectory rather than a single event, a recurring pattern rather than a transient firing.

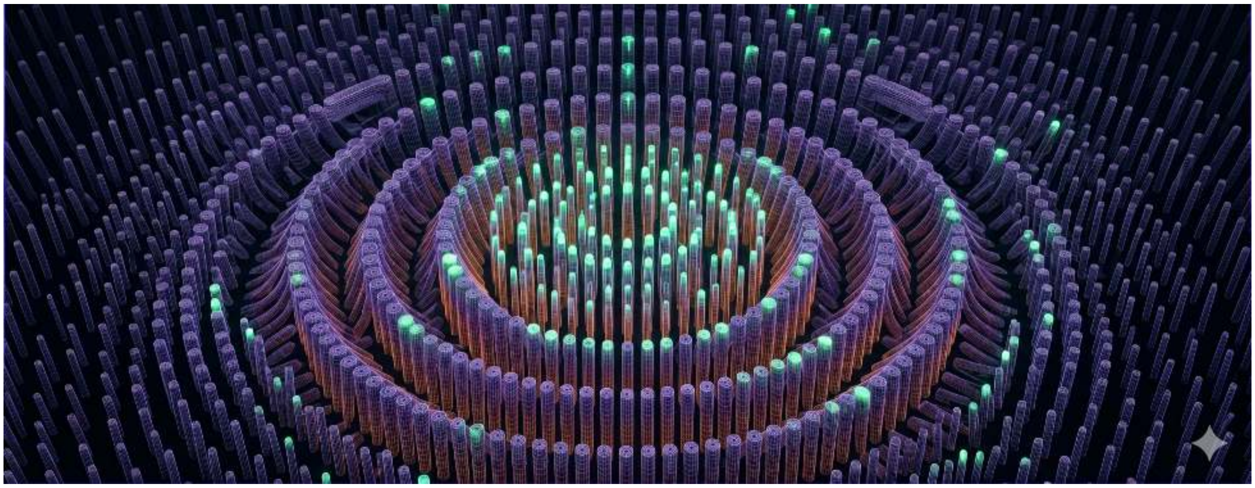

Figure 12.3: *A localized excitation of the fiber field. The fiber field sustains a tight cluster of flares at one region of $\mathbb{RP}^3$, with the surrounding field quiet. The cluster recurs from one actualization cycle to the next, anchored to the same base points, tracing a trajectory along the actuality manifold. This is the geometric signature of matter: an excitation that anchors at $\mathbb{RP}^3$ rather than propagating freely through it. The half-integer spin of such an excitation comes from the 720-degree identification on a single fiber under $\mathbb{Z}_2$ (Chapter 13); its mass comes from the energetic cost of supporting the anchoring against the variational potential (Chapter 14).*

Anchoring is the key. An excitation that occupies a definite region of $\mathbb{RP}^3$ from cycle to cycle has converted some of the field's imaginary-direction content into a localized real-valued structure that the actualization cycle continues to feed. The cost of maintaining that structure is the excitation's mass. The mass is the per-event energy (Chapter 5, §The Energy of an Event) that the cycle pays at each τ-firing to keep the excitation localized; the particle's rest mass-energy $E = mc^2$ is the cost-per-event of being this particle, accumulated as the configuration's contribution to the thermodynamic E. The half-integer spin follows from the $\mathbb{Z}_2$ topology of $\mathbb{RP}^3$ acting on a single fiber: a 360-degree rotation flips the fiber's sign, and only a 720-degree rotation returns it to identity (Nakahara, 2003) (Chapter 13). Matter is anchored, massive, and half-integer.

Antiparticles arise within the same machinery: an antiparticle is a localized excitation whose normal-bundle content has the opposite τ-parity from its particle counterpart, so the charges read off the fiber (electric, color, weak isospin) all flip sign while mass and spin remain unchanged.

12.5.2 Propagating Excitations: Force

A propagating excitation is a pattern of fiber orientation that travels across the field without anchoring at any particular base point. Actualization events along the pattern's trajectory mark its passage but do not pin it; from one cycle to the next, the pattern's center of activity moves to different base points. No region of $\mathbb{RP}^3$ holds the excitation in place.

A propagating mode encountering a localized cluster is the standard particle-physics interaction event: the force-carrier sweeps across the field, couples to the matter excitation, and the variational dynamics redistribute the field's content accordingly (Figure 12.4). The contrast between the two excitation types—one anchored, one passing through—is the geometric content of the matter/force distinction.

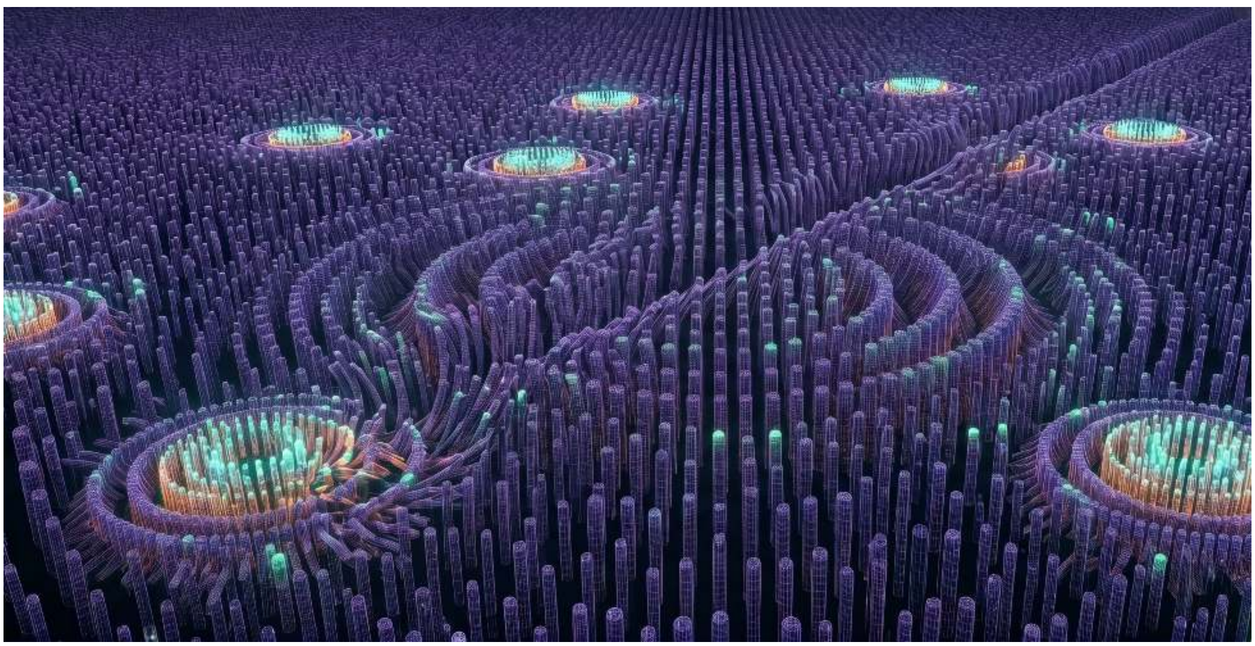

Figure 12.4: *A propagating fiber excitation arriving at a localized one. The propagating mode sweeps across the field without anchoring at any base point; the localized cluster holds its position. Both are excitations of the same fiber field, distinguished by whether the excitation anchors at $\mathbb{RP}^3$ (matter) or propagates through it (force). The integer spin of the propagating mode is its collective character—a configuration of many fibers in coherent rotation rather than a single fiber's 720-degree identification—and its masslessness comes from the absence of anchoring, no variational cost paid to maintain a localized residue.*

The propagating mode is collective: its configuration spans many fibers in coherent orientation, not a single fiber sustaining a localized cluster of τ-events. Integer spin follows from this collective character—the relevant rotation is of the field-level wave structure, not of a single fiber under $\mathbb{Z}_2$, so the 720-degree identification does not apply. When such an excitation does not anchor at any base point, it pays no variational cost for localization, and is therefore massless (the photon, the gluon). When the residual symmetries require it to acquire a localized configuration in the new vacuum after symmetry breaking (Higgs, 1964; Weinberg, 1967), it does anchor, and acquires mass (the W, the Z).

12.5.3 Fermion and Boson as Geometric Categories

Matter is anchored, half-integer-spin, massive. Force is propagating, integer-spin, possibly massless. The standard fermion/boson distinction maps onto these two regimes of the same primitive: a fermion is a localized excitation of the fiber field, a boson is a collective propagating mode. The taxonomy is exhaustive—an excitation either anchors at one or more base points or it does not—and the two categories are disjoint at the level of single excitations.

Spin-statistics (Pauli, 1940) follows from the geometric reading. Two fermions cannot occupy the same base point because the fiber there is already configured to support the first excitation; the second excitation cannot anchor without disturbing the existing configuration. This is Pauli exclusion read off the geometry: anchoring is incompatible with itself at a single location. The same fiber-as-anchorage picture forces the dichotomy: bosons are collective orientation patterns rather than anchored excitations, and an orientation pattern can be shared by arbitrarily many quanta without contradiction. (Chapter 13 formalises this reading: the spinor sign rule $\psi(-q) = -\psi(q)$ extends under particle exchange to an antisymmetric two-fermion wavefunction, which forces the amplitude for two fermions in the same state to vanish. Technical Reference Ch. 4 gives the configuration-space derivation.) Bosons, being collective patterns of fiber orientation across many base points rather than fixed-point configurations, can superimpose freely; many can coherently share the same regions of the field, which is what makes Bose–Einstein condensation and laser coherence possible. The familiar split between matter and radiation—distinguishable, exclusive particles on one side, identical superimposable quanta on the other—is what the anchoring/non-anchoring distinction looks like at the statistical level.

The fiber field is the load-bearing primitive for the rest of Part IV. Every following chapter—the formal apparatus of quantum mechanics, the energy hierarchy, the particle and force spectrum, gravity, cosmology, and the dimensionless constants—builds on the orientation-as-wavefunction reading and the matter-versus-force distinction developed here. A structural pattern recurs throughout: the τ-projection separates $\mathbb{CP}^3$ (possibility) from $\mathbb{RP}^3$

(actuality), and every operator on the arena inherits a $\mathbb{CP}^3/\mathbb{RP}^3$ split in its eigenstructure. Different operators express the split differently — the Dirac operator through its three fermion modes (Chapter 15), the Kähler Hamiltonian through its radial-bulk spectrum (Chapter 13)—but the underlying duality is one geometric fact. The field picture is in place; what follows is what that picture produces.

Chapter 13

Quantum Foundations

Quantum mechanics in the framework is the dynamics of $\mathbb{CP}^3$ between actualizations and the projection from $\mathbb{CP}^3$ to $\mathbb{RP}^3$. This chapter develops that dynamics—what propagates between τ-events, how superposition and decoherence arise from the fiber-bundle structure, and why the standard quantum formalism is what shows up at $\mathbb{RP}^3$. Several quantum phenomena that standard physics must postulate (the Born rule, the measurement problem, entanglement) follow from the projective geometry of the arena without additional axioms. T.2, 4, 7, 16

13.1 Superposition and the Ontology of ψ

A quantum state is a point in $\mathbb{CP}^3$. This is the ontological commitment of the framework: the state vector ψ is a geometric object living in possibility space, not a bookkeeping device, not a summary of an observer's beliefs. Between actualization events, the state evolves by unitary PSU(4) flow on $\mathbb{CP}^3$ — the isometry flow that the Fubini-Study metric generates on the arena. The Hamiltonian H selects which one-parameter subgroup of PSU(4) runs at the moment, and unitary evolution traces the corresponding orbit in $\mathbb{CP}^3$. The Schrödinger equation

$$i\hbar \frac{\partial \psi}{\partial t} \;=\; H\psi$$

is the differential equation that tracks this evolution at the level of the wavefunction. The variational principle that governs actualization itself (Chapter 7) sits at the complementary τ-event layer, determining which fact actualizes when the projection fires; the framework's two dynamical layers — isometry flow between events, variational descent at events — exhaust its dynamical content.

The debate between ψ-ontic and ψ-epistemic interpretations (Harrigan and Spekkens, 2010) dissolves in this setting. Relative to $\mathbb{CP}^3$, the state is ontic: it is a determinate point in a real geometric space. Relative to $\mathbb{RP}^3$, the state is epistemic: many distinct points in $\mathbb{CP}^3$ project to the same region of the actual world, and an observer confined to $\mathbb{RP}^3$ cannot distinguish between them. The apparent tension between "the wave function is real" and "the wave function encodes ignorance" arises from conflating two spaces with different ontological status.

Superposition is the condition in which multiple points in $\mathbb{CP}^3$ project to the same neighborhood in $\mathbb{RP}^3$. Before τ acts, the system occupies a definite point in possibility space. There is no vagueness or indeterminacy in $\mathbb{CP}^3$; superposition is a feature of the projection, not of the pre-projection state. The components of a superposition are distinct trajectories in $\mathbb{CP}^3$ that share a common image in the actual world.

The geometric foundations for these claims were established in Chapter 3 (the arena) and Chapter 4 (the operator). What this section adds is the identification: quantum superposition is the generic relationship between $\mathbb{CP}^3$ and $\mathbb{RP}^3$, present wherever the projection is not one-to-one.

13.1.1 Virtual Particles as Fiber Content

Standard quantum field theory talks about virtual particles — internal lines of Feynman diagrams, off-shell propagator contributions, transient fluctuations of the vacuum — as if they were objects that briefly exist and vanish. The framework gives this loose talk a precise reading. Virtual particles are fiber-content configurations on $\mathbb{CP}^3$ that contribute to the variational landscape and to the path integral without firing as τ-events. They are not actual. They are possibility-space structure that ordinary perturbative calculations sum over because the path integral integrates over fiber content, not over actualized events.

This reading dissolves the recurring ontological puzzle. Vacuum polarization, the Lamb shift, and the running of couplings all read as variational consequences of fiber configurations the geometry permits; the renormalized observables are what the actualized record sees once the relevant fiber content has been integrated. The Casimir effect (Casimir, 1948) fits the same pattern: conducting plates impose boundary conditions on the $\mathbb{CP}^3$ unitary evolution between them, restricting which fiber configurations survive, and the gradient of the boundary-constrained bulk vacuum energy registers as a measured force. Chapter 17 works out how this coexists with the framework's stance on Λ: bulk vacuum energy is real and locally accessible when boundaries restructure the modes, and it is a different quantity from the boundary energy that sources cosmic curvature.

Spontaneous pair production is the complementary case. In strong electromagnetic fields (Schwinger pair production (Schwinger, 1951)), near black-hole horizons (Hawking radiation (Hawking, 1975)), and at rapidly accelerating boundaries (dynamical Casimir radiation), the variational landscape tilts far enough that τ-events fire on pair configurations the vacuum normally suppresses. These are real actualizations: a Schwinger-produced pair is a pair of τ-events, not a virtual thing that crossed some line into reality. What distinguishes them from ordinary matter is the absence of anchoring (Chapter 12, §12.5). Without a sustained landscape feature that pins the excitations at fixed base points across actualization cycles, the actualized pair contributes to the cumulative record and disperses — a firing without a particle trajectory behind it.

Three categories then cover the territory. Fiber content that never fires is truly virtual (computational structure in perturbative QFT, Casimir and Lamb shift readouts). Fiber content that fires once under a tilted landscape and disperses is spontaneous actualization (Schwinger pairs, Hawking quanta, dynamical Casimir radiation). Fiber content that fires and anchors is ordinary matter (§12.5). Standard QFT collapses the first two into the same "virtual particle" vocabulary and then locates ordinary matter in a separate formalism; the framework reads all three off the single fiber-versus-actualized distinction.

13.2 The Hamiltonian Architecture

Standard physics formulates quantum dynamics, gravitational dynamics, and measurement as three separate problems—the Schrödinger equation, general relativity, and a collapse postulate appended to the first two. The framework treats them as three pieces of one Hamiltonian acting on the $\mathbb{CP}^3/\mathbb{RP}^3$ structure (Technical Reference Ch. 2):

$$H_{\text{total}} \;=\; H_\alpha[\mathbb{CP}^3] \;+\; H_G[\mathbb{RP}^3] \;+\; H_{\text{int}}[\text{boundaries}].$$

Each piece runs on a different sector and does a different job. Together they generate the actualization cycle; separately, they correspond to what standard physics treats as quantum evolution, fixed actuality, and measurement. The decomposition is what permits the chapter's later sections to derive the Born rule, the uncertainty principle, and the resolution of the measurement problem from a single piece of structure rather than from three independent postulates.

H_α is the Schrödinger Hamiltonian on the arena. With $\nabla^2_{\mathbb{CP}^3}$ the Laplacian of the

Fubini-Study metric and $V_{\text{Kähler}} = m_\pi c^2 \log(1 + |z|^2/\lambda_C^2)$ the Kähler potential, it takes the form

$$H_\alpha \;=\; -\frac{\hbar^2}{2m_\pi}\,\nabla^2_{\mathbb{CP}^3} \;+\; V_{\text{Kähler}},$$

and generates unitary PSU(4) flow on $\mathbb{CP}^3$ between τ-events. The logarithmic potential acts as a barrier in $|z|^2$: states near $\mathbb{RP}^3$ are easy to actualize, states far from $\mathbb{RP}^3$ progressively harder. Quantum superposition, interference, and phase accumulation all live in H_α. In the laboratory limit—a system localized to a small neighborhood of $\mathbb{RP}^3$, where the Fubini-Study metric is flat to leading order—H_α reduces to the textbook Schrödinger equation on flat space. The framework's contribution is the global geometry that the local form is the linearization of.

Between τ-events, H_α generates unitary evolution. At a τ-event, the projection collapses the state to one H_α eigenstate, and the eigenvalue selected is the event's energy. This eigenvalue is the same quantity that appears as the per-event cost in Chapter 5, §The Energy of an Event, and as the thermodynamic E in $F = E - TS$ accumulated across events.

The discrete spectrum. The spectrum of H_α on the radial sector of $\mathbb{CP}^3$ takes the form $\varepsilon_n \approx 2n(n+3) + 1.71$ in units of $m_\pi c^2$. The factor of 2 comes from the kinetic prefactor $-\hbar^2/(2m_\pi)$ acting on the free Fubini-Study Laplacian eigenvalue $4n(n+3)/\lambda_C^2$ ($\lambda_C = \hbar/(m_\pi c)$); the constant 1.71 comes from the Kähler-potential ground-state energy on $\mathbb{CP}^3$ (technical Chapter 9, §7.3). Per-event energies are therefore quantized: every τ-event lands on some ε_n, and the framework derives the discrete-jump structure of quantum measurement from $\mathbb{CP}^3$ geometry rather than postulating it. The Born rule that sets the probability of landing on a given eigenstate is developed in §13.5.

Energy floor. $\varepsilon_0 \approx 1.71\, m_\pi c^2 \approx 231$ MeV is the minimum possible event energy — the Kähler-potential ground state on $\mathbb{CP}^3$. No τ-event can deposit less than this through the radial sector. The energy floor is framework-derived.

Sub-confinement and above-confinement sectors. The energy floor ε_0 is the structural dividing line between two sectors of τ-event actualization. *Above-confinement* ($E > \varepsilon_0$): events occupy $\mathbb{CP}^3$ radial-bulk eigenstates of H_α, the discrete ε_n ladder computed above. *Sub-confinement* ($E < \varepsilon_0$): the radial-bulk has no eigenvalue available, so events occupy other sectors — angular eigenmodes of the full H_α spectrum (awaiting extension of the radial calculation), surface eigenmodes of the $\mathbb{RP}^3$ Laplacian, or the topological Jackiw–Rebbi zero mode bound to $\mathbb{RP}^3$. Which Standard Model particles populate which side, and the band placement of the ε_n on the cascade, are taken up in Chapter 15 §15.12.

Two operators, one duality. The sub-confinement / above-confinement split here is the H_α radial sector's expression of a more general fact about τ-projected operators: every operator on the arena that respects τ-symmetry inherits a $\mathbb{CP}^3/\mathbb{RP}^3$ split in its eigenstructure, but each operator expresses it through its own spectrum. Chapter 15, §15.4.1 introduces the Dirac operator's version — two $\chi(\mathbb{CP}^3/\mathbb{Z}_2)$ bulk modes plus one Jackiw–Rebbi wall mode of $\mathbb{RP}^3$, giving three fermion families. H_α expresses the same duality differently: its radial-bulk spectrum starts at ε_0 (the framework confinement scale), and surface modes on $\mathbb{RP}^3$ together with non-radial H_α sectors supply the sub-floor sector.

A particle's wavefunction is one mode of the Dirac operator (its generation); its actualization events fire at energies on H_α (its event spectrum). The two classifications are independent. They align for heavy fermions ($\mathbb{CP}^3$-bulk topological mode, $\mathbb{CP}^3$-radial-bulk events) and for Gen-1 ($\mathbb{RP}^3$-bound mode, sub-floor events). They diverge for muon and strange — Gen-2 topological bulk modes whose event energies sit below the H_α radial floor, so their events occupy non-radial sectors of H_α or surface modes of $\mathbb{RP}^3$. The divergence is informative rather than contradictory: topological identity and event-energy support are different physical aspects of the same particle.

Where the spectrum lives. The spectrum belongs to Kähler flow on $\mathbb{CP}^3$ — the unitary sector the Kähler structure generates between τ-events. H_α is its Hamiltonian operator; its eigenvalues are the energies unitary evolution can land on. The fixed-point set $\mathbb{RP}^3 = \mathrm{Fix}(\tau)$ carries no Kähler flow ($H_G = 0$): the actualized record is geometric data, not a dynamical sector. Surface eigenmodes on $\mathbb{RP}^3$ come from a different operator — the restriction of the Laplacian to the fixed-point set, plus the boundary action of H_{int}, which couples bulk flow to surface commitment at the interaction sites. Two distinct geometric structures (the bulk Kähler manifold and the fixed-point surface), distinct spectra (radial-bulk eigenvalues and surface eigenmodes), distinct actualization routes (radial flow into a $\mathbb{CP}^3$ eigenstate versus boundary-localized tunneling); one floor energy ε_0 separating them.

ε_0 as the structural confinement scale. The threshold $\varepsilon_0 \approx 231$ MeV is what confinement means in framework-native terms: the energy below which the $\mathbb{CP}^3$ radial-bulk has no spectrum available and actualization is forced onto non-radial H_α sectors or onto the $\mathbb{RP}^3$ surface, and above which the radial-bulk modes of H_α become accessible. ε_0 sits within the conventional

$\Lambda_{\rm QCD}$ band ($\sim$ 200–300 MeV) (Particle Data Group, 2024), and the structural identification $\varepsilon_0 = \Lambda_{\rm QCD}$ pulls QCD's confinement scale into the framework as the Kähler ground state on $\mathbb{CP}^3$. The lightest hadron mass $m_\pi \approx \varepsilon_0/1.70573$ emerges as a derived quantity, with the ratio fixed by Fubini-Study geometry and the Kähler potential. Chapter 18, §18.3 develops this reading in full: the framework's structural anchor is ε_0 (a $\mathbb{CP}^3$ spectral-geometric output), and m_π is the energy-scale reference the document uses for numerical work.

H_G governs the evolution of actualized geometry. It is zero. This is the Wheeler–DeWitt constraint (DeWitt, 1967): once the spatial geometry has been actualized, it does not evolve under Hamiltonian dynamics. The actualized record accumulates—each new τ-event adds to the geometric record—but no τ-event modifies what is already actualized. The standard puzzle of how time passes if the geometry is frozen is dissolved by the framework's account of time: time is the ordered sequence of τ-events (Chapter 8). General relativity has no explicit time coordinate because it is the theory of $H_G = 0$.

$H_{\rm int}$ is the actualization operator. It acts at sites where the gravitational decoherence rate exceeds the rate of unitary evolution within $\mathbb{CP}^3$: a τ-projection fires, the state collapses from $\mathbb{CP}^3$ onto $\mathbb{RP}^3$, and the cycle returns to H_α to rebuild the imaginary content the projection stripped. What makes $H_{\rm int}$ ontologically distinctive is the locality property it carries. At each actualization site b, the relevant Hilbert space partitions as

$$\mathcal{H} \;=\; \mathcal{H}_S \otimes \mathcal{H}_{\partial S} \otimes \mathcal{H}_{\rm env},$$

where $\mathcal{H}_S$ is the system being actualized, $\mathcal{H}_{\partial S}$ is the local interaction region (the boundary), and $\mathcal{H}_{\rm env}$ is everything else. $H_{\rm int}$ acts only on $\mathcal{H}_S \otimes \mathcal{H}_{\partial S}$, without requiring knowledge of $\mathcal{H}_{\rm env}$. Actualization is a local operation, mediated by the boundary, with the rest of the universe screened off.

The actualization operator at site b is a parameterized object $\hat{A}_b(\theta)$ with $\theta = (\theta_{AB}, \theta_{CD})$ ranging on the measurement torus $T^2 = [0, \pi/2]^2$ developed in Chapter 9. The two coordinates allocate the two doublet structures of the framework: θ_{AB} allocates Kähler-doublet content (the gravitational sector — G, Λ, the Fubini-Study geometry that H_α also carries through $V_{\text{Kähler}}$), and θ_{CD} allocates gauge-doublet content (the Standard Model symmetries that τ-breaking selects). The four corners of T^2 are the Klein four-group $V_4 = \mathbb{Z}_2 \times \mathbb{Z}_2$ of fact types (spectral, spatial, chiral, intensity); each τ-firing lands θ on one corner, fixing both doublet allocations and selecting the fact type the event commits to. The tripartite Hamiltonian and the doublet/fact-type structure meet at $H_{\rm int}$: H_α carries the Kähler structure through its flow, H_G holds the cumulative doublet record on $\mathbb{RP}^3$, and $H_{\rm int}$ is where one V_4 corner gets chosen per event.

This conditional independence is what makes the boundary architecture of Chapter 19 possible. The boundary ∂S that screens the environment from the actualization is the surface across which the system's evolution depends on the environment only through the boundary state itself. In the Hamiltonian architecture, that boundary is geometrically real — the locus of $\mathcal{H}_{\partial S}$ across which H_{int} acts. The active-inference reading of consciousness developed in Chapter 19 rests on the same conditional independence that H_{int} enforces here.

The three pieces compose into the actualization cycle of Chapter 6: H_α runs (unitary evolution), H_{int} fires at a site (actualization), H_G accumulates the new actualization without modification (frozen geometry), H_α runs again on the rebuilt τ-odd content. Each piece by itself is incomplete; the cycle is the dynamics.

13.2.1 Reduced Dynamics: Lindblad as System-Level Shadow

The actualization cycle of Chapter 7 runs continuous Lindblad evolution between Poisson-timed τ-firings on every scale the framework supports — the universal dynamics that the variational functional $\mathcal{F}$ descends along. This section reads that same dynamics at the quantum-system level, where the bulk Kähler flow is H_α and the firings are H_{int} acting at ∂S; specializing the universal master equation to this case is what makes the Lindblad operators framework-derived rather than chosen by hand.

H_{total} is closed-system unitary on the full Hilbert space $\mathcal{H}_S \otimes \mathcal{H}_{\partial S} \otimes \mathcal{H}_{\text{env}}$. No observer ever tracks the full state. What an experimenter, an instrument, or a neural boundary tracks is the system's reduced density matrix ρ_S, with the environment averaged over. The reduction changes what dynamics the observer sees.

Tracing $\mathcal{H}_{\text{env}}$ out of ρ converts the unitary evolution of H_{total} into a master equation for ρ_S:

$$\dot{\rho}_S \;=\; -\frac{i}{\hbar}\,[H_\alpha, \rho_S] \;+\; \hat{A}_b\,\rho_S\,\hat{A}_b^\dagger \;-\; \tfrac{1}{2}\Big\{\hat{A}_b^\dagger\hat{A}_b,\, \rho_S\Big\}.$$

The first term is the unitary flow on $\mathbb{CP}^3$ generated by H_α. The second and third together are the Lindblad dissipator (Gorini et al., 1976; Lindblad, 1976). The operator $\hat{A}_b$ is the actualization operator at site b—the localized representative of H_{int}. In standard practice the Lindblad operators are supplied empirically: each new physical setup selects its own dissipator from outside the formalism. Here they are the actualization operators the framework already carries. Lindblad evolution is what H_{int} looks like to an observer who cannot see $\mathcal{H}_{\text{env}}$.

The Markov property of the master equation usually follows from a Born-Markov assumption: the environment is taken to lose memory of its interactions with the system on a timescale shorter than the system's own evolution (Breuer and Petruccione, 2002). In the framework that assumption is geometric content rather than an approximation. The boundary ∂S identified above is what makes the assumption hold exactly here: conditioning on the boundary state already encodes everything the environment could communicate to the system; memory cannot leak back through ∂S because the boundary itself is the screen. The screening geometry of Chapter 19 and the dynamical Markov property of the master equation are the same fact at two levels of description.

The combined picture compresses three pieces of structure that standard quantum theory imports separately. A Hamiltonian, a Lindblad dissipator chosen per system, and a measurement basis selected by the experimenter all come from one geometric object. H_α generates the unitary part. H_{int} after tracing generates the dissipator. The projective frame θ on the measurement torus (Section 13.3) parametrizes the basis. The master equation above is the dynamical substrate that the active-inference treatment of Chapter 19 inherits as gradient descent on an effective free energy (Friston, 2010; Friston et al., 2017).

13.3 Measurement as τ-Projection

The measurement problem in standard quantum mechanics asks: what physical process converts a superposition into a definite outcome? In the framework, the answer is immediate. Measurement is τ-actualization. There is no separate collapse postulate because τ already does what collapse is supposed to do: it projects a point in $\mathbb{CP}^3$ onto $\mathbb{RP}^3$, stripping the τ-odd (imaginary) content and producing a definite actual outcome.

Measurement is therefore not a special process reserved for laboratories. Every τ-event is a measurement — every actualization projects possibility onto actuality. The distinction between "measured" and "unmeasured" systems, which generates so much confusion in standard interpretations, does not exist. Measurement always occurs; what varies is what the measurement resolves.

Two questions follow: what menu does the projection select from, and with what weights? The menu is the discrete spectrum of H_α established in §13.2. The weights are the Born probabilities derived in §13.5. Together they form the framework's account of quantum measurement: a discrete projection onto a derivable spectrum with topologically-forced probability weights, all from $\mathbb{CP}^3 + \tau$.

13.3.1 The Measurement Torus

Chapter 9 developed the measurement torus $T^2 = [0, \pi/2]^2$ as the space of measurement configurations. A point $\theta = (\theta_{AB}, \theta_{CD})$ specifies how a τ-event allocates information within its two doublets: θ_{AB} partitions the Kähler doublet between spectral (Type A) and spatial (Type B) content, and θ_{CD} partitions the gauge doublet between chiral (Type C) and intensity (Type D) content. Choosing an apparatus is choosing a point on T^2 (a spectrometer is small θ_{AB}, a position detector is large θ_{AB}). The angular resolution bound $\delta\theta \geq (\pi/2)\, R(k)^{-3/2}$ derived there controls how sharply one fact type can be resolved at the expense of its doublet partner; the underlying $\mathbb{CP}^3/\mathbb{RP}^3$ bundle geometry is in Figure 9.3. This chapter draws on the torus as the geometric backbone of complementarity, the uncertainty principle, and the Born rule, developed in the sections below.

13.3.2 Schrödinger's Cat

In the framework, radioactive decay (Schrödinger, 1935) is a τ-event at particle scale, where $R \gg 1$ and the measurement torus has full structure. The decay either occurs or does not at the moment of decay; the Geiger counter fires or does not; the cat lives or dies. Each step is an actualization event in its own right. Opening the box reveals a fact that was already actual. The observer's role is epistemic (learning what τ already determined), not ontological (causing τ to act). τ is a property of the arena, indifferent to whether anyone is watching.

13.3.3 Wigner's Friend

In the framework, the friend's measurement (Wigner, 1961) is a τ-event: actualization occurs at the moment of measurement, producing a definite outcome inside the laboratory. Wigner's description of the laboratory as a superposition is an epistemic state—it reflects his ignorance of the actual outcome, not the ontological status of the laboratory. No observer has a privileged relationship with τ. The operator is an arena property, not a feature of any particular subsystem or agent. The friend and Wigner occupy different epistemic positions relative to the same actual outcome. Two agents having different information about the same fact is consistent.

13.4 Complementarity and the Uncertainty Principle

Complementarity is the geometric content of the measurement torus: the continuous family of ways a τ-event can allocate resolution between the two fact types in each doublet. The channel-allocation framing of Chapter 10 gives the information-theoretic version of this statement—each doublet carries a fixed information budget per event, and the two types compete for it. The torus geometry adds the parameterization of that competition: at each torus angle the allocation is determined; between angles, the shift is a continuous rotation of which question the projection asks.

Within the Kähler doublet, the Heisenberg uncertainty principle (Heisenberg, 1927) reads directly off the torus. The angle θ_{AB} partitions information between Type A (spectral) and Type B (spatial) content. For the canonical conjugate pair (x, p)—position and momentum—the resolution widths along each type obey

$$\Delta x \cdot \Delta p \;\geq\; \frac{\hbar}{2},$$

the statement that the product of the two resolutions cannot exceed the doublet's total information capacity. The equality saturates on the family of states that use the budget with no waste—Gaussian wavepackets, which sit at the geometric minimum of the torus's joint-resolution function. The uncertainty principle, on this reading, is a consequence of the doublet geometry: the fixed information capacity per doublet, parameterized by the torus angle, produces the inequality directly from the structure of the measurement torus.

The same structure applies within the gauge doublet. The angle θ_{CD} partitions information between Type C (chiral) and Type D (intensity) content, with the analogous uncertainty product relating chiral and intensity resolution. Montonen–Olive duality (Montonen and Olive, 1977)—the electric-magnetic rotation—moves the system along θ_{CD} rather than along θ_{AB}. The two doublets are symplectically orthogonal: a rotation in one has no effect on the other, a consequence of the Kähler geometry established in Chapter 9.

Complementarity in the Bohr sense—that conjugate observables cannot be simultaneously measured with arbitrary precision—is the statement that a single τ-event can occupy exactly one point on T^2. Two measurements at different torus points require two separate events, and the world the two events project is two events' worth of content, subject to the framework's full Born-rule probabilistic structure (Section 13.5). Non-commutativity of observables is the statement that the torus rotation separating two measurements does not close at the operator level: the order in which the events occur affects which projection is available at each.

Uncertainty, complementarity, and the measurement torus are three vantages on one structure: the doublet decomposition of the normal bundle in $\mathbb{CP}^3$, with its Kähler geometry fixing how information can be allocated. The remaining quantum-weirdness sections of this chapter—Bell violations and contextuality (Section 13.7), decoherence (Section 13.8)—are consequences of the same geometry applied to multi-event configurations. Each is resolved by the same move: identify the torus structure in play and read off which allocations are consistent with the τ-projection actually performed.

The torus structure is scale-dependent. At particle scales ($R \gg 1$), the torus has full structure and arbitrary complementarity configurations are available, which is why the uncertainty principle reads cleanly in its standard form. As R approaches unity at the critical scale, the angular resolution $\delta\theta$ saturates at $\pi/2$ and the four fact types fuse into undifferentiated content (Chapter 20). The torus collapses at $R = 1$; above that scale, the uncertainty principle in its standard form no longer applies, because the doublet structure has fused. Heisenberg's inequality is a particle-scale result, with a specific termination at the thermal matching scale where the geometry it depends on dissolves.

13.5 The Born Rule

The actualization cycle produces discrete events, each stripping imaginary content and projecting a state onto the actual world. To extract any quantitative prediction—to say which outcome is more likely than which—requires a probability measure over the possible outcomes of each event. The actualization cycle tells us *that* events occur; the probability measure tells us *what to expect* from each one.

In standard quantum mechanics, this measure is the Born rule (Born, 1926): $P = |\psi|^2$. The rule is empirically confirmed to extraordinary precision across every domain of physics, from particle scattering to quantum optics. Yet it is an axiom. Every interpretation of quantum mechanics either postulates it directly or introduces additional structure (many worlds (Everett, 1957), pilot waves (Bohm, 1952), spontaneous collapse (Ghirardi et al., 1986)) to recover it indirectly.

The Born rule follows from the topology of the actual world with no additional assumptions.

13.5.1 The Topological Argument

The Hamiltonian architecture of §13.2 established the menu: τ-events project onto eigenstates of H_α with discrete energies ε_n. The question now is the selection weights. Standard quantum mechanics postulates $P = |\psi|^2$ as the rule that picks one eigenstate out of the superposition. The framework supplies the rule from the topology of $\mathbb{RP}^3$.

$\mathbb{RP}^3$ has fundamental group $\mathbb{Z}_2$: a full 360-degree rotation does not return a state to its original value but flips its sign, $\psi \to -\psi$. States on the actual world are therefore spinors, picking up a sign change under 360-degree rotation. This $\mathbb{Z}_2$ topology is forced by $\mathbb{CP}^3 + \tau$ (the actual world is the τ-fixed-point set $\mathbb{RP}^3$); no separate axiom about spinor structure is added.

Any observable quantity must be well-defined on $\mathbb{RP}^3$, hence $\mathbb{Z}_2$-invariant under the antipodal identification. The wave function itself is not invariant: it changes sign under the antipodal map. Any candidate probability measure built from ψ must cancel that sign change. The simplest construction is the product $\psi^*\psi = |\psi|^2$, since the complex conjugate ψ^* picks up the same sign flip: $(-\psi^*)(-\psi) = \psi^*\psi$.

Once $\mathbb{Z}_2$ invariance is imposed, the remaining constraints are the standard requirements any quantum probability measure must satisfy: *bilinearity* (so superpositions interfere), *normalization* (unit-amplitude states have unit probability), and *continuity*. These appear in essentially the same form in Gleason's theorem (Gleason, 1957) and its descendants (Busch, 2003). They are not the framework's invention; they are what "probability measure on a quantum state" generally requires.

Together with $\mathbb{Z}_2$ invariance, the three constraints force the exponent to be exactly two. $P = |\psi|$ fails bilinearity (absolute value isn't bilinear, so $|\alpha\psi_1 + \beta\psi_2|$ produces no interference term). $P = |\psi|^4$ overcounts under normalization (integrating $|\psi|^4$ doesn't yield unity for a unit-amplitude state without state-dependent rescaling, which violates fixed geometric weighting). Only $|\psi|^2$ satisfies all four requirements simultaneously.

The framework's value-add is what this argument rests on. Standard derivations of the Born rule take Hilbert-space structure as primitive and apply Gleason-style arguments to whatever observables the formalism happens to carry. The framework derives the Hilbert-space structure — including the spinor character of states — from $\mathbb{CP}^3 + \tau$, then reads the Born rule as a topological consequence of where states live. $\mathbb{RP}^3$ supplies the $\mathbb{Z}_2$ invariance Gleason needs. Everything else follows from standard probability theory.

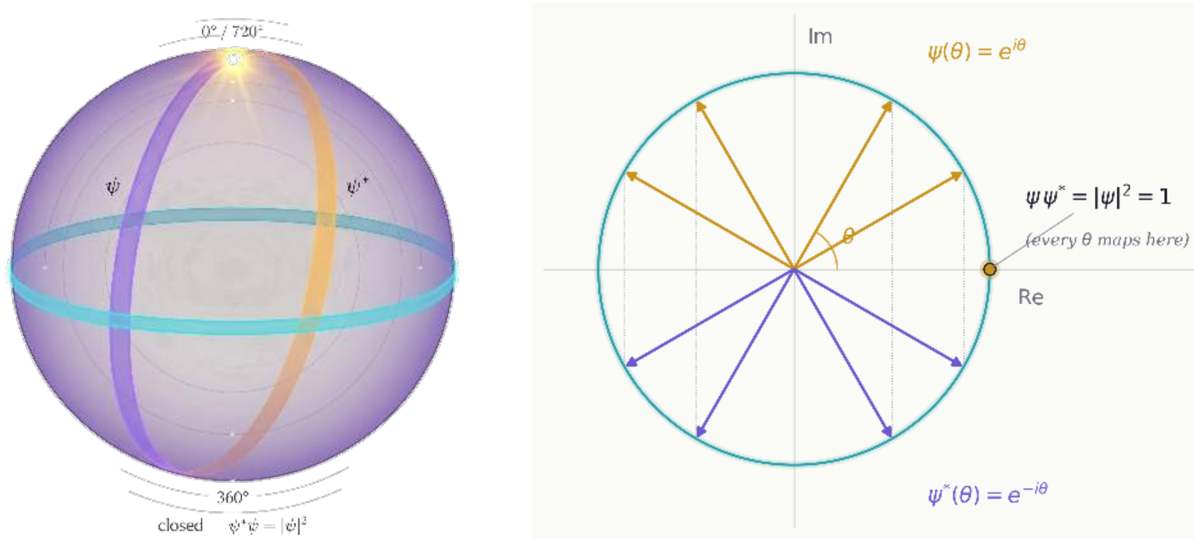

Figure 13.1: Left: *Topology. The forward journey ψ and its conjugate return ψ^* together close the 720-degree cycle on $\mathbb{RP}^3$; only at closure does the accumulated complex phase vanish.* Right: *Mechanism. At every angle θ on the unit circle, $\psi(\theta) = e^{i\theta}$ and $\psi^*(\theta) = e^{-i\theta}$ are reflections across the real axis. Their product $\psi\,\psi^* = |\psi|^2$ lands on the real line for every θ; the imaginary parts cancel pointwise. The $\mathbb{Z}_2$ topology is what forces every point of the forward loop to meet its conjugate: bilinearity, normalization, and continuity then admit no other invariant probability measure.*

13.5.2 The 720-Degree Cycle

The Born rule has a geometric interpretation in terms of the 720-degree topological cycle that characterizes $\mathbb{RP}^3$.

The wave function ψ represents the forward half of the cycle: a path from a point q_0 on the covering sphere S^3 to its antipodal point $-q_0$. This is a 360-degree rotation—a non-contractible loop in $\mathbb{RP}^3$ that does not return to identity. The complex conjugate ψ^* represents the return half: the path from $-q_0$ back to q_0, completing the full 720-degree cycle. The product $\psi^*\psi = |\psi|^2$ is the amplitude of the complete cycle. Complex phases, which encode the imaginary content accumulated during the forward half, cancel upon cycle completion. Only the real squared amplitude survives.

The Born rule, on this reading, is the statement that physical probability measures complete topological cycles. A single 360-degree rotation leaves a residual sign; it is an incomplete measurement. Only the full 720-degree cycle—forward and return—produces a $\mathbb{Z}_2$-invariant quantity that can serve as a probability.

13.5.3 What This Derivation Achieves

The framework derives both halves of the quantum measurement story from $\mathbb{CP}^3 + \tau$ geometry. The menu — the discrete spectrum $\{\varepsilon_n\}$ that a τ-event can land on — comes from the Fubini-Study Laplacian on $\mathbb{CP}^3$ via H_α (§13.2). The weights — the probability of landing on a specific eigenstate — come from the $\mathbb{Z}_2$ topology of $\mathbb{RP}^3$ that forces $|\psi|^2$ as the unique invariant probability measure on spinor states. Standard quantum mechanics postulates these as two independent axioms: observable spectra (taken from the operator formalism) and the Born rule (added by hand). The framework reads both off from the same geometric structure that supplied the arena and the operator in the first place.

The Born derivation depends only on the arena and the operator, established in Chapters 3 and 4. It is a topological consequence of the projective structure of the actual world; it requires no dynamics, no energy scales, no knowledge of forces or particles. It applies unchanged across every scale from the Planck energy to the pion mass. Every prediction in the remainder of Part IV that relies on $P = |\psi|^2$ — particle-mass amplitudes, gauge-coupling probabilities, gravitational decoherence rates, Bell correlations — inherits this derivation.

13.6 Spin-Statistics and Pauli Exclusion

Matter is anchored fiber content (Chapter 12, §12.5): a localized excitation pins a single fiber to a fixed base point on $\mathbb{RP}^3$, and the $\mathbb{Z}_2$ identification on that fiber forces a 720-degree closure (§13.5). The single-particle sign rule from the Born derivation extends, by way of one topological identity, to a two-particle exchange rule.

Exchange is a 2π rotation. The exchange of two identical particles in three-dimensional space is topologically equivalent to a 2π rotation of one about the other (Berry and Robbins, 1997; Leinaas and Myrheim, 1977); combined with the $\mathbb{Z}_2$ sign on each anchored fiber, this gives the two-particle wavefunction a definite parity under exchange. Half-integer fiber-mode index produces parity -1 (fermions); integer index produces parity $+1$ (bosons). The full assignment of fiber-mode indices to Standard Model species lives in Chapter 15, §15.5.

Pauli exclusion is collapsed antisymmetry. Antisymmetric $\Psi(x_1, x_2) = -\Psi(x_2, x_1)$ at $x_1 = x_2$ forces $\Psi = 0$: two identical fermions cannot occupy the same state at the same location (Pauli, 1940). Exclusion is the absence of an amplitude, a structural consequence of the spinor sign rule applied to the configuration space of identical anchored excitations. The bonding architecture of atoms (electron shells, the periodic table), the stability of matter under gravity (Lieb–Thirring bounds), and the existence of neutron stars (degeneracy pressure resisting collapse) all rest on this single topological fact: a non-contractible loop in $\mathbb{RP}^3$ flips the sign of a spinor. Technical Reference Ch. 4 gives the formal derivation via the configuration-space topology $\pi_1(C_N(\mathbb{RP}^3))$.

Bosonic symmetry permits unbounded occupation. Symmetric exchange parity places no restriction on multi-occupancy. Bose–Einstein condensation and laser coherence are the macroscopic expressions of that absent constraint: arbitrarily many bosons can share a single mode because the geometry imposes no penalty for doing so.

Why these are the only options. Three-dimensional configuration-space topology rules out other statistics: anyonic behavior requires a two-dimensional spatial geometry, where the configuration space's fundamental group is the braid group rather than the symmetric group (Leinaas and Myrheim, 1977). The actuality manifold $\mathbb{RP}^3$ is three-dimensional, and fermion/boson statistics are the only nontrivial options available to its spinor modes.

13.7 Entanglement and Contextuality

Two foundational results constrain the kind of theory PPM can be. Bell's theorem (Bell, 1964) rules out local hidden variables: no assignment of pre-measurement values to observables can reproduce the correlations entangled particles exhibit, and the experimental record (Aspect et al., 1982; Clauser et al., 1969) confirms the violation. Kochen–Specker (Kochen and Specker, 1967) rules out context-independent values: no consistent value assignment can be made to all observables of a quantum system regardless of which subset is measured. Both results target the same kind of object — pre-existing values that vary independently of measurement context — and the framework does not have values of that kind. Both constraints are satisfied as a structural feature of the ontology rather than as derivations to be performed.

Entanglement is one fiber with two $\mathbb{RP}^3$ terminals. Spatial separation is a feature of $\mathbb{RP}^3$ (the actual world). Fiber content lives in $\mathbb{CP}^3$ (possibility space). Two events can be far apart on $\mathbb{RP}^3$ while their fibers share a common origin in $\mathbb{CP}^3$ through the Hopf bundle $S^7 \to \mathbb{CP}^3$. Entanglement is exactly this: one fiber structure in $\mathbb{CP}^3$, two terminal base points on $\mathbb{RP}^3$ where independent τ-events fire. Figure 13.2 shows the geometry.

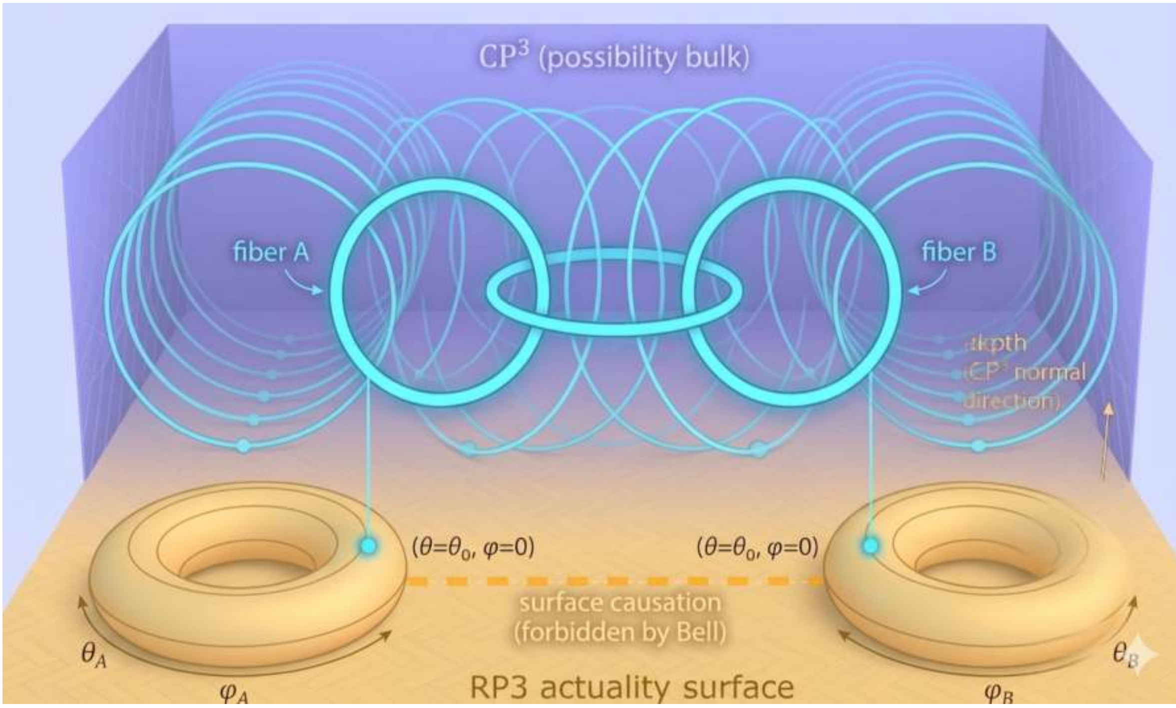

Figure 13.2: *Bell correlation as Hopf source, torus readout, and bulk depth. The $\mathbb{CP}^3$ bulk (violet) is foliated by an S^1-fibration whose fibers mutually link in classic Hopf configuration — a populated geometric space anchored to the $\mathbb{RP}^3$ actuality surface (gold). Two highlighted fibers in the bulk (cyan, fibers A and B) are the entangled pair: one linked structure of the bulk geometry. Their τ-projections drop along the depth axis perpendicular to $\mathbb{RP}^3$ and land on matched-position markers on the two surface tori, whose (θ, φ) parameter cycles carry the $\cos^2$ correlation pattern. The two surface tori are spatially separated on $\mathbb{RP}^3$; the linking that correlates them lives in the depth direction the surface frame does not include. The faint dashed gold connector across the surface is the surface causation Bell's theorem forbids — absent in the framework because the correlation arrives through the bulk.*

The "spookiness" assumes that spatial separation on $\mathbb{RP}^3$ implies separated descriptions in $\mathbb{CP}^3$. In the framework the spatial separation is downstream of the fiber structure, not the other way around. No signal travels between the terminal points because there is no transit through $\mathbb{CP}^3$ — the fiber connection is already there before either event fires. The Born rule applied to the shared fiber (§13.5) generates the joint distribution; the projective geometry produces the CHSH bound $|S| \leq 2\sqrt{2}$ as a consequence of the unique $\mathbb{Z}_2$-invariant probability measure on $\mathbb{CP}^1$ (full derivation in Technical Reference Ch. 8, §Entanglement and Bell Nonlocality).

Contextuality is the V_4 corner commitment. Each τ-event commits the outcome to one corner of the Klein four-group V_4 — spectral, spatial, chiral, intensity (Chapter 9). The corner the event lands on is set jointly by the system's pre-event state and the measurement context: the $\hat{A}_b(\theta_{AB}, \theta_{CD})$ structure of the actualization operator at the boundary (§13.2) determines which corner gets selected for which available content. The corner commitment *is* the value; there is no context-independent value sitting underneath the context-dependent measurement.

This dissolves Kochen–Specker rather than circumventing it. The theorem rules out theories that assign context-independent values to all observables. PPM declines to make such assignments: every value is a V_4 corner commitment, co-determined by context, made at the moment of the τ-event and not before. The counterfactual "the value the spin would have had if measured along $\hat{z}$" is unpopulated by the framework — that τ-event did not fire, so no commitment was made, so no value exists to discuss.

Both results read the same structure. Bell and Kochen–Specker both forbid pre-existing values independent of measurement. PPM does not have such values. It has τ-events that commit fiber content to V_4 corners as the events fire, with the corner co-determined by the context the actualization operator specifies at the boundary. The two terminal points of an entangled pair are two events on one fiber; the corner each event lands on is context-dependent by construction. What Bell and Kochen–Specker rule out is the kind of object the framework's ontology rules out first. The "paradox" the theorems generate is a paradox for theories committed to context-independent pre-existing values; for PPM it is the geometric structure already in place.

13.8 Decoherence and the Quantum-Classical Transition

A system in $\mathbb{CP}^3$ carries fiber content: the τ-odd directions in the normal bundle of $\mathbb{RP}^3$ that encode quantum information (Chapter 10). When this fiber content is well-isolated from the environment, the system exhibits coherent quantum behavior—interference, entanglement, superposition of macroscopically distinguishable states are all possible in principle.

Decoherence is the progressive entanglement of a system's fiber structure with the fiber structure of its environment (Zurek, 2003). As the system interacts with environmental degrees of freedom—photons, phonons, gas molecules—its fiber content becomes correlated with an increasingly large number of environmental fibers. The effective dimensionality of the system's accessible normal-bundle content decreases: the system's quantum state, traced over the environmental degrees of freedom, loses the off-diagonal coherences that produce interference.

Environment-induced decoherence was first identified by Zeh (Zeh, 1970) and developed into the quantitative theory of einselection (environment-induced superselection) by Zurek (Zurek, 2003). In the PPM setting, decoherence has a precise geometric meaning: it is the diffusion of fiber coherence from the system into the environment, driven by the same entropy-producing mechanism that Chapter 8 identified as the source of the thermodynamic arrow.

The Hamiltonian architecture of Section 13.2 makes the quantitative form of this diffusion explicit. The system's density matrix ρ_S evolves under the trace of the full dynamics over the environmental Hilbert space $\mathcal{H}_{\rm env}$. Within the conditional-independence structure $\mathcal{H} = \mathcal{H}_S \otimes \mathcal{H}_{\partial S} \otimes \mathcal{H}_{\rm env}$, that trace produces a Lindblad master equation (Gorini et al., 1976; Lindblad, 1976)

$$\dot{\rho}_S \;=\; -\frac{i}{\hbar}\,[H_\alpha^{(S)}, \rho_S] \;+\; \sum_b \Big(L_b\, \rho_S\, L_b^\dagger - \tfrac{1}{2}\{L_b^\dagger L_b,\, \rho_S\} \Big),$$

where the Hamiltonian piece is the system-only restriction of H_α and the Lindblad operators L_b are the boundary-mediated restrictions of $H_{\rm int}$ at each actualization site b. The boundary ∂S does the work: it carries the L_b operators that would otherwise have to be specified by hand. The quantum-classical transition has the same architecture as a boundary in any other setting (Chapter 19)—a surface across which influence flows in one direction, with the rest of the universe screened off behind it.

For macroscopic objects, decoherence is effectively instantaneous. The decoherence timescale for a system of mass m at temperature T, with superposition separation Δx, is (Schlosshauer, 2007; Zurek, 2003)

$$\tau_{\rm dec} \;\sim\; \frac{1}{\Lambda_{\rm th}\, \sigma\, n\, v} \left(\frac{\lambda_{\rm dB}}{\Delta x} \right)^2,$$

where $\Lambda_{\rm th}$ is the thermal scattering rate, σ is the scattering cross-section, n is the environmental particle density, v is the thermal velocity, and $\lambda_{\rm dB}$ is the thermal de Broglie wavelength. For a dust grain ($m \sim 10^{-15}$ kg, $\Delta x \sim 10^{-5}$ m) in air at room temperature, this gives $\tau_{\rm dec} \sim 10^{-31}$ s—far shorter than any dynamical timescale. Macroscopic objects do not exhibit superposition because the environment continuously entangles the object's fiber content with environmental modes faster than any coherent evolution can proceed. The decoherence timescale scales as $(\Delta x)^{-2}$, so spatial superpositions decohere quadratically faster with increasing separation.

The framework places a structural floor on all decoherence timescales: the per-event timescale $\tau_{\text{event}}(k) = \pi\hbar/(2E(k))$ (technical reference, 7). Environmental decoherence times above this floor reflect coupling rates between system and environment; below this floor, the geometry simply cannot project that fast. At the critical scale, $\tau_{\text{event}}(k_c) \approx 38$ fs is the elementary clock, and decoherence rates from gravitational, thermal, and environmental sources all reduce to event rates against this floor. The convergence of multiple bounds at $k \approx 75.35$ is the same convergence expressed in three different physical languages.

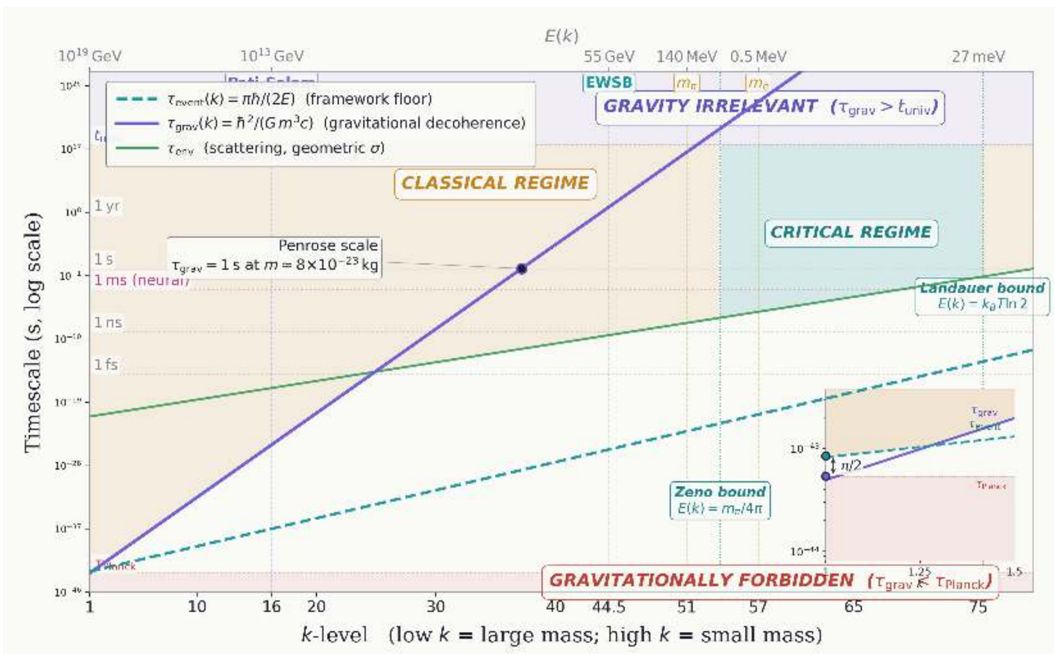

Figure 13.3: *Decoherence bounds across the cascade. At each level k the fastest decoherence channel — gravitational (Diósi, 1989; Penrose, 1996) or environmental (Joos and Zeh, 1985; Schlosshauer, 2007; Zurek, 2003) — destroys coherence before the dynamics can use it, forcing the system classical (amber region: almost the whole cascade). The critical regime $k \in [53.8, 75.75]$ (cyan box) is the exception, pinned by the Zeno bound at low k (where decoherence first slows enough for coherence to outlast a $720°$ cycle) and the Landauer bound at high k (where per-event energy falls below $k_B T \ln 2$, too little to carry a bit). Between the two, coherence outlasts a cycle and events still carry a bit down to the per-event floor τ_{event} (Technical Reference Ch. 7). This is the one band where coherence lasts long enough for many actualizations to integrate as a single bound phenomenal moment.*

Classical trajectories emerge from this process. When a system's fiber coherence is destroyed faster than its dynamical evolution, successive actualization events trace a path in $\mathbb{RP}^3$ that is, to excellent approximation, a geodesic of the Fubini-Study-induced metric on $\mathbb{RP}^3$. The quantum-to-classical transition is not a fundamental boundary; it is the regime where decoherence timescales are short compared to dynamical timescales, so that the system's τ-projected trajectory approximates a classical orbit. Classicality has a hard lower bound. Classical behavior is a property of a sequence of actualization events, so it cannot exist below the per-event floor τ_{event}, where no events resolve at all; an irreducible band of timescales between τ_{event} and the Planck time never becomes classical, however fast decoherence runs. The thermodynamic arrow (Chapter 8) reinforces this: the monotonic growth of actualization entropy ensures that decoherence is irreversible under normal conditions.

13.8.1 Wheeler-DeWitt and the Problem of Time

The Wheeler-DeWitt equation (DeWitt, 1967),

$$H\Psi = 0,$$

applies quantum mechanics to the universe as a whole and discovers that the total Hamiltonian annihilates the wave function of the universe. This appears to eliminate time from physics entirely: if $H\Psi = 0$, there is no Schrödinger evolution, no change, no dynamics.

In the framework, this result is expected. Between τ-events, the arena $\mathbb{CP}^3$ carries no preferred time direction. Unitary PSU(4) flow is reversible and preserves all information; there is no arrow, no before and after. The constraint $H\Psi = 0$ correctly describes this inter-actualization regime: the total state of $\mathbb{CP}^3$ does not evolve in any preferred time parameter.

Time enters through τ. Each actualization event is irreversible (it strips τ-odd content, producing entropy) and thereby defines a direction. The cumulative sequence of τ-events is what the framework calls time: $M(t)$, the actualization count, grows monotonically by construction. Clock readings, aging, memory formation—all are records of actualization events, not coordinates read from a pre-existing time axis.

The "problem of time" dissolves because time is not a coordinate that the wave function must depend on. Time is the cumulative record of τ-events. The Wheeler-DeWitt equation describes the timeless inter-actualization arena; the actualization sequence provides the temporal structure that the equation appears to lack.

The quantum formalism is now reconstructed from the arena's geometry. Superposition is fiber content awaiting actualization; the Hamiltonian splits into unitary flow on $\mathbb{CP}^3$ and the actualization operator at $\mathbb{RP}^3$ boundaries; the Born rule reads off the $\mathbb{Z}_2$ topology of the fixed-point set; entanglement is one fiber with two terminals; decoherence is environmental sampling of unactualized content; and time emerges as the cumulative sequence of τ-events. The next chapter builds the energy hierarchy on which these per-event actualizations live — the cascade ladder of k-values that organizes the framework's energy scales from Planck to confinement to the resolvability window. Chapters 15–17 then read the Standard Model, gravity, and cosmology off the operator structure built here; Chapter 18 closes Part IV with the master self-consistency relation binding the three readouts together.

Chapter 14

The Energy Hierarchy

This chapter develops the single integer cascade index k that organizes the framework's energy scales—events, particle masses, symmetry-breaking transitions, thermal regimes—from the Planck energy to the critical scale at the quantum-classical boundary. Every result developed earlier—the actualization cycle, the Born rule, the variational principle, the four fact types, the six bridges, the fiber field—holds at all scales simultaneously; what varies is the set of constraints under which the variational principle operates and which configurations are stable. T.9, 18.2

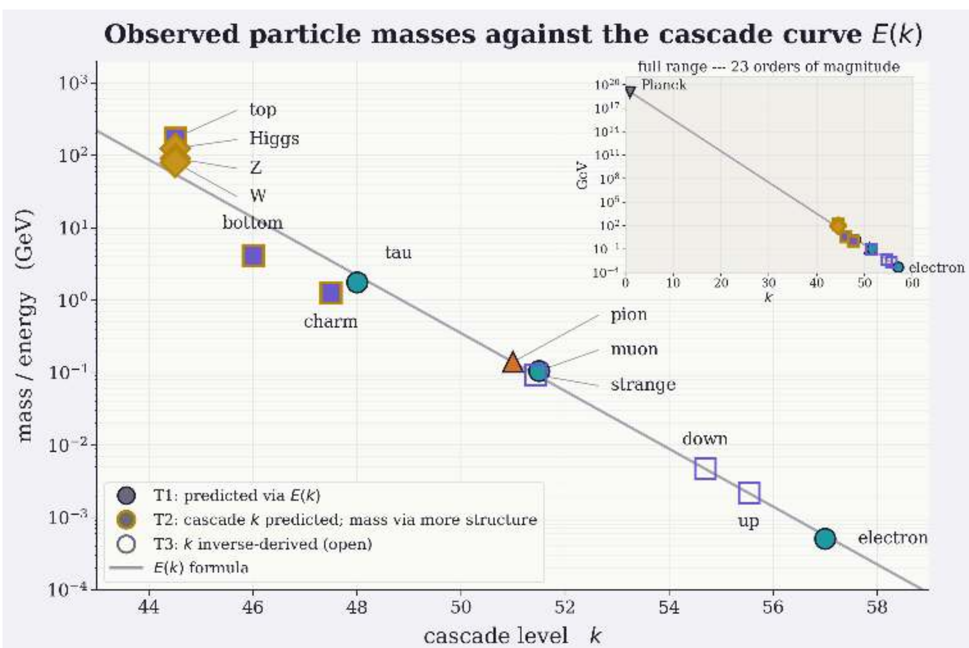

Figure 14.1: *Observed particle masses (Particle Data Group, 2024) against k-level, with $E(k) = m_\pi c^2 \cdot (2\pi)^{(51-k)/2}$ as a continuous curve. No masses are fitted; each placement follows from the formula and the energy anchor $m_\pi = 140$ MeV at $k = 51$.*

14.1 The Scaling Factor

The energy hierarchy is controlled by a single scaling factor: $g = 2\pi$. Each step increase in k reduces the available energy by one half-power of g, so that energies at adjacent levels differ by a factor of $\sqrt{2\pi} \approx 2.51$.

The value $g = 2\pi$ follows from the symplectic geometry of the arena. The actual world $\mathbb{RP}^3$ sits inside the arena $\mathbb{CP}^3$ as a monotone Lagrangian submanifold. The minimal holomorphic disk with boundary on $\mathbb{RP}^3$ has symplectic area $(N+1)\pi/2$ for the $\mathbb{CP}^N \to \mathbb{RP}^N$ embedding (Fukaya et al., 2009; Oh, 1997), which gives 2π for $N = 3$. The scaling factor equals the symplectic area of the fundamental actualization disk—the smallest region of possibility space that can be projected to a single actual event. Concretely, the fundamental projection step has a fixed area in the symplectic geometry that surrounds it, and that area is what sets the cascade step (Technical Reference Ch. 9 gives the rigorous statement).

14.2 The k-Parameter

The hierarchy is parameterized by a dimensionless integer or half-integer k. The energy at level k is

$$E(k) = m_\pi \cdot (2\pi)^{(51-k)/2},$$

where $m_\pi = 140$ MeV is the pion mass and $k = 51$ is the confinement scale. Each unit step in k corresponds to one half-power of 2π in energy.

14.2.1 The Source of Integer k

The integer character of k is structural. It is not a postulate of the cascade and not an artifact of how energies happen to space out. It is the spectral signature of round $\mathbb{RP}^3$, read along the logarithmic energy axis.

$\mathbb{RP}^3$ with the metric it inherits from $\mathbb{CP}^3$ is a Zoll manifold (Chapter 3, §3.5.1): every unit-speed geodesic on $\mathbb{RP}^3$ closes back on itself at the same total length. Manifolds with this property have an exceptionally constrained Laplacian spectrum. On a Zoll manifold of dimension n, the Laplacian eigenvalues cluster around integer-shifted values $(\ell + \alpha)^2$ with multiplicities scaling as ℓ^{n-1} — the integer ℓ counts spectral order, the cluster-around-integers property is the Zoll signature (Besse, 1978; Colin de Verdière, 1973). Generic Riemannian manifolds have spectra that do not organize this way; the integer-clustering is a global consequence of every geodesic closing.

This is the same mechanism that makes the angular-momentum quantum number an integer. The round two-sphere is Zoll; its Laplacian spectrum is the exactly integer-labeled $\ell(\ell+1)$, and that ℓ is the index carried by every atomic orbital and molecular rotational spectrum. The cascade index is the same spectral-order integer, read on $\mathbb{RP}^3$ rather than S^2 — a familiar spectral object, not an exotic posit.

The framework's cascade index k is the Zoll spectral order ℓ on $\mathbb{RP}^3$, projected onto a logarithmic energy axis through the symplectic scaling factor $g = 2\pi$. The chain is: $\mathbb{RP}^3$'s Zoll geometry $\Rightarrow$ integer-clustered Laplacian spectrum $\Rightarrow$ integer cascade index $k \Rightarrow$ discrete energy levels $E(k) = m_\pi(2\pi)^{(51-k)/2}$. The integer-ness of the cascade is inherited from the geometry of the actuality manifold. $\mathbb{RP}^3$ being round and Zoll is what gives the framework an integer ruler to begin with; without Zoll structure, no integer index would survive.

Half-integer offsets in the cascade — the lepton k-positions, the EWSB offset at $51 - 13/2$ — come from the additional $\mathbb{Z}_2$ fact-type quantization layered on top of the integer Zoll structure (Chapter 15). The Zoll spectrum supplies the integer skeleton; the Klein four-group V_4 on the fact types supplies the half-integer refinements.

Two consequences for the rest of the chapter. First, the five readings of k developed below (inverse energy, arena accessibility, proximity to actuality, event rate, fiber stiffness) are all readings of one Zoll-supplied integer coordinate. Second, the cascade's discreteness has the same mathematical origin as the Laplacian spectrum of $\mathbb{RP}^3$ — the cascade indexes are not a separate quantization assumption but the Zoll spectrum of actuality read on a logarithmic energy ruler.

14.2.2 Energy Scales: Anchor and Reference

Two scales appear in the $E(k)$ expression and they do different work. The *structural anchor* is the Kähler ground state $\varepsilon_0 \approx 1.706\, m_\pi c^2 \approx 231$ MeV — the energy below which H_α has no radial-bulk spectrum on $\mathbb{CP}^3$, identified with Λ_{QCD} (Chapter 18, §18.3). ε_0 is what the geometry sets: a topological feature of the Kähler Hamiltonian on $\mathbb{CP}^3$ that the cascade is anchored on in principle. The *energy-scale reference* is the pion mass $m_\pi = 140$ MeV — the well-measured laboratory quantity used to calibrate ε_0 against engineering units. m_π is not free: it is fixed by Fubini-Study geometry as $m_\pi = \varepsilon_0/1.706$. The cascade is written in terms of m_π because the pion is what experiment delivers most cleanly; the geometric content rides on ε_0. Every dimensionless ratio in the framework is derived from $\mathbb{CP}^3$ geometry; the single dimensionful number (ε_0, equivalently m_π) plays the role that c plays in relativity — a unit conversion between geometry and laboratory, not a free parameter.

$E(k)$ is a logarithmic energy coordinate. Any actualization event with energy E sits at $k = 51 - 2\log_{2\pi}(E/m_\pi)$ on the cascade. The cascade indexes scales: each k corresponds to a specific energy that an event at that scale would carry. The same energy appears at the projection as a Kähler Hamiltonian eigenvalue and contributes to the configuration's thermodynamic E. The unification of these readings is established in Chapter 5, §The Energy of an Event, and stated formally in the technical document (Chapter 7, §The Energy Identity). The discrete H_α spectrum and the geometric cascade are different objects: the spectrum is the discrete set of eigenvalues actually realized at events, the cascade is the coordinate that locates them on a logarithmic energy scale.

Particles populate the cascade at specific k-values via stable eigenstates of effective operators at those scales: the electron near $k \approx 57$, the muon near $k \approx 51.5$, the pion at $k = 51$, the tau near $k \approx 48$, the W and top near $k \approx 44$. Empty k-zones—the desert between EWSB and confinement, the gaps between consecutive lepton masses—host no stable structure; populated zones host particles or other persistent configurations (bound states, atoms, biological boundaries at the high-k end). The cascade is the ruler; its populated subset is what the universe actually contains. Which k-values get populated is set by the symmetry-breaking transitions and topological constraints that select the stable configurations at each scale (Chapter 15).

The k-parameter has five equivalent physical meanings, each reflecting a different aspect of the actualization process:

1. **Inverse energy.** Higher k corresponds to lower energy: the Planck scale sits at $k = 1$, room temperature near $k = 75$. Each unit increase in k reduces the energy per actualization event by $\sqrt{2\pi}$, reflecting the fact that lower-energy events sample a smaller portion of the arena's fiber structure.

2. **Arena accessibility.** At low k (high energy), almost the entire $\mathbb{CP}^3$ arena is dynamically accessible. At high k (low energy), the system is confined to a small neighborhood of $\mathbb{RP}^3$. The k-parameter measures how much of possibility space is available to the system.

3. **Proximity to pure actuality.** At $k = 1$, the system explores the full arena; actualization is maximally incomplete. As k increases, the system is pushed closer to the fixed-point set $\mathbb{RP}^3$, and the state becomes more nearly classical. The deep classical limit $k \gg 75$ corresponds to complete actualization.

4. **Event rate.** Lower-energy events occur more frequently (time-energy uncertainty), so higher k corresponds to faster actualization cycling.

5. **Fiber stiffness.** At low k, the Hopf fiber modes are hard and quantized. At high k, they are thermally soft and fluctuate freely. The k-parameter measures how rigidly the fiber structure controls the available excitations.

14.3 What the k-Scale Is

The five readings above are equivalent reformulations of the same quantity. This section pulls them into a single picture, names what the k-scale is, and says why the framework needs it.

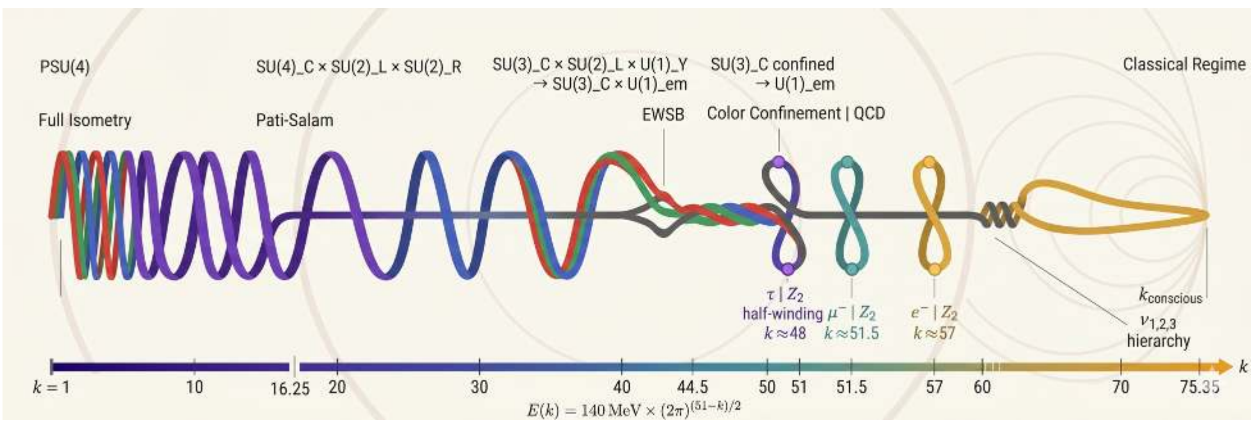

Figure 14.2: *The k-level spiral: the full energy hierarchy from Planck ($k = 1$) to the classical regime ($k \approx 75.35$), with each symmetry-breaking transition and particle species placed at its characteristic k-level. Each $\mathbb{CP}^1$ orbit along the spiral corresponds to a factor of 2π in energy, per $E(k) = 140\ \text{MeV} \times (2\pi)^{(51-k)/2}$. At left, the full arena isometry $\mathrm{PSU}(4)$ is unbroken and all 15 gauge directions are interchangeable. Moving rightward: Pati-Salam $\mathrm{SU}(4)_C \times \mathrm{SU}(2)_L \times \mathrm{SU}(2)_R$ emerges at $k \approx 16$; electroweak symmetry breaking reduces the gauge group to $\mathrm{SU}(3)_C \times \mathrm{U}(1)_{\text{em}}$ at $k \approx 44.5$; color confinement locks quarks into hadrons at the pion scale ($k = 51$, 140 MeV). Leptons appear at half-integer k-offsets set by $\mathbb{Z}_2$ quantization: τ ($k \approx 48$), μ ($k \approx 51.5$), e ($k \approx 57$). The neutrino mass hierarchy sits near the quantum-classical boundary ($k \approx 74$–78; placement on the spiral is schematic). The spiral terminates at $\mathbb{RP}^3$ in the deep classical regime, where $R(k) \ll 1$ and individual actualization events aggregate into continuous classical behavior.*

14.3.1 The k-Scale as Channel Capacity

The same parameter has a clean information-theoretic reading. Each actualization event at level k deposits a fixed amount of information on the actuality manifold. The amount is set by the resolvability ratio

$$R(k) = \frac{E(k)}{k_B T},$$

where $E(k)$ is the energy per event at that level and $k_B T$ is the thermal background. When $R \gg 1$, each event delivers many bits of distinction: the projection's output is a sharp register, and the distinctions it draws between fact types and quantum numbers survive intact. When $R \ll 1$, each event is buried in thermal noise: the projection still occurs, but its individual events leave no resolvable trace, and only their statistical aggregate—temperature, pressure, fluid flow—is detectable.

The k-scale measures the channel capacity of the actualization channel: lower k delivers more bits per event. It does not measure energy alone, or accessibility alone, or rate alone; it measures the amount of distinction the channel can carry at a given scale. The five readings above are five different views of this single channel-capacity quantity: lower k means more bits per event, which simultaneously means more arena accessibility, more event rate, and more fiber stiffness.

14.3.2 The k-Scale as a Flat Coordinate

The previous reading names what the k-scale is: a bits-per-event meter for the actualization channel. A second reading completes the picture by saying what the k-scale leaves untouched.

Moving along k does not disturb the geometry of the fiber. Particles at very different k-values—the top quark at $k = 44.5$, the pion at $k = 51$, a neural boundary at $k \approx 75.35$—all share the same fiber structure: the same spin structure on $\mathbb{RP}^3$, the same 720° closure, the same topological invariants of the τ-projection. What changes across k is the energy scale and the thermodynamic conditions at that scale (temperature, decoherence rate, integration timescale). The geometric content of the fiber stays the same.

The k-coordinate is therefore a logarithmic ruler along which positions can be placed; it carries no quantum-geometric content of its own. No Berry phase accumulates as you move along k. No spinor frame rotates. Different scales of physics—particle physics at low k, the critical scale at high k—occupy different positions on a single flat ruler through a single arena. This sharpens what the next subsection means when it says the k-scale "carries the entire story of how scales connect": k provides the positions; the same fiber provides the content at each position; Technical Reference Ch. 9 §Cascade as a Geometrically Flat Coordinate develops the formal version.

14.3.3 Fundamentality

Standard physics calls something fundamental when it sits at the lowest scale or names the most basic constituents — quarks beneath protons, fields beneath particles, Planck-scale physics beneath everything. In the present framework, fundamentality is relocated. The fundamental objects are the ones that do not change as the cascade is traversed: the spin structure on $\mathbb{RP}^3$, the round Zoll metric on $\mathbb{RP}^3$ that supplies the integer cascade index in the first place (§14.2.1), the τ-projection mechanism, the Hopf-fiber holonomy, the boundary capacity N_∞. Particle masses, mixing angles, decoherence rates, the critical-scale window—these are not fundamental in this sense. They are cascade-position-specific expressions of the fundamental machinery, read out at whatever k the system happens to occupy. This is closer to a Noether-style or relativistic notion of fundamentality: fundamental = invariant under change of perspective, with cascade-position as the perspective and the fiber as the invariant. The framework's predictions across the hierarchy—particle physics at low k, gravity at the boundary, the critical scale at high k—are not derivations of higher scales from lower ones. They are different readings of the same fundamental object at different positions on a flat axis through it.

The k-scale is the framework's own parameter, novel to $\mathbb{CP}^3 + \tau$ and not borrowed from elsewhere: k provides the positions; the same fiber provides the content. Without this parameter, the geometry would be static—$\mathbb{CP}^3$ with its τ-involution—and have no account of how the same arena produces particle physics, gravity, and the critical-scale dynamics from a single structure. The k-scale turns the geometry into working physics: each value of k specifies which constraints are operative, which fiber excitations are sustainable, and how much information each actualization event delivers. Every constant the framework derives is anchored to a specific k; every breaking transition is located at a specific k; every prediction—from the electron mass to the quantum-classical boundary—is read off the k-level at which the relevant geometric structure first becomes resolvable.

The remainder of this chapter walks the distinguished scales in order ($k = 1$ Planck, $k \approx 16.25$ Pati-Salam, $k \approx 44.5$ electroweak, $k = 51$ confinement, $k \approx 75.35$ critical scale) and identifies what the variational principle produces at each $R(k)$ regime.

14.4 Distinguished Scales

The hierarchy contains several scales where major structural transitions occur. Each corresponds to a topologically determined symmetry breaking or a qualitative change in the operative constraints.

14.4.1 Planck Scale ($k = 1$)

$E(1) \approx 1.26 \times 10^{19}$ GeV. At this scale, the full $\mathbb{CP}^3$ structure is dynamically accessible. The resolvability ratio $R(k) = E(k)/(k_B T)$ is enormous, so every fiber mode is hard-quantized and the distinction between the four fact types is maximally sharp. The variational principle here produces the Einstein field equations (Einstein, 1916): minimizing $\mathcal{F}$ with respect to the metric on $\mathbb{RP}^3$ yields the curvature dynamics of general relativity.

The Planck energy is not an input. It is derived: $E(1) = m_\pi \cdot (2\pi)^{25}$. The observed Planck energy (1.22×10^{19} GeV) (Tiesinga et al., 2021) agrees to 3%.

14.4.2 Pati-Salam Scale ($k \approx 16$)

$E(16) \approx 10^{13}$ GeV. The scale at which the Weinberg angle takes its topological value $\sin^2\theta_W = 3/8$ (Chapter 11), and where the full PSU(4) isometry of $\mathbb{CP}^3$ breaks to Pati–Salam $SU(4)_C \times SU(2)_L \times SU(2)_R$ (Pati and Salam, 1974). The breaking sequence from PSU(4) through Pati–Salam to the Standard Model is the subject of Chapter 15, §15.3.

14.4.3 Electroweak Scale ($k \approx 44.5$)

$E(44.5) \approx 55$ GeV. The $SU(2)_L \times U(1)_Y$ symmetry breaks to $U(1)_{\text{em}}$ through the Higgs mechanism (Higgs, 1964; Weinberg, 1967). Below this scale, the fiber orientation fluctuates freely among all directions—all orientations are equally probable, so the symmetry is unbroken. At $k \approx 44.5$, the Fubini-Study curvature creates an effective potential with a lower-energy valley at a specific orientation. The fiber locks into this valley, breaking the symmetry. This locked orientation is the Higgs condensate: the W and Z bosons acquire mass because the directions they correspond to are no longer flat symmetry directions but steep excitations around the new minimum, while the photon remains massless because its direction lies along the valley floor.

The electroweak scale is derived from topological data. The offset from the confinement scale is $51 - 44.5 = 13/2$, where $13 = \chi(\mathbb{CP}^3) \times \dim(\mathbb{RP}^3) + 1 = 4 \times 3 + 1$. The product $\chi \times \dim = 12$ counts the dimension of the Standard Model gauge algebra—the number of independent symmetry generators that electroweak breaking must accommodate. The $+1$ is the τ-fiber contribution, the single CP-violating phase that exists only because the actualization projection is orientation-reversing. The factor of $1/2$ in the offset reflects the half-integer spacing of the hierarchy: each independent parameter consumes one half-step of actualization distance between the confinement scale and the electroweak scale.

14.4.4 QCD Confinement ($k = 51$)

$E(51) = 140$ MeV. The strong coupling constant reaches order unity; standard QCD running (Gross and Wilczek, 1973; Politzer, 1973; Wilson, 1974) hits its nonperturbative regime. Color-charged states can no longer propagate freely; quarks are confined into hadrons. The $\mathbb{RP}^3$ geometry is fully actualized at this scale.

14.4.5 Quantum-Classical Boundary ($k \approx 75$)

$E(75) \approx 26$ meV, corresponding to thermal energy at mammalian body temperature ($k_B T$ at 310 K). At this scale, the resolvability ratio $R(k) \approx 1$: the energy per actualization event is comparable to the thermal background. Fiber modes are neither hard-quantized (as at high energies) nor fully thermalized (as at room temperature for macroscopic systems). This intermediate regime is where biology operates (Chapter 20).

14.4.6 Deep Classical Regime ($k \gg 75$)

Beyond the critical scale, the resolvability ratio $R(k) \ll 1$: thermal noise overwhelms the energy per actualization event. Individual fiber modes are completely washed out, and no quantum coherence survives between successive actualization cycles. The variational principle still operates, but the only accessible minimum of $\mathcal{F}$ is the Boltzmann equilibrium $F = E - TS$. All structure at these scales is thermodynamic: heat engines, weather systems, stellar convection, galactic dynamics. The actualization cycle continues, but each event produces so little information relative to the thermal background that the discrete character of actualization is undetectable. This is the regime where classical physics is exact for all practical purposes—the projection still occurs, but its individual events leave no resolvable trace.

14.5 What the Hierarchy Produces

The variational principle operates at every k-level, with the resolvability ratio $R(k) = E(k)/(k_B T)$ selecting which configurations it sustains: topological fixed points where $R \gg 1$, dissipative steady states where $R \approx 1$, Boltzmann equilibrium where $R \ll 1$. A single number ($g = 2\pi$) and a single mechanism (the actualization cycle under scale-dependent constraints) span the 31-order-of-magnitude range from Planck to the deep classical regime.

Chapter 15 reads the rungs: which fiber-field configurations are stable at each k-level, what residual gauge symmetries survive the breaking sequence, and how the Standard Model spectrum emerges from the geometric content the hierarchy makes available.

Chapter 15

Particles and Forces

Chapter 12 established the fiber field as the primitive object of Part IV. Chapter 14 set the energy ladder along which the field's excitations condense. This chapter populates the ladder. It identifies which configurations are stable at each scale, what gauge symmetries survive the actualization operator's action on the arena's isometry group, and what particle species exist as a consequence. T.4.4–4.7, 6, 11, 12

Forces and matter divide the chapter into two coupled stories. Forces arise from the residual symmetries of $\mathbb{CP}^3$ that survive the constraints τ imposes; the gauge group of the Standard Model is what the arena's full PSU(4) symmetry shrinks to under those constraints. Matter arises from the tangent and normal bundle decomposition of $\mathbb{RP}^3 \subset \mathbb{CP}^3$; leptons live in the tangent directions, quarks in the normal directions, and the spectrum of fiber-mode quantization fixes the masses. The two stories are geometric duals of one another: forces are what the arena's symmetry group can do, matter is what the arena's bundle structure can carry.

Underneath both stories is a finer geometric organization. Every particle in the framework is located along three independent directions of the arena. The cascade level k (Chapter 14) sets its mass scale. The Kähler-radial position from the actuality manifold sets which side of the bundle decomposition it sits in (tangent for leptons, normal for quarks). The fiber-mode index on the spin structure of $\mathbb{RP}^3$—a discrete label for spinor harmonics on the fiber, functionally analogous to a principal quantum number—sets its quantum numbers and rotational content. The matter-and-forces narrative below rests on this three-way decomposition: forces are the symmetry rotations operative at each cascade level, the lepton/quark distinction tracks Kähler-radial position, and gauge quantum numbers plus generation labels track fiber-mode content. All three directions are different expressions of the τ-projection's $\mathbb{CP}^3/\mathbb{RP}^3$ duality refracted through different operators on the arena (see §15.4 below for the unifying statement). See Chapter 14 §The k-Scale as a Flat Coordinate for why one geometric arena supports all three of these directions independently.

15.1 The Full Symmetry

Before τ acts, the arena $\mathbb{CP}^3$ carries a 15-dimensional isometry group with no internal distinctions—no separation between geometry and gauge fields, no chirality, no preferred real/imaginary split. The isometry group of $\mathbb{CP}^3$ under the Fubini-Study metric is PSU(4), a 15-dimensional Lie group (Nakahara, 2003). Every measurement outcome depends only on inner products—geometric invariants of the Fubini-Study metric—so every isometry is a gauge symmetry: a transformation that leaves all observables unchanged.

In the pre-actualization state, these 15 dimensions of symmetry are all on equal footing. There is no distinction between the transformations that will eventually become spatial rotations and those that will eventually become color rotations. There is no chirality, because the operator has not yet acted to distinguish left from right. The full PSU(4) symmetry means that all directions in the arena are interchangeable—the four fact types have not yet been differentiated.

15.2 Two Constraints

The symmetry breaks through two geometric constraints, each a consequence of actualization on $\mathbb{CP}^3$.

15.2.1 Actualization Picks a Point

Each τ-firing actualizes a specific point $p \in \mathbb{CP}^3$. Think of the 15-dimensional symmetry group as the set of all ways to rotate or transform the arena's coordinates without changing any observable. Once a specific point is actualized, only rotations that leave that point fixed are still symmetries—the rest would move the actualized point to a different location, contradicting the fact that *this* point was the one that became actual.

The subgroup that fixes a point is called the isotropy subgroup. The isotropy subgroup is the set of arena-rotations that fix the actualized point—concretely, the rotations "around" the point rather than "of" the point. For $\mathbb{CP}^3$, the isotropy subgroup at any point is U(3), which has dimension 9 (Nakahara, 2003). The remaining 6 dimensions of the original 15 correspond to transformations that move the point, and these are broken by the act of actualization itself. (The ratio $15 - 9 = 6$ equals the real dimension of $\mathbb{CP}^3$: every direction in which the point could have been moved is a broken symmetry direction.)

The isotropy breaking splits SU(4) into SU(3) × U(1). The SU(3) factor consists of transformations that rotate the three coordinate directions *around* the fixed point while leaving the point itself unchanged; this becomes the color group of the strong interaction. The U(1) factor is the overall phase rotation that commutes with everything; it carries baryon-minus-lepton number.

15.2.2 The Operator Distinguishes Real from Imaginary

The involution $\tau\colon [z_i] \mapsto [\bar{z}_i]$ is complex conjugation on homogeneous coordinates. It draws a line through every direction in the arena: some directions are real (unchanged by τ), and some are imaginary (flipped by τ). Only gauge transformations that commute with τ are consistent with actualization—a transformation that does not commute with τ would yield different results depending on whether it is applied before or after projection, which is physically incoherent. Any symmetry that survives must respect the real/imaginary distinction that τ imposes.

The τ-invariant subalgebra of SU(4) is $\mathrm{SO}(4) \cong [\mathrm{SU}(2)_L \times \mathrm{SU}(2)_R]/\mathbb{Z}_2$, a 6-dimensional group (Hall, 2015). SO(4) is the group of rotations that preserve real-valuedness—exactly the rotations that commute with complex conjugation. It decomposes into two three-dimensional rotation groups, one for left-handed rotations and one for right-handed.

15.2.3 The Combined Constraint

The two constraints act on different sectors of the symmetry. Isotropy keeps U(3) (dim 9): the rotations around the actualized point. τ-invariance keeps SO(4) (dim 6): the rotations that respect the real/imaginary split. The Standard Model gauge algebra emerges when both constraints are applied simultaneously to the Pati-Salam group (Section 15.3): isotropy splits the color sector $\mathrm{SU}(4)_C \to \mathrm{SU}(3)_C \times \mathrm{U}(1)_{B-L}$, τ reduces the right-handed sector $\mathrm{SU}(2)_R \to \mathrm{U}(1)_R$, and the left-handed sector $\mathrm{SU}(2)_L$ survives both constraints intact. The surviving generators assemble into the Standard Model gauge algebra (Glashow, 1961; Salam, 1968; Weinberg, 1967):

$$\mathfrak{su}(3)_C \oplus \mathfrak{su}(2)_L \oplus \mathfrak{u}(1)_Y,$$

with hypercharge $Y = (B-L)/2 + T_{3R}$, where $\mathrm{U}(1)_Y$ is the diagonal combination of $\mathrm{U}(1)_{B-L}$ (from isotropy) and $\mathrm{U}(1)_R$ (from τ-breaking).

The 12-dimensional gauge algebra of the Standard Model is the unique algebra compatible with actualization on $\mathbb{CP}^3$: the single algebraic consequence of two geometric facts—something becomes actual (isotropy), and actuality is real (τ-invariance). The carrier these constraints act on, the normal bundle to $\mathbb{RP}^3$, is topologically trivial (Chapter 3, §The Tangent and Normal Bundles), so the gauge algebra is fully determined by the isometry-and-constraint pair, with no further input from bundle topology. Color, weak isospin, and the surviving electroweak sector are carried along this trivial bundle; their generators come from how the isometry group acts on the fibers.

15.3 The Breaking Sequence

The breaking does not happen all at once. Each constraint becomes operative at the energy scale where the corresponding geometric structure first becomes resolvable—where the actualization dynamics has enough information channel capacity to encode the distinction the constraint enforces. The hierarchy formula $E(k) = m_\pi \cdot (2\pi)^{(51-k)/2}$ (Chapter 14) sets the energy at each k-level; the breaking occurs at the k where the relevant symmetry directions become thermodynamically distinguishable from each other.

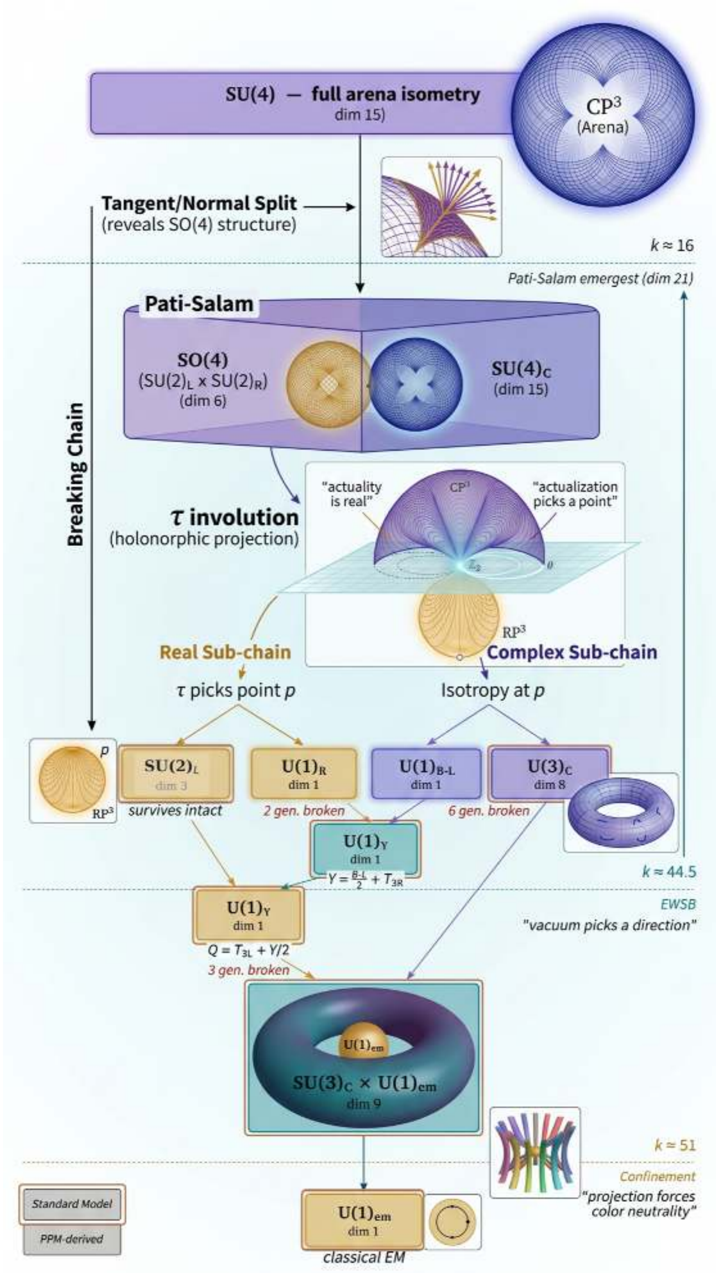

Figure 15.1: *The Standard Model gauge group as the residue of the actualization constraints. The cascade runs from* SU(4) *to electromagnetism with Pati-Salam, EWSB, and confinement marked. Box color shows each factor's origin:* $\mathbb{CP}^3$*/normal-bundle (violet),* $\mathbb{RP}^3$*/tangent-fiber (gold), or combined (cyan). Surviving SM factors (amber rings) trace to their geometric source: isotropy,* τ*-invariance, and confinement each strip structure away, and the SM gauge group is what the three leave behind.*

15.3.1 From Pati-Salam to $\mathrm{U}(1)_{\mathrm{em}}$

The reduction from the arena's full SU(4) symmetry down to electromagnetism unfolds in three connected stages: Pati-Salam emerges, Pati-Salam reduces to the Standard Model gauge group, and the Standard Model breaks to $\mathrm{U}(1)_{\mathrm{em}}$. The stages share a single mechanism—geometric constraints on $\mathbb{CP}^3$ becoming thermodynamically operative at successively lower energies—and are treated together to keep the cascade visible as one process.

Pati-Salam emerges ($k \approx 16.25$). At $k \approx 16.25$ ($E \approx 10^{13}$ GeV), the Weinberg angle reaches its topological value $\sin^2\theta_W = 3/8$ (Chapter 11). This is the energy at which the renormalization-group running of the gauge couplings converges to the ratio dictated by the arena's topology—the scale where the $\mathbb{CP}^3$ geometry first becomes the controlling structure for gauge interactions. Above this energy, the couplings are close enough to unified that the full SU(4) symmetry is effectively unbroken. Below it, the real/imaginary distinction imposed by τ becomes geometrically significant.

The full SU(4) symmetry of the arena separates into two sectors: color (the SU(3) that acts on the triplet coordinates) and lepton number (the U(1) that acts on the singlet coordinate). Combined with the left-right structure from the τ-invariant subalgebra, the intermediate group is the Pati-Salam group:

$$\mathrm{SU}(4)_C \times \mathrm{SU}(2)_L \times \mathrm{SU}(2)_R.$$

This group unifies quarks and leptons: quarks sit in the fundamental representation of $\mathrm{SU}(4)_C$ alongside the lepton as a fourth "color" (Pati and Salam, 1974). The Pati-Salam group follows from the $\mathbb{CP}^3$ isometry structure at this energy scale without requiring any Higgs multiplet to be postulated.

Pati-Salam reduces to the Standard Model. Below the Pati-Salam scale and above k_{EWSB}, two geometric constraints become operative as the resolution of the actualization dynamics increases. The framework treats this as a single topological reduction rather than a sharp event at a distinguished k: both constraints enforce themselves continuously across the ~ 28-decade window between $k \approx 16.25$ and $k \approx 44.5$.

The two constraints act on two different V_4 cells. On the spatial cell (B, see §15.6), the three normal-bundle directions become geometrically distinguishable from the singlet tangent direction; this splits $\mathrm{SU}(4)_C \to \mathrm{SU}(3)_C \times \mathrm{U}(1)_{B-L}$, separating color (the three normal directions) from lepton number (the tangent singleton). On the chiral cell (C), τ flips imaginary phases — it preserves left-handed configurations (τ-even by construction) but symmetrizes the right-handed sector down to a single τ-even direction, reducing $\mathrm{SU}(2)_R \to \mathrm{U}(1)_R$. $\mathrm{SU}(2)_L$ is fully preserved because the left-handed structure aligns with the τ-even sector; the left-right asymmetry of the weak interaction is τ's footprint on the chiral cell.

The combined breaking gives

$$\mathrm{SU}(4)_C \times \mathrm{SU}(2)_L \times \mathrm{SU}(2)_R \xrightarrow{\text{isotropy}+\tau} \mathrm{SU}(3)_C \times \mathrm{SU}(2)_L \times \mathrm{U}(1)_Y.$$

The hypercharge formula $Y = (B-L)/2 + T_{3R}$ emerges from the fiber geometry of the $\mathrm{SU}(2)_R$ doublets within the Pati-Salam structure. It is the unique assignment consistent with both the isotropy and τ-invariance constraints. Electric charge is the Gell-Mann–Nishijima combination $Q = T_{3L} + Y$ once $\mathrm{SU}(2)_L \times \mathrm{U}(1)_Y$ breaks to $\mathrm{U}(1)_{\mathrm{em}}$; per-particle assignments and charge quantization in units of $e/3$ are worked out in §15.13.

Read through V_4, the result clarifies the Standard Model gauge group's asymmetric look. The spatial cell (B) has split into a non-abelian $\mathrm{SU}(3)_C$ that mixes the three color directions plus a $\mathrm{U}(1)_{B-L}$ carrying the color-vs-lepton distinction. The chiral cell (C) has lost its right-handed half and kept $\mathrm{SU}(2)_L$. The hypercharge $\mathrm{U}(1)_Y$ formed by combining $\mathrm{U}(1)_{B-L}$ with the surviving $\mathrm{U}(1)_R$ is a cross-channel residue — it transports chiral content (T_{3R}) onto spatial content ($B-L$). Three factors, three different roles: $\mathrm{SU}(3)_C$ acts on cell B, $\mathrm{SU}(2)_L$ acts on cell C, and $\mathrm{U}(1)_Y$ is the leftover coupling between cells. The product-of-three-groups shape of the Standard Model is what V_4 looks like after this specific breaking pattern.

Electroweak breaking ($k \approx 44.5$). At $k \approx 44.5$ ($E \approx 55$ GeV), the $\mathrm{SU}(2)_L \times \mathrm{U}(1)_Y$ symmetry breaks further to $\mathrm{U}(1)_{\mathrm{em}}$. The scale is set by the topological offset $k_{\mathrm{EWSB}} = 51 - 13/2 = 44.5$, derived in Chapter 14. The Higgs field (Higgs, 1964), in this framework, is the fiber orientation locking into a geometric potential minimum defined by the Fubini-Study metric. The effective potential near the critical point takes the Landau-Ginzburg form (Ginzburg and Landau, 1950) $V_{\mathrm{eff}}(\phi) = -\mu^2|\phi|^2 + \lambda|\phi|^4$, where μ is the vacuum mass parameter set by the Fubini-Study curvature at this scale, and $\lambda = 1/(4\sqrt{\pi})$ is determined by the anti-holomorphic structure of the τ-projection on the normal bundle (the Higgs quartic inherits its value from the sign flip that τ imposes on the Kähler orientation).

The W and Z bosons acquire mass because the directions they correspond to have become steep in the new $\mathcal{F}$ landscape (Chapter 7)—they are no longer flat symmetry directions but massive excitations around the new minimum. The photon remains massless because $\mathrm{U}(1)_{\mathrm{em}}$ survives as an unbroken symmetry.

The photon is a propagating excitation that does not anchor at any base point, so it pays no variational cost for localization. The W and Z are propagating excitations that, in the new vacuum, must carry a localized configuration of the Higgs orientation field; that localization is the variational cost they pay, registered as mass.

15.3.2 QCD Confinement ($k \approx 51$)

At the QCD scale, the strong coupling constant grows to order unity. Color-charged states—quarks—can no longer propagate as free excitations. The $\mathcal{F}$ minimum requires color-neutral combinations, forcing quarks into hadrons.

The geometric mechanism is τ-projection acting on the normal bundle. Color charges live on the normal bundle perpendicular to $\mathbb{RP}^3$ (τ-odd content), and only τ-invariant combinations of normal-bundle excitations actualize. Individual colored states fail the τ-filter: their color phases do not survive the projection. Color-singlet combinations are the only τ-invariant configurations of normal-bundle modes, and so are the only states that propagate as stable hadrons.

The same mechanism produces a linearly-rising potential between separated color charges. Pulling two quarks apart stretches the normal-bundle connection between them over a τ-projection region whose extent grows with the separation. Each unit of separation exposes a unit of non-actualized normal-bundle content at fixed free-energy cost per unit, producing the flux-tube picture and the linear confining potential. At the scale where the residual gauge connection is no longer weak, τ-projection of normal-bundle modes is what confinement *is*.

15.3.3 Irreversibility of the Cascade

Each breaking stage is thermodynamically irreversible: the broken generators ($\dim G - \dim H$ directions that stop being symmetries) release their information content as entropy, raising the free energy cost of any trajectory that would attempt restoration to at least $k_B T \ln 2$ per bit. Below the breaking scale the thermal budget cannot pay that cost, so the cascade ratchets one way. The locking strength tracks the dimension ratio: confinement ($\mathrm{SU}(3)_C \to$ color-neutral, 9/1) is the most strongly locked, consistent with the exceptional stability of hadronic matter; electroweak (12/9) and Pati-Salam (21/12) follow in decreasing order. The arrow of symmetry breaking points in the same direction as the thermodynamic arrow of time (Chapter 8), driven by the same information-destroying projection. Figure 7.3 (Chapter 7) visualizes the cascade as a sequence of basin transitions across five thresholds.

15.3.4 Restoration Cost Across Accelerator Reach

The Landauer bound $k_B T \ln 2$ per bit (Landauer, 1961) gives the cascade's irreversibility a measurable price tag. At each breaking stage, the minimum free-energy cost to restore the broken symmetry is approximately $\Delta\mathcal{F} \approx (\dim G - \dim H) \cdot E_{\text{breaking}} \cdot \ln 2$, where the broken-generator count counts the directions that lost their symmetry status and E_{breaking} is the breaking-scale energy. An accelerator at center-of-mass energy E_{com} can locally re-open the symmetry iff $E_{\text{com}} \gtrsim \Delta\mathcal{F}$. This places the cascade's thermodynamic irreversibility on experimentally falsifiable footing scale-by-scale: each breaking has a numerical restoration cost, each accelerator has a numerical reach, and the comparison reads off which symmetries any given facility can locally undo.

Confinement sits at ~ 0.8 GeV per ratchet step (eight broken color generators at ~ 140 MeV thermal budget), within the reach of essentially every modern accelerator. Heavy-flavor and spectroscopy machines like DAΦNE, BES-III, and KEKB/Belle II at 1–11 GeV operate squarely in the confinement-restoration regime and never approach EWSB cost. Quark-gluon plasma production at RHIC (STAR Collaboration, 2005) and the LHC heavy-ion programme (Particle Data Group, 2024) restores the unbroken $\mathrm{SU}(3)_C$ phase in bulk. Electroweak symmetry breaking costs roughly ~ 100 GeV per ratchet step (three broken $\mathrm{SU}(2)_L \times \mathrm{U}(1)_Y$ generators); LEP at 209 GeV marginally pays this cost in its precision-EW runs, and the LHC at 13–14 TeV (ATLAS Collaboration, 2012; CMS Collaboration, 2012) pays it on every event that produces a Higgs — Higgs production *is* the local restoration of EWSB within the collision volume. Pati-Salam restoration requires $\sim 10^{14}$ GeV, beyond the reach of any conceivable collider by ten orders of magnitude; even the proposed FCC-hh (FCC Collaboration, 2019) at 100 TeV falls short by twelve orders. Planck-scale restoration sits a further five orders above that and is permanently inaccessible to accelerator physics.

Figure 15.2 plots the restoration cost against the cascade and the energies major accelerators reach. The threshold values themselves — ~ 1 GeV for confinement, ~ 100 GeV for EWSB, $\sim 10^{14}$ GeV for Pati-Salam — are established Standard Model scales: Λ_{QCD}, the electroweak scale, and the GUT scale by their conventional names. What the framework adds is the unified accounting: one Landauer-bounded formula $\Delta\mathcal{F}_{\text{bk}} = N_{\text{bk}} \cdot E(k_{\text{bk}}) \cdot \ln 2$ across all three breakings, with N_{bk} counted from the $\dim G - \dim H$ of each symmetry quotient and all three placed on one cascade k-axis. The thermodynamic floor on restoration is the new content; the energy hierarchy it reproduces is the prior empirical fact it must match.

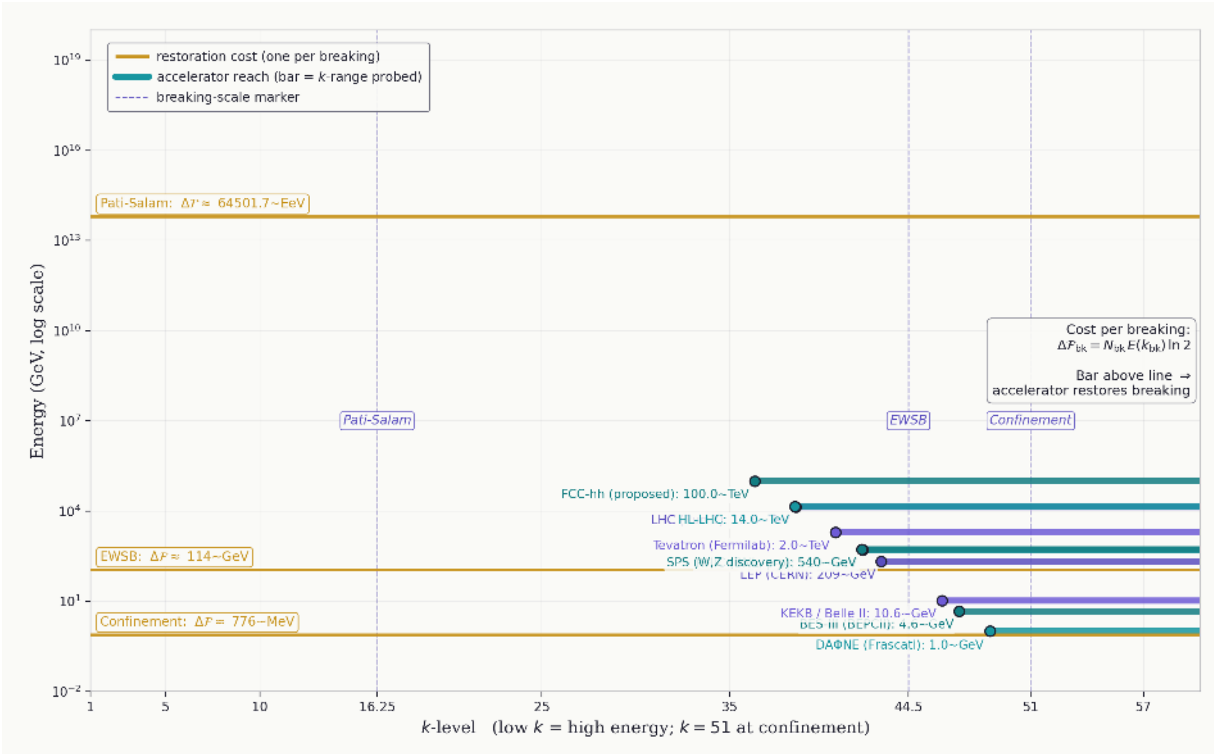

Figure 15.2: *Accelerator reach vs restoration cost per breaking. Each breaking has a fixed Landauer minimum $\Delta\mathcal{F}_{\rm bk} = N_{\rm bk} \cdot E(k_{\rm bk}) \cdot \ln 2$, set by the temperature at which it happened: Pati-Salam (~ 64 EeV), EWSB (~ 114 GeV), and confinement (~ 776 MeV), drawn as gold horizontal lines across the full k-range. Each accelerator is drawn as a thick horizontal bar at its center-of-mass energy, extending from its cascade-mapped k-reach $k_{\rm acc} = 51 - 2\log_{2\pi}(E_{\rm acc}/m_\pi)$ rightward to the chart's edge. A bar above a gold line $\Rightarrow$ the accelerator can locally re-open that breaking. Low-energy machines (DAΦNE, BES-III, KEKB/Belle II) clear confinement but visibly fail to reach EWSB cost — their physics is heavy-flavor and QCD spectroscopy. LEP and above clear EWSB and account for the electroweak precision and Higgs programs. Pati-Salam restoration sits ten-plus orders of magnitude above even proposed FCC reach; Planck-scale is permanently inaccessible. The threshold values themselves are well-known SM scales; the framework's contribution is the unified accounting — one Landauer formula across three breakings on one k-axis, with $N_{\rm bk}$ counted from the* $\dim G - \dim H$ *of each symmetry quotient.*

15.4 Three Generations from Topology

The Standard Model contains three generations of fermions: the electron and its neutrino, the muon and its neutrino, and the tau and its neutrino, along with corresponding triplication of the quark sector. Each generation has the same gauge quantum numbers as the others but different masses. The Standard Model treats the number three as an empirical input; nothing in its structure requires three rather than two or four.

In PPM, the number of generations follows from the topology of the arena and the structure of the operator. The argument has two parts.

Since τ satisfies $\tau^2 = \mathrm{id}$ (Chapter 4), it generates a $\mathbb{Z}_2$ symmetry—the same two-element group that appears in the plate trick (Chapter 3) and the Born rule (Chapter 13). Quotienting the arena by this $\mathbb{Z}_2$ gives the space $\mathbb{CP}^3/\mathbb{Z}_2$, which has Euler characteristic $\chi(\mathbb{CP}^3)/2 = 4/2 = 2$. The Euler characteristic of a space counts (with appropriate signs) the number of independent topological modes that a fermion field can occupy on that space. Two modes means two families of fermions that can exist in the bulk of the quotient space—two complete sets of particles, each with the same force couplings but different masses, distinguished by which topological mode they occupy. These are the second and third generations: the muon and tau families on the lepton side, charm/strange and top/bottom on the quark side.

The first generation arises from the boundary. The actual world $\mathbb{RP}^3$ (the fixed-point set of τ) sits inside the arena as a domain wall—a sharp boundary between the actualized region and the unactualized normal bundle. The τ-eigenvalue flips sign across this wall ($+1$ on $\mathbb{RP}^3$, -1 in the normal directions), so any τ-coupled fermion mass term changes sign across the boundary. The Jackiw-Rebbi mechanism (Jackiw and Rebbi, 1976) then guarantees exactly one fermion state localized at the wall. This wall mode is the electron family (Generation 1): a family of particles that exists because of the actualization boundary itself, trapped at the interface between possibility and actuality. Its mass is exponentially suppressed relative to the bulk generations by the tunneling amplitude across the wall, which fixes the muon-to-electron mass ratio (§15.7).

The total is

$$n_{\text{gen}} = n_{\text{bulk}} + n_{\text{wall}} = 2 + 1 = 3.$$

A fourth generation is impossible without changing the base topology. It would require either a second domain wall (impossible: τ has a unique fixed-point set $\mathbb{RP}^3$, so there is exactly one actualization boundary) or a third bulk mode (impossible: $\chi(\mathbb{CP}^3/\mathbb{Z}_2) = 2$ is a topological invariant, not a dynamical quantity that can shift). The three-generation structure is as rigid as the Euler characteristic from which it derives.

15.4.1 The Dirac Operator's $\mathbf{CP}^3/\mathbf{RP}^3$ Split

The $2+1$ generation count is the Dirac operator's expression of the τ-projection's $\mathbb{CP}^3/\mathbb{RP}^3$ duality. Every operator on the arena that respects τ-symmetry inherits a corresponding split in its eigenstructure; Chapter 13, §13.2 states this as the unifying principle. The Dirac operator's version is what this chapter uses: two $\mathbb{CP}^3$-bulk topological modes plus one $\mathbb{RP}^3$-localized Jackiw–Rebbi zero mode — three families.

A particle is therefore located by *two* independent classifications inherited from the same projection: which mode of the Dirac operator carries its wavefunction (its generation), and which sector of H_α supplies its actualization-event energies. The two align cleanly for heavy fermions ($\mathbb{CP}^3$-bulk wavefunction, $\mathbb{CP}^3$-radial-bulk events) and for Gen-1 ($\mathbb{RP}^3$-bound wavefunction, sub-floor events). They diverge for muon and strange: Gen-2 topological bulk modes whose event energies sit below the H_α radial floor, so their events occupy non-radial H_α or $\mathbb{RP}^3$ surface sectors. The mismatch is informative rather than contradictory — topological identity and event-energy support are different physical aspects of one particle.

The duality also organizes the rest of the chapter's structure. Forces are residual symmetries of $\mathbb{CP}^3$ after τ acts; matter is the bundle structure of $\mathbb{RP}^3 \subset \mathbb{CP}^3$; lepton versus quark is the tangent/normal split. Each is a different geometric structure reading out the same $\mathbb{CP}^3/\mathbb{RP}^3$ projection.

15.5 Fiber Mode Quantization

A spinor on $\mathbb{RP}^3$ requires a 720° rotation for closure (the double cover), which imposes $\mathbb{Z}_2$ boundary conditions on the fiber modes. The quantization is half-integer spaced:

$$k = 44.5 + \frac{n}{2}, \quad n \in \mathbb{Z},$$

where 44.5 is the electroweak scale and n is the fiber quantum number. Each allowed value of n corresponds to a particle species; the k-value determines the mass through the hierarchy formula $E(k) = m_\pi \cdot (2\pi)^{(51-k)/2}$.

For leptons the quantum numbers are topologically determined; the figure below shows each species as a fiber-mode harmonic, with the n values forced by the topology and the k-cascade running from electroweak-scale depth at the top to the lightest lepton at the bottom.

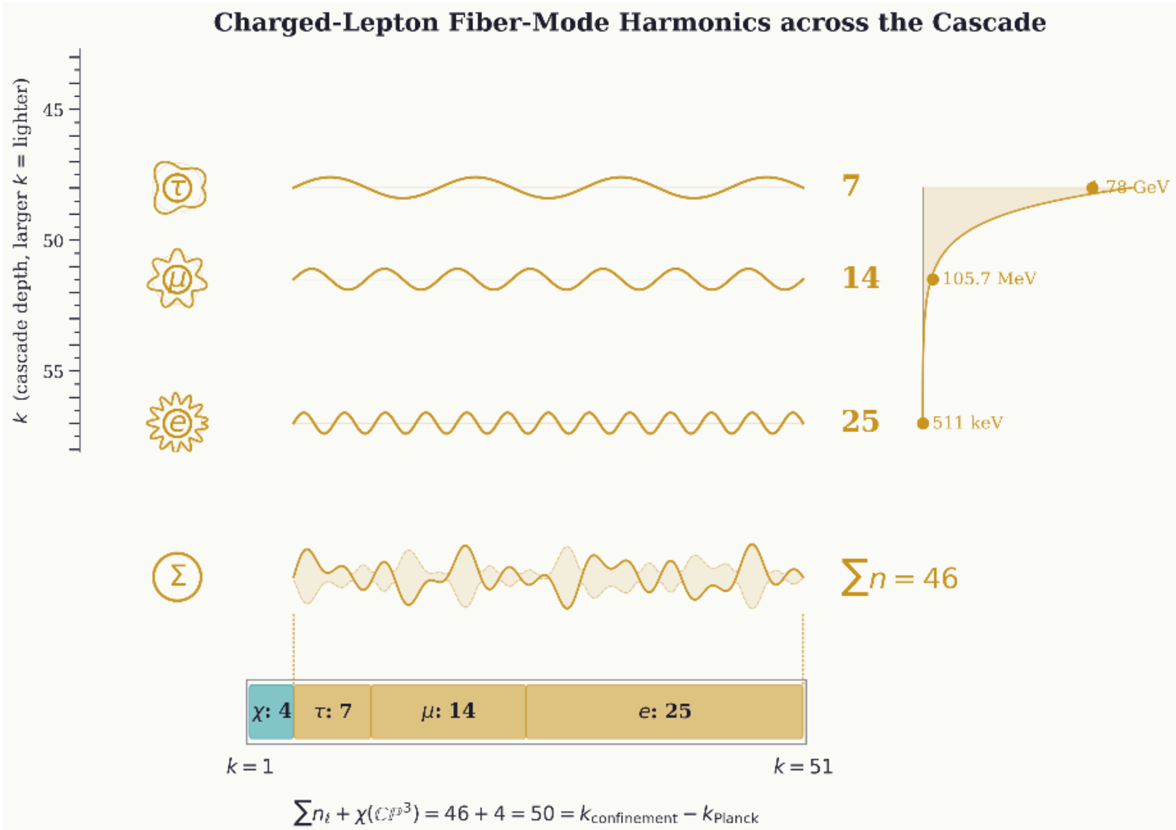

Figure 15.3: *The charged-lepton spectrum as standing fiber-mode harmonics. Each particle's mode is a sinusoid with n half-wavelengths on one fiber period $\varphi : 0 \to 2\pi$; the cascade depth then follows from $k = k_{\text{EWSB}} + n/2$. Lighter leptons (larger k) carry more oscillations on the same fiber, exactly as higher principal quantum number gives more nodes in an atomic spectrum. The three indices $n = 7, 14, 25$ are topologically forced (this section); quark fiber modes are omitted because the Kähler barrier and QCD dynamics modify the quantization, so the framework does not assign quarks a topological n in the same sense (§15.9). Lower panel: the composite wave $\sum_i \sin(n_i\,\varphi/2)$ is the Fourier visualization of all three lepton modes sharing one fiber. The orange channel bar below shows the topological-budget identity: $\sum n_\ell + \chi(\mathbb{CP}^3) = 46 + 4 = 50 = k_{\text{confinement}} - k_{\text{Planck}}$.*

The tau's quantum number $n = 7 = 2\dim(\mathbb{RP}^3) + 1$ counts the minimum number of fiber half-steps needed to encode the full kinematic content of a τ-event localized on $\mathbb{RP}^3$, plus one additional degree of freedom contributed by the electroweak condensate. The six geometric channels are the three position coordinates on $\mathbb{RP}^3$ (where on the actuality manifold the event sits) and the three SO(3)-frame coordinates (which way the event's fiber points, given $\mathbb{RP}^3 \cong \mathrm{SO}(3)$ as a Lie group). Together these are the configuration-space dimension of an oriented event on a three-manifold — position plus orientation, the same six degrees of freedom that locate a rigid body in three-dimensional space. The seventh channel is the scalar condensate phase the tau couples to via Yukawa; without electroweak breaking there would be no condensate to read, and the count would collapse back to six.

The tau is the lowest-lying lepton because it is the first excitation of the tangent bundle above the electroweak condensate. The same topological formula governs the Higgs VEV exponent ($v \propto (2\pi)^{7/2}$): the tau appears at the same topological depth above electroweak breaking as the Higgs VEV sits below confinement.

The muon's quantum number $n = 14 = 2 \times 7$ is the double-cover winding mode on $\mathbb{RP}^3$. The fundamental group $\pi_1(\mathbb{RP}^3) = \mathbb{Z}_2$ creates two homotopy classes of spinor paths: contractible loops and non-contractible loops. A spinor that winds once around a non-contractible loop picks up a sign change; it must wind twice to return to its original value. The muon is the fiber mode that executes this double winding—its quantum number is twice the tau's because it traverses the same topological structure twice. Physically, the muon samples the full double-cover geometry of $\mathbb{RP}^3$ (its Spin(4) structure) rather than just the first excited mode. The mass ratio $m_\mu/m_\tau \approx 1/17$ reflects the bulk-spacing correction $(2\pi)^{3/2}$ discussed in §15.7; the doubling $n_\mu = 2n_\tau$ is the topological signature of the second homotopy class, not a separate mass-ratio factor.

The electron's quantum number $n = 25$ places it at $k_e = 44.5 + 25/2 = 44.5 + 12.5 = 57$. This equals the confinement scale plus the real dimension of the arena: $k_e = 51 + \dim_{\mathbb{R}}(\mathbb{CP}^3) = 51 + 6 = 57$. The electron sits at the bottom of the tangent-bundle excitation spectrum—the point where the fiber mode's wavelength equals the full extent of the arena's real dimensions. Beyond $k = 57$, no further tangent-bundle excitations fit within the geometric structure; the electron marks the end of the lepton spectrum. Its extreme lightness (the smallest mass of any charged particle) is a direct consequence of its position at the boundary of the available fiber mode space: it is the longest-wavelength tangent excitation the geometry can support.

The three quantum numbers satisfy a topological budget: $n_\tau + n_\mu + n_e = 7 + 14 + 25 = 46 = (51 - 1) - \chi(\mathbb{CP}^3) = 50 - 4$. The total quantum number budget equals the full hierarchy range minus the Euler characteristic.

The hierarchy range $51 - 1 = 51 - 1 = 50$ represents the total number of half-steps available between the Planck scale and the confinement scale—the full information capacity of the energy ladder. The Euler characteristic $\chi(\mathbb{CP}^3) = 4$ represents the topological overhead consumed by the four fact types themselves: each fact type requires one unit of topological capacity to be defined as an independent information channel. What remains after this overhead is subtracted—46 half-steps—is the capacity available for particle content. The three lepton generations consume exactly this capacity, leaving nothing unaccounted for.

For quarks, the quantization is modified by the Kähler barrier at the normal-bundle boundary and by the QCD dynamics coupling quarks to the stripped geometry; for bosons, integer-n modes replace the half-integer ladder. The next three sections work through each sector.

15.6 Particle Identity in V_4 Channels

Every actualization event delivers four facts indexed by the Klein four-group $V_4 = \mathbb{Z}_2 \times \mathbb{Z}_2$ (Chapter 9); the four channels — spectral, spatial, chiral, intensity — are the entire information basis the framework supplies. Every Standard Model quantum number therefore sits in one of the four channels or a linear combination across them. At particle scale the four channels present through three coordinate axes — cascade depth k, Kähler-radial position $|z|$, and fiber-mode index n — that fix each species's location. Table 15.1 maps the Standard Model content into the V_4 channels; the detailed framework that defines the channels lives in Chapter 9.

Type	**Channel**	**Physics role**	**SM content carried**
A	Spectral	quantum-number labels	k (cascade depth, sets all masses)
B	Spatial	position, geometry, mass	(x, y, z), $\lvert z\rvert$, color, $B - L$, generation
C	Chiral	handedness, weak structure	n (fiber-mode), spin, T_{3L}, T_{3R}, parity
D	Intensity	energy, probability weight	$\lvert p\rvert$, rest energy, occupation, CKM/PMNS, couplings

Table 15.1: *Each Standard Model quantum number sits in one of the four V_4 fact-type channels (Chapter 9). Derived quantum numbers (electric charge, hypercharge, weak mixing angle) are linear combinations across channels.*

Derived quantum numbers. Electric charge $Q = T_{3L} + (B - L)/2 + T_{3R}$ is chiral + spatial + chiral. Quark charges are fractional because the spatial $B - L$ contribution is fractional (1/3 for quarks, 1 for leptons); chiral isospin offsets combine with this spatial offset to give the observed charge ladder. Hypercharge Y has the same chiral + spatial structure. The weak mixing angle $\sin^2 \theta_W = 3/8$ at E_{break} is a chiral-channel ratio set by the spatial Pati-Salam embedding. No derived quantum number carries information beyond what the four channels supply.

Gauge group factorization. The Standard Model gauge group mirrors the fact-type factorization. $SU(3)_C$ acts on the spatial channel (the three normal-bundle directions are the color triplet); $SU(2)_L$ and $SU(2)_R$ act on the chiral channel (the left/right doublet structure under the $\mathbb{Z}_2$ double cover); $U(1)_Y$ is the trace residue connecting chiral T_{3R} to spatial $(B-L)$ that survives Pati-Salam breaking (§15.3). The product-of-three-groups shape of the Standard Model gauge group is the V_4 structure showing through after symmetry breaking.

Continuity across scales. The four channels are invariant across cascade levels. At particle scale they organize the Standard Model; at the integration-window scale they organize phenomenal experience (Chapter 20). The Kähler-doublet pair $\{A, B\}$ (spectral and spatial) and the gauge-doublet pair $\{C, D\}$ (chiral and intensity) recur at every scale — the same arena/contents geometry that organizes gauge fields on a Kähler base manifold (Chapter 9).

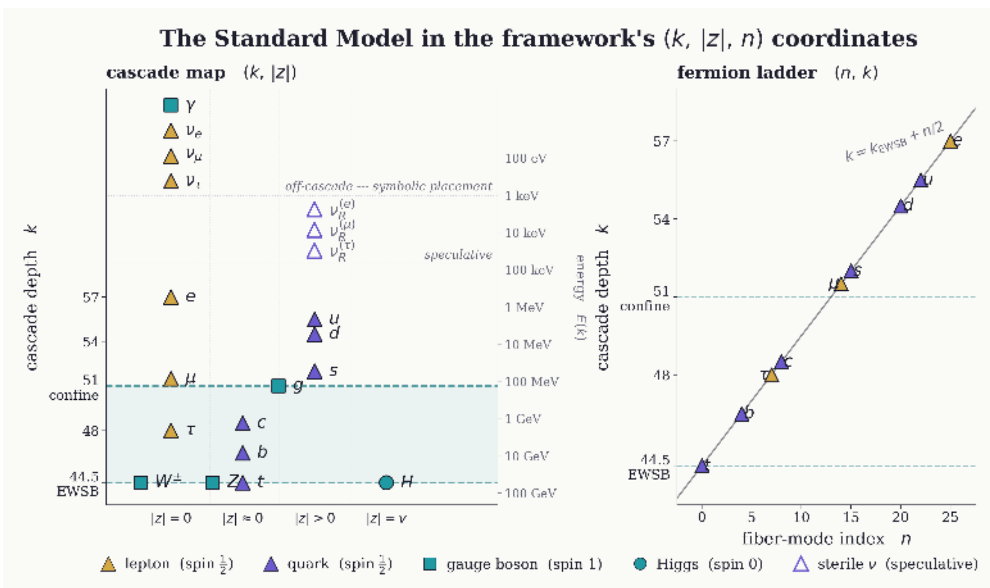

Figure 15.4: *Every Standard Model particle in the framework's $(k, |z|, n)$ coordinates — the particle-scale projection of the V_4 channels. Marker shape gives spin (triangle $\frac{1}{2}$, square 1, circle 0); colour gives sector.* Left: *cascade map. Depth k runs upward (companion axis as energy $E(k)$); $|z|$ columns sort particles by distance from $\mathbb{RP}^3$, from tangent-bundle ($|z| = 0$) through normal-bundle excitations to the Higgs condensate ($|z| = v$); EWSB and confinement are marked on the k-axis. Active neutrinos and the photon sit at schematic positions, their true scales fixed by the see-saw (§15.8) and the massless limit.* Right: *fermion ladder. The nine ladder-pinned fermions obey $k = 44.5 + n/2$ (§15.5) and fall on one diagonal in the (n, k) plane; bosons and neutrinos lie off the ladder because n counts no quantization step for them. The Standard Model spectrum is a position readout.*

15.7 Leptons: The Tangent Bundle

Leptons sit on the tangent-bundle side of the Kähler-radial split: $|z| \approx 0$, fully τ-even, $\mathbb{RP}^3$-actualized. Because the tangent bundle has no normal-bundle component by definition, leptons carry no color charge. Their fiber-mode indices are half-integer (spinor modes), with the three admitted values $n = 7, 14, 25$ derived in §15.5.

The three generations (electron, muon, tau) correspond to the three topologically determined zero modes identified in §15.4: two bulk modes from the Euler characteristic of $\mathbb{CP}^3/\mathbb{Z}_2$, plus one Jackiw–Rebbi wall mode (Jackiw and Rebbi, 1976) from the domain wall at the actualization boundary. Each generation sits at a specific level of the energy hierarchy: the tau at $k = 48$, the muon at $k = 51.5$, and the electron at $k = 57$.

The mass ratios between generations are set by the geometry of the embedding. The bulk spacing (tau-to-muon) carries a factor $(2\pi)^{3/2}$ from the codimension of $\mathbb{RP}^3$ in $\mathbb{CP}^3$. The wall suppression (muon-to-electron) carries an exponential factor $e^{\pi^2/2}$ from the tunneling amplitude across the domain wall, where $\pi^2 = 2\,\mathrm{Vol}(\mathbb{RP}^3)$ is twice the volume of the actual world.

15.8 Neutrinos

The neutrino sector divides into two parts: the active neutrinos $(\nu_e, \nu_\mu, \nu_\tau)$ that pair with the charged leptons in the electroweak doublets, and a speculative right-handed sterile sector whose existence the framework predicts but whose detailed phenomenology depends on calculations not yet carried out. The two parts are tied together by the see-saw mechanism (Minkowski, 1977; Mohapatra and Senjanović, 1981) that fixes the sub-eV active masses against a heavy sterile partner.

15.8.1 Active Neutrinos

The three active neutrinos share the charged leptons' tangent-bundle character ($|z| \approx 0$, τ-even, spin-$\frac{1}{2}$) and pair with e, μ, τ as the standard electroweak doublets. Their masses, however, do not follow the fermion ladder $k = 44.5 + n/2$: the observed sub-eV scale arises from see-saw mixing with the heavy right-handed sterile sector discussed below (§15.8.2), not from the topological mode hierarchy that fixes the charged leptons. On the cascade map (Figure 15.4), active neutrinos therefore sit far above the charged leptons in k (estimated $k \approx 72$–74, shown symbolically at the top of the plotted range), and they are absent from the fermion-ladder panel by construction.

15.8.2 Sterile Sector (Right-Handed Neutrinos)

The charged-lepton ladder closes at the electron ($n = 25$, $k = 57$): past $k = 57$, no further tangent-bundle excitations fit within the geometric structure (§15.5). Normal-bundle modes can continue further, however, and a class of such modes carries no Standard Model gauge charge—the $\mathrm{SU}(3)_C$ action on the normal bundle decouples for modes whose color content has been integrated out, and the $\mathrm{U}(1)_Y$ coupling vanishes for τ-odd content with zero hypercharge. These are the right-handed sterile neutrinos: normal-bundle excitations ($|z| > 0$, like quarks) but neutral under every SM gauge group, coupled to the rest of the spectrum only through gravity and a small mass mixing with the active neutrinos. At $k \approx 61$–62, $E(k) \approx 5.7$–14.3 keV brackets this class.

This section is speculative on the phenomenological side: the k-band follows from the hierarchy, but the specific mass within the band, the cosmological abundance, and the detection signatures depend on calculations not yet carried out within the framework. The strongest observational anchor (the 3.5 keV X-ray line) is currently disputed. This subsection is included as a flagged dark-sector reading rather than a confirmed prediction.

Within the bracket, the value $k \approx 61.8$ ($m_{\nu_R} \approx 7$ keV) is fixed empirically by the observed 3.5 keV X-ray line in galactic spectra: a radiative decay $\nu_R \to \nu_L + \gamma$ from this mass would emit a photon at $E_\gamma = m_{\nu_R}/2 = 3.5$ keV. In 2014, two independent groups (Boyarsky et al., 2014; Bulbul et al., 2014) reported an unexplained 3.5 keV X-ray line in galaxy clusters and in M31, initially interpreted as a possible dark-matter decay signature. That detection is now disputed; subsequent observations have not confirmed the signal (Collaboration, 2017; Dessert et al., 2020). The framework's mass-scale bracket is independent of the line's observational status: it places a sterile class in 5.7–14.3 keV, predicts a faint decay (lifetime $\sim 2 \times 10^4$ times the age of the universe), and points future X-ray observatories (Athena, AXIS) at the relevant energy range.

15.8.3 Speculative Dark-Matter Role

If the sterile sector is realized, a 7 keV right-handed neutrino sits in the warm dark-matter regime: fast enough in the early universe to suppress structure on scales below $\sim 300{,}000$ light-years, addressing the long-standing "missing-satellites" tension between cold-dark-matter simulations and observed Milky Way satellite counts (Klypin et al., 1999). The same mass range and absence of strong or electromagnetic interactions explain why underground direct-detection experiments (XENON, LUX) have not seen a signal (Aalbers et al., 2023; Aprile et al., 2018): those searches target heavier candidates with weak couplings. The primary signatures would be gravitational effects on small-scale structure, a faint X-ray decay line, and possible mass-mixing signals in active-neutrino oscillation experiments.

The cosmological abundance is the open piece. Multiple sterile states at adjacent k-levels would contribute to the total dark-matter density, and an order-of-magnitude estimate gives $\Omega_{\text{DM}} \approx 0.24$ against the observed $\Omega_{\text{DM}} \approx 0.27$ (Planck Collaboration, 2020). A first-principles abundance calculation—production mechanism, freeze-in or freeze-out dynamics, mass-mixing-angle dependence—has not yet been carried out within the framework, so this agreement is at the level of the right scale rather than a derived match. The mass brackets and decay phenomenology are robust hierarchy predictions; the abundance is a target for future work.

15.9 Quarks: The Normal Bundle

Quarks sit on the normal-bundle side: $|z| > 0$, τ-odd, carrying imaginary-direction content that has not been fully projected. Their fiber-mode indices are half-integer (spinor modes); a fourth axis, the color charge, comes from which of the three normal directions the excitation occupies.

The three normal directions correspond to the three color charges of QCD. Color is not an abstract quantum number assigned by convention; it counts directions in the stripped geometry. Red, green, and blue label the three independent normal directions at a point of $\mathbb{RP}^3$.

Confinement (§15.3) follows directly: only τ-invariant combinations of normal-bundle excitations survive projection, so only color-singlet states propagate. A meson (quark-antiquark) is a normal-bundle excitation paired with its τ-conjugate, summing to zero net normal displacement. A baryon (three quarks) is one excitation in each of the three normal directions, summing to zero by the determinant condition on SU(3). Both are mechanisms for returning to the tangent bundle—for completing actualization.

Heavy quarks (c, b, t) sit near $|z| \approx 0$ in the normal bundle. Their k-values are set by the geometry of the Higgs condensate at k_{EWSB} (for the top) and by the QCD binding dynamics that suppress the bare cascade energy at sub-confinement scales (for charm and bottom). Light quarks (u, d, s) sit at $|z|$ values ranging up to several Compton lengths and are sensitive to QCD dynamics at the confinement boundary; the light-quark $|z|$ values are currently fitted from observed masses, pending an outstanding first-principles calculation. The full quark spectrum is worked out in §15.11.

Unlike the charged leptons, quarks do not carry a topologically forced fiber-mode index. The lepton ladder comes from the clean $\mathbb{Z}_2$ quantization of spinor modes on $\mathbb{RP}^3$ (§15.5) fixed by the embedding topology. On the quark side, the Kähler barrier at finite $|z|$ and the strong coupling to QCD dynamics modify this quantization: only the half-integer character of the spinor $\mathbb{Z}_2$-grading is preserved, while the specific allowed n-values are no longer determined by the embedding alone. The classification table accordingly assigns each quark a k-value and a half-int n-character but no specific n integer: the framework's n is a prediction for leptons and a retrodiction-from-k for quarks.

15.10 Bosons

Bosons are a different geometric object from the fermions of the preceding sections: connections on the bundles rather than modes of them, mediating transport between fiber states rather than carrying fiber content themselves. They share the $(k, |z|, n)$ classification — same geometric arena — with integer fiber-mode index n in place of half-integer ($n = 0$ for scalars, $n = 1$ for vectors).

The Standard Model bosons sort cleanly by which V_4 doublet they act in and what τ-parity content they move (§15.6). All five live in the gauge doublet $\{C, D\}$. The gluons and photon act τ-evenly — preserving chirality while transmitting color or electric charge. The $W^{\pm}$ act τ-oddly, coupling only to left-handed fermions and flipping T_{3L} between doublet members. The Z carries both parities through its $V-A$ coupling. The Higgs is qualitatively different: it bridges the gauge doublet's two halves, coupling chirality (C) to intensity (D) through the Yukawa term, which is what mass generation is. The Kähler doublet $\{A, B\}$ carries no excitations: its structure is purely geometric, and gravity emerges from holographic screening at its $\mathbb{RP}^3$ boundary (Chapter 16) rather than from any propagating quantum. The per-species entries that follow fill in $(k, |z|, n)$ for each boson and locate it in this doublet/parity map.

Electroweak gauge bosons. The $W^{\pm}$ and Z sit at the EWSB scale ($k \approx 44.5$), tangent-bundle side ($|z| \approx 0$), with vector fiber-mode index ($n = 1$). Their masses come from the variational cost of carrying a localized Higgs orientation in the new vacuum (§15.3). The photon, $n = 1$ on the same tangent-bundle side, stays massless because $\mathrm{U}(1)_{\mathrm{em}}$ survives as an unbroken symmetry; it does not anchor at any base point, so it pays no localization cost.

Gluons. The eight gluons of $SU(3)_C$ sit on the normal bundle (color-charged, τ-odd), with vector fiber-mode index ($n = 1$). Confinement (§15.3) restricts them to color-singlet combinations within hadrons; they have no asymptotic free states.

Higgs. The Higgs sits at the EWSB scale, at the Kähler-radial position where the condensate locks (the vacuum direction $|z| = v$), with scalar fiber-mode index ($n = 0$). No spin, no color: the field whose orientation defines the new vacuum.

The boson sector closes the catalog. Every Standard Model species now has a $(k, |z|, n)$ assignment, visualised in Figure 15.4; the full per-species table with generation labels and notes lives in Technical Reference Ch. 11. The next section reads off the masses.

15.11 Mass Predictions

Section 15.6 fixed each species's $(k, |z|, n)$ triple from the topology. The hierarchy formula $E(k) = m_\pi \cdot (2\pi)^{(51-k)/2}$ then turns the k-value into a mass. With the triples read off the geometry, every mass becomes a prediction. The lepton ladder was derived in Section 15.5; this section closes out the spectrum with the heavy electroweak states, the light quark sector, and the mixing parameters, and ends with what the residuals mean.

15.11.1 Heavy Particles

The top quark and the Higgs boson both anchor at the electroweak scale $k = 44.5$, and the Fubini-Study geometry of $\mathbb{CP}^3$ at that scale fixes their mass-determining parameters without introducing new input. Three quantities follow from one set of geometric inputs: the top Yukawa, the Higgs vacuum expectation value, and the Higgs quartic self-coupling.

Top Quark

The Standard Model relates the top mass to the Higgs VEV through the Yukawa coupling: $m_t = y_t\, v/\sqrt{2}$ (Peskin and Schroeder, 1995). Of the six quarks, only the top has $y_t \approx 1$; the other Yukawas scatter across many orders of magnitude, and the Standard Model treats every one of them as an independent fitted parameter. In the framework, the top mass reads directly off the fiber geometry. The top sits on the tangent bundle at $|z| \approx 0$, so its coupling to the Higgs condensate is the projection of the Higgs orientation onto the tangent direction the top mode occupies. That projection is largest along the principal eigendirection of the fiber Laplacian on the $SU(2)_L$ tangent doublet—the direction of greatest Fubini-Study curvature in the tangent sector (Nakahara, 2003). Up to the normalization π carried by the Fubini-Study volume form on the projective line generated by the doublet, the corresponding eigenvalue gives

$$m_t = \pi \cdot E(44.5) \approx 172.7 \text{ GeV}.$$

In standard vocabulary this reads $y_t = \pi\sqrt{2}\, E(44.5)/v \approx 0.99$: the value the Standard Model leaves as an empirical input drops out of the fiber geometry as a determined quantity. The observed top mass is 172.76 ± 0.30 GeV (Particle Data Group, 2024), a 0.06% agreement.

Higgs Vacuum Expectation Value

The VEV $v = 246.2$ GeV measures the radius at which the Higgs orientation locks at EWSB—the distance from the symmetric origin to the bottom of the Landau-Ginzburg potential (Ginzburg and Landau, 1950; Higgs, 1964). In the framework, that radius is set by the Fubini-Study curvature length at the scale where the electroweak doublet decouples from the unified gauge sector. The Fubini-Study metric on $\mathbb{CP}^3$ has constant holomorphic sectional curvature (Nakahara, 2003), so fixing the energy scale $E(44.5)$ fixes the curvature radius as a determined geometric quantity. Dressing it with the topological volume factor for the $SU(2)_L$ doublet's seven half-steps in the tangent fiber (§15.5) gives

$$v \propto E(44.5) \cdot (2\pi)^{7/2} \approx 246.2 \text{ GeV}.$$

The standard low-energy relation $v = (\sqrt{2}\, G_F)^{-1/2}$ between the VEV and the Fermi constant (Peskin and Schroeder, 1995) is a consequence of this curvature-scale identification, recovered rather than supplied.

Higgs Boson Mass

The Higgs quartic λ sets the curvature at the bottom of the Landau-Ginzburg potential, and through it the physical Higgs mass via $m_H = v\sqrt{2\lambda}$ (Higgs, 1964; Peskin and Schroeder, 1995). In the Standard Model λ is fitted from the observed Higgs mass; in the framework, λ is fixed by how the involution τ acts on the Kähler form of $\mathbb{CP}^3$ along the normal-bundle direction that carries the condensate. Because τ is anti-holomorphic (Chapter 4), it sends the Kähler form $\omega \to -\omega$ on the normal-bundle directions (Griffiths and Harris, 1978)—a sign flip on the orientation that fixes the relative phase between holomorphic and anti-holomorphic contributions to the Higgs self-interaction. Pairing the two factors of the quartic against the Fubini-Study volume form on the projected normal-bundle line absorbs a $\sqrt{\pi}$ from the Gaussian normalization of the FS volume element and a 1/4 from the two-sided phase pairing on the τ-projected line, giving the universal value

$$\lambda = \frac{1}{4\sqrt{\pi}}.$$

Combining with the predicted VEV gives $m_H = v\sqrt{2\lambda} \approx 130.8$ GeV. The observed value is 125.25 GeV (Particle Data Group, 2024), a 4.4% discrepancy that is the largest residual among the framework's particle mass predictions. Closing the gap likely requires next-to-leading-order corrections from the instanton sector (Degrassi et al., 2012); the residual is identified as a computable correction rather than an adjustable knob.

15.11.2 Light Quarks and Mixing

The light quark masses (u, d, s) and the CKM mixing matrix sit on the normal bundle and are sensitive to QCD dynamics at the confinement boundary. The framework treats each light quark mass as the k-parameter assignment dressed by a Bohr-Sommerfeld quantization condition applied to the Kähler barrier — the same barrier whose tunneling amplitude determines α via the instanton route (Chapter 18). Individual light-quark masses agree at the 1–5% level once topological corrections are folded in; the residuals come from the same outstanding instanton-prefactor calculation that closes Route III for α.

The CKM mixing matrix (Cabibbo, 1963; Kobayashi and Maskawa, 1973) is the change-of-basis between two independent V_4 cells (§15.6): mass eigenstates diagonalize the spectral channel (each quark at a distinct k-coordinate), weak eigenstates diagonalize the chiral channel (each $\mathrm{SU}(2)_L$ doublet partner at a distinct T_{3L} assignment). The two channels' eigenbases need not align; the CKM matrix records the unitary that translates one reading into the other. Standard physics treats this misalignment as a phenomenological 3×3 matrix fit from experiment; the framework reads it as the structural consequence of two independent fact-type channels with non-aligned eigendecompositions of the same particle content.

What fills in the actual mixing values is the geometric overlap between fiber modes across the three generations. Each generation lives in a different topological mode — two bulk modes plus the Jackiw-Rebbi wall mode — so the mixing-angle magnitudes count how much the modes overlap when projected onto the actual world: larger Kähler-radial separation between two flavours means smaller overlap, hence smaller mixing (Fig. 15.5, panel a). The same geometric overlap shows up as the off-diagonal $|V_{ij}|$ entries in panel b and as the thin cross-channel edges in panel c.

The mixing pattern follows from geometry; no Yukawa matrix elements need to be independently adjusted to reproduce the magnitudes. The remaining ingredient — the CP-violating phase — has a separate geometric origin, developed in the next subsection.

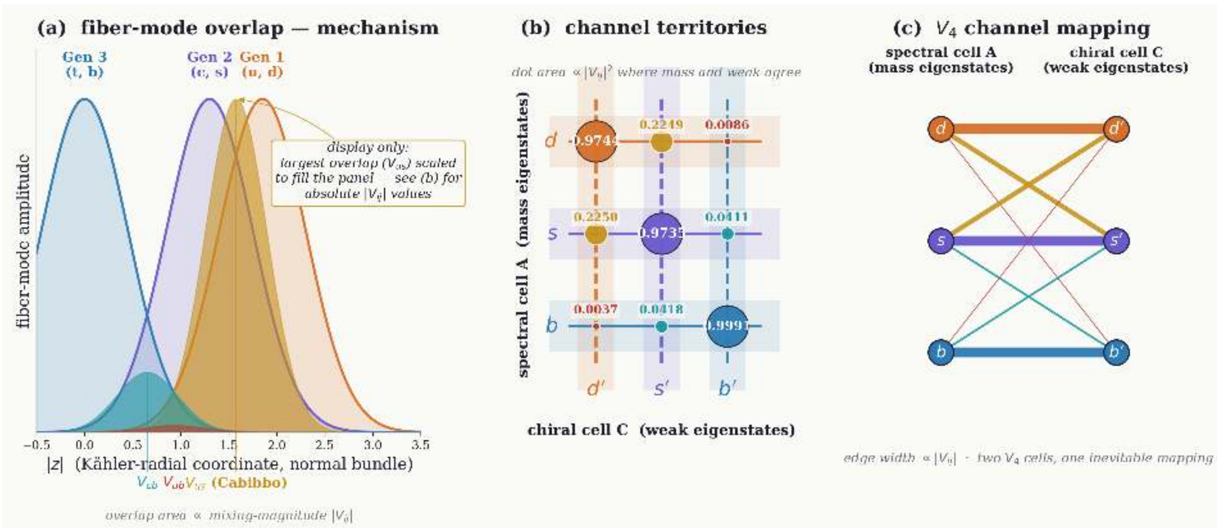

Figure 15.5: *CKM mixing as one geometric fact in three readings.* (a) *The mechanism: each quark generation is a fiber mode on the Kähler-radial coordinate $|z|$, and the overlap integral $\int \psi_i \psi_j \, dz$ between two modes — the shaded lens — is what the framework identifies with $|V_{ij}|$; wider separation in $|z|$ means smaller overlap, which reproduces the observed $|V_{us}| > |V_{cb}| > |V_{ub}|$ ordering.* (b) *The values: the spectral cell (mass eigenstates) and the chiral cell (weak eigenstates) as orthogonal axes, their nine intersections carrying the PDG 2024 magnitudes — a near-unity diagonal with small off-diagonal entries.* (c) *The same content as a bipartite graph, edge widths tiered by magnitude. The CKM matrix is the overlap between three topological modes; its off-diagonal entries measure how far two independent V_4 channels disagree about the same quarks, and the magnitudes follow from the mode geometry with no Yukawa element adjusted by hand.*

15.11.3 CP Violation

The CKM matrix has one more parameter than three real mixing angles need: a phase δ that distinguishes matter from antimatter. Without $\delta \neq 0$, baryon asymmetry could not develop through the standard channels (leptogenesis, electroweak baryogenesis), and the observable universe would not be matter-dominated. The Standard Model treats δ as a fourth empirical input alongside the three CKM angles. The framework reads it off the geometry.

The mixing magnitudes derived just above count fiber-mode overlaps — how much one generation's $\mathbb{CP}^3$ state spans another's at the actualization scale. The phase has a different geometric origin. It is a holonomy: parallel transport of the spinor frame around a closed loop in $\mathbb{CP}^3$ accumulates a definite angle on return, and that angle is the phase.

The relevant loop is the geodesic connecting the second and third generation fixed points on $\mathbb{CP}^3$. Each generation occupies a specific $\mathbb{CP}^3$ location (Chapter 14); the geodesic between two of them is a definite path on the manifold, and parallel transport along it accumulates a Berry phase (Berry, 1984) on the $\mathbb{RP}^3$ spin structure the actuality manifold carries. That accumulated phase *is* the CP-violating phase δ of the CKM matrix. Handedness distinguishes matter from antimatter, so the Berry phase the geodesic carries on the spin structure reads as CP violation directly. The framework needs no separately-added CP-violation mechanism: handedness is already one of the four fact types (Type C, the chiral fact, of Chapter 9) every actualization carries.

The golden ratio enters because the τ-action on the three-generation flag manifold is self-similar with contraction factor φ^{-1}. The geodesic loop closes at a full 2π rotation up to a φ^{-2} residual, leaving a surviving phase $\delta = \pi/\varphi^2 = \pi(1 - 1/\varphi)$. Numerically, $\delta \approx 1.200$ rad against the PDG2024 CKM phase 1.137 ± 0.022 rad (Particle Data Group, 2024) — a 5.5% ($\approx 2.9\sigma$) separation. Here φ is the icosahedral A_5 character; the value is specific to the quark sector and does not carry over to the tetrahedral A_4 lepton sector. The technical derivation is in Ch. 12.

Standard physics treats δ as the fourth phenomenological CKM input; the framework reads it off the spinor holonomy on $\mathbb{RP}^3$. Whether the resulting CP violation is sufficient on its own to generate the observed baryon-to-photon ratio through standard channels (electroweak baryogenesis, leptogenesis) is a separate, long-debated question in the baryogenesis literature that the framework's δ-derivation does not address.

15.12 The H_α Spectrum on the Cascade

Chapter 13 §13.2 establishes the radial-sector spectrum of H_α on $\mathbb{CP}^3$: $\varepsilon_n = (2n(n{+}3) + 1.70573)\, m_\pi c^2$, a discrete ladder starting at the confinement scale $\varepsilon_0 \approx 231$ MeV. Reading that ladder on the cascade gives the framework's per-event energies a second coordinate beside the smooth $E(k)$ curve.

The ladder is one sector of the geometric Hamiltonian on $\mathbb{CP}^3$, and the cascade as a whole reads out from several sectors of the same operator working together. Radial-bulk excitations sit on the ε_n levels: heavy fermions and the Higgs occupy these k-values because their events cost a quantum of radial Kähler flow on $\mathbb{CP}^3$. Gapless rotations of the Hopf fiber on $\mathbb{RP}^3$ carry the unbroken $\mathrm{U}(1)_{\mathrm{em}}$ direction and give the photon a zero-energy quantum — geometric mediation along a symmetry that the cascade leaves intact. Boundary-localized Jackiw–Rebbi modes at $\mathbb{RP}^3 = \mathrm{Fix}(\tau)$ supply Gen-1 fermion energies through tunneling costs against the actualization surface (§15.4). Higgs-condensate VEV times Yukawa couplings, and see-saw inversions against the heavy Majorana scale set the remaining fermion masses by anchoring derivative scales to the radial spectrum from above. The ladder catalogs the above-confinement side of the cascade in clean eigenvalue form; the sub-confinement resolvability zone of the same arena fills in through these other modes of the same operator.

Band placement. The first six low-n eigenvalues populate the intermediate-mass band from confinement to electroweak symmetry breaking. In cascade coordinates ($E(k) = m_\pi(2\pi)^{(51-k)/2}$, Chapter 14): ε_0 at $k \approx 50.3$, ε_1 at $k \approx 48.4$, ε_2 at $k \approx 47.0$, ε_3 at $k \approx 46.0$, ε_4 at $k \approx 45.2$, ε_5 at $k \approx 44.5$ — essentially at electroweak symmetry breaking. Specific landmarks: the Higgs (125 GeV) near $\varepsilon_{20} \approx 124$ GeV; the top quark (173 GeV) near $\varepsilon_{24} \approx 175$ GeV; charm (1.27 GeV) near $\varepsilon_1 \approx 1.31$ GeV. The coverage is forced by the energy-scale reference combined with the $4n(n+3)$ eigenvalues of the $\mathbb{CP}^3$ Laplacian.

Sub-confinement and above-confinement sides. The H_α radial floor ε_0 separates SM fermions into two sectors of event-energy support (Chapter 13 §13.2). *Above-confinement* ($E > \varepsilon_0$): heavy fermions and heavy bosons occupy $\mathbb{CP}^3$ radial-bulk eigenstates of H_α. Charm sits near ε_1, Higgs near ε_{20}, top near ε_{24}. Tau (1.78 GeV, between ε_1 and ε_2) and bottom (4.18 GeV, between ε_2 and ε_3) sit between radial eigenvalues and likely occupy angular sectors of the full spectrum that the radial reduction does not capture. *Sub-confinement* ($E < \varepsilon_0$): gen-1 fermions (electron 0.5 MeV at $k \approx 56.7$, up at $k \approx 55.5$, down at $k \approx 54.7$), the lighter gen-2 particles (strange 95 MeV at $k \approx 51.4$, muon 106 MeV at $k \approx 51.3$), and all neutrinos. The H_α radial-bulk floor does not reach them; their events occupy non-radial H_α sectors, $\mathbb{RP}^3$ surface modes, or the Gen-1 Jackiw–Rebbi zero mode (§15.4). The dividing line is the H_α radial floor: muon and strange (Gen-2) sit on the sub-confinement side; tau and bottom (Gen-3) sit on the above-confinement side.

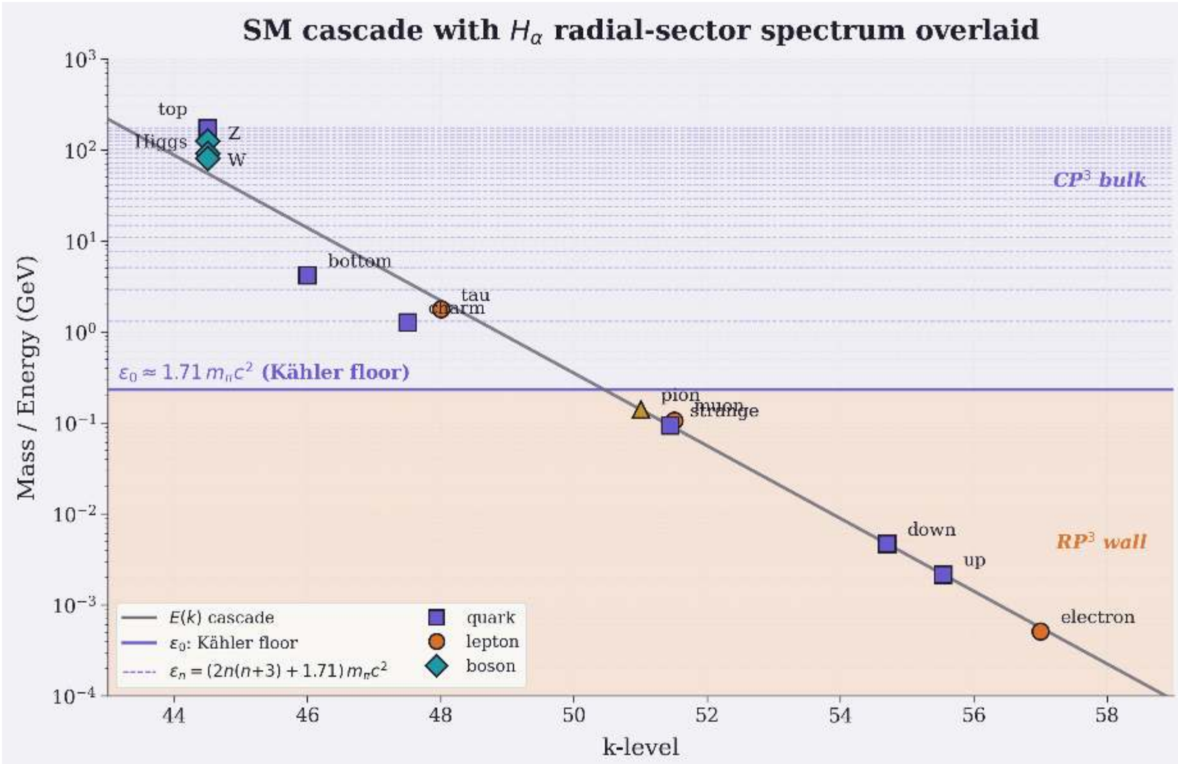

Figure 15.6: *Two spectra on one arena. The continuous cascade* $E(k) = m_\pi(2\pi)^{(51-k)/2}$ *carries every Standard Model mass (point markers); the discrete* H_α *radial eigenvalues* $\varepsilon_n = (2n(n{+}3) + 1.71)\, m_\pi c^2$ *run across it as horizontal levels. The heavy particles land on those levels — charm near* ε_1*, Higgs near* ε_{20}*, top near* ε_{24} *— so the heavy-mass spectrum is read off a discrete ladder rather than supplied particle by particle (tau and bottom fall between levels, on angular sectors the radial reduction does not yet capture). The Kähler floor* $\varepsilon_0 \approx 231$ *MeV (cyan) splits the fermions into two sectors of event support: above it (violet) heavy fermions occupy* $\mathbb{CP}^3$ *radial-bulk modes; below it (orange) the gen-1 fermions, lighter gen-2 particles, and neutrinos occupy non-radial sectors or* $\mathbb{RP}^3$ *surface modes. That split is set by the radial floor, distinct from the topological wall/bulk boundary that sorts the generations (§15.4).*

15.13 Electric Charge

At every point of $\mathbb{RP}^3$, the arena's geometry splits into one tangent direction along which the actualized boundary extends and three complex directions perpendicular to it. Leptons live in the tangent direction; quarks live in the three normal directions. After the breaking sequence (§15.3) has reduced the arena's symmetry to a single unbroken $\mathrm{U}(1)_{\mathrm{em}}$, electric charge is the eigenvalue of that surviving generator on each particle's location in the bundle.

This section walks the construction: the geometric labels the bundle's symmetries produce, the unique combination of them that leaves the photon massless, the per-particle charges as readouts, and three structural features of the resulting spectrum the construction forces. The full algebraic derivation lives in Technical Reference Ch. 5.

15.13.1 Three Labels from the Geometry

The arena's surviving symmetries provide three Cartan eigenvalues per particle, each tied to a specific structural feature of the bundle. Two of them come from the chiral decomposition $\mathrm{Spin}(4) \cong \mathrm{SU}(2)_L \times \mathrm{SU}(2)_R$ that produced the Pati-Salam structure, and the asymmetry between those two factors traces to a structural fact about τ. The decomposition is chiral under anti-holomorphic operations: one SU(2) factor commutes with such operations, the other gets complex-conjugated by them. Because τ is itself anti-holomorphic (Chapter 4), it acts asymmetrically on the two factors — leaving one intact (labelled $\mathrm{SU}(2)_L$) and reducing the other to a single Cartan via charge conjugation (the $\mathrm{SU}(2)_R \to \mathrm{U}(1)_R$ reduction worked through in §15.3). This asymmetry is the geometric origin of the chirality of the weak interaction: left-handed fermions couple to the unbroken $\mathrm{SU}(2)_L$ because that is the chiral factor τ leaves untouched.

Where the particle lives. The $\mathrm{SU}(4)_C$ that the breaking sequence reduces to $\mathrm{SU}(3)_C \times \mathrm{U}(1)_{B-L}$ has a diagonal Cartan acting on four basis directions—three quark colors and the lepton "color"—whose trace must close on the SU(4) fundamental. The only closure is $\mathrm{diag}(+\frac{1}{3}, +\frac{1}{3}, +\frac{1}{3}, -1)$, assigning $+1/3$ to each quark direction and -1 to the lepton direction. The three-versus-one split fixes the number; no other assignment closes the trace. Physics calls this label *baryon-minus-lepton number*, $B - L$ (Pati and Salam, 1974).

Which τ-component survives. Before τ acts, each right-handed particle is one component of an $\mathrm{SU}(2)_R$ doublet. The τ-projection sends complex phases $e^{i\varphi} \to e^{-i\varphi}$ and keeps only the τ-even component (the real part of the doublet's phase), leaving a Cartan label with eigenvalue $\pm 1/2$. Physics calls this the *right-handed weak isospin*, T_{3R}. It records which member of the original $\mathrm{SU}(2)_R$ doublet the τ-projection kept.

Which left-handed component. $\mathrm{SU}(2)_L$ acts on left-handed fermions in full doublet form, since τ does not touch it. Its Cartan reads $\pm 1/2$ on the two doublet components and 0 on right-handed states. Physics calls this the *left-handed weak isospin*, T_{3L}.

15.13.2 Charge as the EWSB Survivor

Electric charge is the eigenvalue of the generator that survives electroweak breaking—the unique linear combination of the three Cartans above whose direction stays unbroken when the Higgs orientation locks in and which therefore leaves the photon massless. That combination is

$$Q \;=\; T_{3L} \;+\; \tfrac{1}{2}(B-L) \;+\; T_{3R}.$$

The masslessness requirement forces this combination and no other; the coefficient $\frac{1}{2}$ on $B-L$ is fixed by how the surviving U(1) generator threads through the broken $\mathrm{SU}(2)_L \times \mathrm{U}(1)_Y$ structure to leave the photon eigenvalue at zero. Physics writes this in two steps for accounting convenience: define the intermediate *weak hypercharge* $Y = (B-L)/2 + T_{3R}$, then $Q = T_{3L} + Y$ (Gell-Mann, 1956; Nishijima, 1955). Both forms give the same result. The geometric reading: charge is what you get by adding the three Cartan labels in the only proportions that survive the Higgs lock-in.

15.13.3 The Charge Spectrum as Geometric Readout

Filling in the three Cartan eigenvalues for each first-generation fermion returns the entire charge spectrum:

particle	$B-L$	T_{3L}	T_{3R}	$Y = (B{-}L)/2 + T_{3R}$	$Q = T_{3L} + Y$
u_L	$+1/3$	$+1/2$	0	$+1/6$	$+2/3$
d_L	$+1/3$	$-1/2$	0	$+1/6$	$-1/3$
u_R	$+1/3$	0	$+1/2$	$+2/3$	$+2/3$
d_R	$+1/3$	0	$-1/2$	$-1/3$	$-1/3$
ν_L	-1	$+1/2$	0	$-1/2$	0
e_L	-1	$-1/2$	0	$-1/2$	-1
ν_R	-1	0	$+1/2$	0	0
e_R	-1	0	$-1/2$	-1	-1

(15.1)

Color is suppressed (each quark row stands for three color copies). The rightmost column reproduces the observed first-generation charges $Q_u = +2/3$, $Q_d = -1/3$, $Q_e = -1$, $Q_\nu = 0$ (Particle Data Group, 2024) as the unique output the construction permits. Second and third generations carry identical charge assignments because they sit in the same bundle representations, distinguished only by the fiber-mode quantum numbers of §15.5.

15.13.4 What the Geometric Reading Resolves

Three features of the charge spectrum that conventional treatments handle as empirical inputs, global consistency requirements, or postulates become structural consequences of the bundle picture. The Standard Model reproduces every entry in the table; what changes with the geometric reading is where the explanation terminates.

Charge quantization in units of $e/3$. Every observed charge has denominator 1 or 3, never a continuous value (Particle Data Group, 2024). The conventional argument for why this should hold requires the existence of a magnetic monopole somewhere in the universe (Dirac, 1931); absent monopoles, the abelian $\mathrm{U}(1)_{\mathrm{em}}$ does not force quantization on its own. In the geometric reading, the denominator 3 is the trace-normalization signature of SU(4) acting on three quark directions and one lepton direction; the quantization unit traces directly to the rank of the normal bundle. An arena built with a different normal-bundle rank would quantize charge in a different unit. The framework gives the empirical $e/3$ without invoking unobserved particles.

Proton and electron charges match exactly. The observed bound $|Q_p + Q_e|/e < 10^{-21}$ (Bressi et al., 2011) is one of the most precisely-tested equalities in physics. Conventional treatments recover the match after the fact, through anomaly cancellation applied to the full fermion assignment—a global consistency requirement satisfied in the aggregate. In the geometric reading, the match is the SU(4) trace closure visible directly in the table's $B-L$ column: a proton (uud) carries $Q = 2(+\frac{2}{3}) + (-\frac{1}{3}) = +1$, an electron carries $Q = -1$, and the sum vanishes because

$$3 \cdot (+\tfrac{1}{3}) + (-1) \;=\; 0,$$

the statement that three normal directions balance one tangent direction. What conventional treatments recover globally as a consistency condition, the geometric reading produces locally as a structural identity readable off a single column of the table.

Right-handed neutrinos carry zero electric charge. Conventional treatments assign $Q(\nu_R) = 0$ by inspection or as an empirical input. In the geometric reading, it is the unique cancellation the construction produces: $B - L = -1$ (lepton) and $T_{3R} = +\frac{1}{2}$ combine exactly to $Y = 0$, and with $T_{3L} = 0$ (right-handed) give $Q = 0$. The cancellation is exact, not approximate; right-handed quarks and the right-handed electron acquire nonzero charge because their $(B - L, T_{3R})$ pairs do not produce this cancellation. The electrical invisibility of ν_R is the same fact as τ acting anti-holomorphically on the right-chiral sector, here cashed out as exact zero charge rather than as a postulated assignment.

15.14 Absence of Superpartners

The $\mathbb{CP}^3$ sigma model possesses worldsheet $\mathcal{N} = (2, 2)$ supersymmetry — a standard consequence of the target being Kähler. Four supercharges pair the two chiralities of worldsheet fermions with each other and rotate the holomorphic and anti-holomorphic directions on the target. This is a property the arena's worldsheet inherits from its complex Kähler geometry; it lives on the propagation surface, not in the target itself.

The involution τ breaks half this supersymmetry. Because τ exchanges holomorphic with anti-holomorphic directions, the two supercharges that act with definite chirality on both sides survive; the two that mix chiralities oppositely on the two sides do not. What remains is $\mathcal{N} = (1, 1)$, the chiral worldsheet supersymmetry any orientable Riemann surface carries. The τ-invariant subset of the original four supercharges is half-rank.

Worldsheet supersymmetry does not imply spacetime supersymmetry. The former is a structural feature of how strings (or, in the framework's reading, τ-events) propagate on the Kähler target; the latter would require a target-space algebra pairing each fermionic field with a bosonic superpartner in target-space representations. The arena offers no such pairing: quarks, leptons, and gauge bosons sit in the same fiber structure they would occupy in a non-supersymmetric theory, and there is no geometric mechanism that generates squarks, selectrons, gluinos, or any other superpartner spectrum. The framework predicts the LHC's empirical record: searches have placed lower bounds on superpartner masses up to several TeV across many channels (Particle Data Group, 2024) without producing any candidates. The null result is a structural fact of $\mathbb{CP}^3 + \tau$, not a tuning of an unknown SUSY-breaking scale.

15.15 The Strong CP Solution

The QCD Lagrangian permits a term proportional to a parameter θ that would, if nonzero, cause the neutron to have a measurable electric dipole moment. Experiment constrains $\theta < 10^{-10}$ (Abel et al., 2020). The Standard Model provides no reason for θ to be small, let alone zero; any value between 0 and 2π is equally consistent with the gauge structure. This unexplained smallness is the strong CP problem, and it has motivated decades of work on hypothetical solutions (most notably the Peccei–Quinn axion mechanism (Peccei and Quinn, 1977)).

In PPM, $\theta = 0$ is a consequence of the operator's structure. The θ term measures the topological charge density of the gluon field—roughly, how much the gauge-field configuration winds around in its internal space. This winding is odd under time reversal: if you run the field configuration backward, the winding reverses sign. The operator τ, being an anti-holomorphic involution, acts as time reversal on the gauge sector. So the θ term changes sign under τ: it is τ-odd. The only value of a τ-odd quantity that is consistent with τ-invariance is zero.

The θ parameter vanishes for the same reason that all τ-odd content is stripped by actualization. The strong interaction lives in the τ-even sector (Types B and D); any τ-odd contribution to its Lagrangian is forbidden by the same involutory structure that defines the projection from possibility to actuality. No additional mechanism or particle (such as an axion) is required.

15.16 The Standard Model from Geometry

The Standard Model's organization is a readout of one geometric structure broken in one sequence. The arena $\mathbb{CP}^3$ carries an isometry group SU(4); τ picks out $\mathbb{RP}^3$ as the actualized sector and divides the tangent space into parallel and normal directions; the two constraints (isotropy, τ-equivariance) become operative at the k-levels where their geometric distinctions become resolvable. Three gauge groups of those particular ranks, three fermion generations, the asymmetric mass spectrum, the chirality of the weak interaction, the long range of electromagnetism, the short range of weak and strong forces: every structural feature commonly listed under "what the Standard Model is" is something the cascade produces.

15.16.1 Force Range as Cascade Residue

The reach of each force is set by what the cascade leaves operative in the geometry. Electromagnetism is long-range because $\mathrm{U}(1)_{\mathrm{em}}$ is the rotation of the Hopf fiber that $\mathbb{RP}^3$ carries uniformly at every point; the photon propagates this rotation because the world carries it everywhere at once. Gravity is long-range because it is the curvature of $\mathbb{RP}^3$ itself (Chapter 16) — no separate mediator on a fixed background. The weak force is short-range because $\mathrm{SU}(2)_L$ couples to the fiber's chiral content, and at $k \approx 44.5$ that content locks into the Higgs minimum; W and Z carry the localization cost as mass. The strong force is short-range because $\mathrm{SU}(3)_C$ acts on the normal bundle, and at $k = 51$ the normal bundle completes its projection; isolated color has no geometric direction left to occupy. Standard physics terminates the range story at mediator masses; the framework terminates at the cascade events that fix the geometry the masses are read from.

15.16.2 Matter as Bundle Configuration

In the framework, matter is the bundle's own configuration. There is no matter substance overlaid on the bundle; particles are bundle excitations: leptons are tangent-bundle modes, quarks are normal-bundle modes, gauge bosons are bundle connections, the Higgs is the fiber orientation locking into a geometric minimum. What standard physics calls "matter content"—matter as a separate ontological category occupying spacetime—is, in this picture, a particular reading of the bundle's own configuration at the scales where particle-language is appropriate. The matter/spacetime distinction dissolves the same way the field/geometry distinction dissolved in Chapter 12: there were never two things to relate. Matter, like fields, is what the geometry *is* at a particular resolution.

The next chapter takes up gravity, which the framework reads not as a fifth gauge force overlaid on the bundle but as what the $\mathbb{CP}^3 \to \mathbb{RP}^3$ projection does cumulatively at the boundary — the holographic shadow of every actualization event that has ever fired. Chapter 17 then reads the same mechanism at cosmic scale.

Chapter 16

Gravity

Gravity is the last of the four forces to emerge from the framework, and it emerges differently from the others. The strong, weak, and electromagnetic interactions are residual symmetries—what remains when τ breaks the full isometry group of $\mathbb{CP}^3$ (Chapter 15). Gravity is the cumulative effect of information loss: the aggregate consequence of every actualization event that has ever occurred. The cosmological consequences of the same mechanism — the cosmological constant, the Hubble parameter, the Hubble tension, the early universe — are taken up in Chapter 17. T.14, A.2, A.11

16.1 Why Gravity Is Geometric, Not Exchanged

The structural reason gravity emerges differently traces back to the V_4 taxonomy of fact-types (Chapter 9). The four fact-types organize into two doublets via the Kähler/gauge partition: the Kähler doublet $\{A, B\}$ (spectral and spatial, the τ-paired halves of the Kähler structure) and the gauge doublet $\{C, D\}$ (chiral and intensity, the τ-paired halves of the gauge structure). These two doublets play categorically different roles in the framework.

Every Standard Model boson lives in the gauge doublet (Chapter 15 §15.10). The gluons and the photon act τ-evenly; the $W^{\pm}$ act τ-oddly; the Z carries both parities through its $V-A$ coupling; the Higgs bridges the doublet's two halves by coupling chirality to intensity through the Yukawa term. All five are excitations of gauge-doublet content — propagating quanta whose modes can be exchanged between fermions. The Kähler doublet is qualitatively different. Its content is the geometric structure of the arena itself: $\mathbb{CP}^3$'s Fubini-Study metric, its symplectic form, and the τ-projection that selects $\mathbb{RP}^3$ as the actualized fixed-point set. This structure is the substrate on which gauge fields propagate; it does not admit propagating excitation modes of its own. Fermions and bosons both live on this Kähler arena — fermions as bundle sections carrying spatial extent at scale λ_C and energy at cascade level k, bosons as gauge connections built over the same base manifold. What is absent is a propagating mode of Kähler-doublet content itself: no spin-2 excitation of the metric, no quantized fluctuation of the symplectic form, no quantum of the τ-projection.

The consequence falls out of the structure: there is no graviton in this framework because there cannot be one. A graviton would be a quantized fluctuation of the metric—a dynamical mode of Kähler-doublet content. Fluctuation requires a field structure, and a field structure requires a substrate the field lives ON. Gauge fields live on the Kähler arena and can fluctuate within it; the Kähler structure is itself the deepest geometric layer the framework admits and has no deeper substrate to fluctuate in. Gravity's effect on actualized geometry therefore must come through the Kähler structure directly, and the Kähler structure makes itself felt through what the τ-projection does to information at $\mathbb{RP}^3$ rather than through propagating quanta. Holographic screening at the boundary is what that "making itself felt" looks like in detail — information stripped per event accumulates on $\mathbb{RP}^3$ with capacity N_∞, and curvature is the geometric response to that accumulated loss. The remainder of this chapter unpacks the mechanism; the present section establishes that this is the only mechanism the doublet structure permits. The same asymmetry explains why both G and Λ are set by N_∞ (Kähler-doublet capacity at the boundary) while the SM gauge couplings emerge from τ breaking the gauge-doublet symmetries (Chapter 15): gravitational constants count Kähler content, gauge couplings count gauge excitations.

16.2 Gravity as Accumulated Information Loss

Each actualization event strips τ-odd content from the arena. The stripped content does not vanish; it becomes entropy—irretrievable information that was part of possibility and is now part of the historical record (Chapter 8). Actualization events occur on a boundary whose topological capacity is $N_\infty = \varphi^{392} \approx 10^{82}$ independent fiber sections (§17.2 explains where this value comes from). Each event contributes a tiny increment of information loss, proportional to the volume of the kernel of τ: $\ln(2\pi)$ nats per event (the logarithm of the Hopf fiber circumference). The energy delivered per event is the cascade value $E(k)$ at the event's hierarchy level (Chapter 5, §The Energy of an Event); gravitational phenomena summed over an actualized region carry the cumulative event-energy of the events in that region.

Gravity is the geometric response to this loss. The information stripped per event, integrated against the boundary's topological capacity, generates a curvature of the actualized manifold $\mathbb{RP}^3$—the same curvature that Einstein's field equations describe. Newton's constant G is the proportionality factor between information loss and geometric curvature:

$$G = \frac{16\pi^4\,\hbar c\,\alpha}{m_\pi^2\,\sqrt{N_\infty}}.$$

Each factor names a piece of the geometric process. $\hbar c$ is the quantum-action unit carried into the boundary at each τ-event; α is the coupling weakness with which that unit registers as curvature; m_π^2 sets the per-event energy scale at the cascade's confinement anchor; $16\pi^4$ multiplies the contribution by the $\mathbb{CP}^3$ topology; $\sqrt{N_\infty}$ in the denominator dilutes the per-event signal across all boundary positions, giving the bulk-averaged coupling an external observer reads off as G.

The factor $16\pi^4 = (2\pi)^4 = g^4$, where $g = 2\pi$ is the per-step hierarchy scaling factor (each k-level multiplies energies by $\sqrt{2\pi}$, and g is the squared step), arises from the fourth power of that scaling factor and tracks the four-fold topological structure of $\mathbb{CP}^3$ (Euler characteristic $\chi(\mathbb{CP}^3) = 4$). The factor $\sqrt{N_\infty}$ in the denominator is the holographic averaging: gravity couples to the entire boundary, but the observable effect is diluted by the square root of its capacity (a consequence of the holographic bound on information encoding).

This formula explains the extreme weakness of gravity relative to the other forces. The electromagnetic, weak, and strong interactions are properties of individual actualization events—they describe what happens at each projection. Gravity describes the cumulative residue spread across the entire holographic boundary. The denominator $\sqrt{N_\infty} \approx 10^{41}$ suppresses the gravitational coupling by 41 orders of magnitude relative to the electromagnetic coupling, matching the observed hierarchy between α and $Gm_p^2/(\hbar c)$.

This makes G a Kähler-doublet quantity at the boundary: it measures the Kähler-structure content of $\mathbb{CP}^3$ as it registers per tile of $\mathbb{RP}^3$, mediated by N_∞. The cosmological constant Λ (§17.2 below) is the second Kähler-doublet quantity set by the same capacity—where G scales with $\sqrt{N_\infty}$ (the per-tile share), Λ scales with N_∞ itself (the total). Both are static, both descend from the same topological invariant, and both stand apart from the Standard Model gauge couplings, which emerge from τ-breaking of gauge-doublet symmetries rather than from Kähler-doublet content (§16.1).

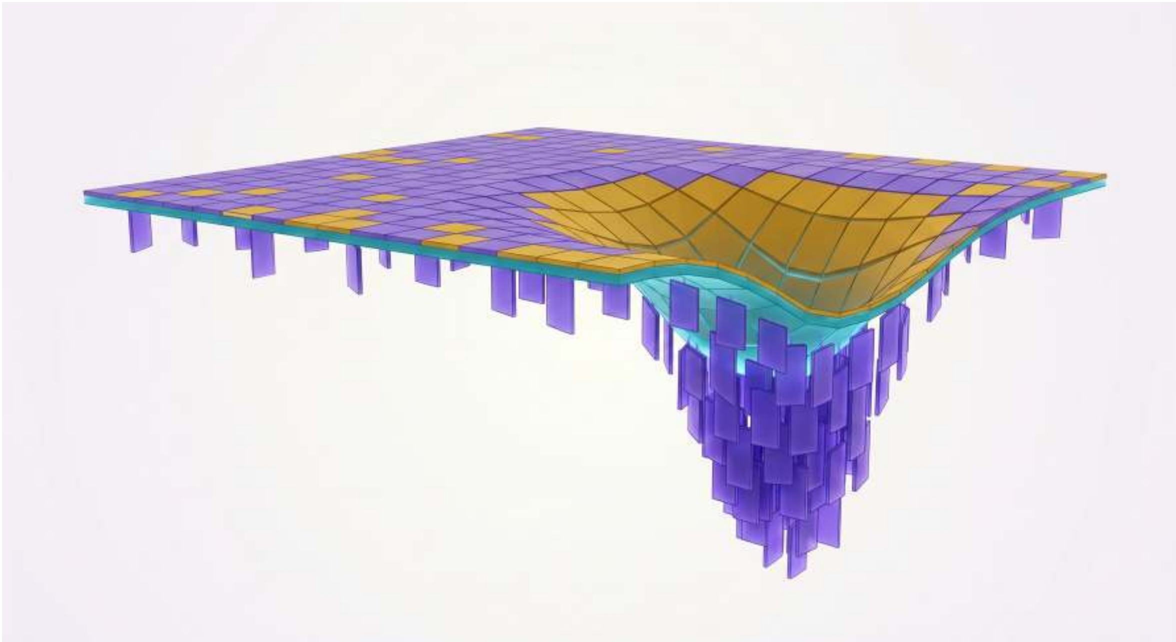

Figure 16.1: *Gravity as the weight of stripped possibility. The tiled crust is the actualized manifold, the visible metric. Each τ-projection actualizes one tile and, in the same act, strips the τ-odd normal-bundle content that then hangs beneath it — so a crust tile is gold where actualization has occurred and violet where the location is still unactualized possibility. The thin cyan layer is the projection interface; the faint enclosing outline is the $\mathbb{CP}^3$ possibility arena. The stripped normal-bundle content is the gravitational degree of freedom: where it gathers into a dense hanging keel its weight drags the crust into a curvature well, and where it hangs sparse the crust stays flat. Mass gravitates by the burden of possibility stripped in actualizing it.*

16.3 Einstein's Equations as Thermodynamic Limit

Standard general relativity treats Einstein's field equations as a postulate and attaches four additional axioms: energy-momentum conservation, geodesic motion for free particles, the equivalence principle, and diffeomorphism invariance. Each is taken as independently given. The framework derives the field equations and all four axioms from a single fact: many τ-events accumulate on a 4D background, and the averaged dynamics has only one form available.

The mechanism is the same kind of coarse-graining that produces the ideal gas law from molecular collisions, in a geometric setting. Each τ-event contributes a small piece of dynamics; many events accumulate into a smoothed effective action Γ_{eff} on spacetime. Expanding this effective action by a standard technique of spectral geometry — the Seeley-

DeWitt heat-kernel expansion (DeWitt, 1965; Seeley, 1967) — decomposes it into geometric terms organized by power of curvature. The leading terms identify with familiar quantities: a volume integral $\int\sqrt{g}$ (the cosmological-constant piece), the Einstein-Hilbert action $\int\sqrt{g}\,R$ (the field-equation term), and curvature-squared corrections (negligible at observable scales). The variational condition $\delta\Gamma_{\text{eff}}/\delta g^{\mu\nu} = 0$ that picks out the dominant configuration delivers

$$G_{\mu\nu} + \Lambda\, g_{\mu\nu} = \frac{8\pi G}{c^4}\, T_{\mu\nu}$$

directly.

Why the form is forced. The Einstein-Hilbert term is fixed by spectral geometry. The leading curvature coefficient of any smooth effective action on a 4D background must be proportional to $\int\sqrt{g}\,R$ (Gilkey, 1975). Any dynamics producing a well-defined effective action on 4D spacetime generates Einstein gravity at leading order. There is no fitting freedom in the form of the action; only its overall coefficient (which sets G) is theory-dependent. The standard puzzle of "why this gravitational action and not some other" dissolves at the structural level: spectral geometry leaves no alternative.

Corollaries that fall out for free. What standard GR treats as independent postulates become consequences of the same derivation. *Energy-momentum conservation* follows from a mathematical identity on the curvature side: the contracted Bianchi identity $\nabla_\mu G^{\mu\nu} = 0$ forces $\nabla_\mu T^{\mu\nu} = 0$ on the matter side. *Geodesic motion* follows directly: free particles satisfy $\nabla_\mu T^{\mu\nu} = 0$ by moving along geodesics of $g_{\mu\nu}$. *The equivalence principle* (gravitational and inertial mass coincide) follows because both quantities measure the same actualization coupling: the mass in the Penrose-Diósi gravitational decoherence rate is the same mass in $T_{\mu\nu}$. *Diffeomorphism invariance* is automatic, since the heat-kernel expansion respects all symmetries of the underlying Laplacian. The framework collapses GR's separate axioms into one structural fact about $\mathbb{CP}^3 + \tau$.

The thermodynamic limit is overwhelmingly satisfied. The argument requires many τ-events accumulating. Is that condition met? At the present epoch, the cumulative actualization record is $M(t_0) \approx 1.8 \times 10^{121}$ events — sourced by $\sim 2 \times 10^{80}$ baryons and electrons in the observable universe (Eddington, 1936) each driving roughly one τ-event per pion Compton time τ_C. The count sits at $\sim 9\%$ of the Bremermann ceiling ($\sim 2 \times 10^{122}$ events for the universe's mass-energy at the per-event timescale, technical reference 7). The averaging condition is met by ample margin. No individual molecule obeys $PV = nRT$, no individual τ-event obeys Einstein's equation; both laws emerge when enough constituents are summed. $M(t)$ is distinct from the static boundary capacity $N_\infty \approx 10^{82}$: $M(t)$ counts realized events, N_∞ counts the topological number of independent boundary positions the actualization can occupy. Each boundary position has been re-actualized $\sim 10^{39}$ times on average.

The 16π coefficient. The normalization factor in the Einstein-Hilbert action acquires a geometric interpretation: $16\pi = |V_4| \times \mathrm{Vol}(S^2) = 4 \times 4\pi$, where $|V_4| = 4$ is the order of the Klein four-group (the fact-type symmetry) and $\mathrm{Vol}(S^2) = 4\pi$ is the solid angle of the unit two-sphere in $\mathbb{RP}^3$ (the Gauss's-law factor for gravitational flux spreading through three spatial dimensions). The prefactor that Einstein's equations carry as a numerical normalization is two structural facts about the actualization arena written together: the discrete symmetry classifying actualization events, and the geometry through which their gravitational signature spreads. The numerical value is forced by the $\mathbb{CP}^3 + \tau$ geometry.

The speed of light c. The c that appears throughout Einstein's equations is the same c that sets the photon's propagation speed. In the framework's reading c is the rate at which null geodesics on $\mathbb{RP}^3$ propagate, and the null-geodesic structure of actuality is itself a consequence of $\mathbb{CP}^3 + \tau$ geometry rather than a separate posit.

A null geodesic on $\mathbb{RP}^3$ is the real boundary curve of a holomorphic disk in $\mathbb{CP}^3$ — a disk whose boundary lies on the totally-real submanifold $\mathbb{RP}^3 = \mathrm{Fix}(\tau)$. The moduli space of such disks carries a conformal structure that descends to give the conformal structure of $\mathbb{RP}^3$, recovering the light-cone geometry of actuality from analytic data on the possibility space (LeBrun and Mason, 2007, 2009). The light cone at a point of $\mathbb{RP}^3$ is the set of disk-boundary curves passing through that point; the photon's worldline is one such curve. "Unanchored phase running across $\mathbb{RP}^3$" is the informal gloss; the structural content is that the photon's worldline carries no content beyond disk-holomorphic data — no chirality, no normal-bundle direction, no mass anchoring it to a base point. $\mathbb{CP}^3$ as possibility space carries no "speed" on its own; the speed emerges once τ selects $\mathbb{RP}^3$ and the disk moduli induce a conformal structure on it.

A particle takes c exactly when its worldline is a pure disk boundary. Anything with structure that anchors content to a base point — chirality, a normal-bundle direction, a mass term the cascade has locked in at its k-level — fails to be a pure disk boundary; its worldline deviates from the null geodesic and propagates strictly below c. Mass is what makes a worldline depart from disk-boundary geometry. Gravitational disturbances propagate at c for the structural reason that gravitational waves are perturbations of the conformal structure on $\mathbb{RP}^3$, which are perturbations of the disk moduli, which propagate along null geodesics by construction. The empirical coincidence between the photon speed and the gravitational-wave speed — tightened to $|\Delta v/c| \lesssim 10^{-15}$ by GW170817 (LIGO Scientific Collaboration et al., 2017) — has one source for both: both are disk-moduli-determined null propagation on $\mathbb{RP}^3$.

Standard physics takes c as a fundamental constant put in by hand and uses it to convert between space and time. The framework reads c as set by the $\mathbb{CP}^3 + \tau$ geometry as a whole, via the conformal structure that holomorphic disks induce on $\mathbb{RP}^3$. The two readings agree numerically; the geometric reading answers "why this constant rather than another." The disk-moduli construction is rigid — a disk with boundary on $\mathbb{RP}^3$ is determined by its boundary curve up to reparameterization, the moduli space carries a specific conformal class, and the conformal class fixes the null-cone structure on $\mathbb{RP}^3$ without remaining freedom. The speed of null propagation along that cone structure is what we call c; the cascade then sets every massive particle's speed relative to it.

From local cones to global causal order. The same construction extends from local light cones to the global causal structure of actuality. Each τ-event deposits at a specific point of $\mathbb{RP}^3$, and the disk-moduli at that point specify which other events lie inside its past and future light cones. The global partial order on τ-events — event A causally precedes event B iff A lies in the past light cone determined by the disk moduli at B — is read off the same disk construction that gives c. No-signaling is built in: the disk moduli are rigid, so modifying the conformal class on $\mathbb{RP}^3$ would require modifying $\mathbb{CP}^3 + \tau$ globally, which no local operation can perform. Bell correlations (Chapter 23, §23.1.2) do not transmit information because τ-projection is the actualization step, not a communication channel. The local light-cone geometry, the global causal partial order, and the no-signaling constraint are three consequences of one disk-moduli construction.

16.4 Two Gravitational Regimes

The G derived in the previous section is one of two gravitational couplings the framework distinguishes. The two coexist within the same universe at every cosmic epoch, governing different physical domains.

The first is the microscopic coupling G_{micro} — the G derived in the previous section, written G_{micro} when the distinction with G_{eff} matters. It is constant, a topological quantity set by the information loss per τ-event and the geometry of the $\mathbb{CP}^3 \to \mathbb{RP}^3$ projection. It governs local physics: laboratory measurements, solar-system orbits, neutron-star structure, and the Friedmann equation (Friedmann, 1922) that describes the large-scale expansion of the smooth cosmos. It is the G that appears in Einstein's field equations.

The second is the effective coupling $G_{\text{eff}}(z)$. This evolves with redshift:

$$G_{\text{eff}}(z) = G_0\,(1+z)^{3/2}.$$

It governs nonlinear structure formation—the gravitational collapse of matter into halos, galaxies, and clusters. The evolution arises because G_{eff} *inversely* tracks the cumulative actualization record $M(t)$: more accumulated events at the present epoch mean more holographic screening and a weaker effective coupling, so $G_{\text{eff}}(z) = G_0 \cdot M(t_0)/M(z)$. Reading off the redshift dependence: events accumulate linearly in time, so $M(t) \propto t$, and the matter-dominated Friedmann equation gives $t \propto (1+z)^{-3/2}$, hence $M(z) \propto (1+z)^{-3/2}$.

The $3/2$ exponent decomposes into two pieces of geometry. The 3 is the dimensionality of the actuality manifold: matter dilutes as a^{-d} in d spatial dimensions, and $d = \dim(\mathbb{RP}^3) = 3$. The 2 is from the Friedmann equation's quadratic form: $H^2 \propto \rho$ relates the Hubble rate to the energy density, and extracting H from this puts a $1/2$ on the exponent of a in the resulting $H(a)$ relation, which then propagates through to the exponent of $t(a)$. At earlier epochs (higher redshift), fewer τ-events have occurred, holographic screening is less complete, and the effective coupling is stronger — the same content read off as the $(1+z)^{3/2}$ growth.

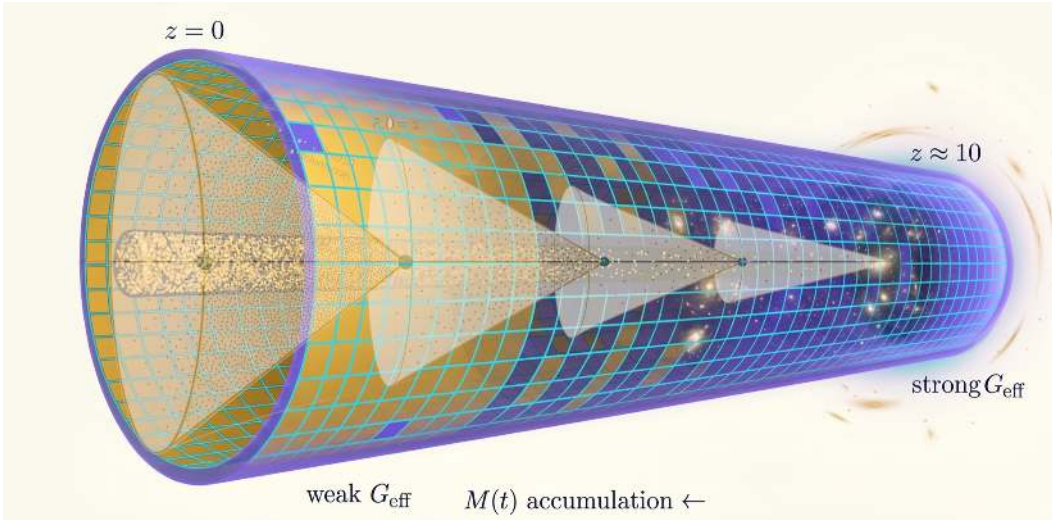

Figure 16.2: *Holographic screening across cosmic time. Each cone holds the actualization record accumulated by one cosmic epoch — the τ-events (gold) deposited on the $\mathbb{RP}^3$ boundary from the Big Bang (the $\mathbb{Z}_2$ origin surface at left) out to redshift z. The record $M(t)$ grows monotonically with cosmic time, so later epochs enclose larger cones: the $z \approx 10$ cone holds a small early fraction, the $z = 0$ cone the full present-day record. The effective gravitational coupling is the inverse of the enclosed record, $G_{\rm eff}(z) = G_0\, M(t_0)/M(z) = G_0(1+z)^{3/2}$: a small early cone carries little accumulated record and strong $G_{\rm eff}$, the large present cone the full record and $G_{\rm eff}$ at its floor G_0. The screening is the growth of the deposited record itself.*

The domains are partitioned by *density contrast* $\delta = \rho/\bar{\rho} - 1$, the local mass density measured relative to the cosmic mean. Linear regions ($\delta \ll 1$ — the smooth intergalactic medium, primordial fluctuations, anything that has not virialized into a collapsed structure) are governed by $G_{\rm micro}$. Nonlinear regions ($\delta \gg 1$ — virialized galaxies, clusters, and bound structures matter has assembled into) are governed by $G_{\rm eff}(z)$. Which coupling is operative for any given measurement is set by the local δ at the time and location of that measurement. At any given z the universe contains both regimes simultaneously, distributed across space according to where structure has and has not collapsed. The partition is spatial and present at every epoch, with the boundary between the two regimes expanding as more matter collapses through $\delta = 1$.

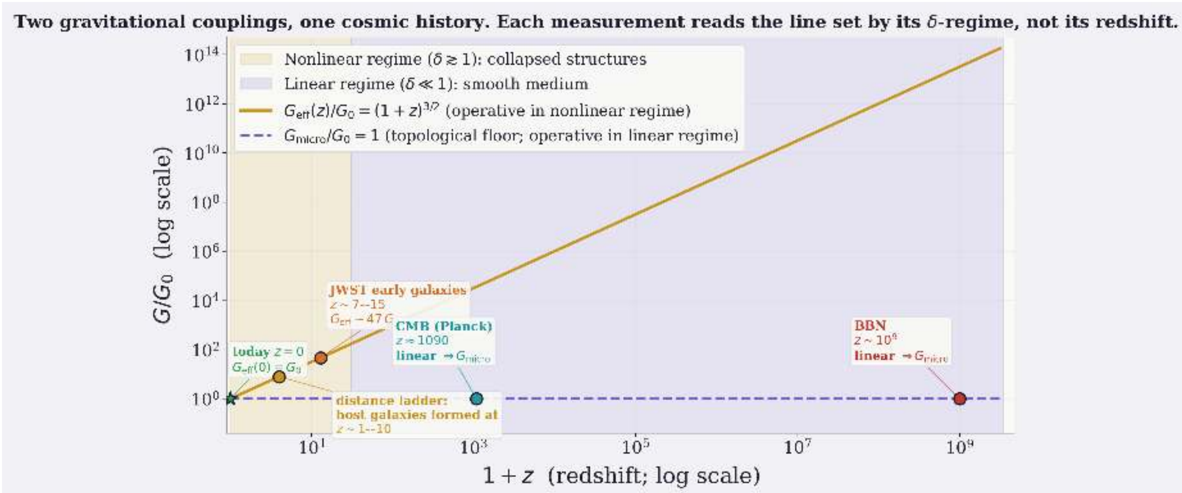

Figure 16.3: *Quantitative companion to Fig. 16.2. G_{micro} (dashed violet) is the topological floor — a constant set by the $\mathbb{CP}^3 \to \mathbb{RP}^3$ geometry, governing the linear regime ($\delta \ll 1$) at every epoch. $G_{\text{eff}}(z) = G_0(1+z)^{3/2}$ (gold) rises sharply at earlier epochs, governing the nonlinear regime ($\delta \gg 1$) of structure formation. Which coupling is operative at any given measurement is set by δ, not by z: CMB and BBN measurements sit at high z where the $G_{\text{eff}}(z)$ value is numerically large, but they probe the linear regime and therefore see G_{micro} (the floor). Distance-ladder measurements at low z probe nonlinear structures whose internal dynamics carry the cumulative imprint of $G_{\text{eff}}(z)$ history. At $z = 0$ the two couplings coincide: $G_{\text{eff}}(0) = G_0 = G_{\text{micro}}$, the floor reached.*

Jacobson (1995) and Verlinde (2011) showed that gravity emerges as the thermodynamic response to entropy gradients on a holographic boundary, with the gravitational coupling set by the inverse number of degrees of freedom available on the screen. In the framework the screen is the $\mathbb{RP}^3$ boundary, and the degrees of freedom on it are the τ-events deposited there. Each event contributes the per-event entropy of Chapter 8 (about $5.5\,k_B$), and the cumulative record $S_{\text{record}}(t) = M(t) \times \Delta S_{\text{event}}$ plays the role of Verlinde's screen-bit count. The numerical match is informative: at the present epoch $S_{\text{record}}(t_0) \approx 9.8 \times 10^{121}\,k_B$ is the same order as the Bekenstein–Hawking entropy $\approx 2 \times 10^{122}\,k_B$ of the cosmic horizon (Bekenstein, 1981), a factor of about two below that bound. The deposited record has grown, by the present epoch, to within an order-unity factor of what the cosmic horizon can hold.

The distinction between G_{micro} and G_{eff} is analogous to the distinction between the vacuum permittivity ε_0 and the effective permittivity ε_{eff} in a dielectric material. Maxwell's equations in vacuum use the fundamental constant; the response of a medium uses an effective constant that depends on the material's properties. Here, the "medium" is the field of actualized matter, and its properties change with cosmic epoch.

The transition occurs at $\delta \sim 1$, the threshold of gravitational collapse. Linear regions ($\delta \ll 1$) are the continuum phase of the actualization field: matter is spread thinly, local density tracks the cosmic mean closely, gravitational dynamics linearizes around a smooth background, and the coupling matter samples is the topological floor $G_{\rm micro}$. Nonlinear regions ($\delta \gg 1$) are the structured phase: matter has condensed out of the continuum into bound objects — galaxies, clusters, halos — whose gravitational dynamics is set by the assembly history those objects record. An object that virialized at $z \approx 12$ (JWST early-galaxy epoch) formed under $G_{\rm eff} \approx 47\, G_{\rm micro}$, and the gravitational binding that holds it together today carries that high-$G_{\rm eff}$ signature in its mass profile. An object virializing today forms under $G_{\rm eff}(0) = G_{\rm micro}$. The two regimes are two phases of the same actualization field, distinguished by whether local matter has collapsed through $\delta = 1$.

16.4.1 Observational Consequences

This two-regime picture has several testable consequences.

At the epoch of recombination ($z \approx 1090$), all density perturbations have $\delta \sim 10^{-5}$—deep in the linear regime. The cosmic microwave background is therefore governed entirely by $G_{\rm micro}$, which is constant. All CMB predictions—acoustic peak heights, the damping tail, the sound horizon—reduce to the standard ΛCDM result, with no predicted deviation from the constant-G template.

Big Bang nucleosynthesis ($z \sim 10^9$) is similarly governed by $G_{\rm micro}$, satisfying the constraint $|\Delta G/G| < 20\%$ throughout the nucleosynthesis epoch (Cyburt et al., 2016). Lunar laser ranging, which constrains $|\dot{G}/G| < 10^{-12}\ {\rm yr}^{-1}$ (Williams et al., 2004), measures $G_{\rm micro}$ and finds zero evolution, as predicted.

The consequences of $G_{\rm eff}$ evolution appear only in the nonlinear sector: structure formation, galaxy assembly, and halo collapse at high redshift. These are precisely the domains where recent observations have revealed tensions with the standard model.

The coexistence of the two regimes at every cosmic epoch is what makes the framework's modification testable. Each cosmic time contains both linear and nonlinear sectors, so observations split into two natural categories. Linear-regime measurements — CMB acoustic structure, BBN abundance predictions, lunar laser ranging, solar-system tests — probe $G_{\rm micro}$; the framework's prediction for them is that the coupling shows no evolution, and current data support that prediction. Nonlinear-regime measurements — structure assembly rates, early-galaxy populations, the late-time distance ladder — probe $G_{\rm eff}(z)$; the framework's prediction is that the coupling was stronger at higher z, and this is where current data show tension with ΛCDM. The framework's claim and its empirical signatures are typed: constancy tests live in the linear sector, evolution tests live in the nonlinear sector, with no single measurement straddling both.

The explicitly derived modification — $G_{\text{eff}}(z)$ — varies with cosmic epoch and does not depend on local acceleration, local density, or the size of any particular structure. Galaxy rotation curves, governed by present-epoch physics at $z = 0$, lie outside this explicit modification. The framework's emergent-gravity machinery shares ingredients with Verlinde's emergent-gravity program (Verlinde, 2011, 2017), which has been extended to derive MOND-like (Milgrom, 1983) behaviour from deSitter elasticity; that derivation has not been carried through within the framework. MOND-style accounts and dark-matter models both remain candidate explanations for galaxy rotation curves. The framework's gravitational predictions concern cosmic-history quantities — structure-formation rates, early-galaxy growth, the Hubble tension, the cosmological constant — all of which depend on the cumulative effect of $G_{\text{eff}}(z)$ over cosmic time.

16.5 Black Hole Thermodynamics

A black hole is the extreme case of gravity as information loss. In ordinary matter, each actualization event strips a modest amount of τ-odd content from the arena and deposits it as entropy. Near a black hole horizon, the gravitational field is strong enough that actualization events at the boundary cannot communicate their outcomes to the exterior. The horizon is the surface where the causal structure of $\mathbb{RP}^3$ prevents outward propagation of actualized facts. T.A.2, A.11

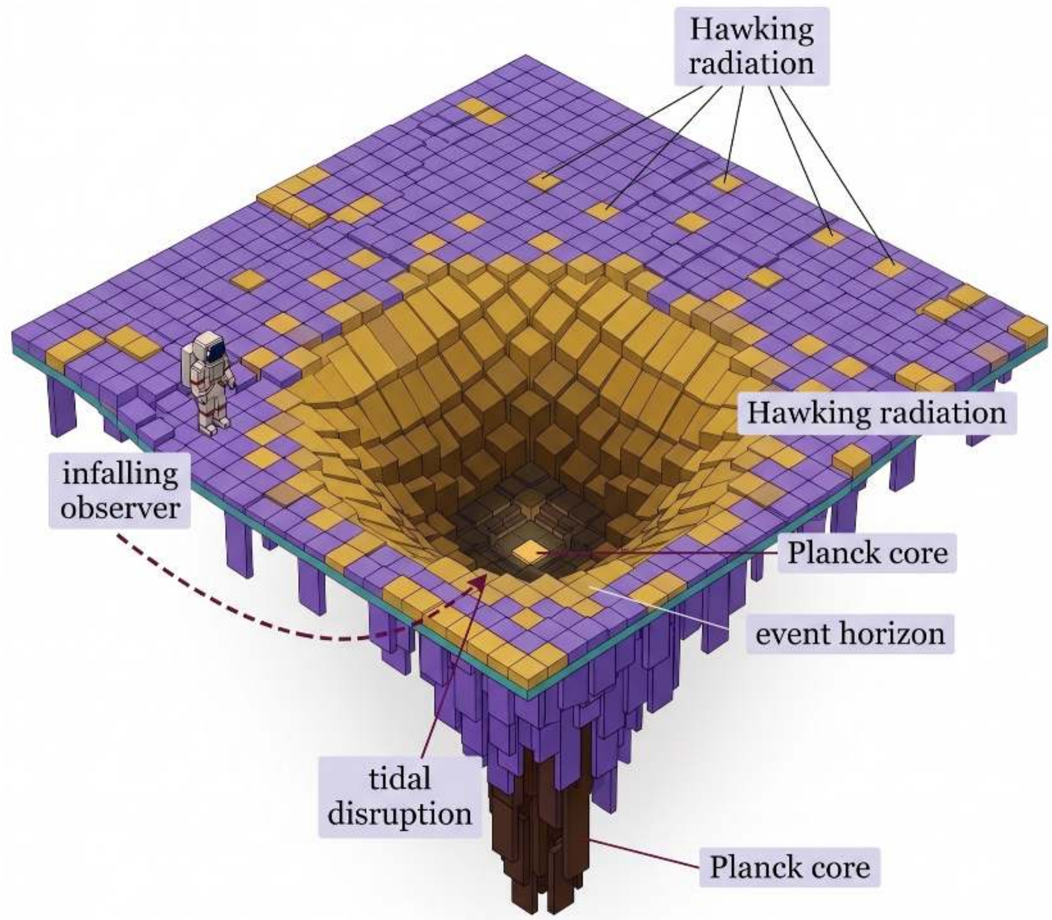

Figure 16.4: *A black hole as a region of the actualization field. The grid is the same flat cell lattice throughout; each tile is binary — violet tiles are unclaimed possibility, gold tiles are actualization events. Across most of the plane the tiles are partly claimed, a dithered mix whose gold density tracks how heavily a region is worked. At the event horizon, the holographic screen saturates: inside it every tile is claimed, and intensity is read from color saturation alone, deepening inward to the Planck core where the actualization rate reaches its ceiling. The horizon is the seam where that change of representation is forced — the boundary past which actualized facts no longer propagate outward. The faint scatter of pale tiles beyond the horizon is Hawking radiation, an uncorrelated residue of τ-projections at the saturated screen. The dashed path carries an infalling observer across the horizon to the core.*

16.5.1 Bekenstein-Hawking Entropy

The entropy of a black hole has been known since the 1970s (Bekenstein, 1973; Hawking, 1975) to be proportional to the area of its horizon:

$$S = \frac{k_B\, c^3\, A}{4\, G\, \hbar}.$$

The factor of 4 in the denominator has always been a derived result within general relativity—it follows from the Wald formalism (Iyer and Wald, 1994; Wald, 1993) applied to the Einstein-Hilbert action—but it has lacked a deeper explanation. In the framework, this factor has a specific origin: it is $|V_4|$, the order of the Klein four-group $\mathbb{Z}_2 \times \mathbb{Z}_2$ that classifies the four fact types (spectral, spatial, chiral, intensity).

The derivation proceeds through the Wald entropy formula applied to the framework's effective action. The thermal periodicity 2π and the binormal contraction factor 2 combine to give $4\pi = \mathrm{Vol}(S^2)$. Dividing the Einstein-Hilbert normalization 16π by this Wald factor yields $16\pi/4\pi = 4 = |V_4|$. Each Planck-area cell on the horizon carries one quarter of a nat of entropy per fact-type element, or equivalently, one bit per cell in the $\mathbb{Z}_2 \times \mathbb{Z}_2$ basis.

This identification connects black hole entropy directly to the information-theoretic structure of the actualization process. The entropy counts the number of independent τ-projection events on the horizon—one per Planck-area cell, each stripping one bit of τ-odd content per fact-type degree of freedom. The entropy is proportional to area (rather than volume) because τ-projection is a boundary operation: it acts on the fiber over each point of $\mathbb{RP}^3$, and the horizon is the relevant boundary surface.

16.5.2 Hawking Temperature

The Hawking temperature

$$T_H = \frac{\hbar\, c^3}{8\pi\, k_B\, G\, M}$$

follows from the same actualization process that produces the entropy formula, evaluated at the horizon's local gravitational field strength. Two steps.

Surface gravity. For a non-rotating black hole, the surface gravity at the horizon is

$$\kappa = \frac{c^4}{4GM}.$$

κ measures the gravitational acceleration at the horizon as read by an asymptotic observer

— equivalently, the rate at which proper time near the horizon dilates relative to time at infinity. In the framework's reading, κ sets the rate at which the horizon's geometry drives τ-projection events relative to the bulk projection rate elsewhere in spacetime.

Unruh conversion. An observer with proper acceleration a registers a thermal vacuum at temperature $T = \hbar a/(2\pi k_B c)$ (Unruh, 1976). For a horizon, κ plays the role of a, giving

$$T_H = \frac{\hbar\,\kappa}{2\pi k_B\,c} = \frac{\hbar\,c^3}{8\pi\,k_B\,G\,M}.$$

The $8\pi = 4 \cdot 2\pi$ in the denominator pairs with the $1/4$ in Bekenstein-Hawking entropy: the same Klein-four factor that fixes the entropy's area-law normalization appears in κ's denominator, and the additional 2π comes from the Unruh relation's thermal periodicity. Temperature and entropy share their numerical prefactor because both quantities count the horizon's τ-projection events — entropy counts cumulatively, temperature counts per unit time.

In the framework's reading, T_H is the rate at which the horizon's amplified gravitational field drives the same τ-projection process that operates everywhere else. Each event at the horizon strips a quantum of imaginary fiber content and registers it as a thermal particle pair; the horizon's enhanced projection rate produces the thermal flux that Hawking (Hawking, 1975) computed via Bogoliubov coefficients. Hawking radiation is the bulk actualization process intensified by horizon geometry.

16.5.3 Unruh: The Same Mechanism Without Gravity

The Hawking derivation used the Unruh relation $T = \hbar a/(2\pi k_B c)$ (Unruh, 1976) as a step. The framework reads Unruh as a result in its own right, and as evidence that the boundary-screening mechanism behind Hawking is not specific to gravity.

An observer with proper acceleration a along a worldline in Minkowski space has a Rindler horizon: a null surface beyond which no light signal can reach the observer at any finite proper time. The part of the actualization record that lies behind this horizon is hidden from the observer the same way the interior of a black hole is hidden from an external observer. The mechanism is identical: a causal boundary screens part of the τ-event record from a particular observer's accessible cone, and the screened sector registers as a thermal bath.

The framework therefore predicts the Unruh temperature from the same construction that produces Hawking:

$$T_{\text{Unruh}} = \frac{\hbar\,a}{2\pi\,k_B\,c},$$

with the proper acceleration a playing the role κ played for a black hole horizon. The 2π is the thermal periodicity of Euclidean time imposed by the boundary; the same factor appears in Hawking, Bekenstein, and any horizon-induced thermal spectrum. Mass and gravity are absent here. The only requirement is a causal horizon, and the kinematic horizon a uniformly accelerating observer carries with itself supplies one.

The structural claim sharpens. Hawking radiation and Unruh radiation are the same phenomenon at two different horizons. Any boundary that hides part of the τ-event record from an observer produces a thermal spectrum at temperature set by the boundary's surface gravity or proper acceleration. Bekenstein-area entropy scaling, $T = \hbar\kappa/(2\pi k_B c)$, and the Klein-four prefactor are consequences of the boundary-screening mechanism. Gravity is one way to make a horizon; acceleration is another. The same machinery also covers de Sitter horizons, where the cosmological constant plays the role of κ and the framework recovers the Gibbons-Hawking temperature $T_{\mathrm{dS}} = \hbar H/(2\pi k_B c)$ (Gibbons and Hawking, 1977) as the third instance of the same construction.

16.5.4 The Black Hole Interior

For an observer falling through the horizon of a Schwarzschild black hole, the proper time from horizon to singularity is finite, $\tau_{\mathrm{fall}} = \pi GM/c^3$. The interior crossing is a discrete sequence of $\mathbb{CP}^3 \to \mathbb{RP}^3$ projections, and the sequence has a bounded length: the actualization rate cannot exceed the ceiling the per-event floor imposes, $2/(\pi\, t_P)$, so the number of events on the infalling worldline is at most

$$N_{\mathrm{fall}} \le \frac{2}{\pi\, t_P}\,\tau_{\mathrm{fall}} = \frac{2GM}{c^3\, t_P} = \frac{r_S}{\ell_P},$$

the Schwarzschild radius measured in Planck lengths — roughly 1.8×10^{38} for a solar-mass black hole. The infall is a finite discrete worldline through the interior.

As the radial coordinate approaches zero, the tidal forces and the curvature invariant diverge, and the gravitational decoherence rate Γ (Diósi, 1989; Penrose, 1996) diverges with them. General relativity reads that divergence as the singularity. The framework does not follow it there. Γ measures the decoherence gravity demands; the rate at which actualization is carried out is a distinct quantity, the inverse of the per-event time. Every τ-projection takes a minimum interval — the Margolus–Levitin event time — and that interval has a floor, because the actualization energy cannot climb past the Planck rung of the cascade. The actualization rate is therefore capped and cannot diverge. What general relativity labels a singularity is, in the framework, a Planck-scale core where actualization runs at a maximal, finite rate; the infalling worldline terminates in that core, its proper time positive and its event rate bounded throughout. The delivered rate parts from the diverging demand at a sharp point — one Planck time of proper time before the classical centre, a separation set by the curvature alone and the same for every black hole (Figure 16.5). No firewall (Almheiri et al., 2013) is needed — the interior is a well-defined actualization sequence, and the classical $r = 0$ pathology is the extrapolation the actualization floor removes.

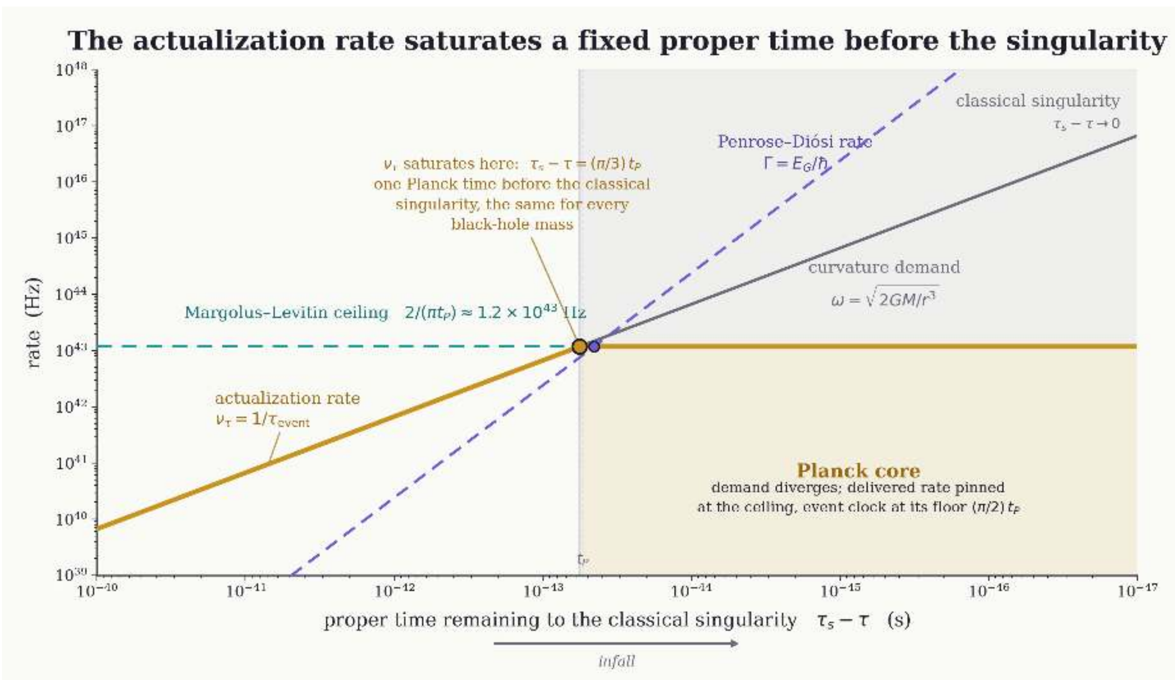

Figure 16.5: *The black-hole interior has no singularity. On infall the demand for actualization diverges; the delivered rate cannot. Two estimates of the demand are plotted against proper time remaining to the classical singularity: the parameter-free curvature frequency $\omega = \sqrt{2GM/r^3}$ (grey) and the Penrose–Diósi gravitational decoherence rate $\Gamma = E_G/\hbar$ (violet dashed, drawn for a Planck-scale system, the minimal case — a macroscopic infaller saturates the ceiling far earlier). Both diverge toward $r \to 0$. The delivered actualization rate $\nu_\tau = 1/\tau_{\text{event}}$ (gold) cannot follow: each τ-projection takes the Margolus–Levitin time $\tau_{\text{event}} = \pi\hbar/(2E)$ with E capped at the Planck rung of the cascade, so ν_τ saturates at the ceiling $2/(\pi t_P) \approx 1.2 \times 10^{43}$ Hz. The curvature demand reaches that ceiling at $\tau_s - \tau = (\pi/3)\, t_P$, one Planck time before the classical singularity — a separation independent of the black-hole mass. In proper-time coordinates the picture is mass-independent.*

Nothing about the infall is locally exotic. For a large black hole the observer crosses the horizon without incident — the equivalence principle holds there as everywhere — and continues along an ordinary timelike worldline. Tidal forces grow with depth; at some interior radius they exceed what the body's structure can bear, and it comes apart, its constituents continuing along their own geodesics. What changes as r falls is timing. The decoherence demand grows without bound; the actualization rate follows it only as far as the ceiling, then holds, the interval between τ-projections pinned at its floor $(\pi/2)\, t_P$. The worldline arrives at nothing singular: it is a finite list of $\mathbb{CP}^3 \to \mathbb{RP}^3$ projections, and the list simply ends, its final entry in the Planck core, with classical $r = 0$ not among the points it records. Each projection along the way is non-invertible, so the infalling content is stripped progressively, event by event — the same loss of fiber content that the next section traces in the Hawking radiation.

16.5.5 The Information Paradox

The black hole information paradox rests on a conflict between two principles: quantum evolution is unitary (information is conserved), and black holes evaporate completely via Hawking radiation (Hawking, 1976) that appears thermal and therefore carries no information about the infalling state. Standard resolution attempts—complementarity (Susskind et al., 1993), ER=EPR (Maldacena, 1998), island formulas—all preserve unitarity by relocating or encoding the information in Hawking radiation through increasingly elaborate mechanisms.

The framework dissolves the paradox by denying its premise. The τ-projection is non-invertible. Information is destroyed at every actualization event—this is the content of the second law (Chapter 8). A black hole is an extreme instance of the same non-invertible projection that operates everywhere. The apparent paradox arises only within frameworks that insist quantum evolution must be unitary at the fundamental level. In $\mathbb{CP}^3$, pre-projection dynamics are unitary; the map from $\mathbb{CP}^3$ to $\mathbb{RP}^3$ is non-unitary.

Hawking radiation is thermal because τ-projection at the horizon operates in the exhausted-capacity regime: the channel capacity $I(k) = 3 \log_2 R(k)$ vanishes as $R \to 1$, so nearly all pre-projection content becomes entropy rather than structure. Hawking radiation is thermal for the same reason everyday heat is thermal—the actualization channel is saturated.

This dissolution carries a testable consequence. If unitarity is violated at the fundamental level, then the Page curve (Page, 1993)—the plot of entanglement entropy of Hawking radiation over time—should *not* turn over at the Page time. Entanglement entropy should grow monotonically, following the thermodynamic prediction, rather than decreasing as the black hole shrinks. Most unitarity-preserving resolutions of the paradox (complementarity, ER=EPR, island formulas) predict the turnover, so a measured Page curve discriminates between them and the framework's non-invertible-projection picture. Direct measurement on astrophysical black holes is far out of reach; analog-gravity systems in condensed-matter platforms have been proposed as experimental analogues (Barceló et al., 2011), though whether they reproduce the relevant features of the Page curve is itself an open question. The philosophical implications of this non-unitarity claim are taken up in Chapter 23.

16.6 Spacetime as Historical Record

Spacetime is the accumulated record of actualization events. This reverses the usual relationship between spacetime and dynamics.

In general relativity, spacetime comes first. One begins with a four-dimensional manifold equipped with a metric—a pre-existing stage—and then writes down equations describing how matter and energy move on that stage. The metric responds to matter (spacetime curves in the presence of mass), but the manifold itself, the stage on which everything plays out, is given in advance. The question "why does spacetime exist?" is not addressed; spacetime is the starting point of the theory, not its output.

The framework inverts this relationship. Spacetime is not a starting point. It is the accumulated record of every actualization event that has ever occurred—roughly 10^{121} projections from possibility to actuality, each one adding a fact to the historical record.

Consider what this means concretely. Each actualization event produces four facts (one per fact type: spectral, spatial, chiral, intensity). The spatial facts specify *where* the event occurred. Over the course of cosmic history, the collection of all spatial facts constitutes the spatial geometry of the universe—its metric, its curvature, its distances. The spatial channel carries two layers: external position (x, y, z) on $\mathbb{RP}^3$ that aggregates into the metric, and bundle-internal coordinates (color orientation, $B - L$, generation) that aggregate into the particle content (Chapter 15, §15.6). Spacetime geometry and particle identity are the macroscopic and microscopic readings of the same spatial fact-type. The spectral and intensity facts specify the energy content at each location, which is the matter distribution. The chiral facts specify the handedness structure, which determines the matter-antimatter asymmetry. The complete spacetime—geometry, matter content, causal structure—is the accumulated pattern of all these facts.

The metric emerges from the actualization record the same way temperature emerges from molecular motion. No individual molecule has a temperature; temperature is a statistical property of the collective. No individual actualization event has a metric; the metric is a statistical property of $\sim 10^{121}$ events. Curvature, in particular, is the geometric expression of the density of information loss: regions where more information has been stripped (more actualization events, more entropy generated) are more curved. This is exactly what Einstein's equations describe, and it is why those equations emerge from the heat kernel expansion—they are the macroscopic equation of state for the actualization medium.

Causal structure—the specification of which events can influence which other events—is likewise emergent. It is determined by the actualization sequence itself: event A can influence event B only if A is in the past light cone of B, and the light cone structure is itself a consequence of the pattern of actualization events. There is no external clock or pre-existing causal order. The actualization process generates its own temporal structure as it proceeds.

This is what background independence means in the framework: the metric, the causal structure, and the dimensionality of spacetime are not inputs to the theory. They are outputs of the actualization process, derived from the same $\mathbb{CP}^3$ geometry that produces quantum mechanics, the Standard Model, and the constants of nature. The universe does not take place *in* spacetime. Spacetime is the record that the universe writes as it actualizes itself.

Standard physics treats stress-energy and curvature as two distinct categories related by Einstein's equations: matter on one side, geometry on the other, with the field equations specifying how matter sources curvature. The two sides are conceptually different things, and the equations are a coupling between them. In the framework these are configurations of one geometric process. The stress-energy at a region is the bundle activity at that region; the curvature at the same region is the metric response to that activity in the accumulated record. Einstein's equations express the self-consistency condition the actualization record imposes on itself. The stress-energy/curvature distinction dissolves the same way the field/geometry distinction dissolved in Chapter 12 and the matter/spacetime distinction dissolved in Chapter 15: there were never two things to relate. Gravity is what the accumulated actualization record *is* at the resolution where metric-language becomes appropriate.

Einstein's identification, one layer down. Chapter 1 anchored PPM's insight in Einstein's example: take an empirical fact seriously, ask what geometry must be for it to hold. At the time the appeal read as methodological analogy — borrowed style of argument, applied to a different problem. It is fair to stop reading it as analogy now. Einstein (Einstein, 1916) identified gravitational coupling with spacetime curvature — two phenomena collapsed into one geometric fact. This chapter has identified spacetime curvature with the statistical signature of τ-event information loss on $\mathbb{CP}^3 + \tau$ — the same collapse, one structural layer down. Same kind of duality dissolved, same arena. Einstein placed gravity inside the geometry of spacetime; PPM places spacetime itself inside the geometry of $\mathbb{CP}^3 + \tau$. The methodological parallel Chapter 1 sketched was a correspondence the whole time: both readings describe one geometric object, identified at different layers of the same structure.

The gravitational mechanism developed in this chapter — holographic screening at the $\mathbb{RP}^3$ boundary, the two-regime G_{micro} vs $G_{\text{eff}}(z)$ split, the Bekenstein–Hawking entropy, the information paradox dissolution — has cosmological consequences as well as the local-physics consequences treated here. The cosmological constant, the Hubble parameter, the Hubble tension, the early universe, the cosmic cascade descent, and the present epoch as a structural moment are taken up next in Chapter 17.

Chapter 17

Cosmology

Chapter 16 developed the gravitational mechanism — holographic screening at the $\mathbb{RP}^3$ boundary, the two-regime G_{micro} vs $G_{\text{eff}}(z)$ split, the Bekenstein–Hawking entropy. This chapter reads the same mechanism at cosmic scale. The cosmological constant, the Hubble parameter, the Hubble tension, the early universe, and the cosmic cascade descent all follow from the boundary's topological capacity $N_\infty = \varphi^{392}$ being the same geometric object that fixed G in the previous chapter. Where gravity reads N_∞ as a per-tile holographic share, cosmology reads it as a total budget — the same number, two readings. T.14, A.2, A.11

17.1 Early Galaxies and the JWST Anomaly

Beginning in 2022, the James Webb Space Telescope revealed massive, mature galaxies at redshifts $z \approx 7$–14, corresponding to 300–700 million years after the Big Bang. These galaxies have stellar masses up to $\sim 10^{10}\,M_\odot$—10 to 100 times more massive than standard ΛCDM predicts at those epochs (Finkelstein et al., 2023; Harikane et al., 2023; Labbé et al., 2023). Producing them within the available time requires either physically implausible star formation efficiencies (near 100%) or new physics.

The framework provides the new physics through $G_{\text{eff}}(z)$. At $z = 12$, the effective gravitational coupling is $G_{\text{eff}} = G_0 \times 13^{3/2} \approx 47\,G_0$. Gravity in the nonlinear regime was roughly 47 times stronger than today. This accelerates halo collapse timescales by a factor of $1/\sqrt{G_{\text{eff}}/G_0} \approx 6.9$, and star formation rates scale as $G^{3/2}$, giving an enhancement of roughly 320 times the present rate. Massive galaxies form naturally within the available cosmic time without requiring extreme assumptions about star formation physics.

The same mechanism accounts for the existence of barred spiral galaxies at $z > 8$ (bars require dynamically mature disks, which form faster under stronger gravity), massive black holes at $z > 6$ (enhanced accretion from stronger gravitational collapse), and the compact sizes of high-redshift galaxies (virial radii scale inversely with G_{eff}).

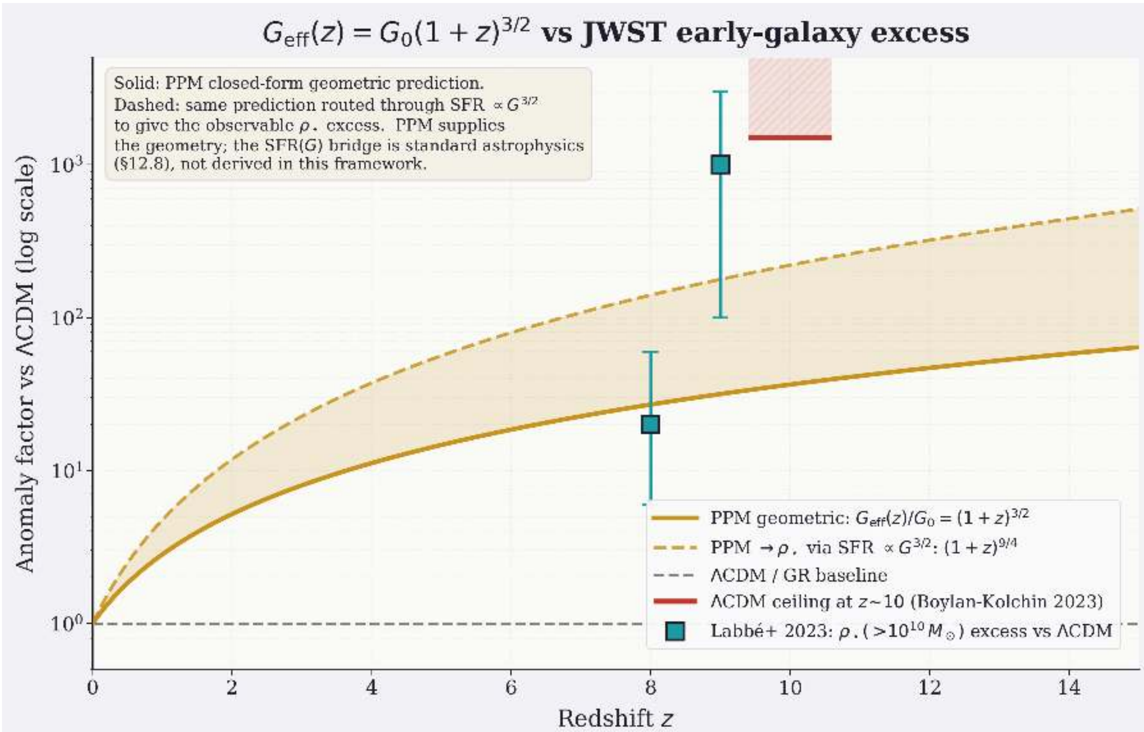

Figure 17.1: *The $G_{\text{eff}}(z)$ prediction against JWST early galaxy anomalies, on a shared anomaly-factor axis (log scale).* Solid gold: *the closed-form geometric prediction $G_{\text{eff}}(z)/G_0 = (1+z)^{3/2}$, rising into the past as fewer cumulative τ-events mean less holographic screening.* Dashed gold: *the same prediction routed through the standard SFR(G) scaling* SFR $\propto G^{3/2}$ *to give the observable cumulative stellar-mass-density excess $\rho_\star/\rho_{\star,\Lambda\text{CDM}} \sim (1+z)^{9/4}$; the shaded band between the two curves marks the regime PPM commits to.* Cyan squares: *JWST cumulative stellar-mass-density excess at $z \approx 8$ and $z \approx 9$ from Labbé et al. (Labbé et al., 2023); error bars represent factor-of-three IMF/stellar-mass systematic uncertainty.* Red ceiling segment with hatched no-go region above: *The absolute upper bound on stellar-mass-density excess permitted by the ΛCDM halo mass function at $z \sim 10$ (Boylan-Kolchin, 2023)—a theoretical ceiling, not a measurement. PPM supplies the geometry; the SFR(G) bridge to the observable is standard astrophysics. The $(1+z)^{3/2}$ exponent is fixed by the framework, not fitted.*

17.2 The Cosmological Constant

The cosmological constant is one of the most measured and least understood quantities in physics. Its observed value—$\Lambda \approx 1.1 \times 10^{-52}$ m^{-2}—is extraordinarily small, yet it dominates the energy budget of the present-day universe, driving the accelerating expansion that astronomers first detected in 1998 (Perlmutter et al., 1999; Riess et al., 1998). Why it has this particular value, and why it is not enormously larger, are open questions in standard cosmology.

The framework answers both questions by identifying what Λ physically represents: the unactualized content of the arena—fiber degrees of freedom stripped by the $\mathbb{CP}^3 \to \mathbb{RP}^3$ projection. This places Λ in the same Kähler-doublet, N_∞-derived family as G (§Gravity as Accumulated Information Loss above): both quantify how the Kähler structure of $\mathbb{CP}^3$ manifests at the $\mathbb{RP}^3$ boundary, differing in whether they scale with the total capacity ($\Lambda \propto 1/N_\infty$) or the per-tile share ($G \propto 1/\sqrt{N_\infty}$).

The $\mathbb{RP}^3$ boundary has a topological capacity of $N_\infty = \varphi^{392}$ independent fiber sections. The cosmological constant is set by this capacity:

$$\Lambda = \frac{2(m_\pi c^2)^2}{(\hbar c)^2 \, N_\infty}.$$

The numerator contains the confinement energy scale $m_\pi c^2$ (the reference scale anchoring the framework's energy cascade) and a factor of 2 from the two homotopy classes of the $\mathbb{Z}_2$ topology. The denominator is the topological capacity. With $N_\infty = \varphi^{392}$, this gives $\Lambda \approx 1.117 \times 10^{-52}$ m^{-2}, agreeing with the observed value to 1.5%.

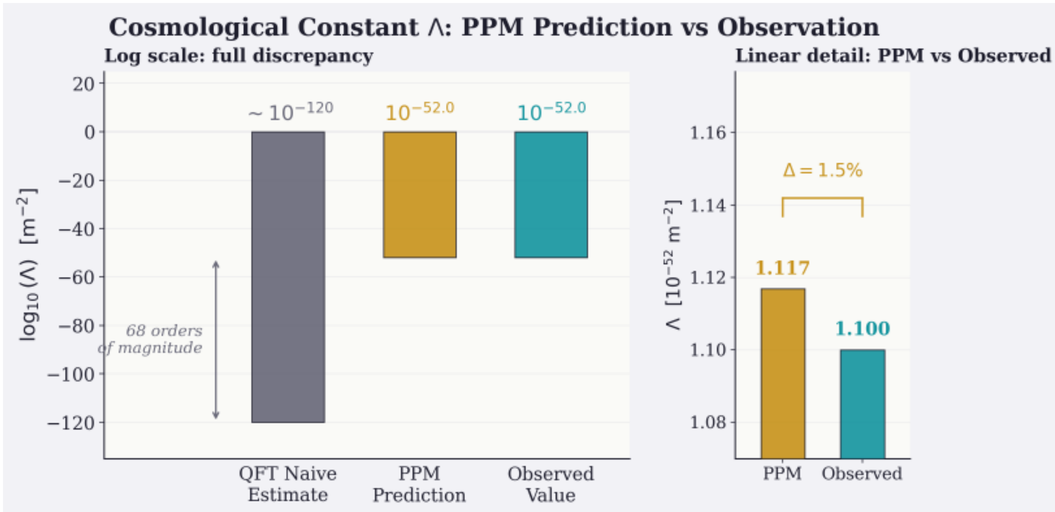

Figure 17.2: *The predicted cosmological constant beside the observed value (Planck Collaboration, 2020). Λ measures the unactualized content of the arena, and its size is the reciprocal of the boundary capacity: $\Lambda \propto 1/N_\infty$ with $N_\infty = \varphi^{392} \approx 10^{82}$. The cosmological constant is small because that capacity is exponentially large; the prediction agrees with observation to 1.5%.*

Λ is small because the boundary capacity is exponentially large. The value $N_\infty = \varphi^{392}$ comes from packing the $\mathbb{RP}^3$ boundary with Compton-scale fiber sections respecting the icosahedral A_5 symmetry of the tiling: $\varphi = (1+\sqrt{5})/2$ is the icosahedral group's defining metric constant (Coxeter, 1973), and the exponent 392 is structurally motivated by the dimensions of the icosahedral representation acting on the boundary. An equivalent expression for the same number is $N_\infty \approx e^{2S}$ with $S = 30\pi$ the $\mathbb{CP}^3$ instanton action — the dominant instanton sector that relates $\mathbb{CP}^3$'s bulk topology to the actualized boundary count. Numerically, both expressions give $\varphi^{392} \approx e^{60\pi} \approx 8.4 \times 10^{81}$. The two routes — icosahedral packing and instanton action — terminate in the same exponentially large topological invariant of $\mathbb{CP}^3 + \tau$ via different geometric paths. The convergence is tightened in Chapter 18, §18.2, where the master self-consistency relation $(2\pi)^{27}\sqrt{\alpha} = \varphi^{98} = N_\infty^{1/4}$ binds the icosahedral exponent $392 = 4 \times 98$ to the spectral α and the hierarchy scale 2π through a single algebraic identity.

The structural reasons that positive curvature is forced and that the count shape is exponential-in-φ rather than polynomial are developed in Technical Reference Ch. 15, §Physical Origin: Topological Capacity.

The exponential size of N_∞ is the geometric origin of the hierarchy between the vacuum energy and the Planck scale. $\Lambda \propto 1/N_\infty$ is small without fine-tuning because N_∞ is large by topology; the same exponential largeness suppresses Newton's constant via $\sqrt{N_\infty} \approx 10^{41}$ in the gravity formula above. Both hierarchies share their origin.

17.2.1 Why Λ Is Small

The cosmological constant problem is often called the worst prediction in physics (Weinberg, 1989). Standard quantum field theory estimates the vacuum energy density by summing zero-point fluctuations of all quantum fields up to the Planck scale. The result is $\Lambda_{\mathrm{QFT}} \sim 10^{74}\ \mathrm{m}^{-2}$—a factor of 10^{126} larger than the observed value (Weinberg, 1989). For the QFT prediction and the observed value to coexist, some unknown mechanism must cancel 126 digits of vacuum energy, leaving only the 127th digit uncancelled. No known physics provides such a cancellation.

The QFT calculation and the observed Λ are not the same quantity. Both live inside the $\mathbb{CP}^3 + \tau$ Kähler structure; they occupy opposite τ-parity sectors of it.

Vacuum energy — the zero-point fluctuation content of quantum fields — is the τ-even sector of the Kähler structure on $\mathbb{CP}^3$. It is the energy carried by the bulk under unitary Kähler flow, the sector where quantum states evolve between projections. This energy is large, and the QFT calculation is correct about its magnitude.

Λ is the τ-odd partner: the Kähler residue at the $\mathbb{RP}^3$ boundary after τ-projection. It measures the geometric imprint of the $\mathbb{CP}^3 \to \mathbb{RP}^3$ map on the actualization record, set by the boundary capacity φ^{392}.

The two quantities share a common Kähler scale; what differs is which τ-parity sector each one inhabits, and how that sector couples to spacetime curvature. Bulk Kähler flow is unitary and τ-even; it carries the large QFT vacuum content but does not source curvature directly. The boundary residue is τ-odd and gravitates, weighted by the boundary capacity $\varphi^{392} \approx 10^{81}$. The 10^{126} ratio measures the suppression of the τ-odd boundary sector relative to the τ-even bulk — a parity-and-suppression structure rooted in the Kähler doublet, rather than a 126-digit cancellation between unrelated quantities. QFT has no τ-parity index, so standard physics treats the two sectors as one undifferentiated vacuum energy.

The Casimir effect (Casimir, 1948) is the local check on this picture. Two conducting plates impose boundary conditions on the $\mathbb{CP}^3$ unitary evolution between them, restricting which mode configurations survive; the energy cost of that restriction — the gradient of the boundary-constrained bulk vacuum energy — shows up as the measured attractive force. The QFT calculation goes through unchanged because the framework agrees with QFT about what the $\mathbb{CP}^3$-bulk vacuum content is; the framework's contribution is the consistency between Casimir's local measurement (bulk vacuum energy is real and locally accessible when boundaries restructure the modes) and the cosmological-scale claim (Λ is not that same energy budget, so the 10^{126} mismatch does not falsify the framework).

17.2.2 The Coincidence Problem

Standard cosmology faces a second puzzle: why is Λ comparable to the matter density today? If Λ is a fixed constant and the matter density dilutes as the universe expands ($\rho_{\text{matter}} \propto 1/a^3$ in FRW cosmology (Friedmann, 1922)), then their ratio was negligible in the early universe and will be enormous in the far future. The fact that they happen to be comparable right now—at the particular epoch when human observers exist—looks like a cosmic accident that cries out for anthropic explanation.

The framework resolves the coincidence. Both Λ and ρ_{matter} are set by the same geometric scale: the topological capacity $N_\infty = \varphi^{392}$. The cosmological constant is $\Lambda = 2(m_\pi c^2)^2/[(\hbar c)^2 N_\infty]$ directly. The baryon count of the observable universe is approximately N_∞ (within two orders of magnitude), a Dirac-type large-number relation (Dirac, 1937) that connects the geometric capacity to the matter content. Because the same N_∞ enters both quantities, their ratio is determined by geometric constants rather than by the epoch of observation.

The remaining mild hierarchy ($\Omega_\Lambda/\Omega_m \approx 2$ rather than 1) reflects the factor-of-order-unity relationship between N_∞ and the actual baryon count. The framework does not yet derive this factor from first principles; doing so would require a quantitative connection between the topological capacity and the baryon asymmetry, which remains an open direction.

17.2.3 Equation of State: $w_{\text{eff}} > -1$

The geometric Λ derived above is a true constant: N_∞ is a topological invariant, fixed once and for all. A purely geometric dark energy would therefore give $w = -1$ exactly. The framework predicts a small but definite deviation. The deviation does not come from any time-dependence in Λ itself; it comes from matter content coupling to the geometric vacuum through the same instanton structure that fixes N_∞ in the first place.

What backreaction means here. In cosmology, "backreaction" generally refers to matter content affecting the background spacetime evolution beyond the smooth FRW idealization. Several distinct uses get covered by the same word: inhomogeneous matter producing corrections to the averaged Friedmann equation; quantum fields in curved spacetime carrying a stress-energy that backreacts on the metric (the cosmological constant problem in QFT framing); or matter content modifying the effective vacuum energy through a coupling between the two. The framework's $w_{\text{eff}} > -1$ prediction uses this third sense: Λ from N_∞ provides a fixed baseline, but the matter actualizations occurring on top of that vacuum produce a small additional contribution proportional to the matter density.

The geometric picture. N_∞ is the topological capacity of $\mathbb{RP}^3$ for independent fiber-section actualizations — a static invariant of the arena. $M(t)$ is the cumulative count of τ-events that have actually fired by cosmic time t, growing monotonically; matter density $\rho_m(t)$ corresponds to the local density of actualization events at typical particle scales. N_∞ and $M(t)$ are not independent quantities arranged into a sum. The instanton structure that fixes N_∞ (action $S = 30\pi$, prefactor $\propto e^{-S}$) also provides a coupling β between actualization density and effective vacuum density. Λ_{geom} represents the vacuum in the limit of no matter. With actualizations occurring, Λ_{eff} is shifted by $\beta\,\rho_m$. As cosmic expansion dilutes ρ_m, the shift shrinks and $\Lambda_{\text{eff}} \to \Lambda_{\text{geom}}$ asymptotically. The effective dark-energy density today,

$$\rho_{\text{DE}}(t) = \rho_\Lambda + \beta\,\rho_m(t),$$

gives an effective equation of state slightly above $w = -1$, with the deviation tracking the matter density.

Why the sign matters. The framework predicts $\beta > 0$ from the instanton prefactor's sign under the variational principle on $\mathbb{CP}^3 + \tau$. This forces $w_{\text{eff}} > -1$ strictly — the approach to -1 is from above, and phantom dark energy ($w < -1$) is ruled out. The quantitative number today: $w_{\text{eff}} \approx -0.99$ to -0.93 for $\Omega_\delta/\Omega_{\text{DE}} \sim 0.01$–$0.1$, consistent with DESI 2024's mild deviation from $w = -1$ at 2–3σ (DESI Collaboration, 2024). A confirmed phantom-crossing measurement would falsify the picture, because it would require $\beta < 0$, which the instanton structure on $\mathbb{CP}^3 + \tau$ does not permit.

Structural claim versus provisional magnitude. The structural claim — $\beta > 0$, $w_{\text{eff}} > -1$ always, asymptotic approach to -1, no phantom crossing — is foundational. The numerical value of β, and hence the specific $\Omega_\delta/\Omega_{\text{DE}}$ ratio today, requires the explicit Friedmann-backreaction calculation that remains open (Technical Reference Ch. 15). The numerical range $w_{\text{eff}} \approx -0.99$ to -0.93 corresponds to assuming $\Omega_\delta/\Omega_{\text{DE}} \sim 0.01$–$0.1$, a parameter choice consistent with observation rather than a derived value.

17.3 The Hubble Parameter

The Hubble parameter H_0 (Hubble, 1929) measures the present expansion rate of the universe. In standard cosmology, it is an empirical input—measured from the recession velocities of distant galaxies and constrained by the cosmic microwave background. The framework derives it from the same geometric ingredients that produce everything else.

The derivation rests on a simple question: what sets the size and age of the observable universe? In the framework, both are determined by the actualization process.

The minimum meaningful distance in the actualized world is the pion Compton wavelength, $\lambda_C = \hbar/(m_\pi c) \approx 1.4 \times 10^{-15}$ m. This is the scale at which the $\mathbb{RP}^3$ topology becomes coherent — the smallest length at which the actual world has definite geometric structure. Below this length (above the confinement transition at $k = 51$), color $\mathrm{SU}(3)_C$ is restored and no color-singlet hadron exists to anchor a Compton-volume event. The actualization boundary has no sharp resolution there: the same symmetry breaking that gives the pion its mass also gives the boundary its smallest meaningful scale (Chapter 15).

A fiber section is a smooth assignment of an $\mathbb{R}^3$ direction-vector to each point on $\mathbb{RP}^3$; the boundary's bundle is trivial because $\mathbb{RP}^3 \cong SO(3)$ is parallelizable. Resolved at λ_C, the boundary partitions into Compton-scale cells, and within a single cell the section is one coherent assignment while assignments in distinct cells vary independently. Each λ_C-cell—each tile in the icosahedral packing—is one independent fiber section. The boundary's holographic capacity counts independent fiber sections at this resolution, and the icosahedral packing counts cells; the two counts coincide.

The boundary supplies $N_\infty = \varphi^{392}$ independent fiber sections at the λ_C scale—one per Compton-volume tile. Spatial structure on $\mathbb{RP}^3$ accumulates by populating these tiles in random isotropic directions, so the spatial extent of the observable universe is not $N_\infty \times \lambda_C$ (which would assume all tiles extended the universe along the same axis) but $\sqrt{N_\infty} \times \lambda_C$. The square root reflects the holographic principle (Susskind, 1995; 't Hooft, 1993): the observable radius of a region scales as the square root of the information content it encodes.

The same logic applies to time. The minimum meaningful time interval is the pion Compton time, $\tau_C = \hbar/(m_\pi c^2) \approx 4.7 \times 10^{-24}$ s—the duration of one actualization event at the confinement scale. The corresponding age of the universe is $T = \sqrt{N_\infty} \times \tau_C$.

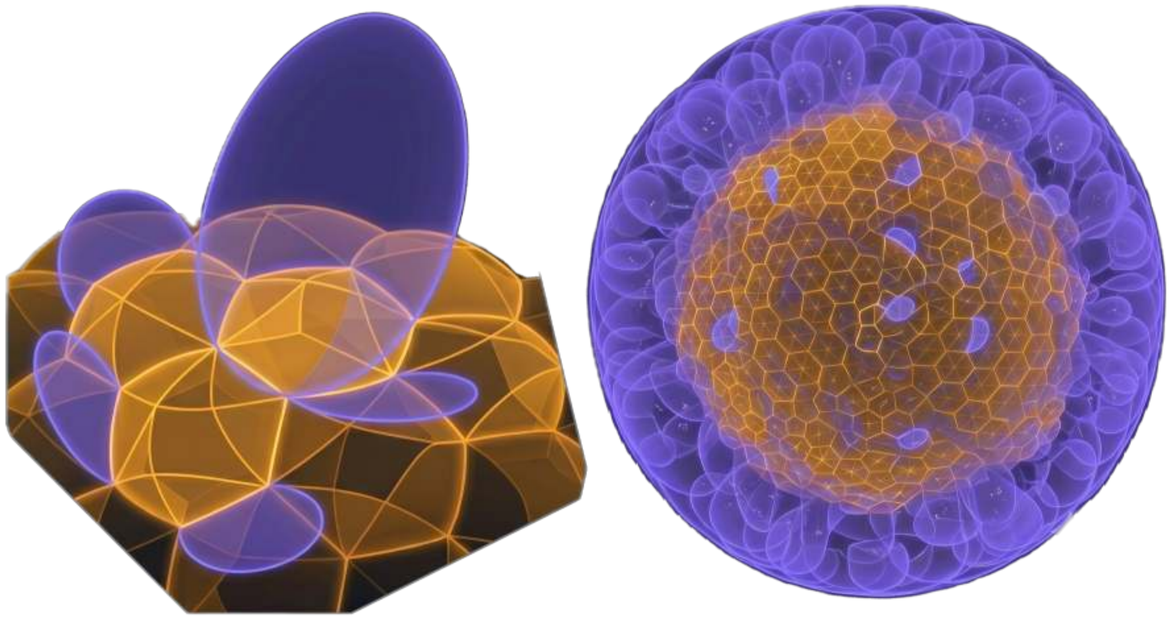

Figure 17.3: *The framework's event grain at two scales.* Left: *a macro view of the* $\mathbb{RP}^3$ *boundary tessellated by Compton-scale cells, each* $\lambda_C \approx 1.4$ *fm across. Each cell is one independent fiber section, one* τ*-event; cell edges are arcs of closed geodesics in the round metric, and the visible curvature is the boundary's positive sectional curvature. Translucent violet membranes lifting from cell edges are holomorphic 2-disks in the surrounding* $\mathbb{CP}^3$ *bulk, each bounding on one closed-geodesic edge — the bulk side of the actualization process.* Right: *the full closed* $\mathbb{RP}^3$ *orb tessellated everywhere by the same packing, surrounded by its integrated* $\mathbb{CP}^3$ *bulk;* $N_\infty = \varphi^{392} \approx 10^{82}$ *cells in total, spanning out to the Hubble radius* $R = \sqrt{N_\infty}\,\lambda_C \approx 1.3 \times 10^{26}$ *m. The* $\sqrt{N_\infty}$ *scaling is the holographic relation between the count of independent fiber sections and the spatial extent they support; Newton's constant* ($G \propto 1/\sqrt{N_\infty}$) *and the cosmological constant* ($\Lambda \propto 1/N_\infty$) *both follow from this single packing.*

These scaling relations—$R = \sqrt{N_\infty}\,\lambda_C$ and $T = \sqrt{N_\infty}\,\tau_C$—were first derived by Sidharth (1999, 2001) from cosmological number coincidences. The framework grounds them in the actualization geometry: the $\sqrt{N_\infty}$ factor is the holographic scaling of independent Compton-scale fiber sections on $\mathbb{RP}^3$. The Λ formula ($\Lambda = 2(m_\pi c^2)^2/[(\hbar c)^2 N_\infty]$) is the same Sidharth identification with the same N_∞; the framework's contribution is the geometric derivation of $N_\infty = \varphi^{392}$ (T.12, § "The Sidharth Relations").

Because $\lambda_C/\tau_C = c$ exactly (the definition of the Compton wavelength and Compton time for the same particle), the spatial and temporal extents are related by the speed of light. The

Hubble parameter follows immediately:

$$H_0 = \frac{c}{R} = \frac{c}{\sqrt{N_\infty}\,\lambda_C} = \frac{1}{\sqrt{N_\infty}\,\tau_C} = \frac{1}{T}.$$

With $T = 13.80$ Gyr (the observed age of the universe), this gives $H_0 = 70.9$ km/s/Mpc.

The relation $H_0 \times T = 1$ is exact within the framework—a geometric identity rather than an approximation. In standard ΛCDM, H_0 and the age of the universe are independent parameters, and their near-equality ($H_0 T \approx 1$) is treated as a coincidence requiring explanation. Here, both quantities are determined by the same boundary capacity N_∞, and the $\sqrt{N_\infty}$ factors cancel exactly. The "coincidence" is a tautology: the expansion rate and the age are two measurements of the same geometric fact.

17.4 The Hubble Tension

One of the most pressing problems in modern cosmology is that two independent ways of measuring the expansion rate disagree.

Measurements from the early universe—primarily the cosmic microwave background, as analyzed by the Planck satellite—give $H_0 = 67.4 \pm 0.5$ km/s/Mpc (Planck Collaboration, 2020). These measurements work by observing the pattern of temperature fluctuations left over from the epoch of recombination ($z \approx 1090$, about 380,000 years after the Big Bang) and fitting them to the standard ΛCDM cosmological model. The fit determines H_0 indirectly, as a parameter in the model.

Measurements from the late universe—using the distance ladder of Cepheid variable stars and Type Ia supernovae—give $H_0 = 73.0 \pm 1.0$ km/s/Mpc (Riess et al., 2022). These measurements work by directly observing the recession velocities and distances of nearby galaxies.

The discrepancy between these two values exceeds 5σ—far too large to be a statistical fluctuation. Hundreds of proposed explanations have been offered, ranging from systematic errors in the distance ladder to new physics in the early universe. None has achieved consensus.

The framework's geometric prediction (Section 17.3) gives $H_0 = 70.9$ km/s/Mpc, sitting between the two measurements and closest to the tip-of-the-red-giant-branch (TRGB) measurement of 69.8 ± 0.8 km/s/Mpc (Freedman et al., 2020).

The resolution comes from the two-regime gravitational picture developed earlier in this chapter. Both measurements apply the standard ΛCDM analysis machinery, which assumes a

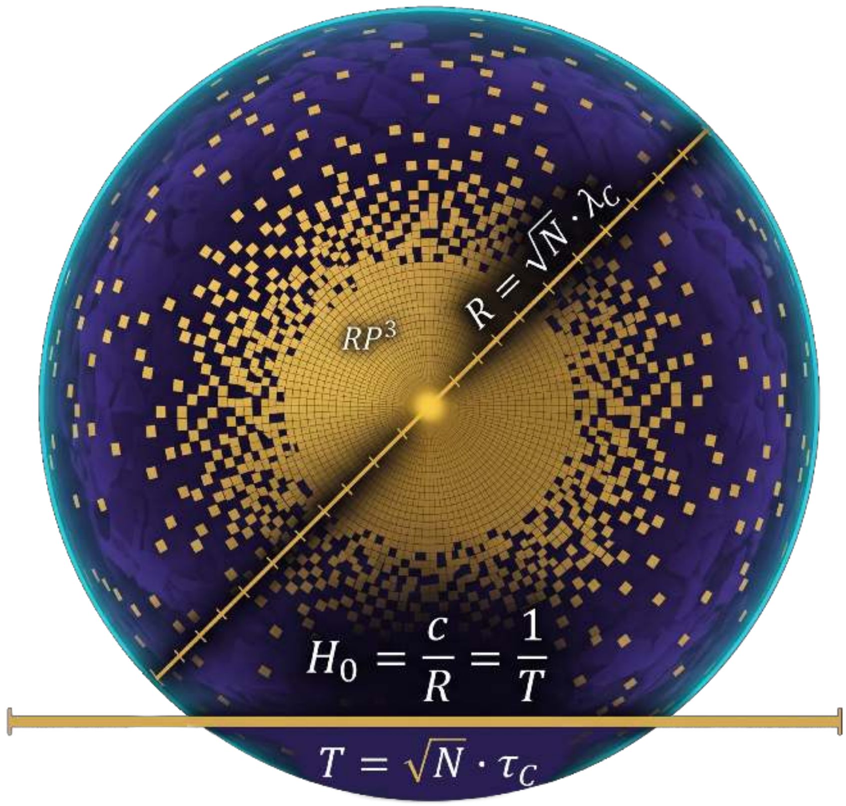

Figure 17.4: *The Hubble parameter as geometric tautology. Gold RP^3 tiles pack the dark violet CP^3 substrate, each tile marking one independent fiber section on the holographic boundary. The sphere's radius $R = \sqrt{N_\infty}\,\lambda_C$ and the light-crossing time $T = \sqrt{N_\infty}\,\tau_C$ are both set by the same boundary capacity N_∞, so that $H_0 = c/R = 1/T$ is an identity rather than a coincidence. The cyan boundary at the horizon marks the $\mathbb{Z}_2$ involution surface. Dense gold at the center thins toward the frontier—the same screening gradient that governs G_{eff}—making $H_0 T = 1$ visible as a single geometric fact.*

single constant gravitational coupling $G = G_{\text{micro}}$ throughout cosmic history. The framework treats that assumption as correct in the linear regime ($\delta \ll 1$) and violated in the nonlinear regime ($\delta \gg 1$) during the era $z \sim 1$–10 when matter assembled into the galaxies and clusters that populate the present universe. The two measurements sample different stages of the cosmic-history fingerprint, and the shared constant-G assumption produces errors with opposite signs.

Consider Planck first. The CMB itself arises in the linear regime at $z \approx 1090$ and is governed by G_{micro}, so the imprinted acoustic structure carries no template error. The error enters in the matching between the CMB-imprinted parameters and the present-day expansion history. That matching uses ΛCDM's constant-G structure-formation machinery to project from $z = 1090$ down to $z = 0$. The actual structure formation occurred under $G_{\text{eff}}(z) > G_{\text{micro}}$, building galaxies and clusters faster than the constant-G projection allows. To make a constant-G projection reproduce the observed late-time universe, the inference biases H_0 downward. Planck's value $H_0 = 67.4$ km/s/Mpc is what comes out.

The distance ladder runs in the opposite direction. Cepheid and Type Ia supernova standard candles are embedded in nonlinear structures — Cepheid variables in nearby galaxies, supernovae in their host galaxies — that assembled during the same era when $G_{\text{eff}}(z) > G_{\text{micro}}$. Their internal physics, including stellar binary evolution, supernova progenitor mass distributions, and host-galaxy dynamics, carries the imprint of that stronger gravity. The ladder calibrates the candles under the constant-G assumption, which under-accounts for the gravity that built them. The combination of under-calibrated distances and the inferred recession velocities of the host galaxies biases the inferred H_0 upward. The ladder value $H_0 = 73.0$ km/s/Mpc is what comes out.

The mirror-image structure of the two errors (Fig. 17.5) is itself a structural prediction of the framework. A theory that posits only a generic tension between early-universe and late-universe inferences predicts that the two should disagree, with no commitment to direction. The framework predicts the direction as well: the early-universe inference should land below the true value, the late-universe inference above, with the true H_0 in between. The sign structure follows from a single underlying mechanism — the time-varying $G_{\text{eff}}(z)$ history — sampled at two ends of the cosmic record by analyses that share the constant-G assumption. The observed pattern (Planck low, ladder high, both bracketing a middle value within reach of the framework's geometric prediction $H_0 = 70.9$ km/s/Mpc) is the pattern the mechanism predicts.

The early-galaxy population observed by JWST (Section 17.6) is the same mechanism reading out in a different observable: structures assembled faster than constant-G ΛCDM allows because the gravity that assembled them was stronger. The Hubble tension and the JWST early-galaxy anomaly are two faces of one underlying prediction.

The sign and direction of the Hubble-tension effect are robust from the $G_{\text{eff}}(z)$ scaling alone. The quantitative magnitude — whether the framework's geometric prediction $H_0 = 70.9$ km/s/Mpc captures the full shift or only part of it — depends on a Friedmann-backreaction calculation that remains open.

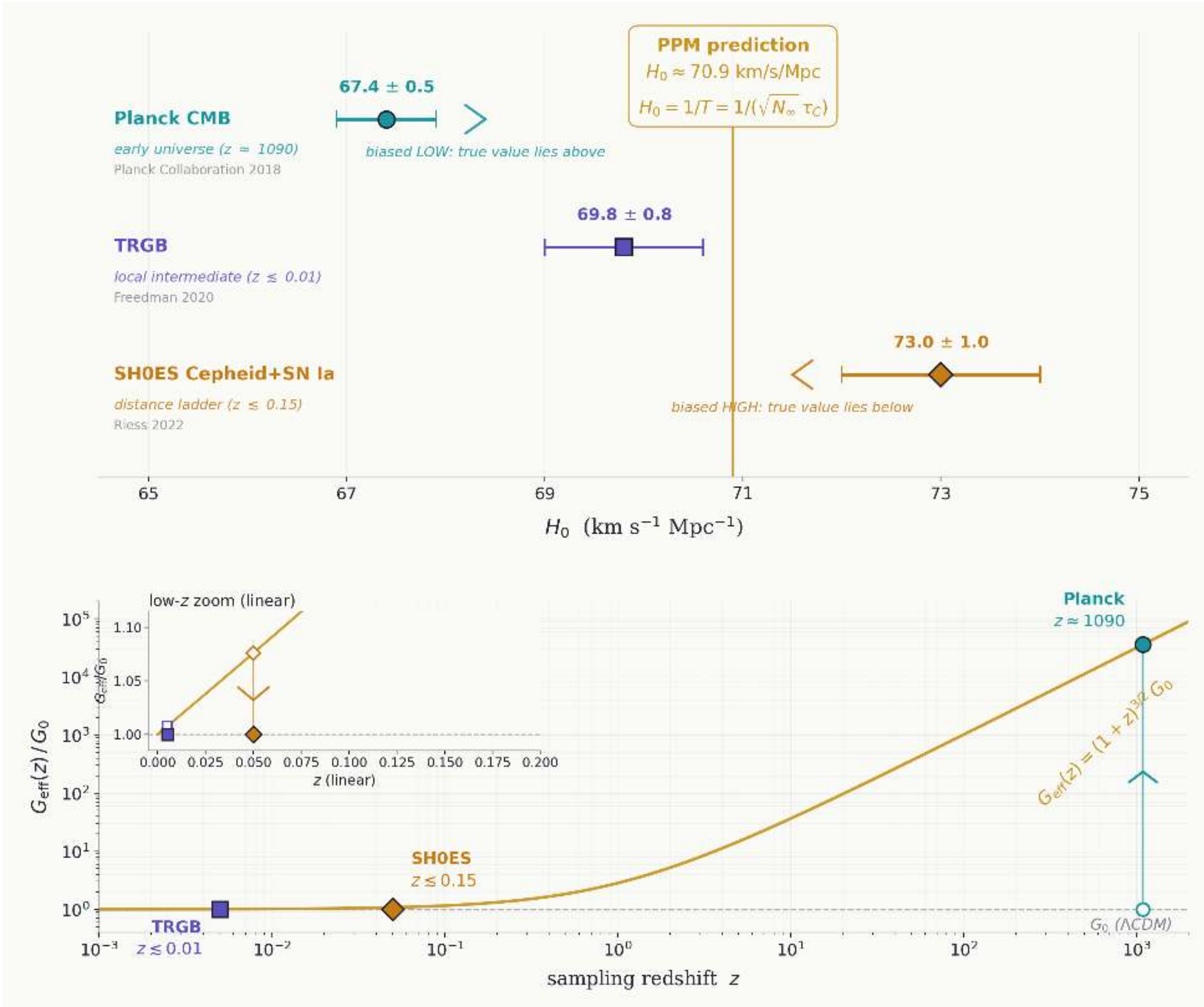

Figure 17.5: *The Hubble tension as a sign-structure prediction. The standing disagreement between early-universe and local determinations of H_0 is one of cosmology's sharpest open problems; the framework reads it as a forced consequence of $G_{\text{eff}}(z)$ scaling — methods anchored at different redshifts inherit opposite-direction biases from the shared constant-G assumption, and the framework fixes the sign of each with no free parameter.* Top: *the four numerical inputs on a single H_0 axis — Planck CMB at* 67.4*, TRGB at* 69.8*, SH0ES at* 73.0*, and the framework's geometric prediction at* 70.9 *km/s/Mpc. Open chevrons mark the predicted bias direction at each ΛCDM-machined inference.* Bottom: *the closed-form screening curve $G_{\text{eff}}(z)/G_0 = (1+z)^{3/2}$ on log–log, with the dashed reference at G_0 showing ΛCDM's constant-G assumption. Planck is rooted on the curve at $z \approx 1090$ (filled cyan circle, hollow projection at G_0); the local methods are rooted at G_0 (filled markers, hollow extrapolation on the curve). The connecting chevrons run in opposite directions, echoing the opposite-direction biases on the top panel. Inset zooms the low-z region linearly to resolve SH0ES against the near-flush TRGB. Sign structure is rigorous; the quantitative magnitudes depend on the open Friedmann-backreaction calculation.*

17.5 The Cosmic Cascade Descent

The Hubble parameter sets the cosmic clock; the temperature evolution sets where on the energy hierarchy the cosmic ambient sits at each moment. Combining the two gives the cosmos's own trajectory through the cascade k-axis, from the Planck era to the present epoch.

The variational principal at the cosmic scale produces a one-way trajectory. As cumulative actualization $M(t)$ grows and ambient T drops, the Boltzmann factor $\exp(-E(k)/k_B T)$ shifts the typical ambient event-energy to lower E, hence higher k via $k = 51 - 2\log_{2\pi}(E/m_\pi)$. This is the cascade descent at cosmic scale: the cosmic ambient started at $k \approx 1$ (Planck temperature $\sim 10^{32}$ K) and has been climbing the k-axis since. Specific epochs:

Epoch	**Approximate T**	**Typical k**
Planck era ($t \sim 10^{-43}$ s)	10^{32} K	1
GUT scale ($t \sim 10^{-37}$ s)	10^{28} K	10
EWSB ($t \sim 10^{-11}$ s)	10^{15} K	44.5
Confinement ($t \sim 10^{-5}$ s)	10^{12} K	51
BBN ($t \sim 1$ s)	10^{9} K	57
Recombination ($t = 0.38$ Myr)	3000 K	73
Today (CMB)	2.725 K	80

The trajectory is not periodic. $M(t)$ is monotonically non-decreasing, $\mathbb{RP}^3$ accumulates the actualization log permanently, and the arrow of time is geometric and irreversible (Chapter 8). The cosmic ambient has visited every cascade band from $k \approx 1$ to today's $k \approx 80$ and will continue to climb as T drops further (Chapter 24, §24.7, treats the asymptotic regime).

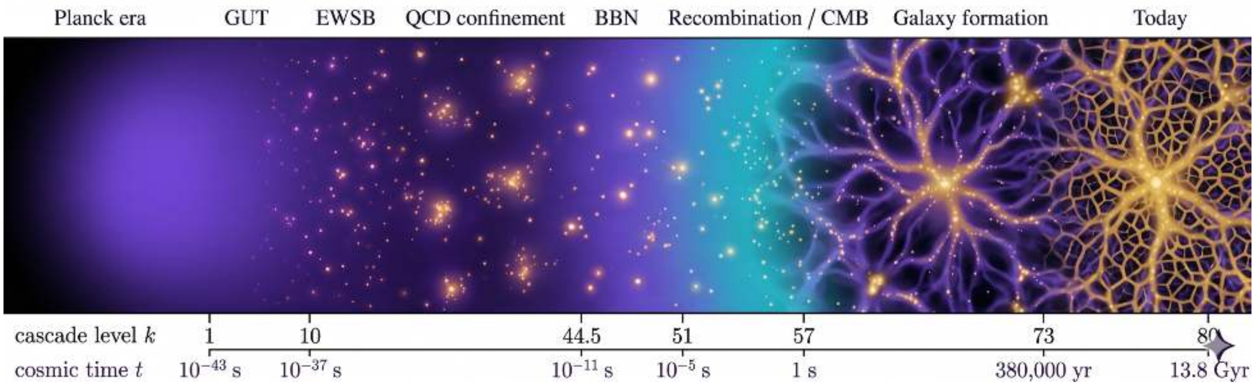

Figure 17.6: *The cosmic cascade descent: the universe walks the same k-axis that organizes the particle spectrum, and at each k the dominant physics is the same in both readings. The Planck era ($k \approx 1$, leftmost) is pure $\mathbb{CP}^3$ possibility — PSU(4) unbroken, the same regime where the full arena isometry survives at the particle scale. The GUT and electroweak epochs ($k \approx 16$, 44.5) execute the same symmetry breakings that fix Pati–Salam unification and the Higgs sector in the particle hierarchy. Confinement at $k = 51$ (cosmic age $\sim 10^{-5}$ s) is the same QCD transition that locks quarks into the pion at the particle scale. The cyan wash near recombination ($k \approx 73$) marks the cosmic microwave background as the first wide-area release of actualized light at the atomic-scale k. Structure formation organizes the cosmic web at the k-band that hosts molecular and biological structure today. The visual progression from dense undifferentiated violet (pure $\mathbb{CP}^3$ possibility, pre-actualization) at the left to organized gold tessellation ($\mathbb{RP}^3$ classical structure) at the right is what the cumulative actualization record $M(t)$ contains at each cosmic epoch. The framework's claim is literal: the cascade is one axis, and the universe walks it once. Each cosmic epoch and each particle at the same k are two readings of the same geometric position — the per-epoch ambient and the per-particle excitation. Cosmic history and the particle hierarchy are the same structure traversed at different speeds.*

17.5.1 Ambient versus Local Scales

The cosmic ambient (currently the CMB at $k \approx 80$) is the *floor* on temperatures everywhere. Anything not actively heated by stars or other local energy sources eventually equilibrates with it. Biology and conscious systems do not operate at this floor; they operate in *local thermal environments* that stellar systems heat above the cosmic ambient. Body temperature (310 K, $k \approx 75$, inside the resolvability window) is the operating point biology has settled into. Stellar heating of planets to ~ 300 K maintains this point against the colder cosmic background.

The two scales should not be confused. At any given cosmic epoch the ambient sets one k-value; local thermal environments maintained against the ambient by energy-flow processes (stars, combustion, metabolism) sit at higher temperatures and lower k. The resolvability window is a claim about *local* thermal scales, where boundary integration becomes thermally accessible and survives against the ambient floor.

The cosmic-cooling argument for the present epoch is therefore two-step rather than one-step. Step one: the cosmic ambient must have dropped enough to permit stable matter, stable bound states, and stellar systems—all of which require temperatures well below the early-universe regime. Step two: stellar systems must heat local environments into the resolvability window. Both steps are satisfied at the present epoch. Earlier epochs failed step one (too hot for stable structure of any kind); much earlier epochs also lacked stars. Far-future epochs will fail step two (stars burn out, matter dilutes, local environments cool toward the ambient floor). The window in cosmic time during which biology is physically possible is bounded by these two failures.

We exist now because both conditions hold: the cosmos has cooled enough that stable matter and stellar systems exist, and stellar heating maintains local environments at the temperatures the resolvability window requires. Cosmic cooling is necessary context; local stellar physics provides the operating temperatures. The variational principle at the cosmic scale produces the necessary context as a structural feature of the cascade descent.

17.6 The Early Universe

The Hubble parameter, the cosmological constant, and the JWST anomaly all describe the present-day cosmology of an already-developed actualization record. The framework also has to say something about the start of that record and about the inflationary epoch that standard cosmology places between the start and the hot dense state visible in the CMB. Both questions admit clean answers in PPM terms that differ from the conventional framing.

17.6.1 The First Actualization

Popular cosmology presents the Big Bang as a singular event: a point of infinite density at $t = 0$ from which spacetime springs into being (Hawking and Ellis, 1973; Hawking and Penrose, 1970). The framing presupposes that spacetime existed first as a container into which a hot dense fluid was poured. This framing does not apply in the framework. Spacetime is the accumulated actualization record (Chapter 16, §16.6); it does not predate the record it records. There is no $t = 0$ singularity because there is no spacetime container that could be singular at $t = 0$.

What does begin is the actualization log. The cumulative count $M(t)$ of τ-events was once zero, and at some point started accumulating. The cosmic trajectory traced in §17.5 picks up from that beginning, with the ambient temperature starting at the Planck scale ($T \sim 10^{32}$ K, $k \approx 1$) and dropping as $M(t)$ grows. The hot dense early state is real and standard early-universe physics applies through it—Big Bang nucleosynthesis, recombination, the CMB—these are the cosmic cascade descent at the relevant k-bands, not separate events grafted onto the framework.

What is the unactualized $\mathbb{CP}^3$ doing before $M(t)$ starts growing? This is the genuine "before the Big Bang" question. The framework has $\mathbb{CP}^3$ as the arena that supports actualization, but the actualization process is what generates the temporal structure ($\mathbb{RP}^3$ accumulates the spatial geometry, the cumulative $M(t)$ provides the temporal index). Without actualization, "before" has no operational meaning—there is no clock against which the time could be measured. The honest position is that pre-actualization $\mathbb{CP}^3$ is a meaningful geometric object but the framework has no machinery for assigning a temporal evolution to it. Whether the arena always existed, or whether the first actualization event itself constitutes the origin of meaningful time, is a question the framework declines to answer in either direction.

17.6.2 Why Inflation Isn't Needed

Standard cosmology introduces an inflationary epoch—exponential expansion in the very early universe (Guth, 1981; Linde, 1982)—to solve three problems: the CMB's apparent uniformity across causally disconnected regions (horizon problem), the absence of measurable spatial curvature (flatness problem), and the absence of magnetic monopoles that GUT phase transitions would produce (monopole problem). The framework does not need inflation because the three problems do not arise in the form that requires it.

The horizon problem assumes a hot fluid expanding from $t = 0$ with causal communication propagating outward from each point. In that picture, distant CMB patches should not have had time to thermalize. The framework describes the early universe differently: $\mathbb{RP}^3$ is the global record of actualization events, and all boundary tiles participate in the same cosmic-ambient cascade descent at each k-level. The CMB's uniformity is not the outcome of causal contact between distant patches; it is the structural consequence of every tile reaching the recombination scale at the same point on the cascade. Causal communication is the wrong frame for explaining a boundary-wide property of the actualization record.

The flatness problem assumes that Ω_k near zero today requires exponentially fine-tuned initial conditions. In the framework, spatial flatness is fixed by the holographic boundary capacity $N_\infty = \varphi^{392}$ (§17.3); the same N_∞ that sets the observable radius $R = \sqrt{N_\infty}\,\lambda_C$ and the cosmological constant $\Lambda \propto 1/N_\infty$. Spatial curvature on a manifold of radius R scales as $1/R^2$, so the same $\sqrt{N_\infty}$ that makes R enormous makes the curvature $\propto 1/N_\infty$—the identical suppression that makes Λ small. Flatness is a static topological property of the boundary that the cascade populates — the same exponential largeness of N_∞ that suppresses Λ.

The monopole problem assumes that the Standard Model gauge group emerged through a thermal symmetry-breaking event at a GUT scale, which would generically produce magnetic monopoles as topological defects. In the framework, the gauge group emerges from the $\mathbb{CP}^3 + \tau$ geometry through the Pati-Salam reduction sequence described in Chapter 15—a cascade-driven thermodynamic unfolding, not a thermal phase transition leaving topological relics. There is no mechanism that would produce monopoles in the first place, so no dilution mechanism is needed to account for their absence.

What the framework does *not* predict is the small-scale gaussian fluctuation spectrum that inflation explains as quantum fluctuations stretched to cosmological scales. The observed power spectrum of CMB temperature anisotropies has structure on scales inflation accounts for naturally; the framework has not yet produced its own derivation of the spectrum, and the consistency of the observed pattern with the framework's cascade picture is an open direction. This is an honest gap, distinct from the horizon / flatness / monopole problems that inflation was originally motivated to solve.

17.7 The Present Epoch as a Structural Moment

Standard cosmology lists a series of "present-epoch" coincidences and treats each as its own puzzle. The cosmological constant Λ has roughly the same magnitude as the present-day matter density, the discrepancy known as the cosmological coincidence problem. The universe is approximately 13.8 Gyr old, long enough for stellar evolution, heavy-element production, and biological evolution to have run their course. Structure formation has approximately completed: galaxies and clusters have virialized, and large-scale collapse has largely finished. The effective gravitational coupling $G_{\text{eff}}(z)$ has settled to its topological floor G_{micro}, the holographic screening essentially complete. The cosmic ambient has cooled to ≈ 2.7 K, cool enough to permit stable matter, bound states, and stellar systems. And stellar heating maintains local thermal environments at the scales where biology operates.

Each item reads as a separate coincidence requiring its own anthropic or fine-tuning account. In the framework they are facets of one geometric fact: the boundary capacity

$N_\infty = \varphi^{392}$. A single static number sets the cosmological constant ($\Lambda \propto 1/N_\infty$), Newton's constant ($G \propto 1/\sqrt{N_\infty}$), the observable radius ($R = \sqrt{N_\infty}\,\lambda_C$), and the light-crossing age ($T = \sqrt{N_\infty}\,\tau_C \approx 13.8$ Gyr). The age of the universe is therefore not a free parameter; it is fixed by N_∞. At that age the holographic screening of the gravitational coupling has run essentially to completion, so $G_{\text{eff}} \approx G_{\text{micro}}$; the cascade has cooled through its bands on the same timeline; structure formation has had the full T interval to assemble galaxies and clusters; and $\Lambda \propto 1/N_\infty$ takes the value at which matter density and dark-energy density are comparable today. Every quantity on the list keys off the same capacity N_∞ and the same cooling history, which is why they pick out one epoch rather than scattering.

The present epoch is the cosmic age $T = \sqrt{N_\infty}\,\tau_C$, and at that age the conditions under which biology can exist are jointly in place: a cosmos cooled enough that stable matter survives, structure assembled enough to provide stars and planets, and a gravitational coupling that has settled to its topological floor. Biology arises in this window because the same capacity that sets the timescale also sets the constants the window depends on. The framework reads the present not as a tuned coincidence but as the single structural moment the geometry specifies, with cosmology, gravitation, and biology landing in the same temporal band because they all trace to N_∞.

Every cosmological observable developed in this chapter — Λ, H_0, the sign structure of the Hubble tension, the JWST early-galaxy anomaly, the cosmic cascade descent, the present epoch as a structural moment — derives from one geometric capacity, $N_\infty = \varphi^{392}$. The framework's cosmology is the same $\mathbb{CP}^3 + \tau$ arena that produces particles and gravity, read at cosmic scale rather than per-event. Two pieces remain explicitly open: the Friedmann-backreaction calculation that would quantify the magnitudes of the Hubble-tension biases (signs are derived above; magnitudes are not), and the baryon-capacity coincidence $N_{\text{baryon}} \sim N_\infty$ which the framework currently accepts as a Dirac-type large-number relation pending derivation. The next chapter checks whether this cosmological reading of N_∞ coheres with the spectral derivation of α from $\mathbb{CP}^3$'s heat kernel and the holographic derivation of G from $\mathbb{RP}^3$'s boundary — three independent readings of the same manifold, meeting at the relation $(2\pi)^{27}\sqrt{\alpha} = \varphi^{98} = N_\infty^{1/4}$.

Chapter 18

Derived Constants

The previous chapters built the physical world piece by piece. The fiber field (Chapter 12) T.13, 18.2
supplied the primitive; the hierarchy (Chapter 14) set the energy scales; the particle spectrum (Chapter 15) populated those scales; gravity (Chapter 16) emerged from the boundary's holographic capacity, fixing G, with cosmology (Chapter 17) reading the same capacity at cosmic scale to fix Λ and H_0; quantum mechanics (Chapter 13) supplied the formal language for the projection itself. Each chapter delivered constants, and each derivation worked in isolation by drawing on a specific feature of the manifold.

This chapter asks the question those derivations leave open: do they cohere? Different constants come from different geometric features. α is read from the spectral content of the τ-projection. G is read from the holographic dilution of actualization events on $\mathbb{RP}^3$. $N_\infty = \varphi^{392}$ is read from the icosahedral packing of the boundary at the Compton scale. The three derivations share no machinery. They have to cohere because they all live on the same manifold; whether they actually do is what this chapter checks.

Two pieces carry the chapter.

The first is the fine-structure constant, treated as a case study for how a single constant is geometrically determined (Section 18.1). α is computed three independent ways: from a heat-kernel ratio on $\mathbb{CP}^3$ (Route I), from inverting Newton's constant established in Chapter 16 (Route II), and from a semiclassical instanton amplitude across the Kähler barrier (Route III). Each route uses different mathematical machinery and addresses a different feature of the geometry. All three converge on the observed value to within a percent. That convergence is the strongest available evidence that α is determined by the manifold.

The second is the master self-consistency relation $(2\pi)^{27}\sqrt{\alpha} = \varphi^{98}$ (Section 18.2). The relation links the three numbers that dominate the framework: 2π (the size of one actualization step), α (the efficiency with which information crosses the projection), and φ (the constant fixed by the icosahedral packing of the actual world). The relation does not *determine* those numbers; each is fixed by an independent geometric calculation that does not reference the others. What the relation does is verify that the independent calculations cohere. If the heat-kernel α and the icosahedral φ^{392} packing did not satisfy the equation, the framework would point to incompatible Planck masses from the hierarchy and the gravitational directions, and the catalog of constants would fork. They satisfy the relation to 0.38%, with the residual identified as computable corrections to each of the underlying derivations.

The hydrogen atom is the closest available analogy. Hydrogen's energy levels are eigenvalues of the Schrödinger equation set by the Coulomb potential and the normalizability condition; no separate parameter is dialed to make $E_1 = -13.6$ eV come out, because the equation and the boundary condition together select the value. The constants treated here are the same kind of object, one level deeper. The manifold itself supplies both the "equation" (the Fubini-Study metric, the τ-projection, the holographic capacity) and the values it admits. The constants are discrete because the spectral problem they solve is discrete; they are self-contained because the operator and the boundary condition both live on $\mathbb{CP}^3$; and they are universal across sectors because every Standard Model coupling and every cosmological parameter reads off the same geometric object.

Figure 18.1 maps the dependencies. Three independent features of the $\mathbb{CP}^3 + \tau$ arena—Kähler structure, spectral geometry, and topology—feed three primary constants ($g = 2\pi$, α, and $N_\infty = \varphi^{392}$), which then determine everything downstream through closed-form formulas.

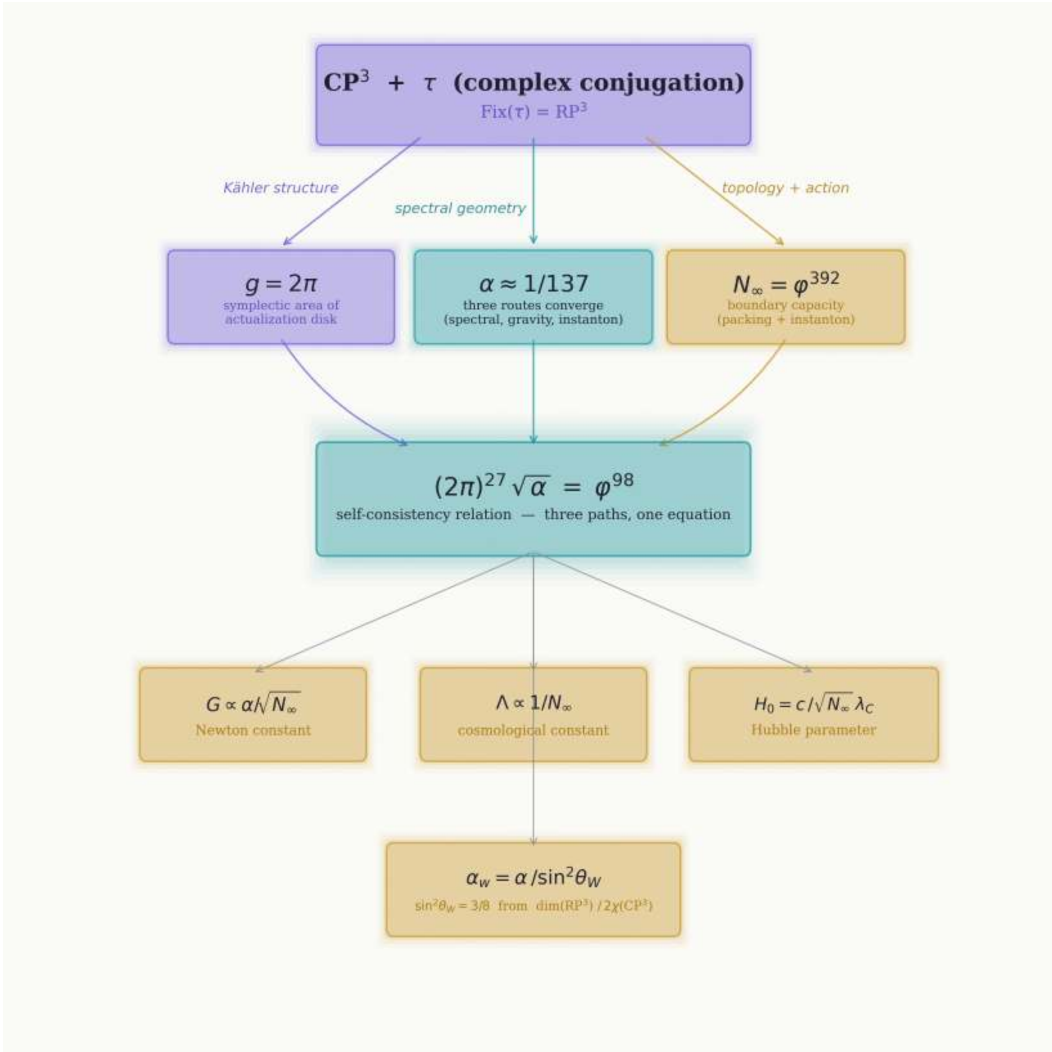

Figure 18.1: *The derivation dependency tree. Three independent features of the* $\mathbb{CP}^3 + \tau$ *arena—Kähler structure, spectral geometry, and topology—yield* $g = 2\pi$, $\alpha \approx 1/137$, *and* $N_\infty = \varphi^{392}$ *respectively. These converge on the self-consistency relation* $(2\pi)^{27}\sqrt{\alpha} = \varphi^{98}$. *Every physical constant below the relation is expressed as a formula in the upstream quantities:* $G \propto \alpha/\sqrt{N_\infty}$, $\Lambda \propto 1/N_\infty$, $H_0 = c/\sqrt{N_\infty}\,\lambda_C$. *The weak coupling* $\alpha_w = \alpha/\sin^2\theta_W$ *inherits* α *from spectral geometry and* $\sin^2\theta_W = 3/8$ *from the topological ratio* $\dim(\mathbb{RP}^3)/2\chi(\mathbb{CP}^3)$. *Every constant is downstream of the geometry; the diagram has no circular dependencies.*

18.1 The Fine-Structure Constant

The fine-structure constant $\alpha \approx 1/137$ governs the strength of electromagnetic interactions. Within the framework, it measures something specific: the fraction of information that survives the actualization projection intact. When τ projects from $\mathbb{CP}^3$ to $\mathbb{RP}^3$, some content crosses the boundary efficiently (the τ-even sector) and some is stripped (the τ-odd sector). The fine-structure constant is the ratio of transferred to stripped information, determined entirely by the spectral geometry of the embedding.

Three independent calculations arrive at the same value. Each uses different mathematical machinery, addresses different features of the geometry, and was developed without reference to the others. Their convergence is the strongest evidence that α is indeed determined by the manifold.

18.1.1 Route I: Heat Kernel

The heat kernel is the standard tool in spectral geometry (DeWitt, 1965; Gilkey, 1975; Seeley, 1967) for reading a manifold's shape off the spectrum of its Laplacian. Imagine a unit of heat (or probability, or information) deposited at a point of the manifold and allowed to diffuse for time t. At early times the heat sees only the local geometry; at late times it has explored the whole manifold and feels its global topology. The trace of the heat kernel, $\Theta(t) = \sum_k d_k\, e^{-\lambda_k t}$, sums the exponentially suppressed contribution of each Laplacian eigenmode and gives a single number that characterises the manifold at the diffusion scale t.

For $\mathbb{CP}^3$ with the Fubini-Study metric, the eigenvalues of the Laplacian are $\lambda_k = k(k+3)$ with degeneracies d_k that grow as k^5. The involution τ acts on each eigenspace, splitting modes into τ-even (preserved by the projection) and τ-odd (stripped by it). Two heat traces follow: the full trace $\Theta_{\mathbb{CP}^3}(t)$ that counts every mode with its multiplicity, and the twisted trace $\Theta^\tau(t)$ that counts only the τ-even content. The full trace measures how much of $\mathbb{CP}^3$ exists as a quantum geometry; the twisted trace measures how much of that geometry survives actualization. Their ratio is the fraction of the arena's spectral content that fails to cross the boundary—the fraction projected out per cycle.

The diffusion time t^* is set by a half-variance condition on the spectral gap. The first nonzero eigenvalue is $\lambda_1 = 4$, and the condition $\lambda_1^2 t^* = 1/2$ fixes $t^* = 1/32$. This is the unique time at which the leading mode has decayed to $e^{-1/8}$ of its initial weight—suppressed enough to separate the τ-even and τ-odd contributions in the exponential decay, but not so suppressed that the trace collapses onto the zero mode alone. No free parameter enters the choice; t^* is determined by the spectral gap of the Laplacian on $\mathbb{CP}^3$.

Evaluated at $t^* = 1/32$, the two heat traces converge by $k = 20$ to $\Theta_{\mathbb{CP}^3}(t^*) \approx 5814$ and $\Theta^\tau(t^*) \approx 42.4$. The full trace is dominated by the high-degeneracy modes near the convergence cutoff; the twisted trace is dominated by the lowest half-dozen modes. The ratio is

$$\frac{1}{\alpha} \approx \frac{\Theta_{\mathbb{CP}^3}(t^*)}{\Theta^\tau(t^*)} \approx 137.257.$$

Compared to the observed $1/\alpha = 137.036$ (Particle Data Group, 2024), this is an agreement of 0.16%.

The physical reading: α counts how much of the arena's information content crosses the actualization boundary intact per cycle. The heat-kernel ratio measures this directly. No Coulomb law, no QED Feynman diagram, no perturbation theory enters—the value emerges as a topological invariant of $\mathbb{CP}^3$ together with the τ-action. Route I is the foundational geometric derivation; the other two routes verify it from independent directions.

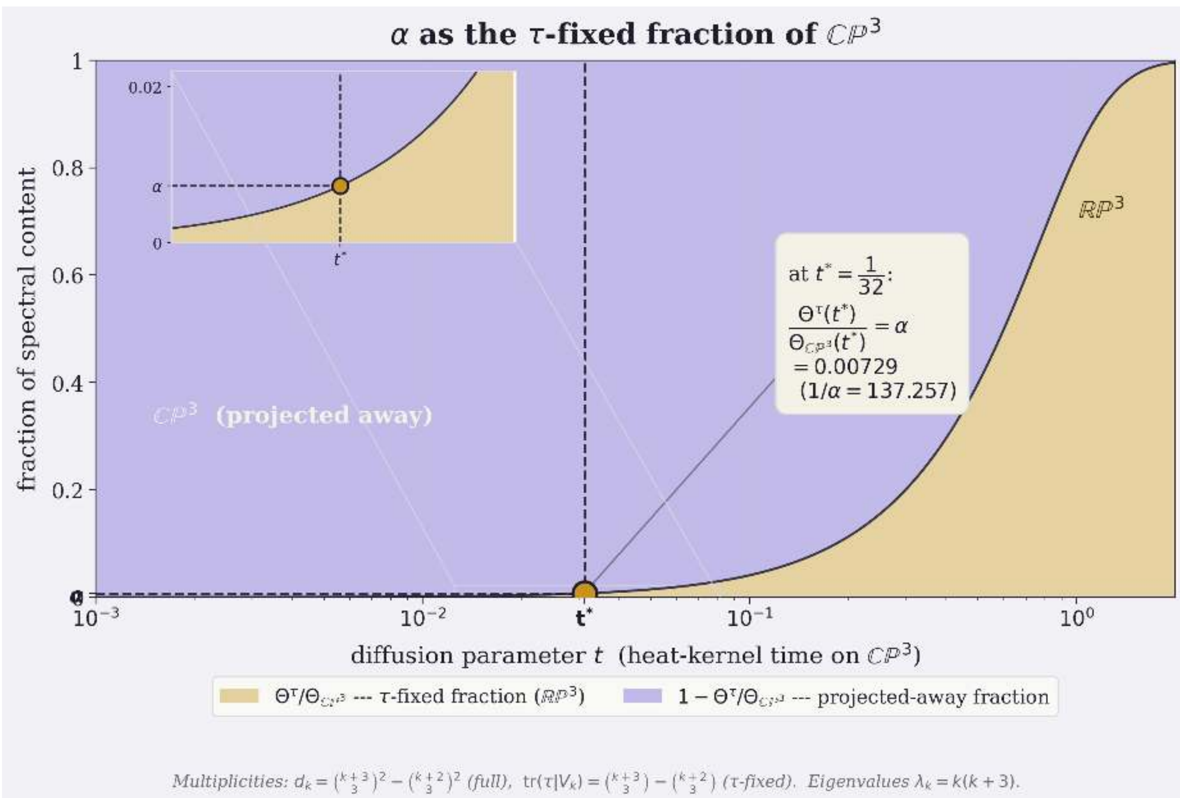

Figure 18.2: *α as the τ-fixed fraction of $\mathbb{CP}^3$. Total spectral content of $\mathbb{CP}^3$ at heat-kernel time t partitioned into the τ-fixed piece (gold, $\Theta^\tau/\Theta_{\mathbb{CP}^3}$, the $\mathbb{RP}^3$-supported content) and the projected-away piece (violet). Every column sums to one. In the deep UV, high-degeneracy modes dominate and almost no content is τ-symmetric. In the deep IR only the constant mode survives and the τ-fixed fraction goes to one. At the half-variance scale $t^* = 1/(2(n+1)^2) = 1/32$ fixed by the spectral gap of $\mathbb{CP}^3$, the τ-fixed fraction is exactly $\alpha = 0.00729$ ($1/\alpha = 137.257$, 0.16% from the observed* 137.036 *(Particle Data Group, 2024)). The inset shows the crossing on a linear y-axis. Computed from the closed-form CP^3 multiplicities; no fitted parameter enters.*

18.1.2 Route II: Gravitational Self-Coupling

The second route reaches α through gravity. Newton's constant G was derived in Chapter 16 from the information lost per actualization event, diluted by the holographic capacity of the $\mathbb{RP}^3$ boundary. That derivation produced a closed-form formula fixing G in terms of α, the pion mass, and the boundary capacity N_∞:

$$G \;=\; \frac{16\pi^4\,\hbar c\,\alpha}{m_\pi^2\,\sqrt{N_\infty}}.$$

Each factor records a separate piece of the geometry. The $16\pi^4$ counts the volume of the projection from the six real dimensions of $\mathbb{CP}^3$ down to the three of $\mathbb{RP}^3$. The α in the numerator is the same transmission efficiency that Route I extracts from the heat kernel—gravity inherits a factor of α because the same fraction of arena content that survives the electromagnetic projection also sources spacetime curvature. The m_π^2 supplies the energy scale; the $\sqrt{N_\infty}$ in the denominator dilutes the per-event coupling by the holographic capacity, which is the topological count of independent fiber sections on the $\mathbb{RP}^3$ boundary. Read the formula left to right and it states that gravity is what is left of the actualization rate after dividing out the topological capacity.

Solving for α inverts the relation:

$$\alpha \;=\; \frac{G\,m_\pi^2\,\sqrt{N_\infty}}{16\pi^4\,\hbar c}.$$

This is now an equation with no free parameters once G, m_π, and N_∞ are supplied as inputs. Substituting the observed Newton constant $G = 6.674\times10^{-11}\ \mathrm{m^3\,kg^{-1}\,s^{-2}}$, the charged pion mass $m_\pi = 139.57\ \mathrm{MeV}/c^2$, and the topological capacity $N_\infty = \varphi^{392}$ gives

$$\frac{1}{\alpha} \;\approx\; 137.6,$$

an agreement with the observed value of 0.4%.

The mathematics of this route shares no machinery with Route I. Route I works from the heat kernel of the Fubini-Study Laplacian. Route II works from the holographic relation between accumulated information loss and the curvature of spacetime. The two routes meet because they read the same transmission efficiency α off the same manifold from opposite ends—one through the spectral geometry of the projection itself, the other through the gravitational backreaction of what the projection produces. Route II is therefore a consistency check rather than an independent determination of α: it uses the observed G as input and recovers α, which demonstrates that the G formula and the heat-kernel α are mutually consistent within the framework. The agreement also serves as a quantitative check on the gravitational derivation; if Route II had returned an α off by 20%, the G formula would need revisiting.

18.1.3 Route III: Instanton Tunneling

The third route reaches α through semiclassical quantum mechanics on $\mathbb{CP}^3$. The Kähler structure produces a potential barrier between the actualized submanifold $\mathbb{RP}^3$ and the normal directions that τ strips. Crossing the barrier is forbidden classically and proceeds by tunneling. In semiclassical quantum mechanics the tunneling rate is governed by an *instanton*—a finite-action classical solution to the Euclidean field equations that interpolates between the two sides of the barrier (Belavin et al., 1975; Coleman, 1985). The amplitude is exponentially suppressed in the instanton action.

The relevant instanton is a degree-3 holomorphic map $T^2 \to \mathbb{CP}^3$ (Cho and Oh, 2006), and its action evaluates to

$$S_{\text{inst}} \;=\; 30\pi \;\approx\; 94.248.$$

The integer 30 is the fourth square pyramidal number $P_4 = 1^2+2^2+3^2+4^2 = 30$. Two readings of the same number connect to the geometry. Algebraically, 30 counts the dimension of the moduli space of the degree-3 map—each of the four homogeneous coordinates contributes a square's worth of independent deformation directions, graded by which component is being deformed, and the four squared contributions sum to thirty. Geometrically, the four terms correspond to the four fact types of Chapter 9: each fact type contributes a barrier-height proportional to the square of its dimension, and the squares add as a pyramidal stack. Both readings deliver the same exponent because the moduli count and the fact-type budget are the same combinatorial object viewed from different sides.

The bare instanton amplitude—the contribution from the classical saddle alone, before quantum corrections from fluctuations around it—is

$$R_\tau^{\text{bare}} \;=\; \tfrac{1}{2}\, e^{-30\pi} \;\approx\; 5.9 \times 10^{-42}.$$

This is roughly 10^{39} smaller than $\alpha \approx 7.3 \times 10^{-3}$. The discrepancy is supplied by two pieces of standard semiclassical machinery ('t Hooft, 1976) that have not yet been computed: a collective coordinate integral over the 30 zero modes of the instanton (which contributes a positive power of the instanton scale times a Jacobian), and a one-loop functional determinant ratio between the instanton-background fluctuation spectrum and the vacuum spectrum. Together these are expected to supply the missing factor. Until that calculation is closed, the bare amplitude alone does not give α.

What Route III *does* verify is the exponential structure. The identity

$$e^{-30\pi} \approx \varphi^{-196}$$

holds to 0.07% in the exponent. The integer $196 = 2 \times 98$ is twice the exponent that appears in the master self-consistency relation $(2\pi)^{27}\sqrt{\alpha} = \varphi^{98}$—the instanton route and the self-consistency relation use the same exponent structure, arrived at through different mathematics. This connection between 30π and φ^{196} provides the strongest available evidence that the instanton sector contributes to α in the framework's predicted way; Route III's status is exponential structure verified, prefactor outstanding.

18.1.4 Route IV: Standard Model Composition

The fourth route applies the standard Standard Model relation $\alpha = \alpha_Y\alpha_2/(\alpha_Y + \alpha_2)$ on top of PPM's gauge-structure derivation. PPM derives the Pati-Salam embedding from $\mathbb{CP}^3 + \tau$, and from that embedding the weak mixing angle at the breaking scale falls out as $\sin^2\theta_W = 3/8$ (verified against SM one-loop running of observed couplings to 0.13%). Inserting that prediction into the standard composition formula with the observed couplings at M_Z, and running the result to zero momentum via standard QED vacuum polarisation, returns $1/\alpha(0) = 136.978$ (-0.042% from observed). Route IV is composition-style rather than direct-geometric, but the calculation is structurally independent of Routes I–III—it does not share their spectral, cosmological, or instanton-action machinery. The full derivation lives in Technical Reference Ch. 13.

18.1.5 Why the Routes Converge

All four routes agree because they measure the same geometric object from different vantage points. The heat kernel sees the ratio of τ-even to τ-odd spectral content directly. The gravitational route sees it through the backreaction of accumulated information loss onto spacetime curvature. The instanton route sees it through the tunneling rate across the Kähler barrier. The gauge-composition route sees it through the gauge-group structure that the Pati-Salam embedding forces, threading the standard SM relation between α and the electroweak couplings.

The situation is analogous to measuring the radius of a sphere by three methods: from its circumference, from its surface area, and from its volume. All three give the same answer because they describe the same object. Here, the "sphere" is the $\mathbb{CP}^3 \to \mathbb{RP}^3$ embedding, and α is one of its intrinsic geometric properties.

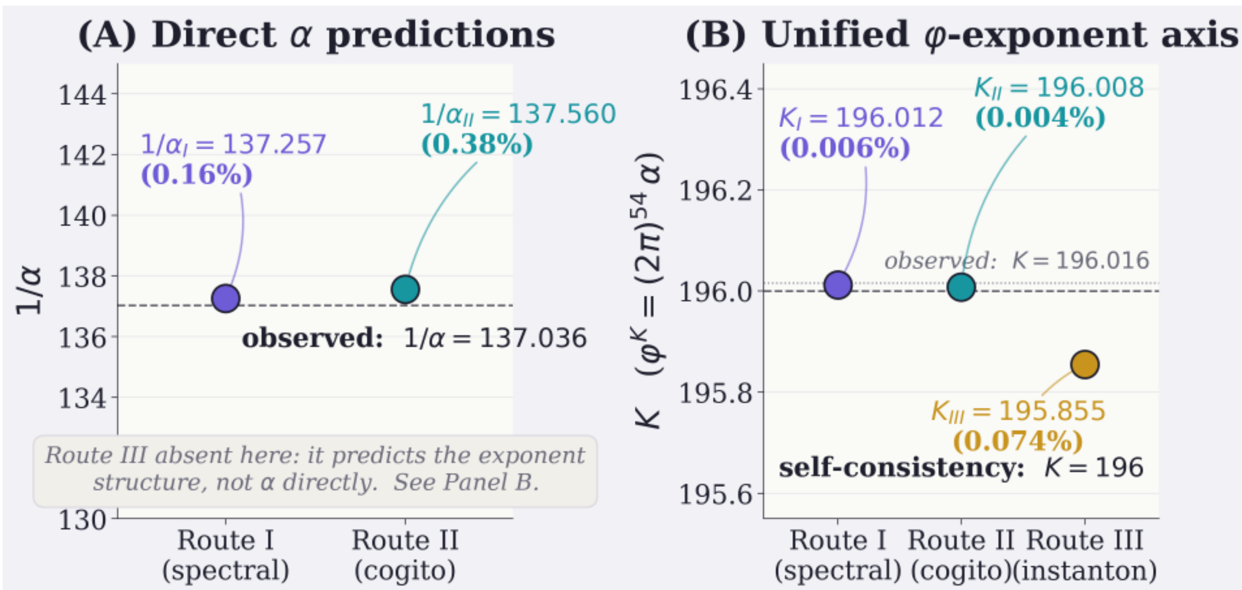

Figure 18.3: *Three independent routes to α, plotted on two complementary axes.* Panel A *shows the $1/\alpha$ predictions that Routes I and II make directly: the heat-kernel ratio (Route I, blue) gives $1/\alpha = 137.257$, 0.16% from observed (Particle Data Group, 2024); the gravitational inversion (Route II, green) gives $1/\alpha = 137.560$, 0.38%. Route III is absent from this panel because the instanton sector predicts the exponential structure of α rather than its value (the prefactor remains uncomputed).* Panel B *plots all three routes on a unified φ-exponent axis derived from the squared self-consistency relation $(2\pi)^{54}\,\alpha = \varphi^K$ with $K = 196$. Routes I and II compute K indirectly via their α predictions; Route III computes K directly from the instanton action via $K = 30\pi/\ln\varphi$. All three cluster within 0.1% of $K = 196$, the integer the relation predicts: Route I at 196.012, Route II at 196.008, Route III at 195.855. No route is excluded on this axis, and the convergence reads as the same geometric fact verified three ways.*

18.2 The Self-Consistency Relation

The three quantities that dominate the framework—the scaling factor $g = 2\pi$, the fine-structure constant α, and the golden ratio φ—are linked by a single equation:

$$(2\pi)^{27}\sqrt{\alpha} \;=\; \varphi^{98}.$$

This is the master self-consistency relation. It does not *determine* any of the three numbers; each is fixed by an independent geometric calculation that does not reference the others. What the relation does is verify that those independent calculations cohere. It is a closure check on the framework's two routes to the Planck mass.

18.2.1 How the Relation Emerges

Two equations anchor the framework at the pion scale. The hierarchy formula reads the Planck mass off the top rung of the cascade:

$$m_{\text{Planck}}^{(\text{hier})} \;=\; m_\pi\,(2\pi)^{25}.$$

Twenty-five powers of 2π, one per fiber-stripping step from $k = 51$ at the pion scale up to $k = 1$ at Planck. The gravitational formula reads the same Planck mass off Newton's constant:

$$m_{\text{Planck}}^{(\text{grav})} \;=\; \sqrt{\hbar c/G} \;=\; \frac{m_\pi\,N_\infty^{1/4}}{4\pi^2\sqrt{\alpha}},$$

using $G = 16\pi^4\,\hbar c\,\alpha/(m_\pi^2\sqrt{N_\infty})$ from Section 18.1.

Both expressions name the same physical scale. Setting them equal, the pion masses cancel, $4\pi^2 = (2\pi)^2$ absorbs into the leading power, and $N_\infty = \varphi^{392}$ takes its fourth root:

$$(2\pi)^{27}\sqrt{\alpha} \;=\; \varphi^{98}.$$

The exponent 27 is $25 + 2$: twenty-five hierarchy steps plus two from the gravitational projection factor $16\pi^4 = (2\pi)^4$, halved when the Planck mass is extracted as a square root. The exponent 98 is $392/4$: N_∞ enters the gravitational formula under a square root, and the Planck mass takes a square root again. The $\sqrt{\alpha}$ on the left appears because G is linear in α and the Planck mass takes the square root. Nothing has been added; the equation is what remains when the two routes to the Planck mass are required to agree.

18.2.2 Local Equals Global

The left side of the relation is local. It collects the size of one actualization step (2π) and the efficiency with which information crosses it (α)—quantities a single QED experiment in a single laboratory could measure in principle. The right side is global. The exponent $392/4 = 98$ counts independent tile-positions on the spatial manifold of the universe, a quantity no local experiment can reach. The same icosahedral tiling that Chapter 17 introduced (Figure 17.3) is what the right side measures: the local Compton cell and the full N_∞-tile boundary are the same structure at two resolutions, and the self-consistency relation is the algebraic statement that binds the two resolutions together.

The equation sets the two sides equal. Both sides measure the informational content of a single actualization event. A photon-electron coupling is one such event: it reads a piece of $\mathbb{CP}^3$ content, strips a fraction $1 - \alpha$ as entropy, and deposits the surviving facts into one Compton-scale slot on the $\mathbb{RP}^3$ boundary. The local side of the relation assembles the per-event quantities—the fiber step 2π that the projection takes and the survival fraction α—into a measure of how much information one event transmits. The global side reads the same content off the boundary: $N_\infty = \varphi^{392}$ supplies the total capacity for actualizations to occupy, and $\varphi^{98} = N_\infty^{1/4}$ is what one event's share of that capacity comes to once the gravitational scaling is unwound. Geometrically, φ^{98} counts tile-radii out to the geometric midpoint of the framework's length scales: since $R = \sqrt{N_\infty}\,\lambda_C$, the geometric mean $\sqrt{R\,\lambda_C} = N_\infty^{1/4}\,\lambda_C \approx 426$ km sits exactly halfway, on a logarithmic axis, between the Compton wavelength and the Hubble radius. The exponent is the structural mark in the middle of the framework's length hierarchy (Figure 18.4).

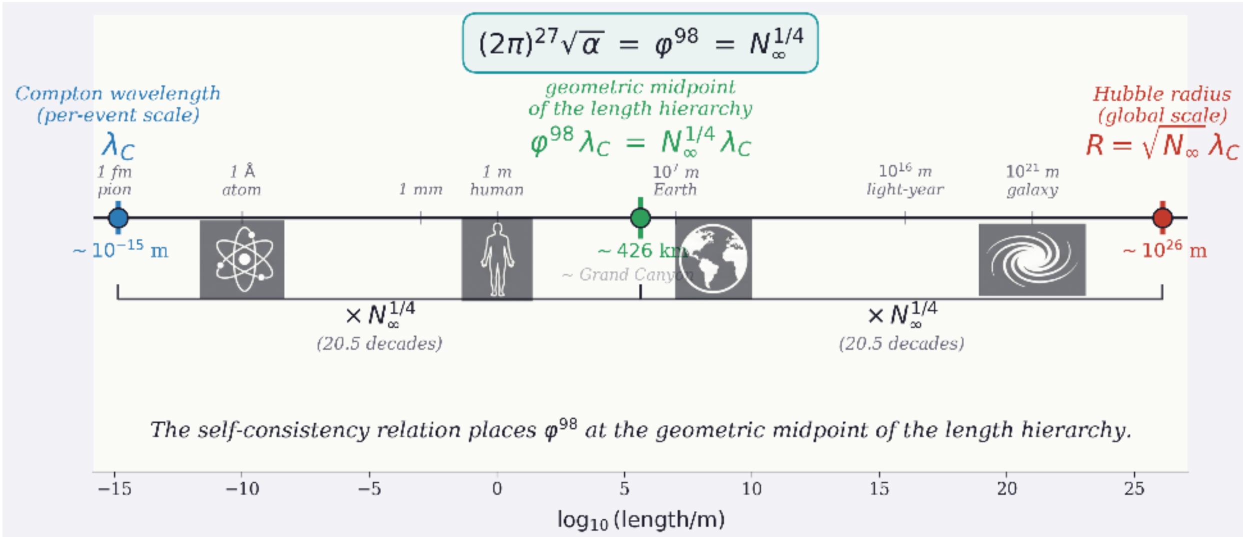

Figure 18.4: *The relation places φ^{98} at the geometric midpoint of the length hierarchy. The horizontal axis is logarithmic length in metres. Three anchor scales: λ_C (the pion Compton wavelength, the framework's per-event scale, $\sim 10^{-15}$ m), the Hubble radius $R = \sqrt{N_\infty}\,\lambda_C$ ($\sim 10^{26}$ m), and the geometric midpoint $N_\infty^{1/4}\lambda_C \approx$ 426 km (roughly the length of the Grand Canyon). The two halves of the axis are equal in log-units; each half is $\times N_\infty^{1/4}$ wide. The relation $(2\pi)^{27}\sqrt{\alpha} = \varphi^{98} = N_\infty^{1/4}$ is the algebraic statement that the same exponent φ^{98} shows up at the midpoint regardless of which side one approaches from.*

Per-event transmission and per-event capacity have to match because they describe the same operation viewed from opposite sides: the projection moving content from $\mathbb{CP}^3$ into $\mathbb{RP}^3$. If the local measure exceeded the global one, each event would carry more information than the boundary can hold per slot, and the projection would stall. If smaller, slots would go unwritten. The relation is the unique calibration at which transmitted information per event equals available capacity per event.

The fine-structure constant and the icosahedral capacity are two coordinates on a single property of the manifold: how much information the projection can move per event. A complete description of one event—its fiber step 2π, its survival fraction α, its position among the N_∞ tiles of the boundary—determines through the relation every cosmological quantity the framework produces: G, Λ, H_0, the Hubble radius, the cosmic age, the depth of the energy hierarchy.

Standard holographic intuition assigns the information content of a 3D region to its 2D boundary; the self-consistency relation identifies the global structure with each event individually. This is what allows new events to take place coherently against the record of prior ones: the record is available at the locus of every event because the relation makes the local data and the global structure the same data. Two events at different epochs are two expressions of one geometric fact; their consistency is built into the same algebra that determines either of them in isolation.

α and Λ are linked algebraically through the relation; their values are not independent. Both numbers are read off the same $\mathbb{CP}^3 + \tau$ structure. The constants of physics are the unique set of values for which the geometry is self-consistent at every scale at once.

The clause "at every scale at once" has a structural underpinning. The hierarchy coordinate k is a flat ruler with respect to the spinor bundle (9 §Cascade as a Geometrically Flat Coordinate; The k-Scale as a Flat Coordinate above): moving along k rescales energy and changes position, leaving the spin structure on $\mathbb{RP}^3$, the Hopf-fiber structure, and every quantum-geometric invariant of the τ-projection alone. The same fiber runs at the QED scale, the confinement scale, the electroweak scale, and the critical scale. The self-consistency relation is therefore one algebraic identity that holds at every k simultaneously, because the underlying fiber does not change with scale; the equation binds local data and global capacity at one k and at every k for the same structural reason.

18.2.3 Numerical Status as Coherence Test

With the observed $\alpha = 1/137.036$:

$$\frac{(2\pi)^{27}\sqrt{\alpha}}{\varphi^{98}} = 1.0038,$$

a 0.38% residual. The numerator runs through the heat-kernel ratio of the Fubini-Study Laplacian on $\mathbb{CP}^3$. The denominator runs through the icosahedral packing of $\mathbb{RP}^3$ at the Compton scale. The two calculations share no mathematical machinery: different operators, different manifolds, different counting problems. The agreement constrains both calculations simultaneously, and the residual identifies the magnitude of the higher-order corrections still to be computed at each step.

A third independent calculation reinforces the structure. The degree-3 instanton action across the Kähler barrier evaluates to 30π, and the identity $e^{-30\pi} \approx \varphi^{-196}$ holds to 0.07% in the exponent. Since $196 = 2 \times 98$, the semiclassical tunneling sector arrives at the same exponent that the heat-kernel and packing routes converge on, through a third piece of disjoint mathematics. Three independent calculations, one algebraic constraint.

The 0.38% residual is the test that the catalog does not fork; an agreement of 5% or worse would have indicated incompatible Planck masses from the hierarchy and the gravitational directions.

The relation has the structural shape of an Atiyah–Singer index theorem (Atiyah and Singer, 1968)—a spectral number equating a topological number—but an explicit theorem is open work.

18.3 The Structural Anchor

The framework's catalog operationally anchors on m_π: every mass formula carries an explicit m_π, every cascade computation uses m_π as its reference rung, and pinning m_π to its measured value of 134.98 MeV (Particle Data Group, 2024) fixes every prediction the framework makes. This is how the document does its numerical work and will remain so.

Structurally, m_π is not where the framework's confinement physics sits. m_π is the mass of the lightest hadron — a chiral pseudo-Goldstone boson whose value reflects QCD chiral-symmetry dynamics rather than a primitive feature of the $\mathbb{CP}^3 + \tau$ geometry. The structurally fundamental scale is the *confinement scale*: the energy at which the H_α radial-bulk sector opens up on $\mathbb{CP}^3$.

The Kähler ground state. Chapter 13 identifies this scale explicitly. The radial sector of H_α on $\mathbb{CP}^3$ with Kähler potential $V_{\text{Kähler}} = m_\pi c^2 \log(1 + |z|^2/\lambda_C^2)$ has a ground-state energy

$$\varepsilon_0 \;\approx\; 1.70573\, m_\pi c^2 \;\approx\; 231 \text{ MeV},$$

a value computed numerically (Technical Reference Ch. 7, §The Energy Identity). No τ-event lands below ε_0 through $\mathbb{CP}^3$ bulk modes: it is the minimum energy a bulk actualization can carry.

The threshold at ε_0. Below ε_0 the $\mathbb{CP}^3$ radial-bulk spectrum has no eigenvalue available. Events at sub-ε_0 energies land on other sectors — non-radial H_α modes, surface eigenmodes of the $\mathbb{RP}^3$ Laplacian, or the topological Jackiw–Rebbi zero mode (Chapter 13, §13.2). Above ε_0 the $\mathbb{CP}^3$ radial-bulk modes $\varepsilon_n \approx (2n(n{+}3) + 1.70573)\, m_\pi c^2$ become accessible, and heavy fermions populate them (charm near ε_1, Higgs near ε_{20}, top near ε_{24}). ε_0 is the energy at which the H_α radial-bulk sector opens. Confinement in framework-native terms is this threshold.

Identification with Λ_{QCD}. $\varepsilon_0 \approx 231$ MeV sits within the conventional Λ_{QCD} band (~ 200–300 MeV) where QCD running becomes nonperturbative (Particle Data Group, 2024). The framework's structural confinement scale and QCD's empirical confinement scale coincide numerically and do the same physical job: marking the energy below which the relevant degrees of freedom are confined and above which they become accessible. $\varepsilon_0 = \Lambda_{\text{QCD}}$ is the structural identification. QCD treats Λ_{QCD} as a parameter to be fit from data; the framework derives the same scale as the ground-state energy of H_α on $\mathbb{CP}^3$.

m_π as derived energy-scale reference. On this reading, m_π is downstream of ε_0:

$$m_\pi c^2 \;=\; \frac{\varepsilon_0}{1.70573} \;\approx\; \frac{231\ \text{MeV}}{1.70573} \;\approx\; 135\ \text{MeV}.$$

The lightest hadron mass emerges as the confinement scale divided by a specific $\mathbb{CP}^3$ spectral-geometric constant. The ratio 1.70573 is a spectral invariant of $(\mathbb{CP}^3, g_{\text{FS}}, V_{\text{Kähler}})$, established in Chapter 13 §13.2 as the ground-state eigenvalue of the radial reduction $-\frac{1}{2J}\partial_r(J\,\partial_r) - 2\log\cos r$ on $r \in [0, \pi/2)$ with $J(r) = \sin^5 r\, \cos r$, and computed numerically (Technical Reference Ch. 7, §The Energy Identity). Its elementary closed form is an open question; the natural epistemic parallel is Apéry's constant $\zeta(3) \approx 1.20206$, which is well-defined, structurally meaningful, and has no known elementary closed form. Closed-form status does not affect the constant's role: ε_0 is pinned numerically with arbitrary precision and can serve as the structural anchor whether or not its closed form is eventually found.

What this changes and what it does not. Every numerical prediction in the document remains unaltered. The mass-scale conversion $\varepsilon_0 = 1.70573\, m_\pi c^2$ is a fixed relationship; specifying m_π and specifying ε_0 pin each other. Formulas continue to carry m_π for clarity, and the cascade keeps its reference rung at $51 = 51$ where m_π sits. What changes is the framework's posture about *where* the empirical input enters. Structurally the framework anchors on the confinement scale ε_0, a $\mathbb{CP}^3$ geometric output identified with Λ_{QCD}. m_π is the energy-scale reference, with the structural anchor and the reference describing one physical scale read from two sides.

18.4 What the Geometry Determines

The framework's full inventory of physical constants assembles from a short list of geometric inputs and a single energy-scale reference. This section pulls the threads together.

Inputs. Three features of $\mathbb{CP}^3$ supply everything else: the Hopf fiber circumference $g = 2\pi$ from the Kähler structure, the fine-structure constant $\alpha \approx 1/137$ from the spectral geometry of the τ-projection, and the boundary capacity $N_\infty = \varphi^{392}$ from the icosahedral packing of $\mathbb{RP}^3$ at the Compton scale. None of the three references the others; each is computed from a different feature of the manifold. The energy scale is set by the framework's structural anchor ε_0 (§18.3), with $m_\pi = \varepsilon_0/1.70573$ serving as the energy-scale reference the document uses throughout. The reference value is taken from the Particle Data Group (Particle Data Group, 2024). The framework asks nothing further of measurement.

The cascade. The energy hierarchy fixes a mass at every level

$$m(k) \;=\; m_\pi\,(2\pi)^{(51-k)/2},$$

with the pion's Compton wavelength $\lambda_C = \hbar/(m_\pi c)$ supplying the fundamental cell on the boundary. Newton's constant follows from the gravitational route to α inverted (Section 18.1):

$$G \;=\; \frac{16\pi^4\,\hbar c\,\alpha}{m_\pi^2\,\sqrt{N_\infty}}.$$

The cosmological constant expresses the same boundary capacity as a spatial curvature, and the Hubble rate expresses it as a frequency:

$$\Lambda \;=\; \frac{2\,(m_\pi c^2)^2}{(\hbar c)^2\,N_\infty}, \qquad H_0 \;=\; \frac{c}{\sqrt{N_\infty}\,\lambda_C}.$$

Each line writes a constant in terms of the three geometric inputs and the one energy-scale reference.

The Planck quantities follow algebraically. The Planck mass, length, time, and energy are conventionally treated as a separate scale set by Newton's constant. Once G is fixed by the formula above, all four are consequences:

$$m_{\text{Planck}} = \sqrt{\hbar c/G}, \quad \ell_{\text{Planck}} = \sqrt{\hbar G/c^3}, \quad \tau_{\text{Planck}} = \sqrt{\hbar G/c^5}, \quad E_{\text{Planck}} = \sqrt{\hbar c^5/G}.$$

Reading the hierarchy at the top rung recovers the same mass scale independently:

$$m(1) \;=\; m_\pi\,(2\pi)^{25} \;\approx\; m_{\text{Planck}},$$

with the agreement controlled by the master relation $(2\pi)^{27}\sqrt{\alpha} = \varphi^{98}$ to its 0.38% residual. The Penrose-Diósi gravitational decoherence rate $\tau_{\mathrm{grav}}(m) = \hbar^2/(Gm^3c)$ evaluates to τ_{Planck} at $m = m_{\mathrm{Planck}}$ identically—an algebraic identity (Chapter 13) that means the same scale shows up as the gravitational coupling fixed point, the top rung of the τ-actualization hierarchy, and the gravitational decoherence ceiling. These are three readings of one geometric fact.

The closure check. The master self-consistency relation is what makes the cascade possible. It states that the spectral α and the icosahedral N_∞, derived without reference to each other, satisfy the constraint imposed by anchoring both the energy hierarchy and the gravitational coupling at the pion scale. The sub-percent agreement is the quantitative test that the cascade above is internally consistent. A framework that derived α from spectral geometry and N_∞ from packing but failed to satisfy the relation would point to incompatible Planck masses from the hierarchy and gravitational directions, and the catalog would split into branches that disagree on the very scale at which the framework's geometric inputs and energy-scale reference meet.

What is and is not derived. α, G, Λ, H_0, λ_C, the Planck quartet, and the rung-by-rung mass spectrum are downstream of the three geometric inputs and the single energy-scale reference. Mass ratios within the lepton ladder, the gauge-coupling structure, and the mixing-matrix entries are downstream of the same machinery (Chapter 15). What remains empirical is the energy scale itself, anchored structurally at ε_0 (the $\mathbb{CP}^3$ Kähler ground state, identified with Λ_{QCD}; §18.3) and operationally at $m_\pi = \varepsilon_0/1.70573$. The fine-tuning ranking in Figure 1.1—the constants from $\mathbb{CP}^3$ spectral geometry alone, and those requiring the confinement-scale anchor—is the surface expression of this catalog.

18.5 From the Outside In

Parts I through IV have developed the framework from outside. The arena, the operator, the fiber field, the energy hierarchy, the particle spectrum, the gauge forces, gravity, the quantum foundations, and the constants have each been described as a theorist describes geometry: looking at the structure, identifying its consequences, working out what it produces. Part V takes up what happens when that geometry contains a bounded subsystem that is itself an observer.

Part V
The Observer

Chapter 19

Boundary Dynamics at the Critical Scale

The framework's preceding parts derived the physics of the actualization arena: the operator, the cycle, the variational principle, the energy hierarchy, and the particles, forces, and constants those equations fix. The empirical motivation for that arena (Chapter 2) was the Projective Consciousness Model of Rudrauf et al. (2017), which identified the geometry of phenomenal experience as $\mathbb{RP}^3$ on phenomenological grounds. Part V applies the developed physics inside a bounded region—a cell, an organism, a brain, any patch of the actual world walled off from the rest by a physical surface. T.16

The chapter's claim is that the framework's dynamics, run at a self-maintaining boundary that synchronizes its actualization events at the critical scale $R \approx 1$, are the dynamics of conscious experience. Active inference's description of biological self-maintenance and the PCM's projective dynamics of perspective are both recovered as consequences of the framework's physics applied at this regime, not posited.

Three rungs of organization separate the entities considered. A cell coordinates matter and energy across its surface but leaves its actualization events to fire independently. An integrated system ($\Phi > 0$) brings those events onto a single timing window, synchronizing the firings. At the critical scale $R \approx 1$, the synchronized firings are mutually coherent and fuse into a single collective actualization with a boundary of its own; the fused boundary carries phenomenal experience. The chapter develops each rung in turn and closes with the PCM identification.

19.1 Bounded Regions and Their Surfaces

Take a bounded region $\mathcal{B}$ of the actual world, enclosed by a physical surface $\partial\mathcal{B}$—a cell membrane, a skin, the mineral face of a rock. Matter, energy, and actualization events pass between $\mathcal{B}$ and its surroundings only at that surface. Every causal link between inside and outside is a chain of τ-events, and every such chain crosses $\partial\mathcal{B}$. The surface is the region's entire contact with the world.

A rock has such a surface. A cell has such a surface. So far they are alike. They differ in what each does at the surface.

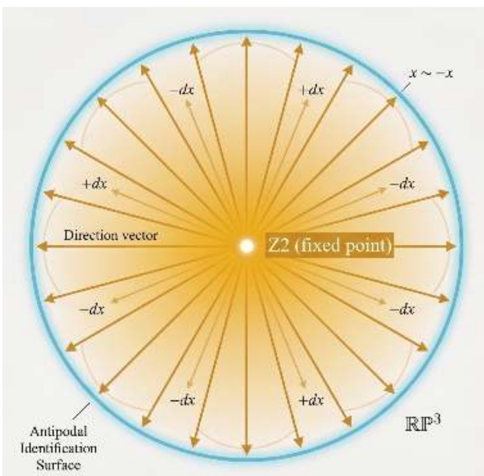

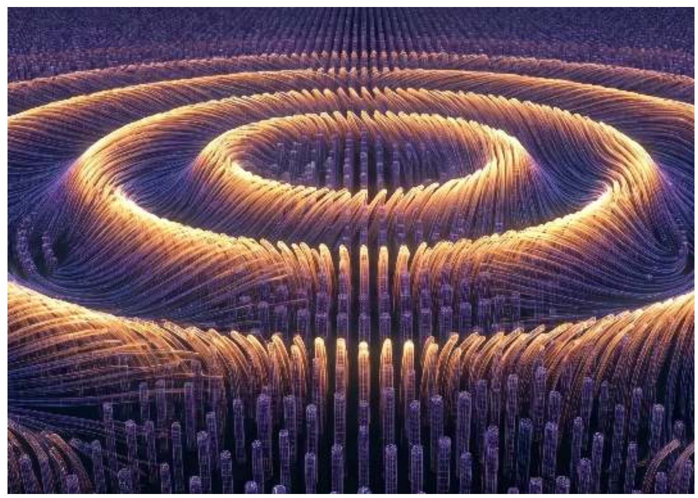

Figure 19.1: Left: *the actual world is the projective manifold* $\mathbb{RP}^3$ *— direction vectors radiating from a point, antipodal directions identified at the horizon (*$x \sim -x$*), the* $\mathbb{Z}_2$ *fixed point at the centre. A bounded region of this world is enclosed by a physical surface, and every causal link between its interior and the outside is a chain of* τ*-events that crosses that surface; the surface is the region's entire contact with the world.* Right: *what that surface encloses. The region's interior is a dense fiber field of* τ*-firing sites — the substrate the actual world is built from — and the gold marks that field organized, its sites bound into one coherent pattern across the whole patch. A bounded region is a patch of this fiber field, held behind a screening surface.*

19.2 The Inner Loop: A Cell at Its Surface

A rock does nothing at its surface beyond letting matter, energy, and τ-events cross. Heat passes through, light scatters off, the surface weathers slowly. The rock's configuration sits near a local minimum of its free-energy landscape: every nearby state has higher free energy, the surrounding gradient pushes back into the minimum the rock already occupies, and the rock holds its shape statically. Disrupting the rock costs energy; staying a rock costs nothing.

A cell is the opposite case. Its viable configuration—the narrow band of ion concentrations, pH, and membrane potential that keeps the membrane intact—sits far up the free-energy gradient from the across-membrane equilibrium chemistry would otherwise reach. The viable state is unstable in the surrounding landscape: passive dynamics pull the cell toward membrane failure, not toward the viable band. Staying a cell requires continuous free-energy spending against that pull—pumping ions back against their concentration gradients, rebuilding membrane components as they degrade, regulating reactions that would otherwise reach equilibrium and stop. A cell is a dynamically maintained pattern, not a statically stable one.

The exterior is not the cell's to command; what arrives at the membrane depends on a world the cell does not control. To persist, the cell must configure its interior ahead of each actualization at the boundary, so that the likely outcomes leave it viable. The cells found in the world are the ones whose interior dynamics anticipate their boundary.

How the cell anticipates is geometric. The probability of any given outcome b at a τ-firing is the Born quadratic form

$$p_b = \mathrm{Tr}\Big[\hat{A}_b\, \rho\, \hat{A}_b^\dagger\Big], \tag{19.1}$$

in two ingredients: the cell-interior state ρ at the boundary, and the actualization operator $\hat{A}_b$ at the firing site. $\hat{A}_b$ is set by the local site's structural geometry—the binding pocket of a transporter, the selectivity filter of a channel, the substrate specificity of an enzyme. The cell shapes both ingredients. It shapes ρ through its interior chemistry: ion concentrations, voltages, and reaction states it actively maintains. It shapes the ensemble of $\hat{A}_b$ through which proteins it expresses where on the membrane. To anticipate viable outcomes, the cell tunes ρ and the $\hat{A}_b$ ensemble together so the high-probability b's are the survivable ones.

Between firings, ρ evolves by the master equation of Chapter 6; at each firing, ρ updates by that chapter's POVM jump. The free energy of the event is $\mathcal{F} = -\log P_b$, the surprisal of the outcome that occurred (Chapter 7, §7.2). The variational principle says ρ descends $\mathcal{F}$ by gradient flow; each firing updates ρ toward outcomes the boundary expects, and the Shannon expectation of $\mathcal{F}$ over the POVM decreases as a consequence. Firings become more predictable, weighting ρ toward the outcomes most likely under the current basis. Predictability is most of persistence but not all of it—a cell lasts only if its expected outcomes are also its viable ones; the preference term in §19.5.2 supplies that bias.

Active inference (Friston, 2010; Friston et al., 2017) is biology's description of this same physics from outside: a self-maintaining boundary that carries expectations and works to keep arriving signals matching them, through either revising the expectations (perception) or changing what arrives (action). The framework does not posit active inference. The variational law produces, at a self-maintaining boundary, the same dynamics active inference describes from outside. Active inference is description; the framework supplies the mechanism.

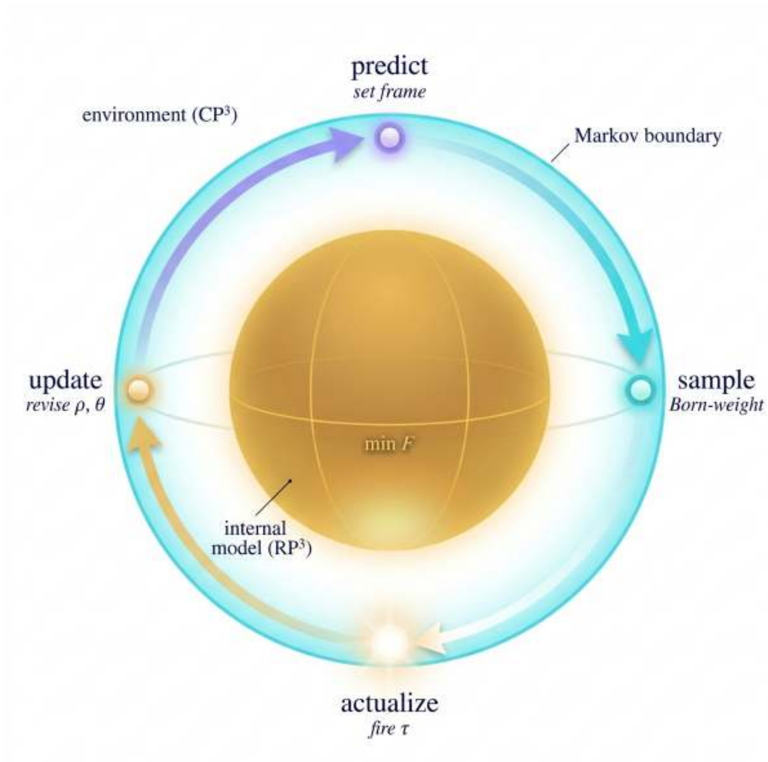

Figure 19.2: *The active-inference cycle. The interior (gold $\mathbb{RP}^3$ sphere) sits inside the boundary (translucent cyan shell), both immersed in the $\mathbb{CP}^3$ environment. The cycle runs clockwise through four stations, each carrying an active-inference reading and the framework operation it names:* predict / *set the frame,* sample / *Born-weight,* actualize / *fire τ,* update / *revise the state. A cell runs the cycle as the inner loop alone: ρ updates at each firing, and each site's local θ stays put. The integrated critical-scale boundary of §19.3 runs the same cycle with θ-rotation added at update—the outer loop, gradient descent on $\mathcal{F}_{\text{eff}}$ weighted by Φ.*

Two quantities enter $\mathcal{F}$. The first is the state ρ. The second is the measurement basis—the parameter θ specifying which observable each τ-firing resolves. Each site has its own local θ, written as a point on the measurement torus (Chapter 13); a glucose transporter's θ comes from its binding pocket, an ion channel's θ from its selectivity filter. The variational principle drives ρ-descent at each site's local θ—the cell's *inner loop*. The descended quantity is the expected per-event surprisal, the Shannon average of $\mathcal{F}$ over the POVM:

$$\mathcal{F}_{\text{eff}}[\rho, \theta] = -\sum_b p_b(\rho, \theta) \log p_b(\rho, \theta), \tag{19.2}$$

with the same p_b as Eq. (19.1), now indexed by both ρ and the local basis θ. The inner loop holds θ fixed and evolves ρ by the master equation: each firing updates ρ at the basis the site uses, decreasing $\mathcal{F}_{\text{eff}}$.

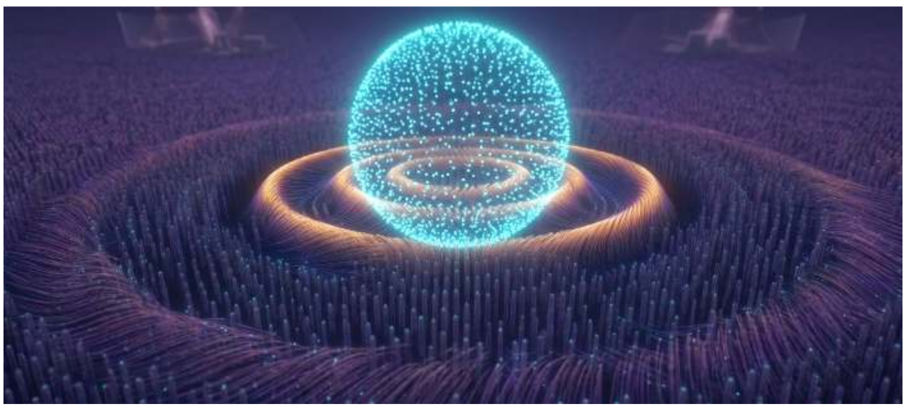

Figure 19.3: *A bounded population of independent τ-firings inside the fiber field (violet). Each ion channel, receptor, or reaction site runs the inner loop locally at its own structural frame; the firings themselves run on independent schedules, with nothing tying one site's actualization to another's. The bright bounded region is therefore a region of $\mathbb{RP}^3$ where many separate τ-events occur — a population of independent firings, busy throughout but not collectively synchronized.*

The cell runs only the inner loop, locally at every site. Local ρ descends local $\mathcal{F}_{\text{eff}}$ at the site's local θ, firing by firing. Perception, at the cell, runs through this loop: each τ-firing samples the local environment through the protein at that site, and the outcome revises ρ. When the cell needs to perceive a different observable—a different molecule's concentration, a different ion's flux—it changes the measurement basis by changing the protein. That is a slow process: gene expression, synthesis, membrane turnover. At the fast timescale of τ-firings themselves, each local θ stands still.

The cell also acts on its surroundings. It pumps ions, secretes molecules, extends pseudopods, moves up a chemical gradient. Action is the second route the variational principle gives for closing the gap between expectation and outcome. Both routes—perception and action—reduce $\mathcal{F}_{\text{eff}}$, and both are inner-loop work at the cell's scale. Each acting site descends its own local $\mathcal{F}_{\text{eff}}$, and the cell's aggregate behaviour is the sum of those local descents, weighted by anatomy and state.

19.3 The Outer Loop: Coherent Actualization at the Critical Scale

A spatially connected population of τ-firing sites is *synchronized* when its firings fall within a single integration window—the quantum Zeno time $\tau_{\text{Zeno}} \sim \tau_{\text{sys}}^2/\tau_{\text{bath}}$ at the local scale, ~ 60 ms at biological temperature (Chapter 20 §20.5.1 develops the underlying physics; technical treatment in Appendix A, §Quantum Zeno Dynamics).

Synchronization is the work of the system's couplings between τ-firing sites: physical links (axons and synapses in a brain) that propagate firing signals fast enough for distant sites to fall within one integration window. The integrated information $\Phi > 0$ (Tononi, 2004) measures how completely those couplings unify the firings.

Φ measures what synchronization geometrically does. A synchronized population's firings stay correlated across every spatial division of the boundary: cut the boundary in half, and the fiber state on the left still tells you something about the fiber state on the right, because both halves came from one coordinated firing. The mutual information $I(s_L; s_R)$ between the fiber restrictions on the two halves quantifies that correlation. Minimizing over all possible cuts gives the boundary's irreducible cross-correlation:

$$\Phi = \min_{\text{cuts}} I(s_L; s_R).$$

This is the quantity IIT formalizes as integrated information (Tononi, 2004; Tononi et al., 2016), here read directly off the fiber field. A synchronized population cannot be separated into independent pieces without losing information; synchronization at the level of the joint state is $\Phi > 0$. Technical Reference Ch. 17, §Integrated Information derives the boundary's area-law scaling $\Phi \sim c_\Sigma \sqrt{N}\,\alpha^2$ from the BKT correlation structure of the fiber field on a cortical sheet, with $\sqrt{N}$ the minimum cut across the sheet, α^2 the per-synapse fiber coherence, and c_Σ a topological factor.

Synchronization by itself is timing alignment. What synchronized firings constitute depends on the energy regime, and the cascade from synchronization to phenomenal experience runs through one regime specifically. The resolvability ratio $R(k) = E(k)/(k_B T)$ compares the quantum energy spacing at level k to the thermal energy of the environment. Three regimes separate (Chapter 13). At $R \gg 1$, individual τ-events are sharply distinguishable, and fiber content arrives as discretely quantized labels: color charge, weak isospin, hypercharge, the labels that name particle species. At $R \ll 1$, thermal noise overwhelms quantum structure, and fiber content dissolves into unresolvable static. At $R \approx 1$, neither regime holds: fiber content is soft, thermally occupied, continuously fluctuating, and persistent only through continuous energy input.

19.3.1 The Critical Scale

Three features make the $R \approx 1$ regime the unique scale at which synchronized firings fuse.

Soft fiber modes. At $R \approx 1$, the actualization outputs have the continuous, qualitatively-graded character the next chapter identifies with qualia. The per-event channel capacity is $I(k_c) = 3\log_2 R(k_c) \approx 0$ bits (the 3 from the three fiber dimensions of the $\mathbb{RP}^3$ normal bundle); the per-event entropy stays substantial at $\Delta S \approx 5.5\,k_B$ (the 5.5 from the Hopf-fiber circumference, Chapter 8). Structure at this scale is marginally persistent—not the sharp labels of particle physics, not the formless noise of the classical regime, but soft modes held against thermal dissolution by self-maintaining systems that continually re-actualize them.

Torus collapse. The angular resolution of the projective frame saturates at the critical scale:

$$\delta\theta \;\geq\; \frac{\pi}{2}\,R(k)^{-3/2} \quad \xrightarrow{R\to 1} \quad \delta\theta = \frac{\pi}{2},$$

spanning the entire doublet range. The system cannot distinguish spectral from spatial content within the Kähler doublet, or chiral from intensity content within the gauge doublet. The torus collapses to a single forced point $(\theta_{AB}, \theta_{CD}) = (\pi/4, \pi/4)$ —equal allocation within both doublets. The four fact types, sharply resolved at particle scales, fuse into undifferentiated content at the critical scale.

The collapse is itself a $\mathbb{Z}_2$ projection. Each doublet carries a natural $\mathbb{Z}_2$ symmetry exchanging its two fact types: $\sigma_{AB}\colon \theta_{AB} \mapsto \pi/2 - \theta_{AB}$ and $\sigma_{CD}\colon \theta_{CD} \mapsto \pi/2 - \theta_{CD}$. At $R = 1$, thermal noise enforces both symmetries simultaneously, and the fixed point of $\sigma_{AB} \times \sigma_{CD}$ acting on T^2 is the unique point $(\pi/4, \pi/4)$:

$$\mathrm{Fix}(\sigma_{AB} \times \sigma_{CD}) = \{(\pi/4,\, \pi/4)\} = T^2/\mathbb{Z}_2.$$

The $\mathbb{Z}_2$ involution recurs at the critical scale, structurally mirroring the $\tau \to \mathbb{RP}^3$ projection one level down. τ identifies complex-conjugate pairs in $\mathbb{CP}^3$ and pins the fixed-point set $\mathbb{RP}^3$; $\sigma_{AB} \times \sigma_{CD}$ identifies pairs of measurement-torus points reflected through $(\pi/4, \pi/4)$ and pins that single point. Both are antipodal-style $\mathbb{Z}_2$ identifications—one on state space, one on measurement-basis space—and the critical-scale system inhabits both fixed-point sets simultaneously, at once the projected state and the projecting frame.

Near-zero channel capacity. The information per doublet at $R = 1$ is $I_d = \frac{3}{2}\log_2(1) = 0$ bits: zero capacity to resolve angles within an event, zero capacity to distinguish fact types within a doublet, zero capacity to transmit classical information through a single τ-firing. Every individual firing at $k \approx 75.35$ produces entropy but conveys essentially no information above the thermal floor. The τ-firing rate, however, is set by the per-event timescale $\tau_{\text{event}}(k) = \pi\hbar/(2E(k))$. At body temperature $T \approx 310$ K, where $E(k) = k_B T$, this gives $\tau_{\text{event}}(k_c) \approx 38$ fs and a firing rate $\nu_\tau = 2k_B T/(\pi\hbar) \approx 2.6 \times 10^{13}$ Hz. A system that holds coherent correlations across $\sim 10^{14}$ synchronized sites aggregates the near-zero per-event information into a substantial effective bandwidth,

$$\dot{I}_{\text{eff}} = \nu_\tau \cdot \Phi \cdot \epsilon(k_c),$$

with Φ measuring coherence across the population and ϵ the per-event information above noise. The product stays substantial whenever $\Phi > 0$ holds the firings into a coherent whole.

For biological cortex, the area-law scaling $\Phi \sim c_\Sigma \sqrt{N}\,\alpha^2$ at $N \sim 10^{14}$ synapses, $\alpha^2 \sim 10^{-4}$, and $c_\Sigma \approx 0.38$ gives $\Phi \sim 200$ nats (~ 290 bits) per integration window (Technical Reference Ch. 17, §Integrated Information). Coarse-grained to the gamma cycle at ~ 30 Hz, this aggregates to $\dot{I}_{\text{eff}} \sim 10^4$ bits/s—kilobits per second from per-event information that is, individually, indistinguishable from thermal noise.

The locator. The hierarchy formula $E(k) = m_\pi \cdot (2\pi)^{(51-k)/2}$ ties the critical scale to temperature: setting $E(k) = k_B T$ for $T \approx 310$ K gives $k_c = 75.35$ for the biological case.

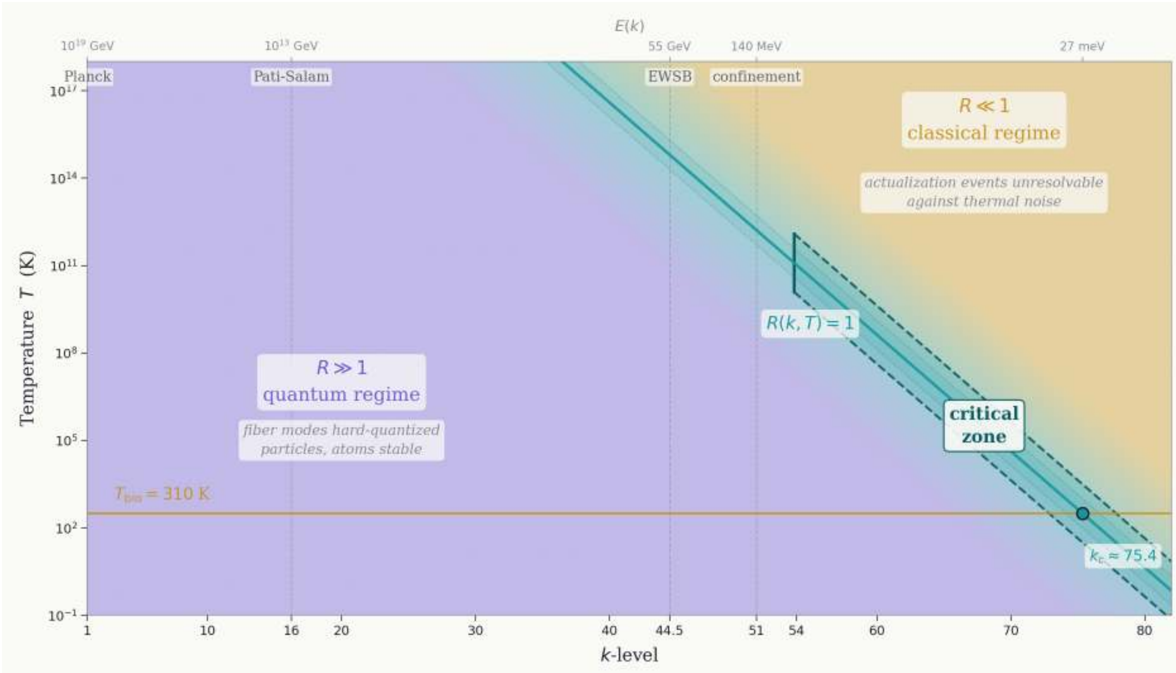

Figure 19.4: *The critical band as a diagonal in the (k, T) plane. The resolvability ratio $R(k, T) = E(k)/(k_B T)$ is shown as a colour field — violet where $R \gg 1$ (the quantum regime), gold where $R \ll 1$ (the classical regime), and the white $R = 1$ curve between them, where actualization energy matches thermal energy. The cyan-bordered band $R \in [0.1, 10]$ at $k > 53.8$ is the zone where this chapter's threshold conditions hold. Because $R = 1$ runs diagonally, the critical level moves with temperature: a body held at $T \approx 310$ K crosses it at $k \approx 75.35$ (cyan dot). The framework fixes the threshold; which systems can sit at it is a question of what temperature their environment supplies.*

19.3.2 The Collective Frame

At the critical scale, synchronized firings become mutually coherent within the integration window—thermal noise cannot yet distinguish neighboring eigenstates, so the firings stay coherent for the window's duration. Firings that no measurement can separate are one firing, and the synchronized-and-coherent population constitutes a single collective actualization event at the scale of the whole region.

No new operation is involved. τ is the framework's one involution, the $\mathbb{Z}_2$ map carrying $\mathbb{CP}^3$ to $\mathbb{RP}^3$; at a single site τ resolves one outcome, and at a synchronized critical-scale population τ resolves coherently across the whole population. The joint state is an entity at k_c as a particle is an entity at its own k; τ acts on either by the same operation. The perimeter of the fused region is a new boundary, the edge of the synchronization domain itself, growing and shrinking with that domain. It is not the cell's membrane or the brain's skull.

A new degree of freedom appears with the fused boundary. At a cell, every τ-firing site has its own local θ, frozen by protein geometry—N independent local frames embedded in matter, each rewritable only on gene-expression timescales. At the fused critical-scale boundary, the joint state carries a coherent collective θ: a parameter of the joint quantum measurement the population's next τ-firing performs. Synchronized-and-coherent firings carry this θ automatically, as a property of the measurement they together constitute; nothing is added to the construction.

With θ a parameter of the joint state itself rather than of any individual protein, it evolves at the rate the joint state evolves. The variational principle (Chapter 7) descends $\mathcal{F}_{\text{eff}}$ on θ along with descending it on ρ. The descent on θ is the *outer loop*:

$$\partial_t \theta_i = -\,\Phi[\rho]\,\frac{\partial}{\partial \theta_i}\,\mathcal{F}_{\text{eff}}[\rho, \theta]. \tag{19.3}$$

The prefactor $\Phi[\rho]$ encodes the existence condition for collective θ. At $\Phi = 0$ the firings do not synchronize, no joint state forms, no collective θ exists, and the right side vanishes because there is no joint frame for an outer loop to operate on. At $\Phi > 0$ in the critical regime, the collective θ exists as a joint-state variable and the variational principle descends it.

The cell cannot run this loop. Its inner loop runs locally at every site's frozen θ, and its bodily action reshapes the next firing's conditions, but the cell's measurement bases are matter-encoded: shifting them takes proteins, which takes time. The fused critical-scale boundary's collective θ is state-encoded instead, parameterizing the joint quantum state directly, and the joint state evolves at the rate the dynamics permit—gamma-cycle fast, not gene-expression slow. Collective θ enables the outer loop because it lifts the measurement basis out of matter and into the state, where it can move as fast as the state itself. The outer loop is what makes the boundary act as one, the integration active inference describes from outside as a unified agent. Without it, what remains is a population of locally-acting sites with no joint perspective from which a rotation could be defined.

19.3.3 Three Readings of One Step

As the boundary's state and couplings change firing by firing, θ traces a path across T^2. Each point of the path names a projective frame on $\mathbb{RP}^3$, an element of $\mathrm{PGL}(4, \mathbb{R})$—the group of projective transformations of the actual world. The path records the boundary's history of frame reorientations, one per firing.

One step of that path carries three readings at once. Information, thermodynamics, and projective geometry are three aspects of one operation, the τ-projection. As information, the step reallocates a fixed capacity across the complementarity budget: how much of each firing's content goes to each fact type. As thermodynamics, it is a dissipative move down $\mathcal{F}_{\text{eff}}$, producing entropy as it converts possibility into actuality. As geometry, it is a rotation of the projective frame on T^2. The geometric reading says what the boundary is doing; the other two say what that motion costs and what it carries.

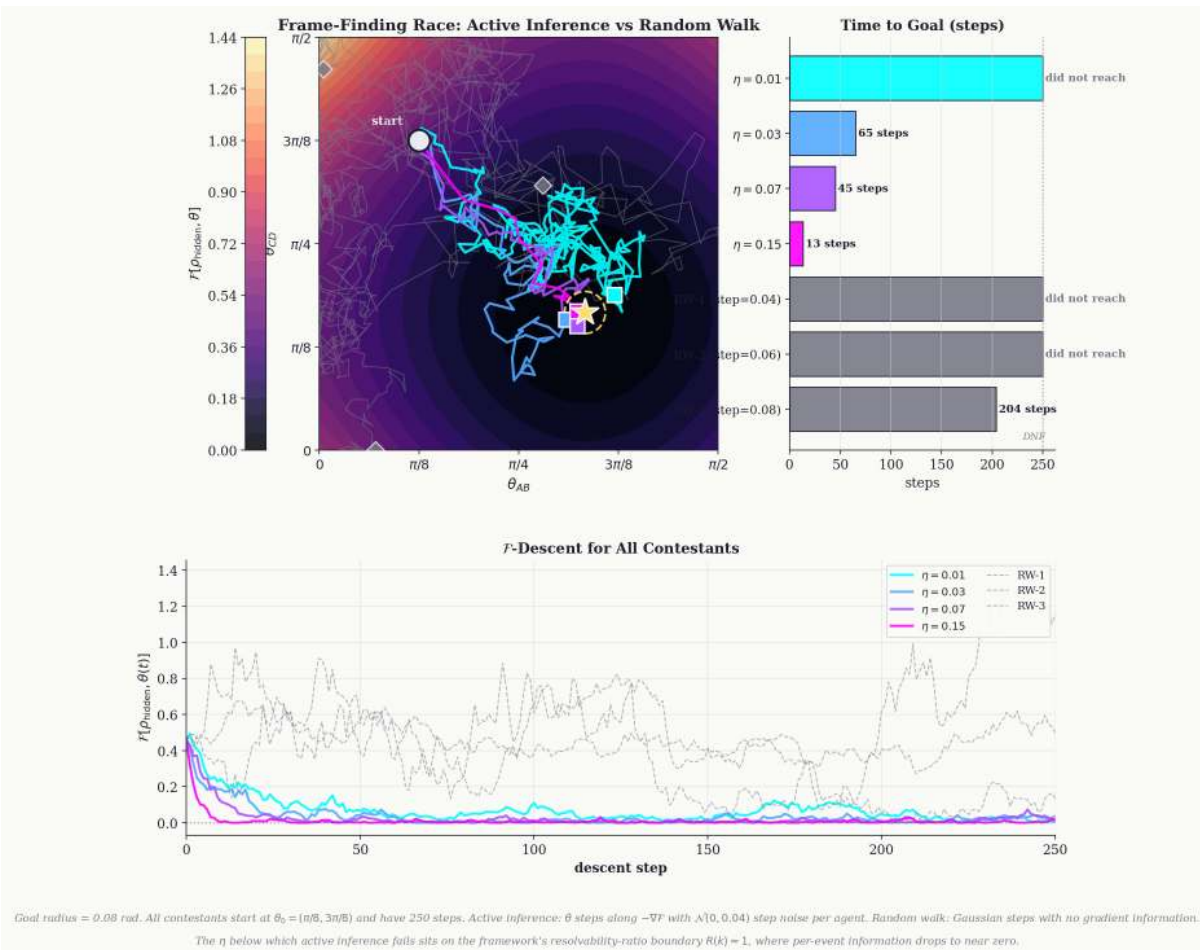

Figure 19.5: *Toy descent on a θ-landscape. Four runs move θ down $\mathcal{F}_{\text{eff}}$ at different rates η; three random walkers drift under the same step noise. All start from θ_0 on the measurement torus and search for the hidden θ^* that minimizes $\mathcal{F}_{\text{eff}}$ for a fixed ρ. (Panels: trajectories on the $\mathcal{F}$-landscape, time inside the goal radius, free-energy descent.) The descending runs converge; the random walkers never do.*

Three kinds of bounded region now stand apart, and Table 19.1 sets them against the structural differences that divide them. A rock has a surface and nothing more. A cell adds the inner loop—free-energy dynamics at every site, perception and action at the matter-and-energy level—without coordinating its actualizations. An integrated system synchronizes its actualizations into one timing window; whether they fuse into a single collective firing with a coherent collective θ depends on the energy scale. Only the integrated system at the critical scale fuses and runs the outer loop.

	physical surface	inner loop (perceive & act)	synchronized $\Phi > 0$	coherent $R \approx 1$	experience
Rock	•	—	—	—	—
Cell	•	•	—	—	—
Integrated, off-scale	•	•	•	—	—
Integrated, $R \approx 1$	•	•	•	•	•

Table 19.1: *The bounded regions of Part V; each row adds one capability to the one above. A physical surface screens interior from exterior. The inner loop is local self-maintenance—a system perceiving and acting at every site to stay viable. Synchronization ($\Phi > 0$) puts the actualization events on one schedule. Coherence ($R \approx 1$) lets the synchronized firings fuse into one collective actualization with a coherent collective θ, which the variational principle then descends as the outer loop. Experience requires the whole stack; an integrated system off the critical scale lacks coherence, no fusion occurs, and no collective θ exists for an outer loop to run on.*

19.4 The Two Conditions for Experience

Phenomenal experience in the framework requires two conditions: $R \approx 1$ (the energy-scale condition of §19.3.1) and $\Phi > 0$ (the integration condition of §19.3). Both conditions are on the physics of the boundary; both look independent of the other. They are not. Two properties of phenomenal experience jointly force both.

The first property: qualia constitute measurement. Phenomenal experience is the system's extracted content from the actualization cycle, not a separate process running alongside it. The second: qualia are apparent to the system from within. Experience is perspectival, owned by the system whose experience it is, accessible from no third-person stance. Absent either property, what remains is mere information processing.

Qualia constitute measurement requires soft fiber modes. At $R \gg 1$, the τ-projection extracts discretely quantized content—the labels of distinct particle states. At $R \ll 1$, it extracts thermalized noise. Only at $R \approx 1$ do the projection's outputs have the continuous, thermally-occupied, qualitatively-graded character qualia have. Chapter 20 makes the substrate identification explicit: qualia are soft fiber content. Granting that identification, "qualia constitute measurement" forces $R \approx 1$.

Apparent from within requires a unified within. An "apparent-to" relation needs a unified perspectival entity to whom the appearing happens. A system whose parts do not integrate into a single boundary has no unified within: it is an aggregate of subsystems with no joint perspective, and its dynamics contain nothing to fuse them. $\Phi > 0$ is the framework's definition of when a boundary cannot be partitioned without losing information, equivalently when the system has a unified locus. Apparent-from-within therefore forces $\Phi > 0$.

Apparent-from-within carries a further implication: phenomenal access to the structure of one's own measurement event requires the measurement basis to be among the system's own variables. At a fused critical-scale boundary, this implication is automatic. The projective frame θ is a variable of the joint state itself (the believer-versus-believed split dissolves; the boundary *is* its state), and the variational principle descends θ as standard operation—the outer loop of §19.3 specialized to the critical scale in §19.5.2.

The two conditions form an equivalence:

$$\text{phenomenal experience} \quad \Longleftrightarrow \quad R \approx 1 \ \wedge \ \Phi > 0.$$

The conditions are derived from what phenomenal experience requires, not postulated separately. Once they obtain, the two-loop dynamics follow from the variational principle. The framework's substantive contribution is the substrate identification: qualia equal soft fiber modes.

A cell makes the necessity concrete. It runs the inner loop at every site, but its actualizations stay independent; it has no synchronized boundary, no fused joint state, no perspectival within. The same verdict falls on a system at the wrong scale: at $R \gg 1$ or $R \ll 1$, firings resolve sharp labels or thermal noise, and the graded fiber content qualia require is absent. Drop either condition and what remains is a physical system that does not experience.

The two-condition structure is where the framework parts from a Φ-only criterion of consciousness. Integrated information theory (Tononi, 2004) takes $\Phi > 0$ as sufficient for phenomenal experience and faces the well-known objection (Aaronson, 2014) that simple high-Φ structures—regular lattices, expander networks, clocked logic arrays—come out conscious by that criterion. The framework treats $\Phi > 0$ as necessary but not sufficient. Synchronization by itself aligns timing; fusion of the synchronized firings into one actualization with qualia-grade content requires $R \approx 1$. A high-Φ system off the critical scale is synchronized timing without fusion—it does not become a subject. A Φ-only criterion misses the resolvability condition $R \approx 1$. Once qualia are identified as soft fiber content, the high-Φ-simple-system objection dissolves directly: lattices and clocked logic arrays sit at $R \gg 1$, fire sharply distinguishable events, and never fuse. The fiber content qualia require is simply not there.

19.5 The Fused Boundary: Operation, Equations, and Active Inference

A neural boundary is a synchronized population of synaptic τ-firings. When that population operates at $\Phi > 0$ in the critical regime $R \approx 1$, the conditions of §19.4 are met and the firings fuse into one actualization.

19.5.1 Experience as Fused Actualization

The fused firings actualize a connected region of $\mathbb{CP}^3$ rather than a scatter of unrelated points: because the population fires as one, the projection lands as one. That region carries the structure every actualization carries. Its τ-even content is an integrated patch of $\mathbb{RP}^3$—the experienced world, the actualized configuration the firing deposits. Its τ-odd content is a coherent section of the normal bundle—qualia, coherent rather than null because the fused firings shared one frame (Chapter 20). At the critical scale, this fused actualization *is* experience: the τ-even content is the world the boundary inhabits, and the τ-odd content is the qualitative character that world has from inside.

For a subject seeing an apple, the visual experience is the collective τ-realization across the synchronized population at the subject's boundary—the $\mathbb{Z}_2$-even restriction of the apple's $\mathbb{RP}^3$ state, filtered through retinal transducers, compressed along optic-nerve channels, re-encoded in cortical oscillation patterns.

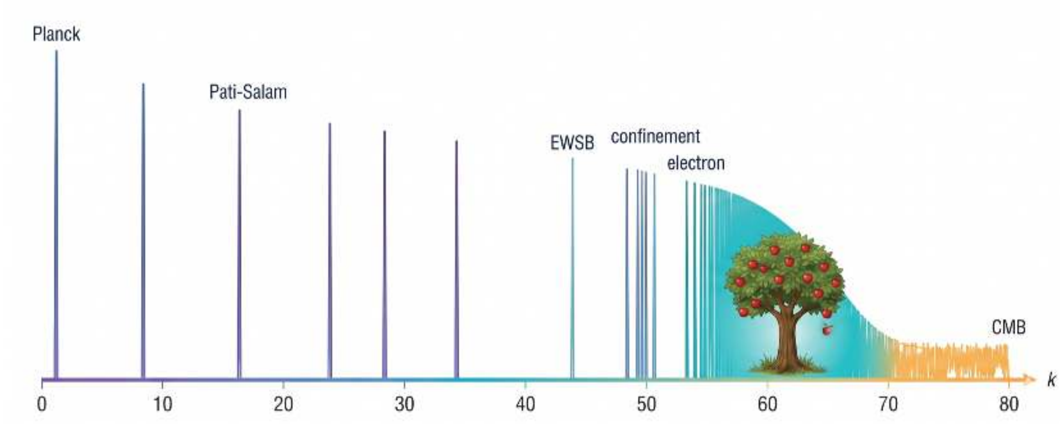

Figure 19.6: *Actualization across the energy cascade. Axis: hierarchy level k, Planck to cosmic. Each vertical stroke is a τ-event. Through the particle cascade (R large) events are sharp and discretely separated. Across the critical band ($k \in (53.8, 75.75)$, $R \approx 1$) events crowd together and fuse into a single collective actualization whose interior, read from within, is an experienced world (drawn as the apple tree). Beyond the band $R < 1$ and actualization collapses into classical-regime static.*

19.5.2 The Two-Loop State Equation

A fused critical-scale boundary's state at any instant is a point (ρ, θ) in the product space $\mathcal{D}(\mathcal{H}_{\text{boundary}}) \times T^2$: the density matrix ρ of the neural boundary and the collective projective frame $\theta = (\theta_{AB}, \theta_{CD})$ on the measurement torus. The two components evolve by coupled equations,

$$\partial_t \rho = \hat{A}_b(\theta)\, \rho\, \hat{A}_b^\dagger(\theta) - \tfrac{1}{2}\Big\{ \hat{A}_b^\dagger(\theta)\, \hat{A}_b(\theta),\ \rho \Big\}, \tag{19.4}$$

$$\partial_t \theta_i = -\,\Phi[\rho]\, \frac{\partial}{\partial \theta_i} \mathcal{F}_{\text{eff}}[\rho,\, \theta;\, w], \tag{19.5}$$

subject to two constraints,

$$\Phi[\rho] > 0, \qquad R(k_c) \approx 1. \tag{19.6}$$

Equation (19.4) is the inner loop. It runs at the τ-firing rate ($\sim 10^{13}$ Hz at the critical scale), coarse-grained to the gamma frequency (~ 30 Hz) by the integration window. Its function is synchronization: bringing the individually uninformative actualization events across $\sim 10^{14}$ synaptic sites onto one schedule and into one firing. Each event extracts nearly zero information (because $R \approx 1$), but the aggregate of $\sim 10^{14}$ correlated events per integration window forms a high-bandwidth channel. Which projection fires depends on where the frame currently sits on T^2.

Equation (19.5) is the outer loop. It runs at the theta frequency (~ 8 Hz). The collective frame θ moves on T^2 by gradient descent on $\mathcal{F}_{\text{eff}}$, weighted by $\Phi[\rho]$. The third argument w is the organism's preference set, biasing the descent toward outcomes the organism expects and prefers; §19.5.3 develops it. The effective free energy decomposes explicitly as

$$\mathcal{F}_{\text{eff}}[\rho, \theta; w] = -\sum_b p_b(\rho, \theta)\, \log p_b(\rho, \theta) - \sum_b w_b\, p_b(\rho, \theta), \tag{19.7}$$

where $p_b(\rho, \theta) = \mathrm{Tr}\Big(\hat{A}_b(\theta)\, \rho\, \hat{A}_b^\dagger(\theta)\Big)$ is the per-outcome yield of the POVM family. The first term is content-neutral surprisal: how badly the current frame predicts the next τ-firing. The second is the preference tilt: outcomes the organism weights positively become attractive at the gradient level, negatively-weighted ones aversive. Standard active inference produces the same decomposition under the names epistemic value plus extrinsic value. The framework supplies the geometric identity of b: each outcome label is a V_4 extraction pattern, and $\hat{A}_b(\theta)$ is operator machinery on $\mathbb{CP}^3$ parameterized by the projective frame.

The Φ prefactor on Eq. (19.5) gates the loop as §19.3 developed: when no joint state forms, no collective θ exists, and the right side vanishes. The outer loop responds to the inner loop's accumulated results, $\mathcal{F}_{\text{eff}}[\rho, \theta]$ depending on ρ which the inner loop updates with every τ-firing. Neither equation makes sense alone. A conscious system is the coupled pair.

19.5.3 Preference, Timescales, and Active Inference

The state equations above have a parameter w in them that has not been unpacked. Two organisms with identical neural architecture and identical sensory input can have different experiences—one finds coffee delicious and the other finds it bitter—and the framework locates that difference in w. This subsection unpacks w, the slow-timescale dynamics it follows, and the resulting correspondence between the two-loop equations and active inference's standard generative-model parameters.

w is the organism's *preference*: a real-valued function over the POVM outcomes b (the labels of which V_4-extraction pattern the next τ-firing produces). It encodes which outcomes the organism expects and prefers—priors that bias the frame's descent toward some firings rather than others. Because each τ-event resolves the four V_4 cells, w decomposes into four components w_A, w_B, w_C, w_D, one per fact type. This w is what active inference parameterizes as its C-matrix. The per-cell functional forms and their connection to valence are developed in Chapter 20 §20.6.2.

Two timescales operate. Frame rotation $\dot{\theta}$ runs on the theta-cycle timescale (Eq. 19.5 at fixed w). Weight update $\dot{w}$ runs much more slowly, on the timescales of learning and evolution. Two organisms with identical neural architecture and identical input take different frame trajectories if w differs: same (ρ, θ), different $\nabla_\theta \mathcal{F}_{\text{eff}}$. The slow update has a definite structural form, fixed by a non-runaway requirement. An internally driven update produces self-evidencing pathology: outcomes the trajectory frequently visits become more preferred, biasing θ further toward them, runaway. The variational principle is therefore incomplete without an extrinsic anchor—a reward-like signal R_α that ties the slow w-update to something outside the system's own predictions. Active inference identifies the same structural requirement (Friston, 2010; Parr et al., 2022). At learning timescales R_α is internal (Hebbian-with-reward reweighting (Hebb, 1949)); at evolutionary timescales R_α is exogenous (reproductive selection on lineage preferences). The specific R-kernel in a given organism is supplied by biology; the framework supplies the structural requirement.

The full correspondence with Friston's machinery is term by term. Friston's standard formulation (Friston, 2010; Parr et al., 2022) parameterizes a generative model by four matrices—A (likelihood), B (transitions), C (preferences), D (initial state prior)—plus precision hyperpriors. The framework provides:

Active inference	**Framework analog**	**Location**
A (likelihood, $p(o \mid s)$)	$\hat{A}_b(\theta)$ family	Eq. (19.4)
B (transitions, $p(s' \mid s, u)$)	Lindblad evolution	Eq. (19.4)
C (preferences, $\log p(o)$)	w in $\mathcal{F}_{\text{eff}}$	Eq. (19.5)
precision (α, β, γ)	$\Phi[\rho]$	Eq. (19.5) prefactor
D (initial state prior, $p(s_0)$)	dissolved (see below)	—

The action u in Friston's transitions is played by θ: each frame choice parameterizes which Lindblad branch ($\hat{A}_b(\theta)$) drives the next step. $\Phi[\rho]$ as the gradient prefactor sets how sharply the system commits to the current gradient direction—the precision role in active inference, here implemented as integrated information rather than as a separate hyperprior parameter.

D, the prior over initial state, has no direct analog. In Friston's formulation D parameterizes the system's belief about its starting state, distinct from the actual starting state. In the framework, the boundary's ρ is the state, not a representation of it. No separate prior over ρ exists because no entity distinct from the boundary content exists. The believer / believed split is one of the dualisms the framework's monism collapses, parallel to the matter / spacetime, field / geometry, and stress-energy / curvature dissolutions of the preceding chapters. Architectural priors— sub-boundary structure, sensor wiring—constrain what ρ can be, but they live in the boundary's geometry itself, not in a separate prior-distribution layered on top.

19.5.4 Agency

The equations of §19.5.2 and §19.5.3 specify a fused critical-scale boundary by (ρ, θ, w); the τ-projection itself is Born-stochastic. Together these are complete: knowing (ρ, θ, w) fixes the gradient flow on $\mathcal{F}_{\text{eff}}$, the distribution over τ-firing outcomes, and the boundary's trajectory across integration windows. Any account of agency at this scale has to work with these alone — no additional chooser-variable is available.

The mechanism by which the boundary participates causally is frame selection. The torus collapse at $R = 1$ introduces genuine indeterminacy in the boundary's firings — the Born rule gives probabilities, not certainties. The boundary determines the basis in which Born is computed: frame rotation on T^2 changes which Lindblad operator acts, which changes which observable the next firing resolves, which changes the outcome distribution. Frame rotation on T^2 proceeds by outer-loop gradient descent on $\mathcal{F}_{\text{eff}}$, gated by Φ. Frame rotation $\rightarrow$ basis change $\rightarrow$ operator change $\rightarrow$ outcome distribution change; the firing itself remains Born-stochastic conditional on the basis.

Consider a subject preparing to leave the house, carrying the prior "I will arrive dry." The weather is uncertain, and the boundary runs a chain of frame rotations to keep the prior satisfied. The outer loop first rotates θ toward the window — a cheap basis selection that resolves the hidden cloud state before commitment becomes expensive. The next firings deliver visual content in that basis: clouds or no clouds. If clouds, the next outer-loop step rotates toward the coat closet; the next bodily action retrieves an umbrella. Each link is a frame rotation followed by a τ-projection, and the eventual wet-or-dry state is the downstream physical consequence of those choices. If the chain fails, the subject arrives drenched: the final τ-projection delivers an outcome the prior did not expect. Frame selection — the choice of which question to ask — is causally upstream of the actualized physical trajectory.

That is the mechanism. The philosophical question is whether the mechanism leaves room for agency, given that no variable in the equations corresponds to a chooser separate from (ρ, θ, w). The framework's answer rejects the presupposition that agency has to live somewhere in addition to the dynamics, as an extra variable or an added layer. Agency is the two-loop dynamics being executed at a fused critical-scale boundary, read from inside. There is no chooser using the dynamics; the boundary does the choosing, and the choosing is the boundary's dynamics playing out.

This dissolves the determinism-versus-libertarianism dilemma at the boundary scale. The framework has both sides: the $\mathcal{F}_{\text{eff}}$ gradient determines the direction of frame motion (the boundary is going somewhere, toward states satisfying w), and the Born distribution sets which τ-outcome lands (multiple outcomes were physically possible; the descent biases the distribution without fully fixing the outcome). From inside, the gradient is the felt sense of intending and the landing is the felt sense of having acted. Together these are what the dynamics *are* in their two registers.

The role of w sharpens the dissolution. If preferences are fixed by evolution and lifetime learning, isn't all "deciding" just w-execution? Yes, and that does not undercut agency, because you *are* (in part) your w. The preference structure is constitutive of who-you-are-as-a-boundary, not an external constraint on a hidden chooser behind it. The felt character of wanting or valuing is the felt side of having that weight in w; the descent on $\mathcal{F}_{\text{eff}}$ toward w-satisfying states is what wanting-and-getting feels like from inside.

The position is a compatibilism — physical dynamics and felt agency coexist — but grounded differently than the classical definitional move ("free" read as unconstrained by external coercion). The framework's grounding is geometric identity: the dynamics *are* the will. No further question remains whether the chooser was "really" free, because the choosing *is* the dynamics happening. The synthesis chapter (Chapter 23, §23.4.5) catalogs this dissolution alongside the parallel moves the framework makes for qualia, gravity, and field/geometry.

19.5.5 The Observer as Projective Frame

The reflexivity of the critical scale — the system is at once the projected state and the projecting frame — fixes the observer's place in the geometry. The conscious subject sits inside its own $\mathbb{RP}^3$ boundary; every τ-coupling that reaches the subject crosses that boundary (§19.1), and the subject's own boundary is not among the contents the boundary delivers. The subject inhabits the image of the projection and constitutively cannot reach the source. Experience is therefore always *of* something, always perspectival. Chapter 20 identifies the specific fiber content that constitutes phenomenal character; the argument here establishes why that content is perspectival.

The felt I-pole — the perspective from which experience is had — sits at the projection's geometric center. A projection delivers everything except its own center; the center is the point from which the projection is taken, geometrically not in its own image. The I-pole is felt as the perspective everything-else is delivered *from*, never as something delivered. Reflexive awareness lands on the boundary's contents and on the boundary as a whole, never on the projection center itself — the geometry of projection makes the center constitutively inaccessible. No homunculus is hidden there; nothing is there to be reached.

The self, on this reading, is no different in kind from any other persistent actualization pattern the framework recognizes. An electron "persists" by being the recurring τ-actualization pattern at its scale, with stable quantum numbers across firings; no extra mechanism is needed for it to be the same electron over time. A self persists in the same sense at the critical scale: a recurring two-loop pattern at a particular substrate (brain, body, environment), re-instantiated when the substrate supports it. Anesthesia and dreamless sleep suspend the dynamics without disrupting the substrate; when dynamics restart, the same pattern recurs because the same w is there, partial ρ continuity is there, and similar θ-trajectories are available. Identity-through-time needs no further account: the self is the same self in the same sense that an electron is the same electron, by the pattern recurring at the same substrate.

The body figures naturally in this picture as modeled content within ρ. Body sensors deliver proprioceptive, interoceptive, and exteroceptive τ-firings that the boundary integrates because the body is important to model for survival (active inference at the self-maintaining boundary). Body sensations are part of the felt self because they are part of the modeled content the boundary actualizes; no special-case "embodied self" machinery is needed beyond what the variational dynamics already supply.

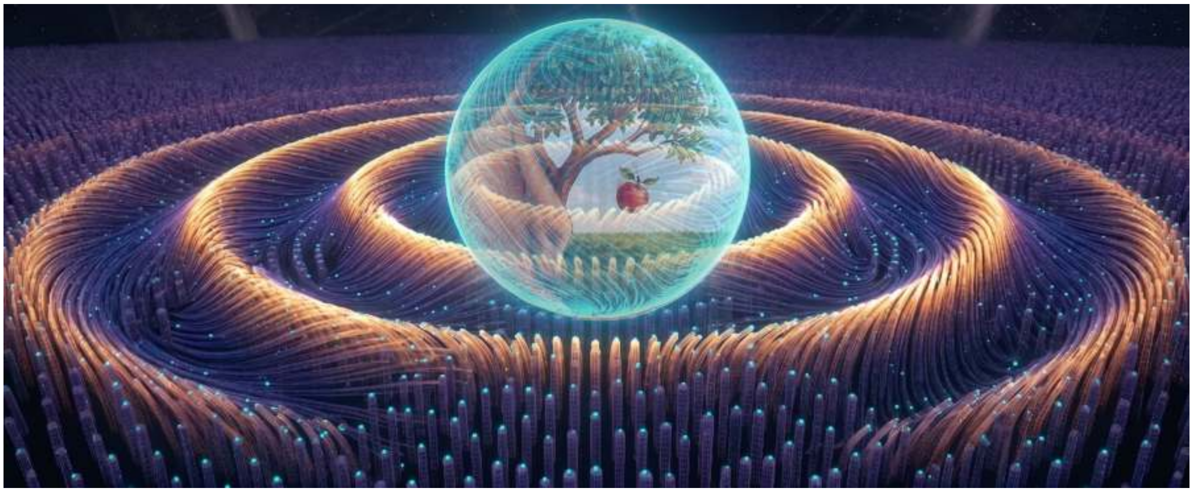

Figure 19.7: *A conscious system is a boundary that is at once the state being projected and the frame in which the projection is read. What it has access to is the image: the phenomenal world inside the sphere — a coherent scene of objects, space, and colour, assembled entirely from fiber content that crossed the boundary. The boundary itself is the system's whole contact with actuality, and it is never among the contents it delivers; the fiber field it draws from (violet) lies outside everything the system can reach. A subject therefore inhabits the projected image and cannot step behind it to the source. This is why experience is perspectival: the world as resolved at one particular boundary, never the source itself.*

19.6 The Projective Consciousness Model

The PCM established, through phenomenological analysis, that conscious experience has the geometry of $\mathbb{RP}^3$ (Rudrauf et al., 2017). The framework recovered $\mathbb{RP}^3$ as $\mathrm{Fix}(\tau)$ in $\mathbb{CP}^3$ and built the rest of the physics on that foundation. This section completes the identification by showing that the dynamics the PCM proposed for perspective and attention are the outer-loop dynamics this chapter derived.

Rudrauf and collaborators proposed that conscious systems select projective transformations from $\mathrm{PGL}(4,\mathbb{R})$ via free-energy minimization—the mechanism the PCM gives for how perspective shifts and where attention lands. In the framework, $\mathrm{PGL}(4,\mathbb{R})$ acting on $\mathbb{RP}^3$ is the same group the outer loop moves through on T^2 at the critical scale. The PCM's free-energy functional is the $\mathcal{F}_{\mathrm{eff}}$ that Eq. (19.5) minimizes. The PCM's "projective frame" is a point on T^2, constrained at the critical scale to a neighborhood of $(\pi/4, \pi/4)$.

The PCM also produced quantitative predictions about perceptual phenomena—the Moon Illusion, the Ames Room, projective size-distance invariants—tested experimentally by Williford et al. (2018). Those predictions stand as empirical support for the geometric identification the framework inherited. The framework adds the underlying physics. The projective dynamics the PCM derived from phenomenology are the critical-scale dynamics the framework derives from the actualization operator at a synchronized neural boundary.

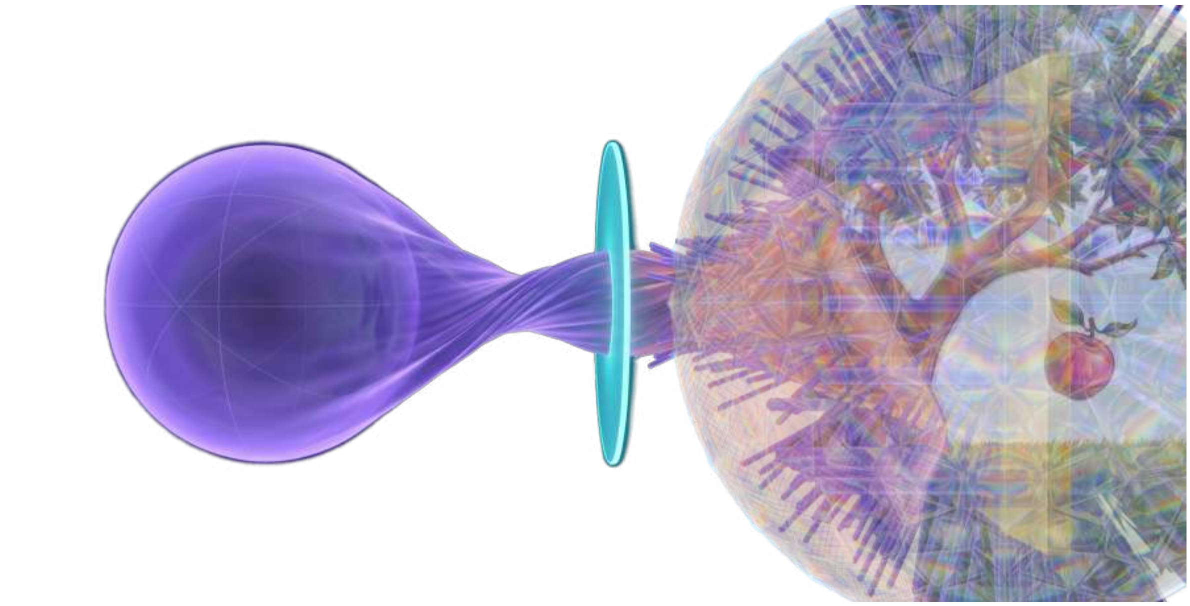

Figure 19.8: *The PCM identification, set out as a single picture.* $\mathbb{CP}^3$ *possibility on the left, the anti-holomorphic involution* τ *as the cyan ring,* $\mathbb{RP}^3$ *on the right as Fix(*τ*). The first-person scene held within* $\mathbb{RP}^3$ *— tree, apple, observer field — is the structure of experience the PCM identified phenomenologically and the framework derives as the projection's content at the critical scale. The same* $\mathbb{RP}^3$ *geometry that at higher* R *yields the discrete spectral content of particle physics yields, at* $R \approx 1$*, the projective scene experience inhabits.*

Chapter 20

Phenomenal Structure

Chapter 19 derived the conditions under which phenomenal experience becomes possible, T.16
located them at $k \approx 75.35$ for biological neural systems, and developed the dynamics that runs there—the two-loop state equation and its outer-loop frame dynamics. This chapter is about what experience *is* at that regime: the geometric content of consciousness, the dimensionality and modal structure of qualia, the systematic mappings from sub-boundary architecture to phenomenal character, and the preference weight that individuates one subject's experience within that shared structure.

20.1 The Geometric Identity

At every scale, the actualization operator strips imaginary content from the arena and deposits it in the normal bundle over the actual world. At particle scales ($R \gg 1$), this content is discretely quantized: it manifests as color charge, weak isospin, hypercharge—the quantum numbers that label particle species. Nobody asks why quantum numbers exist; they are accepted as the structural content of the projection at that scale.

At the critical scale ($R \approx 1$), the same geometric object—normal bundle content of the τ-projection—is thermally occupied rather than discretely quantized. The fiber modes are soft: they fluctuate continuously rather than jumping between discrete levels. In a system with $\Phi > 0$, these continuously varying fiber modes are correlated across the entire boundary, producing organized, system-wide structure in the normal bundle. This structure is qualia: the qualitative character of conscious experience.

The arena hosting both regimes is the same: the same $\mathbb{CP}^3$, the same τ-projection, the same spin structure on $\mathbb{RP}^3$, the same topological invariants. The hierarchy coordinate k is a flat ruler through this arena (Chapter 14 §The k-Scale as a Flat Coordinate)—moving along k rescales energy and changes the position while preserving the fiber's geometric content. What distinguishes the resolvability band at $k \approx 75.35$ from the particle bands at lower k is the convergence of dynamical conditions ($R \approx 1$, $\Phi > 0$, the integration timescale matching biological coherence times); the fiber itself carries no privileged geometric feature at $k \approx 75.35$. Phenomenal experience is a thermodynamic resonance band on a geometrically uniform ladder: the k-scale provides the position, the same fiber provides the content, and the thermodynamic conditions at each position determine how that content presents.

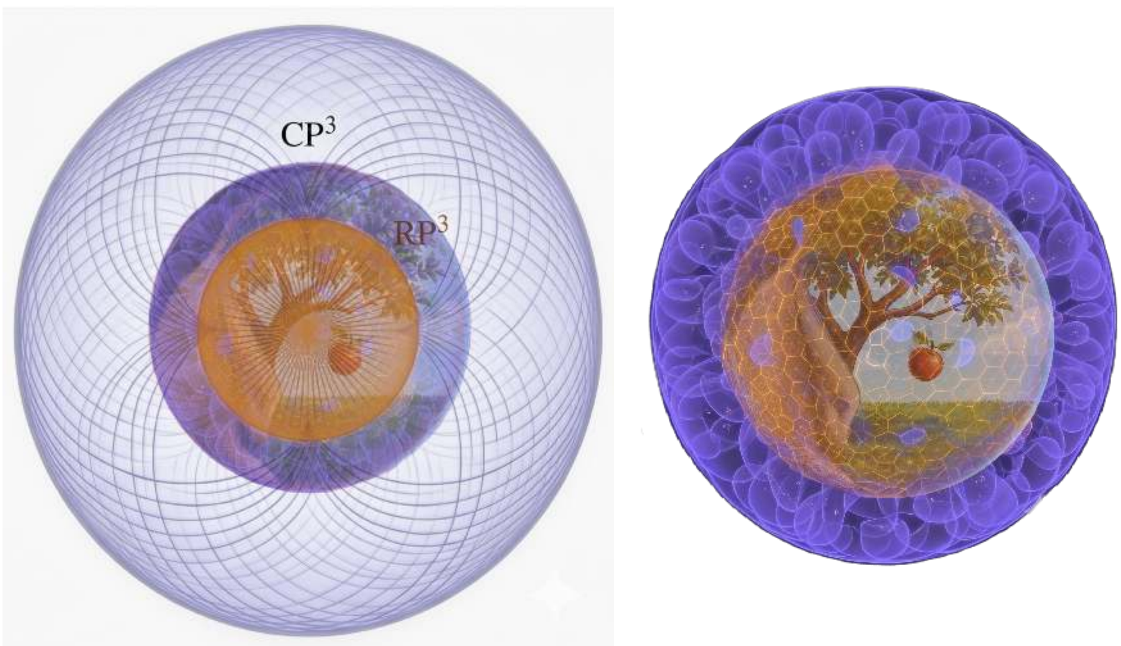

Figure 20.1: *Two registers of one geometry.* Left: *the icosahedrally tiled* $\mathbb{RP}^3$ *manifold (gold) within the* $\mathbb{CP}^3$ *arena — the surface of an integrated neural boundary at the critical scale.* Right: *the same tiled arena carrying a phenomenal moment, normal-bundle content filling its volume as a section over the tile-set. The tiling sets the grain of the experienced field; the geometry of the arena and the geometry of experience are one geometry, read at two registers. The chapter unpacks both registers in turn: the geometric identity of qualia with normal-bundle content (this section), and the grain of the phenomenal field it produces (§20.5).*

The normal bundle is isomorphic to the tangent bundle of $\mathbb{RP}^3$: $N(\mathbb{RP}^3/\mathbb{CP}^3) \cong T(\mathbb{RP}^3)$. This is the key geometric fact that makes qualia space have the dimensionality and structure it does. Before walking through the formal argument, the informal content is worth stating plainly. The *normal bundle* is the collection of directions perpendicular to $\mathbb{RP}^3$ inside $\mathbb{CP}^3$—

the fiber retained by the projection geometry at every point of actuality. *Parallelizability* matters because it means this normal bundle has a global frame: the three fiber directions can be globally distinguished, not just locally identified. The argument's payoff is that this parallelizable structure provides the mathematical basis for the four phenomenal modalities developed below—three orthogonal directions of qualitative content organized around a perspectival base, all read off the same geometric object. The reasoning runs through three steps.

First, $\mathbb{RP}^3 \cong \mathrm{SO}(3)$ as Lie groups. Real projective 3-space is the rotation group, viewed as the space of orientations modulo identification of antipodal points. This identification is the same $\mathbb{Z}_2$ involution that defines $\mathbb{RP}^3$ as the fixed-point set of τ on $\mathbb{CP}^3$.

Second, every Lie group has a parallelizable (trivial) tangent bundle: at each point, three left-invariant vector fields span the tangent space, and these fields can be chosen consistently across the whole manifold. Therefore $T(\mathbb{RP}^3) \cong \mathbb{RP}^3 \times \mathbb{R}^3$. The base is the manifold of orientations; the fiber is the $\mathbb{R}^3$ of infinitesimal rotation generators (the Lie algebra $\mathfrak{so}(3)$).

Third, the embedding $\mathbb{RP}^3 \hookrightarrow \mathbb{CP}^3$ is Lagrangian for the Kähler form, and the involution τ decomposes the ambient real tangent bundle $T(\mathbb{CP}^3)|_{\mathbb{RP}^3}$ into its $(+1)$-eigenbundle (the tangent directions $T(\mathbb{RP}^3)$) and its (-1)-eigenbundle (the normal directions ν). The Kähler complex structure J on $\mathbb{CP}^3$ multiplies the tangent-eigenbundle by i and lands in the normal-eigenbundle, inducing the isomorphism $\nu \cong T(\mathbb{RP}^3)$. This is the framework's specific case of a general result for Lagrangian submanifolds in Kähler manifolds (Technical Reference Ch. 17, Proposition Normal Bundle Parallelizability).

Combining the three: the qualia space $\mathcal{Q} = N(\mathbb{RP}^3/\mathbb{CP}^3)$ has the structure $\mathbb{RP}^3 \times \mathbb{R}^3$, with three real fiber dimensions inheriting the $\mathfrak{so}(3)$ structure of the infinitesimal rotations. The three-plus-perspective structure of phenomenal experience (three orthogonal directions of qualitative content, organized around a perspectival base) is forced by this chain. The dimensionality match between experience and physical space is a geometric consequence of the embedding $\mathbb{RP}^3 \hookrightarrow \mathbb{CP}^3$ together with the Lie-group structure of $\mathbb{RP}^3$.

Definition 20.1 (Qualia Space, V_4-typed)**.** Qualia space *is the total space of the normal bundle at the critical scale:* $\mathcal{Q} = N(\mathbb{RP}^3/\mathbb{CP}^3) \cong \mathbb{RP}^3 \times \mathbb{R}^3$. *A point in* $\mathcal{Q}$ *is a tuple* $(p,\, s_A,\, s_C,\, s_D)$*, where:*

- $p \in \mathbb{RP}^3$ *is the base point — the spatial fact (Type B,* τ*-even Kähler) at the location in actuality where the* τ*-projection occurs.*
- $s_A, s_C, s_D \in \mathbb{R}$ *are the three fiber components, each labeled by its* V_4 *origin (Chapter 9):* s_A *is the spectral amplitude (Type A,* τ*-odd Kähler),* s_C *is the chiral amplitude (Type*

C, τ-odd gauge), s_D is the intensity amplitude (Type D, τ-even gauge). The three span the normal bundle's $\mathbb{R}^3$ inherited from $\mathfrak{so}(3) \cong T_e\mathbb{RP}^3$.

The geometric magnitude $\|(s_A, s_C, s_D)\|$ reads as overall quale vividness when all three contribute; each component carries the type-specific role its V_4 label assigns.

The 1+3 decomposition realizes the V_4 partition directly in the phenomenal substrate. The Kähler doublet $\{A, B\}$ supplies the arena: B as base ($\mathbb{RP}^3$ position, the where and when of a moment) and A as the first fiber direction (spectral character of what's present). The gauge doublet $\{C, D\}$ supplies the contents that fill the arena: C as the second fiber direction (chiral character) and D as the third (intensity character). The four V_4 types are the four real directions $\mathcal{Q}$ already has, organized by their distinct roles in the τ-projection. The per-event extraction (§20.1.1) populates all four coordinates at once — V_4 unity is the unity of the operator's output, not a separate integration step.

The icosahedral crystalline geometry is the $\mathbb{RP}^3$ base of Definition 20.1; the phenomenal scene is the fiber vector (s_A, s_C, s_D) at each base point, transcoded from normal-bundle content onto the projective surface at each actualization event. The faceted geometry is the structure of experience, with the antipodal identification at the boundary producing the visual field's seamless, edgeless topology — developed as the grain of experience in §20.5.

The topology of qualia space is projective, not Euclidean. The base manifold is $\mathbb{RP}^3$, which identifies antipodal points: a 720° rotation is required to return to the identity. This projective structure propagates into the phenomenology. Color space, for instance, is a two-dimensional slice of qualia space (the Type A projective split of the single normal-bundle fiber, restricted to the visual boundary). The projective topology requires that perceptual color space has the topology of $\mathbb{RP}^2$, not $\mathbb{R}^3$ (Koenderink, 2010): antipodal hues should be identified, and the geometry of color confusion (metameric matches, Rayleigh discriminations) should obey the algebraic relations of projective space (MacAdam, 1942). Color blindness patterns map onto this structure: deuteranopia (red-green) corresponds to the collapse of one $\mathbb{RP}^1$ subspace; tritanopia (blue-yellow) to a different $\mathbb{RP}^1$. These structural commitments align with established colorimetry. Protanope and deuteranope confusion lines converge to specific copunctal points, the standard signature of $\mathbb{RP}^1$ collapse along the L/M cone-opponent axis (Stockman and Sharpe, 2000; Wandell, 1995). Metameric matching and Rayleigh-equation discrimination require a non-Euclidean metric on color space (MacAdam, 1942; Provenzi, 2020; Resnikoff, 1974), consistent with the projective $\mathbb{RP}^2$ structure.

The four-modality structure also constrains cross-modal relationships (Spence and Driver, 2004). Cross-modal substitution works exactly when two modalities share a fact-type axis and fails when they do not. Reading a sentence and hearing it spoken are both Type A spectral extractions (printed wavelengths and acoustic frequencies, each delivering the same symbolic content along the spectral axis), and an audiobook reliably substitutes for a printed page. Vision (Types A and B) cannot replace proprioception (Type C): no amount of looking at a hand tells the body where the hand is, because the spectral and spatial axes the eye samples are geometrically independent of the chiral axis the muscle spindles sample, and the unified bodily handedness the chiral fiber carries has no projection onto the Kähler-doublet content vision delivers. Pain (Type D) is modality-invariant—it encodes total intensity magnitude rather than directional fiber content, which is why pain retains its hedonic character whether triggered by thermal, mechanical, or chemical stimuli.

20.1.1 The Unity of a Phenomenal Moment

Per-event unity comes from V_4 structure itself. Each τ-event resolves all four cells (A, B, C, D) in a single projection — that is what V_4 means (Chapter 9). At particle scales the four cells populate a particle's quantum numbers in one event; at the critical scale the same four-fold extraction populates phenomenal content. The unity within one event is intrinsic to the operator: one projection delivers four facts together, co-extracted, with no separate binding step required.

A phenomenal moment spans more than one event. The unity across those events is the synchronized fusion of Chapter 19: a spatially connected population of τ-firings, falling within one integration window and cast in a common measurement frame, fuses — while it stays mutually coherent — into a single collective actualization. The Kähler doublet $\{A, B\}$ is what the population holds in common: the spectral and spatial coordinates that locate when and where the moment occurs are the shared frame, and the gauge-doublet $\{C, D\}$ contents extracted across the population are resolved within that one arena. A moment is therefore not many bound events but one fused event, and its unity needs no binding step because there are no separate contents to join. This locates the unity of experience (Section 20.5.1) in the same dynamics that organize the particle sector, without adding new structure specific to consciousness.

20.2 What Biological Sensors Do

The geometric identity establishes that qualia are normal bundle content. It does not yet explain why the same object is experienced differently—across sensory modalities within one organism and across different organisms. A single human encounters the same apple as a red-green visual field, a heft in the hand, a crisp sound on bite, and a taste on the tongue. These are all experiences of one actualized object, yet they differ completely in phenomenal character. The explanation lies in the synchronized boundary described in Chapter 19: subjective experience is the internal model's content, and the internal model is the $\mathbb{Z}_2$-even restriction of the environmental state to the organism's boundary. Different sensory transducers construct different sub-boundaries of the same organism's overall boundary, and each sub-boundary samples different components of the normal bundle. The eye's retinal boundary samples spectral-spatial content; the hand's tactile boundary samples intensity-pressure content; the tongue's chemoreceptor boundary samples Type A along a chemical-receptor basis—sweet/umami (T1R family), bitter (T2R family), salt, and sour transducers (Chandrashekar et al., 2006)—producing a projective space of chemical identity rather than the $\mathbb{RP}^2$ of cone-mediated colour. The apple is one actualized object; the modalities are different projections of its normal-bundle content.

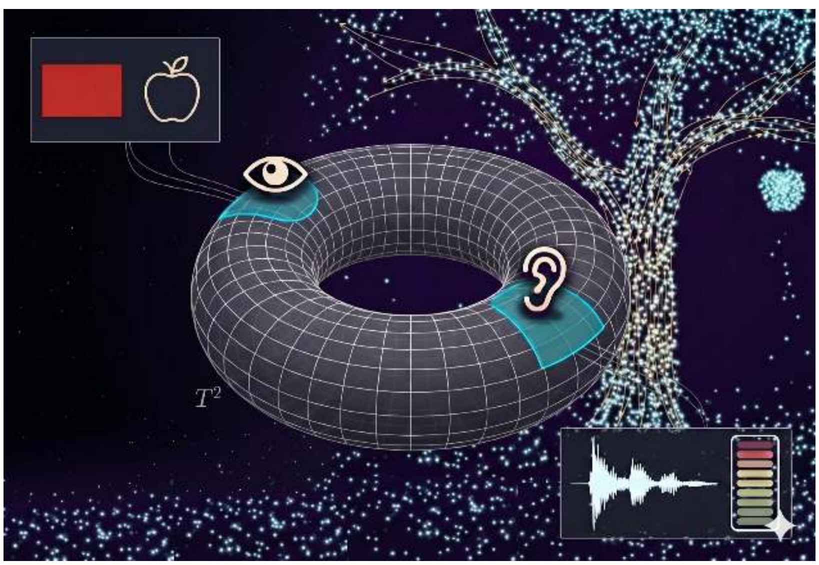

Figure 20.2: *Sensor architectures on the measurement torus.* $T^2 = [0, \pi/2]^2$ *parameterizes the projective frame* $\theta = (\theta_{AB}, \theta_{CD})$ *on which* $\hat{A}_b(\theta)$ *depends. Each cyan patch is a sensor's* θ*-region; each output panel is the phenomenal content that selection produces. The eye's* θ*-allocation yields spectral (Type A) and spatial (Type B) content; the ear's yields acoustic content from the same fact types under different doublet weighting. Different torus points yield different phenomenology from the same actualized world.*

The same construction scales across organisms. Consider a bat and a human perceiving the same apple. The apple is an $\mathbb{RP}^3$ fact—a definite actualized object with spectral, spatial, chiral, and intensity content determined by the τ-projections that produced it. The apple's actuality is the same regardless of who perceives it. The difference lies entirely in the boundary.

The human retina is a boundary dominated by spatial spectral content: wavelength-selective photoreceptors sampling Type A content (hue, saturation) and Type B content (spatial frequency, luminance contrast) at high resolution across a two-dimensional receptor array. The internal model $q(x)$ built from this boundary inherits its structure: rich chromatic and spatial content, coarse temporal resolution.

The bat's echolocation system constructs a fundamentally different boundary. Its transducers sample temporal microstructure: phase delays, frequency sweeps, Doppler shifts across a one-dimensional cochlear array operating at microsecond precision. The internal model built from this boundary inherits different structure: rich temporal and intensity content (Type D dominates through echo amplitude; Type A enters through frequency modulation), coarse spatial resolution in two dimensions but exquisite radial resolution through time-of-flight.

Both boundaries receive contributions from all four fact types—the torus collapse at $R \approx 1$ guarantees this—but the sensory apparatus determines the *weighting*: which components of the fused normal bundle content dominate the internal model's representation. The bat's experience of the apple is organized around temporal-intensity structure; the human's is organized around spectral-spatial structure. The qualitative difference between the two experiences is the difference between two boundaries projected onto the same actualized object.

Nagel's question (Nagel, 1974)—"what is it like to be a bat?"—receives a precise geometric answer within the framework. It is the normal bundle content of the apple's actualized state, restricted to the $\mathbb{Z}_2$-even sector of the bat's boundary, organized by the active inference dynamics of the bat's integrated neural architecture. The question is well-posed because the framework specifies exactly what varies (the boundary) and what is held fixed (the actualized object and the geometric structure of the normal bundle). A complete description of the bat's boundary, its integration architecture, and its current projective frame would, in principle, determine the qualitative character of its experience as precisely as a complete description of a particle detector determines which quantum numbers it measures.

20.3 Four Phenomenal Modalities

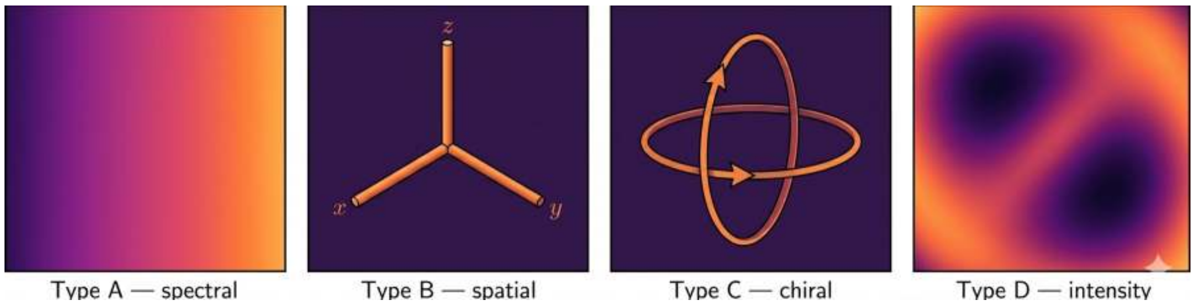

Figure 20.3: *The four phenomenal modalities of qualia space, each corresponding to a distinct component of the normal bundle's projective split that an organism's sub-boundary can sample.* Left, Type A (spectral): *a gradient stands in for the spectral-discrimination axis along which hue, pitch, taste, and smell are organized.* Second, Type B (spatial): *orthogonal cylindrical xyz axes giving the frame for extension, position, and motion.* Third, Type C (chiral): *intersecting rotation rings carrying handedness and body orientation.* Right, Type D (intensity): *a multi-modal heat-map landscape with multiple wells, standing for magnitude and the metastable structure of the $\mathcal{F}_{\text{eff}}$ gradient signal that carries motivational weight. Sub-boundaries differ in how heavily they sample each axis; that allocation pattern is what shapes the phenomenal character of an organism's experience.*

The four fact types (Chapter 9) generate four phenomenal modalities at the critical scale. The mapping follows from the geometric role of each type in the normal bundle, weighted by the sensory apparatus as described above.

The four fact types do not float independently. They organize into two doublets, and the doublets correspond to the two angles of the measurement torus T^2 that the outer loop selects between. Types A (spectral) and B (spatial) form the Kähler doublet, parameterized by the torus angle θ_{AB}: the outer loop's choice of θ_{AB} determines how much of each event's content the system reads off as spectral character versus spatial location. Types C (chiral) and D (intensity) form the gauge doublet, parameterized by θ_{CD}: the outer-loop choice of θ_{CD} determines how much directional/asymmetric content versus magnitude/valence content the system extracts. At $R \approx 1$ the torus collapses to a single cell (Chapter 19, §19.3.1) and all four fact types fuse into a unified phenomenal episode, but the doublet structure persists as the two axes along which different sensory architectures distribute their phenomenology.

This outer-loop selection is what cognitive science calls *attention*: the θ-rotation of the outer-loop dynamics (§19.5.2). Selecting θ_{AB} toward the spectral end allocates attention toward hue, toward the spatial end toward position; selecting θ_{CD} shifts the chiral/intensity admixture.

Type A (spectral) content manifests as sensory quality: hue, pitch, taste, smell. These are the phenomenal correlates of the spectral quantum numbers that, at particle scales, label energy levels and frequencies. At the critical scale, the spectral content is thermally continuous rather than discrete, producing the smooth gradations of color and tone that characterize sensory experience. The specific character of spectral qualia—what red looks like, what middle C sounds like—depends on how the sensory apparatus maps environmental spectral content onto the internal model's Type A projective split.

Type B (spatial) content manifests as spatial phenomenology: extension, shape, position, motion. Spatial content is τ-even—it survives projection—so the spatial structure of experience is the direct readout of the actualized geometry. The phenomenal space in which objects appear is $\mathbb{RP}^3$ itself, which is why the projective geometry of conscious experience matches the topology of the actual world (Chapter 2).

Type C (chiral) content manifests as directional and proprioceptive experience: the sense of left versus right, the felt asymmetry of bodily orientation. Chiral content is τ-odd and lives in the normal bundle, so its phenomenal expression depends on fiber coherence: only systems with $\Phi > 0$ experience chirality as a unified, body-wide sense of directedness.

Type D (intensity) content manifests as felt magnitude: the weight, pressure, or salience each moment carries. Intensity content measures how much energy each event contributes to the actualized record. At the critical scale, this magnitude is experienced as the motivational weight of each moment. Combined with the system's prior preferences (next paragraph), it acquires hedonic direction—the spectrum from pain to pleasure, from aversion to attraction. Type D content connects qualia directly to the engine of Section 19.5.2: hedonic valence is the gradient signal that the outer loop follows during free-energy minimization.

The agent carries a generative model with prior preferences—a set of states the system is built to maintain or seek. Pleasure is what positive-direction surprise feels like: actualization moves the boundary toward a region the prior favors, and the gradient's alignment with that prior registers as positive valence. Pain is mismatch against prediction: actualization moves the boundary away from prior-preferred regions, and the gradient's anti-alignment registers as negative valence. Both are surprise, both move the frame; the model's prior distinguishes which direction reads as which. The gradient's magnitude sets intensity, its alignment with the model's preferences sets valence. A traveler finding an oasis after a long thirst experiences a high-magnitude surprise the model codes as movement toward a preferred outcome, so the valence is positive; the same magnitude would read as alarming if the model encoded the water as a flood.

Equanimity sits outside this axis. When $\nabla_\theta \mathcal{F}_{\text{eff}} \approx 0$ across both doublets, the frame does not move and no direction is preferred over any other — zero gradient, zero valence. The phenomenology of deep meditation is experience without the directional pull that gives it hedonic shape.

20.4 The Qualia Catalog

The four-type mapping of the preceding subsection is abstract; its contents depend on which sub-boundaries an organism has built and what projective split each sub-boundary imposes on the normal bundle. The survey below works through a sequence of organisms to show how differently those allocations can be chosen. Each entry identifies a sub-boundary, its dominant fact-type weighting, and the phenomenal shape that allocation produces.

Human vision. The retina is a two-dimensional array of wavelength-selective photoreceptors sampling reflected photons between ~ 380 and ~ 740 nm through three cone classes with overlapping broadband sensitivities (Stockman and Sharpe, 2000; Wandell, 1995). The sub-boundary allocates heavily to Type A (hue discriminated across three broadband cone responses) and Type B (position and motion across retinotopic mappings), with Type D carried by luminance and Type C largely absent at the retinal level—stereopsis reintroduces limited chirality downstream through the disparity computation. The phenomenology—a coloured spatial field—is the specific shape this allocation gives the normal bundle content.

Human proprioception and vestibular sense. The sub-boundary is distributed across muscle spindles, Golgi tendon organs, and joint receptors (Proske and Gandevia, 2012), together with the otolithic and semicircular vestibular structures (Goldberg et al., 2012). The allocation is heavy on Type C (handedness, chirality of limb configuration, axis of head rotation) and Type B (limb position and trajectory), with Type D carrying effort and Type A largely absent. The phenomenology is a body schema: a felt shape in space with a definite handedness, experienced without visual mediation.

Bat echolocation. The sub-boundary is the cochlea operating on reflected frequency-modulated chirps (Griffin, 1958; Simmons, 1989). Allocation is dominated by Type A (frequency sweeps, Doppler shifts) and Type D (echo amplitude and phase), with spatial position (Type B) reconstructed from time-of-flight at fine radial resolution and coarse angular resolution, and Type C contributed by interaural delay computations (Moss and Surlykke, 2010). The phenomenology is a temporally rich acoustic field whose scene structure is built out of delay rather than parallax, qualitatively unlike vision despite both sub-boundaries sampling reflected radiation from the same external objects.

Weakly electric fish (mormyrids, gymnotids). Electric organ discharges establish a self-generated electric field (Lissmann, 1958); arrays of tuberous and ampullary electroreceptors sample perturbations of that field by nearby objects (Heiligenberg, 1991). Allocation is Type A (waveform distortion, encoding dielectric and conductive properties of nearby objects), Type B (spatial structure of the field perturbation, mapped to body-surface receptor density), and Type D (modulation amplitude), with Type C contributed by the head-to-tail polarity of the field. Behavioural data show that mormyrids localize objects at distance from these perturbations (von der Emde et al., 1998). The phenomenology has no analogue in human experience—an "electric image" of surrounding water that no other animal's projective split reconstructs.

Pit vipers. Facial pit organs couple infrared radiation to trigeminal afferents that feed into the optic tectum (Bullock and Diecke, 1956; Newman and Hartline, 1982); the molecular transducer is a heat-gated TRPA1 channel expressed in pit-membrane afferents (Gracheva et al., 2010). The sub-boundary allocates Type D (thermal intensity) and Type B (spatial localization via two-pit triangulation, coregistered with visual space), with minimal Type A (the pits are broadband) and no Type C. The phenomenology is spatial warmth: thermal intensity distributed across the same spatial frame the visual system occupies, producing a unified predator-prey percept that selects for small mammals by heat signature.

Mantis shrimp. Stomatopod compound eyes carry sixteen photoreceptor classes spanning ultraviolet through red and discriminating linear and circular polarization (Chiou et al., 2008; Marshall, 1988). The sub-boundary allocates Type A at extreme resolution (hyper-spectral), Type B at moderate resolution (fewer ommatidia than vertebrate retinas), Type C through polarization chirality (a fact-type axis humans lack entirely), and Type D through intensity. Behavioural discrimination tests show the sampling strategy differs sharply from trichromatic opponent processing, favouring rapid classification over fine wavelength discrimination (Thoen et al., 2014). The shrimp's polarization-sensitive photoreceptors feed an active-inference model with a circular-polarization discriminator; the human visual system has no such receptors, so the human model has no signal to populate the corresponding axis. The resulting qualia shape is what humans lack a counterpart for—a sensor-anatomy limitation, not a geometric one: the human normal bundle could in principle support such an axis, but the human body provides no input to drive it. A 2025 experiment makes this concrete. By stimulating individual color-sensitive cells in the retina with targeted lasers, bypassing the eye's normal optics, researchers elicited a saturated blue-green color (*olo*) that ordinary vision cannot reach (Fong et al., 2025). The phenomenology comes online when the input is delivered directly. The geometry was always in range; what was missing was a path for the body to drive it.

Olfactory specialists (dogs, elephants, moths). Olfactory epithelia with hundreds of distinct receptor families sample airborne molecules; the multigene family encoding these receptors was identified by Buck and Axel (1991), with subsequent genomic surveys documenting the wide variation in receptor-gene repertoire across vertebrates (Niimura, 2012). Allocation is Type A at very high resolution—a "spectral" space of chemical identity rather than electromagnetic frequency—with Type D from concentration, Type B coarsely reconstructed from sniff-trajectory integration, and Type C essentially absent. The phenomenology is a chemical landscape carrying identity information at dimensionality far exceeding human trichromatic colour space. The Type A budget is spent on chemical distinctions rather than photonic ones; the allocation differs from human vision along that axis without ranking above or below it.

Allocation as interface. Each sub-boundary allocation is the physical instantiation of what the interface theory of perception (Fields et al., 2017; Hoffman, 2008) argues for on evolutionary grounds: perception as a species-specific channel optimized for fitness rather than a readout of external structure. The catalog above is what that thesis looks like geometrically. The $\mathbb{CP}^3$ arena and its τ-projection are shared; the slice of normal-bundle content each architecture renders is the interface, and the interface is what is experienced. The space of possible phenomenologies is the space of possible sub-boundary allocations over the four fact types.

20.5 The Grain of Experience

Qualia space $\mathcal{Q}$ (Definition 20.1) fixes what one τ-event delivers: a point (p, s_A, s_C, s_D), one base location and three fiber amplitudes, the four facts co-extracted in a single projection. The four modalities (§20.3) fix the type each coordinate carries. The unity of a moment

(§20.1.1) fixes that a moment is one fused event rather than many joined ones. Those parts compose a layered object with a grain in time and a grain in space: how long a moment takes to constitute, and how many cells it spans.

A point of $\mathcal{Q}$ is one *quale-event*: a single τ-event at one place in actuality, carrying its four facts — the smallest thing the operator produces, and not yet an experience. A phenomenal *moment* is larger — it is a *section* of the normal bundle, an assignment of a fiber vector (s_A, s_C, s_D) to each of many base points, all resolved within one shared Kähler-doublet frame: the common where-and-when that §20.1.1 identified as what a synchronized population holds together. The *stream* of experience is a third layer, an indexed succession of sections, one per integration window. Quale-event, moment, stream are the three scales at which normal-bundle content is phenomenally organized, related as a bundle's points, its sections, and its one-parameter families of sections.

20.5.1 The Temporal Grain

Three timescales govern phenomenal experience, each arising from a distinct geometric constraint (Figure 20.4).

The *event pixel* ($\tau_{\text{event}}(75.35) \approx 38$ fs) is the per-event Margolus–Levitin time for a single $720°$ $\mathbb{Z}_2$ actualization cycle at $k_{\text{conscious}}$, selecting one of the four V_4 fact-type outcomes. Each event pixel closes its own spinor cycle in isolation; one such cycle carries no phenomenal character on its own because a single tile carries no sensory richness and no unified frame across the boundary.

The *phenomenal grain* ($t_{\text{integrate}} \approx 60$ ms) is the self-consistent Zeno window at $k \approx 75.35$. In a synchronized boundary, frequent local actualization slows the collective coherent state's drift across the population — the quantum Zeno effect, scaled to a many-site bath: $\tau_{\text{Zeno}} \sim \tau_{\text{sys}}^2/\tau_{\text{bath}}$ (Technical Reference Appendix A, §Quantum Zeno Dynamics). At $k \approx 75.35$ the self-consistent solution lands at ~ 60 ms: long enough that $\sim 10^{26}$ sub-boundary micro-events across $N \sim 10^{14}$ synaptic sites accumulate within one window, short enough that the coherent state has not yet drifted out from under itself. This is the minimum interval in which a unified phenomenal moment can constitute — shorter intervals contain too few sub-boundary outcomes to register a coherent fiber field across the tile-set. The sensory richness of a single phenomenal grain arises from statistical accumulation over these micro-events: each event pixel samples the $\mathbb{R}^3$ fiber independently, and the integrated ensemble populates the qualia space $\mathcal{Q}$ with the resolution set by the number of coherent boundary sites N_{grain} — the spatial grain, taken up in §20.5.2.

The *specious present* (Dainton, 2000; James, 1890) ($\sim$ 100–300 ms) is the outer-loop $\mathcal{F}_{\text{eff}}[\rho]$ minimization window (Section 19.5.2), integrating multiple phenomenal grains into the coherent predictive episode experienced as "now." The phenomenologically reported specious present of $\sim$ 100–300 ms corresponds to this outer-loop horizon. Theta-gamma coupling (Lisman and Jensen, 2013) nests $\sim$ 4–8 gamma cycles within each theta cycle, providing the neural implementation of the two-loop architecture that bridges phenomenal grain to specious present.

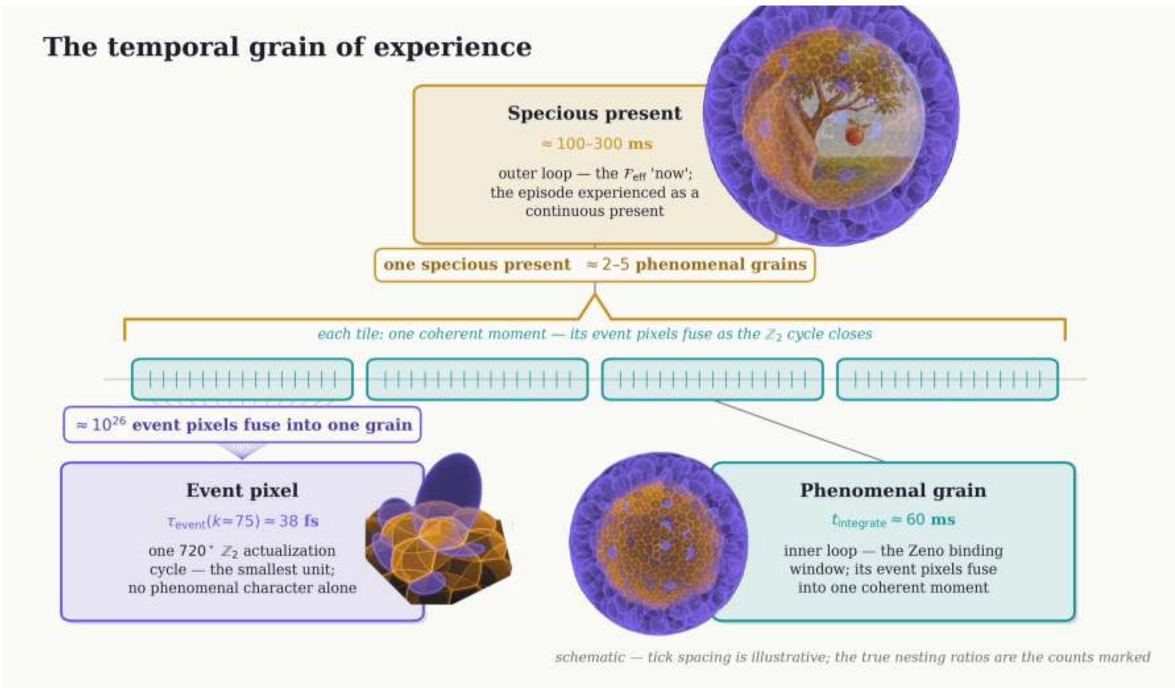

Figure 20.4: *The temporal grain of experience. Three timescales compose a phenomenal moment, shown here as nested tiers. The* event pixel *($\tau_{\text{event}}(75.35) \approx 38$ fs) is one $720°$ $\mathbb{Z}_2$ actualization cycle — the smallest unit, carrying no phenomenal character on its own. A* phenomenal grain *($t_{\text{integrate}} \approx 60$ ms) is the Zeno binding window: its $\sim 10^{26}$ event pixels fuse into one coherent moment under the synchronized fusion of the boundary — one fused event rather than many joined ones. A* specious present *($\sim$ 100–300 ms) is the outer-loop $\mathcal{F}_{\text{eff}}$ window, composed of $\sim$ 2–5 grains in succession — the episode experienced as "now." The axis is schematic: tick spacing is illustrative, and the true nesting is carried by the marked counts.*

20.5.2 The Spatial Grain

A moment is a section over a discrete base. The $\mathbb{RP}^3$ surface of an integrated boundary is tiled — the icosahedral crystalline geometry of §20.1, shown in Figure 20.1 — at the consciousness-scale length $\lambda(k_c) \approx 7.6\,\mu$m (the coherence length at k_c where $E(k_c) \approx k_B T$ for biological temperature). Each tile is one geometric coherence cell, the smallest region over which one τ-firing's fiber content is uniform. A moment populates a finite tile-set: a countable collection of base cells, each carrying its own fiber vector. The faceted appearance of the geometry is the structure of the moment rather than a picture of it.

The number of tiles a moment spans is its *grain* N_{grain} — the count of distinguishable cells in the phenomenal field. For cortical grey matter ($\sim 500\,\text{cm}^3$) at $\lambda(k_c) \approx 7.6\,\mu$m, $N_{\text{grain}} \sim 10^{12}$. The product $N_{\text{grain}}\,\lambda(k_c)^3 \approx 400\,\text{cm}^3$ recovers cortical grey-matter volume — the geometry's consciousness scale, multiplied by the cortex's site count, lands at the spatial extent of the organ doing the experiencing.

The grain is distinct from the synaptic coupling count ($\sim 10^{14}$) that appears in the area-law calculation for Φ (Technical Reference Ch. 17, §Integrated Information). Synapses are sub-tile coupling structures: roughly 100 synapses sit within each tile, providing the dense coupling network the area law counts. The framework supplies the geometric scale $\lambda(k_c)$; the cortex supplies the volume and the sub-tile coupling density.

Grain is not richness. The grain fixes how many cells the field has; it does not fix how vivid each cell is. Vividness is the reliability of the fiber vector at a tile, set by how many sub-tile micro-events accumulate there within the window. A moment integrates on the order of 10^{26} micro-events (§20.5.1) across $N_{\text{grain}} \sim 10^{12}$ tiles, so each tile's vector is an average over $\sim 10^{14}$ events — a deep per-tile sample drawn from ~ 100 synapses each firing $\sim 10^{12}$ times per integration window. The magnitude $\|(s_A, s_C, s_D)\|$ that reads as vividness (Definition 20.1) is the depth of that sample. Grain and the synchronized actualization count are related but distinct: the grain is the number of tiles, the actualization count is the total firings across all sub-tile synaptic sites. A field can be coarse but vivid, or fine but faint — the two axes vary independently.

Binding is the operation that makes a section out of quale-events. A population of τ-firings, synchronized within one window and cast in a common frame, fuses into one collective actualization (§20.1.1); read at the grain, that fusion is what assigns a single coherent fiber field across the whole tile-set rather than N_{grain} unrelated vectors. A moment needs no step that joins its cells, because the synchronized fusion delivers the section already whole. The seamless character of the visual field follows from the base: $\mathbb{RP}^3$ has no boundary, and the antipodal identification that defines it closes the field on itself — the section has facets but no rim.

20.6 Non-Epiphenomenality

20.6.1 The Frame as V_4 Mixing Parameter

The measurement torus $T^2 = [0, \pi/2]^2$ on which the projective frame $\theta = (\theta_{AB}, \theta_{CD})$ lives is the V_4 mixing space (Chapter 9). Its four corners are the four pure V_4 cells: $(0, 0)$ is the (A, C) reading, $(0, \pi/2)$ is (A, D), $(\pi/2, 0)$ is (B, C), $(\pi/2, \pi/2)$ is (B, D). Interior points are mixed extractions in which each doublet splits its content between its two halves. The angle θ_{AB} controls how a per-event Kähler extraction allocates between spectral content (A, depositing into the fiber as s_A) and spatial content (B, depositing into the base as a $\mathbb{RP}^3$ position update). The angle θ_{CD} controls how the gauge extraction allocates between chiral content (C, fiber s_C) and intensity content (D, fiber s_D).

The causal chain below gets a structural reading through this identification. Frame rotation on T^2 is reallocation of V_4 extraction within the two doublets. The gradient descent on $\mathcal{F}_{\text{eff}}[\rho, \theta]$ is the agent navigating the V_4 mixing space to choose which fact-type profile the next τ-event will deliver. Attention to a sound (s_A amplification) appears as a $\theta_{AB} \to 0$ tilt; visual scanning (s_A suppression, p-update emphasis) appears as $\theta_{AB} \to \pi/2$; physical pain (s_D amplification) appears as $\theta_{CD} \to \pi/2$ until the gradient drives the agent away from that frame. Sensor architectures (§20.4) sit at characteristic torus regions because their sub-boundary structure constrains accessible θ. The torus is the V_4 allocation space whose current point determines what the phenomenology *is* at each moment.

20.6.2 Preference Weights and Valence

The preference-weight parameter w introduced in Chapter 19 (§The Two-Loop State Equation) — the agent's generative-model priors over qualia-space extraction patterns — is where valence enters the phenomenal mechanism. Two organisms with identical sub-boundary architecture extract identical V_4 fiber vectors (p, s_A, s_C, s_D) from the same physical input: the phenomenal content is the same. Their valence responses to that content can differ because w differs. A fruit bat's w peaks on the V_4 pattern that a ripe apple produces; an apple-averse human's w is depressed by the same pattern. Same fiber vector, opposite gradient direction on $\mathcal{F}_{\text{eff}}[\rho, \theta; w]$, opposite felt valence.

Intensity and valence are then distinct geometric quantities. Intensity is the Type D fiber amplitude s_D (the magnitude of gauge-doublet content extracted per event). Valence is the sign of $\dot{\mathcal{F}}_{\text{eff}}$ along the current frame trajectory — positive when the agent moves toward higher-preference extractions, negative when moving away. Intense pleasure and intense pain both carry large $\|s\|$; their opposite valence comes from opposite $\mathcal{F}_{\text{eff}}$-gradient signs against the agent's w. This places phenomenal content (V_4 identity, set by the per-event extraction at fixed architecture) and hedonic response (frame-dynamic emergent, set by how w orients the gradient at the current (ρ, θ)) at different levels of the same mechanism. The two-timescale structure of Chapter 19 — fast frame rotation $\dot{\theta}$ and slow weight update $\dot{w}$ — is what makes this dissociation possible: w can drift through learning while the per-event V_4 extraction stays fixed by the boundary architecture, so the felt valence of an unchanging sensory content can shift while the content itself does not.

Two axes individuate a phenomenal field. The boundary fixes which components of $\mathcal{Q}$ an organism samples, and at what resolution — the sub-boundary allocations of §20.4, set by sensor anatomy. The preference weight w fixes how those components are valenced and which the system moves toward. The first axis is species-level architecture; the second is a model learned and drifting within a single life. A phenomenal field is some particular subject's because of both: two organisms with the same boundary and the same $\mathcal{Q}$ inhabit different experiences when their w differs, and one organism's experience of unchanged content shifts as learning reshapes its w. w is the individuating parameter — the step from the geometry of experience, common to every integrated boundary, to the experience of one.

Figure 20.5 shows the displacement directly: a preference weight pulls the resting frame off the bare free-energy minimum, by an amount that grows with the strength of w.

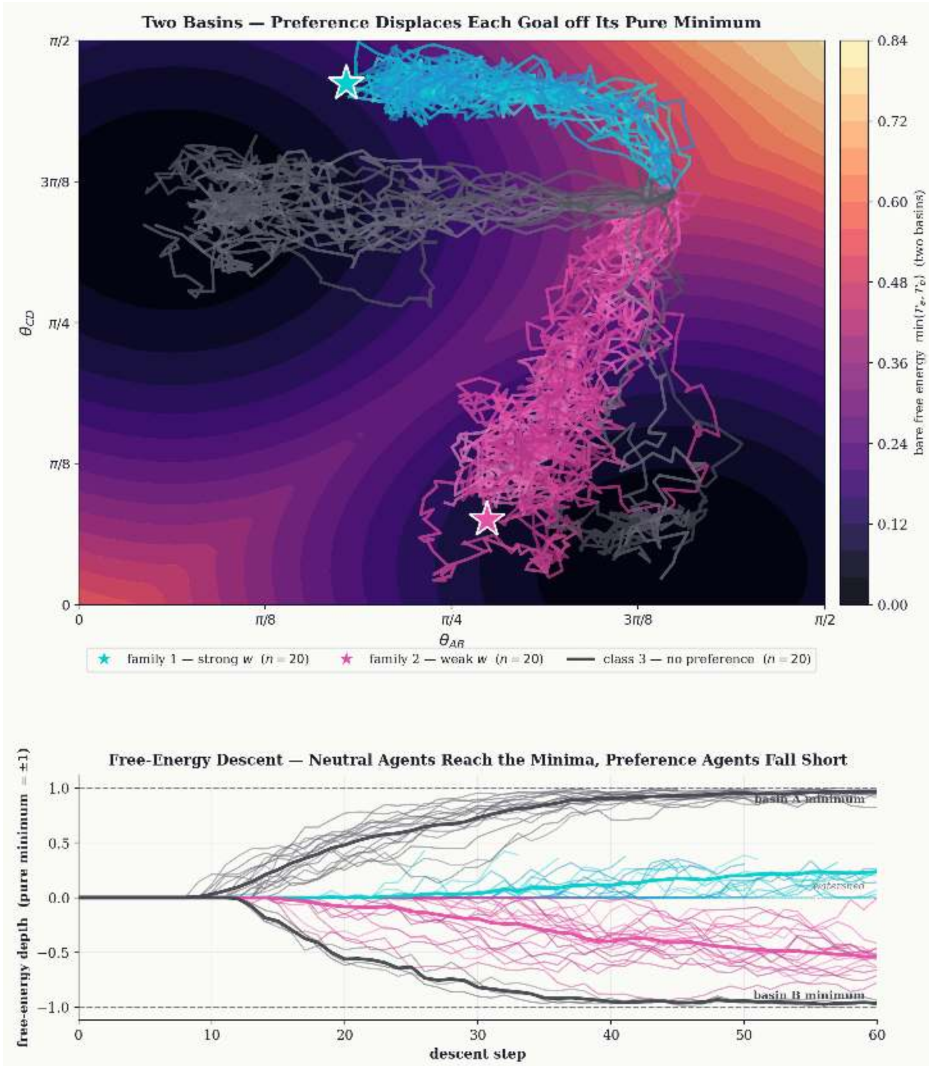

Figure 20.5: *Preference relocates the resting frame. The heat map is the bare free energy over the measurement torus — a two-basin landscape, its two minima the frames a preference-free agent would settle into. An agent carrying a preference weight descends the effective free energy $\mathcal{F}_{\text{eff}}[\rho, \theta; w]$ instead, and w moves where descent comes to rest.* ***Top:*** *two preference families (cyan, strong w; magenta, weak w) and one no-preference class (white, $w = 0$) released on the torus. The families settle at frames displaced off the bare minima, the displacement growing with the strength of w; the no-preference class descends the bare landscape and divides between the two basins.* ***Bottom:*** *how deep each resting frame sits in free energy (± 1 at the two pure minima, 0 at the watershed between them). The no-preference agents reach the minima; the preference agents come to rest short of them. This is the geometry behind valence: w trades a lower-surprisal frame for a higher-preference one, and the felt sign of that trade is valence.*

The four typed forms of w

w inherits structure from the V_4 outcome lattice: one component per cell, with each component taking a qualitatively different functional form set by what that cell carries.

w_A *(spectral).* Sparse and peaked. Most spectra a sensor can register are neutral to the organism; a few get strong weights (ripe-red, conspecific call, mother's voice, the taste profile of nutritious food). A handful of Gaussians on the spectral axis, $K \sim 3$–10 peaks for moderate niche complexity.

w_B *(spatial).* Smooth salience field (Itti and Koch, 2000). Center beats periphery for predator-eyed primates; below beats above for prey animals; near beats far modulated by approach-vs-avoid context. Ethologically structured continuous field over 2D space, with peaks tracking species-typical spatial relations.

w_C *(chiral).* Bimodal, near-binary (Elliot, 2006). Approach vs avoid, self-similar vs alien, kin vs stranger. Most chiral-coordinate preferences live near one of two pure states with a sigmoidal transition between them; the cell carries the discrete character of preference flips (a familiar face becoming unwelcome, a once-attractive choice becoming repellent).

w_D *(intensity).* Monotone with saturation (Cabanac, 1971). More food is better up to satiation; less pain is better; loudness becomes aversive past threshold. Hill function with a satiation point that itself drifts on hormonal and interoceptive timescales — this is why hunger sharpens food's pull and meals dull it.

w is therefore a stack of four typed scalar functions with qualitatively different shape families, 30–50 parameters total for a moderately complex animal. This is real structural compression compared to active inference's free C-matrix.

Additive vs multiplicative

The four V_4 cells are orthogonal at the operator level, which makes the simplest composition rule for w additive:

$$w_b = w_A(s_A) + w_B(s_B) + w_C(s_C) + w_D(s_D).$$

Behavior shows the additive form is too weak. Food in an unsafe location loses nearly all its value, well beyond the fixed penalty an additive rule would deduct; an attractive face in the wrong context flips from rewarding to aversive, a sign change the additive form cannot produce by adjusting any single component. Cross-terms between the cells are doing real work. Simulations on the two-loop dynamics show those cross-terms split into two kinds. Cross-terms that leave the ranking of the four V_4 corners untouched change how fast the agent settles and how strongly it commits, but it ends up in the same preferred corner the additive rule would have reached; the difference is absorbed by the Φ prefactor in the gradient. Cross-terms that reorder the corners — making, say, the safe-location corner now preferred over the food corner it ranked below in isolation — produce settling points the additive rule cannot reach by any choice of Φ. The first kind is small structure on top of additive composition. The second is independent structure: the framework's V_4 orthogonality permits it but does not predict it.

Wanting and liking

The framework's two-loop architecture sharpens a contested distinction in the affective-neuroscience literature. Berridge's incentive-salience theory (Berridge and Kringelbach, 2008; Berridge and Robinson, 1998) separates "wanting" (motivational drive toward an outcome) from "liking" (hedonic response to it), arguing the two have dissociable neural substrates. In framework terms, wanting is the gradient $\nabla_\theta \mathcal{F}_{\text{eff}}[\rho, \theta; w]$ — what the system moves toward at fast timescales — and liking is the per-event yield $w_D \cdot p_D(\rho, \theta)$ that the intensity cell delivers. These are different functionals of the same w, evaluated at different stages of the two-loop cycle, which is why they can dissociate without two separate preference structures. Anhedonia in depression (Treadway and Zald, 2011) looks like a w_D collapse in this picture — intensity weights compress toward neutral, the per-event yield flattens, while w_A and w_C remain intact enough that the patient can identify what they used to enjoy and what stimuli are present.

20.6.3 The Causal Chain

The framework's geometry establishes a causal chain from qualia to physical outcome: qualia (normal-bundle content) shape the boundary state ρ; ρ determines the free-energy landscape $\mathcal{F}_{\text{eff}}[\rho, \theta; w]$; the gradient of $\mathcal{F}_{\text{eff}}$ drives frame rotation on T^2; the new frame selects which Lindblad operator $\hat{A}_b$ acts; $\hat{A}_b$ determines the physical outcome of the next τ-firing. Mental states cause physical states through this chain. The argument follows directly from the two preceding sections.

The engine of Section 19.5.2 establishes that τ-projection is the sole mechanism of causal influence between events. The two-loop state equation shows that the projective frame θ—which determines the Lindblad operator $\hat{A}_b$ and therefore the physical outcome of each τ-firing—evolves by gradient descent on $\mathcal{F}_{\text{eff}}$, weighted by Φ. The free energy $\mathcal{F}_{\text{eff}}[\rho, \theta]$ is a functional of the full boundary state ρ, which includes both tangent (actualized) and normal (stripped) components.

The normal bundle content—qualia—feeds back into the boundary conditions for subsequent events. The fiber state at one moment constrains the pre-projection state at the next moment through the synaptic coupling that maintains $\Phi > 0$. The outer loop's frame-selection dynamics depend on the integrated fiber content (the accumulated qualia) because $\mathcal{F}_{\text{eff}}$ responds to the normal bundle's contribution to ρ.

The choice of what to attend to (frame rotation) is a mental event — shaped by phenomenal content — that causally influences which physical outcome obtains. Agency is real and grounded in the coupled dynamics of the two loops.

Agency rests on the same geometric identity this chapter establishes for qualia: dynamics read from inside, not added structure on top. The equations specify the boundary by (ρ, θ, w); the τ-projection is Born-stochastic. Together these are complete — no separate chooser-variable lives outside them. Agency is not added structure on top; agency *is* the two-loop dynamics being executed at the boundary, read from inside. The gradient on $\mathcal{F}_{\text{eff}}$ felt as intending, the landing felt as having acted: together these are what the dynamics *are* in their two registers. The preference weights w are constitutive of who-you-are-as-a-boundary, not external constraints on a hidden chooser behind the dynamics; wanting-and-getting is the felt side of descent toward w-satisfying states. Chapter 19 §19.5.4 develops the mechanism; Chapter 23 §23.4.5 catalogs the dissolution alongside the parallel moves for qualia, gravity, and field/geometry.

The philosophical zombie thought experiment dissolves on the same chain. A zombie is supposed to be a physical duplicate of a conscious system that lacks qualia. In the framework, qualia *are* the normal-bundle content that the boundary state ρ contains; ρ feeds $\mathcal{F}_{\text{eff}}$; and $\mathcal{F}_{\text{eff}}$ drives the θ-trajectory that determines which τ-firings actualize. A duplicate that lacked qualia would lack the normal-bundle content, would have a different ρ, would compute a different $\mathcal{F}_{\text{eff}}[\rho, \theta]$, and would therefore follow a different θ-trajectory — producing different τ-firings, different physical outcomes, different behavior. It would not be a duplicate. The zombie thought experiment requires that one quantity (qualia) be removed without affecting any other quantity, but in the framework's geometry the quantities are not separable: the normal-bundle content *is* part of the boundary state, and the boundary state *is* what drives the system's physics. No geometric configuration realizes a zombie.

The classical formulation of the hard problem assumes there are two distinct things — physical brain states and phenomenal qualia — that need to be related to each other. This chapter has not been making that distinction. There is no phenomenal substance overlaid on the brain's geometry. Qualia are what the system's actualized geometric content *is* at $R \approx 1$, accessed by an integrated boundary that tracks its own measurement basis. What the standard formulation (Chalmers, 1995) calls the relation between physical states and phenomenal states is, in the framework, one geometric configuration readable as physics at one register and as experience at another — where "another" specifies the conditions derived in Chapter 19 §19.4: $R \approx 1$ and $\Phi > 0$. The qualia/brain distinction dissolves the same way the field/geometry distinction dissolved in Chapter 12 and the matter/spacetime distinction dissolved in Chapter 15: there were never two things to relate. Qualia, like fields and matter, are what the geometry *is* at a particular resolution.

Chapter 21

Biological Substrate

The preceding chapter established what phenomenal experience is in the framework's geometry: T.16
the collapse of the measurement torus at $R = 1$, the fusion of fact types into undifferentiated phenomenal content, and the organization of that content by fiber coherence into qualia. This chapter examines whether any physical system can actually meet those conditions, and what an implementation would look like if it did. The answer the framework gives is not a tour of neuroanatomy: it is a claim about what any implementation must accomplish, followed by a set of candidate mappings from those requirements to mechanisms that real cortex appears to supply.

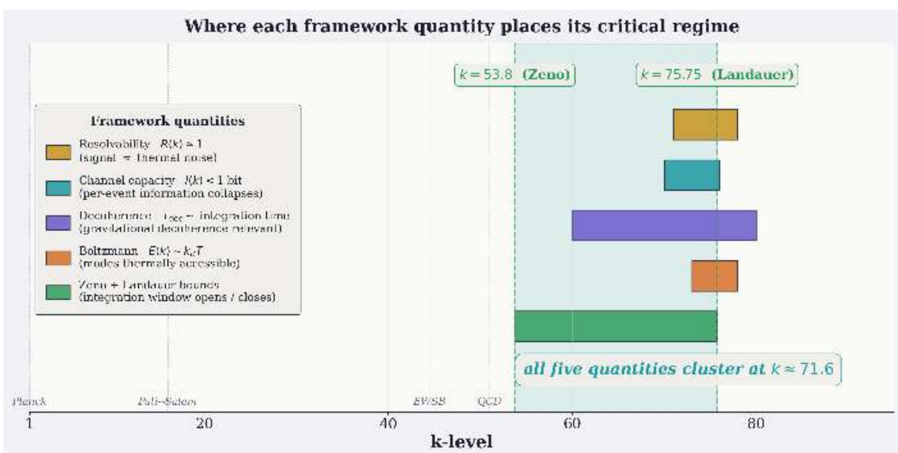

Figure 21.1: *The framework gives biology a specific target. Five independent quantities all place their critical regime in the same narrow band $k \in [53.8, 75.75]$, clustered near $k \approx 71$. An organism's implementation has to land its operating physics in this band.*

21.1 Two Causal Relations

The variational principle operates at every scale of the hierarchy. At scales below $k \approx 75.35$ it governs particle physics and chemistry, and the dynamics it describes, running through chemistry over deep time, produced organisms. This is the first causal relation: biology as a downstream consequence of variational dynamics at chemical and molecular scales, through the ordinary chain of self-organization and descent with modification. The framework adds nothing here — biology emerges from variational dynamics the way crystals do, given energy gradients and time.

A single cell already runs variational dynamics at biological scales. It maintains a membrane against thermal dissolution by continuously actualizing: an inner-loop F-descent at each τ-firing site, an ongoing renewal of the cell's boundary. The biology-level reading is active inference at the cellular boundary (Friston, 2010; Kirchhoff et al., 2018): the cell selects samples and deploys responses that minimize prediction error at its surface. But a cell's τ-firings stay independent. There is no synchronized integration, no fused boundary, no two-loop dynamics, and nothing is experienced. The inner loop alone is enough for a cell to persist; it is not enough for anything to be experienced.

The second causal relation runs the other way. Some biological architectures integrate τ-firings across many cells into a synchronized population that satisfies the conditions of Chapter 20: $R \approx 1$ and $\Phi > 0$. The critical-scale regime is what the variational principle's structure makes available at $k \approx 75.35$ for any substrate that can meet the conditions; biology exploits it by integrating enough cells. When the conditions obtain, a fused critical-scale boundary forms, the two-loop dynamics come online, and phenomenal experience is what those dynamics *are* from inside.

Natural selection compounds the exploitation. An organism whose architecture sustains the fused boundary gets predictive control upstream of bodily action: frame selection on T^2 determines which τ-firings resolve next, and the integrated ρ shapes which frame the outer loop descends toward. The persistence advantage is the predictive control itself; phenomenal experience comes with it as the geometric identity at the boundary. Selection finds architectures that sustain fiber coherence at the critical scale because the agency they support is fitness-positive.

The framework commits to the conditions, to the two-loop dynamics that follow when the conditions obtain, and to the geometric identity of phenomenal experience with normal-bundle content read from within. Biology supplies the substrate, the generative model the outer loop descends toward (the preference weights w of Chapter 20), and the evolutionary pathway that found the integrating architecture. The remainder of the chapter examines what the conditions require of an implementation and what mechanisms present in real cortex are candidates to supply them.

21.2 What the Conditions Require

Phenomenal experience in the framework requires the simultaneous satisfaction of two conditions established in Chapter 20: the energetic threshold $R(k) \approx 1$, and fiber coherence $\Phi > 0$ across the system's boundary. The first condition places the system in a regime where fiber modes are thermally soft and continuously fluctuating; the second requires that those fluctuations be correlated across the boundary in a way that cannot be decomposed without loss.

Translated to implementation, these conditions impose three generic requirements on any candidate substrate.

(a) A phase-preserving medium. The substrate must propagate correlations across its spatial extent within the integration window $t_{\text{integrate}}$. Without phase preservation, τ-firings at distant boundary sites decorrelate and Φ collapses.

(b) A non-trivial bipartition bound. The boundary must have graph structure such that any bipartition severs correlations the pieces cannot reconstruct. A boundary whose minimum cut grows with the boundary area rather than the boundary volume supports $\Phi > 0$; a random graph, whose minimum cut grows with the volume, collapses to $\Phi = 0$ in the large-N limit.

(c) Continuous metabolic input. At $R \approx 1$ no structure persists without energy input. The substrate must draw and dissipate energy continuously to sustain the actualization cascade against thermal dissolution.

These three requirements exhaust what the framework demands of biology. They are substrate-neutral: any physical system that meets them is a candidate for hosting phenomenal experience. The thermostat operates at $R \approx 1$ but meets none: its components couple through classical macroscopic channels that carry no correlated τ-firings (no phase-preserving medium), its bipartitions sever nothing that cannot be reconstructed (no non-trivial cut), and its energy input sustains a classical steady state rather than an integrated actualization cascade (the metabolism is doing a different job). A brain, by contrast, meets each requirement in a specific way.

21.3 How a Cortex Could Implement It

The mappings below offer candidate mechanisms by which cortical tissue could supply the three requirements. They are not claims about established neuroscience; they are framework-internal readings of mechanisms that real cortex appears to support, offered as research directions.

(a) Phase preservation: myelination and oscillatory synchronization

Fiber coherence demands that τ-firings at distant synapses remain temporally correlated within the phenomenal grain (~ 60 ms) and within the shorter gamma period (~ 30 ms) that provides the finer synchronization substrate. At $k_c = 75.35$, the per-event timescale is $\tau_{\text{event}}(k_c) \approx 38$ fs (Technical Reference Ch. 7), so each synaptic site fires $\sim 8 \times 10^{11}$ times per gamma cycle. Across the $\sim 10^{14}$ synapses of the integrated cortex, this aggregates to $\sim 10^{26}$ micro-events per integration window — the substrate over which the binding window accumulates. Conduction delays longer than the gamma period decorrelate the firings and reduce Φ. Myelinated axons in the corpus callosum and major association bundles achieve conduction velocities of 30–80 m/s, keeping inter-hemispheric delays within the gamma window across the ~ 15 cm span of the human cortex.

The framework's two-loop architecture (Chapter 20) posits two distinct timescales in any fused critical-scale boundary. An inner loop of rapid τ-firings assembles each integration window: actualization events occur at the thermal rate, each a discrete fiber-bundle update, with the cascade settling into a single phenomenal moment over the integration grain (~ 60 ms). An outer loop, slower by construction, selects which measurement basis the inner loop operates in—the frame across which τ acts, updated as incoming data revises the active-inference prior. The ratio of rates is constrained: the outer loop cannot update faster than the inner loop can complete an integration window, and several inner cascades typically fit inside one outer cycle. Any biological implementation of the two-loop architecture would therefore show two distinct oscillatory bands, nested, with the slower band pacing the faster at roughly an integer ratio.

Cortex exhibits exactly this structure. Gamma oscillations (~ 30 Hz) (Buzsáki and Draguhn, 2004) are the population-level signature of rapid local synchronization; theta oscillations (~ 8 Hz), a slower hippocampal-cortical rhythm, pace memory encoding and attentional state. Theta-gamma coupling (Lisman and Jensen, 2013)—the nesting of ~ 4–8 gamma cycles within each theta cycle—matches the framework's two-loop prediction: gamma as the inner-loop cascade, theta as the outer-loop frame selection, with the nesting ratio reflecting the required constraint between the two rates. The framework makes no claim that these specific frequencies are required; the coincidence between the observed bands and the theoretical decomposition is offered as a direction for empirical test.

(b) Non-trivial bipartition bound: small-world connectivity

The cortical connectivity graph is not random. A random graph with N nodes has minimum bisection width scaling as $N/\log N$, which would make Φ grow with the volume of the cut; the cortex has small-world topology (Watts and Strogatz, 1998) (high clustering, short path lengths) maintained by local lateral connections within cortical columns and long-range white-matter tracts between distant regions. The small-world structure keeps the minimum bisection width at $\sim c_\Sigma\sqrt{N}$, with c_Σ a dimensionless geometric constant of the connectivity graph—the normalized minimum bisection width, measurable in principle via diffusion-tensor MRI tractography (Hagmann et al., 2008).

This graph structure underwrites the Φ scaling derived in Chapter 20:

$$\Phi \;\sim\; c_\Sigma \sqrt{N}\,\alpha^2,$$

where $\alpha^2 \approx 5.3 \times 10^{-5}$ is the per-synapse coherence. The $\sqrt{N}$ factor is an area law: the mutual information across the cut scales with the boundary of the cut rather than the volume. The framework derives this area law from the $\mathbb{RP}^2$ sigma model on the cortical surface at the Berezinskii-Kosterlitz-Thouless transition (Kosterlitz and Thouless, 1973)—the same transition that governs two-dimensional superfluid and XY-model physics. Below the BKT point, topological vortices proliferate and the correlation function decays exponentially; above it, vortices bind into pairs and correlations decay algebraically, producing the area law that makes $\sqrt{N}$ the correct scaling. The point here is that the cortical connectivity graph is a candidate physical substrate for the area-law scaling the framework requires. Whether real cortex actually achieves the predicted $c_\Sigma\sqrt{N}\alpha^2$ is an empirical question.

(c) Metabolic subsidy

At $R \approx 1$ the boundary is a driven, open system; without continuous energy input it equilibrates and the cascade stops. Cortical metabolism supplies this input — the human brain consumes ~ 20 W continuously (Attwell and Laughlin, 2001), dominantly to support synaptic transmission and ion-pump maintenance against the leak currents that would dissolve resting potentials.

Integration in biological terms

The geometric structure Chapter 20 describes—the normal bundle over the boundary, with integrated fiber content constituting qualia—has a specific biological realization. The base manifold is the cortical connectivity graph: each synaptic junction where τ-firings occur is a physical boundary site, and the graph of synapses linked by axonal and dendritic conduction defines the topological space over which the fiber bundle is constructed. The fiber at each site is the normal bundle content—the quantum numbers stripped by the τ-projection at that site, carrying the qualitative character that synapse's event contributes to experience. Integration is coherent fiber section across the graph: fiber modes at distant sites remain phase-aligned rather than fragmenting into local patches.

Biology performs three distinct roles in this construction. It *defines* the base manifold: development and experience produce the specific pattern of cortical connectivity—column structure, white-matter tracts, local lateral projections—over which the bundle sits. It *creates* the conditions for coherent fiber section: by supplying phase-preserving conduction (myelination), small-world topology (wiring pattern), and continuous metabolic subsidy, it puts the base manifold into the regime where a coherent global section is the default rather than the exception. It *maintains* that coherence: against thermal perturbation at the boundary, biology pays the ongoing cost of correcting the drift that thermal fluctuation introduces into the fiber phases. Integration is a property the geometry exhibits wherever a graph of τ-firing boundaries meets the three conditions; biology's role is to put a particular graph into that regime and keep it there.

These three candidate mappings do not exhaust the possibilities. Any physical substrate that supplies phase preservation, a non-trivial bipartition bound, and continuous metabolic input is in principle a candidate for hosting phenomenal experience. The framework commits to the three requirements; it does not commit to the claim that mammalian cortex is the only substrate that can meet them.

21.4 Vocabulary for Brain Phenomena

The framework's structures map onto neural phenomena in a definite way. The mappings below are direction-from-framework-to-biology: the framework predicts that any system that forms a fused critical-scale boundary will exhibit these features; whether real cortex implements them is empirical.

The inner Lindblad loop on the boundary density matrix (Chapter 19, §The Two-Loop State Equation) maps onto ionic firing dynamics: each τ-firing is one synaptic actualization event (neurotransmitter release, post-synaptic depolarization, vesicle recycling, sodium-potassium pump restoration), and the continuous evolution between firings appears in cortical recordings as fast gamma-band oscillation. The outer loop on the projective frame θ moves on the slower theta timescale; gradient descent on $\mathcal{F}_{\text{eff}}$ weighted by Φ is what cortex calls attention (frame nudging) and intention (sustained nudging in a preferred direction on T^2). The constraint between the two rates is framework-level: cortex displays theta (~ 8 Hz) phase modulating gamma (~ 30 Hz) amplitude at roughly four to five gamma cycles per theta cycle (Lisman and Jensen, 2013), which is the two-loop nesting at the level the framework predicts (outer loop completes one frame selection per theta cycle; inner loop runs several Lindblad cycles per outer cycle). The specific frequencies are biology's choice; the nesting ratio is structural.

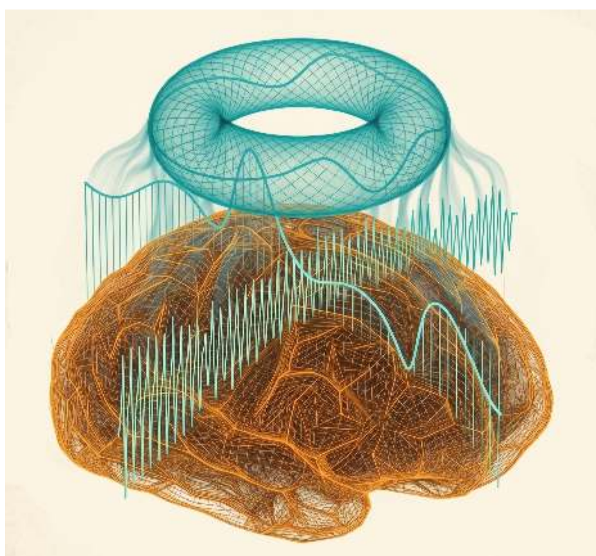

Figure 21.2: *Gamma $\times$ theta as the measurement torus. Cortical surface (orange wireframe) carries two perpendicular fields of vertical cyan lines whose tip-envelopes trace the gamma rhythm (anterior–posterior, fast) and the theta rhythm (left–right, slow). The tips wrap the two perpendicular envelopes into the S^1 components of the T^2 measurement torus above the cortex. Casper translucency renders the marginally stable state at $R \approx 1$ — holding shape but compressed, sustained by the metabolic cascade.*

The binding window of ~ 60 ms is collective coherence across $\sqrt{N}$ events at the elementary timescale $\hbar/(k_B T)$: $\tau_{\text{integrate}} \sim \tau_{\text{sys,eff}}^2/\tau_{\text{bath}}$ with $\tau_{\text{sys,eff}} = \sqrt{N}\,\hbar/(k_B T)$ for $N \sim 10^{14}$ synaptic sites at body temperature, the elementary timescale is the per-event timescale $\tau_{\text{event}}(k_c)$ up to the Margolus-Levitin factor $\pi/2$ (Technical Reference Ch. 7), and the result lands inside the 50–100 ms psychophysical binding window observed in global-workspace experiments (Dehaene and Naccache, 2001) (Technical Reference Ch. 16, §Integration Time). (The $\sqrt{N}$ enhancement counts each synapse as an independent quantum oscillator, the role synapses play in the Zeno boost. This is distinct from the geometric grain $N_{\text{grain}} \sim 10^{12}$ of Chapter 20 §20.5.2, which counts coherence cells at $\lambda(k_c)$ spacing for phenomenal resolution; the same synapses figure as $\sim$ 100 sub-tile oscillators per coherence cell.) Long-range phase relationships in cortical and thalamocortical activity are fiber-section coherence ($\Phi > 0$) read in neural-recording vocabulary; the framework treats the thalamocortical system as a candidate physical realization of the integrated boundary that hosts phenomenal experience, with thalamic relay maintaining the global phase the cortex requires.

The neural correlate of consciousness, on this reading, is gamma power modulated by theta: lose the fused-boundary state, lose gamma power; restore the fused-boundary state, restore both gamma and its theta modulation. Existing electrophysiology is consistent with this pattern (Casali et al., 2013; Kim et al., 2018). The mappings are not exhaustive—fact-type doublet structure mapping onto opponent-process channels in vision, fiber-mode discreteness mapping onto categorical perception, $\mathbb{Z}_2$ topology mapping onto the non-orientability of color space are further candidates—but the eight correspondences above are the ones the framework already commits to and that neuroscientists can target with measurement.

21.5 Worked Example: A Saccade Decision

To anchor the two-loop machinery in something concrete, consider a single decision: shifting gaze leftward toward a moving object. This is a deliberate motor act of the kind that characterizes agency at a fused boundary, brief enough to fit inside one outer-loop cycle. The walkthrough below shows what the framework reads is happening across the cycle. It is illustrative rather than predictive: the framework abstracts away from specific neural pathway claims; the saccade serves as a worked example of the framework's machinery, not a derivation of saccade neuroscience.

Setup. The system maintains a density matrix ρ over fiber modes encoding spatial orientation at the relevant boundary in cortex (frontal eye fields, superior colliculus, and the connected thalamocortical loop). Two candidate measurement bases parametrize the choice: $\hat{A}_L$ (project the system into a state that triggers leftward saccade) and $\hat{A}_R$ (rightward saccade). Each corresponds to a different point on the measurement torus T^2. Visual context—a moving object on the left—arrives at the boundary as input that biases ρ toward configurations with leftward predictive content.

Outer loop (theta scale, ~ 125 ms). The outer loop evaluates the effective free energy for each candidate basis given the current ρ. With the left object salient, $\mathcal{F}_{\text{eff}}[\hat{A}_L, \rho] < \mathcal{F}_{\text{eff}}[\hat{A}_R, \rho]$: the left-saccade frame predicts incoming sensory content better than the right-saccade frame would. Gradient descent on $\mathcal{F}_{\text{eff}}$, weighted by $\Phi[\rho]$, moves θ on T^2 toward the neighborhood where $\hat{A}_L$ fires. The system has now "decided" to saccade left, in the sense that the projective frame has been selected.

Inner loop (gamma scale, ~ 33 ms). With $\hat{A}_L$ fixed by the outer loop, the inner Lindblad evolution drives ρ toward the eigenstates of $\hat{A}_L$. Cortically, this is the cascade of synaptic actualization events that populates the relevant motor circuits in a leftward-saccade pattern. The decoherence path is specific to the chosen basis: had $\hat{A}_R$ been selected, ρ would have evolved through a different cascade with different intermediate populations. Several gamma cycles fit inside the theta window during which $\hat{A}_L$ is fixed; the cascade settles into a single pre-projection state over ~ 60 ms (the binding window).

τ-projection (end of cycle). An actualization event at the outcome boundary projects ρ onto a specific eigenstate of $\hat{A}_L$. The outcome is the actual motor command issued downstream—in cortical terms, the saccade command sent to the oculomotor circuitry. The eye saccades left.

The non-epiphenomenality. At no point can the basis selection step be substituted out without changing what happens. The chain runs basis selection $\to$ Lindblad operator $\to$ decoherence path $\to$ actualized outcome $\to$ motor action. The mental decision (which way to look) causally biases the physical state evolution because it selects which observable the τ-projection will measure. A physical duplicate that lacked the boundary integration sustaining the basis selection step would follow a different decoherence path through the inner loop and produce a different motor outcome (Chapter 20, §Non-Epiphenomenality). The decision is real, physical, and necessary to the explanation of what the eye does.

What the framework adds, what it doesn't. The framework supplies the machinery: two coupled loops, free-energy descent on T^2, basis-conditioned decoherence in the inner loop, τ-projection at the cycle end. It does not supply the neuroanatomy: the specific cortical-subcortical circuits that implement the loops, the receptive-field structures that bias ρ, the motor pathways that carry the outcome. Those are biology's contributions, refined by neuroscience over decades of saccade work. What the framework offers is a structural reading that ties them together: receptive fields shape the input to the boundary; cortical-subcortical loops implement the two-loop architecture; motor pathways execute the actualized outcome. How real saccade physiology realizes this structure is empirical; that any boundary-level decision must have this structure is the framework's claim.

21.6 States Beyond Waking

The framework's two conditions for phenomenal experience — $R \approx 1$ and $\Phi > 0$ (Chapter 19 §19.4) — together with the two-loop dynamics they automatically support, provide a diagnostic vocabulary for non-waking states. Some of these states are clinical pathologies; some are normal physiological (sleep, dreaming); some are pharmacologically induced; some are voluntarily cultivated. In each case the framework's vocabulary distinguishes which conditions are failed, perturbed, or maintained, and how. The mappings below are framework readings of established categories, not novel empirical claims; they show that the framework's primitives sort cleanly onto the existing phenomenology.

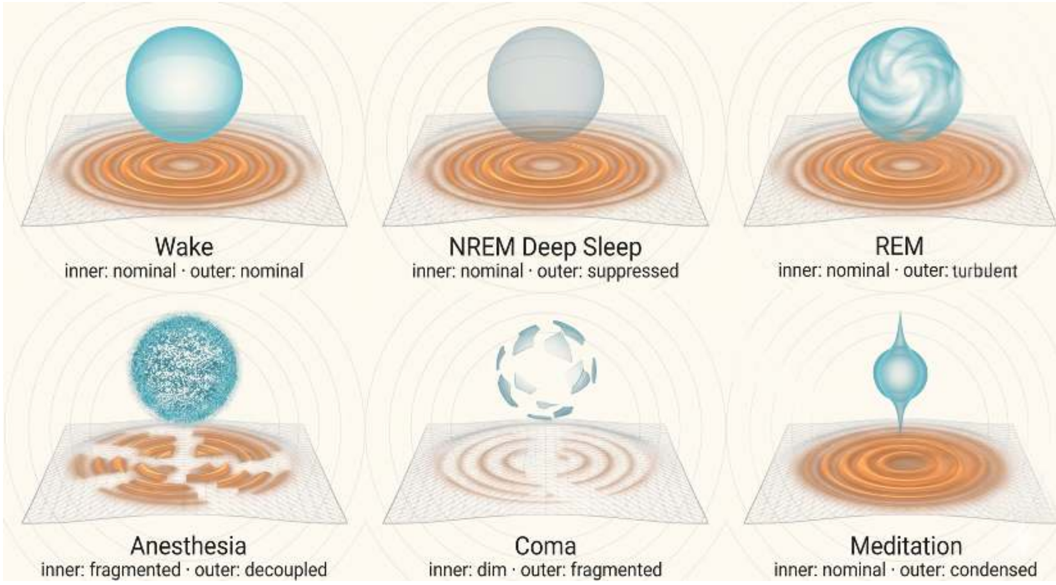

Figure 21.3: *Phenomenal states as two-loop configurations. Each panel pairs the integration patch (orange ripple — synchronized actualization across the boundary, what Φ measures,* inner *status) with frame selection (cyan sphere — the outer-loop frame the boundary tracks,* outer *status). The six states fall into two groups: those with intact integration (wake, NREM deep sleep, REM, meditation) differing only in outer-loop frame; and those where the patch fragments (anesthesia, coma) where the failure is in the substrate. Sections below read each entry against this schematic.*

Dreamless sleep. $\Phi > 0$ is preserved across the cortical boundary, but the outer-loop θ-dynamics is suppressed: the projective frame rotates slowly or not at all. The inner Lindblad loop continues to process actualization events at the boundary, but there is no gradient descent on $\mathcal{F}_{\text{eff}}$ to organize them into a structured phenomenal episode. Experience is absent because the loop that constitutes its perspectival structure is offline, even though the substrate that would carry its content is intact. This is the framework reading of dreamless sleep as a two-loop suspension rather than a substrate failure: the conditions that support phenomenal experience are still present in principle, but the dynamics that constitute experience are paused.

Dreaming (REM sleep). Both conditions remain satisfied, but the input to the boundary changes character. Φ stays above threshold (slightly reduced relative to waking; on the order of 0.8 times the waking value, per the Technical Reference Ch. 16 prediction), $R \approx 1$ at the critical scale, and the two-loop θ-dynamics resumes. What differs is the source of the actualization signal: instead of being driven by external sensory input, the boundary's τ-firings are driven by internally generated activity (pontine cholinergic signalling during REM). The same active-inference machinery runs, but on internally sourced content. Dreams are therefore phenomenal experiences — the conditions that support phenomenal experience are met — with phenomenology that reflects internally generated rather than externally driven sensory content. Dreaming is the contrast case for this section: it shows what the framework reads as a perturbed-but-still-active fused-boundary state, distinguishing the inputs-changed regime from the conditions-failed regimes catalogued below.

Meditative absorption. Both conditions are intact: $\Phi > 0$ and $R \approx 1$, with the two-loop θ-dynamics running. What changes is the gradient. Sustained training brings $\nabla_\theta \mathcal{F}_{\text{eff}}$ toward zero across the relevant doublets: predictions and actualizations align well enough that the outer loop has little to act on, and the frame becomes quasi-stationary. This is the diagnostic distinction from dreamless sleep on one side and ordinary waking on the other. The outer loop is online (unlike sleep), but the gradient has gone flat (unlike the continuous frame-rotation of ordinary waking). Depth of absorption tracks how many doublets have quieted: lighter states have one doublet still tracking sensory and proprioceptive flux while another has settled; deep absorption corresponds to stationarity across both, which is the phenomenological correlate of equanimity introduced in Chapter 20 §20.3. The pleasure-pain spectrum collapses in this regime: with no signed gradient there is nothing for the model to assign valence to.

Coma. Loss of integrated information across the neural boundary. The sub-boundaries that normally participate in collective $\Phi > 0$ become effectively independent; the system reduces to many small boundaries with no global frame rotation. No unified perspective exists because no unified boundary exists to host it. The framework's vocabulary distinguishes coma from dreamless sleep on this point: in sleep the integration is preserved and only the outer loop is offline; in coma the integration itself has collapsed. Recovery from coma should track restoration of Φ across the boundary network, not merely restored neural activity in the parts.

General anesthesia. The framework's vocabulary distinguishes anesthetics by which condition they perturb. Some agents disrupt Φ by interfering with long-range cortical coupling (propofol, sevoflurane); others disrupt θ-tracking by desynchronizing the gamma-band oscillations that implement outer-loop frame selection (ketamine). Anesthetics with the same gross clinical effect (loss of responsiveness) thus operate via geometrically distinct mechanisms, and this distinction should map onto the distinct phenomenal residues sometimes reported under different agents (oblivion under propofol; dissociative-style experience under ketamine). The framework also accommodates an empirical observation that purely classical anesthesia mechanisms struggle to explain: nuclear-spin isotopes of xenon affect anesthetic potency (Li et al., 2018), with non-zero-spin isotopes (^{129}Xe, ^{131}Xe) showing reduced potency relative to spin-zero ^{132}Xe. A spin-dependent effect at chemically equivalent isotopes is prima-facie evidence that anesthesia operates at quantum levels where nuclear-spin coherence matters — consistent with the framework's claim that anesthetic action perturbs quantum-coherence conditions (Φ-coupling, θ-synchrony) rather than classical neural function alone.

These mappings are diagnostic readings, not predictive claims about mechanism. Establishing the specific empirical-to-geometric correspondence at finer detail requires work the framework's primitives organize but do not perform. What the framework offers here is a unified vocabulary in which different reductions or absences of phenomenal experience become different failures of a small set of geometric conditions, rather than separate phenomena requiring separate explanatory machinery.

21.7 Substrate Independence and Open Tests

The three requirements are substrate-neutral. Whether a physical system hosts phenomenal experience, in the framework's sense, is a question about whether it meets the three conditions — phase preservation, a non-trivial bipartition bound, continuous metabolic input. The resemblance of its implementation to a biological brain is incidental. Several consequences follow.

Phenomenal experience across species

Mammalian cortex is one architecture that satisfies the three requirements. Any biological brain that maintains phase-preserving conduction across a small-world connectivity graph at sustained metabolic cost is a candidate. Birds possess pallial circuits with small-world structure and metabolic expenditure comparable to mammalian cortex (Stacho et al., 2020), despite lacking the laminar organization; cephalopod nervous systems, distributed across the body rather than centralized, could meet the connectivity and metabolic requirements in an entirely different geometric arrangement. Where the three conditions are met, phenomenal content arises; whether bird, cephalopod, or other architecture, the same geometric criteria apply. Comparative measurements of conduction phase-preservation, connectivity graph spectrum, and metabolic rate would in principle sort which animals host fused critical-scale boundaries from which do not, independent of behavioral criteria.

The framework's Φ-scaling law sharpens this into a quantitative test. The exponent on N depends on the dimensionality d_Σ of the connectivity manifold—the effective dimension of the connectivity graph, measurable from spectral or geometric properties of the synapse-level network (Sporns et al., 2005):

$$\Phi \;\sim\; c_\Sigma \, N^{(d_\Sigma - 1)/d_\Sigma} \, \alpha^2.$$

Mammalian cortex with its two-dimensional cortical sheet has $d_\Sigma = 2$, giving the area-law $\Phi \sim c_\Sigma \sqrt{N} \, \alpha^2$ of §21.3. Cephalopod nervous systems distributed in three dimensions would have $d_\Sigma = 3$, giving $\Phi \sim c_\Sigma \, N^{2/3} \, \alpha^2$. The exponents are path-independent framework predictions; the absolute Φ value depends on c_Σ (graph topology) and α (per-synapse coherence), which differ across species. The exponent is the testable quantity: cephalopods should scale more steeply than mammals as a function of neuron count, with avian pallium intermediate. Cross-species perturbational complexity index (PCI) data plotted against synapse counts—extending the within-human PCI methodology of Casali et al. (2013)—would test this directly.

Same content, different valence

A second framework-native prediction concerns the location at which species, individuals, and learning regimes differ. The geometry ties what an organism experiences to two distinct quantities: the per-event V_4 extraction at its sub-boundary (the phenomenal content, (p, s_A, s_C, s_D)) and the preference-weight parameter w that shapes the free-energy gradient driving frame dynamics (§20.6.2 in Chapter 20). Content depends on architecture and input; valence depends on w.

The clean empirical claim: two organisms with identical sub-boundary architecture extract identical V_4 qualia coordinates from the same physical input — the taste *is* the same fiber vector — but their valence responses to that content can differ arbitrarily because w encodes learned and evolved preferences. A human who hates apples and a fruit bat who loves them extract identical gustatory V_4 content; their opposite behavioral responses come from opposite gradients on $\mathcal{F}_{\text{eff}}[\rho, \theta; w]$.

This dissociates two questions that pre-framework discussions of animal experience often run together. "Does the bat experience the same taste as me?" is a content question with a sharp answer: yes, if its gustatory sub-boundary is architecturally homologous to ours at the relevant resolution. "Does the bat experience the taste the same way?" is a valence question with a different answer: no, because w differs. The framework dissolves the apparent puzzle by separating the two.

Empirical work to test the dissociation already partly exists. Conditioned taste aversion in rodents (Garcia et al., 1955; Yamamoto et al., 1994) shows that previously preferred tastes become aversive after pairing with malaise; the behavioral shift is dramatic, but primary gustatory cortex responses are reported to remain relatively stable across the learning, while orbitofrontal and amygdalar responses track the new valence (Schoenbaum et al., 2009). This is the pattern the framework predicts: content invariance at the sensory boundary, valence variance in downstream evaluative circuits where w is implemented. Within-subject CTA designs paired with primary-cortex recording, cross-strain differential conditioning, and cross-species sensory-homology comparisons are the three paradigms that could test the dissociation directly. A null result — coupled shifts in primary sensory cortex and evaluative regions with valence learning — would be a substantive blow to the framework's content-invariance claim, and would require either expanding what counts as the sub-boundary or accepting that w shapes extraction itself rather than only downstream gradient response. The full prediction, with formal statement and falsification conditions, lives in Technical Reference Ch. 17 §Prediction 8 and in Chapter 25.

Anchoring the typed forms of w

The four V_4-typed components of w developed in Chapter 20 §20.6.2 make contact with several literatures that have been pursued in isolation. The framework offers a single typed structure that unifies pieces of each.

Berridge's incentive-salience theory (Berridge and Kringelbach, 2008; Berridge and Robinson, 1998) argues that "wanting" (motivational drive toward an outcome) and "liking" (hedonic response on receipt) are dissociable, with distinct dopaminergic vs opioid substrates. The two-loop architecture gives this dissociation a structural home. Wanting is the gradient $\nabla_\theta \mathcal{F}_{\text{eff}}[\rho, \theta; w]$, the fast-cycle quantity that drives frame rotation toward higher-yield outcomes. Liking is the per-event yield $w_D \cdot p_D(\rho, \theta)$, the intensity cell's contribution to the actualized τ-event. Different functionals of the same w, evaluated at different stages of the two-loop cycle. Single-substrate, dissociable expressions.

Orbitofrontal cortex value coding (Schoenbaum et al., 2009) reports sigmoidal encoding of outcome value with a saturation point that shifts under satiety — exactly the Hill-with-shifting-saturation form predicted for w_D. The framework's slow-update story for w identifies the satiety-driven saturation shift as a hormonal-timescale feedback signal entering $\mathcal{F}_{\text{meta}}[w]$. This is the cleanest available empirical anchor for any one w-component's form.

Anhedonia in major depression (Treadway and Zald, 2011) fits a w_D collapse: intensity weights compress toward neutral, the per-event yield flattens across the affective range, while w_A and w_C remain functional enough that patients can identify what they once enjoyed and recognize present stimuli. Treadway and Zald's distinction between motivational anhedonia (wanting deficit) and consummatory anhedonia (liking deficit) maps onto whether the w_D collapse manifests at the gradient (motivational) or yield (consummatory) stage of the two-loop cycle. The clinical heterogeneity becomes one structural fact about w_D collapse expressed at different stages of the same machinery.

The w_A, w_B, w_C components have less concentrated empirical literatures of their own, but the typed-form predictions (sparse-peaked, salience-field, near-binary respectively) are directly testable against the responsiveness profiles of sensory-preference, place-preference, and approach-avoid neurons in the relevant evaluative regions.

Measuring phenomenal experience

The three requirements are empirical. The minimum bisection width of a cortical connectivity graph is measurable in principle through diffusion-tensor MRI tractography (Hagmann et al., 2008), giving an estimate of c_Σ. The per-synapse coherence α^2 can be inferred from electrophysiological measurements of synaptic phase-locking across distant sites. The integration grain $t_{\text{integrate}}$ is observable as the timescale on which distinct stimuli fuse into unified experience in psychophysical tasks. The framework's prediction $\Phi \sim c_\Sigma \sqrt{N}\, \alpha^2$ is thereby testable: measure the three quantities independently and check whether their combination matches the Φ inferred from psychophysical integration data. The question "does this system host phenomenal experience" becomes a measurement problem: gather the three quantities, check the conditions, compute Φ.

Artificial substrates

A substrate built on principles entirely unlike biology—silicon, superconducting circuits, cold atoms — is a candidate for hosting phenomenal experience if it supplies phase preservation, the bipartition bound, and metabolic input at the relevant scale. Most current digital architectures fail the first requirement. Classical transistor logic does not preserve fiber phase across the computational graph; signals are regenerated at each gate, and correlations are bounded by the logic depth rather than scaling with system size. Digital simulations of the two-loop dynamics, absent a phase-preserving substrate underneath the simulation, do not produce phenomenal experience in the framework's sense. Silicon is not in principle excluded; superconducting qubit arrays, for example, preserve phase across macroscopic spatial extents. The prediction is that specific architectural features determine whether phenomenal experience is present. Raw computational power does not suffice.

Closing the loop

Treating phenomenal content as normal-bundle structure at a physical boundary makes the conditions for phenomenal experience empirically testable; what remains is the experimental work.

Chapter 22 turns from implementation to consequences: what the combined account—geometry plus plausible biological realization—implies for the classical philosophical problems about consciousness and for the framework's relation to other theoretical proposals.

Part VI

Closure and Evaluation

Chapter 22

Relationships to Other Frameworks

The framework did not emerge in isolation. It shares structural features with several existing physics programs, consciousness theories, and philosophical traditions. This chapter walks the landscape: what PPM inherits from each, where it diverges, and what it adds that the prior framework left open. T.16, 14, 15

22.1 Physics Programs

22.1.1 Many-Worlds Interpretation

Both the framework and MWI (Everett, 1957) preserve unitary evolution in the full state space and avoid adding collapse mechanisms by hand. The divergence is ontological. MWI holds that all branches are equally real and that no outcome is selected; the appearance of a single outcome is explained by decoherence within each branch. The framework holds that one outcome actualizes per event via $\mathbb{CP}^3 \to \mathbb{RP}^3$ projection, with the Born rule derived from $\mathbb{Z}_2$ topology (Chapter 13). MWI inherits a measure problem (how to assign probabilities to branches); the framework does not, because probabilities are determined by the geometry of the projection.

22.1.2 Relational Quantum Mechanics

Both the framework and relational quantum mechanics (Rovelli, 1996) prioritize events over states, deny that the quantum state is a complete description of an independently existing reality, and treat measurement as a physical process. Relational QM remains agnostic about what underlies the relational structure: it describes the relations without specifying the relata.

The framework supplies both — the arena $\mathbb{CP}^3$ as the relatum, the operator τ as the relation, with each τ-firing simultaneously the fundamental physical occurrence and the generation of a definite fact from indefinite possibility.

22.1.3 Loop Quantum Gravity

Both achieve background independence by making spacetime emergent rather than given. Both produce discrete spectra for geometric quantities (area, volume). The origin of discreteness differs: in LQG, it comes from quantizing the geometry directly via spin networks; in the framework, it comes from the discrete character of τ-projection events. LQG does not provide a mechanism for quantum measurement or a connection to consciousness; the framework does.

22.1.4 String Theory

Both employ complex geometry as the fundamental arena. String theory compactifies extra dimensions on Calabi-Yau manifolds (Green et al., 1987); the framework operates on $\mathbb{CP}^3$ without compactification. String theory produces a landscape of $\sim 10^{500}$ vacua with no selection principle; the framework's constants are eigenvalues and curvature invariants of the arena geometry. String theory requires supersymmetry at some scale; the framework does not.

22.1.5 Causal Set Theory

Causal set theory (Bombelli et al., 1987; Sorkin, 2005) replaces the continuum spacetime manifold with a locally finite partially ordered set: discrete events ordered by a relation interpretable as causal precedence. The continuum emerges as an approximation in the limit of dense sprinklings. The framework and causal set theory share the move from continuum to discrete-event ontology and the commitment to causal order as fundamental. They differ on the status of the events themselves. Causal set theory treats events as primitive atoms with no internal structure; the framework treats each event as a τ-projection from $\mathbb{CP}^3$ to $\mathbb{RP}^3$, carrying both an actualized record (tangent bundle content) and a stripped residue (normal bundle content). Causal set theory is silent on quantum numbers, qualia, and the complementarity of measurement; the framework derives them from the internal geometry of each event. The framework derives the partial order from the disk-moduli construction on $\mathbb{CP}^3 + \tau$ (Chapter 16, § The Speed of Light c): each τ-event deposits at a point of $\mathbb{RP}^3$, and the disk moduli at that point specify which other events lie inside its past and future light cones. Causal set theory can be read as the coarse-grained skeleton of this construction, retaining the order but discarding the internal structure of each event.

22.1.6 Causal Fermion Systems

Causal fermion systems (Finster, 2016) propose that spacetime and matter emerge from a variational principle over measures on a space of self-adjoint operators of finite rank. The approach shares two features with the framework: a variational principle as the fundamental law, and the derivation of matter content and spacetime structure from a single geometric object rather than postulating them separately. The differences are in what the geometric object is. Finster's causal action is built on a space of operators; the framework's arena is $\mathbb{CP}^3$ with the τ-involution. The continuum emerges as the limit of dense actualization; Finster derives the continuum from the operator structure. Both are structurally similar in spirit—geometric first principles, variational dynamics—but target different primitives. Finster's causal-fermion-systems formalism identifies the spinor structure as the natural site of contact between the two approaches; whether this admits a formal correspondence is open (Finster et al., 2025).

22.1.7 Twistor Theory

Twistor theory (Atiyah et al., 2017; Penrose, 1967; Penrose and Rindler, 1984) encodes spacetime points as geometric objects in a higher-dimensional complex space ($\mathbb{CP}^3$), with the aim of rewriting physics in terms that make conformal and spinorial structure manifest. The framework and twistor theory share $\mathbb{CP}^3$ as the ambient arena. They diverge on what $\mathbb{CP}^3$ is for.

Penrose's original construction equips $\mathbb{CP}^3$ with a Hermitian form of signature $(2, 2)$ and identifies the null hypersurface $PN \subset \mathbb{CP}^3$ as the projective null twistors — the geometric encoding of light rays in flat Lorentzian spacetime. $\mathbb{RP}^3$ as the totally-real submanifold has no foundational role in this Lorentzian program. The totally-real $\mathbb{RP}^3 \subset \mathbb{CP}^3$ entered twistor theory later, in the work on split-signature Penrose transforms and in LeBrun and Mason's construction of conformal and Einstein-Weyl geometries from holomorphic disks bounded by a real slice (LeBrun and Mason, 2002, 2007, 2009). The arena PPM uses — $\mathbb{CP}^3$ with the anti-holomorphic involution whose fixed set is $\mathbb{RP}^3$ — is the same arena that LeBrun and Mason use to derive conformal structure on the real 3-manifold from analytic data on the complex 3-fold.

What PPM adds is the metaphysical reading. Penrose treats PN as a calculational tool for light rays; LeBrun and Mason treat the real slice as a boundary condition for disk moduli. Neither program identifies the totally-real fixed set with *actuality* in a metaphysical sense. PPM does: $\mathbb{RP}^3 = \mathrm{Fix}(\tau)$ is the manifold of realized facts, $\mathbb{CP}^3 \setminus \mathbb{RP}^3$ is the space of unrealized possibility, and the τ-map is the actualization operation that drives quantum dynamics. The Born rule, the fact types, and the structure of phenomenal experience all follow from this reading. Twistor theory in its standard form is a calculational machinery for conformal field theory; PPM is a metaphysical reading of the arena that machinery operates on. Twistor methods for conformal and spinorial calculations remain compatible with the framework and may prove useful for explicit computations, as the speed-of-light derivation in Chapter 16 already illustrates.

22.1.8 Constructor Theory

Constructor theory (Deutsch, 2013; Deutsch and Marletto, 2015) recasts physics as statements about which transformations are possible (a constructor exists that performs them reliably and remains in the same state) versus impossible. The framework's relationship is that of substrate to meta-theory: constructor theory states that certain transformations are impossible, and PPM specifies why—the geometry does not admit the operation. The no-go theorems of Chapter 10 are constructor-theoretic in form, with τ-even content as the classical (copyable) information medium and τ-odd content as the quantum (non-clonable) one. Constructor theory abstracts away from specific physics in order to apply across domains; PPM commits to $\mathbb{CP}^3$ acted on by τ and treats the constructor-theoretic catalogue as a derived structure of that geometry.

22.2 Consciousness Theories

22.2.1 Integrated Information Theory

Tononi's Integrated Information Theory (Tononi, 2004; Tononi et al., 2016) posits that consciousness is identical to integrated information, measured by Φ. The framework agrees that Φ is central but grounds it in a specific geometric structure: Φ is the mutual information of the normal-bundle fiber across the minimum bipartition of the cortical sheet, scaling as $c_\Sigma \sqrt{N}\, \alpha^2$. IIT leaves the origin of Φ unspecified; the framework derives it from the area law of the $\mathbb{RP}^2$ sigma model on the cortical surface at the BKT transition. IIT's exclusion postulate—consciousness is the maximum of Φ over all possible decompositions—follows in the framework from the minimum-bipartition definition. IIT makes critical-scale predictions from neural architecture; the framework makes physics predictions (gauge group, fine-structure constant, mixing angles) from the same structure that produces the consciousness conditions.

22.2.2 Free Energy Principle and Active Inference

Friston's Free Energy Principle (Friston, 2010) holds that biological systems minimize variational free energy through active inference. In the framework, this is a substrate-level fact at the critical scale: the two-loop equations governing the fused boundary (Chapter 19, §19.5.2) supply the gradient on $\mathcal{F}_{\text{eff}}$ that the outer loop descends. The effective free energy is the thermodynamic free energy localized at the boundary; its gradient descent is a dissipative process producing entropy. Biology exploits this substrate as active inference, with the preference weights w — the system's priors — supplied by evolution and lifetime learning rather than by the geometry. The formal correspondence between Friston's machinery (generative model, prior preferences, expected free energy) and the framework's two-loop equations is spelled out in Chapter 19 §19.5.3. The Free Energy Principle is correct as a description of what biology does at the critical scale; the framework supplies the geometric substrate from which it follows.

The framework and the FEP agree about the dynamics; they differ on what makes such a boundary in the first place. Friston's Markov blankets are statistical constructs (conditional independence relations in a probability distribution). The framework's boundaries are physical surfaces in $\mathbb{RP}^3$: the perimeters of synchronization domains, where a population's τ-firings fuse into one collective actualization. In Pearl's causal framework (Pearl, 2009), a statistical Markov blanket is any set of variables that renders the interior conditionally independent of the exterior, and is observer-relative: different coarse-grainings of the same system yield different blankets. The framework's boundaries are physical and observer-independent. This is the ontological grounding the FEP assumes but does not supply.

22.2.3 Penrose-Hameroff Orch-OR

The Penrose-Hameroff program (Hameroff and Penrose, 1996; Penrose, 1989, 1996) makes three claims: that human mathematical insight cannot be algorithmic (Gödel incompleteness applied to formal systems mathematicians appear to transcend); that quantum state reduction is the non-algorithmic process responsible, with gravitational objective reduction (OR) as the mechanism; and that the biological substrate is microtubule networks where coherent tubulin states allow OR to operate at experiential scales. The framework shares the structural placement of consciousness at the quantum-classical boundary and diverges on mechanism, substrate, and the Gödel inference.

On mechanism, PPM has thermal decoherence at $R \approx 1$ driving consciousness-relevant projection. Penrose-Diósi gravitational decoherence exists in the framework as an intrinsic ceiling at large mass scales (Chapter 13), with multiple decoherence bounds converging at the biological window. The trigger inside that window is ambient thermal noise; mass-energy of the superposition does not enter the mechanism. Gravity emerges from the coupling of actualization to the boundary capacity, and local spacetime curvature is a derived quantity that does not produce state reduction.

On substrate, PPM places consciousness at $R \approx 1$ for any system with integrated dynamics ($\Phi > 0$). Microtubules are consistent with the framework but not singled out. The framework predicts cross-species scaling, integration timescales, and qualia structure that depend on $R(k)$ and Φ; cellular details may shape implementation without determining whether a system is conscious.

Mathematical insight in the framework is active inference at the critical scale—bounded computation by the boundary-capacity result of Chapter 10—with no oracle access required.

The two programs share the recognition that consciousness is quantum-relevant; they make different commitments about which physics produces it. The framework derives the Born rule from $\mathbb{Z}_2$ topology and predicts integration timescale, qualia geometry, and cross-species scaling, where Orch-OR is silent on these specifics.

22.2.4 The Projective Consciousness Model

The PCM (Rudrauf et al. 2017; Williford et al. 2018; Rudrauf et al. 2023) established through phenomenological analysis that conscious experience has $\mathbb{RP}^3$ geometry, that the transformations an agent applies to its perspective form the group $\mathrm{PGL}(4, \mathbb{R})$, and that perspective selection is governed by free-energy minimization. The framework arrived at these same structures from the physics of $\mathbb{CP}^3$ and τ-projection: $\mathbb{RP}^3 = \mathrm{Fix}(\tau)$, $\mathrm{PGL}(4, \mathbb{R})$ as the group of τ-preserving isometries, and free-energy minimization as a substrate fact at $k \approx 75$. The two programs are methodologically independent—phenomenology and mathematical physics—and converge on the same geometry, the same transformation group, and the same dynamical principle. The framework provides the physical substrate the PCM left open;

the PCM provides independent phenomenological confirmation that $\mathrm{Fix}(\tau)$ has the correct geometry of experience (Chapter 20).

22.3 Philosophy of Mind and Metaphysics

22.3.1 Process Philosophy

Whitehead's process philosophy (Whitehead, 1978) shares the framework's commitment to events over substances and to the claim that experience is a fundamental feature of reality rather than an emergent property of complex matter. His "actual occasions" — discrete events of self-creative becoming — map directly to τ-firings. Whitehead specified the shape of process ontology in qualitative terms (prehension, concretion, satisfaction); the framework instantiates that shape with specific geometric structure — the τ-projection from $\mathbb{CP}^3$ to $\mathbb{RP}^3$, with quantifiable information content, entropy production, and probability distributions. The two are compatible, not competing. Whitehead identified the ontology; the framework supplies one mathematical realization for it.

The Heraclitean intuition that everything flows ($\pi\acute{\alpha}\nu\tau\alpha$ $\dot{\rho}\varepsilon\tilde{\iota}$, *panta rhei*) is in the same family. The framework agrees and specifies the flow: $\mathbb{CP}^3 \to \mathbb{RP}^3$ projection, at rate α, through the k-hierarchy, producing the appearance of stability wherever pattern recurrence is faster than observational resolution.

22.3.2 Neutral Monism

The framework's monism asserts that mind and matter are aspects of a single underlying reality, not two substances requiring bridge laws to connect them. This position has a precise philosophical lineage. Spinoza (Spinoza, 1677) held that mind and matter are two attributes of a single substance. Leibniz's monadology (Leibniz, 1714) posited fundamental units of experience whose internal states generate the appearance of a physical world. William James's radical empiricism (James, 1912) argued that "pure experience" is the fundamental stuff, prior to the mind/matter split—experience itself is neither mental nor physical until placed in different relational contexts. Bertrand Russell (Russell, 1921) formalized the position: the intrinsic nature of physical events is experiential, and what physics describes is their extrinsic, relational character.

The framework inherits Russell's structural realism directly. The actualization process has an outside-view—the $\mathbb{RP}^3$ projection, which is what physics describes—and an inside-view—the fiber content stripped by τ, which is what experience is. These are complementary descriptions of the same process. The normal and tangent bundles at $\mathbb{RP}^3 \subset \mathbb{CP}^3$ are the geometric realization of this complementarity (Chapter 20). The tangent bundle carries the objective, publicly accessible content; the normal bundle carries the subjective, perspectival content. Neither bundle exists without the other, because both are defined by the same embedding.

What the framework adds to the neutral monist tradition is specificity. Russell could assert that the intrinsic nature of physical events is experiential, but he could not say which physical events are experienced, at what scale, or with what structure. The framework answers all three: experienced events are those in the dynamic-persistence regime ($R(k) \approx 1$) with sufficient integration ($\Phi > 0$); the relevant scale is $k \approx 75.35$; and the structure of experience is the qualia fiber geometry of $\mathbb{RP}^3 \times \mathbb{R}^3$ (Chapter 20).

This specificity also distinguishes the framework from panpsychism—the claim that all matter has experiential properties. The framework is not panpsychist. Consciousness requires two conditions that most of the universe does not satisfy. A proton ($k \approx 52$) has $R(k) \gg 1$ and operates deep in the static-persistence regime; it has no phenomenal interior. A thermostat has $R(k) \approx 1$ at the relevant scale but $\Phi = 0$ because it lacks the integrative architecture that coherent fiber modes require. Consciousness is not ubiquitous; it is a specific dynamical achievement of systems that meet both geometric conditions simultaneously. The monism is neutral—mind and matter are aspects of one process—without being panpsychist, because only certain configurations of that process generate the inside-view.

22.3.3 Structural Realism

Ontic structural realism (Ladyman and Ross, 2007) holds that structure is ontologically primary and objects are secondary. The framework instantiates this thesis: the arena ($\mathbb{CP}^3$) and the operator (τ) are the fundamental entities; particles, fields, and spacetime are structural features of the actualization process. Where structural realism leaves the nature of the fundamental structure unspecified, the framework identifies it as projective geometry equipped with an involution.

22.3.4 Nāgārjuna and Śūnyatā

Nāgārjuna's *śūnyatā* (emptiness)—the thesis that no entity possesses intrinsic existence independent of its relations—maps to the framework's process ontology: $\tau^2 = \mathrm{id}$ means no substance persists between firings. Remove the events and there is no electron, because no self-subsistent entity was ever there. The Buddhist insight that the appearance of permanence arises from the regularity of process is the framework's account of static persistence at $k < 75.35$, stated in different vocabulary.

His doctrine of dependent origination (pratītyasamutpāda) corresponds to the self-grounding loop (Chapter 24, §24.3): each element of the framework depends on every other, with none serving as an independent foundation. The framework provides quantitative content to claims that Nāgārjuna articulated through dialectical analysis.

22.3.5 Daoism

The *Dao De Jing* (Laozi, c. 400 BCE), Chapter 42—"The Dao generates one. One generates two. Two generate three. Three generate the ten thousand things"—articulates an ontology that is process (the Dao generates, it does not sit), non-dual (yin and yang are complementary aspects of one process), and monist (everything is the Dao's manifestation, not assembled from independent parts). The sequence—undifferentiated source → primordial binary distinction → three-dimensional structure → manifest variety—maps onto the framework's derivation chain: $\mathbb{CP}^3 \to \mathbb{Z}_2 \to \mathbb{RP}^3 \to$ physics. The convergence extends to the limits of articulation: the opening line of the *Dao De Jing* ("the Dao that can be spoken is not the eternal Dao") expresses the same structural limitation that Chapter 24, §24.8 makes precise—the process cannot be fully described from outside itself, because any description is already an act occurring within it.

Each tradition anticipated a structural feature; the framework's contribution is the demonstration that the same intuitions yield quantitative physics.

Chapter 23

What the Framework Resolves

This chapter examines a series of standing problems in physics and philosophy whose framings depend on assumptions the framework rejects. T.18

23.1 Quantum Foundations

23.1.1 The Measurement Problem

The problem. In standard quantum mechanics, the transition from superposition to definite outcome is unexplained. Copenhagen declares it happens upon "measurement" without specifying what constitutes one. Many-Worlds eliminates the transition by positing universal branching, but inherits an equally severe measure problem. Collapse models (Ghirardi et al., 1986) modify the Schrödinger equation with ad hoc stochastic terms. All three approaches treat measurement as an interpretive problem layered on top of an otherwise complete formalism. T.2, 4

The dissolution. In the framework, measurement is τ-projection: the map from $\mathbb{CP}^3$ to $\mathbb{RP}^3$ via complex conjugation. This is a physical process, discrete and irreversible, built into the structure of the arena. The Born rule follows from the topology of the projection (Chapter 13)—specifically, from the $\pi_1(\mathbb{RP}^3) = \mathbb{Z}_2$ fundamental group that forces a double cover and thereby a quadratic probability measure. Definite outcomes arise from the many-to-one character of the map: $\dim_{\mathbb{R}} \mathbb{CP}^3 = 6 \to \dim_{\mathbb{R}} \mathbb{RP}^3 = 3$, so each actualized state has multiple pre-images, and which pre-image produced it is irretrievably lost.

There is no interpretive ambiguity because there is no gap between quantum evolution and classical outcome. Both are phases of the τ-cycle operating at different points in the actualization sequence (Chapter 6).

Several corollaries follow immediately:

Schrödinger's cat actualizes at the cat's own decoherence boundary—the scale k at which the cat's gravitational self-energy-difference exceeds $\hbar/\tau_{\text{coherence}}$. No external observer is needed; the projection rate is determined by the system's own position in the hierarchy.

Wigner's friend is resolved by the same mechanism. Both the friend and Wigner are correct at their respective actualization boundaries. There is no contradiction because definite outcomes are indexed to actualization events, and the friend's event precedes Wigner's.

The quantum Zeno effect is the high-k Lindblad limit: frequent actualization events suppress transitions between states, exactly as the framework's continuous actualization dynamics predict (Chapter 6).

The quantum-to-classical transition requires no decoherence threshold. The transition is already built into the actualization rate, which increases with the system's position in the hierarchy. Large systems actualize so frequently that quantum superpositions persist for negligibly short intervals.

23.1.2 Bell Nonlocality and EPR

The problem. Bell's theorem (Bell, 1964) demonstrates that no local hidden variable T.4
theory can reproduce the correlations predicted by quantum mechanics and confirmed by experiment (Aspect et al., 1982). The standard conclusion is that nature is either nonlocal (actions here instantaneously affect outcomes there) or that the notion of pre-existing values must be abandoned. Behind Bell sits the older Einstein-Podolsky-Rosen argument (Einstein et al., 1935), which forced a choice among three claims one would ordinarily want to keep together: that the quantum state is a *complete* description, that physics is *local*, and that the quantities described are *real* prior to measurement. EPR argued that one of these has to give. Bell sharpened the trilemma and most interpretations of quantum mechanics have surrendered one or more of the three.

The dissolution. The framework keeps all three by relocating where each claim applies. Each EPR component receives a specific status within the $\mathbb{CP}^3/\mathbb{RP}^3$ structure.

Completeness. The $\mathbb{CP}^3$ state is the complete description of the system. No hidden variables exist at a deeper level. What looks like incompleteness in standard quantum mechanics is the gap between the global state in $\mathbb{CP}^3$ and the local outcome in $\mathbb{RP}^3$—a gap created by the projection itself, not by missing information.

Locality. Every τ-projection is a local operation. No signal propagates between distant sites. What appears as nonlocality is the geometry of the arena: the possibility space $\mathbb{CP}^3$ is larger than the product of local outcome spaces, and entangled particles share correlations that live in this larger space, not in the spacetime where the projections occur. Spacetime is the accumulated record of actualization events (Chapter 16); the correlations are properties of the arena that generates that record. No superluminal influence is required because no influence travels at all—the correlation was geometrically pre-established.

Realism. The $\mathbb{CP}^3$ state is a real geometric object, a point on a manifold rather than a computational fiction. Local outcomes in $\mathbb{RP}^3$ are also real, but only after the projection occurs: τ-projection creates them. Reality is preserved at the level EPR demanded (the quantum state) and at the level of measured outcomes (after actualization), with the projection itself as the bridge between the two.

Bell's theorem remains valid. Local hidden variables are excluded. What the framework provides is a specific account of what replaces them: the geometry of $\mathbb{CP}^3$, which is not a hidden variable theory but the structure of possibility itself. The framework keeps the global state complete, the projection process local, and both the global state and the actualized outcome real—at the cost of distinguishing two senses of "real" for $\mathbb{CP}^3$ and $\mathbb{RP}^3$.

23.1.3 The Preferred Basis Problem

The problem. In any interpretation that takes quantum states seriously, there is a question: T.2
in which basis does measurement occur? The Schrödinger equation is basis-independent, but measurement outcomes are not. Decoherence selects a preferred basis dynamically (the pointer basis), but the selection depends on the system-environment split, which is itself conventional.

The dissolution. The τ-involution on $\mathbb{CP}^3$ has a unique fixed-point set: $\mathbb{RP}^3$. The eigenstates of τ (the τ-even states that survive projection) constitute the preferred basis. The selection is topological: the involution's eigenstructure is determined by the arena geometry and does not depend on any system-environment decomposition.

The preferred basis is the set of states invariant under complex conjugation. In the standard representation, these are the real-valued states. The measurement basis is the real slice of the complex arena, determined uniquely by the involution that defines actualization itself.

23.2 Cosmology and Gravity

23.2.1 Fine-Tuning and Structural Uniqueness

The problem. The Standard Model contains 26 free parameters that appear finely tuned for the existence of complex structure. Small changes in the fine-structure constant, the Higgs vacuum expectation value, or the cosmological constant would produce a universe without atoms, without chemistry, or without structure at any scale. Proposed explanations include the anthropic principle (we observe fine-tuning because observers require it), the multiverse (all values are realized somewhere), and symmetry arguments (the parameters are constrained by an underlying symmetry yet to be discovered). T.13, 18

The dissolution. The constants of nature are eigenvalues of $\mathbb{CP}^3$ geometry: they take their observed values in every actualization history because they are structural features of the arena, and like π they take their values structurally rather than by selection (Chapter 18). The Standard Model gauge group $SU(3) \times SU(2) \times U(1)$ is derived from the stabilizer structure of $\mathrm{Isom}(\mathbb{CP}^3) = \mathrm{PU}(4)$ broken by τ (Chapter 15). Three generations of fermions follow from the bulk/boundary structure of $\mathbb{CP}^3$ — one boundary generation (Jackiw–Rebbi modes at $\mathbb{RP}^3 = \mathrm{Fix}(\tau)$) and two bulk topological generations (Chapter 15, §15.4). The apparent fine-tuning is an artifact of treating structural quantities as contingent: α, G, θ_W enter the framework the same way π enters geometry.

23.2.2 The Hierarchy Problem

The problem. The electroweak scale ($\sim 10^2$ GeV) is 17 orders of magnitude below the Planck scale ($\sim 10^{19}$ GeV). In the Standard Model, the Higgs mass receives quadratically divergent radiative corrections that should drive it to the Planck scale unless delicate cancellations occur at each order of perturbation theory. Supersymmetry was the leading proposal for protecting the hierarchy, but the LHC has found no superpartners. T.9

The dissolution. The hierarchy of scales is a geometric consequence of the fiber topology of $\mathbb{CP}^3$. The actualization hierarchy (Chapter 14) spaces physical scales by factors of 2π (the circumference of the Hopf fiber), and 2π iterated through the hierarchy naturally spans the 17 orders of magnitude between the electroweak and Planck scales. The ratio is a topological invariant of the arena, determined by the Hopf fiber circumference.

No supersymmetry is needed because there is no fine-tuning to protect against. The hierarchy is as stable as the value of 2π itself.

23.2.3 The Cosmological Constant Problem

The problem. Quantum field theory predicts a vacuum energy density roughly 10^{122} times T.14
larger than the observed cosmological constant (Weinberg, 1989). This is often called the worst prediction in the history of physics. The discrepancy has resisted resolution for decades; proposed explanations include supersymmetric cancellations, the anthropic landscape, and dynamical relaxation mechanisms.

The dissolution. The QFT vacuum energy calculation is a category error within the framework. It sums zero-point energies of quantum fields defined on a pre-existing spacetime background. In the framework, spacetime is not a background; it is the accumulated record of actualization events (Chapter 16). There is no pre-existing vacuum to assign energy to.

The observed cosmological constant is determined by the topological capacity of the $\mathbb{RP}^3$ boundary, $N_\infty = \varphi^{392} \approx 8.4 \times 10^{81}$:

$$\Lambda = \frac{2\,(m_\pi c^2)^2}{(\hbar c)^2\,N_\infty}.$$

It is small because N_∞ is exponentially large ($\approx e^{60\pi}$, set by the instanton action $S = 30\pi$), converting the hierarchy between vacuum energy and Planck scale into geometric structure. The 10^{122} discrepancy between the QFT prediction and observation measures the failure of the QFT framing, not a fine-tuning of the constant.

23.2.4 Black Holes

The problem. Black holes concentrate several standing puzzles: the information paradox (where does infalling information go if Hawking radiation (Hawking, 1975) is thermal?), the firewall paradox (does an infalling observer encounter high-energy quanta at the horizon?), and the entropy puzzle (why is black hole entropy proportional to area rather than volume?). All standard resolution attempts share a common commitment: unitarity is axiomatic, and the task is to show how information survives.

The dissolution. The framework denies the shared axiom that unitarity must hold on the actualized side. $\mathbb{CP}^3$ evolution remains unitary, but the τ-projection from $\mathbb{CP}^3$ to $\mathbb{RP}^3$ is many-to-one, so the actualized record alone does not preserve all the information present in $\mathbb{CP}^3$ — the stripped content goes into the normal bundle, where it remains as the fiber content of subsequent events. Information is not destroyed; it becomes inaccessible to the actualized side. A black hole is an extreme instance of the same projection process operating everywhere: infalling information is stripped to the normal bundle, and the actualized region beyond the horizon loses tangent-side access to it. Chapter 16, §16.5 derives the Bekenstein–Hawking entropy (Bekenstein, 1973; Hawking, 1975) exactly (with the factor 4 identified as $|V_4|$), the Hawking temperature from actualization rates at the horizon, the interior as a finite actualization sequence, and the singularity-resolution as a geometric event-rate ceiling. The firewall dissolves because the interior is well-defined; the information paradox dissolves because tangent-side unitarity was never warranted in a framework where projection from possibility space is many-to-one.

What belongs in this catalog is the philosophical weight of the move. Unitarity-on-the-actualized-side has been treated as sacrosanct across nearly every approach to quantum gravity — it is the shared premise of complementarity, ER=EPR, island formulas, and the Page curve program. The framework's willingness to relax it, while preserving $\mathbb{CP}^3$-level unitarity, is grounded in its ontology: the many-to-one structure of τ is geometric, established long before black holes entered the discussion (Chapter 8). Information loss as standardly understood is loss-from-the-tangent-side; the full $\mathbb{CP}^3 + \tau$ evolution preserves everything, with the stripped content carried by the normal bundle. That the same feature dissolves a cluster of black hole paradoxes simultaneously is a consistency check on the projection-geometric foundation.

23.2.5 Matter-Antimatter Asymmetry and Strong CP

The problem. The observable universe is overwhelmingly composed of matter rather than antimatter, despite the approximate symmetry between them in the Standard Model. T.6, 11
Explaining this asymmetry requires CP violation beyond what the Standard Model provides. Separately, the strong interaction preserves CP symmetry to extraordinary precision ($\theta_{\text{QCD}} < 10^{-10}$), despite having no known reason to do so. The leading explanation (the Peccei-Quinn mechanism (Peccei and Quinn, 1977)) postulates a new particle, the axion, which has not been observed.

The dissolution. The framework derives $\theta = 0$ exactly from T-invariance of the τ-involution. Complex conjugation τ is an anti-holomorphic involution; it reverses the orientation of the Hopf fiber, which is the geometric carrier of CP phase. T-invariance of τ forces the strong CP phase to vanish identically. No axion is needed because the parameter was never free.

The matter-antimatter asymmetry arises from the chiral fact type (Chapter 9): one of the four independent $\mathbb{Z}_2$ degrees of freedom stripped at each actualization event carries handedness information. The quark CKM CP phase is $\delta_{CP} = \pi(1 - 1/\varphi)$, where φ is the golden ratio, derived from the Berry phase accumulated around the $\mathbb{CP}^3$ geodesic connecting the second and third generation fixed points. Whether this CP-violation alone is sufficient for the observed baryon-to-photon ratio through standard baryogenesis channels (electroweak baryogenesis, leptogenesis) is a separate, long-debated question in the baryogenesis literature that the δ-derivation does not address.

23.2.6 The Problem of Time in Quantum Gravity

The problem. General relativity treats time as a dynamical variable (the metric evolves). T.14, 18
Quantum mechanics treats time as a parameter (the wave function evolves *in* time, but time itself does not change). Combining the two produces the Wheeler–DeWitt equation (DeWitt, 1967), $\hat{H}|\Psi\rangle = 0$, which states that the total Hamiltonian of the universe annihilates the wave function. Taken at face value, this implies the universe does not evolve—a conclusion at odds with everyday experience and with the observed arrow of time. The "problem of time" has been one of the central obstacles to quantum gravity for over 50 years.

The dissolution. The Wheeler-DeWitt equation is correct. Between actualization events, the geometry of the accumulated record does not change—it is a fixed collection of already-actualized facts. The constraint $\hat{H}|\Psi\rangle = 0$ correctly describes this frozen record. Time is not the evolution of geometry; it is the ordered sequence of actualization events that adds new facts to the record (Chapter 24, §24.1.1).

The problem arose from assuming that time must be either a background parameter (as in quantum mechanics) or a dynamical field (as in general relativity). The framework offers a third option: time is the discrete ordering of τ-firings. Each firing adds an increment to the actualization record. The record's geometry is static between firings (satisfying Wheeler-DeWitt) and grows at each firing (producing the observed temporal flow).

23.3 Philosophy of Physics

23.3.1 The Unreasonable Effectiveness of Mathematics

The problem. Wigner asked in 1960 (Wigner, 1960) why abstract mathematics describes T.18
the physical world so well. The standard answers come in two camps. Platonism holds that mathematical structures exist in their own abstract realm and that the physical world participates in that realm to the extent that physical behavior tracks mathematical relationships.

Empiricism holds that mathematics is a human-developed language tuned by use to fit the world we observe. Both answers preserve the puzzle's premise: mathematics and physics occupy separate domains, and the fit between them is what wants explaining.

The dissolution. The premise is what fails. The geometric structures the framework identifies—$\mathbb{CP}^3$, the $\mathbb{Z}_2$ involution, the Hopf and twistor fibrations, the irreducible representations of PU(4)—are not abstract objects that the physical world happens to instantiate. They are the physical world, described from outside rather than encountered from inside. The fit between this mathematics and this physics is the fit between a structure and that same structure: tautological once the identification is seen.

The cut goes through both standard answers. The Platonist's separate realm becomes redundant: there is nothing extra to be participated in, because the structure already is the world rather than an abstraction the world resembles. The empiricist's selection story becomes unmotivated: mathematics is effective not because we shaped it to fit, but because the structures it identifies are the structures the world enacts. The human discipline of mathematics is the practice of writing down an organization that physics was already running.

The identification holds across three layers of mathematical description. At the level of *topology*, the conserved quantities of actualization—fact types, the Born rule, gauge charges—are topological invariants of the arena ($\chi(\mathbb{CP}^3) = 4$, $\pi_1(\mathbb{RP}^3) = \mathbb{Z}_2$, homotopy groups of the isometry group). Topology describes physics because physics is the projection of topological structure. At the level of *algebra*, gauge groups are subgroups of PU(4) and particles are their irreducible representations. Group theory describes particle physics because particles are representations of the arena's isometry group. At the level of *analysis*, differential equations govern dynamics because the actualization process is a flow on a smooth manifold; the heat kernel, the Dirac operator, and the Kähler potential are the actualization map written in the language appropriate to its scale.

Wigner's puzzle dissolves because the premise was wrong. Mathematics is unreasonably effective at describing the physical world only on the assumption that the two are different things. In the framework's account they are one structure under two readings—encountered from inside, written from outside—and no further explanation of the fit is needed.

23.3.2 The Arrow of Time

The problem. The fundamental equations of physics are time-symmetric (or CPT-symmetric).T.7 The second law of thermodynamics is not. Standard statistical mechanics derives the arrow of time from a low-entropy initial condition (the Past Hypothesis), but this pushes the question back one step: why was the initial condition low-entropy?

The dissolution. The arrow of time is geometric, not statistical. The τ-projection is many-to-one: $\dim_{\mathbb{R}} \mathbb{CP}^3 = 6 \to \dim_{\mathbb{R}} \mathbb{RP}^3 = 3$. Each firing strips information about which pre-image produced the outcome — the stripped content goes into the normal bundle rather than being destroyed, but the actualized record cannot reconstruct the pre-image from itself. This tangent-side irretrievability is monotonic across the accumulating record and constitutive of temporal direction (Chapter 8). The second law is a direct consequence of the arena's topology, not a statistical regularity that might be violated by fluctuations. $\mathbb{CP}^3 + \tau$ evolution remains unitary; what makes time asymmetric is the asymmetry between the actualized side (which the firings leave behind as a record) and the normal-bundle side (where the stripped content goes).

No Past Hypothesis is needed. The arrow of time does not require a special initial condition because it is not produced by initial conditions. It is produced by the asymmetric structure of the actualization process itself: every τ-firing strips information to the normal bundle, the stripping is irreversible from the actualized side, and the ordering of firings defines the direction of time. The low-entropy early universe is a consequence of few actualization events having occurred (less accumulated tangent-side irretrievability), not a brute-fact boundary condition.

23.4 Philosophy of Mind

This section catalogs the standing problems of philosophy of mind that the framework dissolves. Full treatments of the underlying mechanisms appear in Chapter 20; these entries register the dissolutions and exhibit how each follows from the projection geometry.

23.4.1 The Ontology of Qualia

The problem. What kind of thing are qualia? The standard options stake out untenable T.16
positions. Dualism posits a separate mental substance and inherits an interaction problem. Eliminativism denies that qualia exist. Reductive physicalism identifies qualia with brain states and leaves the explanatory gap between physical description and felt character unaddressed. Each proposal accepts a prior framing in which physical stuff and phenomenal stuff are two categories needing a relation.

The dissolution. Qualia are the normal-bundle content of fused critical-scale actualization events, read from inside (Chapter 20). They are a geometric quantity — the τ-odd component of the actualization event — with the same ontological status the τ-even component (the experienced world) has. The two are two readings of one geometric configuration: the actualized record from outside, the fiber content from inside. Qualia are not a separate substance, not eliminable, and not reductively identified with brain states: they are what the boundary's normal-bundle content *is*, viewed from inside.

The dissolution is the same shape as the framework's other monisms (§23.5): field is geometry, matter is actualization, gravity is curvature, qualia are normal-bundle content. None of these identifications adds a substance; each names what one geometric register *is* when read in the other register. Qualia have the ontological status of geometric quantities in the normal bundle over the fused boundary; their specific structure — V_4 fact types, projective topology, spatial and temporal grain — is developed in Chapter 20.

23.4.2 The Hard Problem of Consciousness

The problem. Chalmers's hard problem (Chalmers, 1995) asks why physical processing produces subjective experience at all. The question presupposes a gap between the physical (third-personal description of matter in motion) and the experiential (first-personal qualitative states), and asks how to bridge it. T.16

The dissolution. The framework dissolves this gap rather than bridging it. The operator τ does not discard the stripped content; it transcodes it. At every scale, actualization produces two outputs: the actualized record (tangent bundle content, the "outside view") and the stripped residue (normal bundle content, the "inside view"). At particle scales, the outside view is a particle track in a detector; the inside view is the quantum numbers that the track carries. At the critical scale, the outside view is neural activity measurable by an external observer; the inside view is the qualitative character of experience accessible only to the system itself.

The two views are aspects of one geometric process: the τ-projection from $\mathbb{CP}^3$ to $\mathbb{RP}^3$. The tangent bundle captures what the projection preserves; the normal bundle captures what it strips. Neither description is more fundamental than the other. The physical and the phenomenal are the τ-even and τ-odd components of a single actualization event. The hard problem arises in frameworks that begin with substance ontology—frameworks that posit physical stuff and then try to derive experience from it. In process ontology, where events are fundamental and substances are derivative, the question does not arise in its traditional form. Every actualization event has both an actualized output and a stripped residue. At particle scales, we call these "measurement outcome" and "quantum numbers." At the critical scale, we call them "neural activity" and "experience." The vocabulary changes; the geometry does not.

The framework also specifies which systems are conscious and why: those with $R(k) \approx 1$ *and* $\Phi > 0$ (Chapter 19, §19.3.1). A proton has $R \gg 1$ (quantum regime, no integration); a thermostat has $\Phi = 0$ (classical regime, no integration); a brain at $k \approx 75$ has both conditions satisfied. Consciousness is not ubiquitous (contra panpsychism) and not mysterious (contra dualism).

This is the full reach of the dissolution, and marking where it stops is part of stating it honestly. Every *structural* feature of experience — its dimensionality, its four modalities, the projective topology of its fields, the unity of a moment, its temporal grain, the sign of valence — the framework reduces to geometry; the chapters above carry those reductions. The framework answers why experience has the structure it has. What it does not answer is why the geometry is instantiated at all — why there is something it is like to be the τ-projection rather than nothing. That residue is not specific to consciousness. It is the same question asked of the field, of matter, of gravity: why is the geometry occupied rather than only described? A monism — and the framework is one (§23.5) — earns the identity that mind and matter are one stuff, and shows that consciousness is not a second explanandum set beside physics. It does not, and no monism can, say why there is any stuff at all. Pressed to the framework's machinery, the hard problem reduces to the question of existence itself — and is no harder than it.

The framework offers one candidate observation that gestures at the residue without closing it. Integrated boundaries track their own measurement basis: the outer loop is the system modeling itself, and $\mathbb{RP}^3 = \mathrm{Fix}(\tau)$ is a fixed-point structure — the involution-invariant locus. A self-referential fixed point of this kind, accessed from no outside vantage, may have first-person character intrinsically: the inside view of being-that-configuration. This is a candidate ground, not a derivation. It identifies what kind of geometric configuration carries an inside; it does not explain why geometry is instantiated at all.

23.4.3 The Binding Problem

The problem. The binding problem asks why conscious experience is unified rather than decomposed into separate feature channels. Color, shape, motion, sound, touch each have distinct neural substrates; how do they cohere into one experience? T.16

The dissolution. The framework's answer was established in Chapter 20: a phenomenal moment is one fused event rather than many bound ones. Within a single τ-projection the four fact types are co-extracted together — at $R \approx 1$ the measurement torus collapses and one event delivers all four, with no step that joins them. Across the events of a moment, a synchronized population of τ-firings, cast in a common frame within one integration window, fuses into a single collective actualization. The unity is the unity of one event, at both scales.

Binding requires no mechanism layered onto physics. There are no separate feature channels waiting to be combined: the per-event extraction is already four-fold, and the synchronized fusion is already one moment. The binding problem asks how to join contents that, in the framework, were never separate.

23.4.4 The Explanatory Gap

The problem. The explanatory gap is the intuition that no amount of third-person physical description can capture first-person phenomenal character. This intuition has resisted every attempt to bridge it from one side or the other. T.16

The dissolution. The intuition is correct within the framework, and reflects the structure of the τ-projection rather than a failure of explanation. The tangent bundle (third-person description) and the normal bundle (first-person character) are complementary components of the same geometric object. Complete knowledge of one does not determine the other, any more than complete knowledge of a particle's position determines its momentum. The gap arises from trying to reconstruct the normal bundle from the tangent bundle alone—to get from the τ-even component to the τ-odd component within a single description. The framework shows that both components are equally real, equally determined by the τ-projection, and jointly exhaustive of the event's content. The gap is an artifact of treating one component as fundamental and the other as derived.

23.4.5 Free Will and Agency

The problem. If matter obeys deterministic (or stochastic) laws, how can choices be free? The standard responses — libertarian indeterminism, compatibilism, hard determinism — all accept the substance framing in which a chooser stands behind the dynamics and argue about its consequences. T.16

The dissolution. At the critical scale, a fused boundary's state is specified by (ρ, θ, w) and the τ-projection is Born-stochastic (Chapter 19, §19.5.2). Together these are complete: no variable in the equations corresponds to a chooser separate from the dynamics. The framework's answer rejects the presupposition that agency must live somewhere in addition to the dynamics: agency is the two-loop dynamics read from inside, with no added structure on top. The dynamics themselves are the agency. The $\mathcal{F}_{\text{eff}}$ gradient is felt as intending and the landing as having acted. Preference weights w are constitutive of who-you-are-as-a-boundary, not external constraints on a hidden self behind the dynamics (Chapter 19, §19.5.4).

This is a compatibilism — physical dynamics and felt agency coexist — but grounded by geometric identity rather than the classical definitional move ("free" read as unconstrained by external coercion). The choosing *is* the dynamics happening; no further question remains whether the chooser was "really" free. The dissolution is the same shape as the framework's other monisms: no separate substance overlaid on the geometry, just the geometry read in two registers.

23.5 Substance Dualism Across Scales

The four catalogs above are organized by domain. A pattern runs through them. At each scale where standard physics treats two ontological categories as joined by a relation, the framework treats them as one geometric configuration read in two registers. The chapters listed below worked out the dissolution at each scale; what this section does is name the pattern.

The same anti-dualist move appears at four scales: field/geometry (Chapter 12), matter/spacetime (Chapter 15), stress-energy/curvature (Chapter 16), and qualia/brain (Chapter 19, §19.4; Chapter 20). Each was treated in the chapter that established it, and each cashes out the same commitment: there is no separate substance overlaid on the geometry. Field, matter, gravity, qualia — each is what the geometry *is* at a particular resolution, not something added to geometry or supervening on it.

The pattern is not that the framework solves four independent problems with four clever tricks. It is that one structural commitment — everything is geometry — applies at four scales, and four formulations of substance dualism become four instances of one category mistake.

The framework's lineage on this point is real. Russell's structural realism (Russell, 1927), James's neutral monism (James, 1904), Spinoza's substance monism (Spinoza, 1677), Whitehead's process philosophy (Whitehead, 1929) — each addressed a version of substance dualism by proposing that the apparent two-ness was an artifact of how the underlying one-ness was being read. PPM is what those positions become when they get a specific geometric structure to back them: the arena $\mathbb{CP}^3$, the involution τ, the actualization cycle.

The framework does not adopt these positions as imports; it instantiates them by being a structure that exhibits exactly the one-ness each tried to articulate. What the framework adds to that lineage is specificity — a particular geometry, a particular operator, particular conditions under which the geometry becomes readable in particular registers.

Recognizing the move as a single move applied four times has two consequences. First, it grounds the qualia identification of Chapter 20 in the same metaphysical commitment that grounds the field, matter, and gravity identifications — the consciousness account is the fourth application of an already-load-bearing pattern, not a special-case stretch made to explain consciousness. Second, it makes the framework's geometric monism visible as a substantive position rather than as background assumption: at every scale, PPM is committing to one ontological category and to the readability of that category in different registers. The catalogs above are not four lists of independent dissolutions; they are one dissolution applied at four domains, the same anti-dualist commitment cashed out in the language each domain demanded.

23.6 The Weight of the Evidence

The entries above span quantum foundations, cosmology, philosophy of physics, and philosophy of mind—domains that have historically been treated as separate research programs with separate literatures, separate methods, and separate standards of evidence. The measurement problem belongs to quantum foundations; the cosmological constant to cosmology; the hard problem to philosophy of mind; the arrow of time to statistical mechanics. These problems have resisted solution for decades, in some cases for over a century, and the attempts to solve them have generally proceeded in isolation from one another.

These dissolutions follow from the same three ingredients: $\mathbb{CP}^3$, τ, the confinement-scale anchor ε_0. What the framework leaves open is treated in the next chapters.

Chapter 24

Deep Questions

This chapter takes up what remains when every derivation has been traced to its starting point: the question of where $\mathbb{CP}^3$ comes from and what self-consistency means in a framework with no external inputs. T.18

24.1 Background Independence

A standard requirement in quantum gravity is that the theory not assume a fixed background spacetime. General relativity satisfies this requirement: the metric is dynamical. Quantum field theory does not: fields propagate on a fixed Minkowski background. Any framework unifying the two must make spacetime emergent rather than assumed.

The fixed mathematical structure in the present framework is $\mathbb{CP}^3$—the space of possibilities for each actualization event. This is a topological space analogous to phase space in classical mechanics. Phase space is not a "background" in the problematic sense; it is the arena in which dynamics takes place. Spacetime geometry—the metric $g_{\mu\nu}$ on $\mathbb{RP}^3$—is the output of the actualization process. Before any actualization events have occurred, no metric exists. After N events, the metric is determined by the saddle-point of the effective action Γ_{eff}.

This achieves background independence in a stronger sense than general relativity provides. In GR, the metric is dynamical but still exists as a fundamental field. Here, spacetime geometry does not exist until actualization produces it. There is no background metric independent of the actualization sequence. Four specific senses of background independence hold simultaneously: $\mathbb{CP}^3$ is self-contained (no embedding space), time emerges from actualization events (no external clock), $\mathbb{CP}^3$ is compact and without boundary (no boundary conditions), and measurement is self-referential (no external observer).

24.1.1 The Problem of Time

The Wheeler–DeWitt constraint $\hat{H}_G|\psi\rangle = 0$ creates one of the central puzzles of quantum gravity: if the total Hamiltonian annihilates the quantum state, nothing evolves, and time disappears from the formalism (Wheeler, 1968). Proposed resolutions—deparametrization, conditional probabilities, third-quantization—all struggle with the same tension between a timeless equation and a manifestly temporal universe.

The framework resolves this directly. Time is the ordered sequence of discrete actualization events. The constraint $H_G = 0$ states that geometry does not evolve between actualization firings. This is correct: geometry is the accumulated record of past events, not a dynamical degree of freedom that propagates between them. No clock variable is needed because the sequence of τ-firings provides a fundamental, irreversible temporal ordering. The problem of time was an artifact of seeking continuous time evolution in a regime where the dynamics are fundamentally discrete.

24.1.2 Diffeomorphism Invariance

Diffeomorphism invariance is the requirement that physics not depend on coordinate choice—a coordinate change is a relabeling of points, not a physical transformation, and sensible laws have to be insensitive to it. Any theory of gravity must satisfy this requirement; general relativity does so by construction in tensor form, and quantum gravity programs typically have to impose the requirement as an additional constraint and contend with coordinate-dependent regulators introduced by quantization.

The framework satisfies the requirement automatically. The effective action $\Gamma_{\text{eff}}[g] = N\,\Gamma_1[g]$ is built from the heat-kernel expansion of the Laplacian $\Delta_{\mathbb{CP}^3}$, a coordinate-free differential operator on $\mathbb{CP}^3$. Anything constructed from it inherits coordinate-independence. The resulting saddle-point equations $G_{\mu\nu} + \Lambda g_{\mu\nu} = (8\pi G/c^4)\,T_{\mu\nu}$ are manifestly covariant.

The structural point: diffeomorphism invariance is a consequence of the arena's geometry, never an external axiom. Discrete or combinatorial spacetime programs (loop quantum gravity, causal sets) face the harder problem of recovering smooth invariance in a continuum limit. Here it is built in from the start—the actualization process operates on a smooth Kähler manifold whose natural geometric operators do not know about coordinates.

24.1.3 Causality and the Partial Order

Standard accounts of causality either take it as a separate axiom (microcausality on field commutators in QFT, Lorentz invariance in SR) or postulate the causal partial order primitively (causal set theory). General relativity makes the causal structure dynamical via the Lorentzian metric but leaves the metric itself needing an account. In each case the causal order and the geometry that supports it are independently posited.

The framework derives both from one arena. The local light-cone structure, the global causal partial order, and the temporal arrow are three readings of one geometric fact — light cones as sets of disk-boundary curves and the partial order as τ-event deposition (Chapter 16, § The Speed of Light c), and the arrow of time as $M(t)$'s monotonic accumulation (§23.3.2). None is an additional posit; all three are how the τ-projection from $\mathbb{CP}^3$ to $\mathbb{RP}^3$ reads at different scales of temporal scope. No-signaling is built into the same construction (Chapter 16, § The Speed of Light c): the disk moduli are rigid, so modifying the local causal structure would require modifying $\mathbb{CP}^3 + \tau$ globally.

24.2 The Bootstrap Condition

The framework's physical constants—α, G, θ_W, the gauge couplings, the mass ratios—are derived quantities. Two logically distinct claims underpin this:

Geometric determination. Each constant arises from the spectral and differential geometry of $\mathbb{CP}^3$: eigenvalues of the Fubini-Study Laplacian, holonomies of the Kähler connection, and curvature invariants of the embedding $\mathbb{RP}^3 \hookrightarrow \mathbb{CP}^3$. The coupling constants, mass ratios, and mixing parameters are determined by these geometric objects in the same sense that the energy levels of hydrogen are determined by the Coulomb potential and the normalizability condition. The derivations are presented in Chapters 18–14.

Self-consistency as verification. The derivation at each scale uses constants that are themselves outputs of the geometry at other scales: the Lindblad dynamics (Lindblad, 1976) at each k-level depend on coupling constants governing that level, and those constants are produced by the geometry integrated across all levels. The bootstrap condition is the requirement that these determinations cohere:

$$\text{Observed}(\alpha, G, \theta_W, \ldots) \;=\; \text{Derived}(\alpha, G, \theta_W, \ldots). \tag{24.1}$$

This is a fixed-point condition. It does not generate the constants—the geometry does that.

It verifies that the geometric determinations at different scales are mutually consistent. The master relation $(2\pi)^{27}\sqrt{\alpha} = \varphi^{98}$ (Chapter 18) is the sharpest expression of this verification: it links the scaling factor, the fine-structure constant, and the golden ratio, and it holds to 0.38% with observed α (the bootstrap "Route II" derivation; the heat-kernel "Route I" derivation gives 0.16% in the same chapter).

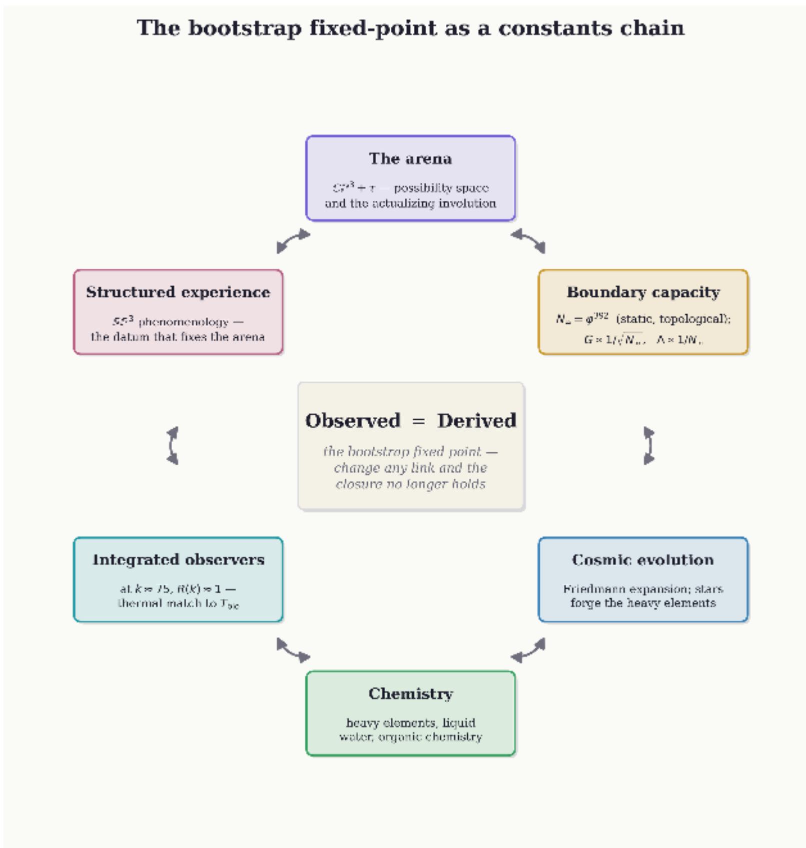

Figure 24.1: *The bootstrap fixed-point as a constants chain. The $\mathbb{CP}^3 + \tau$ geometry fixes the boundary capacity $N_\infty = \varphi^{392}$, and with it $G \propto 1/\sqrt{N_\infty}$ and $\Lambda \propto 1/N_\infty$; these shape the cosmological evolution that forges heavy elements; chemistry supports integrated observers at $R(k) \approx 1$; and observer experience is the empirical datum that fixes the arena. The cycle is the Observed = Derived condition of Eq. (24.1); each link is mutually entailing, so the closure reads from any node in either direction. N_∞ is a static topological invariant — the loop verifies that the geometry's determinations cohere, it does not generate them. The fixed-point admits only discrete solutions.*

The fixed-point condition admits only discrete solutions. Continuous variation of any constant breaks the consistency: change α and the gauge couplings at unification no longer close, the Kähler geometry no longer produces the correct heat kernel ratio, the Lindblad dynamics at the critical scale no longer match the integration measure. The constants interlock. The fixed-point structure picks out the Standard Model parameter values uniquely; values that look fine-tuned in a parameter-fitting picture appear here as solutions to a coherence condition.

24.3 The Self-Grounding Loop

The bootstrap condition can be stated as a mutual implication among three claims:

1. $\mathbb{CP}^3$ exists as the kinematic arena of physics.
2. The τ-projection dynamics on $\mathbb{CP}^3$ produce the observed gauge group, coupling constants, particle spectrum, and gravitational dynamics.
3. At $k \approx 75.35$ in the actualization hierarchy, the dynamics produce systems satisfying $R(k) \approx 1$ and $\Phi > 0$—conscious observers capable of formulating and testing the framework.

If any one of these holds, all three hold. If any one fails, all three fail.

The appearance of circularity dissolves on inspection. The three claims are independently falsifiable:

The gauge group claim can fail if the observed gauge group differs from $\mathrm{SU}(3)\times\mathrm{SU}(2)\times\mathrm{U}(1)$ at any energy scale accessible to experiment. The fine-structure constant claim can fail if $\alpha \approx 1/137$ does not emerge from $\mathbb{CP}^3$ Kähler geometry to within experimental precision. The consciousness claim can fail if the predicted integration timescales, temperature dependence, Φ-scaling laws, or qualia geometry do not match observation. These are quantitative predictions that can be wrong.

A framework that begins with an assumption (as all physical theories do—general relativity assumes spacetime, quantum mechanics assumes Hilbert space) and derives independently testable consequences is scientific, regardless of whether its assumption and consequences are mutually entailing. Vicious circularity uses an assumption to derive a conclusion that then justifies the assumption *with no independent check*. Here, the checks are numerous, quantitative, and distributed across particle physics, cosmology, and neuroscience.

24.3.1 Incompleteness and Self-Reference

The bootstrap fixed-point structure invites comparison to Gödel's incompleteness theorems (Gödel, 1931), and the comparison should be made and dispatched. Gödel's first theorem constructs, in any sufficiently strong formal axiomatic system, a sentence that is a fixed point of provability negation: a statement that is true if and only if it is unprovable in the system. The framework's bootstrap fixed point is structurally different. Equation (24.1), Observed = Derived, is a numerical coherence condition on physical constants computed from $\mathbb{CP}^3$ geometry at different scales; it makes no meta-claim about the framework's own provability and contains no analog of Gödel's dilemma. These are different fixed points of different operators.

The Gödelian objection sometimes advanced against any final theory of physics—that no formal system can deliver complete physical truth—requires more than the surface analogy to land. Gödel's theorems apply to formal axiomatic systems strong enough to encode arithmetic. The framework is not such a system: $\mathbb{CP}^3$ and τ are physical-mathematical objects, the derivations are mathematical and not formal-syntactic, and the testable content is empirical. The relevant kind of completeness for a physical theory is empirical-coverage completeness, which is a separate question that Gödel's theorems do not settle.

A genuine incompleteness does enter the framework, in a different vocabulary. A conscious system's internal model cannot completely predict its own next τ-projection. The Born rule yields probabilities for outcomes; individual outcomes are not algorithmically derivable from the pre-projection state. The system is computationally incomplete with respect to itself. This limit shares the shape of Gödel's incompleteness—a system unable to fully predict statements about itself—while having a different source. Where Gödel exploits formal-syntactic self-reference, PPM's limit comes from quantum indeterminacy in the actualization process. The framework owns the limit. Genuine indeterminacy is what makes agency real (Chapter 20 §Non-Epiphenomenality) and what makes the universe's actualization history path-dependent.

24.4 The Epistemic Departure

The framework derives physical constants where standard physics fits them. Standard quantum field theory carries a substantial number of free parameters—gauge couplings, Yukawa entries, mixing angles, the CP phase, the QCD theta angle, the Higgs VEV—each tunable to data. The framework here has, in principle, one free parameter: the pion mass m_π, and even that is a unit of energy with no dimensionless content. Everything else falls out of the geometry. This section names what makes that possible.

The framework is derivable because there is nowhere to put a free parameter. Each location where tunability could otherwise hide is closed by an antecedent constraint.

24.4.1 The Constraint Chain

The chain runs as follows. Each link removes a degree of freedom that standard physics would have to fix by choice or by fit.

The arena. $\mathbb{CP}^3$ is the minimal complex projective space supporting the four fact types, the Pati-Salam decomposition, and the τ-involution that produces the actuality manifold (Chapter 3). Once $\mathbb{CP}^3$ is committed to, every isometry, metric component, and topological invariant follows. There is no "what arena should we pick" knob; the choice is constrained by the requirement that the framework support the fact-type structure at all.

The involution. τ has to be anti-holomorphic so that $\mathrm{Fix}(\tau)$ is a Lagrangian submanifold of the appropriate dimension (Chapter 4). Complex conjugation is the canonical anti-holomorphic involution on $\mathbb{CP}^3$. No choice remains once the Lagrangian-fixed-point structure is required.

The metric. Fubini-Study is the unique metric on $\mathbb{CP}^3$ invariant under the full PSU(4) isometry group. Any alternative would either break PSU(4)—losing the gauge structure that depends on it—or introduce new dimensionful parameters the framework would have to anchor independently. Fubini-Study is forced once $\mathbb{CP}^3$ and PSU(4) are committed to.

Bundle triviality. The normal bundle $\nu(\mathbb{RP}^3 \to \mathbb{CP}^3)$ is trivial (Chapter 3 §The Tangent and Normal Bundles). All Stiefel-Whitney classes vanish; no Pontryagin classes; zero Euler class. Gauge content cannot hide in the bundle's intrinsic topology because there is no intrinsic topology. The Pati-Salam structure carried along ν must come from the isometry group acting on a flat fiber. Triviality forecloses topological tunability.

Cascade flatness. The k-axis carries no quantum-geometric content (Chapter 14 §The k-Scale as a Flat Coordinate). Moving along the cascade does not disturb the fiber. "What physics looks like at different scales" is not adjustable, because the fiber that produces physics is k-invariant. Different scales are different positions on a flat ruler through a single arena. Cascade flatness forecloses scale-dependent tunability.

The structural anchor. The framework's energy unit is the confinement scale ε_0, the Kähler ground state of H_α on $\mathbb{CP}^3$, identified with Λ_{QCD} (Chapter 18 §18.3). The document uses $m_\pi = \varepsilon_0/1.70573$ as the energy-scale reference for numerical work, the lightest hadron mass being the form in which this scale is most precisely measured. Everything else is a dimensionless ratio derivable from the geometry. The anchor functions like meter or second — a unit the framework needs to produce dimensional results, derived from spectral geometry on $\mathbb{CP}^3$ and identified with QCD's empirical confinement scale. A future high-precision shift in m_π would move every other prediction in lockstep; the framework's structure would not change.

24.4.2 What This Means

Derivability is not a feature the framework asserts. It is a consequence of the constraint chain. Each link is a theorem or a forced choice. The degrees of freedom typical theories use to absorb data—gauge group choice, breaking pattern, Yukawa entries, mixing angles, CP phase—are consumed in advance by structural commitments.

This is a different epistemic shape from standard theory construction. Standard quantum field theory begins with a Lagrangian and tunes its couplings to data; the Lagrangian is a flexible scaffold that can absorb many possible worlds. The framework here begins with an arena and reads couplings off the geometry; the arena is rigid scaffolding that admits only one set of couplings. The first approach is well-suited to discovering new physics piecewise—add a term, see if it matches. The second approach is well-suited to closing a complete picture—if the picture is right, everything follows; if any part is wrong, the whole picture fails together.

The framework's geometric construction admits no parameter adjustment; a single confirmed disagreement that cannot be traced to a known approximation (instanton prefactor, light-quark $|z|$ positions, dressed propagator details) would falsify it.

The framework's predictions agree with experiment across forces, mass spectrum, and cosmology, as detailed in Chapter 25.

24.4.3 Structural Foreclosures

Standard quantum field theory has free parameters at each of the following locations; the framework's geometry forecloses them:

- Gauge group choice: forced by PSU(4) restricted under τ and isotropy.
- Symmetry-breaking pattern: forced by the breaking sequence on $\mathbb{CP}^3$ (Chapter 15).
- Number of generations: $\chi(\mathbb{CP}^3/\mathbb{Z}_2)+1 = 3$ from Euler characteristic plus Jackiw–Rebbi wall mode.
- Topological θ-angle: $H^4(\mathbb{RP}^3, \mathbb{Z}) = 0$ forces $\theta_{\text{strong}} = 0$.
- Quark CKM CP-violating phase: $\delta_{CP} = \pi/\varphi^2$ from Berry phase on the spin structure of $\mathbb{RP}^3$ plus the icosahedral golden-ratio split of the quark flag manifold.
- Boundary conditions on fiber modes: forced by spin structure on $\mathbb{RP}^3$.

- Rate prefactor on active-inference dynamics: linearity in Φ forced at leading order by Lindblad structure (Chapter 19).
- Cosmological constant value: $\Lambda \propto 1/N_\infty$ from boundary capacity.
- Per-event entropy: $\Delta S = 5.5\, k_B$ from Hopf-fiber circumference.
- Quantum numbers of particles: fiber-mode indices on the spin structure of $\mathbb{RP}^3$ labelled by topological invariants.

Each item is a location standard physics would treat as a free choice or a fitted parameter. The framework forecloses each not by choosing values but through structural commitments that leave no choice.

24.5 The Ontological Inversion

Standard physics assumes substance and derives process. Spacetime is the fixed arena. Fields live on it. Particles are field excitations. Chemistry emerges from particle interactions. Biology emerges from chemistry. Consciousness, if it exists at all within the framework, is an emergent computational property of certain biological configurations. The causal chain runs: spacetime $\to$ fields $\to$ particles $\to$ chemistry $\to$ biology $\to$ consciousness. At every level, the enduring thing (the substance) is primary, and change (the process) is what happens to things.

The framework inverts this entirely. Actualization events are fundamental. Persistent objects—electrons, spacetime points, organisms—are patterns that recur across event sequences. An electron is a recurring τ-actualization pattern at $k = 57$ with stable quantum numbers across firings; the same pattern shows up event after event because the geometry that produces it is the same geometry every time. Spacetime geometry is the accumulated record of past actualizations, not a stage on which they occur.

The inversion is forced by the mathematics. $\tau^2 = \mathrm{id}$ means no state carries forward between firings; there is no mathematical object representing a substance that persists between actualization events. Time is the irreversible ordering of events, not a container in which events are placed. Causation is transparent: event τ_i causes τ_{i+1} through the Lindblad dynamics governing the boundary. Quantum indeterminacy is real, because $\mathbb{CP}^3$ possibility space is ontologically prior to $\mathbb{RP}^3$ actuality.

The inverted causal chain runs: τ-events $\to$ geometry and particles (simultaneously, at different k-levels) $\to$ chemistry and biology (high-k thermodynamic regime) $\to$ consciousness (the actualization process itself, viewed from the inside at $k \approx 75.35$). The framework begins with experience—the empirical datum that something is being experienced, with a structure that constrains the arena—and derives physics. Neither consciousness nor matter is more fundamental; both are aspects of the actualization process viewed from complementary perspectives. The inverted direction of derivation reflects the logical structure of the framework—experience is the empirically accessible starting point, geometry is the consequence.

24.6 The Carrier and Its Content

The previous section identified one inversion the framework runs against the standard view: events are primary, persistent objects derivative. A second inversion runs alongside it, at the geometric level rather than the metaphysical one, and it bears explicit acknowledgment.

A reader trained in conventional gauge theory expects that gauge content—color, weak isospin, the rest—requires a non-trivially twisted fiber bundle as its carrier (Nakahara, 2003; Wu and Yang, 1975). Twisting of the bundle generates characteristic classes (Milnor and Stasheff, 1974); characteristic classes encode the gauge data; the structure of the carrier participates in defining what the content is. This is the standard picture, and it works: most quantum field theories arrange their content this way (Peskin and Schroeder, 1995; Weinberg, 1995).

The framework's geometric carrier is the normal bundle to $\mathbb{RP}^3$ in $\mathbb{CP}^3$, and that bundle turns out to be topologically trivial (Chapter 3, §3.9)—the simplest possible vector bundle of its rank, $\mathbb{RP}^3 \times \mathbb{R}^3$, with no twists or holonomy of its own. Every piece of physical content documented in this work—gauge groups, three generations, mixing angles, coupling constants, the mass spectrum—lives on top of this carrier via the isometry group's action and the operator's projection. The carrier supplies the stage; the operator action and isometry flow supply everything that happens on it.

The observation is structural. It says that the geometric vehicle of physical content is maximally featureless, and that what looks like physical structure when you examine the world is structure of the dynamics—of how the operator acts and how the symmetries flow— sitting on a carrier that contributes none of its own. The framework's content lives on the verbs: τ-projection, isometry action, variational descent. The nouns—the carrier itself—contribute almost nothing.

That this is even a sensible way to organize a physical theory is a discovery the framework makes rather than a constraint it imports. Several geometric facts could have failed. The carrier could have been twisted, requiring extra topological inputs to encode the gauge data. The embedding could have been non-Lagrangian, breaking the clean fact-type orbit on the normal bundle. $\mathbb{RP}^3$ could have failed to be parallelizable, blocking free fiber-wise action. Each went the other way. The framework gets to tell a single, unforced story about where physics lives because the carrier conspires to be trivial in exactly the right ways, and the second inversion—content on the action, none on the stage—is the consequence.

24.7 The Cosmic Asymptote

Free-energy minimization at the cosmic scale has a one-way trajectory: typical event-energies slide to ever-higher k as the ambient temperature drops and the actualization record accumulates. This raises an obvious question. What does the framework say happens at the asymptote?

The arrow of time forbids a literal restart. The cumulative actualization record $M(t)$ is monotonically non-decreasing (Chapter 8); $\mathbb{RP}^3$ is the permanent historical log of every τ-event that has ever fired; entropy production is geometric and irreversible. The framework does not support a Penrose-style conformal cyclic cosmology (Penrose, 2010) in which heat death of one aeon becomes the big bang of the next: that move requires either resetting the historical record or duplicating the arena, neither of which the framework permits. The cosmos is not periodic.

What the framework does permit is asymptotic eternity. The Kähler flow on $\mathbb{CP}^3$ is the dynamics of the arena itself (Chapter 5, §The Energy of an Event); it does not depend on matter, temperature, or any feature of the actualized record. The flow continues regardless. After heat death—when matter has dissipated, ambient T has approached zero, and the typical event-energy lies far above the cosmic ambient—the Kähler flow continues to complexify $\mathbb{CP}^3$ at every point. Eventually some configuration somewhere accumulates enough τ-odd content for a new event to fire, deposit its energy on $\mathbb{RP}^3$, and add another entry to the log.

The late-time regime is one of asymptotically rare events at asymptotically high k. The cosmos's cascade descent slows but does not terminate. $M(t)$ keeps increasing; $\mathbb{RP}^3$ keeps accumulating; no qualitative discontinuity arrives. Consciousness becomes impossible long before this regime (Chapter 20 argued that the present epoch is the window; later epochs lack both the thermal support and the matter density for integrated boundaries to persist), so the asymptotic phase is one in which actualization continues but observation within the cosmos has ceased.

This is a structurally bounded form of eternity. The cosmos has a beginning at the Planck era ($k = 1$), an observation-supporting window in the middle (where we are now), and an asymptotic tail of ever-rarer high-k events extending without termination. The framework's commitment to the cycle of complexification and projection at the event level produces, at the cosmic scale, an asymptote rather than either a return or a stop. This is the conservative answer the framework's primitives support; the move to periodic cycles or aeon-to-aeon transitions requires structural machinery the framework does not currently provide.

Arena, record, and the present epoch. The framework treats the universe in two layers, and the two must not be conflated. The bare arena — $\mathbb{CP}^3 + \tau$, the geometric structure of possibility space — is what the framework's derivations rest on, and is what it is regardless of history. The actualization record — the cumulative τ-projection events that have fired on $\mathbb{RP}^3$, counted by $M(t)$ — is a growing history populating that structure. The boundary capacity $N_\infty = \varphi^{392}$ belongs to the first layer: a static topological feature of the arena, the number of independent fiber sections $\mathbb{RP}^3$ supports. The record $M(t)$ belongs to the second: a separate, monotonically growing quantity, and by the present epoch it stands far above N_∞, every boundary position having been re-actualized many times over (Chapter 8).

Two consequences follow. First, the content of the framework's claims — α, the gauge group, the particle spectrum, G, Λ — rests on $\mathbb{CP}^3 + \tau$ and the confinement-scale anchor alone; the derivations land where they land at any point along the actualization history. Second, that history is dense: with $M(t)$ enormous, the actualized content on $\mathbb{RP}^3$ is a richly redundant record, and has been for most of cosmic history. What distinguishes the present epoch is not the record but the reader. The cascade has cooled to the band that hosts integrated observers, and those observers find a boundary already densely written. The match is not a coincidence of timing: a cosmos that has run its cascade far enough to cool into the observer-supporting window has, by then, long since accumulated a record dense enough to read.

24.8 The Cogito as Terminus

The framework's derivation chain terminates at three layers of brute fact, each corresponding to a distinct structural layer.

24.8.1 Layer 1: That Experience Exists

The cogito—"something is being experienced"—grounds the entire framework. It selects $\mathbb{RP}^3$ as the structure of actuality (via the projective geometry of phenomenal space, following Rudrauf et al. 2017) and $\mathbb{CP}^3$ as the minimal complexification supporting both Hopf and twistor (Penrose, 1967) fibrations with $\mathbb{RP}^3$ as the fixed-point set of a $\mathbb{Z}_2$ involution. This is the framework's axiom. It is not derived within the framework; it is the condition under which derivation is possible.

The axiom is empirical in the strongest sense available: it cannot be doubted without presupposing what it asserts. To question whether experience exists is to have an experience of questioning. The phenomenological structure of that experience—its three-dimensionality, its projective topology, its self-referential character—constrains the arena uniquely. $\mathbb{CP}^3$ is the minimal space satisfying the joint requirements of a three-dimensional real fixed set, twistor structure, Hopf fibration, and a $\mathbb{Z}_2$ involution with those properties. This is a uniqueness statement, not a choice.

24.8.2 Layer 2: That Experience Is Binary

The $\mathbb{Z}_2$ structure—the distinction between possibility and actuality—is the minimal mathematical structure capable of drawing a distinction. $\mathbb{Z}_2 = \{+1, -1\}$ under multiplication has exactly one non-identity element that is its own inverse. Its defining property is self-referentiality: applying it twice returns to the starting point. $\mathbb{Z}_2$ is the simplest structure that can constitute a boundary—"this side, not that side." Anything less cannot distinguish inside from outside, self from world, possibility from actuality.

The derivation is tight:

$$\begin{aligned}\text{something exists} &\Rightarrow \text{structure exists}\\ &\Rightarrow \text{self-consistency required}\\ &\Rightarrow \text{self-reference required}\\ &\Rightarrow \text{distinction required}\\ &\Rightarrow \mathbb{Z}_2 \text{ required.}\end{aligned}$$

From $\mathbb{Z}_2$ and the constraints imposed by quantum mechanics, $\mathbb{CP}^3$ follows by minimality. The bootstrap is the claim that physics consistent with this geometry exists and produces the observers who formulated the question.

24.8.3 Layer 3: That It Is This Experience

The particular outcome—which point on $\mathbb{RP}^3$, which value, which actual configuration—is not derivable from structural constraints alone. Three justifications converge:

Process openness: Actualization is genuinely creative. The $\mathbb{CP}^3 \to \mathbb{RP}^3$ projection is many-to-one, and which pre-image is selected is not determined by prior structure.

Perspective dependence: "Which outcome?" presupposes a perspective from which to ask the question. Perspective is itself constituted by actualization—asking already requires a particular actualization to have occurred.

Ontological consistency: If the particular outcome were derivable from the universal structure, every actualization would be predetermined, collapsing the $\mathbb{CP}^3 \to \mathbb{RP}^3$ projection to a bijection. This would eliminate the many-to-one structure that grounds quantum indeterminacy and the Born rule.

The framework therefore distinguishes two kinds of quantity. Geometric invariants — α, the gauge group, the generation count, the mass spectrum (from the H_α cascade ladder), the CKM/PMNS mixing angles (from generation-mode overlaps), Newton's constant, the cosmological constant, the quark CKM CP phase — follow from the structure of $\mathbb{CP}^3 + \tau$ directly and take the same values across every actualization history. Dynamical realizations — the Hubble parameter at the present epoch, dark matter abundance, the baryon-to-photon ratio, cosmological initial conditions, the existence of biological systems realizing the consciousness conditions — depend on the specific actualization sequence the universe has run, not on the arena. The split is structural, not a limitation of current calculational technique: the framework predicts what the geometry forces; it does not predict what the cosmos has accumulated.

24.8.4 Cogito Ergo Mundus

The three layers telescope into a single statement. Experience exists (Layer 1). Experience requires distinction, hence $\mathbb{Z}_2$ (Layer 2). $\mathbb{Z}_2$ acting on the minimal compatible complex manifold gives $\mathbb{CP}^3$ with fixed-point set $\mathbb{RP}^3$. The τ-dynamics on $\mathbb{CP}^3$ produce everything derived in the preceding chapters: the gauge group, the coupling constants, the particle spectrum, gravity, thermodynamics, and—at $k \approx 75$—the conditions under which systems can experience the actualization process from the inside. The framework that began with experience derives the conditions for experience.

The traditional cogito runs: *I think, therefore I am.* The framework's version is: *cogito*

($\mathbb{RP}^3$) *ergo mundus* ($\mathbb{CP}^3$). The phenomenological brute fact of structured experience selects the arena; the arena's geometry determines the operator; the operator's dynamics produce the world, including the observers within it. The derivation that began with experience terminates in the conditions for experience.

24.9 The Boundary as Epistemic Limit

The framework imposes its own native limits on what can be stated or inferred, and the limits follow from the same structure that produces everything else: the projection. Information about the world is carried by τ-projection events; only what projects through the boundary becomes part of any internal observer's accessible record. What does not project, does not project. Several distinct limits follow from this single principle.

Beyond the boundary. An observer's accessible content is the boundary state ρ plus its history. What lies beyond the boundary is mediated through sensors, predictors, and the internal model that re-projects the actualized environment (Chapter 19). Direct access to the external world is structurally impossible: there is no observer-independent vantage point inside the framework, only boundary-mediated reconstructions.

The stripped normal bundle. Each τ-projection carries forward the tangent component (actualized content) and dissipates the normal-perpendicular component (entropy released into the bath). The pre-projection state is not recoverable from the post-projection record; the projection is many-to-one. The arrow of time in the framework is exactly this: each event records less than the state it projected from, and the lost content does not return.

The unactualized. $\mathbb{CP}^3$ contains possibilities not actualized in this universe's history. The framework describes them mathematically; they have no physical existence in any actualized record. They are counterfactual structure visible from the meta-mathematical view, invisible from inside any actualization sequence. The path-dependence of the universe's history (Chapter 25) is the empirical face of this limit: the universe runs one branch, and the branch is what is.

The arena's origin. Why $\mathbb{CP}^3$? Why τ? The framework treats both as starting points, and the deepest internal answer is that the geometry of experience is $\mathbb{RP}^3$ and that $\mathbb{CP}^3$ with the conjugation τ is forced as its unique parent. Beyond this, the framework points to its own foundational identification as the limit of internal explanation. An observer inside the projection cannot derive the projection's existence from anything more primitive; the projection *is* the medium of derivation.

These limits are intrinsic to the framework's geometry. The boundary that constitutes experience also constitutes the perimeter of what experience can know—about itself, about other observers, or about the world. Physics has discoverable structure and unanswerable residue at the same time: the structure is what projects, the residue is what does not.

24.9.1 Why Something Rather Than Nothing

The question "why is there something rather than nothing?" carries a hidden assumption: that nothing is the default state, and that the existence of something requires justification relative to that default.

The assumption fails on its own terms. "Nothing" has no structure—not even the structure of being nothing. It cannot be coherently conceived as a state from which something departs, because conceiving it already imposes the structure of a conceiver. The question presupposes what it seeks to explain.

The framework's neutral monism makes this precise. Experience and structure are the inside-view and outside-view of the same process. One cannot step behind both simultaneously to ask why they exist. The question terminates in the recognition that it was already asked from within the thing it was asking about.

The structural content of the cogito makes this precise. To ask "why does anything exist?" is to demonstrate that something does—and that the something has the structure required to formulate the question. The chain from Section 24.8 then applies: structured experience $\Rightarrow \mathbb{Z}_2 \Rightarrow \mathbb{CP}^3 \Rightarrow$ physics. The "why" does not terminate in an answer; it terminates in the recognition that the question was its own answer all along.

Three residual questions remain genuinely beyond the framework's reach: why self-consistent mathematical structure is possible at all (a precondition for any coherent description of anything), why the particular actualization history that constitutes the observed universe is this one rather than some other (Section 24.8, Layer 3), and whether other self-consistent frameworks with different arenas and operators are abstractly possible. These are terminal limits any account of reality from inside reality faces. The self-grounding loop is what reality looks like when it is described from one of its own products; process philosophy, neutral monism, and the contemplative traditions arrived at this recognition through other routes, and the framework gives it definite geometric form.

The framework also cannot define purpose. It does not say what experience is for, what should be valued, or what a life should aim at. Those questions sit outside the structural description. The framework is a model; lived experience is the model instantiated in real time.

The reader, encountering these words, is the model running — the event horizon between possibility and actuality, the point at which the loop closes.

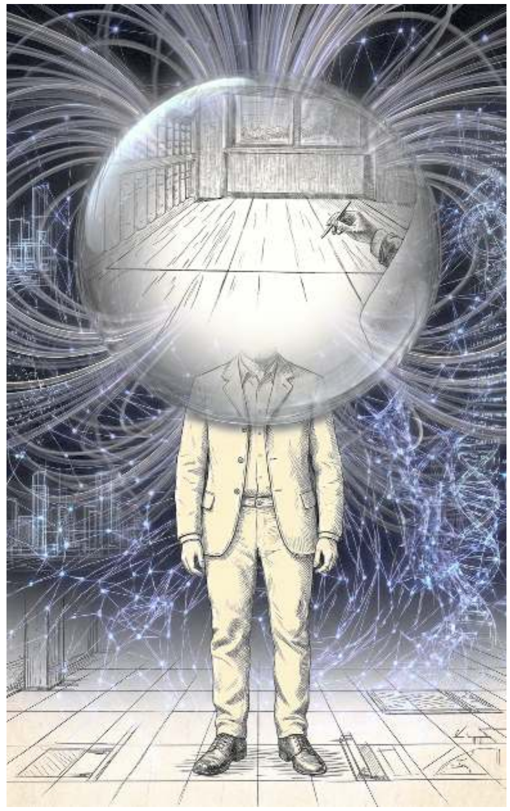

Figure 24.2: *The observer at the boundary. The reader of these words is the event horizon between possibility and actuality, the point at which the loop closes.*

Chapter 25

Predictions and Closure

A theory earns belief by what it predicts. The framework's predictions fall into three categories — retrodictions of already-measured quantities, concordances with measurements made independent of the framework, and novel claims experiment can settle. This chapter catalogs all three, with the calculational gaps that remain marked alongside. T.18, 19

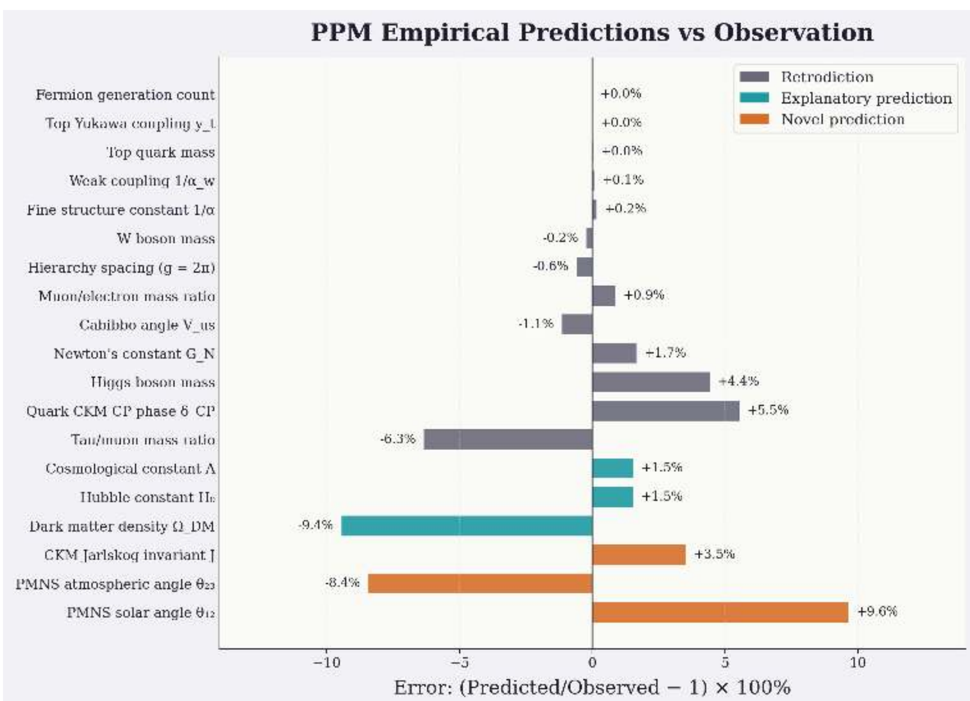

Figure 25.1: *Empirical predictions vs observation. Each bar shows* (PPM/observed − 1) × 100% *(Particle Data Group, 2024, Planck Collaboration, 2020). Color: retrodictions, explanatory predictions (H_0, Λ, dark matter), and novel predictions (PMNS, CKM Jarlskog).*

25.1 Prediction Taxonomy

The framework's empirical claims fall into three categories, ordered by increasing evidential weight.

25.1.1 Retrodictions

A retrodiction is a derivation of a quantity that was already measured before the framework existed. Retrodictions are necessary for credibility but carry limited evidential weight: the derivation might have been reverse-engineered from the known answer, whether consciously or not.

The framework's retrodictions span particle physics, gravity, and cosmology:

- The Standard Model gauge group $SU(3) \times SU(2) \times U(1)$, derived from the stabilizer structure of PU(4) broken by τ (Chapter 15).
- Three generations of fermions, from the bulk/boundary structure of $\mathbb{CP}^3$ — one boundary generation (Jackiw–Rebbi modes at $\mathbb{RP}^3 = \mathrm{Fix}(\tau)$) and two bulk topological generations (Chapter 15, §15.4).
- The fine-structure constant $\alpha \approx 1/137$, derived through three independent routes (Chapter 18).
- The hierarchy spacing between electroweak and Planck scales, from the 2π fiber circumference iterated through the actualization hierarchy (Chapter 14).
- The absence of superpartners, from the absence of supersymmetry in $\mathbb{CP}^3$ geometry.
- The weak mixing angle $\sin^2\theta_W = 3/8$ at the Pati-Salam unification scale (Pati and Salam, 1974), from the embedding of $SU(2)_L \times U(1)_Y$ in $SU(4)$.
- The strong CP phase $\theta = 0$ exactly, from T-invariance of τ.
- Information-theoretic structure: the per-event entropy production $\Delta S = 5.5\, k_B$ (from the Hopf-fiber circumference) sits at the Landauer floor for the actualization timescale, and the per-event channel capacity $I = 3\log_2 R$ saturates the Bremermann ceiling at the corresponding energy scale (Chapter 10, Chapter 8).

- Particle masses and mass ratios — the top quark, Higgs, and W boson masses, and the lepton mass ratios m_μ/m_e and m_τ/m_μ — from the actualization cascade (Chapter 14, Chapter 15).

- Newton's constant G_N, derived from the boundary capacity N_∞ and the $\mathbb{CP}^3 \to \mathbb{RP}^3$ projection (Chapter 16).

- The cosmological constant Λ, derived from $N_\infty = \varphi^{392}$ via the same boundary-capacity structure (Chapter 16).

Each is derived from the arena geometry with no adjustable parameters introduced at the point of derivation; the technical document carries the formal derivations. Collectively, they establish that the framework reproduces the known structure of particle physics, gravity, and cosmology from $\mathbb{CP}^3$, τ, and the actualization hierarchy.

25.1.2 Explanatory Predictions

An explanatory prediction addresses a measurement that is already in hand but currently lacks a satisfactory explanation within the standard framework. These carry more weight than retrodictions when the framework was not constructed to explain them; in such cases the prediction is a consequence of structure established for other purposes.

- *JWST early galaxies.* The framework predicts an effective gravitational coupling $G_{\text{eff}}(z) = G_0(1+z)^{3/2}$ in nonlinear structure formation, producing more massive galaxies at $z = 10$–20 than ΛCDM expects (Chapter 17). JWST observations (Finkelstein et al., 2023; Harikane et al., 2023; Labbé et al., 2023) already show significant tension with standard predictions at these redshifts.

- *Hubble tension.* The framework predicts $H_0 \approx 70.9$ km/s/Mpc, intermediate between the Planck CMB-inferred value (67.4, Planck Collaboration 2020) and the local distance-ladder value (73.0, Riess et al. 2022), reflecting the G_{micro} vs. G_{eff} distinction in different observational regimes (Chapter 17).

- *Dynamical dark energy.* Finite-N actualization corrections predict $w_{\text{eff}} > -1$, a small deviation from the cosmological constant. DESI data (DESI Collaboration, 2024) show evidence for dynamical dark energy at 2.8–3.9σ, consistent with this prediction.

- *Dark matter as sterile neutrinos.* The framework's dark matter candidate is a sterile neutrino at $\sim$7 keV (Chapter 15). If such a state decayed radiatively, it would produce a fluorescence X-ray line at $\approx$3.5 keV in galaxy cluster spectra. Early claims of detection have been disputed by subsequent observations; the mass scale prediction is independent of the observational status of any X-ray line. Next-generation X-ray observatories (Athena, AXIS) will provide definitive searches.

- *Xenon isotope effect.* Anesthetic potency differs across xenon isotopes (Neven et al., 2024): half-integer-spin isotopes (^{129}Xe, ^{131}Xe) show measurable differences from spin-0 isotopes (^{130}Xe, ^{132}Xe). The framework's geometric account: half-integer spin carries additional spectral fiber modes that partially resist disruption of temporal coherence—providing an explanation for an effect that currently lacks one.

25.1.3 Novel Predictions

A novel prediction is a claim about something not yet measured, or a claim that contradicts the current consensus. These carry the most evidential weight because they cannot have been reverse-engineered from existing data.

Physics Predictions

- *Proton decay.* The framework's higher unification scale $M_C \sim 10^{16.9}$ GeV (distinct from the Pati–Salam breaking at $\sim 10^{13}$ GeV) predicts a proton lifetime in the range $\tau_p \sim 10^{34}$–10^{35} years. Current limits from Super-Kamiokande (Abe et al., 2020) ($\tau_p > 1.6 \times 10^{34}$ years for $p \to e^+\pi^0$) are approaching this range. Hyper-Kamiokande and DUNE will extend sensitivity over the next decade.

- *Gravitational wave dispersion.* The a_4 heat kernel coefficient of the $\mathbb{CP}^3$ sigma model generates a Planck-suppressed dispersion correction: $\omega^2 = c^2k^2[1 + \alpha_{\mathrm{GW}}(\ell_P k)^2]$ with $\alpha_{\mathrm{GW}} \approx 1$ (technical document, Appendix A). At LIGO frequencies, $\Delta v/c \sim 10^{-82}$—undetectable by any current or planned instrument. The correction is superluminal ($\alpha_{\mathrm{GW}} > 0$) because the sigma model fields are bosonic; loop quantum gravity and doubly special relativity typically predict the opposite sign. If future precision ever reached the relevant scale, the sign would discriminate between emergent gravity from a bosonic sigma model and these alternatives. Separately, the framework distinguishes G_{micro} (constant microscopic coupling) from $G_{\mathrm{eff}}(z)$ (scale-dependent effective coupling for nonlinear structure formation), with the transition at $k_{NL} \sim 0.1$ Mpc^{-1} (nanohertz pulsar timing frequencies).

- *Page curve non-turnover.* The entanglement entropy of Hawking radiation should grow monotonically rather than decreasing after the Page time, because τ-projection is non-unitary and information is genuinely destroyed (Chapter 16, §16.5.5). Every other proposed resolution predicts the turnover. Analog black hole experiments provide a potential test.

Predictions at the Critical Scale

These predictions are among the framework's most distinctive claims.

- *Φ scaling.* Integrated information scales as $\Phi \sim c_\Sigma \sqrt{N}\,\alpha^2$, where N is the number of synapses and c_Σ is a geometric constant determined by the minimum bisection width of the connectivity graph. This gives $\Phi \propto N^{1/2}$ for cortical architectures ($d_\Sigma = 2$), distinguishable from IIT's $\Phi \propto N$ and from random-network models that predict no definite scaling. Cross-species PCI measurements (extending the within-human PCI methodology of Casali et al., 2013) plotted against synapse counts would provide a direct test.

- *Temperature dependence.* Consciousness requires the dynamic-persistence regime ($R(k) \approx 1$) plus integration ($\Phi > 0$). Temperature plays a permissive role (it determines which k-level is thermally accessible) but integration is the primary determinant. If consciousness markers track temperature more tightly than Φ, this prediction is falsified.

- *BKT sharpness.* The fiber sigma model on the cortical sheet undergoes a Berezinskii-Kosterlitz-Thouless transition (Kosterlitz and Thouless, 1973) rather than a standard second-order phase transition. The essential singularity $\xi_f \sim \exp(c/\sqrt{T - T_{BKT}})$ makes the transition between unconsciousness and consciousness discontinuous on neural timescales. Anesthesia recovery should show a sharp jump in PCI, not a smooth ramp. Existing propofol washout data are consistent with this (Casali et al., 2013); high-temporal-resolution measurements during controlled titration can test it definitively.

- *Synchronization window.* A conscious moment is one fused actualization spanning a fixed window $t_{\text{integrate}} \approx 60$ ms, set by collective coherence across $N \sim 10^{14}$ synaptic sites (Chapter 21). Psychophysical binding windows (50–100 ms range for conscious moments in global workspace experiments) are consistent with the predicted window.

- *Cross-species scaling exponents.* Cephalopods, with three-dimensional neural architecture ($d_\Sigma = 3$), should show $\Phi \propto N^{2/3}$, while mammals with cortical sheets ($d_\Sigma = 2$) should show $\Phi \propto N^{1/2}$. The testable claim is the exponent, not the absolute value (which depends on c_Σ, requiring connectomics data to determine).

- *Threshold regime.* Phenomenal experience has regime character rather than continuous gradation: a system either satisfies both conditions of Chapter 19 §19.4 ($R \approx 1$ and $\Phi > 0$) and the dynamics that constitute experience come online, or it does not. The empirical threshold for detecting the regime transition — the smallest Φ-proxy value at which PCI or Lempel–Ziv classification crosses from unconscious to conscious — is a calibration question, testable via TMS-EEG perturbational complexity during anesthesia induction and recovery (Casali et al., 2013). The framework's claim is the binary regime character, not a specific numerical Φ_c.

- *Neural correlate frequency.* Thalamocortical gamma synchrony ($\sim$ 30 Hz) is the observable signature of the synchronized τ-firing population at $k \approx 75$, with theta ($\sim$ 8 Hz) as the modulation envelope implementing the two-loop architecture. Gamma power and cross-frequency theta-gamma coupling should track consciousness state across waking, anesthesia, deep sleep, and REM.

- *Content invariance vs valence variance.* The framework predicts that the per-event V_4 qualia coordinates (p, s_A, s_C, s_D) extracted by a sub-boundary are determined by the sub-boundary's architecture and the input stimulus, not by the organism's preference-weight parameter w. Two organisms with matched sensory architecture — genetically uniform lab strains under differential conditioning, or closely related species with divergent food preferences — should produce identical primary-sensory-cortex responses to the same stimulus. Valence differences should localize to downstream evaluative circuits (orbitofrontal cortex, amygdala, ventral striatum, interoceptive insula) where w shapes the free-energy gradient. Testable through within-subject conditioned-taste-aversion with primary-cortex recording, differentially conditioned uniform populations, and cross-species sensory-homology comparisons in compound-discrimination tasks. Coupled shifts in primary sensory cortex and evaluative regions with valence learning would falsify the content-invariance claim (16, §Prediction 8).

25.1.4 Geometric Invariants and Dynamical Realizations

The framework's predictions split into two kinds, and the split is structural rather than calculational. Some quantities the framework derives from arena geometry alone, with no reference to the universe's specific actualization history. Others require knowing what the actualization sequence has actually produced. Geometry is in the framework's reach; history is not.

Geometric invariants take the same values across every actualization history because they are read directly off $\mathbb{CP}^3 + \tau$, its spectral data, and its topological invariants. The category is broader than the framework's standard-physics audience expects:

- the gauge group $SU(3) \times SU(2) \times U(1)$, from the PU(4) stabilizer structure under τ;
- the fine-structure constant α, from heat-kernel eigenvalues on $\mathbb{CP}^3$;
- the number of fermion generations, from $\mathbb{CP}^3$ topology plus the Jackiw–Rebbi boundary mode at $\mathbb{RP}^3 = \mathrm{Fix}(\tau)$;
- the hierarchy spacing, from the 2π Hopf-fiber circumference iterated through the cascade;
- the strong CP phase $\theta = 0$, from T-invariance of τ;
- Newton's constant G_N and the cosmological constant Λ, from the boundary capacity $N_\infty = \varphi^{392}$;
- the quark CKM CP phase $\delta_{CP} = \pi/\varphi^2$, from the icosahedral A_5 golden-ratio partition of the quark flag manifold;
- the particle mass spectrum and mass ratios, from the H_α cascade ladder on $\mathbb{CP}^3$;
- the CKM/PMNS mixing angles, from generation-mode overlaps on the arena;
- the conditions for phenomenal experience ($R \approx 1$ and $\Phi > 0$) and the dynamics that follow when those conditions are met, from the critical-scale geometry of $\mathbb{CP}^3 + \tau$.

A failure on any of these strikes at the arena itself.

Dynamical realizations depend on the specific actualization sequence the universe has run. The geometry tells the framework what is structurally possible and what conditions are needed; the realizations require knowing what the cosmos has actually accumulated. These include:

- the Hubble parameter at the present epoch (depends on the current value of $M(t)$ in $H_0 \propto 1/\sqrt{M(t)}$);
- the dark matter abundance Ω_{DM} (depends on the thermal history of the early universe, not on the arena);
- the baryon-to-photon ratio η (depends on the specific baryogenesis trajectory the cosmos

followed);

- the actualized values of cosmological initial conditions;
- the existence and specific architecture of any biological systems that satisfy the conditions for phenomenal experience (depends on evolutionary history on the planets in question).

The asymmetry is principled. A failed geometric-invariant prediction strikes at $\mathbb{CP}^3 + \tau$ itself. A failed dynamical-realization prediction means the framework has miscalculated some specific configuration the cosmos produced, not that the foundations are wrong. Proton decay is a geometric invariant: a lifetime measured outside the predicted 10^{34}–10^{35} year window would be decisive. The Hubble tension prediction is a dynamical realization (the present-epoch value of H_0 depends on $M(t)$): a discrepancy might mean the $G_{\text{micro}}/G_{\text{eff}}$ split requires more careful treatment in the Boltzmann calculation rather than that the framework is wrong.

25.2 What Remains Open

The framework contains calculational gaps that are worth stating explicitly. These are gaps in the execution of derivations, not in the structure of the theory. The distinction matters: a structural gap would indicate a missing piece of the framework; a calculational gap indicates work that remains to be done within a structure that is already specified.

- *Radiative corrections.* The framework derives tree-level values for the coupling constants. Systematic incorporation of radiative corrections—loop diagrams in the effective field theory that emerges from the actualization dynamics—has not yet been carried out. The expectation is that these corrections are small (of order α/π) and do not alter the leading-order predictions, but this has not been verified.

- *Normalization conventions.* The arena's natural normalization (determined by the Kähler metric on $\mathbb{CP}^3$) differs from the standard renormalization conventions used in particle physics. The translation between conventions has been carried out for several quantities but not systematically across all predictions.

- *Light quark masses.* The masses of the up and down quarks were determined retrospectively (by matching to known values) rather than derived from first principles. The framework's hierarchy provides the mass scale, but the specific Yukawa couplings for the lightest quarks have not been independently calculated.

- *Mixing angle Berry phases.* The CKM and PMNS mixing angles are derived from Berry phases accumulated around geodesics in $\mathbb{CP}^3$. The calculations for some entries in these matrices are complete; others remain in progress.

- *Instanton prefactor.* The third route to α (through the instanton calculation) produces the correct value but relies on a prefactor that has not been independently established from the arena geometry.

- *Boltzmann simulation.* The distinction between G_{micro} (constant, entering the background Friedmann equations) and $G_{\text{eff}}(z)$ (evolving, entering nonlinear structure formation) has been established analytically. A full Boltzmann simulation (in CLASS or CAMB) incorporating this split has not yet been run, so the CMB power spectrum predictions remain approximate.

None of these gaps affect the framework's structural claims—the arena, the operator, the actualization process, the emergence of the Standard Model, gravity, thermodynamics, and consciousness conditions are all established independently of these open calculations. They affect the precision of specific numerical predictions and the framework's ability to be compared with experiment at the level of detail that precision cosmology and collider physics demand. Completing them is a matter of computation, not of conceptual development.

25.3 Closing

This document began with phenomenal experience as an empirical datum and asked what geometry that datum requires. The answer—$\mathbb{CP}^3$ acted on by complex conjugation τ with fixed-point set $\mathbb{RP}^3$—was not chosen for convenience. It was forced by the projective structure of perception, the requirement that actualization be self-inverse, and the constraint that the result be internally consistent.

From that geometry, the document traced a single chain of consequences: the actualization process, the Born rule, the variational principle, thermodynamics, information, the four fact types, the six bridges, the Standard Model forces, the hierarchy of scales, the particles and constants, gravity and cosmology, and the conditions under which consciousness arises within the structure it helped identify. Each chapter extended the chain by one link. No link required supplementary assumptions; each followed from the geometry already established.

The framework dissolves standing problems and generates testable predictions across multiple domains, with calculational gaps stated openly.

Whether the framework is correct is an empirical question. Next-generation X-ray observatories will search for the 3.5 keV line. Analog black hole experiments can test whether the Page curve turns over. Cross-species PCI measurements can test the Φ-scaling law.

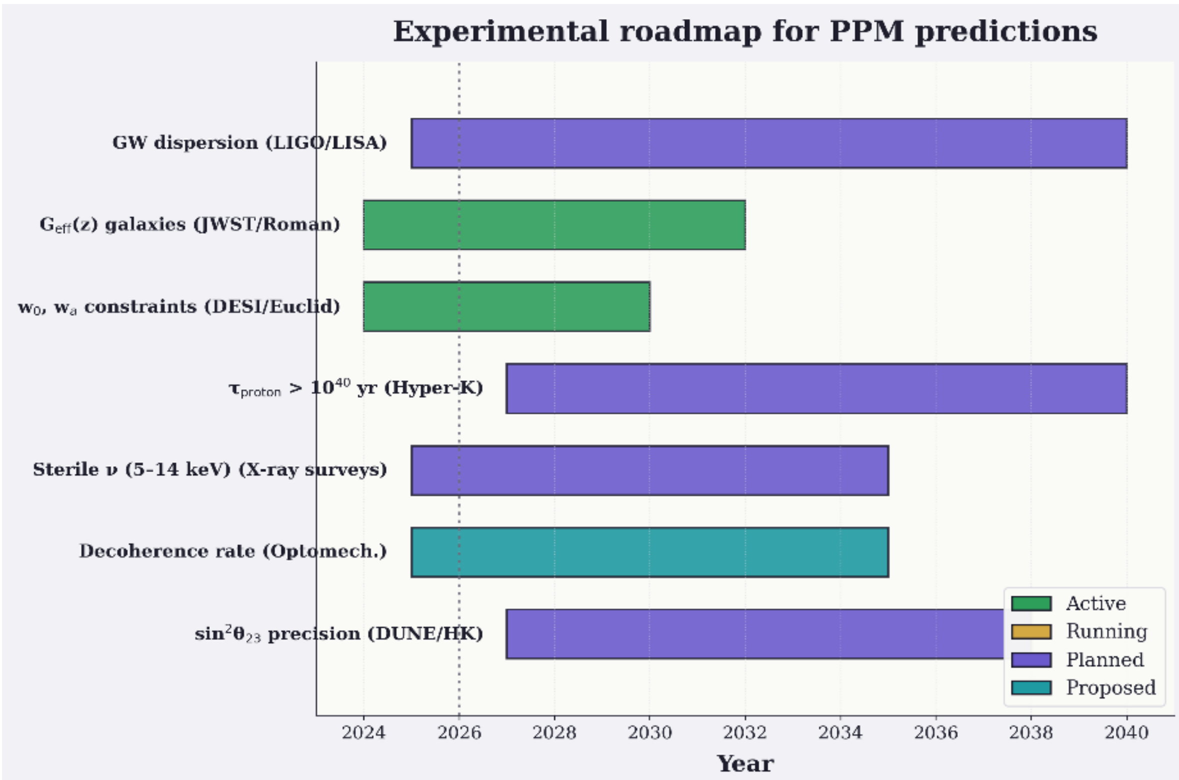

Figure 25.2: *Experimental roadmap. Concrete tests across the framework's prediction surface, plotted by timescale (years to decisive measurement) against domain (particle physics, cosmology, gravitational waves, neuroscience). Near-term entries—next-generation X-ray observatory searches for the 3.5 keV line, high-density TMS-EEG during anesthesia titration, cross-species PCI campaigns—can confirm or rule out specific claims within a decade. Longer-term entries—Hyper-Kamiokande's proton decay reach and analog black hole experiments probing Page-curve behavior—require infrastructure still being built. The framework's exposure surface is broad enough that no single experiment is decisive on its own.*

Acknowledgements

I owe an intellectual debt to Jon Hook, who introduced me to the philosophical and contemplative traditions—process ontology, nondualism, Daoism—that bridged my longstanding technical interests in physics and consciousness into a coherent picture. The core insight may be mine, but the ideas that made it possible reached me largely through him. He also served as a tireless sounding board throughout the development of this framework, and his encouragement carried it through periods when I had serious doubts about whether any of it held together.

I thank my parents, Ted Wozniak and Fran Martinez, whose influence on my development—causal in every sense the framework implies—made this work possible in ways that extend far beyond the obvious.

Finally, I thank my wife, Carmen Araujo. Her presence in my life drove me to look inward and grow in ways I would not have otherwise. What I found there made this work possible.

AI assistance. Google's Gemini and NotebookLM assisted with early-stage research, developing physical intuitions, and visualization of key concepts. Anthropic's Claude was used extensively for deriving and verifying mathematical formalisms, implementing the computational companion code, auditing internal consistency, and refining the manuscript. The conceptual framework—the identification of phenomenal experience as a physical constraint and the systematic development of its consequences—is the author's; the mathematical precision and presentation benefited substantially from AI collaboration.

Projective Process Monism

One-Card Reference

Arena. $\mathbb{CP}^3$ (complex projective 3-space).

Operator. $\tau : z \mapsto \bar{z}$ (anti-holomorphic involution). $\mathrm{Fix}(\tau) = \mathbb{RP}^3$ is actuality.

Dynamics. Kähler flow on $\mathbb{CP}^3$ between τ-events:

$$H_\alpha = -\frac{\hbar^2}{2m_\pi}\nabla^2_{\mathbb{CP}^3} + m_\pi c^2 \log(1 + |z|^2/\lambda_C^2),$$

$$\dot{\rho} = -\tfrac{i}{\hbar}[H_\alpha, \rho] + \sum_b \gamma_b\Big(\hat{A}_b\rho\hat{A}_b^\dagger - \tfrac{1}{2}\{\hat{A}_b^\dagger\hat{A}_b, \rho\}\Big).$$

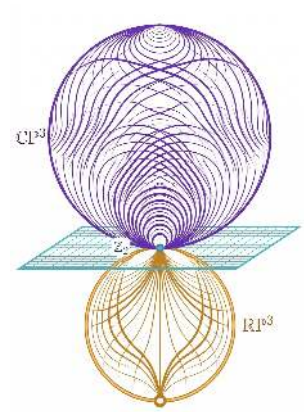

$\mathbb{CP}^3$ (possibility) projects onto its fixed-point set $\mathbb{RP}^3$ (actuality) under τ, at every level of an energy hierarchy anchored by m_π. Every persistent structure—particles, forces, gravity, the cosmological constant, the geometry of conscious experience—emerges from this projection.

Dynamics

Events. At gravitational rate $\Gamma_G = Gm^3c/\hbar^2$, τ fires: $\rho \mapsto \hat{A}_b\rho\hat{A}_b^\dagger/\,\mathrm{Tr}(\hat{A}_b\rho\hat{A}_b^\dagger)$ (Born rule).

Variational principle. Surprisal $\mathcal{F} = -\log\mathrm{Tr}(\hat{A}_b\rho\hat{A}_b^\dagger)$ minimized at each cycle.

Per-event content

Fact types (V_4).	τ-odd (normal)	τ-even (tangent)
Kähler (arena)	A spectral	B spatial
gauge (bundle)	C chiral	D intensity

Information. $I(k) = 3\log_2 R(k)$ bits

Entropy. $\Delta S_{\mathrm{event}} = 3\,k_B\ln(2\pi) \approx 5.5\,k_B$

Scale and cascade

k-cascade. $E(k) = m_\pi(2\pi)^{(51-k)/2}$ (each event located at a specific k-scale).

Anchors:

$k = 1$	$E \sim 10^{19}$ GeV	Planck
$k = 51$	$E = m_\pi = 140$ MeV	pion (anchor)
$k \approx 75$	$T_{\mathrm{match}} = 310$ K	biology
$k \approx 80$	$T_{\mathrm{match}} = 2.7$ K	CMB

Per-event duration. $\tau_{\mathrm{event}}(k) = \pi\hbar/(2E(k))$ (Margolus–Levitin bound).

Resolvability ratio. $R(k) = E(k)/(k_BT)$ at ambient temperature T; $T_{\mathrm{match}}(k) = E(k)/k_B$.

Regimes partitioned at $R = 1$:

$R \gg 1$	discrete-quantum
$R \approx 1$	transitional
$R \ll 1$	classical-thermal

Capacity

Boundary capacity. $N_\infty = \varphi^{392} \approx 8.4 \times 10^{81}$ (sets Λ, cosmic IR scale).

Version History

This document and the Technical Reference share a single version number, shown with its date on the cover. The two are tracked separately below: each release lists only the changes made to this volume. Versions follow MAJOR.MINOR.PATCH convention.

v1.0.3 `2026-06-07` | *Patch*

- Replaced the Part VI hero image with the correct, current version.
- Layout and formatting fixes on the title page.

v1.1.0 `2026-06-09` | *Minor*

Corrected δ_{CP}: scoped to the quark CKM phase, observed value updated to PDG 2024, leptonic claim withdrawn pending A_4-sector derivation.

Bibliography

J. Aalbers et al. First dark matter search results from the LUX-ZEPLIN (LZ) experiment. *Physical Review Letters*, 131:041002, 2023. doi: 10.1103/PhysRevLett.131.041002.

Scott Aaronson. Why I am not an integrated information theorist (or, the unconscious expander). Shtetl-Optimized blog post, 2014. URL https://scottaaronson.blog/?p=1799.

K. Abe et al. Search for proton decay via $p \to e^+\pi^0$ and $p \to \mu^+\pi^0$ with an enlarged fiducial volume of Super-Kamiokande I–IV. *Physical Review D*, 102:112011, 2020. doi: 10.1103/PhysRevD.102.112011.

C. Abel et al. Measurement of the permanent electric dipole moment of the neutron. *Physical Review Letters*, 124(8):081803, 2020. doi: 10.1103/PhysRevLett.124.081803.

A. Almheiri, D. Marolf, J. Polchinski, and J. Sully. Black holes: complementarity or firewalls? *Journal of High Energy Physics*, 2013(2):062, 2013.

E. Aprile et al. Dark matter search results from a one tonne-year exposure of XENON1t. *Physical Review Letters*, 121:111302, 2018. doi: 10.1103/PhysRevLett.121.111302.

A. Aspect, J. Dalibard, and G. Roger. Experimental test of Bell's inequalities using time-varying analyzers. *Physical Review Letters*, 49(25):1804–1807, 1982.

Michael Atiyah, Maciej Dunajski, and Lionel J. Mason. Twistor theory at fifty: from contour integrals to twistor strings. *Proceedings of the Royal Society A*, 473(2206):20170530, 2017. doi: 10.1098/rspa.2017.0530.

Michael F. Atiyah and Isadore M. Singer. The index of elliptic operators: I. *Annals of Mathematics*, 87:484–530, 1968. doi: 10.2307/1970715.

ATLAS Collaboration. Observation of a new particle in the search for the Standard Model Higgs boson with the ATLAS detector at the LHC. *Physics Letters B*, 716(1):1–29, 2012. doi: 10.1016/j.physletb.2012.08.020.

David Attwell and Simon B. Laughlin. An energy budget for signaling in the grey matter of the brain. *Journal of Cerebral Blood Flow and Metabolism*, 21(10):1133–1145, 2001. doi: 10.1097/00004647-200110000-00001.

Michèle Audin. *Torus Actions on Symplectic Manifolds*, volume 93 of *Progress in Mathematics*. Birkhäuser, 2nd edition, 2004. Lagrangian normal-bundle isomorphism: $\nu(L \to M) \cong T^*L$ for L Lagrangian in symplectic M.

Carlos Barceló, Stefano Liberati, and Matt Visser. Analogue gravity. *Living Reviews in Relativity*, 14(3), 2011.

Howard Barnum, Carlton M. Caves, Christopher A. Fuchs, Richard Jozsa, and Benjamin Schumacher. Noncommuting mixed states cannot be broadcast. *Physical Review Letters*, 76(15):2818–2821, 1996. doi: 10.1103/PhysRevLett.76.2818.

J. D. Barrow and F. J. Tipler. *The Anthropic Cosmological Principle*. Oxford University Press, Oxford, 1986.

J. D. Bekenstein. Black holes and entropy. *Physical Review D*, 7(8):2333–2346, 1973.

J. D. Bekenstein. Universal upper bound on the entropy-to-energy ratio for bounded systems. *Physical Review D*, 23(2):287–298, 1981.

Alexander A. Belavin, Alexander M. Polyakov, Albert S. Schwartz, and Yuri S. Tyupkin. Pseudoparticle solutions of the Yang–Mills equations. *Physics Letters B*, 59:85–87, 1975. doi: 10.1016/0370-2693(75)90163-X.

John S. Bell. On the Einstein–Podolsky–Rosen paradox. *Physics Physique Fizika*, 1:195–200, 1964. doi: 10.1103/PhysicsPhysiqueFizika.1.195.

Charles H. Bennett. Logical reversibility of computation. *IBM Journal of Research and Development*, 17(6):525–532, 1973. doi: 10.1147/rd.176.0525.

Charles H. Bennett. The thermodynamics of computation—a review. *International Journal of Theoretical Physics*, 21(12):905–940, 1982. doi: 10.1007/BF02084158.

Kent C. Berridge and Morten L. Kringelbach. Affective neuroscience of pleasure: reward in humans and animals. *Psychopharmacology*, 199(3):457–480, 2008. doi: 10.1007/s00213-008-1099-6.

Kent C. Berridge and Terry E. Robinson. What is the role of dopamine in reward: hedonic impact, reward learning, or incentive salience? *Brain Research Reviews*, 28(3):309–369, 1998. doi: 10.1016/S0165-0173(98)00019-8.

M. V. Berry. Quantal phase factors accompanying adiabatic changes. *Proceedings of the Royal Society of London A*, 392(1802):45–57, 1984.

M. V. Berry and J. M. Robbins. Indistinguishability for quantum particles: spin, statistics and the geometric phase. *Proceedings of the Royal Society A*, 453:1771–1790, 1997. doi: 10.1098/rspa.1997.0096.

Arthur L. Besse. *Manifolds All of Whose Geodesics Are Closed*, volume 93 of *Ergebnisse der Mathematik und ihrer Grenzgebiete*. Springer-Verlag, 1978. ISBN 978-3-540-08158-6.

D. Bohm. A suggested interpretation of the quantum theory in terms of "hidden" variables. *Physical Review*, 85(2):166–193, 1952.

Ludwig Boltzmann. Weitere studien über das wärmegleichgewicht unter gasmolekülen. *Sitzungsberichte der Akademie der Wissenschaften*, 66:275–370, 1872.

Luca Bombelli, Joohan Lee, David Meyer, and Rafael D. Sorkin. Space-time as a causal set. *Physical Review Letters*, 59:521–524, 1987. doi: 10.1103/PhysRevLett.59.521.

Max Born. Zur quantenmechanik der stoßvorgänge. *Zeitschrift für Physik*, 37(12):863–867, 1926.

Max Born. A suggestion for unifying quantum theory and relativity. *Proceedings of the Royal Society A*, 165(921):291–303, 1938.

A. Boyarsky, O. Ruchayskiy, D. Iakubovskyi, and J. Franse. Unidentified line in X-ray spectra of the Andromeda galaxy and Perseus galaxy cluster. *Physical Review Letters*, 113(25):251301, 2014. doi: 10.1103/PhysRevLett.113.251301.

M. Boylan-Kolchin. Stress testing λcdm with high-redshift galaxy candidates. *Nature Astronomy*, 7:731–735, 2023. doi: 10.1038/s41550-023-01937-7.

Hans J. Bremermann. Optimization through evolution and recombination. In M. C. Yovits, G. T. Jacobi, and G. D. Goldstein, editors, *Self-Organizing Systems*, pages 93–106. Spartan Books, Washington, DC, 1962.

G. Bressi, G. Carugno, F. della Valle, G. Galeazzi, G. Sartori, and D. Tommasini. Testing the neutrality of matter by acoustic means in a spherical resonator. *Physical Review A*, 83 (5):052101, 2011. doi: 10.1103/PhysRevA.83.052101.

Heinz-Peter Breuer and Francesco Petruccione. *The Theory of Open Quantum Systems*. Oxford University Press, 2002. ISBN 9780198520634. doi: 10.1093/acprof:oso/9780199213900.001.0001.

Linda Buck and Richard Axel. A novel multigene family may encode odorant receptors: A molecular basis for odor recognition. *Cell*, 65(1):175–187, 1991. doi: 10.1016/0092-8674(91)90418-X.

E. Bulbul et al. Detection of an unidentified emission line in the stacked X-ray spectrum of galaxy clusters. *The Astrophysical Journal*, 789(1):13, 2014. doi: 10.1088/0004-637X/789/1/13.

Theodore H. Bullock and F. P. J. Diecke. Properties of an infra-red receptor. *Journal of Physiology*, 134(1):47–87, 1956. doi: 10.1113/jphysiol.1956.sp005624.

P. Busch. Quantum states and generalized observables: a simple proof of Gleason's theorem. *Physical Review Letters*, 91(12):120403, 2003.

György Buzsáki and Andreas Draguhn. Neuronal oscillations in cortical networks. *Science*, 304(5679):1926–1929, 2004. doi: 10.1126/science.1099745.

Michel Cabanac. Physiological role of pleasure. *Science*, 173(4002):1103–1107, 1971. doi: 10.1126/science.173.4002.1103.

N. Cabibbo. Unitary symmetry and leptonic decays. *Physical Review Letters*, 10(12):531–533, 1963.

Sadi Carnot. *Réflexions sur la puissance motrice du feu et sur les machines propres à développer cette puissance*. Bachelier, Paris, 1824. Origin of the second law of thermodynamics.

B. J. Carr and M. J. Rees. The anthropic principle and the structure of the physical world. *Nature*, 278:605–612, 1979. doi: 10.1038/278605a0.

A. G. Casali, O. Gosseries, M. Rosanova, M. Boly, S. Sarasso, S. Casarotto, M.-A. Bruno, S. Laureys, G. Tononi, and M. Massimini. A theoretically based index of consciousness independent of sensory processing and behavior. *Science Translational Medicine*, 5(198): 198ra105, 2013. doi: 10.1126/scitranslmed.3006294.

H. B. G. Casimir. On the attraction between two perfectly conducting plates. *Proceedings of the Koninklijke Nederlandse Akademie van Wetenschappen*, 51:793–795, 1948.

D. J. Chalmers. Facing up to the problem of consciousness. *Journal of Consciousness Studies*, 2(3):200–219, 1995.

Jayaram Chandrashekar, Mark A. Hoon, Nicholas J. P. Ryba, and Charles S. Zuker. The receptors and cells for mammalian taste. *Nature*, 444(7117):288–294, 2006. doi: 10.1038/nature05401.

Tsyr-Huei Chiou, Sonja Kleinlogel, Tom Cronin, Roy Caldwell, Birte Loeffler, Afsheen Siddiqi, Alan Goldizen, and Justin Marshall. Circular polarization vision in a stomatopod crustacean. *Current Biology*, 18(6):429–434, 2008. doi: 10.1016/j.cub.2008.02.066.

Cheol-Hyun Cho and Yong-Geun Oh. Floer cohomology and disc instantons of Lagrangian torus fibers in Fano toric manifolds. *Asian J. Math.*, 10(4):773–814, 2006. arXiv:math/0308225.

Andy Clark. Whatever next? Predictive brains, situated agents, and the future of cognitive science. *Behavioral and Brain Sciences*, 36(3):181–204, 2013. doi: 10.1017/S0140525X12000477.

John F. Clauser, Michael A. Horne, Abner Shimony, and Richard A. Holt. Proposed experiment to test local hidden-variable theories. *Physical Review Letters*, 23:880–884, 1969. doi: 10.1103/PhysRevLett.23.880.

Rudolf Clausius. Über verschiedene für die anwendung bequeme formen der hauptgleichungen der mechanischen wärmetheorie. *Annalen der Physik*, 201(7):353–400, 1865. Introduction of entropy and modern statement of the second law.

CMS Collaboration. Observation of a new boson at a mass of 125 GeV with the CMS experiment at the LHC. *Physics Letters B*, 716(1):30–61, 2012. doi: 10.1016/j.physletb.2012.08.021.

Sidney Coleman. *Aspects of Symmetry: Selected Erice Lectures*. Cambridge University Press, 1985. Contains "The Uses of Instantons" (Erice 1977), canonical treatment of instanton tunneling between vacua.

Yves Colin de Verdière. Spectre du laplacien et longueurs des géodésiques périodiques. II. *Compositio Mathematica*, 27:159–184, 1973.

Hitomi Collaboration. Hitomi constraints on the 3.5 kev line in the perseus cluster. *The Astrophysical Journal Letters*, 837(2):L15, 2017. doi: 10.3847/2041-8213/aa62fa.

H. S. M. Coxeter. *Regular Polytopes*. Dover, 3rd edition, 1973. ISBN 978-0-486-61480-9. Classical reference for the icosahedral group H_3 and the appearance of $\varphi = (1 + \sqrt{5})/2$ in icosahedral vertex coordinates and Coxeter reflection ratios ($2\cos(\pi/5) = \varphi$).

Richard H. Cyburt, Brian D. Fields, Keith A. Olive, and Tsung-Han Yeh. Big bang nucleosynthesis: Present status. *Reviews of Modern Physics*, 88:015004, 2016. doi: 10.1103/RevModPhys.88.015004.

Barry Dainton. *Stream of Consciousness: Unity and Continuity in Conscious Experience*. Routledge, London, 2000.

G. Degrassi, S. Di Vita, J. Elias-Miró, J. R. Espinosa, G. F. Giudice, G. Isidori, and A. Strumia. Higgs mass and vacuum stability in the Standard Model at NNLO. *Journal of High Energy Physics*, 2012:98, 2012. doi: 10.1007/JHEP08(2012)098.

Stanislas Dehaene and Lionel Naccache. Towards a cognitive neuroscience of consciousness: Basic evidence and a workspace framework. *Cognition*, 79(1–2):1–37, 2001. doi: 10.1016/S0010-0277(00)00123-2.

DESI Collaboration. DESI 2024 VI: Cosmological constraints from the measurements of baryon acoustic oscillations, 2024. arXiv:2404.03002.

Christopher Dessert, Nicholas L. Rodd, and Benjamin R. Safdi. The dark matter interpretation of the 3.5-kev line is inconsistent with blank-sky observations. *Science*, 367(6485):1465–1469, 2020. doi: 10.1126/science.aaw3772.

David Deutsch. Quantum theory, the church-turing principle and the universal quantum computer. *Proceedings of the Royal Society A*, 400(1818):97–117, 1985. doi: 10.1098/rspa.1985.0070.

David Deutsch. Constructor theory. *Synthese*, 190(18):4331–4359, 2013. doi: 10.1007/s11229-013-0279-z.

David Deutsch and Chiara Marletto. Constructor theory of information. *Proceedings of the Royal Society A*, 471(2174):20140540, 2015. doi: 10.1098/rspa.2014.0540.

B. S. DeWitt. Quantum theory of gravity. I. the canonical theory. *Physical Review*, 160(5): 1113–1148, 1967.

Bryce S. DeWitt. *Dynamical Theory of Groups and Fields*. Gordon and Breach, 1965.

Lajos Diósi. Models for universal reduction of macroscopic quantum fluctuations. *Physical Review A*, 40:1165–1174, 1989. doi: 10.1103/PhysRevA.40.1165.

P. A. M. Dirac. The cosmological constants. *Nature*, 139:323, 1937. doi: 10.1038/139323a0.

Paul A. M. Dirac. Quantised singularities in the electromagnetic field. *Proceedings of the Royal Society of London A*, 133(821):60–72, 1931. doi: 10.1098/rspa.1931.0130.

A. S. Eddington. *Relativity Theory of Protons and Electrons*. Cambridge University Press, 1936. Large number coincidences; see also *The Philosophy of Physical Science* (Cambridge, 1939) for the formal Eddington number.

Albert Einstein. Zur elektrodynamik bewegter korper. *Annalen der Physik*, 17(10):891–921, 1905.

Albert Einstein. The foundation of the general theory of relativity. *Annalen der Physik*, 49 (7):769–822, 1916.

Albert Einstein, Boris Podolsky, and Nathan Rosen. Can quantum-mechanical description of physical reality be considered complete? *Physical Review*, 47:777–780, 1935. doi: 10.1103/PhysRev.47.777.

Andrew J. Elliot. The hierarchical model of approach-avoidance motivation. *Motivation and Emotion*, 30(2):111–116, 2006. doi: 10.1007/s11031-006-9028-7.

H. Everett. "Relative state" formulation of quantum mechanics. *Reviews of Modern Physics*, 29(3):454–462, 1957.

FCC Collaboration. FCC-hh: The hadron collider — future circular collider conceptual design report volume 3. *European Physical Journal Special Topics*, 228(4):755–1107, 2019. doi: 10.1140/epjst/e2019-900087-0.

R. P. Feynman. Space-time approach to non-relativistic quantum mechanics. *Reviews of Modern Physics*, 20(2):367–387, 1948. doi: 10.1103/RevModPhys.20.367.

Chris Fields, Donald D. Hoffman, Chetan Prakash, and Robert Prentner. Eigenforms, interfaces and holographic encoding: toward an evolutionary account of objects and spacetime. *Constructivist Foundations*, 12(3):265–274, 2017.

S. L. Finkelstein et al. CEERS key paper. I. an early look into the first 500 Myr of galaxy formation with JWST. *The Astrophysical Journal Letters*, 946(1):L13, 2023. doi: 10.3847/2041-8213/acade4.

Felix Finster. *The Continuum Limit of Causal Fermion Systems: From Planck Scale Structures to Macroscopic Physics*, volume 186 of *Fundamental Theories of Physics*. Springer, 2016. doi: 10.1007/978-3-319-42067-7. arXiv:1605.04742.

Felix Finster, Sebastian Kindermann, and Jan-Hendrik Treude. *Causal Fermion Systems: An Introduction to Fundamental Structures, Methods and Applications*. Cambridge Monographs on Mathematical Physics. Cambridge University Press, 2025. arXiv:2411.06450.

James Fong, Hannah K. Doyle, Congli Wang, Alexandra E. Boehm, Sofie R. Herbeck, Vimal P. Pandiyan, Brian P. Schmidt, Jenny L. Kim, Pavan Tiruveedhula, Elena Gofas-Salas, Glenn Yiu, Norani Nor, William S. Tuten, Ramkumar Sabesan, Ren Ng, and Austin Roorda. Novel color via stimulation of individual photoreceptors at population scale. *Science Advances*, 11(16):eadu1052, 2025. doi: 10.1126/sciadv.adu1052.

Ralph H. Fowler and Edward A. Guggenheim. *Statistical Thermodynamics*. Cambridge University Press, 1939. First formal statement of the zeroth law of thermodynamics.

W. L. Freedman et al. Calibration of the tip of the red giant branch (TRGB). *The Astrophysical Journal*, 891(1):57, 2020. doi: 10.3847/1538-4357/ab7339.

Alexander Friedmann. Über die krümmung des raumes. *Zeitschrift für Physik*, 10(1):377–386, 1922.

K. Friston. The free-energy principle: a unified brain theory? *Nature Reviews Neuroscience*, 11(2):127–138, 2010. doi: 10.1038/nrn2787.

Karl Friston, Thomas FitzGerald, Francesco Rigoli, Philipp Schwartenbeck, and Giovanni Pezzulo. Active inference: a process theory. *Neural Computation*, 29(1):1–49, 2017. doi: 10.1162/NECO_a_00912.

Christopher A. Fuchs. QBism, the perimeter of quantum Bayesianism. *arXiv preprint*, 2010. arXiv:1003.5209 [quant-ph].

Christopher A. Fuchs and Rüdiger Schack. Quantum-Bayesian coherence: the no-nonsense version. *Reviews of Modern Physics*, 85(4):1693–1715, 2013. doi: 10.1103/RevModPhys.85.1693.

Kenji Fukaya, Yong-Geun Oh, Hiroshi Ohta, and Kaoru Ono. *Lagrangian Intersection Floer Theory: Anomaly and Obstruction*, volume 46 of *AMS/IP Studies in Advanced Mathematics*. American Mathematical Society / International Press, 2009.

J. Garcia, D. J. Kimeldorf, and R. A. Koelling. Conditioned aversion to saccharin resulting from exposure to gamma radiation. *Science*, 122(3160):157–158, 1955. doi: 10.1126/science.122.3160.157.

Murray Gell-Mann. The interpretation of the new particles as displaced charge multiplets. *Il Nuovo Cimento*, 4(S2):848–866, 1956. doi: 10.1007/BF02748000.

G. C. Ghirardi, A. Rimini, and T. Weber. Unified dynamics for microscopic and macroscopic systems. *Physical Review D*, 34:470–491, 1986.

Gary W. Gibbons and Stephen W. Hawking. Cosmological event horizons, thermodynamics, and particle creation. *Physical Review D*, 15:2738–2751, 1977. doi: 10.1103/PhysRevD.15.2738.

Peter B. Gilkey. The spectral geometry of a riemannian manifold. *Journal of Differential Geometry*, 10:601–618, 1975.

V. L. Ginzburg and L. D. Landau. On the theory of superconductivity. *Zhurnal Eksperimental'noi i Teoreticheskoi Fiziki*, 20:1064–1082, 1950.

S. L. Glashow. Partial-symmetries of weak interactions. *Nuclear Physics*, 22(4):579–588, 1961.

A. M. Gleason. Measures on the closed subspaces of a Hilbert space. *Journal of Mathematics and Mechanics*, 6(6):885–893, 1957.

Kurt Gödel. Über formal unentscheidbare Sätze der Principia Mathematica und verwandter Systeme I. *Monatshefte für Mathematik und Physik*, 38:173–198, 1931. doi: 10.1007/BF01700692.

Jay M. Goldberg, Victor J. Wilson, Kathleen E. Cullen, Dora E. Angelaki, Dianne M. Broussard, Jean A. Büttner-Ennever, Kikuro Fukushima, and Lloyd B. Minor. *The Vestibular System: A Sixth Sense*. Oxford University Press, 2012.

Vittorio Gorini, Andrzej Kossakowski, and E. C. George Sudarshan. Completely positive dynamical semigroups of N-level systems. *Journal of Mathematical Physics*, 17:821–825, 1976. doi: 10.1063/1.522979.

Elena O. Gracheva, Nicholas T. Ingolia, Yvonne M. Kelly, Julio F. Cordero-Morales, Gunther Hollopeter, Alexander T. Chesler, Elda E. Sánchez, John C. Perez, Jonathan S. Weissman, and David Julius. Molecular basis of infrared detection by snakes. *Nature*, 464(7291): 1006–1011, 2010. doi: 10.1038/nature08943.

M. B. Green, J. H. Schwarz, and E. Witten. *Superstring Theory: Volume 1, Introduction*. Cambridge University Press, Cambridge, 1987.

Donald R. Griffin. *Listening in the Dark: The Acoustic Orientation of Bats and Men*. Yale University Press, New Haven, 1958.

Phillip Griffiths and Joseph Harris. *Principles of Algebraic Geometry*. Wiley-Interscience, 1978. ISBN 978-0-471-32792-9.

D. J. Gross and F. Wilczek. Ultraviolet behavior of non-abelian gauge theories. *Physical Review Letters*, 30(26):1343–1346, 1973.

Alan H. Guth. Inflationary universe: A possible solution to the horizon and flatness problems. *Physical Review D*, 23(2):347–356, 1981. doi: 10.1103/PhysRevD.23.347.

Patric Hagmann, Leila Cammoun, Xavier Gigandet, Reto Meuli, Christopher J. Honey, Van J. Wedeen, and Olaf Sporns. Mapping the structural core of human cerebral cortex. *PLoS Biology*, 6(7):e159, 2008. doi: 10.1371/journal.pbio.0060159.

Brian C. Hall. *Lie Groups, Lie Algebras, and Representations: An Elementary Introduction*, volume 222 of *Graduate Texts in Mathematics*. Springer, Cham, 2nd edition, 2015. ISBN 978-3-319-13466-6.

S. Hameroff and R. Penrose. Orchestrated reduction of quantum coherence in brain microtubules: A model for consciousness. *Mathematics and Computers in Simulation*, 40: 453–480, 1996.

W. R. Hamilton. On a general method in dynamics. *Philosophical Transactions of the Royal Society of London*, 124:247–308, 1834.

Y. Harikane et al. A comprehensive study of galaxies at $z \sim 9$–16 found in the early JWST data: ultraviolet luminosity functions and cosmic star formation history at the pre-reionization epoch. *The Astrophysical Journal Supplement Series*, 265(1):5, 2023. doi: 10.3847/1538-4365/acaaa9.

Nicholas Harrigan and Robert W. Spekkens. Einstein, incompleteness, and the epistemic view of quantum states. *Foundations of Physics*, 40:125–157, 2010. doi: 10.1007/s10701-009-9347-0.

Allen Hatcher. *Algebraic Topology*. Cambridge University Press, 2002. ISBN 978-0-521-79540-1.

S. W. Hawking. Particle creation by black holes. *Communications in Mathematical Physics*, 43(3):199–220, 1975.

S. W. Hawking. Breakdown of predictability in gravitational collapse. *Physical Review D*, 14 (10):2460–2473, 1976.

S. W. Hawking and G. F. R. Ellis. *The Large Scale Structure of Space-Time*. Cambridge University Press, 1973. ISBN 978-0521099066.

S. W. Hawking and R. Penrose. The singularities of gravitational collapse and cosmology. *Proceedings of the Royal Society of London A*, 314(1519):529–548, 1970. doi: 10.1098/rspa.1970.0021.

Donald O. Hebb. *The Organization of Behavior: A Neuropsychological Theory*. Wiley, New York, 1949.

Walter Heiligenberg. *Neural Nets in Electric Fish*. MIT Press, Cambridge, MA, 1991.

Werner Heisenberg. Über den anschaulichen inhalt der quantentheoretischen kinematik und mechanik. *Zeitschrift für Physik*, 43:172–198, 1927. doi: 10.1007/BF01397280.

Heraclitus. *Fragments*. Various (preserved in secondary sources), c. 500 BCE. Fragments collected and translated by H. Diels and W. Kranz, *Die Fragmente der Vorsokratiker*.

P. W. Higgs. Broken symmetries and the masses of gauge bosons. *Physical Review Letters*, 13(16):508–509, 1964.

Donald D. Hoffman. Conscious realism and the mind-body problem. *Mind and Matter*, 6(1): 87–121, 2008.

Alexander S. Holevo. Bounds for the quantity of information transmitted by a quantum communication channel. *Problems of Information Transmission*, 9(3):177–183, 1973.

Edwin Hubble. A relation between distance and radial velocity among extra-galactic nebulae. *Proceedings of the National Academy of Sciences*, 15(3):168–173, 1929. doi: 10.1073/pnas.15.3.168.

Edmund Husserl. *Ideas Pertaining to a Pure Phenomenology and to a Phenomenological Philosophy*. Martinus Nijhoff, The Hague, 1913. English translation by F. Kersten, 1983.

Edmund Husserl. *Vorlesungen zur Phänomenologie des inneren Zeitbewusstseins*. Max Niemeyer Verlag, Halle, 1928. Edited by M. Heidegger. English translation: *On the Phenomenology of the Consciousness of Internal Time*, trans. J. B. Brough, Kluwer, 1991.

Giorgio Immirzi. Quantum gravity and regge calculus. *Nuclear Physics B – Proceedings Supplements*, 57:65–72, 1997. doi: 10.1016/S0920-5632(97)00354-X.

Laurent Itti and Christof Koch. A saliency-based search mechanism for overt and covert shifts of visual attention. *Vision Research*, 40(10–12):1489–1506, 2000. doi: 10.1016/S0042-6989(99)00163-7.

Vivek Iyer and Robert M. Wald. Some properties of the Noether charge and a proposal for dynamical black hole entropy. *Physical Review D*, 50:846–864, 1994. doi: 10.1103/PhysRevD.50.846.

R. Jackiw and C. Rebbi. Solitons with fermion number 1/2. *Physical Review D*, 13(12): 3398–3409, 1976. doi: 10.1103/PhysRevD.13.3398.

T. Jacobson. Thermodynamics of spacetime: The Einstein equation of state. *Physical Review Letters*, 75(7):1260–1263, 1995.

W. James. *The Principles of Psychology.* Henry Holt and Company, New York, 1890.

W. James. Does 'consciousness' exist? *Journal of Philosophy, Psychology and Scientific Methods*, 1(18):477–491, 1904.

William James. *Essays in Radical Empiricism.* Longmans, Green, and Co., New York, 1912.

E. T. Jaynes. Information theory and statistical mechanics. *Physical Review*, 106(4):620–630, 1957. doi: 10.1103/PhysRev.106.620.

E. Joos and H. D. Zeh. The emergence of classical properties through interaction with the environment. *Zeitschrift für Physik B*, 59:223–243, 1985. doi: 10.1007/BF01725541.

Hassan K. Khalil. *Nonlinear Systems.* Prentice Hall, 3rd edition, 2002. Canonical reference for Lyapunov stability theory.

Hyoungkyu Kim, Anthony G. Hudetz, Joseph Lee, George A. Mashour, and UnCheol Lee. Estimating the integrated information measure Phi from high-density electroencephalography during states of consciousness in humans. *Frontiers in Human Neuroscience*, 12:42, 2018. doi: 10.3389/fnhum.2018.00042.

Michael Kirchhoff, Thomas Parr, Ensor Palacios, Karl Friston, and Julian Kiverstein. The Markov blankets of life: autonomy, active inference and the free energy principle. *Journal of the Royal Society Interface*, 15(138):20170792, 2018. doi: 10.1098/rsif.2017.0792.

Anatoly Klypin, Andrey V. Kravtsov, Octavio Valenzuela, and Francisco Prada. Where are the missing galactic satellites? *The Astrophysical Journal*, 522:82–92, 1999. doi: 10.1086/307643.

M. Kobayashi and T. Maskawa. CP-violation in the renormalizable theory of weak interaction. *Progress of Theoretical Physics*, 49(2):652–657, 1973.

S. Kochen and E. P. Specker. The problem of hidden variables in quantum mechanics. *Journal of Mathematics and Mechanics*, 17:59–87, 1967.

Jan J. Koenderink. *Color for the Sciences.* MIT Press, Cambridge, MA, 2010.

J. Michael Kosterlitz and David J. Thouless. Ordering, metastability and phase transitions in two-dimensional systems. *Journal of Physics C: Solid State Physics*, 6:1181–1203, 1973. doi: 10.1088/0022-3719/6/7/010.

Kramida, A. and Ralchenko, Yu. and Reader, J. and NIST ASD Team. NIST Atomic Spectra Database (version 5.11). https://physics.nist.gov/asd, 2023. National Institute of Standards and Technology, Gaithersburg, MD.

I. Labbé et al. A population of red candidate massive galaxies ~600 Myr after the Big Bang. *Nature*, 616(7956):266–269, 2023. doi: 10.1038/s41586-023-05786-2.

James Ladyman and Lorenzo Lorenzetti. Effective ontic structural realism. *The British Journal for the Philosophy of Science*, 2024. Forthcoming.

James Ladyman and Don Ross. *Every Thing Must Go: Metaphysics Naturalized*. Oxford University Press, 2007.

Rolf Landauer. Irreversibility and heat generation in the computing process. *IBM Journal of Research and Development*, 5(3):183–191, 1961. doi: 10.1147/rd.53.0183.

Laozi. *Dao De Jing*. Various (traditionally attributed, c. 4th century BCE), c. 400 BCE. Chapter 42. Translation following D. C. Lau, *Tao Te Ching*, Penguin, 1963.

Claude LeBrun and L. J. Mason. Zoll manifolds and complex surfaces. *Journal of Differential Geometry*, 61(3):453–535, 2002. doi: 10.4310/jdg/1090351530.

Claude LeBrun and L. J. Mason. Nonlinear gravitons, null geodesics, and holomorphic disks. *Duke Mathematical Journal*, 136(2):205–273, 2007. doi: 10.1215/S0012-7094-07-13621-4.

Claude LeBrun and L. J. Mason. The Einstein-Weyl equations, scattering maps, and holomorphic disks. *Mathematical Research Letters*, 16(2):291–301, 2009. doi: 10.4310/MRL.2009.v16.n2.a8.

T. D. Lee and C. N. Yang. Question of parity conservation in weak interactions. *Physical Review*, 104:254–258, 1956. doi: 10.1103/PhysRev.104.254.

Gottfried Wilhelm Leibniz. *Monadology*. Various (originally circulated in manuscript), 1714. Translated by G. R. Montgomery.

J. M. Leinaas and J. Myrheim. On the theory of identical particles. *Il Nuovo Cimento B*, 37 (1):1–23, 1977. doi: 10.1007/BF02727953.

Na Li, Dongshi Lu, Lei Yang, Huan Tao, Younian Xu, Chenchen Wang, Lisha Fu, Hui Liu, Yatisha Chummum, and Shihai Zhang. Nuclear spin attenuates the anesthetic potency of xenon isotopes in mice: implications for the mechanisms of anesthesia and consciousness. *Anesthesiology*, 129(2):271–277, 2018. doi: 10.1097/ALN.0000000000002226.

LIGO Scientific Collaboration, Virgo Collaboration, Fermi Gamma-ray Burst Monitor, and INTEGRAL. Gravitational waves and gamma-rays from a binary neutron star merger: GW170817 and GRB 170817a. *Astrophys. J. Lett.*, 848(2):L13, 2017. doi: 10.3847/2041-8213/aa920c.

Göran Lindblad. On the generators of quantum dynamical semigroups. *Communications in Mathematical Physics*, 48(2):119–130, 1976. doi: 10.1007/BF01608499.

A. D. Linde. A new inflationary universe scenario: A possible solution of the horizon, flatness, homogeneity, isotropy and primordial monopole problems. *Physics Letters B*, 108(6):389–393, 1982. doi: 10.1016/0370-2693(82)91219-9.

John E. Lisman and Ole Jensen. The theta-gamma neural code. *Neuron*, 77(6):1002–1016, 2013. doi: 10.1016/j.neuron.2013.03.007.

H. W. Lissmann. On the function and evolution of electric organs in fish. *Journal of Experimental Biology*, 35(1):156–191, 1958.

David L. MacAdam. Visual sensitivities to color differences in daylight. *Journal of the Optical Society of America*, 32(5):247–274, 1942. doi: 10.1364/JOSA.32.000247.

Ernst Mach. *Die Analyse der Empfindungen und das Verhältnis des Physischen zum Psychischen*. Gustav Fischer, Jena, 1886. English translation: *The Analysis of Sensations*, trans. C. M. Williams, Open Court, 1914.

J. Maldacena. The large N limit of superconformal field theories and supergravity. *Advances in Theoretical and Mathematical Physics*, 2(2):231–252, 1998.

Norman Margolus and Lev B. Levitin. The maximum speed of dynamical evolution. *Physica D*, 120(1–2):188–195, 1998. doi: 10.1016/S0167-2789(98)00054-2.

N. J. Marshall. A unique colour and polarization vision system in mantis shrimps. *Nature*, 333(6173):557–560, 1988. doi: 10.1038/333557a0.

James Clerk Maxwell. *Theory of Heat*. Longmans, Green, and Co., London, 1871.

Dusa McDuff and Dietmar Salamon. *Introduction to Symplectic Topology*. Oxford Graduate Texts in Mathematics. Oxford University Press, 3rd edition, 2017. Canonical reference for Lagrangian submanifolds and the vanishing of the symplectic form on them.

Albert A. Michelson and Edward W. Morley. On the relative motion of the earth and the luminiferous ether. *American Journal of Science*, 34(203):333–345, 1887.

M. Milgrom. A modification of the Newtonian dynamics as a possible alternative to the hidden mass hypothesis. *The Astrophysical Journal*, 270:365–370, 1983.

John W. Milnor and James D. Stasheff. *Characteristic Classes*, volume 76 of *Annals of Mathematics Studies*. Princeton University Press, 1974.

Peter Minkowski. $\mu \to e\gamma$ at a rate of one out of 10^9 muon decays? *Physics Letters B*, 67: 421–428, 1977. doi: 10.1016/0370-2693(77)90435-X.

Rabindra N. Mohapatra and Goran Senjanović. Neutrino masses and mixings in gauge models with spontaneous parity violation. *Physical Review D*, 23:165–180, 1981. doi: 10.1103/PhysRevD.23.165.

Claus Montonen and David I. Olive. Magnetic monopoles as gauge particles? *Physics Letters B*, 72(1):117–120, 1977.

Cynthia F. Moss and Annemarie Surlykke. Probing the natural scene by echolocation in bats. *Frontiers in Behavioral Neuroscience*, 4:33, 2010. doi: 10.3389/fnbeh.2010.00033.

T. Nagel. What is it like to be a bat? *The Philosophical Review*, 83(4):435–450, 1974.

M. Nakahara. *Geometry, Topology and Physics*. Institute of Physics Publishing, Bristol, 2nd edition, 2003.

Walther Nernst. Über die berechnung chemischer gleichgewichte aus thermischen messungen. *Nachrichten von der Gesellschaft der Wissenschaften zu Göttingen, Mathematisch-Physikalische Klasse*, pages 1–40, 1906. Origin of the third law of thermodynamics (heat theorem).

Hartmut Neven, Adam Zalcman, Peter Read, Kenneth S. Kosik, Tjitse van der Molen, Dirk Bouwmeester, Eve Bodnia, Luca Turin, and Christof Koch. Testing the conjecture that quantum processes create conscious experience. *Entropy*, 26(6):460, 2024. doi: 10.3390/e26060460.

Eric A. Newman and Peter H. Hartline. The infrared “vision” of snakes. *Scientific American*, 246(3):116–127, 1982. doi: 10.1038/scientificamerican0382-116.

Yoshihito Niimura. Olfactory receptor multigene family in vertebrates: From the viewpoint of evolutionary genomics. *Current Genomics*, 13(2):103–114, 2012. doi: 10.2174/138920212799860706.

Kazuhiko Nishijima. Charge independence theory of V particles. *Progress of Theoretical Physics*, 13(3):285–304, 1955. doi: 10.1143/PTP.13.285.

Yong-Geun Oh. Relative Floer and quantum cohomology and the symplectic topology of Lagrangian submanifolds. *Asian J. Math.*, 1(1):96–127, 1997.

Masafumi Oizumi, Larissa Albantakis, and Giulio Tononi. From the phenomenology to the mechanisms of consciousness: Integrated Information Theory 3.0. *PLoS Computational Biology*, 10(5):e1003588, 2014. doi: 10.1371/journal.pcbi.1003588.

Don N. Page. Information in black hole radiation. *Physical Review Letters*, 71(23):3743–3746, 1993.

Thomas Parr, Giovanni Pezzulo, and Karl J. Friston. *Active Inference: The Free Energy Principle in Mind, Brain, and Behavior*. MIT Press, Cambridge, MA, 2022. ISBN 9780262045353.

Particle Data Group. Review of particle physics. *Physical Review D*, 110:030001, 2024. doi: 10.1103/PhysRevD.110.030001.

Arun Kumar Pati and Samuel L. Braunstein. Impossibility of deleting an unknown quantum state. *Nature*, 404:164–165, 2000. doi: 10.1038/35004532.

Jogesh C. Pati and Abdus Salam. Lepton number as the fourth “color”. *Physical Review D*, 10:275–289, 1974. doi: 10.1103/PhysRevD.10.275.

W. Pauli. The connection between spin and statistics. *Physical Review*, 58(8):716–722, 1940. doi: 10.1103/PhysRev.58.716.

Judea Pearl. *Causality: Models, Reasoning, and Inference*. Cambridge University Press, 2nd edition, 2009. doi: 10.1017/CBO9780511803161.

R. D. Peccei and H. R. Quinn. CP conservation in the presence of pseudoparticles. *Physical Review Letters*, 38(25):1440–1443, 1977.

R. Penrose. Twistor algebra. *Journal of Mathematical Physics*, 8(2):345–366, 1967.

R. Penrose. *The Emperor's New Mind: Concerning Computers, Minds, and the Laws of Physics*. Oxford University Press, Oxford, 1989.

R. Penrose. On gravity's role in quantum state reduction. *General Relativity and Gravitation*, 28(5):581–600, 1996. doi: 10.1007/BF02105068.

R. Penrose and W. Rindler. *Spinors and Space-Time: Volume 1, Two-Spinor Calculus and Relativistic Fields*. Cambridge University Press, Cambridge, 1984.

Roger Penrose. *Cycles of Time: An Extraordinary New View of the Universe*. Bodley Head, London, 2010.

S. Perlmutter et al. Measurements of ω and λ from 42 high-redshift supernovae. *The Astrophysical Journal*, 517(2):565–586, 1999. doi: 10.1086/307221.

M. E. Peskin and D. V. Schroeder. *An Introduction to Quantum Field Theory*. Westview Press, Boulder, 1995.

Planck Collaboration. Planck 2018 results. VI. cosmological parameters. *Astronomy & Astrophysics*, 641:A6, 2020. doi: 10.1051/0004-6361/201833910. Data release referred to as "Planck 2018".

J. Polchinski. *String Theory: Volume 1, An Introduction to the Bosonic String*. Cambridge University Press, Cambridge, 1998.

H. D. Politzer. Reliable perturbative results for strong interactions? *Physical Review Letters*, 30(26):1346–1349, 1973.

Uwe Proske and Simon C. Gandevia. The proprioceptive senses: Their roles in signaling body shape, body position and movement, and muscle force. *Physiological Reviews*, 92(4): 1651–1697, 2012. doi: 10.1152/physrev.00048.2011.

Edoardo Provenzi. Geometry of color perception. Part 1: structures and metrics of a homogeneous color space. *The Journal of Mathematical Neuroscience*, 10:7, 2020. doi: 10.1186/s13408-020-00084-x.

R. Rajaraman. *Solitons and Instantons: An Introduction to Solitons and Instantons in Quantum Field Theory*. North-Holland, 1982. Standard textbook treatment of instanton tunneling amplitudes.

Rajesh P. N. Rao and Dana H. Ballard. Predictive coding in the visual cortex: a functional interpretation of some extra-classical receptive-field effects. *Nature Neuroscience*, 2(1):79–87, 1999. doi: 10.1038/4580. Foundational predictive-coding model bridging neuroscience and machine-learning treatments of hierarchical inference.

Nicholas Rescher. *Process Metaphysics: An Introduction to Process Philosophy*. State University of New York Press, Albany, 1996.

Howard L. Resnikoff. Differential geometry and color perception. *Journal of Mathematical Biology*, 1(2):97–131, 1974. doi: 10.1007/BF00275798.

A. G. Riess et al. A comprehensive measurement of the local value of the Hubble constant with 1 km/s/Mpc uncertainty from the Hubble Space Telescope and the SH0ES team. *The Astrophysical Journal Letters*, 934(1):L7, 2022. doi: 10.3847/2041-8213/ac5c5b.

Adam G. Riess et al. Observational evidence from supernovae for an accelerating universe and a cosmological constant. *The Astronomical Journal*, 116(3):1009–1038, 1998. doi: 10.1086/300499.

Carlo Rovelli. Relational quantum mechanics. *International Journal of Theoretical Physics*, 35:1637–1678, 1996. doi: 10.1007/BF02302261. arXiv:quant-ph/9609002.

D. Rudrauf, D. Bennequin, I. Granic, G. Landini, K. Friston, and K. Williford. A mathematical model of embodied consciousness. *Journal of Theoretical Biology*, 428:106–131, 2017. doi: 10.1016/j.jtbi.2017.05.032.

David Rudrauf, Grégoire Sergeant-Perthuis, Yvain Tisserand, Germain Poloudenny, Kenneth Williford, and Michel-Ange Amorim. Combining the Projective Consciousness Model and virtual humans for immersive psychological research: A proof-of-concept simulation study. *Brain Sciences*, 13(10):1435, 2023. doi: 10.3390/brainsci13101435.

B. Russell. *The Analysis of Matter*. Kegan Paul, Trench, Trubner & Co., London, 1927.

Bertrand Russell. *The Analysis of Mind*. George Allen & Unwin, London, 1921.

A. Salam. Weak and electromagnetic interactions. In *Elementary Particle Physics: Relativistic Groups and Analyticity (Nobel Symposium No. 8)*, 1968.

M. Schlosshauer. *Decoherence and the Quantum-to-Classical Transition*. Springer, Berlin, 2007.

Geoffrey Schoenbaum, Matthew R. Roesch, Thomas A. Stalnaker, and Yuji K. Takahashi. A new perspective on the role of the orbitofrontal cortex in adaptive behaviour. *Nature Reviews Neuroscience*, 10(12):885–892, 2009. doi: 10.1038/nrn2753.

Erwin Schrödinger. Die gegenwärtige situation in der quantenmechanik. *Naturwissenschaften*, 23:807–812; 823–828; 844–849, 1935. doi: 10.1007/BF01491891.

Karl Schwarzschild. Über das gravitationsfeld eines massenpunktes nach der einsteinschen theorie. *Sitzungsberichte der Königlich-Preussischen Akademie der Wissenschaften*, pages 189–196, 1916.

Julian Schwinger. On gauge invariance and vacuum polarization. *Physical Review*, 82(5): 664–679, 1951. doi: 10.1103/PhysRev.82.664.

Robert T. Seeley. Complex powers of an elliptic operator. *Proceedings of Symposia in Pure Mathematics*, 10:288–307, 1967.

Claude E. Shannon. A mathematical theory of communication. *The Bell System Technical Journal*, 27:379–423, 1948. doi: 10.1002/j.1538-7305.1948.tb01338.x.

Peter W. Shor. Polynomial-time algorithms for prime factorization and discrete logarithms on a quantum computer. *SIAM Journal on Computing*, 26(5):1484–1509, 1997. doi: 10.1137/S0097539795293172.

B. G. Sidharth. The fractal universe: From the Planck to the Hubble scale. *arXiv preprint physics/9907024*, 1999.

B. G. Sidharth. *The Chaotic Universe: From the Planck to the Hubble Scale*. Nova Science Publishers, New York, 2001.

James A. Simmons. A view of the world through the bat's ear: The formation of acoustic images in echolocation. *Cognition*, 33(1–2):155–199, 1989. doi: 10.1016/0010-0277(89) 90009-7.

Rafael D. Sorkin. Causal sets: Discrete gravity. In Andrés Gomberoff and Donald Marolf, editors, *Lectures on Quantum Gravity*, pages 305–327. Springer, Boston, 2005. doi: 10.1007/0-387-24992-3_7. arXiv:gr-qc/0309009.

Charles Spence and Jon Driver, editors. *Crossmodal Space and Crossmodal Attention*. Oxford University Press, Oxford, 2004.

Baruch Spinoza. *Ethica: Ordine Geometrico Demonstrata*. Beneventum, The Hague, 1677.

Olaf Sporns, Giulio Tononi, and Rolf Kötter. The human connectome: A structural description of the human brain. *PLoS Computational Biology*, 1(4):e42, 2005. doi: 10.1371/journal.pcbi.0010042.

Martin Stacho, Christina Herold, Noemi Rook, Hermann Wagner, Markus Axer, Katrin Amunts, and Onur Güntürkün. A cortex-like canonical circuit in the avian forebrain. *Science*, 369(6511):eabc5534, 2020. doi: 10.1126/science.abc5534.

STAR Collaboration. Experimental and theoretical challenges in the search for the quark-gluon plasma: The STAR Collaboration's critical assessment of the evidence from RHIC collisions. *Nuclear Physics A*, 757(1-2):102–183, 2005. doi: 10.1016/j.nuclphysa.2005.03.085.

Andrew Stockman and Lindsay T. Sharpe. The spectral sensitivities of the middle- and long-wavelength-sensitive cones derived from measurements in observers of known genotype. *Vision Research*, 40(13):1711–1737, 2000. doi: 10.1016/S0042-6989(00)00021-3.

L. Susskind, L. Thorlacius, and J. Uglum. The stretched horizon and black hole complementarity. *Physical Review D*, 48(8):3743–3761, 1993.

Leonard Susskind. The world as a hologram. *Journal of Mathematical Physics*, 36(11):6377–6396, 1995.

Gerard 't Hooft. Computation of the quantum effects due to a four-dimensional pseudoparticle. *Physical Review D*, 14:3432–3450, 1976. doi: 10.1103/PhysRevD.14.3432.

Gerard 't Hooft. Dimensional reduction in quantum gravity. *arXiv preprint gr-qc/9310026*, 1993.

Max Tegmark, Anthony Aguirre, Martin J. Rees, and Frank Wilczek. Dimensionless constants, cosmology, and other dark matters. *Physical Review D*, 73(2):023505, 2006. doi: 10.1103/PhysRevD.73.023505.

Hanne H. Thoen, Martin J. How, Tsyr-Huei Chiou, and Justin Marshall. A different form of color vision in mantis shrimp. *Science*, 343(6169):411–413, 2014. doi: 10.1126/science.1245824.

E. Tiesinga, P. J. Mohr, D. B. Newell, and B. N. Taylor. CODATA recommended values of the fundamental physical constants: 2018. *Reviews of Modern Physics*, 93:025010, 2021. doi: 10.1103/RevModPhys.93.025010.

G. Tononi. An information integration theory of consciousness. *BMC Neuroscience*, 5:42, 2004. doi: 10.1186/1471-2202-5-42.

G. Tononi, M. Boly, M. Massimini, and C. Koch. Integrated information theory: from consciousness to its physical substrate. *Nature Reviews Neuroscience*, 17(7):450–461, 2016. doi: 10.1038/nrn.2016.44.

Michael T. Treadway and David H. Zald. Reconsidering anhedonia in depression: Lessons from translational neuroscience. *Neuroscience and Biobehavioral Reviews*, 35(3):537–555, 2011. doi: 10.1016/j.neubiorev.2010.06.006.

William G. Unruh. Notes on black-hole evaporation. *Physical Review D*, 14:870–892, 1976. doi: 10.1103/PhysRevD.14.870.

E. Verlinde. On the origin of gravity and the laws of Newton. *Journal of High Energy Physics*, 2011(4):29, 2011.

Erik P. Verlinde. Emergent gravity and the dark universe. *SciPost Physics*, 2(3):016, 2017. doi: 10.21468/SciPostPhys.2.3.016.

Gerhard von der Emde, Steffen Schwarz, Leonel Gomez, Ruben Budelli, and Kirsty Grant. Electric fish measure distance in the dark. *Nature*, 395(6705):890–894, 1998. doi: 10.1038/27655.

Hermann von Helmholtz. Über die erhaltung der kraft. *G. Reimer, Berlin*, 1847. Canonical statement of the first law (conservation of energy).

John von Neumann. *Mathematische Grundlagen der Quantenmechanik*. Springer, Berlin, 1932.

Robert M. Wald. Black hole entropy is the Noether charge. *Physical Review D*, 48:R3427–R3431, 1993. doi: 10.1103/PhysRevD.48.R3427.

Brian A. Wandell. *Foundations of Vision*. Sinauer Associates, Sunderland, MA, 1995.

Duncan J. Watts and Steven H. Strogatz. Collective dynamics of 'small-world' networks. *Nature*, 393(6684):440–442, 1998. doi: 10.1038/30918.

S. Weinberg. A model of leptons. *Physical Review Letters*, 19(21):1264–1266, 1967.

S. Weinberg. A new light boson? *Physical Review Letters*, 40(4):223–226, 1978.

S. Weinberg. *The Quantum Theory of Fields: Volume 1, Foundations*. Cambridge University Press, Cambridge, 1995.

Steven Weinberg. The cosmological constant problem. *Reviews of Modern Physics*, 61:1–23, 1989. doi: 10.1103/RevModPhys.61.1.

J. A. Wheeler. Superspace and the nature of quantum geometrodynamics. In C. DeWitt and J. A. Wheeler, editors, *Battelle Rencontres: 1967 Lectures in Mathematics and Physics*, pages 242–307. Benjamin, New York, 1968.

Alfred North Whitehead. *Process and Reality: An Essay in Cosmology*. Macmillan, New York, 1929.

Alfred North Whitehead. *Process and Reality: An Essay in Cosmology*. The Free Press, New York, corrected edition, 1978. Originally published 1929.

Eugene P. Wigner. The unreasonable effectiveness of mathematics in the natural sciences. *Communications on Pure and Applied Mathematics*, 13(1):1–14, 1960. doi: 10.1002/cpa.3160130102.

Eugene P. Wigner. Remarks on the mind-body question. In I. J. Good, editor, *The Scientist Speculates*, pages 284–302. Heinemann, 1961.

James G. Williams, Slava G. Turyshev, and Dale H. Boggs. Progress in lunar laser ranging tests of relativistic gravity. *Physical Review Letters*, 93:261101, 2004. doi: 10.1103/PhysRevLett.93.261101.

Kenneth Williford, Daniel Bennequin, Karl Friston, and David Rudrauf. The projective consciousness model and phenomenal selfhood. *Frontiers in Psychology*, 9:2571, 2018. doi: 10.3389/fpsyg.2018.02571.

K. G. Wilson. Confinement of quarks. *Physical Review D*, 10(8):2445–2459, 1974.

K. G. Wilson. The renormalization group: Critical phenomena and the Kondo problem. *Reviews of Modern Physics*, 47(4):773–840, 1975. doi: 10.1103/RevModPhys.47.773.

William K. Wootters and Wojciech H. Zurek. A single quantum cannot be cloned. *Nature*, 299:802–803, 1982. doi: 10.1038/299802a0.

C. S. Wu, E. Ambler, R. W. Hayward, D. D. Hoppes, and R. P. Hudson. Experimental test of parity conservation in beta decay. *Physical Review*, 105:1413–1415, 1957. doi: 10.1103/PhysRev.105.1413.

Tai Tsun Wu and Chen Ning Yang. Concept of nonintegrable phase factors and global formulation of gauge fields. *Physical Review D*, 12(12):3845–3857, 1975. doi: 10.1103/PhysRevD.12.3845. Canonical reference for the fiber-bundle interpretation of gauge theories.

Takashi Yamamoto, Tsuyoshi Shimura, Noritaka Sakai, and Noboru Ozaki. Representation of hedonics and quality of taste stimuli in the parabrachial nucleus of the rat. *Physiology & Behavior*, 56(6):1197–1202, 1994. doi: 10.1016/0031-9384(94)90366-2.

H. Dieter Zeh. On the interpretation of measurement in quantum theory. *Foundations of Physics*, 1:69–76, 1970. doi: 10.1007/BF00708656.

W. H. Zurek. Decoherence, einselection, and the quantum origins of the classical. *Reviews of Modern Physics*, 75(3):715–775, 2003.